



City Research Online

City, University of London Institutional Repository

Citation: Panchal, J. P. (2018). Minimising ground movements around deep excavations in soft soils. (Unpublished Doctoral thesis, City, University of London)

This is the accepted version of the paper.

This version of the publication may differ from the final published version.

Permanent repository link: <https://openaccess.city.ac.uk/id/eprint/21044/>

Link to published version:

Copyright: City Research Online aims to make research outputs of City, University of London available to a wider audience. Copyright and Moral Rights remain with the author(s) and/or copyright holders. URLs from City Research Online may be freely distributed and linked to.

Reuse: Copies of full items can be used for personal research or study, educational, or not-for-profit purposes without prior permission or charge. Provided that the authors, title and full bibliographic details are credited, a hyperlink and/or URL is given for the original metadata page and the content is not changed in any way.

**MINIMISING GROUND MOVEMENTS
AROUND DEEP EXCAVATIONS
IN SOFT SOILS**

by

Jignasha Prakash Panchal

A dissertation submitted for the Degree of
Doctor of Philosophy

City, University of London
Research Centre for Multi-scale Geotechnical Engineering
Department of Civil Engineering

November 2018

Persevere

Dedicated to

Shantaben Thakorhai Mistry

for her faith and wisdom

CONTENTS

	PAGE NO.
--	-----------------

LIST OF TABLES	VIII
LIST OF FIGURES	IX
ACKNOWLEDGEMENTS	XXV
DECLARATION	XXVI
ABSTRACT	XXVII
LIST OF SYMBOLS	XXVIII
CHAPTER 1 INTRODUCTION	1
1.1 Background	1
1.2 Objectives	3
1.3 Experimental work	3
1.4 Summary of thesis	5
CHAPTER 2 LITERATURE REVIEW	7
2.1 Introduction	7
2.2 Mechanisms of ground movement	7
2.3 Vertical stress relief	9
2.4 Earth pressure at rest	9
2.5 Wall installation effects	11
2.6 Influence of wall stiffness on deformations in soft ground	12
2.7 Numerical analyses of excavations in soft soils	13
2.8 Case studies of excavations in soft soils	15
2.9 Soil displacement trends identified from databases	17
2.9.1 Peck (1969)	17
2.9.2 Mana & Clough (1981)	17
2.9.3 Clough & O'Rourke (1990)	19
2.9.4 Long (2001)	19
2.9.5 Moormann (2004)	20
2.9.6 Wang <i>et al.</i> (2010)	21

2.10	Centrifuge modelling	22
	2.10.1 Modelling excavations in the centrifuge	22
	2.10.2 Centrifuge modelling of excavations in soft ground	24
2.11	Methods of controlling ground movements in soft soils	26
	2.11.1 Soil strengthening: ground improvement techniques	27
	2.11.2 Soil strengthening: additional construction	31
	2.11.3 Surcharging the excavation formation level	33
2.12	Summary	38
CHAPTER 3	CENTRIFUGE MODELLING	41
3.1	Introduction	41
3.2	Principals of centrifuge modelling	41
3.3	Scaling laws	42
3.4	Errors in centrifuge modelling	44
	3.4.1 Variations in stress levels	44
	3.4.2 Radial acceleration error	45
	3.4.3 Grain size scaling effects	45
	3.4.4 Boundary effects	46
3.5	The geotechnical centrifuge	46
	3.5.1 The Acutronic 661 Geotechnical Centrifuge	46
	3.5.2 Data acquisition	47
	3.5.3 Instrumentation and calibration	48
	3.5.4 Image processing – Visimet	49
	3.5.5 Image processing – GeoPIV-RG	50
3.6	Summary	51
CHAPTER 4	APPARATUS DEVELOPMENT	52
4.1	Introduction	52
4.2	Typical approaches to modelling excavations	52

4.3	Model design requirements	53
	4.3.1 Strongbox	54
	4.3.2 Ground water supply	55
	4.3.3 Positioning of LVDTs	55
	4.3.4 Location of PPTs	56
4.4	Apparatus common to all tests; design and development	56
	4.4.1 Simulation of excavation	56
	4.4.2 Retaining wall	57
	4.4.3 Silicone seals	58
	4.4.4 Aluminium excavation support system	60
	4.4.5 Capping beam	61
	4.4.6 Spacer between the retaining wall and airbag	62
	4.4.7 Bespoke LVDT footings	62
4.5	Test specific apparatus	63
	4.5.1 Underwater excavations	63
	4.5.2 Deep soil mixing ground improvement	65
	4.5.3 Double wall excavation	65
	4.5.4 Berm supported excavation	66
4.6	Summary	67
CHAPTER 5	EXPERIMENTAL TEST SERIES	68
5.1	Introduction	68
5.2	Stress history of soil sample	68
5.3	Sample preparation	69
	5.3.1 Sample preparation of lime-stabilised soil	72
5.4	Model making	74
	5.4.1 General model making method	74
	5.4.2 Model making specific to underwater excavations	78
	5.4.3 Deep soil mixing modelling technique	78

5.4.4	Double wall model making procedure	79
5.4.5	Modelling a bermed excavation	80
5.5	Test procedure	81
5.5.1	Underwater excavation test procedure	82
5.5.2	Bermed excavation	82
5.6	Image analysis	83
5.7	Summary	85
CHAPTER 6	CENTRIFUGE TEST RESULTS	86
6.1	Details of tests	86
6.1.1	Preliminary test; JP1	88
6.1.2	Preliminary underwater excavation test; JP3	88
6.1.3	Underwater excavation tests; JP6 and JP8	90
6.1.4	Baseline tests; JP7 and JP9	90
6.1.5	Tension propping tests; JP11 and JP12	91
6.1.6	Deep soil mixing tests; JP10, JP14 and JP15	92
6.1.7	Double wall tests; JP12, JP13, JP18 and JP20	93
6.1.8	Bermed excavation tests; JP16, JP17 and JP19	94
6.1.9	Combined excavation method tests; JP21 and JP22	95
6.2	Observations and results	96
6.2.1	Influence of embedment on ground movements	96
6.2.2	Effects of construction methods on displacements	101
6.3	Pore pressure responses	106
6.4	Correlation between air pressure transducer measurements and digital pressure indicator (DPI) readings	110
6.5	Comparison between LVDT measurements and image processing computations at the retained surface	111
6.6	Summary	113
6.6.1	Wall embedment and surface settlements	114

6.6.2	Effect of wall fixity on ground movements	114
6.6.3	Influence of construction method on settlements	114
CHAPTER 7	DISCUSSION	115
7.1	Introduction	115
7.2	Excavation stiffness support system	115
7.3	Excavation support mechanisms	116
7.3.1	Theorised effectiveness of excavation methods	116
7.4	Heave at formation level	121
7.4.1	Influence of embedment depth on heave	126
7.4.2	Impact of fixity conditions on ground movements	128
7.4.3	Limiting the width of ground improvement or surcharge on excavation formation level	128
7.5	Soil settlements of retained surface	130
7.6	Soil model shear strength profile	134
7.7	Failure mechanisms	136
7.8	Excavation failure pressure	137
7.9	Summary	138
CHAPTER 8	CONCLUSIONS, LIMITATIONS OF RESEARCH AND RECOMMENDATIONS FOR FURTHER WORK	140
8.1	Introduction	140
8.2	Experimental approach	140
8.3	Conclusions	142
8.4	Limitations and implications of this project	145
8.5	Recommendations for further work	147
REFERENCES		148
TABLES		
FIGURES		
APPENDIX A		

LIST OF TABLES

- Table 2.1 Factors affecting increase in strength of DSM treated soil (after Bruce *et al.*, 1998)
- Table 2.2 Typical values of DSM treated soil (after Bruce *et al.*, 1998)
- Table 3.1 Scaling laws for centrifuge tests (Powrie, 1986)
- Table 3.2 Properties of Speswhite kaolin clay (after Grant, 1998)
- Table 6.1 Summary of centrifuge tests conducted including comments on successes and failures
- Table 6.2 Centrifuge test series and notation
- Table 6.3 Excavation camera (angled) calibration check
- Table 6.4 Straight camera (perpendicular) calibration check
- Table 6.5 Comparison between PIV analysis, LVDT and slip gauge results for all excavation camera and far camera data
- Table 7.1 Comparisons between excavation depths at failure calculated from the Peck (1969) stability number, the UB developed solution and the depth at failure measured from overburden pressure in the centrifuge tests.

LIST OF FIGURES

- Figure 2.1 Deep seated inward displacement due to excavations (after Burland *et al.*, 1979)
- Figure 2.2 Vertical stress relief at the base of an excavation (after Burland *et al.*, 1979)
- Figure 2.3 Movements occurring from horizontal stress relief (after Burland *et al.*, 1979)
- Figure 2.4 Influence of stress history on the relationship between horizontal effective stresses and the effective overburden pressure in clays (Gaba *et al.* (2017) after Burland *et al.*, 1979)
- Figure 2.5 Simplified soil stress history under K_0 conditions (after Mayne & Kulhawy, 1982)
- Figure 2.6 Variation in K_0 against overconsolidation ratio for three clays (Ladd & Varallyay, 1965)
- Figure 2.7 Measured lateral earth pressures on a diaphragm wall during excavation of a 17m deep basement in soft silty clay (Sato *et al.*, 1992)
- Figure 2.8 Plan of instrumented site (Finno *et al.*, 1988)
- Figure 2.9 Development of strains during and after sheet pile installation (Finno & Nerby, 1989)
- Figure 2.10 Pore pressure and settlement responses during pile driving and vibration (Finno *et al.*, 1988)
- Figure 2.11 General lateral deformation pattern (after O'Rourke, 1993)
- Figure 2.12 Comparison between field measurements and the computed incremental displacements (O'Rourke, 1993)
- Figure 2.13 Proposed method for predicting wall displacements based on FOS against basal heave and system stiffness (after Clough & O'Rourke, 1990)
- Figure 2.14 Wall displacements of a stiff retaining wall (Gaba *et al.*, 2017)

- Figure 2.15 Lateral wall displacements for a factor of safety of 2 during excavation where (a) $K_0 = 2$ and (b) $K_0 = 0.5$ (Potts & Fourier, 1984)
- Figure 2.16 Corresponding surface settlement profiles for a factor of safety of 2 during excavation where (a) $K_0 = 2$ and (b) $K_0 = 0.5$ (Potts & Fourier, 1984)
- Figure 2.17 Stress contours after 13m excavation in (a) $K_0 = 2$ and (b) $K_0 = 0.5$ (Potts & Fourier, 1984)
- Figure 2.18 Influence of wall embedment on surface settlements and lateral wall deflections in normally consolidated soil ($OCR = 1$) (Hashash & Whittle, 1996)
- Figure 2.19 Influence of prop spacing (h) on surface settlements and lateral wall deflections in normally consolidated soil ($OCR = 1$) for wall embedment of $L=60$ m (Hashash & Whittle, 1996)
- Figure 2.20 Lateral wall deflections arising from good construction sequencing and over-excavation prior to installing props (after Davidson, 1977)
- Figure 2.21 Measured and computed wall displacements of a cantilevered excavation comprising T-section diaphragm wall panels (Sato *et al.*, 1992)
- Figure 2.22 Stress distribution of reinforcement bars along the diaphragm walls (Sato *et al.*, 1992)
- Figure 2.23 Comparison of vertical displacements between greenfield site and those measured in densely developed areas (Ng *et al.*, 2012)
- Figure 2.24 Database of settlements of retained surface across various excavations in a range of ground conditions (Peck, 1969)
- Figure 2.25 Influence of basement level on settlement profile in Chicago (after Peck, 1969)
- Figure 2.26 Influence of FOS against basal heave on lateral wall displacements (after Mana & Clough, 1991)
- Figure 2.27 Additional data superimposed onto the original Mana & Clough (1981) graph (Gaba *et al.*, 2017)

- Figure 2.28 Excavation geometry in soft soil used to calculate the factor of safety against base heave
- Figure 2.29 Settlement at various distances beyond excavation normalised against the maximum recorded settlement (Clough & O'Rourke, 1990)
- Figure 2.30 Case studies included in the Long (2001) database replotted on Clough *et al.* (1989) graph
- Figure 2.31 Maximum vertical and horizontal displacements arising from deep excavations in soft clay ($S_u < 75\text{kN/m}^2$) (Moormann, 2004)
- Figure 2.32 Comparison between maximum vertical displacements in soft and stiff ground (Moormann, 2004)
- Figure 2.33 Moormann (2004) data superimposed on the Peck (1969) graph
- Figure 2.34 Maximum vertical and horizontal displacements arising from deep excavations in soft clay ($20\text{kN/m}^2 < S_u < 40\text{kN/m}^2$) (Wang *et al.*, 2010)
- Figure 2.35 Wang *et al.* (2010) data plotted on the Peck (1969) graph
- Figure 2.36 Image of excavation produced by in-flight excavator (Lim, 2003)
- Figure 2.37 (a) centrifuge test series and (b) experiment set up (Kimura *et al.*, 1994)
- Figure 2.38 Surface settlements measured 25mm from excavation (Kimura *et al.*, 1994)
- Figure 2.39 In-flight excavation test set up (Takemura *et al.*, 1999)
- Figure 2.40 Observed deformations for a 5.5m deep excavation illustrating the effect of embedment in sand and a floating wall (Takemura *et al.*, 1999)
- Figure 2.41 (a) normalised surface settlements for various tests as excavation progresses and (b) corresponding lateral wall deflections (Takemura *et al.*, 1999)
- Figure 2.42 Centrifuge test series (Takemura *et al.*, 1999)
- Figure 2.43 Apparatus set up for simulating in-flight excavation (Lam, 2010)
- Figure 2.44 Centrifuge test series (Lam *et al.*, 2014)

- Figure 2.45 Lateral wall deflections and surface settlements recorded in centrifuge tests (Lam *et al.*, 2014)
- Figure 2.46 Applicability of grouting processes for various soils (Bell, 2012)
- Figure 2.47 Deep soil mixing auger (Bell, 2012)
- Figure 2.48 Centrifuge set up on DSM ground improvements beneath excavation (Ohnishi *et al.*, 2000)
- Figure 2.49 Ground deformations for (a) Reference test were bearing capacity of soil is 60kPa (b) improved soil with 100kPa bearing capacity (c) improved soil with 400kPa bearing capacity (Ohnishi *et al.*, 2000)
- Figure 2.50 Lateral wall deflections in the untreated and ground improved sites (Lee & Yong, 1991)
- Figure 2.51 Cross section of site and proposed treatment (Tanaka, 1993)
- Figure 2.52 Heave measured during each stage of excavation across the entire formation level (Tanaka, 1993)
- Figure 2.53 Lateral deflections measured at two adjacent locations at end of excavation and section illustrating soil strata, final formation levels and depths of DSM treatment.
- Figure 2.54 Typical DSM patterns for use in excavations (Ou *et al.*, 1996)
- Figure 2.55 Comparison between EMS and RAS simulations (Ou *et al.*, 1996)
- Figure 2.56 Comparisons between field measurements on site in Taipei with the 3D RAS, EMS and 2D EMS models (Ou *et al.*, 1996)
- Figure 2.57 Experiment set up to model; (I) reference test; (II) treated strut across entire formation (III) improved soil with the presence of a gap and (IV) an improved soil berm (Lim, 2003)
- Figure 2.58 Typical results from centrifuge tests (Lim, 2003)
- Figure 2.59 Schematic of pin piles used in construction of deep excavation in London Clay and plan of site (Fernie *et al.*, 1991)
- Figure 2.60 Measured displacements after excavation (Fernie *et al.*, 1991)

- Figure 2.61 Schematic of heave reducing pile model (after McNamara, 2001)
- Figure 2.62 Comparable heave developed at formation (McNamara, 2001)
- Figure 2.63 Influence of embedment on ground movements (after McNamara, 2001)
- Figure 2.64 Comparative influence of heave reducing piles on predicted lateral deflections for braced excavation as excavation progresses (Osman & Bolton, 2006)
- Figure 2.65 Pit-in-pit excavation (Sun *et al.*, 2017)
- Figure 2.66 Failure mechanisms of varying wall spacing for pit-in-pit braced excavations (Sun *et al.*, 2017)
- Figure 2.67 Sequence of double walled excavations (Yu *et al.*, 2018)
- Figure 2.68 Plan of modelled tests (Yu *et al.*, 2018)
- Figure 2.69 Singapore Marina Bay station location and cross section (Denman *et al.*, 1987)
- Figure 2.70 Excavation schemes considered for the construction of the Marina Bay station box (Denman *et al.*, 1987)
- Figure 2.71 Excavation sequence at Marina Bay, Singapore (Denman *et al.*, 1987)
- Figure 2.72 Comparisons between measured and predicted deflections (Clarke & Prebaharan, 1987)
- Figure 2.73 Cross section through Oslo Opera excavation site (Karlsrud & Andresen, 2008)
- Figure 2.74 Typical berm geometry
- Figure 2.75 Influence of berm volume on settlements and lateral deflections compared with a cantilevered and propped excavation (Potts *et al.*, 1993)
- Figure 2.76 Experiment set up (Powrie & Daly, 2002)
- Figure 2.77 Short term behaviour on (a) surface settlement profile (a) lateral displacements of wall crest immediately after excavation (Powrie & Daly, 2002)

- Figure 2.78 Long term behaviour on (a) surface settlement profile 5 years after excavation (a) wall crest lateral displacements between 0-20 years (Powrie & Daly, 2002)
- Figure 2.79 Equivalent surcharge method (Daly & Powrie, 2001)
- Figure 2.80 Comparison between modelled and equivalent surcharge method berms on wall deflections and bending moments (Potts *et al.*, 1993)
- Figure 2.81 Berm geometry and soil profile (Powrie *et al.*, 1993)
- Figure 2.82 Raised effective formation level method (Gaba *et al.*, 2017)
- Figure 2.83 Modified limit equilibrium method (Daly & Powrie, 2001)
- Figure 2.84 (a) Classic deformation mechanism where H_c is the critical height that the excavation reaches prior to failure and H is the design excavation depth (b) influence of construction techniques designed to interrupt the classic deformation mechanism and (c) effect of reducing the vertical stress change
- Figure 3.1 Gravitational stress in prototype modelled by inertial stresses induced by rotational acceleration in centrifuge (after Taylor, 1995)
- Figure 3.2 Under and over stress in the centrifuge model (after Taylor, 1995)
- Figure 3.3 Schematic diagram of the Acutronic 661 centrifuge at City, University of London (after Le, 2017)
- Figure 3.4 (a) Original image taken with miniature USB camera and (b) undistorted image, curvature removed, used in Geo_PIV image analysis
- Figure 4.1 General centrifuge test arrangement
- Figure 4.2 Typical apparatus set up
- Figure 4.3 Images of retaining wall with tapered toes
- Figure 4.4 Retaining wall details, where X is the length of the retaining wall
- Figure 4.5 Perspex guide for installation of retaining wall

- Figure 4.6 Gaps forming behind retaining wall owing to rubber membrane being pulled into soil
- Figure 4.7 Template used to prevent application of PlastiDip rubber membrane to excavation void and outer edge of retaining wall
- Figure 4.8 Final PlastiDip layer on surface of clay model
- Figure 4.9 Aluminium channel design to secure silicone seal to retaining wall
- Figure 4.10 Details of silicone seals cast on retaining wall
- Figure 4.11 Aluminium mould used to form silicone seals on retaining wall
- Figure 4.12 General centrifuge model configuration with retaining wall, stiff excavation support (stiffener) and latex airbag
- Figure 4.13 Excavation stiffener details
- Figure 4.14 Capping beam details
- Figure 4.15 Space in capping beam to accommodate LVDT footing
- Figure 4.16 Airbag spacer details
- Figure 4.17 Photograph of airbag spacer with push fitting attachment for underwater test series and silicone rubber seal
- Figure 4.18 Photographs of airbag spacer sealed against retaining wall
- Figure 4.19 Bespoke LVDT footings for soft soil models, 50 x 10mm in plan and 2mm thick in the centre tapered to 0.5mm at the ends
- Figure 4.20 Image taken post-test showing that LVDT footings had settled in sample during reconsolidation
- Figure 4.21 Standpipe arrangement used in underwater excavation test series
- Figure 4.22 Details of consolidation box for lime stabilised clay sample
- Figure 4.23 Photograph of consolidation box being disassembled by sliding out front plate
- Figure 4.24 Details of lower stiffness cut off wall used in double wall series of tests

- Figure 4.25 Guide used for double wall installation clamped to strongbox
- Figure 4.26 Photograph of double wall at formation level
- Figure 4.27 Photographs post simulated excavation of the two positions of vertical support used to model two independent berm widths; (a) 100mm wide berm and (b) 50mm wide berm
- Figure 5.1 Stress profile through sample following 1g and 160g consolidation
- Figure 5.2 Estimated undrained shear strength profile of soil following in-flight consolidation
- Figure 5.3 Soil sample consolidation set up at 160g
- Figure 5.4 Typical settlement curve during in-flight consolidation at 160g
- Figure 5.5 Details of scraper used for trimming soft soil clay samples
- Figure 5.6 Photograph of scraper in model in preparation for the first trim
- Figure 5.7 Unconfined compression test set up illustrating data logging programme, test specimen, loading frame, LVDT and load cell
- Figure 5.8 Images of lime-stabilised soil samples (a) prior to testing and (b) and (c) at failure after developing multiple shear planes in two independent samples
- Figure 5.9 Unconfined compressive strengths of lime-stabilised clay samples compared with a virgin clay sample from centrifuge test samples
- Figure 5.10 Unconfined compressive strengths of lime-stabilised soil after varying time periods (Panchal *et al.*, 2018)
- Figure 5.11 Change in measured water contents of lime stabilised soil with increasing time (after Panchal *et al.*, 2018)
- Figure 5.12 Failure patterns of cement treated soil (Kitazume & Takeyama, 2014)
- Figure 5.13 Influence of time on unconfined compressive strengths (Locat *et al.*, 1990)
- Figure 5.14 Bespoke cutting shelf and guide used for establishing extent of excavation

- Figure 5.15 Voids formed at both ends of the retaining wall to accommodate silicone seals prior to wall installation
- Figure 5.16 Embedment of retaining wall by hand using rectangular plunger
- Figure 5.17 Formation of the excavation (a) using plates to scrape away material and (b) final excavation void
- Figure 5.18 Removal of clay from between the ribs of the retaining wall
- Figure 5.19 Sheet of filter paper, latex airbag, porous plastic and aluminium stiffener placed after formation of the excavation void
- Figure 5.20 3mm acetal targets embedded in model with propping system and latex airbag in test JP1
- Figure 5.21 Typical texture of black ballotini applied to models in main experimental test series
- Figure 5.22 General centrifuge arrangement for dry excavations
- Figure 5.23 General arrangement of an underwater excavation test
- Figure 5.24 Photograph post underwater excavation test with excavation void full of water
- Figure 5.25 (a) Removal of treated soil from consolidation box, (b) series of angles clamped to model to accurately establish extent of ground treatment, (c) plates used to excavate virgin soil and (d) installation of lime-stabilised clay soil block
- Figure 5.26 General arrangement of DSM ground improvement tests
- Figure 5.27 Plan view of double wall after installation
- Figure 5.28 General arrangement of a double walled test
- Figure 5.29 General arrangement of bermed excavation tests
- Figure 6.1 Schematic diagram of pins used to fix crest of wall in test JP11
- Figure 6.2 Settlement profile of retained ground at an overburden pressure of 38kPa

- Figure 6.3 Vertical displacement immediately behind retaining wall during reference test excavations
- Figure 6.4 Settlement profile of retained ground at end of excavation
- Figure 6.5 Vertical displacement immediately behind retaining wall during underwater excavation tests
- Figure 6.6 Loading history on formation level owing to reduction in air pressure and flooding of excavation area
- Figure 6.7 Development of settlements owing to total stress acting on formation level
- Figure 6.8 Contours of horizontal movements at end of excavation (0kPa) (displacement in mm)
- Figure 6.9 Contours of vertical movements at end of excavation (0kPa) (displacement in mm)
- Figure 6.10 Change in surface settlement profile 12 minutes post excavation
- Figure 6.11 Settlement profile of retained ground at end of excavation
- Figure 6.12 Vertical displacement at immediately behind the retaining during double walled excavation tests
- Figure 6.13 Contours of horizontal movements at 25kPa overburden pressure (displacement in mm)
- Figure 6.14 Contours of vertical movements at 25kPa overburden pressure (displacement in mm)
- Figure 6.15 Settlement profile of retained ground at end of excavation
- Figure 6.16 Contours of horizontal movements at end of excavation and complete removal of berm pressure (displacement in mm)
- Figure 6.17 Contours of vertical displacement at end of excavation and complete removal of berm pressure (displacement in mm)
- Figure 6.18 Surface settlements immediately after excavation

- Figure 6.19 Progression of vertical displacements during excavation immediately behind retaining wall
- Figure 6.20 Contours of horizontal movements at 50kPa (displacements in mm)
- Figure 6.21 Contours of vertical movements at 50kPa (displacements in mm)
- Figure 6.22 Settlement during removal of overburden pressure immediately behind retaining wall for a fixed wall crest and an unrestrained wall
- Figure 6.23 Surface settlement profiles at end of excavation for a wall fixed at the crest and an unrestrained wall
- Figure 6.24 Settlement during removal of overburden pressure immediately behind retaining wall for double walled and DSM tests
- Figure 6.25 Settlement troughs at end of excavation for double walled and DSM tests
- Figure 6.26 Contours of horizontal movements at 25kPa overburden pressure (displacement in mm)
- Figure 6.27 Contours of vertical movements at 25kPa overburden pressure (displacement in mm)
- Figure 6.28 Settlement during excavation immediately behind retaining wall for underwater excavation and a double wall or DSM zone
- Figure 6.29 Surface settlement profiles of combined tests (JP21 and JP22) compared with individual tests (JP6, JP13 and JP14)
- Figure 6.30 Influence of combining construction methods with underwater excavation at end of simulated excavation
- Figure 6.31 Location of pore pressure transducers
- Figure 6.32 Influence of excavation methods on excess pore pressures (a) PPT1 and (b) PPT2
- Figure 6.33 Influence of fixity conditions on excess pore pressures (a) PPT1 and (b) PPT2
- Figure 6.34 Influence of wall embedment on excess pore pressures (a) PPT1 and (b) PPT2

- Figure 6.35 Influence of DSM geometry on excess pore pressures (a) PPT1 and (b) PPT2
- Figure 6.36 Influence of berm geometry on excess pore pressures (a) PPT1 and (b) PPT2
- Figure 6.37 Influence of combining a construction method with an underwater excavation on excess pore pressures (a) PPT1 and (b) PPT2
- Figure 6.38 Comparisons between DPI readings and air pressure transducer recordings
- Figure 6.39 Schematic orientation of cameras on centrifuge swing, areas of model captured by each camera and common columns of control point targets
- Figure 6.40 Plan of general arrangement for calibration checks using slip gauges, an LVDT and control board
- Figure 6.41 Horizontal contours from the angled calibration series (camera orientated towards location of excavation) at 5mm displacement and example of field of view
- Figure 6.42 Horizontal contours from the straight calibration series (perpendicular to window) at 5mm displacement and example of field of view
- Figure 6.43 Overlapped data from two cameras and four points used in comparative analysis
- Figure 6.44 Accumulation of errors as displacement increases
- Figure 6.45 Horizontal displacement contours plotted from two cameras
- Figure 6.46 Comparisons between LVDT and PIV surface settlements
- Figure 6.47 Example of mesh generated for PIV analysis and emphasis on the points used as surface targets
- Figure 6.48 Comparisons between PIV and LVDT data at distance $2H$ behind the retaining wall
- Figure 6.49 Surface displacements at early stages of excavation simulation recorded at distance $2H$ behind the retaining wall.
- Figure 7.1 Support offered by underwater excavation method

- Figure 7.2 Passive resistance during underwater excavation method
- Figure 7.3 Comparative support offered from deep soil mixing treatment
- Figure 7.4 Passive resistance during DSM treatment across (a) full width of formation, 37mm deep (b) 100mm wide and 55mm deep and (c) 50mm wide and 112mm deep
- Figure 7.5 Increase in passive pressure afforded to excavation from soil berm
- Figure 7.6 Increase in passive pressure afforded to excavation from soil berm
- Figure 7.7 Increase in passive pressure and mobilised undrained shear strength as a result of a double walled excavation
- Figure 7.8 Increase in passive pressure afforded to excavation from a double walled excavation
- Figure 7.9 Vertical displacements across formation level during various stages of the simulated excavation in test JP18
- Figure 7.10 Expected deformation mechanism during excavation
- Figure 7.11 Expected settlement and heave profiles during excavation owing to soil-wall interaction and settlement of retaining wall
- Figure 7.12 Maximum and minimum measured vertical soil displacements at formation level in test JP18 from PIV analysis of mesh points nearest to and furthest from the retaining wall
- Figure 7.13 Settlement profile of retained soil upon completion of excavation
- Figure 7.14 Positions analysed to determine location where displacements first occurred
- Figure 7.15 Wall crest response and soil response at retained surface and formation level during the removal of the overburden pressure.
- Figure 7.16 (a) typical cosine curve of flexible walls (O'Rourke, 1993) and (b) original and final position of the wall measured from PIV analysis at the end of the excavation

- Figure 7.17 Vertical movements developing from beginning of the excavation to an overburden pressure 120kPa
- Figure 7.18 Mesh points used in the PIV analysis of test JP7
- Figure 7.19 Vertical movements across the formation level of a reference test at varying depths plotted at an overburden pressure of 50kPa where (a) illustrates vertical movements in JP9 (55mm embedment) at 50kPa; (b) JP7 (75mm embedment) at 50kPa plotted on the same scale
- Figure 7.20 Heave profile of formation level at 50kPa overburden pressure for varying wall embedment depths
- Figure 7.21 Vertical movements across the formation level of an underwater excavation at varying depths plotted at an overburden pressure of 50kPa.
- Figure 7.22 Vertical movements across the formation level of a double walled excavation plotted at an overburden pressure of 50kPa
- Figure 7.23 Heave profiles at the end of the excavation for a shallow and deep primary retaining wall in tests JP13 and JP18 respectively
- Figure 7.24 Vertical movements across the formation level of reference excavations plotted at an overburden pressure of 50kPa showing (a) free unrestrained wall crest; (b) wall fixed at crest
- Figure 7.25 Heave profile at 50kPa overburden pressure illustrating the vertical displacement across the formation level for excavations with free and fixed crests
- Figure 7.26 Heave profile at 25kPa overburden pressure illustrating the vertical displacement across the formation level for excavations with free and fixed crests
- Figure 7.27 Vertical displacements for DSM excavations of the following widths (a) B , (b) $2B/3$ and (c) $B/3$
- Figure 7.28 Vertical displacements for bermed excavations of widths (a) $2B/3$ and (b) $B/3$ all of which were taken at an overburden pressure of 80kPa in the main excavation area

- Figure 7.29 Heave profiles of various DSM geometries at 50kPa overburden pressure
- Figure 7.30 Heave profiles of the two bermed excavation widths recorded when the overburden pressure in the main excavation reached 80kPa
- Figure 7.31 Surface settlement profile of the underwater excavations upon complete removal of the overburden pressure
- Figure 7.32 Surface settlement profile of reference tests at an overburden pressure of 74kPa
- Figure 7.33 Comparison of passive pressures acting on wall of 55mm embedment in the underwater excavation and the reference test with an overburden pressure of 74kPa acting at the formation
- Figure 7.34 Surface settlement profiles of various double wall tests under a 74kPa overburden pressure plotted in relation to the underwater surface settlements at the end of the excavation
- Figure 7.35 Surface settlement profiles of the different DSM geometries under a 74kPa overburden pressure compared the underwater surface settlements at the end of the excavation
- Figure 7.36 Surface settlement profiles of the bermed excavations where the pressure in the main excavation bag was 80kPa and the berm applied a surcharge of 100kPa
- Figure 7.37 Example of the quality of images obtained from test JP17 showing extreme light exposure and interference
- Figure 7.38 Surface settlement profiles of underwater excavations combined with a double wall or DSM configuration all taken at the end of the excavation
- Figure 7.39 Undrained shear strength profiles from centrifuge tests and theoretical profile based on Springman (1989) empirical formula and S_u/σ_v' ratio for soft clays
- Figure 7.40 Comparison between undrained shear strengths measured with shear vane and computed from water contents (WC)
- Figure 7.41 JP7 - Reference test with 75mm wall embedment

- Figure 7.42 JP12 – Double wall test with 55mm wall embedment
- Figure 7.43 JP14 – DSM of width $2B/3$ with 55mm wall embedment
- Figure 7.44 General failure mechanism identified in centrifuge tests
- Figure 7.45 Interpretation of bearing capacity at collapse of a simple foundation (Atkinson, 2007)
- Figure 7.46 JP12 settlement against overburden pressure at distance H
- Figure 7.47 Rate of settlement plotted against overburden pressure in test JP12
- Figure 7.48 Rate of settlement against overburden pressure
- Figure 8.1 Graphical representation of relative effectiveness of influence of the retaining wall embedment and wall crest fixity on various excavation methods at an overburden pressure of 74kPa

ACKNOWLEDGEMENTS

I am privileged to have been encouraged to undertake doctoral studies with the Research Centre for Multi-scale Geotechnical Engineering at City, University of London where I spent three years with a group of uniquely skilled individuals.

Any acknowledgement to my supervisor, Dr Andrew McNamara, will not sufficiently express my gratitude for the time, energy, support and, most importantly, the abundant humour he has provided throughout my time at City. My confidence, critical thinking and technical writing abilities have all developed through time spent in discussions; he has been particularly generous in providing valuable feedback. I would not have completed my research within the given timescale without his motivation, guidance and experience, both in physical modelling and in all things related to industry; for that I am most grateful. I have been through a challenging period and I am honoured to have been allowed to work alongside Andrew and to have been involved in a wide range of exciting projects. I hope to continue working with him throughout my career in industry.

I thank Professor Sarah Stallebrass for her theoretical knowledge. Huge thanks are also owed to the group at City including Professor Neil Taylor, for his thought provoking “But, what if...” scenarios; Dr Richard Goodey for his patience when I frequently took the centrifuge out of action; Dr Sam Divall for his anecdotes and Dr Brett McKinley for his understanding off all things non-geotechnics. Thanks are also owed to Ms Paloma Peers for her wit and extraordinary grasp of language; Dr Binh Le who provided endless jest and encouragement; Dr Hitesh Halai for leading by example; Dr Sadegh Nadimi for his computational brilliance; Miss Greta Tanghetti for her kindness and Dr Joana Fonseca. This close-knit group has made my time at City a wonderful and memorable experience and I wish our new arrivals, Mr Eric Ritchie and Mr Ciaran Kennedy, the best of luck.

Considerable effort towards the design and fabrication of centrifuge modelling equipment was given by our dedicated technical staff at City, Mr Jim Hooker and Mr Mervyn Haynes. I also thank Mr Richard Leach, Mr Robert Cherry and the rest of the technician team who made it happen.

I would like to acknowledge Cementation Skanska for part sponsoring this project and supporting my conference attendance. I was fortunate enough to visit site and work with the design team which provided real-life context to this work. Thanks are therefore owed to Ms Zöe Baldwin, Mr James Court, Mr Andy Bell and Dr Jon Morris. Arup Geotechnics moulded the scope of works and offered vast knowledge and experience of deep excavations in soft soils. I thank Mr Chris Barker and Dr Paul Morrison for their time and support throughout this project.

Last, but by no means least, I owe huge praise to my family, especially my mother who encouraged me to accept this opportunity. In doing so, she suffered the late night and early morning drop offs to the station, my invisible presence during write up and subsequent grouchy moods. She taught me to persevere and deserves the success of this degree more than myself. I owe special thanks to my brothers, Mr Manoj Panchal, Mr Nivethithan Tharumarajah, Mr Nimesh Shukla, Mr Ash Sharma and Mr Rashik Bhandari for bearing with me and their understanding throughout my PhD. I also express my deepest gratitude to Ms Helena Norotomo, Mr Robert Hudson and Mr Abel Lugar for being my compassionate family away from home.

DECLARATION

I grant powers of discretion to the University Library to allow this dissertation to be copied in whole or part without further reference to me. The permission covers only single copies made for study purposes, subject to normal conditions of acknowledgement.

ABSTRACT

This research concerns the influence of a range of construction methods, acting at or below excavation formation level, on ground movements of the retained surface attributed to a 12m deep excavation in very soft to soft soil. Movements around excavations arise as a consequence of the removal of soil and lateral wall deformations. The work examined the behaviour of excavations that were supported by a high stiffness embedded retaining wall whilst modelling a variety of construction techniques. Four distinct construction methods were modelled which could be regarded as surcharging the formation level or stiffening the ground below excavation formation level. The specific techniques that were explored include underwater excavations, bermed excavations, deep soil mixing and double walled excavations. This study aimed to determine the efficiency of these construction measures on reducing the magnitude and extent of displacements occurring behind the retaining wall.

Experimental data were obtained from twenty-two plane strain centrifuge model tests undertaken at $160g$. The geometry of the model comprised a pre-formed excavation where the retaining wall was laterally supported by a continuous prop acting over the majority of the height of the wall and the excavation formation level was surcharged by a pressurised rubber bag. Pressure in the bag at formation level was reduced at a constant rate to simulate the stress change caused by the excavation process. Vertical movements at the retained ground surface were measured using displacement transducers whilst subsurface deformations elsewhere in the model were determined from the analysis of digital images captured by cameras viewing the front of the model through a Perspex window. The magnitude and extent of movements were quantified and the general patterns of ground deformation were identified for the construction methods implemented.

A series of reference tests were conducted to provide a baseline against which modified excavation tests were compared. The stiff wall and continuous prop supporting the retaining wall ensured that the reference tests quantified the magnitude of displacements at the retained surface arising simply as a result of heave at the formation level. The main test series investigated a range of construction methods that aimed to surcharge or stiffen the formation level. Additional tests were also undertaken to evaluate the influence of wall embedment on the performance of the excavation system. Direct comparisons were also drawn between tests in an attempt to establish the significance of wall crest fixity on soil movements.

The use of all of the special construction techniques investigated were shown to reduce the magnitude of vertical displacement behind the retaining wall and at the formation level; in addition to reducing horizontal displacements at the toe of the wall. Increasing the retaining wall embedment depth in the main test series generally reduced the magnitude of vertical settlement by a factor of two, however the effect was less pronounced in the reference tests. Improving the fixity of the crest of the wall delayed excavation collapse and, where additional support mechanisms were not employed, pinning the crest of the wall was shown to reduce maximum settlement in the reference test by a factor of three.

Of the four supporting construction methods the underwater excavation was found to be the most effective owing to the reduced change in vertical stress during the simulated excavation. Various deep soil mixing geometries were modelled and similar excavation behaviour was observed, however deep soil mixing ground treatment extending to the toe of the retaining wall and across $\frac{2}{3}$ of the excavation demonstrated a slight reduction in settlement. Similar behaviour was observed for double walled excavations. Combining underwater excavations with a double wall was shown to further reduce maximum settlements however little additional benefit was observed when performing an underwater excavation with a deep soil mixed soil layer at excavation formation level.

LIST OF SYMBOLS

a	Radial acceleration
B	Excavation width
c_v	Coefficient of consolidation
D	Distance behind retaining wall
g	Acceleration due to gravity
H	Height of excavation
h	Prop spacing
h_m	Depth in model
h_p	Depth in prototype
r	Radius
s_u	Undrained shear strength
t	Time
t_m	Time in model
t_p	Time in prototype
u	Pore pressure
E_s	Young's modulus for stainless steel
E_c	Young's modulus for concrete
H	Depth of excavation
I	Moment of inertia
K_0	Coefficient of earth pressure at rest
K_a	Coefficient of active earth pressure
K_p	Coefficient of passive earth pressure
L	Drainage path length
L_e	Wall embedment
N	Gravity scaling factor
N_c	Bearing capacity factor
p'_v	Effective overburden pressure
T_v	Time factor for consolidation
S^*	System stiffness

δ	Displacement
γ	Unit weight of soil
γ_w	Unit weight of water

Γ	Specific volume on the critical state line when $p' = 1\text{kPa}$
κ	Gradient of unload-reload line in $v:\ln p'$ space
λ	Gradient of normal compression line in $v:\ln p'$ space
M	Stress ratio at critical state (q'/p')
v	Specific volume
ρ	Density
σ'_h	Horizontal effective stress
σ'_v	Vertical effective stress
σ_{vm}	Vertical stress in model
σ_{vp}	Vertical stress in prototype
φ	Angle of friction of soil
ω	Angular velocity

Abbreviations

DPI	Digital pressure indicator
DSM	Deep soil mixing
FEA	Finite element analysis
FEM	Finite element modelling
FOS	Factor of safety
LVDT	Linear variable differential transformer
OCR	Overconsolidation ratio
PPT	Pore pressure transducer
rpm	Revolutions per minute
UCS	Unconfined compressive strength
WC	Water content

CHAPTER 1 INTRODUCTION

A global rise in construction projects that are often complicated by stringent building height regulations leads to an increasing challenge to procure lettable space above ground. Developers are tasked with constructing deep underground spaces to provide basements and transport networks whilst controlling ground movements to prevent damage to neighbouring structures. This research investigates the influence of deep basements constructed in very soft soils and evaluates the effectiveness of a range of excavation methods on mitigating ground movements behind the retaining wall.

1.1 BACKGROUND

It is economically feasible for developers to undertake construction projects in urban areas on high value land but this often requires extreme measures to maximise value. This eventually leads to spatial constraints above ground, resulting in engineering deep underground basements in heavily congested areas to provide adequate commercial and retail space. The construction of such spaces inevitably involves excavating significant volumes of soil and this stress relief is one of the major causes of ground movement. Surface settlements are frequently excessive in soft soils and extend far beyond the site boundary. Although ground movements cannot be completely eliminated it is vital that they are controlled and managed to prevent damage to neighbouring structures and services.

Considerable efforts are routinely made in predicting displacements arising from deep excavations. These include empirical solutions and finite element analysis using advanced soil models. However, owing to ground condition variability, differences in stress history, excavation support stiffness, quality of workmanship and construction methods, significant challenges exist in accurately modelling a geotechnical scenario with constitutive numerical models to determine ground movements for a unique site. Despite advances in numerical modelling capabilities, physically modelling the excavation process using real soil has the potential to provide a better indication of the magnitude and extent of patterns of settlement, provided stress similarity and other key parameters can be achieved in the physical model.

With the construction of deeper basements in densely populated and rapidly developing regions such as far-east Asia where thick deposits of soft soil exist, significant efforts have been made to stabilise excavations and minimise the magnitude of movements extending beyond the site boundary. Whilst there is a wide range of measures that could be employed to reduce ground movements, these methods can largely be categorised as surcharging, stiffening or improving the ground conditions of the formation. Some techniques include, but are not limited to, zoned excavations, vibro-compacted columns, deep soil mixing, vertical drainage pipes and underwater excavations and berms. The suitability of any one of the methods needs to be considered in the context of ground conditions as established from site investigation information and site constraints. However, the effectiveness of each technique, in comparison with other methods, is currently unknown. Consequently, excavations and temporary works can often be overdesigned to mitigate ground movements or measures adopted may prove less successful in controlling ground movements than envisaged.

Ground movements around deep excavations are attributed to a wide range of factors, however it is accepted that the wall stiffness, excavation support stiffness and construction sequencing are key parameters governing the magnitude of soil deformations. These movements comprise lateral movements from wall deflections and vertical movements arising from basal heave owing to the vertical stress relief during the removal of overburden material. Considering that these critical factors affect soil deformations it is a reasonable assumption that significantly reducing either or both of wall deformations and basal heave will significantly reduce ground movements generally. Regardless of wall movements which can generally be controlled with the use of stiff walls, stiff propping, jacking etc., surface settlements can also be directly attributed to heave. A study of the measures to reduce heave permits an evaluation of the influence and efficacy of different construction methods on mitigating basal heave and subsequent ground movements in general.

Small scale physical model tests can be conducted to provide a means of observing surface movements and subsurface failure mechanisms arising from excavating to depth in soft soils. This is possible in a geotechnical centrifuge where stress similarity is achieved between the prototype and model. Owing to the variability of ground

conditions and excavation techniques across sites a parametric study is intended to comprise a reference test of an idealised high support stiffness excavation and in which various other parameters can be compared.

1.2 OBJECTIVES

This research aims to provide an insight into the control of ground movements around deep excavations in very soft soils and to develop an understanding of associated deformation mechanisms for stiffly supported excavations. Centrifuge modelling has been used to determine the efficiency of a range of stabilising techniques for an excavation in very soft clay that was normally consolidated below formation level. The following are the main objectives of this research and form the basis for discussion and conclusions:

- Development of apparatus to enable representative simulation of a 12m deep prototype open cut excavation in very soft soils in the geotechnical centrifuge at City, University of London.
- Develop a model making process for very soft clay and testing regime to ensure accuracy, repeatability and consistency between experiments.
- Establish the mechanisms of ground deformation for excavations in soft clay with very high lateral support stiffness.
- Conduct a parametric study on the short term effects of a range of construction methods on ground movements arising during the excavation process. The ground responses are recorded and presented on normalised charts.

1.3 EXPERIMENTAL WORK

Development of the model was governed by the requirement to simulate a 12m deep prototype open excavation in very soft soils under plane strain conditions. Five distinct series of tests were conducted using a very stiff retaining wall and excavation support system which controlled lateral movements and subsequent surface settlements arose only from basal heave. Each test series aimed to determine the influence of a particular construction technique on ground movements arising during an excavation event.

A total of 22 centrifuge tests were conducted under plane strain conditions where a preformed excavation was surcharged by a pressurised airbag and a retaining wall was prevented from moving laterally by a stiff continuous prop. Simulation of the excavation involved gradually reducing the pressure in the airbag at a constant rate to represent the vertical stress change arising from the excavation of overburden material. The stiff prop supported the retaining wall along the majority of its depth, with the lowest 25mm of wall exposed and supported only by the pressurised airbag. An early series of tests made use of a stiff prop to provide lateral restraint in compression only. Following these initial tests, it was observed that the excavation had experienced passive failure in front of the retaining wall toe. A capping beam was therefore designed to fix the top of the retaining wall in the main series of tests. This provided wall propping in tension which was more representative of modelling a prototype propped excavation in which top down construction was employed.

Surface settlements along the centreline of the model were monitored during the excavation using linear variable differential transformers whilst subsurface movements were computed from sequential images captured by on-board cameras. Analysis of these images permitted comparisons between movements measured at the retained surface against those calculated by tracking the movements of target beads embedded in the surface of the clay at the Perspex window interface.

Three reference tests modelling differing wall embedment depths were conducted. In these tests no improvements had been made to the excavation formation and they provided a baseline for a parametric study of the influence of special construction techniques. The following construction methods were simulated in order to reduce the surface settlements during an excavation: (1) surcharging by means of water (submerged excavation), (2) bermed excavation, (3) ground improvement through deep soil mixing, (4) soil stiffening using a double retaining wall. Having established the general behaviour of an excavation without any additional support direct comparisons of the various excavation methods were made. The influence of wall embedment depth was also investigated through additional tests.

1.4 SUMMARY OF THESIS

This thesis describes the approach adopted in researching the influence of a range of construction methods on ground movements arising from deep excavations in soft soils. Development of the model apparatus is described in detail and model making techniques are explained. Test results and interpretations are given together. Significant efforts have previously been made in understanding movements around excavations in soft soils which enabled a comprehensive literature review to be performed. This is presented in Chapter 2 alongside a background to the problem and some of the key factors affecting ground movements associated with excavations.

The principles of centrifuge modelling are described in Chapter 3, with particular attention being paid to boundary effects and the acquisition of data from tests undertaken at the geotechnical centrifuge facility at City, University of London. Chapter 4 details the rationale behind the apparatus adopted in this series of experiments and the development of novel model making solutions to ensure accuracy in modelling deep excavations in soft soils. During the testing phase slight modifications to the apparatus were required and explanations for these adjustments are also presented.

Descriptions of the excavation methods undertaken as part of this research project are presented in Chapter 5. The sample preparation method adopted to ensure tests were repeatable is also detailed. Owing to the range of construction methods investigated the modelling techniques varied between experiments. The generic model making procedures and those specific to each of the various excavation scenarios are also explained in this chapter.

A summary of the tests undertaken and the results from each of the experiments are presented in Chapter 6, illustrating the influence of one particular construction method over others. Raw data from each experiment is presented here to demonstrate the consistency of results and accuracy of the data acquisition systems in place. This also includes a discussion on displacement measurements taken from LVDTs and implied by image analysis.

Chapter 7 compiles the results from the centrifuge tests and draws comparisons between them. Trends in the data are identified, analysed and the significance of the

findings emphasised, with reference to surface settlements as the excavation progresses.

Final conclusions and limitations of the research are presented in Chapter 8. The importance of the results to industrial applications are highlighted and recommendations for further research are made that may provide further detailed insight into the influence of other excavation methods on ground movements in soft soils arising from deep excavations.

CHAPTER 2 LITERATURE REVIEW

2.1 INTRODUCTION

A rise in development projects leads to increasingly congested towns and cities. Additional development of these sites tends to occur underground by constructing progressively deeper basements. Ensuring excavation stability is as critical as managing vertical settlements adjacent the site. Surface settlements arising from deep excavations are a complex combination of basal heave and lateral wall deflection. Relatively slender, unobtrusive embedded retaining walls are preferred over gravity retaining walls and are typically used in urbanised areas. The walls of the excavation will commonly be supported with props; however, the flexible wall will permit a degree of lateral deflection. In very soft soil ($S_u < 20\text{kN/m}^2$) to soft soil ($20\text{kN/m}^2 < S_u < 40\text{kN/m}^2$) the magnitude and extent of surface settlements of the retained ground are frequently excessive. This literature review aims to present the key factors that influence ground movements and expected patterns of deformation. A range of excavation construction techniques published as physical model tests, numerical studies and field trials will also be reviewed.

2.2 MECHANISMS OF GROUND MOVEMENT

In areas where stiff soil is prevalent, such as London, excavation sequences are well established as methods of restricting ground movements are generally understood. However, significant challenges exist where thick layers of soft soil exist, such as Singapore and Hong Kong. For instance, Wang *et al.* (2010) highlighted a number of discrepancies in displacement trends between previously published empirical deformation studies and those measured in Shanghai soft soil. This is owing to the large number of factors that influence soil displacements which include, but are not limited to, wall stiffness, wall embedment, excavation support stiffness, excavation depth, construction sequence, ground conditions and whether additional excavation support techniques are employed. These contribute to the complexities in accurately predicting or successfully mitigating ground movements arising from deep excavations in soft soils.

Gaba *et al.* (2017) and Padfield & Mair (1984) explain that ground movements are a combination of both global and local displacements. Global movements are attributed to the unloading of the formation level and are therefore difficult to control as they are unaffected by the excavation support stiffness. This confirms the theory of Peck (1969) who stated that the magnitude of settlement is governed not by the stiffness of the support system or bracing spacing but the characteristics of the surrounding soil. Peck (1969) presented maximum settlements collected from various sites which were plotted against the distance from excavation, both normalised by the maximum excavation depth. This graph demonstrated that in soft clays settlements of up to $0.2\%H$ were observed to extend as far as $4H$ from the site. However, it is important to appreciate that construction methods and technology have since undergone significant advancements. For instance, timber lagging and low stiffness sheet piles have since been replaced with diaphragm walls and stiff props. A better understanding of how ground movements develop has also lead to an improvement in construction sequencing to prevent loss of ground.

Local movements are plastic deformations that arise in the short term in the active wedge behind the wall and their magnitude is a function of wall stiffness. Consequently, stiffer walls can reduce the magnitude of settlement and affect the final settlement profile. However, in practice the stiffness of the wall or number of props is limited to economic and spatial constraints so additional reductions of surface settlements are limited. Burland *et al.* (1979) explains that horizontal displacements are governed by the mode of wall deformation. The deformation profiles of cantilevered and propped walls would be expected to be different as cantilevered walls develop large horizontal movements at the crest and subsequent settlements are relatively small. This is compared with propped walls that are subjected to larger deflections at depth and consequently may experience larger vertical displacements.

Recent studies by Lam (2014) investigated the influence of toe fixity conditions, wall and prop stiffness and depth to stiff strata of an excavation in soft soils. Unsurprisingly, stiff props limited wall deflections and so the change in horizontal stress behind the wall was minimised. The stiffness of the wall also influenced the surface settlement profile, which was consistent with the findings of Clough and O'Rourke (1990). Although propped excavations tend to experience larger vertical

displacements than cantilevered excavations, surface settlements can be reduced by grouting the toe of the wall or reducing the distance between the toe and a stiffer soil layer.

2.3 VERTICAL STRESS RELIEF

Burland *et al.* (1979) contrasts the soil behaviour from vertical stress relief of overburden pressure from an excavation formation level to that of surcharged ground. During an excavation the unloading of the formation can initiate deep seated movements, as shown in Figure 2.1 which cause the ground within the excavation to heave and surrounding area to settle. In the short term, the pressure relief results in an elastic response. If the formation remains unloaded in the long term the ground continues to heave and drainage occurs resulting in heave across the site, as shown in Figure 2.2. The local effects from unloading the formation cause the excavation walls to deflect as illustrated in Figure 2.3.

The behaviour of the soil and support system is dependent on the stability number (N), representative of all the soil involved in the mechanism (Peck, 1969). This can be calculated using (2.1). However, this stability factor ignores the influence of wall embedment and consequently underestimates excavation stability.

$$N = \frac{\gamma H}{S_u} \quad (2.1)$$

Where γ is the bulk unit weight of the soil

H is the depth of the excavation soil

S_u is the undrained shear strength of the soil beside and beneath the cut to the depth at which shear failure would be expected to occur.

2.4 EARTH PRESSURE AT REST

It is accepted that the vertical stress change arising during an excavation can be determined from the self-weight of soil removed. Similarly, changes in pore pressure can be measured to enable calculations of vertical effective stresses. However, variations in earth pressures must be computed by first considering the in-situ

horizontal stresses (Burland *et al.*, 1979). Lateral earth pressure was defined as a ratio between the horizontal to vertical effective stress. However, Gaba *et al.* (2017) state that this approach does not account for the complex soil/wall friction at the wall interface, particularly in soils and weak rock. Therefore, lateral earth pressures should be computed as a ratio of horizontal effective stress to effective overburden pressure;

$$K = \frac{\sigma'_h}{p'_v} \quad (2.2)$$

Careful consideration of the stress history of a sample is very important in estimating the initial in-situ earth pressure, K_0 . Deposition tends to relate to the 1D compression line (Figure 2.4) and is associated with normally consolidated soils (Mayne & Kulhawy, 1982) as represented by line OA in Figure 2.5. However, variations between the estimated K_0 value and actual value may be owing to clays drying out from exposure to air, weathering or erosions which result in a decrease in pore pressure, increasing the effective stress whilst total stresses remain constant (Burland *et al.*, 1979; Gaba *et al.*, 2017).

An overconsolidated effect occurs during excavations as overburden pressures are removed and the overconsolidation ratio influences the value of K_0 . As overburden unloads the horizontal effective stresses become ‘locked in’ resulting in a steep unload line as the clay approaches the passive failure line. This is owing to the large change in effective overburden pressure over a relatively short period of time compared with the extended period over which excess pore pressures dissipate in clays and plastic strains subsequently develop.

In normally consolidated clays K_0 can be calculated using the empirical formula by Jaky (1944) later validated by Mayne & Kulhawy (1982) during a review of 170 different soil specimens.

$$K_0 = (1 - \sin\varphi') \quad (2.3)$$

Where φ' is the effective angle of shearing resistance which is 23° for Speswhite kaolin clay (Grant, 1998). This gives a value for K_0 of 0.609 for Speswhite kaolin clay, which lies within the range of K_0 values of 0.6 ± 0.2 for normally consolidated clays (Ladd & Varallyay, 1965). Consequently, soft soils have relatively low lateral passive pressures and a retaining structure founded in such soil remains largely

unaffected by the excavation. Figure 2.6 illustrates the difference in variability of K_0 for soft normally consolidated clays to stiff overconsolidated clays. Soft clays tend to exhibit a more linear variation with increasing OCR compared with stiff clays that demonstrate a sudden rise at $\text{OCR} = 5$ and peak K_0 value at around 24. This is consistent with the Burland *et al.* (1979) statement which indicated that overconsolidated clays are more sensitive to changes in stress history.

2.5 WALL INSTALLATION EFFECTS

Where ground conditions permit installation of sheet piles these are a preferred method for shallow retained excavations. Slender driven sections of sheet piles are unlikely to have a significant influence on the in-situ lateral stresses (Gunn & Clayton, 1992). This is owing to soil not needing to be excavated to accommodate the retaining wall. However, it is becoming increasingly popular to incorporate the retaining structure with the permanent works. Therefore, although high stiffness support systems, such as concrete diaphragm walls, are installed the net changes in lateral effective stress are not significant owing to K_0 being lower than unity. Furthermore, a small reduction in in-situ lateral effective stresses is experienced during excavation of a single diaphragm panel which is subsequently supported by bentonite slurry. Following this, there is a slight increase in lateral stresses when bentonite is displaced by wet concrete as the lateral concrete pressure is greater than the at-rest lateral earth pressure (Kantartzzi, 1993). Sato *et al.*, (1992) demonstrated small changes in the lateral pressure exerted on concrete diaphragm walls during the excavation of a 17m deep basement, see Figure 2.7. Consequently, ground movements associated with diaphragm wall installation in soft soils are minimal compared with those arising from similar wall construction in stiff overconsolidated clays.

Finno & Nerby (1989) reported on the installation effects of driving sheet piles through soft and medium to stiff clay. Sheet piles were instrumented with inclinometers and extensometers to aid in the computation of horizontal and vertical strains respectively. Piezometers and settlement points were also used on the site to monitor changes in pore pressure and record settlements, details are illustrated in Figure 2.8. Excavation of a pilot trench began at day 1 and sheet piles were driven in from day 52 to a depth of 28ft before being vibrated to 50ft from day 64. The main excavation commenced

on day 101. Pile driving was shown to have little influence on vertical strains (Figure 2.9) however the soil moved laterally away from the sheet piles and consequently the ground was reported to have heaved. Strains were concentrated at an elevation of 10-20ft which was in the Blodgett till, which was described as stiff, desiccated crust and rubble fill. Therefore, it can be expected that a more homogeneous soil would have developed small strains over a wider area. In addition, during pile driving excess pore pressures rapidly developed before the soil consolidated prior to vibratory installation, as shown in Figure 2.10; the dissipation of excess pore pressures exhibited standard consolidation behaviour.

2.6 INFLUENCE OF WALL STIFFNESS ON DEFORMATIONS IN SOFT GROUND

The general deformation shape of a flexible wall (Figure 2.11) owing to an excavation was proposed by O'Rourke (1993) and was a means of estimating the lateral deflection profile in soft clay. Very good agreement was shown between this prediction and field measurements, as demonstrated in Figure 2.12. Alternatively, the system stiffness approach can be adopted which was developed by Clough & O'Rourke (1990), see Figure 2.13. This method required evaluation of the factor of safety against basal heave, following Terzaghi's (1943) principle and the system stiffness, which was defined as;

$$S^* = \frac{EI}{\gamma_w h^4} \quad (2.4)$$

Where EI is the flexural stiffness of the retaining wall, γ_w is the bulk unit weight of water and h is the spacing between props. Whilst this method is an approximation, it suggests that the higher the system stiffness the lower the magnitude of lateral displacement. It does not appear possible to achieve zero lateral deflection; whilst this may be true in practice, in theory a continuously propped highly stiff wall would not expect to deflect.

Gaba *et al.* (2017) reflect that stiffer walls attract larger bending moments and higher soil stresses compared with flexible walls that are more equipped at redistributing stresses. However, a flexible wall permits greater deflections and consequently larger settlements. Gaba *et al.* (2017) idealise the displacements of a stiff wall in Figure 2.14

and define a stiff wall as one where deflection at the toe is greater than the deflection at formation level. This mechanism is representative of a wall propped at its crest, therefore the greatest rotation is observed at the toe.

Potts & Fourie (1984) simulated an excavation retained by a 1m thick reinforced concrete diaphragm wall using finite element analysis. The walls were propped at the crest and for comparison two scenarios were modelled $K_0 = 2$ and $K_0 = 0.5$. The lateral wall deflections and predicted surface settlements are presented in Figure 2.15 and Figure 2.16 respectively. Although the same wall was modelled in both tests the deformation patterns are noticeably different. Whilst the $K_0 = 0.5$ wall deflects at formation level, no deflection is observed at the toe. On the other hand, stiffer soil results in a more rotational deformation in the $K_0 = 2$ case. The results suggest that the wall and retained surface in normally consolidated soil was not as heavily affected by the excavation compared with the case where $K_0 = 2$. This behaviour was owing to the assumption of linear-elastic soil behaviour prior to failure. The stress distributions are presented in Figure 2.17 and are typical of the stress contours of stiff and flexible walls. A stiffer wall develops larger bending moments and high stresses, whilst flexible walls redistribute these through the soil. This study illustrated that K_0 governs the behaviour of the soil adjacent an excavation.

2.7 NUMERICAL ANALYSES OF EXCAVATIONS IN SOFT SOILS

Hashash & Whittle (1996) reported a series of numerical experiments to investigate the influence of wall embedment, excavation support systems and the soil stress history on ground deformations around a braced excavation in Boston Blue Clay. MIT-E3, an effective stress soil model particularly suited to normally and lightly overconsolidated clays, was used to model top down construction in a deep clay deposit. The retaining wall was modelled as a 0.9m thick diaphragm wall with rigid incompressible bracing. A simplified construction sequence was adopted as follows: excavate to depth h_u unsupported, install prop at ground level and continue excavation to depth h_e in 2.5m increments, install another prop at depth h below ground (where $h < h_e$), repeat until total excavation depth $H = 40\text{m}$ is achieved or until failure. Wall embedment depths ranged from 12.5m to 60m whilst prop spacing varied between 0m (continuous wall support) to 10m (minimal support). Figure 2.18 illustrates the

influence of two wall embedment depths (L) on vertical and lateral ground deformation profiles for constant prop spacing of 2.5m. Unsurprisingly, the shallower embedment ($L = 20\text{m}$) exhibited two dissimilar wall deflection profiles. Larger displacements were noted at the toe of the wall, whilst a deeper embedment depicts the classic O'Rourke (1993) cosine deformation profile and bulge below formation level. However, similar trends and magnitudes of surface settlements were observed for both depths of embedment and, as expected, the shape of the settlement trough is representative of an excavation propped at its crest. Figure 2.19 demonstrates the influence of prop spacing on an excavation with 60m embedment. Providing rigid continuous support along the entire exposed length of retaining wall would obviously develop below the current excavation level and the analyses showed maximum deflections occurring 10m below the excavated level. However, reducing the number of props permits large deflections along the entirety of the wall with maximum movements typically observed at the current excavation depth.

Interestingly, the prop spacing has a more significant influence on the surface settlement profile. This supports the theory presented by Goldberg *et al.* (1976) and Clough and O'Rourke (1990) which states that the system stiffness is governed by prop stiffness and spacing. This was further supported by a case study during an excavation in San Francisco where over-excavating 10m of soil resulted in wall deflections four times greater than those previously experienced when props were installed at the correct stages in the excavation, see Figure 2.20. Having established that wall deflections contribute to the settlement trough, it can be argued that by controlling the spacing, and consequently the stiffness of the support system, the resultant settlement profile can also be influenced.

Dong *et al.* (2016) carried out a detailed investigation into the sensitivity of finite element analyses based on the chosen soil/structure interaction models and parameters used in the numerical model. They found that a high level of detail was required to produce an accurate 3D model for a deep excavation construction in Shanghai. Factors such as post-curing of concrete had a significant effect on the measured displacements and the model was sensitive to slight differences in the K_0 values used.

2.8 CASE STUDIES OF EXCAVATIONS IN SOFT SOILS

Wallace *et al.*, (1992) reported on the construction of a 12m deep bottom up basement in soft Singapore marine clay. A diaphragm wall was constructed up to 1.2m thick and with a maximum embedment of 40m. Field data were obtained and compared with numerical analysis conducted using FREW. Piezometers, inclinometers and ground settlement stations were employed to monitor the site during construction. A clearly defined construction sequence and good workmanship ensured that the props were preloaded and promptly installed to assist in mitigating ground movements. A relatively large difference was observed between the predicted and measured values which was attributed to the conservative undrained shear strengths adopted in the FREW analysis. Reducing the strength parameters by approximately 10% gave more realistic computations of ground and wall movements. This highlights the complexities in using numerical methods to accurately predict the performance of an excavation prior to works commencing. In addition, this paper placed emphasis on the sensitivity of soil strength on predictions in soft soils.

Several excavations were performed in south western Detroit adjacent existing sludge thickener tanks in very soft to soft clays (Abedi *et al.*, 1992). Comparisons were drawn between field measurements and FEM analyses. Three rows of sheet piles were driven about 11m through clay with an undrained shear strength of approximately 17kN/m^2 and retained the toe of a soil berm that remained between the existing sludge tanks and the excavation. The site was instrumented with inclinometers, extensometers and surface markers. Generally, there were discrepancies between the measured and predicted displacements. This was owing to the disparity between the construction sequence modelled in the analysis and that which was conducted on site and an oversimplistic 2D analysis. This underlines the importance of modelling actual construction events in numerical analyses to obtain more representative ground deformation predictions.

Sato *et al.*, (1992) presented the construction of a 25 storey building adjacent the Sumida River in Japan comprising a 3 storey basement. A 17.1m deep excavation was formed using a cantilevered retaining diaphragm wall in thick deposits of alluvial silty clay with strengths ranging from $10\text{-}100\text{kN/m}^2$, overlying diluvial gravels. Inclinometers, earth and water pressure cells were used in monitoring the site during

excavation. T-shaped continuous walls were constructed along the two longest structure spans and were connected using flat diaphragm walls. Bracing was not needed owing to the high flexural rigidity of the T-sections. This was particularly important to minimise construction costs and reduce the project programme. Wall deflections presented for different levels of excavation are shown in Figure 2.21. The results showed that the T-sectioned wall panels minimised wall displacements to less than 30mm. Although data relating to surface settlements is not presented, the influence of wall stiffness and geometry on controlling wall displacements is worth noting. Stresses in the reinforcement bars were measured and are presented in Figure 2.22. The measurements demonstrate that this site layout controlled the development of heave, owing to the low stresses developed at the centre of the formation. Therefore, it can be assumed that having controlled wall displacements and heave, surface settlements of the retained ground would be relatively small.

Details of a 14.5m multi-propped diaphragm wall deep excavation were reported by Ng *et al.* (2012). The excavation was performed on a greenfield site in Shanghai soil in China with particular emphasis on panel 4 of the diaphragm wall. The ground below formation level was treated with jet grouting to further enhance the excavation performance. The wall was heavily instrumented with earth pressure cells to measure total lateral earth pressures, piezometers to monitor pore water pressures and load cells to measure prop forces. Inclinometers and control marker targets were used on the wall whilst settlement markers were used at formation level and along the retained surface at 5m intervals. Similar construction techniques were adopted to those reported by Wang *et al.* (2005); Tan Wei (2011) and Lie *et al.* (2011). However, data obtained during this excavation showed that the surface settlements were larger than those measured in published literature (Figure 2.23). This excavation was conducted in a shorter period of time so the larger settlements could not be attributed to consolidation settlement. Instead it was proposed that the movements were considerably larger than those observed in urbanised areas owing to the excavation being completed in a greenfield site. Vertical displacements in built up areas are less prone to propagation as the general ground is relatively stiffer owing to the presence of other foundations and obstructions.

2.9 SOIL DISPLACEMENT TRENDS IDENTIFIED FROM DATABASES

Ground movements arising from deep excavations in clay are complex to predict owing to a wide range of parameters and factors that influence the excavation behaviour. However, extensive work has been conducted to collate, normalise and publish the responses of various excavation case studies to provide databases and aid in establishing trends. These databases will briefly be discussed here.

2.9.1 Peck (1969)

In the state of the art report Peck (1969) published a graph of maximum settlement against distance from excavation, both normalised against the final excavation depth. This graph, illustrated in Figure 2.24, collated the surface settlements from sites in Chicago and Oslo with soil conditions including sands and clays with strengths ranging from hard to very soft. This plot also accounted for depth between the clay layer and hard strata. Similarity between the cases was drawn from the excavation support system which comprised braced sheet or soldier piles. A further study into the influence of the number of basement levels, and subsequently excavation depth, from 20 sites in Chicago had been conducted by Ireland (1955). Since all the construction projects were founded on underlying rock the main variable was the depth of excavation and the trends were presented in Peck's (1969) report, as illustrated in Figure 2.25. This clearly shows that the deeper the excavation the greater the magnitude of settlement. It is worth noting that whilst these trends are consistent with those of cantilevered excavations, the magnitudes are considerably larger than those expected using modern and advanced construction technologies. This graph provided engineers with an initial means of appreciating the trend of movements and understanding how the strength of the ground influenced the magnitude of settlements.

2.9.2 Mana & Clough (1981)

Mana & Clough (1981) published a plot that illustrates the effect of the factor of safety against basal heave, as shown in Figure 2.26, as defined by Terzaghi (1943) on the dimensionless maximum lateral wall displacement. The plot relates to only 11 cases out of 130 available studies to eliminate cases with dissimilar construction methods,

poor workmanship, first prop being installed at a depth exceeding $2S_u/\gamma$ and where excessive settlements had been observed during wall installation. The envelope defined by Mana & Clough (1981) relate to the case studies where sheet piles had been installed in soft clays. In general, smaller lateral displacements are observed for higher a factor of safety against basal heave. However, data from other databases were included in this graph as shown in Figure 2.27. The wide scatter of this data shows that the factor of safety cannot be used as a sole means of predicting maximum horizontal deflections.

The factor of safety against basal heave were computed using (2.5) when the depth of clay below the base of the excavation (D) exceeds $\sqrt{2}B/2$ as illustrated Figure 2.28.

$$FOS_{\text{basal heave}} = \frac{1}{H} \frac{N_c S_{u2}}{\gamma - \frac{2S_{u1}}{\sqrt{2} B}} \quad (2.5)$$

N_c is dependent on excavation geometry however where $H/B > 1$, $N_c = 5$. Whilst this equation accounts for final excavation depth, width of failure mechanism and two undrained shear strengths above and below formation level, wall embedment was ignored. Increasing embedment has been shown to improve the stability of an excavation and therefore has an influence over the factor of safety. This contributes to the varied scatter of a number of case studies in the Mana & Clough (1981) graph. As expected, the stiffer diaphragm wall displays lower magnitudes of horizontal displacement but over a wider range of factor of safety values. In addition to the simplistic factor of safety equation not accounting for wall embedment, it also ignores the additional support provided by props. The excavation method is not considered and a higher factor of safety would be expected for top down construction compared with an open cut or cantilevered excavation. Over an extended period of time larger lateral deformations will accumulate as excess pore pressures dissipate. Consequently, owing to the range of variables associated with ground movements it is not possible to focus solely on factor of safety against basal heave.

2.9.3 Clough & O'Rourke (1990)

Expanding on the published case studies (Goldberg *et al.*, 1976) Clough & O'Rourke (1990) normalised surface settlements against the maximum recorded settlement arising from a range of construction techniques at varying distances from the wall recorded. The results are presented in Figure 2.29 and, with the exception of two anomalous plots, all lie within the proposed displacement envelope for soft to medium clay. The maximum settlements are described to occur as little as $0.75H$ from the excavation with additional settlements up to $2H$ developing in the transition zone. Whilst this encompasses the data it is not representative of the actual surface settlement profile. It assumes maximum movements commence adjacent the wall and extend as far as $0.75H$. However, propped excavations exhibit an alternative deformation response with small settlements near the wall and larger displacements developing between $0.5H$ and H .

In addition, Clough & O'Rourke (1990) investigated the influence of factor of safety against basal heave and considered the overall stiffness of the excavation on lateral wall movements. The chart, given in Figure 2.13, is an improvement over the Mana & Clough (1981) graph.

2.9.4 Long (2001)

Data relating to 296 case studies were collated by Long (2001) to determine trends in movements based on ground conditions and soil strata in an attempt to validate the findings of Clough & O'Rourke (1990). The data was reanalysed and a factor of safety was computed using the Bjerrum & Eide equation before being replotted on the Clough *et al.* (1989) graph. Although a vague trend could be established between the computed factor of safety values and corresponding stiffness and deflections there were still some inconsistencies.

Long (2001) identified that in circumstances where a low factor of safety exists and a deep layer of soft soil (defined with $S_u < 25\text{kN/m}^2$) is retained with soft soil at formation level the Clough *et al.* (1989) chart provides a reasonable starting point for assessing soil displacements, as shown in Figure 2.30. In general, it agrees with the

Clough & O'Rourke (1990) envelope that in soft soils with a low factor of safety against base heave the stiffness has a significant influence on deflections and that the maximum normalised lateral displacement will be in the region of $3.2\%H$.

2.9.5 Moormann (2004)

Moormann (2004) collated an extensive database of 536 international case studies of deep excavations in soft soils with about 300 cases taken between 1991-2001. In the analysis, soft soils were defined as having $S_u \leq 75\text{kN/m}^2$. Moormann (2004) plotted maximum horizontal and vertical displacements against the final excavation depth in an attempt to ascertain a trend of movements in soft soils. It was concluded that maximum lateral movements typically range between $0.5\%H$ and $1\%H$ and are observed when the excavation depth was between $0.5H$ and H . It was also mentioned that the type of retaining wall influences the wall displacement however it is not clear whether prop stiffness and consequently excavation stiffness was considered. Although Moormann (2004) agrees with the statement presented by Goldberg *et al.* (1976) that the ratio of vertical to horizontal movements ranges between 0.5 and 1, Figure 2.31 shows that the ratio varies across a wider range of 0.5 to 2. The variability in measurements is not only attributed to sheet piled walls but also for diaphragm and secant piled walls. Furthermore, Moormann (2004) displayed maximum vertical settlements associated with excavations in soft and stiff soil (Figure 2.32). Whilst trends in displacements in stiff ground can be easily identified the same cannot be said for soft ground.

Moormann (2004) superimposed the displacements from this database on the Peck (1969) graph (Figure 2.33) and found that the maximum settlements tend to cluster between $0H$ and $0.5H$ at distance $0.5H$ from the retaining wall. Evidently, with improved construction methods, and advancements in technology, settlements in soft ground are well controlled and now lie within Zone I which was initially representative of displacements in sands and soft to hard clay. In agreement with the findings of Long (2001), Moormann (2004) found that a clear relationship between factor of safety against heave, system stiffness and lateral displacements did not exist. The scatter in the graphs produced by Moormann (2004) emphasise the complexities surrounding the ground response to deep excavations in soft soil.

2.9.6 Wang *et al.* (2010)

Wang *et al.* (2010) developed an extensive database on ground movements arising from 300 deep excavations in Shanghai soft soil. This study largely benefitted from relatively comparable soil conditions on each site, in contrast to the databases published by Goldberg *et al.* (1976); Mana & Clough (1981); Clough & O'Rourke (1990) and Moormann (2004). Consequently, should trends exist around soft soil excavations they may be more easily discernible than those presented in previous papers. The methods of construction were segregated; and established that stiffer walls developed maximum horizontal displacements at average distances of $0.4\%H$. Sheet pile walls were the most flexible and measured average horizontal displacements of $1.5\%H$ whilst deep soil mixed walls performed better with average displacements of $0.91\%H$. Displacements were compared with embedment depth ratios, system stiffness and diaphragm wall thickness to identify trends in movements. The data generally fell between the lower end of the Mana & Clough (1981) limits whilst a slight improvement was noted for a high factor of safety, however this was not an obvious trend and is open to interpretation.

Maximum vertical and horizontal displacements were plotted (Figure 2.34) and whilst the wide envelope extends from $0.4\%H$ to $2\%H$ there is arguably less scatter of the data. This is particularly evident when compared with the trend of movements presented by Moormann (2004) in Figure 2.31. Furthermore, the data was also superimposed onto the Peck (1969) graph showing significantly more defined settlement profiles. The displacements generally lie within Zone I and clearly represent the upper bound of settlements proposed by the authors. The proposed settlement trough agreed with that which was proposed by Hsieh & Ou (1998) where vertical displacements at the retaining wall are generally 0.5% of H and maximum displacements are observed at a distance of $0.5H$ from the retaining wall. The primary deformation zone extends as far as $2H$ with minimal displacements occurring beyond this distance.

2.10 CENTRIFUGE MODELLING

2.10.1 Modelling excavations in the centrifuge

2.10.1.1 Increase acceleration field until excavation failure (Lyndon & Schofield, 1970)

At the advent of centrifuge modelling the acceleration field on an excavation model would be gradually increased until the model failed. This was a very simple way of establishing the deformation patterns in an undrained excavation event. This can be achieved by consolidating the model in-flight, removing it and forming the excavation at $1g$. The model will then be rapidly accelerated whilst patterns of deformation are obtained. This method was extensively used by various researchers (Liu 1999; Ma *et al.* 2009; Liang *et al.* 2012). Whilst a short period of time is left before the test is conducted, drawbacks of this method are generally limited to clays. This is owing to excess pore pressure generation during spin up and the low permeability of the soil which requires a lengthy period of time to dissipate the excess pore pressures. Therefore, this method is particularly well suited to modelling excavations in sand. An alternative method (Lyndon & Pearson, 1984; Zhu & Yi, 1988) involved repeatedly starting and stopping the centrifuge between removing layers of soil (glass ballotini) to simulate each stage of the excavation.

2.10.1.2 Remove soil bags from the excavation void (Azevedo, 1983)

An excavation formed at $1g$ was surcharged (Azevedo, 1983) with bags of sand which were then removed to simulate the excavation. This method was also reportedly adopted by Allersma (1988) where sand wrapped in geosynthetic fabric were pulled out of the excavation. This method ensures consistency of lateral stresses on both sides of the retaining wall provided a similar material is used in the bags as the main body of soil. However, this method tends to be used for excavations in sand and the interaction between the wall and soil is affected by the presence of the bag.

2.10.1.3 Heavy fluid discharge (Bolton & Powrie, 1987; 1988)

A common method of simulating excavations also involves forming the excavation void at $1g$ and filling impermeable bags at formation level with a dense fluid, such as zinc choride or sodium polytungstate. Dense fluids can replicate the density of soil

and actuating a motor drains the bag at the desired rate into an on-board reservoir. As the level of dense fluid drops the lateral pressure on the wall and surcharge at formation level are reduced, thus simulating the excavation process. This technique has been used by a number of researchers (Kusakabe, 1982; Richards & Powrie, 1998, McNamara, 2001; Ong *et al.*, 2006; McNamara *et al.*, 2009; Elshafie *et al.*, 2013) however there is considerable disparity between the soil and fluid lateral pressure coefficients and the use of dense fluid assumes that K_0 of the retained soil is unity. Although, in heavily overconsolidated clays the lateral pressure approaches K_0 during the excavation and this approach can be argued a reasonable approximation for stiff clays. However, in normally consolidated samples K_0 ranges between 0.5 and 0.6 and approaches K_p during the excavation.

2.10.1.4 Surcharge formation with pressurised airbag

Airbags are typically employed when modelling tunnelling processes (Atkinson *et al.*, 1975; Wu & Lee, 2003; Ng, 2014; Le, 2017). However, based on the concept proposed by Peck (1969) whereby an excavation can be supported by pressurised air, McNamara (2001) reported using an airbag to surcharge the formation level. An airbag proved more successful than dense fluids, owing to the minimal and simple apparatus. There was no requirement for motors, reservoirs, valves, repairs to leaking polythene bags etc., as a direct connection was established between the bag and the airfeed. Therefore, whilst motors are prone to failure at high g no significant issues were reported as having occurred with the airbag arrangement.

*2.10.1.5 In-flight excavation (Kimura *et al.*, 1994; Takemura *et al.*, 1999)*

The first published records of in-flight excavators suggest they were developed in the early 1990's. Subsequently, many centrifuge facilities have developed bespoke in-flight excavators (Takemura *et al.*, 1999; Gaudin *et al.*, 2004; Lam, 2010) that remove layers of soil to closely model the prototype excavation process. It is necessary for in-flight excavators to operate in two directions. Early excavators (Kimura *et al.*, 1993; Takemura *et al.*, 1999, Ng *et al.*, 2001) were incapable of supporting the wall as the excavation progressed but Lam (2010) addressed this and developed a prop actuating system that installed support after a prescribed depth of soil had been removed. Whilst in-flight excavators permit the correct soil stress paths to develop they may not also produce clean accurate models, see Figure 2.36. A void in the strongbox is required

into which the scraped material is stored. Consequently, the size of the model is reduced and in order to monitor far field responses and minimise boundary effects it may be necessary to accelerate models to a higher g level. In this case modelling accuracy becomes even more critical and the equipment would be even more prone to mechanical failure. Although Lam (2010) designed an excavator that could actuate props in-flight following soil removal a time delay would inevitably exist between the final scrape and application of the prop. Therefore, actuating props would require careful calibration to ensure they applied a force in a controlled manner. This would contribute to an extended time lag between excavation and prop installation. In soft ground displacements rapidly develop and any disturbances will have a measurable influence on movements. This apparatus has recently prompted the development of similar in-flight excavators, as reported by Ma & Xu (2018).

2.10.2 Centrifuge modelling of excavations in soft ground

A number of centrifuge tests into the behaviour of deep excavations in stiff overconsolidated soils have previously been conducted (Powrie & Kantartzi, 1996; Richards & Powrie, 1998; McNamara, 2001; Powrie & Daly, 2002; Powrie & Daly, 2007). Although, limited publications exist relating to the behaviour of deep excavations in soft soils, some literature has been reviewed below.

An investigation into the behaviour of unsupported and sheet piled excavations in overconsolidated and normally consolidated clay was conducted by Kimura *et al.* (1994). The study also examined the effect of tying the sheet piled walls in an attempt to understand how wall support influenced deformations in clays as summarised in Figure 2.37(a). Vertical settlements, pore pressures and toe loads were monitored. Pore pressures were compared with a site at Haneda airport and confirmed that the modelling technique simulated prototype behaviour. Surface settlements measured 25mm away from the excavation and were plotted against the excavation depth, illustrated in Figure 2.37(b) demonstrate better supported excavations can be excavated to greater depths prior to failure. Excavations in the overconsolidated clay samples were approximately 50% deeper than those in normally consolidated clay, upholding the theory that displacements in soft normally consolidated ground are often excessive. In addition, the mode of failure in normally consolidated ground was

shown to be more sudden than in overconsolidated clay, as seen by the abrupt acceleration in settlements (Figure 2.38).

Takemura *et al.* (1999) presented a newly developed in-flight excavator to model a double propped deep excavation in normally consolidated soft clay as shown in Figure 2.39. Relatively flexible walls were used to study deformations influenced by wall embedment, excavation depth below lowest prop, toe fixity and prop forces. Figure 2.40 illustrates the deformations observed in two cases highlighting the reduction in displacement when the toe is founded in sand. Settlement profiles and lateral wall deflections are plotted in Figure 2.41(a) and (b) respectively and reference details of the centrifuge test series are given in Figure 2.42. Interestingly, the magnitudes of settlement are within the range of Peck's (1969) Zone III curve, which was consistent with Peck's theory. Whilst other studies and recent databases demonstrate that the magnitude of settlement is considerably lower than previously predicted, owing to improved construction techniques, this study can be argued to have essentially modelled less sophisticated construction activities and the shapes of the curves are representative of those propping conditions. Deflected wall shapes were computed from measured strains for test cases 7 and 9, with the main difference between the two cases being prop forces. When a larger upper prop force acted on the upper portion of the wall smaller deflections were observed (case 7). However, as the excavation progressed, the lower prop force in case 7 was 25% lower than that of case 9 which resulted in a greater overall deflected profile. The soil approached active conditions prior to placing the lowest prop which resulted in larger displacements developing as the excavation proceeded and therefore displacements can be better controlled if larger resisting forces exist in the lower prop.

Lam *et al.* (2014) reported on a series of 60g centrifuge tests that modelled in-flight excavations in lightly overconsolidated clay. The investigation comprised a series of five tests that evaluated the influence of wall and prop stiffness, toe fixity and depth to a hard stratum. The experiment set up and test series are presented in Figure 2.43 and Figure 2.44. The lateral deflections and surface settlements from each of the tests are plotted in Figure 2.45. The effect of reducing the thickness of the clay layer (tests 2 & 5) gave similar maximum lateral deflections but the magnitude of settlement at the end of the excavation was approximately 25% lower when the depth to hard

stratum was reduced by a factor of about two. Furthermore, it was demonstrated that, unsurprisingly, jet grouting at the toe of the wall (test 3) with infinite stiffness eliminated lateral deflections below formation level. In addition, the fixed toe reduced the maximum magnitude of deflection by about 30% compared with test 2 with significantly smaller settlements. The retained surface response was comparable with that observed in test 5; with a shallower depth of clay. An understanding of influence of prop stiffness was achieved in tests 1 & 4, which highlighted the effectiveness of a stiff system on controlling lateral deflections and surface settlements. Similarly, the influence of overall excavation system stiffness was validated in tests 1 & 2 where a higher system stiffness was shown to minimise displacements. This study provided a broad insight into the influence of a number of variables on surface settlements and provided conclusive evidence of the effect system stiffness has on soil movements. However, owing to the degree of flexibility of the wall it was not possible to ascertain the proportions of settlement owing to deflection and heave.

2.11 METHODS OF CONTROLLING GROUND MOVEMENTS IN SOFT SOILS

A wide range of methods have been adopted to mitigate or control the magnitude of movements in soft ground arising from deep excavations. The popularity of different techniques varies across regions, perhaps owing to availability of plant, materials, local knowledge and of course ground conditions. Phear & Harris (2008) explain that ground improvement is an unusual branch of geotechnical engineering where practice precedes theory as theories are developed following experience (Charles, 2002) with emphasis on improving techniques and defining its limitations. The term ground improvement is also loosely defined as an objective and is also relative to a particular aspect and the degree of improvement is defined by the engineer (Mitchell & Jardine, 2000) Common methods can largely be divided into two classes; soil strengthening and surcharging. For the purpose of simplicity, the soil strengthening measures discussed in this report will be subdivided into ground improvement methods and constructing additional foundations below formation level (Fernie *et al.*, 1991; McNamara, 2001). Case studies relating to these methods will be presented in the following subsection.

2.11.1 Soil strengthening: ground improvement techniques

Soil strengthening can be achieved by adopting a wide range of techniques, for instance faster rates of consolidation can be obtained by means of surcharging the ground around vertical drains (Tomlinson, 1956; McGown & Hughes, 1981; Long & O'Riordan, 2001), vacuum consolidation (Almeida *et al.*, 2000) or electro-osmosis (Casagrande, 1949; Bjerrum *et al.*, 1967; Su & Wang, 2003). On the other hand, mechanical improvement, generally encompassing dynamic or vibratory compaction, stone columns, soil mixing, grouting, can be used to provide not only stronger ground but can also be used in various configurations to suit the needs of the site.

Extensive research into improvement by consolidation has previously been conducted with recent emphasis placed on monitoring long term effects of consolidation (Nash & Ryde, 2001) and modelling consolidation behaviour in specific soils (Long & O'Riordan, 2001). The effects of consolidation can generally be estimated using Terzaghi's consolidation theory (1943). Similarly, although many variables exist for vibro-replacement, or vibro-stone columns, their design can crudely be related to bearing capacity theory or by reasonable agreement with the basic improvement factor developed by Priebe (1995) (McCabe & Egan, 2010).

More than 30 ground improvement methods exist and are commercially available. Reasonable guidelines exist for designing or estimating the effect of a ground improvement method however Phear & Harris (2008) state that limited research exists specifically for lime and cement stabilised soils. Therefore, this study will primarily focus on deep soil mixing owing to its applicability to a range of countries prevalent with soft ground.

Deep soil mixing has been popular from the 1960s and is widely used in Europe, USA and the Far East (Bell, 2012) for a wide range of applications, including improving bearing capacity, slope stability, supporting excavations, cut off barriers and to reduce earth pressures behind retaining walls.

Adding lime to clays improves the strength by inducing an exothermic reaction which results in the pore water in the soil being drawn out. This in turn increases the soil shear strength and lowers its permeability and compressibility (Boardman *et al.*,

2001). Its application was common for improving the stiffness of road foundations but DSM is versatile and can be adapted to provide solutions for a wide range of geotechnical problems. For instance, mass treatment can be used to construct gravity walls or form stronger blocks of soil at excavation formation level, slim columns can be reinforced with H sections to form stiffer structures with increased bending capacity (Bell, 2012). Columns can also vary in size, location and be overlapped to form lines or grids. Factors affecting DSM and typical properties are given in Table 2.1 and Table 2.2 respectively.

Deep soil mixing (DSM) is particularly well suited to clayey soils (Figure 2.46) and the method of installation is dependent on the water content of the soil. Wet soil mixing involves mixing in a grout as the soil may have a relatively low moisture content. Conversely, dry soil mixing combines dry binders, such as lime, cement or fly ash with soils of high moisture content. Mixing blades and auger flights along the tool shaft are rotated as the tool advances into the soil, see Figure 2.47. Grout or dry binder is simultaneously injected through a hollow stem in the shaft. As the auger advances, it blends the soil with the grout or dry binder until the design depth is reached. The shaft then rotates in reverse, thoroughly mixing the grouted soil as it is withdrawn from the ground (Reams *et al.*, 2000).

Hui (2006) carried out centrifuge testing solely to investigate the factors affecting the uniformity of deep soil mixed columns and ease of modelling this technique in-flight but did not investigate the applicability of DSM to construction events. The author established that numerous variables, including dimensionless numbers (Froude and Reynolds number), work done in mixing and centrifugal effects from mixing, installation and extraction time and number of blades all affect the wet mixing process. Difficulties arose in attempting to model the viscous forces in the centrifuge. The research highlighted the difficulties in modelling all variables associated with modelling DSM columns in flight and suggested that further work be undertaken to measure the viscosity of the slurry.

More relevant to this project, Ohnishi *et al.*, (2000) modelled DSM treatment at the formation of a deep excavation at 100g on the centrifuge. Soil was treated with fly ash and cement with the aim of reducing basal heave. A 16m deep, 25m wide excavation with a doubly propped retaining wall of 7m embedment was modelled, see

Figure 2.48. A reference test without any improvement and two improved soil strengths (100kPa and 400kPa) were simulated and extended across the formation to the toe of the wall. The centrifuge tests showed that high strength improvement (400kPa) reduced the prop forces significantly, as the backfill pressure was largely transferred into the improved ground. Image analysis indicated DSM minimised heave in both ground improvement cases, but increasing strength by a factor of 4 reduced soil displacements to 50mm, an order of magnitude lower than the 100kPa test as shown in Figure 2.49. Although the depth between the toe of the wall and bottom of the strongbox was around half the depth of the excavation, comparisons drawn between the reference test and improved soil tests showed a marked reduction in heave. Changes in surface settlement owing to DSM treatment was not discussed in the study.

Clearly, improving a significant depth of soil across the entire formation level reduces ground movements. However, attempts to reduce the depth of treatment should be made in order to design a more cost effective solution. Lee & Yong (1991) presented a case study where an excavation formation had been stabilised with jet grouting to facilitate the development of a 7 storey superstructure and 2 storey basement. Although this is not the same method as DSM the objectives and outcomes are similar and increased the shear strength from 20kN/m^2 to 300kN/m^2 . Sheet piles were driven around the perimeter of the site 2-4m into the medium stiff silty clay layer. A 2m thick layer of jet grouting below the formation level was performed at one corner of the site to mitigate the risk of damaging a neighbouring structure. A comparison of lateral deflections at the treated and untreated sites are presented in Figure 2.50 showing approximately 50% reduction in lateral movement. Reducing the depth of treatment was a cost effective means of controlling movements.

Tanaka (1993) presented a case study of a floating retaining wall that was not founded in hard strata, as shown in Figure 2.51. DSM had been used to strengthen the soil below the formation level and consequently the wall embedment was reduced. Heave and lateral wall deflections were measured during the excavation and the displacements are presented in Figure 2.52 and Figure 2.53. Although excessive heave was noted at formation level the lateral deflections clearly show the presence of the DSM layer and that it had an impact on controlling lateral deflections above formation

level. The paper concludes that the DSM performed unsatisfactorily and was unable to control heave, however the magnitude of improved shear strength is not reported and the shape of the lateral deflection profiles suggest that the treated soil was stiffer than the wall, resulting in excessive deflection.

Although a range of DSM patterns can be constructed (Figure 2.54) Ou *et al.* (1996) investigated DSM columns as they are one of the more common methods. The aim of the study was to establish whether a simplified 3D FEM model that considered the column treatment area as a block (equivalent material simulation, EMS) rather than discrete columns (real allocation simulation, RAS) was an appropriate means of estimating wall deflections. By defining the ratio of treated area to the total excavation area (I_r) and an equivalent material parameter (m) reasonable agreement was achieved between the 3D EMS and RAS models, see Figure 2.55. However, the model was further simplified for 2D plane strain models and all three methods were compared with measurements from a site in Taipei. The results are given in and highlight the efficiency of the 2D EMS method. It can be argued that the treated to untreated soil ratio dilutes the relatively high stiffness columns across the formation level. Therefore, a lower stiffness support acting across the formation level may have a similar influence on wall deflections.

An attempt was made by Lim (2003) to understand the influence of poor or limited contact between the retaining wall and ground improvement zone, as is typical in practice, through a series of centrifuge tests and numerical analysis. The thickness of the treated soil remained constant whilst another test series modelled an improved zone that did not extend across the entire formation level. Two sides of the excavation were modelled and defined as an improved berm, see Figure 2.57. It was found that conventional improved soil struts were very effective at controlling wall deflection but performance was governed by the stiffness of the strut. The presence of a small gap between the improved soil and wall resulted in noticeable movement during early stages of the excavation. This was owing to the reduced stiffness of the whole system, therefore larger gaps had a more significant impact on excavation behaviour. The improved berm was also found to be as effective as the traditional raft owing to the additional end bearing provided and the shear resistance along the base. Therefore, the stiffness of a soil berm does not govern the overall behaviour of the excavation as

the block essentially transfers lateral forces from the wall into the surrounding soil mass. The influence of these various arrangements on measured settlements are illustrated in Figure 2.58.

2.11.2 Soil strengthening: additional construction

Inserting an inclusion, such as piles, anchors, nails etc. into the soil at formation level is another method of improving the ground. This is owing to an increase in stiffness of the ground at and below the formation level. Fernie *et al.* (1991) detailed the finite element analyses for a 24m deep excavation in stiff London Clay and provided short-term wall and settlement data. The scheme and plan of site are provided in Figure 2.59. These measures were required to prevent long term displacements owing to rising groundwater. This was achieved through the use of 15m pin piles around the perimeter of the structure to provide additional vertical support, acting as a reinforced soil block. The ground response immediately after the excavation was recorded and the results are presented in Figure 2.60. There was reasonable agreement between the measured and predicted horizontal deflections, with less displacement measured near the surface owing to the employment of an additional prop. As expected, larger settlements were observed in location 1, closer to the site, and reduced magnitude with increasing distance from the excavation. Whilst this method controlled ground movements to reasonable limits in London Clay there is a lack of literature relating to its use in soft soils.

McNamara (2001) adopted this concept to develop an understanding of the influence of heave reducing piles at formation level. A series of centrifuge tests, see Figure 2.61 and numerical analyses were conducted in stiff clay which modelled a 12m deep top-down propped excavation; the number of rows of piles at formation level was varied. The presence of one row of piles at $3d$ from the retaining wall reduced the magnitude of surface settlements by 25%, whilst an additional row at $6d$ reduced vertical displacements by 40%. Similar magnitudes of lateral wall deflections were observed for one and two rows of piles, whilst more piles were shown to control the development of heave (Figure 2.62). Two rows of piles were shown to have a more significant impact at controlling long term movements than a single row. Wall embedment was also varied and as expected, deeper embedment was better able to

control movements, see Figure 2.63. McNamara (2001) likened the behaviour of the soil at formation to a block owing to the high strength of the clay. It is unknown whether similar benefits or behaviour are likely for deep excavations in soft clay.

McNamara's (2001) concept of heave reducing piles was employed in the design of foundations for a new tower in Singapore. The site was underlain by 30m soft marine clay (Osman & Bolton, 2006) and in order to mitigate lateral deflections heave reducing piles were proposed. Using the mobilised strength design method Osman & Bolton (2006) predicted that heave reducing piles would reduce lateral deflections by more than 50%, as shown in Figure 2.64. Although this was not proven in the field it, the results are comparable with those established by McNamara and highlights the applicability of intrusions at formation level to assist in reducing deformations.

A common method of constructing basements in China has been coined the pit-in-pit excavation (Sun *et al.*, 2017). This technique involves forming an inner and outer retaining wall which essentially achieves deeper but narrowing excavations, similar to benches formed in quarries. The scheme adopted for the Shanghai Museum of Natural History is shown in Figure 2.65. Finite element analysis was conducted to establish the basal-heave failure mechanisms for various arrangements of the embedment ratio of inner to outer wall and the distance between the inner and outer walls. Sun *et al.* (2017) found that the deformation patterns generally resembled slip circles and when the spacing (W) between the inner and outer walls was larger than the critical spacing (W_{cr}) the slip circles tend to be centred about the lowest strut. However, reducing the distance between the walls results in a more integrated mechanism as the origin of the slip circle is assumed to act at a distance halfway between the two walls at the elevation of the lowest prop. These mechanisms are illustrated in Figure 2.66.

Yu *et al.* (2018) investigated the influence of a double retaining wall, where the second, longer retaining walls were constructed as a means of providing a basement extension to a deep elevation; Figure 2.67 illustrates the modelling stages which are typical of double walled excavations. The tests were conducted in silt at $1g$ in a steel tub, 3x3m in plan and 2m high and the spacing of piles and embedment of the front and back rows were varied. The study primarily investigated the bending moments developed during the excavation and found that once the front row of piles is excavated bending moments are transferred to the back row and their magnitude is

considerably greater than those measured in a reference test where a single row of piles was modelled. Although this paper considers the eventual removal of the front retaining wall, it provides an insight into the transfer of loads below formation level and also concludes that contrary to traditional lateral earth pressure design, the soil between the two walls provides negligible active pressure to the front row of piles.

Whilst there has been some research into double walls, a significant study into the influence on ground movements of double retaining walls for one excavation depth has not been published.

2.11.3 Surcharging the excavation formation level

Peck (1969) stated that the only means of significantly reducing the magnitude of movements arising from deep excavations is by decreasing the change in stress on the soil until supports are in place and are capable of withstanding the horizontal forces. This can be accomplished by either removing as little soil as possible until the supports are installed or alternatively, applying a fluid pressure to the excavation equal to that which was exerted by the excavated soil.

A technique employed in Scandinavia uses air pressure to prevent excessive lateral deflections and heave in an excavation (Peck, 1969). Whilst this technique was common for the excavation of tunnels and caissons, its implementation in supporting retaining walls and formation levels is more complex. The retaining wall must first be installed before a roof slab is cast at or near ground level and supported on the retaining wall. A surcharge is placed on roof slab to prevent blow out before compressed air is used to excavate in a similar fashion used in tunnelling. A similar but more manageable surcharge method is by means of underwater excavation. The vertical load from the water minimises the total vertical stress relief whilst the head of water provides lateral support to the wall. There have been a limited number of case reports where this method was employed however two will be briefly discussed here.

The Marina Bay Station project involved the construction of a station box on reclaimed land in the Upper Marine Clay adjacent the East Coast Parkway Expressway (Clarke & Prebaharan, 1987; Denman *et al.*, 1987) see Figure 2.69. Four schemes had been considered (Figure 2.70) which included a conventional ‘dry’ excavation and ground

improvement treatment. Owing to the construction cost, delivery and sequencing the final scheme involved lower stiffness walls than those proposed in alternative schemes in conjunction with a raised water level. This reduced the need for numerous props and those that were required could be installed prior to flooding. The final sequence (Figure 2.71) first involved driving the sheet piles to depths between 15-18m before 6.5m of soil was excavated dry to facilitate installation of props. The remaining soil was removed by means of waterjetting and airlifting. Relief pipes were placed at the final excavation level to counter the effects of long term heave before a tremie was used to cast a 1.5m thick concrete slab in-situ. The cofferdam was then dewatered before the station box was constructed which permanently propped the sides of the diaphragm wall. The reliability of measurements during wall installation was poor, however data from the excavation was more reliable. Inclinometer readings were in very good agreement with the predicted wall movements, as shown in Figure 2.72. This method illustrated the benefits of submerged excavations in mitigating the risk of excessive displacements, expensive and very stiff retaining walls and props at many elevations.

Karlsrud & Andresen (2008) presented a case study where underwater excavation aided in the construction of the Oslo Opera House basement structure, which involved excavation of a 38m diameter shaft with sheet piles extending 20m below ground level, shown in Figure 2.73. The top 6m was excavated dry whilst concrete ring beams were cast before underwater excavation proceeded to formation level. A 500mm thick layer of drainage material and compressible heave void formers bedded the base of the excavation with the purpose of countering the 140kPa uplift pressure with a thinner, more economic base slab. Immediately after the dewatering stage, the authors reported no vertical displacements of the base slab, indicating that heave had been sufficiently controlled. Lateral movements ranged between 78mm and 123mm, which were within 10% of predictions made from an equivalent plane strain FEM analysis.

Although underwater excavations have been shown to support the sides of excavations and reduce the net change in vertical stress relief, data relating to surface settlements and the long term effects are unknown and the effect of soil softening at formation level is not widely publicised.

Passive pressure is a function of the vertical stress acting at formation level. Reducing the change in overburden pressure can therefore increase the passive pressure and assist in stabilising an excavation Fleming *et al.* (1992). Although underwater excavations are an obvious means of surcharging the formation level, divers were required during concreting of the base slab at Marina Bay (Denman *et al.*, 1987). Contractors were therefore subjected to the risk of developing serious health problems, such as the bends. Although technology has now improved and would no longer require divers to level concrete, an alternative surcharge method that does not require large amounts of dewatering is by means of constructing berms.

As described by Potts *et al.* (1993) a berm provides contractors with an option to excavate to the first basement level without prior installation of the ground floor slab. An advantage of this is that contractors can work in well ventilated conditions, with sufficient working room owing to the lack of props, with fewer risks and excavation can be completed in a shorter period. Completing the excavation and constructing the basement with minimal delay is essential as Ou *et al.* (1998) reported that up to 10mm lateral wall displacement was observed during periods of inactivity during a deep top-down excavation. Whether this is due to consolidation settlement owing to the dissipation of excess pore pressures in soft clays or creep, it is accepted that the consequences of a delay during excavation will result in a greater magnitude of ground movements.

Berms are typically defined as a mass of ground that remains in-situ around the perimeter wall during and after the bulk of excavation has been completed. The self-weight of the berm surcharges the ground directly in front of the retaining wall, whilst the height of the berm provides some level of lateral restraint to the wall. Horizontal or raking struts support the top of the wall before the berm is gradually excavated and more struts are installed. Peck explains that lateral displacements may become excessive as the berm deflects, however this can be countered by installing all ground level props before the berm is excavated or pre-stressing an upper raking prop. The berm dimensions are defined in Figure 2.74 where the berm height is referred to as H , the toe width as B , the bench width as W and slope angle as S . The dimensions of a berm are dictated by the size of the site and angle of friction of the soil.

Through finite element analysis Potts *et al.* (1993) assessed the effects of berm geometry, volume and wall embedment on wall movements, modelled in ground conditions typical of London. Analysis for varying berm geometry and constant volume revealed that berm geometry was not a critical factor in controlling lateral deflections, as doubling the height only reduced displacements by 14%. However, for a constant berm volume it was discovered that berm height had a more significant impact on deflections than berm width. The influence of berm volume on wall movements was predictable, the greater the volume the more efficient the berm at reducing displacements. A berm volume equal to 30% of the total excavation gave maximum settlements 20-25% larger than would be expected for a propped excavation, whilst lateral deflections were approximately 60% greater than a propped excavation, which had a computed efficiency of 61.5%. The results from this analysis are presented in Figure 2.75.

Comparisons were made between finite element analyses, hand calculations and field measurements of an earth berm used in the construction of a temporary access route in North Wales (Powrie *et al.*, 1993). The results showed that the use of a berm restricted wall movements to acceptable levels and were in reasonable agreement with the FE analysis. Hand calculations were based on maintaining wall equilibrium after long-term pore pressures had dissipated and assuming a horizontal effective stress profile, thus overestimating wall movements and under-predicting berm efficiency. The analysis was shown to be highly sensitive to parameters including soil stiffness and lateral earth pressures, indicating the complexities in numerically modelling berms.

Centrifuge tests at 100g were conducted by Powrie & Daly (2002) to investigate the behaviour of berms as temporary supports for embedded retaining walls. The study focussed on the impact of wall embedment, groundwater levels and berm volume on reducing surface settlements and wall deflections, as illustrated Figure 2.76. The second series of tests was more representative of an undrained excavation and showed that low groundwater tables reduced displacements owing to the development of suction, which could be possible in the field if the berm was protected by concrete blinding. In the short term (Figure 2.77) there was no significant difference in vertical displacements for different depths of embedment or groundwater table, however the

influence of a lower groundwater table was more pronounced in reducing lateral displacements of the wall crest. As shown in Figure 2.78, berms offered greater contributions in the long term by preventing additional lateral displacements. In addition, the results showed that deeper wall embedment does not significantly contribute to a reduction in settlement. Comparison between the centrifuge results and a numerical analysis gave similar conclusions.

The two common and relatively simple methods for analysing earth berms (Simpson & Powrie, 2001) are summarised below;

2.11.3.1 The equivalent surcharge method (Fleming et al., 2008)

A uniform surcharge (S), equal to the weight of berm, is applied across the width of the passive wedge, as illustrated in Figure 2.79 and can be computed using equation (2.6). This method is considered as a highly conservative method (Simpson & Powrie, 2001) as discovered in the numerical analysis study by Potts *et al.* (1993) where displacements and moments were overestimated as the lateral resistance offered by the berm was ignored, see Figure 2.80.

$$S = \frac{W_b \tan\left(45 - \varphi'_{crit}/2\right)}{d} \quad (2.6)$$

2.11.3.2 Raised effective formation level method (Fleming et al., 2008)

The most recently published guide for the design of embedded retaining walls; CIRIA C760 (Gaba *et al.*, 2017) recommends using this method of analysis which partially considers the lateral pressure acting on the wall. The principle of this analysis is illustrated in Figure 2.82 and the width of the berm (b) remains unchanged and the berm profile is reduced to 1:3 giving a new berm height of $b/3$. The new raised formation level is considered as being half the new berm height, $b/6$, and extends across the full formation level. Any of the original berm above the 1:3 profile and the new effective formation level (shaded area in Figure 2.82) is then considered as an additional surcharge acting across the passive wedge, computed using equation (2.7).

$$S = \frac{W_b \tan \theta}{d + b/6} \quad (2.7)$$

Daly & Powrie (2001) analysed the centrifuge tests published by Powrie & Daly (2002). The equivalent surcharge method, raised effective formation level and a newly proposed modified limit equilibrium method, which accounts for the lateral pressures exerted on the wall at varying depths were used, see Figure 2.83. It was demonstrated that the raised effective formation level gave slightly conservative but comparable results to the modified limit equilibrium method but was considered less conservative than the equivalent surcharge method. Further investigation into the methods of analysis was undertaken by Smethurst & Powrie (2008) who found that the critical passive wedge in the raised effective formation level was estimated to be larger owing to the use of effective stress analysis which results in deeper wall embedment. Consequently, the raised effective formation level method overestimates the effect of the berm by up to 15%. Smethurst & Powrie (2001) therefore suggest using equation (2.8) to determine a more reasonable height by which to raise the formation level.

$$y = \frac{W_b \tan(45 - \varphi'/2)}{\gamma d} \quad (2.8)$$

2.12 SUMMARY

A large body of literature has been published relating to the general ground response to deep excavations, particularly in stiff ground. Obvious displacement trends exist and can be used to help engineers approximate the magnitude of soil movements. However, there is less consistency with the behaviour of soft soil in response to a deep excavation. There are a number of deep excavation databases (Peck, 1969; Goldberg *et al.*, 1976; Mana & Clough, 1981; Clough & O'Rourke, 1990; Long, 2001; Moormann, 2004 and Wong *et al.*, 2010) that critically examine data from various sites worldwide. Whilst numerical analysis has been shown to produce expected trends of movements many attempts have been made to plot field data on the classic curves (Peck, 1969; Mana & Clough, 1981; Clough & O'Rourke, 1990).

Generally, the retained soil displacement patterns are consistent with the Peck (1969) graph, however the magnitudes are significantly smaller owing to considerable developments in technology and construction methods. Efforts to link factors of safety against basal heave and horizontal deflections have been made by Clough & O'Rourke (1990) who suggest that increasing the overall excavation system stiffness and designing to higher factors of safety may contribute to smaller lateral deflections. The theory is logical, plausible and generally true of deep excavations in stiff or competent ground, however, in soft ground there are no consistently conclusive trends to validate this theory.

It is accepted that there are a wide range of factors that influence ground movements and the literature suggests that displacements in soft ground are highly susceptible to these variables; more so than stiff soils. The settlement profile of a retained surface is essentially influenced by global and local displacements. Whilst it is possible, within practical and economic means, to control local displacements, managing movements that arise from the vertical unloading of the overburden is considerably more challenging. Therefore, ground deformations comprise a complex combination of lateral wall deflections and vertical heave. To date, parametric studies by means of centrifuge tests and numerical analyses have been conducted to investigate the influence of a few variables on ground movements. Whilst these provide a snapshot of the influence of an element on general ground movements by means of modelling a realistic flexible wall, no extensive physical modelling studies have been conducted to determine the influence of a parameter on global movements alone. Therefore, there is a lack of understanding of resultant ground movements in soft soils pertaining to a very stiff wall and propped excavation.

This literature review has briefly reflected on various construction methods and measures that can be used to assist in controlling ground deformations. Techniques employed to improve the strength or stiffness of the soil are considered ground improvement measures, which are essentially defined as measures undertaken to increase the capacity of a particular element relative to its original state. Ground improvement has been classified as a branch of geotechnical engineering that is contractor led where practice precedes theory. Consequently, whilst there is some literature available it was noted that owing to this situation there is a distinct lack of

high quality technical papers submitted to leading journals that related to field studies of ground improvement methods and that critically review the techniques. Numerous ground improvement techniques exist that are commercially available and all contribute to reducing displacements arising from an excavation. The ground condition is one of the key elements that should be considered when deciding on the type of improvement, in addition to costs and spatial limitations on site. Some techniques have been extensively researched whilst others less so, in particular deep soil mixing (DSM) and submerged excavations. This exercise found that the literature was largely compiled from a mix of numerical analyses and physical model tests with some field studies. The patterns of movements and extent of settlement propagation in soft soils associated with ground improvement techniques generally follow the general trend of settlements with some degree of reduction in magnitude. However, they can also improve the stability of an excavation.

A significant majority of the ground improvement literature has focussed on effects on lateral wall deflections. Whilst this is an important factor that should be assessed for relatively flexible walls, the information is of limited relevance to this project. Determining the implications of ground improvement measures on heave and surface settlements owing purely to global deformations is the aim of this project.

Ground movements around excavations can be controlled in two ways; either by interrupting the deformation mechanism or reducing the change in vertical stress relief (Figure 2.84). Having conducted this literature review it has become apparent that there is limited published material surrounding some construction techniques that could prove successful in controlling ground movements. The scope of this research project will therefore be limited to deep soil mixing and double walled excavations to investigate their influence on the deformation mechanism. In addition, underwater and bermed excavations will be modelled to establish the effect of reducing the overburden pressure change on ground movements.

CHAPTER 3 CENTRIFUGE MODELLING

3.1 INTRODUCTION

The behaviour of soil is governed by its in-situ stress and the stress history to which it has been subjected. Consequently, physical modelling relies on achieving stress similarity between the model and prototype. The majority of geotechnical problems are large scale, however it is impractical, potentially unsafe and economically unfeasible to perform full scale field tests as a means of understanding the soil behaviour of a particular event. Similarly, downscaling the prototype event to a smaller model and performing tests at $1g$ is not suitable owing to the stress dissimilarity between the prototype and model. The principle of centrifuge modelling involves increasing the self-weight of the soil sample, which in turn increases the stresses in the model. Consequently, centrifuge modelling may be a propitious and practical means of analysing ground deformation behaviour.

3.2 PRINCIPALS OF CENTRIFUGE MODELLING

The aim of centrifuge modelling is to achieve stress similarity between the model and the prototype. This is achieved by accelerating a model to induce an inertial radial acceleration field N times greater than the gravitational field strength on Earth. Hence stress increases with depth through the model, from zero at ground surface to values that are a function of soil density, depth and radial acceleration which are representative of the prototype. Therefore, in the model, the vertical stress, σ_{vm} , at depth h_m should equate to the vertical stress σ_{vp} at depth h_p .

$$\sigma_{vm} = \sigma_{vp} \quad (3.1)$$

The principles of centrifuge modelling were described by Taylor (1995). Newton's second law of motion states radial acceleration is imposed towards the centre of rotation on an object that is pulled out of its straight flight path and around a curve of constant radius.

$$a = \omega^2 r \quad (3.2)$$

Where a = radial acceleration (m/s^2)

ω = angular velocity (rad/s)

r = radius of the curve (m)

On the centrifuge, the radial acceleration increases the self-weight of the model in the direction of the base, hence

$$a = Ng \quad (3.3)$$

Where N = dimensionless gravity scaling factor

g = acceleration due to gravity (9.81m/s^2)

As illustrated in Figure 3.1, centrifuge models subjected to a radial acceleration field can closely represent the prototype provided care is taken to design the model.

3.3 SCALING LAWS

An appreciation of centrifuge scaling laws is required to facilitate the design of a suitable model which reflects the correct stresses at prototype scale. Vertical stresses in the prototype are a function of the bulk unit weight of the soil and the depth at which the stress is determined.

$$\sigma_{vp} = \rho gh_p \quad (3.4)$$

For a model subjected to an acceleration N times greater than that experienced on Earth

$$\sigma_{vm} = \rho N g h_m \quad (3.5)$$

Assuming that the same soil is present in the model and prototype then the condition of stress similarity is achieved if;

$$\text{Recall that} \quad \sigma_{vm} = \sigma_{vp} \quad (3.1)$$

$$\text{Therefore,} \quad \rho N g h_m = \rho g h_p \quad (3.6)$$

Cancel and rearrange

$$N = \frac{h_p}{h_m} \quad (3.7)$$

The scaling law of $1/N$ is not only limited to linear dimensions, but also the geometric properties of elements used in the model. For example, the moment of inertia used to calculate the stiffness of the retaining wall in this series of tests scales to $1/N^4$ in the centrifuge. Powrie (1986) provided a detailed list of scaling factors and those relevant to this project are presented in Table 3.1.

Consolidation plays a significant role in understanding and predicting the settlement behaviour of soil. In the centrifuge, consolidation must be scaled appropriately in order to account for the dissipation of excess pore pressures within the model. This is achieved using a dimensionless consolidation time factor, T_v ;

$$T_v = \frac{c_v t}{L^2} \quad (3.8)$$

Where c_v = coefficient of consolidation (mm^2/s)

t = elapsed time (s)

L = drainage path length (mm)

For an equivalent time factor in the model and prototype;

$$T_{vm} = T_{vp} \quad (3.9)$$

$$\frac{c_{vm} t_m}{L_m^2} = \frac{c_{vp} t_p}{L_p^2} \quad (3.10)$$

Therefore;

$$t_m = t_p \frac{c_{vp}}{c_{vm}} \frac{L_m^2}{L_p^2} \quad (3.11)$$

Since

$$\frac{L_m^2}{L_p^2} = \frac{1}{N^2} \quad (3.12)$$

$$t_m = t_p \frac{c_{vp}}{c_{vm}} \frac{1}{N^2} \quad (3.13)$$

Assuming the soil in the prototype is the same soil used in the model, it can be said that the scaling factor for consolidation time is $1:N^2$. Hence, a small scale model accelerated for one minute at $160g$ equates to approximately 18 days at prototype scale. In terms of consolidation this facilitates the observation of long term ground movements over a short period duration.

3.4 ERRORS IN CENTRIFUGE MODELLING

Centrifuge modelling provides a means of assessing large scale geotechnical engineering problems. As with most modelling techniques however, errors can arise. Understanding the typical errors faced by centrifuge modellers and establishing methods to mitigate these is of paramount importance.

3.4.1 Variations in stress levels

At full scale Taylor (1995) explains that the gravitational field on Earth is relatively uniform, however the increase in radius through the model depth causes a variation in the centrifugal acceleration in the model. This results in areas of under and overstress in the model as illustrated in Figure 3.2.

A reduction in the magnitude of under and overstress in the model can be achieved by using an effective radius, R_e . Applying the effective radius ensures the correct stress is applied at a depth two-thirds from the model surface.

$$R_e = R_t + \frac{h_m}{3} \quad (3.14)$$

Where R_e = effective radius (m)

R_t = radius to top of model (m)

h_m = depth to base of model (m)

3.4.2 Radial acceleration error

The radial acceleration field passes through the axis of the centrifuge, which in turn introduces a horizontal component of acceleration in the model. This is owing to the fact that the radial acceleration field is not parallel to the base of the model. The further away from the model centreline, i.e. the closer to the model boundaries, the greater the magnitude of this horizontal error.

To limit these errors McNamara (2001) states that the strongbox should be orientated such that the smallest dimensions align with the radial acceleration field. Furthermore, critical measurements, such as ground movements, should be made along the centreline of the model as these are likely to be more representative of the prototype.

3.4.3 Grain size scaling effects

The scaling laws of centrifuge modelling apply to the geometry of the model as well as the soil sample, thus fine grained sand may be used to model gravel at 100g. Taylor (1995) explained that if this concept was applied to clays then a $2\mu\text{m}$ clay particle would scale up to a fine grained sand. However, this argument is unreasonable as the stress-strain characteristics of clay vary significantly from granular materials. Fuglsang and Ovesen (1988) stated that grain size effects are particularly noticeable where the grain size exceeds $1/30^{\text{th}}$ of the dimension of a significant component in the model. Considering that the thickness of each wall rib is 1mm and applying the grain size scale it was deemed that there was no grain size scaling effect.

Speswhite kaolin is typically used when performing centrifuge tests in clay owing to its practical properties, with permeability, k , equal to 10^{-9}m/s . For instance, Speswhite kaolin has a relatively high permeability, which reduces the model consolidation time and allows pore pressures to dissipate in the centrifuge quicker than if, for example, London Clay had been used ($k = 10^{-12}$). The properties of Speswhite kaolin have been well researched and established (Al-Tabbaa, 1987; Grant, 1998) and are presented in Table 3.2.

3.4.4 Boundary effects

At City, University of London, plane strain centrifuge tests are conducted in a rectangular Duraluminium strongbox. An 80mm thick Perspex window fitted to the front face of the strongbox allows observation of subsurface movements of the model.

The presence of friction between the soil and the various boundaries is inevitable (Phillips, 1995), however certain measures can be implemented to reduce the magnitude of these boundary effects. Suggestions included designing a sufficiently large model so that side wall friction is negligible and measurements of surface deformations are taken from the centreline of the strongbox.

To further reduce frictional resistance between the clay and the strongbox, waterpump grease can be used to lubricate the internal faces of the strongbox prior to placing the slurry. A colourless high viscosity silicone oil can also be spread across the window to permit visual inspection of the model whilst minimising interface friction and also preventing clogging of a base drain that is provided beneath the model.

3.5 THE GEOTECHNICAL CENTRIFUGE

3.5.1 The Acutronic 661 Geotechnical Centrifuge

The geotechnical facility located at City, University of London is an Acutronic 661 beam centrifuge, details of which were given by Schofield and Taylor (1998). Following renovation, maintenance and upgrades a schematic diagram has been presented in Figure 3.3. This centrifuge can accommodate a 400kg package at 100g, reducing to 200kg at 200g. The swinging platform is 500 x 700mm in plan with a maximum package height of 970mm which is balanced by a counterweight that can be adjusted radially on a screw mechanism. The radius to the swinging platform is 1.8m with an effective radius ranging between 1.5m and 1.6m depending on the model to be tested.

High accelerations are achieved by the centrifuge therefore it is important that it is operated in an enclosed and secure area. The centrifuge is located within a circular reinforced concrete structure which was designed to reduce air resistance within the

chamber. A sacrificial block wall surrounds the chamber that was designed to absorb the impact from any inadequately secured equipment and enable them to become embedded, preventing further damage to the centrifuge whilst operational.

Four strain gauges are positioned in the centrifuge pedestal and are used to measure out-of-balance loads and are constantly monitored by the centrifuge control system. The centrifuge automatically shuts down if the out-of-balance exceeds a maximum pre-set value of 15kN. This safety mechanism allows the centrifuge to remain operational whilst unmanned overnight.

Connections to the swinging platform are supplied through a stack of slip rings located above the central rotating pillar. These include four fluid slip rings that supply compressed air or water at pressures up to 10bar. Sixteen electrical slip rings transmit transducer signals to communicate with the centrifuge control system, instrumentation, data acquisition, cameras, lighting, motors, lead screw actuators and solenoid valves as required. The on-board computer converts analogue transducer signals to digital signals, which can be amplified if necessary.

3.5.2 Data acquisition

Permanent junction boxes mounted to the centrifuge are used to collect signals from the instrumentation. Signals are passed through an on-board signal conditioning unit where they are filtered and amplified. Amplification gains of 1, 10, 100, 500 or 1000 are available and this range also caters for low output voltage instrumentation, such as pore pressure transducers.

Le (2017) describes the in-flight PXI computer, supplied by National Instruments as being mounted to the centrifuge and records real-time data from the instrumentation. This data is logged using a Labview program, which can be accessed remotely in the control room through LAN connection. Motors, solenoids and lead screw actuators used in apparatus on the centrifuge swing are also controlled using this system.

3.5.3 Instrumentation and calibration

This research focussed on ground movements arising from deep excavations which was modelled by means of reducing the surcharge on a preformed excavation and monitoring subsequent movements. It was essential that accurate vertical movements and pressure measurements were recorded. In order to achieve accuracy all transducers were calibrated over the same range prior to each test.

Eleven linear variable differential transformers (LVDTs), manufactured by Schlumberger and supplied by RS Components Ltd, Northants, were used to measure surface settlements of the retained ground surface along the centre line of the centrifuge model. Each LVDT was calibrated at 1mm increments over a range of 10mm with the aid of a screw micrometre clamped within an aluminium block. This is standard practice for similar experimental work at City, University of London.

A minimum of three Druck PDCR81 miniature pore pressure transducers (PPTs) were installed in the clay along the centre line of the model with access through the back wall of the strongbox. These were used to monitor changes in pore pressure during in-flight consolidation to determine when conditions of pore pressure equilibrium were established and during the simulation of the excavation. Porous stones were glued to the PPTs to protect the diaphragms. Prior to use in the model the PPTs were placed in a manifold, sealed within a de-airing chamber and subjected to a vacuum of -100kPa. PPTs are extremely susceptible to inaccuracy if they are not de-aired. Ensuring that the PPTs were saturated and thoroughly de-aired enabled monitoring of pore pressure responses to an excavation. A Bishop ram was used in conjunction with a Druck DPI101 Digital Pressure Indicator (DPI) to pressurise and calibrate the PPTs prior to each test. A PPT without a porous stone was used to monitor the pressure at the base of a standpipe used to maintain the groundwater level in the model.

The surcharge applied to the formation was achieved by means of a pressurised latex bag. The air pressure within this bag was measured using a sub-miniature flush diaphragm pressure transducer, model number PX600-200GV, supplied by Omega Engineering Ltd. A centrifuge hydraulic air feed, controlled using the digital pressure indicator in the control room, was used in the calibration of this pressure transducer.

3.5.4 Image processing – Visimet

Digital image processing has been used as a means of displacement measurement in conjunction with centrifuge modelling at City, University of London since 1998 (Grant, 1998) and the system has been developed specifically to record subsurface movements. In the early stages of testing, a small charge coupled device (CCD) monochrome camera was mounted to the centrifuge swing and was orientated perpendicular to the model.

During model making, 3mm diameter bullet shaped black acetal targets were embedded into the front of the clay model at 10mm centres in a square grid arrangement. Ground movements were then measured by tracking the movement of these targets against fixed control point targets, etched into the front face Perspex window. Images were captured at one second intervals and were fed back to a monitor in the control room via the electrical slip stack and stored on the centrifuge on-board computer.

Image quality plays a vital role in controlling the precision of measurements which can be influenced by lighting, contrast, clarity of targets, camera properties and the number of known control point targets captured in the image sequence. Visimet for Geotechnics was the programme used in the analysis of the images taken in the initial tests. The width of the individual 3mm diameter targets in pixel space was between 6 – 7 pixels, which provided a target area of approximately 30 and 40 pixels. Divall (2003) explains that Visimet for Geotechnics analyses images by applying a greyscale over each target. As the target moves the intensity changes and soil displacements across consecutive images can be quantified by tracking the changes in intensity. Calibration of the images requires details of camera lenses, focal lengths, position, orientation and optical properties of the Perspex window (Divall, 2013). The software converts the target movements from pixels in image space to millimetres in object space.

Grant (1998) reported that the accuracy of this technique was within 50 to 80 μm . In a series of centrifuge tests McNamara (2001) demonstrated that the level of accuracy achieved by Visimet was $\pm 25\mu\text{m}$. This is compared to an accuracy of $\pm 5\mu\text{m}$ for LVDTs.

3.5.5 Image processing – GeoPIV-RG

Whilst Visimet was used during the first tests, the majority of the centrifuge tests conducted as part of this research programme made use of Particle Image Velocimetry (PIV) to measure soil deformations. PIV was initially used in the field of experimental fluid mechanics for high velocity flows but was developed by White (2002) for practical applications in geotechnical engineering. White described the deformation of soils as a “low-velocity flow process” which allows for a slower image capture rate. However, the calculation of displacements can only be achieved if a suitable texture is applied to the model and displacements between consecutive images are small enough to be contained within a discrete patch. In clays, texture is typically accomplished by means of coloured flock material or sand applied at a suitable density which is determined by lighting conditions and the camera focal length.

In these tests, black 1mm diameter glass ballotini (beads) were embedded in the front face of the clay model. The size of the ballotini and a high density texture were used owing to the camera angle, focal length and lighting conditions on the centrifuge. One miniature digital USB camera, model number IS-DFK72BUC02, supplied by Alrad Instruments Ltd., was initially positioned at an angle to focus on the area of interest; the excavation located at the far end of the strongbox. Later tests made use of an identical camera, angled in the opposite direction to capture far field movements.

GeoPIV-RG (Stanier *et al.*, 2015) analysis essentially relies on the tracking of a patch within a larger mesh to establish soil movements. An intensity value is assigned to each patch and analysis of sequential images tracks the movement of this light intensity patch across the main image. Division of the image into appropriate patch sizes is important to ensure that each unique patch is large enough to be identified in the image but small enough such that the shear planes or localised soil displacements can be pinpointed.

Owing to the need to position the cameras at acute angles relative to the model window and the region of interest being at the extreme end of the camera view, the captured images were highly distorted. It was therefore necessary to correct the images prior to analysis. This process used the camera properties to remove the curvature and reduce the noise in the images. A comparison between an image taken with the camera

and its undistorted counterpart are illustrated in Figure 3.4. A similar computational analysis is applied to GeoPIV-RG as used by Visimet for Geotechnics, whereby changes in the intensity of the patch are tracked between the initial reference image and subsequent images. With better analysis a higher degree of match (cross-correlation) was achieved between the reference image and following images. The user can define a cross-correlation coefficient (CCC) value and any patch that falls below this threshold is automatically filtered out from the dataset. A CCC factor of 0.8 was typically used to ensure that data was of a suitably high standard and also to ensure there was a sufficient amount of data available for analysis.

Image analysis conducted GeoPIV-RG has recently become more popular than Visimet for Geotechnics owing to a number of factors. Nadimi *et al.* (2016) showed that the discrepancy between LVDT and GeoPIV-RG measurements were within $5\mu\text{m}$, compared with $25\mu\text{m}$ from Visimet image analysis. Additionally, installation of the black ballotini was considerably quicker than embedding numerous 3mm black acetal targets, thus accelerating the model making stage and prevent excessive drying out of clay samples.

3.6 SUMMARY

This chapter outlined the fundamental methodology for this research. The geotechnical centrifuge at City, University of London was described and the principles of centrifuge modelling have been explained. Errors arising from centrifuge modelling have been discussed and measures to mitigate the magnitude of these errors were implemented. Data acquisition, instrumentation and image processing techniques used in this research have also been detailed.

CHAPTER 4 APPARATUS DEVELOPMENT

4.1 INTRODUCTION

The general apparatus set up used in the tests reported is given in Figure 4.1 showing the excavation model and major elements of apparatus. A pressurised latex airbag was used to surcharge the formation level whilst a spacer protected the bag from a very stiff wall. LVDTs were positioned along the centreline of the model to measure surface settlements and black glass ballotini were embedded in the clay surface to record subsurface deformations. A stiffener, bolted to the strongbox, provided continuous propping to the wall and also supported a capping beam that restrained the crest of the wall in a later series of tests. This apparatus and specific requirements for each test will be described in detail in this section.

4.2 TYPICAL APPROACHES TO MODELLING EXCAVATIONS

Excavations in clays have been extensively researched using the geotechnical centrifuge (Takemura *et al.*, 1999; Powrie and Daly, 2007; Lam *et al.*, 2012 etc.). Numerous efforts have also been made to predict and control ground movements arising from deep excavations using a range of modelling techniques.

Research undertaken at City, University of London (McNamara, 2001; McNamara *et al.*, 2009; Halai, 2017) used a combination of heavy fluid and air pressure to simulate lateral pressures and surcharge the excavation formation level. These systems required a complicated arrangement of motors and reservoirs to drain the excavation. Mechanical failures were regularly encountered with this apparatus set up owing to the unreliability of complex equipment at high g levels. Spatial constraints on the centrifuge swing required careful planning and design of supporting equipment. Air pressurised latex bags were shown to be reliable and less prone to failure than the heavy fluid system. The air pressure provided consistent surcharge across the formation and, during the simulated excavation, the flexible bag deflated and allowed the formation level to heave. One disadvantage of using either air or heavy fluid is that K_0 , the coefficient of lateral pressure at rest equals one for both fluids. Therefore, during the excavation the applied passive pressure is not representative of pressure

experienced in the field, as K_0 approaches K_p . However, since the stress history of the soil used in the reported centrifuge tests resulted in a normally consolidated or a material with a lightly overconsolidated crust suggesting that $K_0 = 1$ is acceptable.

More recently Kimura *et al.* (1994) and Lam (2010) have made use of in-flight excavators, in which an actuator moves both horizontally and vertically. Layers of soil were scraped away from the retaining wall into a void in the strongbox giving a realistic simulated excavation. A prop was actuated once a predefined depth of soil had been removed. Although this modelled the excavation process with a faithful representation of the corresponding lateral stress profile, an additional variable, namely the prop force, had been introduced into the test. Prop installation needed to be well controlled to avoid the application of a large sudden force on the wall, as this may have influenced the stability of the excavation. Therefore, a time delay would have existed between excavating soil and installing the prop. Bearing in mind the scaling laws relating to time this has the potential to increase the magnitude of movements. Modern in-flight excavators (Lam, 2010; Ma & Xu, 2018) are very tall apparatus and owing to the size of the centrifuge platform at City, a similar piece of bespoke and highly complex equipment would require significant design input, development and testing. It would be likely to extend the duration of this three-year research project and such an approach is considered well beyond reach.

4.3 MODEL DESIGN REQUIREMENTS

Previous centrifuge research relating to deep excavations in soft clays has investigated a large number of variables within any one test. For instance, a range of wall flexibilities, prop system stiffness and installation methods have commonly been varied within a single test.

Numerous factors can affect the trend of movements arising from deep excavations. This project focussed on minimising the magnitude of basal heave attributed to deep excavations in soft clay. Particular efforts were made in controlling and significantly limiting movements attributed to wall bending in order to remove this variable from the problem. Owing to the considerably low undrained shear strength of the clay sample it was particularly important to refine an appropriate simple and repeatable model making technique. The apparatus developed and final model making process

will be explained in this section. The general arrangement for a typical centrifuge tests is presented in Figure 4.2.

4.3.1 Strongbox

All centrifuge tests were conducted in a rectangular aluminium alloy box, referred to as a strongbox, which comprises four walls and a base plate. Internally, the strongbox is 550mm wide, 375mm high and 200mm deep. If required, the walls can be unbolted however it is common practice to remove only the front plane strain face as this prevents misalignment of the box between tests. An aluminium front face was typically used for the consolidation process which was replaced with a transparent Perspex window to enable the model to be viewed in plane strain during the test.

Herringbone channels cut into the base of the strongbox provided a suitable drainage path for the pore fluid during $1g$ consolidation in a hydraulic press. The channels were connected to drainage taps which were fitted with 8mm pipes that directed pore fluid to a bucket. Care was taken to ensure that these pipes remained submerged at all times to prevent air entering the sample. A number of tapped holes in the back and side walls of the strongbox enabled the installation of instrumentation, such as pore pressure transducers and air pressure transducers.

Plane strain excavation problems can be modelled in their entirety, i.e. both walls of the excavation or as a half width excavation. Simulating both sides of an excavation permits the modeller to position the excavation at the centre of the strongbox and benefits from reduced boundary effects on recorded measurements. Arguably, a symmetrical excavation problem produced carefully should provide consistent and comparable measurements on both sides of the model. In addition, unless extremely accurate small-scale high g models are produced the modeller will obtain a limited data set and fewer far field measurements when both sides of an excavation are simulated.

On the other hand, half width excavations eliminate the risk of accidentally modelling asymmetric excavations and permit modelling at a reasonable scale. Significantly more far field observations can be made and this technique also reduces the amount of instrumentation used in each experiment. Owing to the low strength of the soil, it

was hypothesised that significant movements arising from the excavation would extend up to $2H$ beyond the excavation with additional movements occurring as far as $4H$. It was therefore decided that a half width excavation should be modelled.

4.3.2 Ground water supply

This research simulated an excavation in very soft soil with a high ground water table. To create such conditions, a standpipe base was bolted to a spacer that was seated on the centrifuge swing and used to centralise the strongbox on the platform. This system comprised a brass standpipe secured to the standpipe base and an overflow tube which prevented the intended water level from being exceeded. A pressure transducer was generally screwed into the standpipe base to monitor the water pressure whilst in-flight. This arrangement was common for all tests and the level in the standpipe was maintained in-flight by a direct water feed from the centrifuge slip ring. A pipe connected the standpipe to the model base drain to set the water table 5mm below ground surface. With the centrifuge spinning at high speed it was extremely important to prevent drying out of the sample whilst it was consolidated in-flight. This was achieved by applying PlastiDip, liberally sprayed across the model, which formed a flexible and impermeable, low stiffness synthetic rubber membrane and protected the sample and established water table. The use of PlastiDip was first established by Gorasia (2013) and this system of model sealing has proved superior to liquid paraffin, silicone oil and plastic wrap.

4.3.3 Positioning of LVDTs

Vertical surface settlements were recorded in two completely independent ways, by means of digital image analysis and through physical recordings obtained from LVDT data. An aluminium gantry was designed to bolt across the full width of the strongbox and comprised two box sections secured to a base plate at either end. These box sections were aligned parallel to each other and LVDT clamps screwed into the sections to secure the LVDTs in place.

A total of eleven LVDTs were located along the centreline of the strongbox at $H/2$ intervals from the retaining wall, where H = excavation depth, with one being

positioned directly behind the wall. This provided a surface settlement profile ranging from points at $0H$ (immediately behind the wall) to $5H$, as shown in Figure 4.2.

4.3.4 Location of PPTs

To provide a baseline for comparison between tests a minimum of three PPTs were used in each centrifuge test and were installed along the centreline of the model through ports in the back wall of the strongbox. Two of the PPTs were installed at the same elevation either side of the toe of the wall approximately $1.5H$ below ground level, whilst the third was installed at a distance $4H$ away from the wall to monitor far field pore pressure changes, illustrated in Figure 4.2.

An additional two PPTs were later used; however, owing to uncertainties about the reliability of these newer PPTs, it was decided that they would be located in other areas of interest; at a higher elevation behind the wall and the middle of the excavation in line with the toe of the retaining wall.

4.4 APPARATUS COMMON TO ALL TESTS; DESIGN AND DEVELOPMENT

4.4.1 Simulation of excavation

Pressurised rubber bags previously used by McNamara (2001) successfully surcharged the formation without the need for elaborate and complex mechanical parts prone to failure at high acceleration.

The simplest of excavations required one large latex airbag 200 x 150mm in plan to surcharge the formation where it was secured through the sidewall of the strongbox by means of a brass manifold. The brass manifold housed an air pressure transducer and provided a secure inlet for an airline pipe from the centrifuge slip ring. A remote data logger in the control room enabled the pressure to be monitored during reconsolidation and the simulated excavation. Care was taken to ensure that the union had been securely fastened to prevent leakages.

4.4.2 Retaining wall

Physical modelling research projects involving the use of embedded retaining walls are typically conducted by forming the excavation void, cutting a trench to cater for the embedded depth of the wall and carefully sliding the wall into place. However, owing to the nature of the soil used in this research project, emphasis was placed on establishing a suitable, accurate and time efficient model making process. Considerable problems were faced when attempts were made to cut clean perpendicular voids in the very soft clay. It was also unlikely that the soft clay could provide sufficient support to the wall during model making had the excavation void been formed prior to wall installation.

A new approach was developed to enable wall installation prior to the removal of any soil. In order to facilitate this a slender wall section was required. However, as this research focussed on reducing movements arising solely from heave, and not wall bending, it was essential that a very stiff but slender wall was fabricated. The final section was inspired by sheet piles and simplified such that the ribs were perpendicular to one another. The ribbed profile wall was machined from a 10mm thick stainless steel plate giving 1mm thick ribs at 10mm centres, as shown in Figure 4.3. Two walls were used in this series of tests, both of which were 190mm wide and were 130mm or 160mm in length. The toes of the walls were tapered to improve ease of installation and reduce wall installation effects. Details of the retaining walls are illustrated in Figure 4.4. Considering the thickness of each wall rib as 1mm and applying the grain size scaling law of 1/30th to clay, it was deemed that there were no grain size scaling effects for this model.

The total cross sectional area of the wall was 331.4mm² and taking the value of Young's Modulus of stainless steel (E_s) as 210kN/mm² the prototype stiffness was 9.6×10^4 kN/m², equivalent to a reinforced diaphragm wall approximately 1.4m thick. This was deemed to suitably represent a high stiffness retaining wall.

4.4.2.1 Retaining wall guide

Maintaining verticality during wall installation was of equal importance therefore a guide was fabricated. The guide comprised a 10mm thick Perspex sheet screwed into a 50mm thick ribbed Perspex block the profile of which matched that of the retaining

walls, see Figure 4.5. The tolerance of the wall plan positioning with the guide was $\pm 0.1\text{mm}$ and, owing to its length, an acceptable verticality of 0.2% was achieved. The exact location of this guide was consistent in each test owing to the careful alignment of the bolt holes in the strongbox and cutting shelf.

4.4.2.2 *Excavation template*

The top surface of the clay was sealed with PlastiDip, a fast curing aerosol applied synthetic rubber membrane, at the beginning of the model making stage before embedding the wall. During early tests it was found that although the rubber membrane was very flexible it was extremely robust and the membrane has a tendency to become dragged down into the soil as the wall was pressed into the soil. This disturbed the soil and voids tended to open behind the retaining wall (Figure 4.6). These were sealed with silicone grease prior to spin up however, the excavation area template was developed to prevent this from occurring in future tests.

A steel template was machined on a computer numerical control (CNC) machine. This prevented the rubber membrane from sealing the clay to the outer edge of the retaining wall, see Figure 4.7. It was not a concern that this area was not sealed as the soil was later removed to pre-form the excavation and any change in water content would not have influenced the performance of the excavation. An image of the clay surface is given in Figure 4.8.

4.4.3 **Silicone seals**

Waterproof seals along the sides of the wall were necessary to prevent water seeping into the excavation. However, owing to the difficulties in machining the wall from stainless steel it was necessary to establish another way of securing silicone seals to the edges of the wall.

4.4.3.1 *Side wall channels*

Side wall channels were fabricated from lightweight aluminium and screwed into the wall flanges. These were designed to sit flush with the wall and provide sufficient anchorage for the silicone seal. The M2 screws securing the channels to the wall also

served the purpose of adequately securing the silicone seal to the channel, see Figure 4.9.

The slot machined through the channel was offset 1mm from the centre to allow for the change in alignment once fixed to the retaining wall. Once fully attached, the slot was located centrally to the overall thickness of the wall and the silicone seal was subsequently centralised.

4.4.3.2 Seal design

The seal was not only required to prevent the ingress of water into the excavation but also to allow the modeller to track wall movements during the excavation process. The seal was therefore required to house imaging targets, in addition to reducing friction between the seal and the strongbox interfaces.

The adopted approach replicated the seal designed by McNamara (2001), which was based on a design by Powrie (1986) where the seal extended 6mm beyond the edge of the wall with a 5.6mm radius. The seal accommodated 3mm diameter targets spaced at 20mm centres, see Figure 4.10. The total width of the wall with seals was 202mm, which ensured that the flexible seals were compressed against the strongbox interfaces to create a watertight seal. The radius ensured minimal friction between the target and the Perspex window and the interface was greased to further minimise friction.

4.4.3.3 Seal mould design

A mould was fabricated in which the seals were formed, as illustrated in Figure 4.11. It was necessary to cast silicone around the M2 screws connecting the aluminium channels to the retaining wall to ensure a secure fixing between the silicone seals. The mould was therefore designed to clamp the entire wall whilst the silicone rubber cured. In order to facilitate this the mould comprised two aluminium plates that secured the full length of the wall and two aluminium blocks located at either end of the wall that bolted to the two plates.

Bullet shaped aluminium targets were fixed at 20mm centres to a half inch diameter aluminium rod. The rod formed the desired radius and the bullet inserts ensured accurate positioning of the targets post curing.

4.4.3.4 Forming the silicone seals

Two-part Addition Cure Silicone Rubber, supplied by Alchemie Limited, Warwick, was used to produce the seals. A room temperature vulcanising silicone rubber (RTV240) was mixed with C250 catalyst to a 10:1 ratio by weight. This particular specification was chosen owing to its low Shore hardness rating of 40A, ensuring both flexibility and durability. Up to 2% white dye was also added which provided sufficient contrast between the seal and the black targets.

With a viscosity ranging between 30-70Pa.s and a pot life of 80 – 140 minutes, the silicone, dye and catalyst mixture was placed in a vacuum chamber and de-aired to remove the majority of air bubbles that had formed during mixing.

The mould was cleaned with acetone, assembled and clamped around the retaining wall and all surfaces sprayed with a thin layer of silicone oil to act as a demoulding agent. Care was taken to ensure that the mould was horizontal to prevent gaps forming from an unlevelled mould. The liquid silicone rubber was slowly poured into the channel to the top of the mould and a thin wire was used to agitate the mixture to encourage any remaining air bubbles to rise to the surface. The aluminium spiked rod was bolted to the mould and the sample left for a minimum of 24 hours before trimming excess silicone and demoulding the wall.

4.4.3.5 Wall targets for image analysis

The targets inserted into the wall were similar to those previously used for tracking soil movements. These were machined from black acetal rod, were 3mm in diameter, had a 4mm long parallel shaft and a cone length of 3mm. Once embedded in the silicone seal and compressed against the Perspex window there was no risk of the targets becoming loose.

4.4.4 Aluminium excavation support system

The main aim of this research investigation was to ascertain the effects of various construction methods on basal heave. It was therefore crucial that the excavation and retaining wall were appropriately supported to limit wall movements.

An aluminium support system, previously designed by McNamara *et al.* (2009) laterally restrained the upper $\frac{2}{3}$ of the wall as shown in Figure 4.12. The void that remained beneath this was used to provide sufficient space for the pressurised latex airbag. In this project, the aluminium support system will be referred to as a stiffener. It comprised two 10mm thick horizontal plates, two vertical plates and a shear block. The bottom base plate effectively propped the wall 25mm above formation level under plane strain conditions. The two vertical plates offered additional support to the wall, however these were at two discrete locations 50mm either side of the model centreline, as illustrated in Figure 4.13.

The stiffener was designed to bolt directly onto the strongbox sidewall; the horizontal base plate was 150 x 200mm in plan, as per the design by McNamara *et al.* (2009). In order to accommodate a bag spacer, details of which will be presented in the next section, a 3mm deep recess was machined from the bottom portion of the spacer. The stiffener reacted against the top 50mm length of wall and acted in compression as a prop. During the simulated excavation, removal of the overburden pressure typically resulted in passive failure and the toe of the wall rotated into the excavation about the lowest prop level. Owing to the high stiffness retaining wall, there were no concerns of the wall failing in bending below the lowest prop level.

4.4.5 Capping beam

Passive failure of the excavation could have been prevented for the two modelled depths had the support acted in tension as a tie. A capping beam that was designed to sit on top of the wall was used in the later series of tests.

The capping beam was L-shaped in cross section and fabricated from a solid bar of aluminium; details of which are illustrated in Figure 4.14. The initial design required that the capping beam be screwed directly into the stiffener apparatus. However, as the model settled by approximately 5mm during in-flight reconsolidation the contact between the beam and wall became significantly reduced. As the excavation progressed and additional movements developed the capping beam served no purpose and the wall failed in a similar passive manner.

It was evident that a sliding mechanism was required to provide support in tension. Development of the capping beam comprised two L-shaped brackets to secure the stiffener to the capping beam. A vertical slot machined along each bracket allowed the capping beam to fall under its own self-weight and remain in contact with the wall whilst also ensuring that the beam remained horizontal.

It was necessary to continue to accommodate the LVDT located immediately behind the retaining wall. A 60mm long slot was cut along the centre of the capping beam to permit positioning of this LVDT footing, as shown in Figure 4.15.

4.4.6 Spacer between the retaining wall and airbag

In these centrifuge tests the airbag reacted against the stiffener, formation level, the strongbox sidewall and the retaining wall. Owing to the profile of the retaining wall, the pressurised airbag would have protruded between the wall ribs and there would be a risk that the sharp edges would consequently burst the airbag.

A profiled spacer was designed to eliminate the risk of an airbag failure. It consisted of 8mm square aluminium sections screwed at 22mm centres to a 1mm thick steel plate as illustrated in Figure 4.16. A silicone layer 1mm thick was cast between the spacer and the retaining wall to prevent water seeping into the excavation during reconsolidation.

A preliminary test using a 25mm high spacer plate resulted in the airbag bursting. As the sample settled during reconsolidation, the spacer was displaced downwards with the wall and the airbag was punctured against the exposed edges of the wall. Consequently, the solid blocks were remounted to a 50mm high plate to prevent a similar recurrence. Images of the spacers are presented in Figure 4.17 and Figure 4.18.

4.4.7 Bespoke LVDT footings

A preliminary test had revealed that the low undrained shear strength soil was incapable of supporting the 10mm diameter LVDT footings typically used by the researchers at City. These footings punched through the layer of PlastiDip and became embedded at a depth of approximately 5mm into the surface of the clay and

consequently no useable LVDT data was recovered. Hence, wider lightweight footings were required to provide vertical movements over a width as narrow as 10mm.

This was achieved by 3D printing numerous rectangular footings, 10 x 50mm in plan tapering from 2mm at the middle to 0.5mm thick at the extreme ends; details of which are given in Figure 4.19. The LVDT footings were orientated such that the longest dimension was aligned perpendicular to the window (see Figure 4.15). However, having implemented these precautions there was still evidence that the footings settled into the soil to some degree, as visible in Figure 4.20 owing to the low strength of the soil.

4.5 TEST SPECIFIC APPARATUS

A range of excavation sequences were investigated in this research project which lead to the development of additional equipment and modifications to the generic apparatus set up. Details of all such developments will be described in this section.

4.5.1 Underwater excavations

4.5.1.1 Water feed

The underwater excavation was accomplished by means of a direct water feed into the excavation area. This comprised a water pipe connected to the centrifuge slip ring directed from the top of the strongbox into the excavation void.

An appropriate flow rate from the pipe was required such that at prototype scale every metre of soil removed would be replaced by 1m of water. In summary, the decrease in pressure per metre of excavation was 16kN/m² and water inflow of 9.81kN/m² was required to partially counter it. The excavation was conducted at a rate of approximately 1kN/m²/sec and a supply from the direct water feed was set to approximately 11.25ml/sec.

4.5.1.2 Supply of water below formation level

This construction technique aimed to model both the benefits from the vertical and lateral support offered by the water as well the soil softening effects of performing an underwater excavation. The excavation was simulated by reducing the pressure in the latex airbag, however concerns were raised over whether water would flow below the bag to the formation level owing to latex being waterproof and creating a barrier. This dictated the provision for a direct water feed below the excavation. Owing to the experiment set up and the limited number of water feeds from the hydraulic slip stack, an alternative approach using valves was adopted, schematically described in Figure 4.21.

One water feed supplied the standpipe (S'Pipe1) to establish the water table 5mm below ground level. The other feed was placed directly in the excavation and was activated when the excavation commenced. To model the effects of soil softening, a second standpipe (S'Pipe2) supplied water below the excavation dredge level. The overflow was set as high as the standpipe tube and an 8mmOD flexible pipe supplied it with water from the overflow of S'Pipe1. The outlet from S'Pipe2 comprised a 4mmOD pipe which was connected to a 6.25mm diameter ball valve. The outlet from the valve was a 4mmOD pipe which was directed to the side of the box and through a port in the sidewall of the strongbox at an elevation consistent with the lowest prop.

The ball valve was controlled by a single acting pneumatic cylinder, model number ORD-86167, supplied by RS Components Ltd. A bespoke connector had been fabricated to secure the actuator stroke to the ball valve handle. The valve and actuator were bolted to the standpipe spacer in the appropriate arrangement to permit opening of the valve once the piston was activated. The piston was secured to the standpipe spacer using a single M8 bolt around which it pivoted. A solid aluminium block supported the actuator to prevent it from bending under elevated **g**-forces.

Water was supplied to the formation through the wall spacer. The central solid aluminium block was replaced with a block that had been drilled for this purpose. A round body stud push fitting was screwed into this block into which the 4mmOD pipe was fed. This particular fitting was chosen owing to its small diameter as it was possible to accommodate this between the ribs of the wall.

4.5.2 Deep soil mixing ground improvement

It was envisaged that the deep soil mixing test series would result in a considerably slower model making time than those involving underwater excavations owing to the additional volume of excavated soil. Significant efforts were made to increase modelling efficiency by designing a consolidation chamber that produced a sample of the correct dimensions to minimise the time needed to trim the sample.

4.5.2.1 Consolidation of lime stabilised clay

The consolidation chamber comprised five 10mm thick aluminium plates assembled as a bottomless box with a lid. The plates slot together to facilitate quick removal of the sample with minimal disturbance to the sample as shown in Figure 4.22. Oversized slots machined along the edges of the two side plates housed the front and back plates. A number of M5 threaded rods and nuts tied the box together and ensured it remained square during consolidation.

Holes drilled along the bottom edge of the box permitted water to drain from the sample and accelerated the consolidation time. The lid distributed the load from the 150mm diameter platen evenly across the full sample area. A photograph of the disassembly of the consolidation chamber is presented in Figure 4.23.

4.5.3 Double wall excavation

This construction technique required the installation of a lower stiffness intrusion in front of the retaining wall to model a slurry cut off wall. Numerous possibilities were explored which included 5mmOD thin walled steel tubes pushed in at 10mm centres to represent a contiguous pile wall. This would require a special jig to maintain verticality, delay model making and increase plugging and installation effects at the base of each tube. Another ribbed profile wall was consequently machined from aluminium, details of which are given in Figure 4.24.

4.5.3.1 Slurry wall

Seals were not required along this wall as the permanent retaining wall mitigated seepage into the excavation. This wall did however have sheets of Teflon adhered to

its sides to reduce the effects of friction against the strongbox boundaries. Taking Young's Modulus of aluminium and concrete as 69kN/mm^2 and 20kN/mm^2 respectively, at prototype scale its stiffness was comparable with a 1m thick slurry wall.

4.5.3.2 Slurry wall guide

To position the wall and install it vertically another Perspex guide was fabricated, as shown in Figure 4.25. This simple guide was clamped to the model making cutting shelf and the back of the strongbox. It rested against the retaining wall and hung inside the box to establish the exact location of the wall. The brackets were close enough to hold the wall in place whilst an aluminium push stick was used to transfer load by hand and embed the wall in the clay. An image of the embedded slurry wall is shown in Figure 4.26.

4.5.4 Berm supported excavation

Bermed excavations are defined as a mass of unexcavated soil at the site perimeter. This soil provides both lateral support to the wall and surcharges the area directly in front of the wall. As the experiments used air pressure to simulate the excavation modifications were made to the common apparatus to segregate the varying surcharges across the formation level.

This construction method was idealised by dividing the preformed excavation into two areas; the berm and the main excavation. Two airbags were required to initially supply the same pressure to the formation during in-flight reconsolidation, however during the excavation they were required to supply different pressures. This was achieved by manufacturing two bag sizes, 50 x 200mm and 100 x 200mm in plan and 1mm thick in parallel and enabled observation of the influence of berms on ground movements. The locations of the latex airbags are shown in Figure 4.27.

An additional port in the back wall of the strongbox was drilled to accommodate an air pressure union to secure the second airbag to the strongbox. With the original air pressure port being in the sidewall of the strongbox the second port was located in the back of the strongbox reasonably close to the retaining wall. This allowed the port to be used for both the 50mm and 100mm wide bags.

4.5.4.1 Support between airbags

The excavation involved decreasing the pressure in both bags until the berm pressure of 100kPa was reached. The berm bag remained at this pressure whilst the excavation bag pressure continued to decrease. It was imperative that a vertical boundary existed between the two bags to prevent the berm bag from expanding into the adjacent void where it would burst.

Owing to the range of tests conducted during this research, the fabrication of new elements was minimised and only minor interchangeable modifications were made to simplify the model making stages. A sufficiently rigid barrier was required between the two bags but it was also necessary to reduce this width to allow adequate observation of basal heave. Aluminium plates 6mm thick, 200mm long and 25mm deep were screwed to the stiffener at 50mm or 100mm intervals depending on the geometry of the test, also visible in Figure 4.27.

4.6 SUMMARY

A brief introduction to the methods of simulating excavations was made and the methods adopted in this series of experiments. Bespoke scrapers were developed to aid in the modelling of excavations in very soft clay to guarantee repeatability, accuracy and consistency between tests. Details of the design and development of general apparatus were outlined in this chapter. More specific requirements for each of the centrifuge tests have been detailed as required. The arrangement of testing elements for each excavation method were also explained.

CHAPTER 5 EXPERIMENTAL TEST SERIES

5.1 INTRODUCTION

This project relied on accurately modelling deep excavations in extremely soft soil. Significant difficulties were faced in preparing the model and numerous stages were undertaken before the sample could be tested. The techniques adopted to achieve a reliable, robust and repeatable model making scheme will be described in this chapter.

5.2 STRESS HISTORY OF SOIL SAMPLE

Previous centrifuge tests conducted on soft soils by Lam *et al.* (2014) used a soil sample consolidated to a stress of 160kN/m² which resulted an undrained shear strength of 25kPa at 60g. This project also required a low strength, normally consolidated, soil sample and consequently a bespoke sample preparation method was developed. The clay slurry in all test cases was first subjected to a pre-consolidation pressure of 100kPa at 1g for about 10 days. The sample was then trimmed to a height of 290mm before being further consolidated in-flight on the centrifuge at 160g overnight before being trimmed again, to give a final depth of 255mm. The stress history of the sample having undergone these stages is illustrated in Figure 5.1. The empirical formula defined in Equations (5.1) and (5.2) by Springman (1989) and Garnier (2002) respectively can be used to predict the upper limit of undrained shear strength of the soil.

$$S_u = 0.19 \sigma'_v OCR^{0.59} \quad (5.1)$$

$$S_u = 0.22 \sigma'_v OCR^{0.706} \quad (5.2)$$

Owing to the thin over-consolidated layer above the formation level the empirical formulae suggest that the soil strength at ground level ranges between 5-8kN/m², increasing to approximately 30kN/m² at depth, see Figure 5.2. By British Standards (BS 5930:2015) this constitutes very soft soil at ground surface and soft soil at depth which fulfilled the requirements for this particular research project.

Accurately producing a model in considerably soft clay whilst maintaining the geometry during reconsolidation proved extremely challenging. However, the preparation method developed and described in detail proved successful in modelling the excavation; applying the correct stress history to the sample and producing a normally consolidated soil sample overlain by a very thin lightly over-consolidated layer above formation level, typical of many ground conditions found in east Asia.

5.3 SAMPLE PREPARATION

The soil sample was prepared from a Speswhite kaolin clay slurry mixed to a water content of approximately 120%. This water content produced a workable slurry as it is twice the liquid limit of the material and could be easily agitated to remove entrapped air bubbles. The slurry was produced in a large industrial ribbon blade mixer from distilled water and kaolin powder or kaolin recycled from previous tests. Where kaolin had been recycled it was left to soak for a period of time and agglomerations of consolidated clay in the mixture were squeezed out by hand. The clay was mixed until a uniform slurry was achieved.

The model depth required in these tests was 255mm however owing to the initial in-flight consolidation stage it was necessary to produce a 290mm deep sample to account for the settlement as the sample consolidated. In order to facilitate this a slurry sample about 515mm deep was consolidated to 100kPa at 1g. This was approximately equal to 60% of the volume of the ribbon blade mixer. The internal depth of a strongbox is only 375mm and therefore a 300mm deep extension was bolted to the top of the strongbox to accommodate the depth of slurry needed. It was sealed with an O-ring and silicone grease to prevent slurry from seeping out under pressure as it was evident that the O-ring alone was not sufficient to contain the slurry. Particular care was essential when bolting the front aluminium face to the strongbox to ensure that the top edge was sufficiently aligned with the sidewalls of the strongbox.

Waterpump grease was liberally and evenly applied to the walls of the strongbox and extension to reduce friction at the interfaces (McNamara, 2001). Sheets of 3mm thick porous plastic and filter paper were placed above the strongbox base in which herringbone drainage channels had been cut. Although the slurry had been mixed to a high water content care was taken when placing the slurry into the strongbox. A

palette knife was used to gently agitate the slurry and encourage air bubbles to rise to the surface between pours. Another layer of filter paper and porous plastic were placed on top of the sample to sandwich the slurry and permit drainage of water from the top as well as the bottom to halve the drainage path length and accelerate the consolidation process.

The initial preconsolidation stage was carried out at $1g$ in a hydraulic press where a tightly fitting platen attached to a ram was lowered onto the sample using the control dial. The pressure on the sample was gradually increased to 100kPa over a period of 24 hours. The movement of the platen was monitored using a potentiometer and after a week these movements were reviewed and judged to be negligible. Drainage was permitted from the top of the model through three holes in the platen and also from the base of the model via the herringbone drainage channels connected to drainage taps at either end of the strongbox. Pipes attached to the drainage taps diverted water into a bucket and care was taken to ensure that the pipes remained submerged to prevent air becoming entrapped in the sample.

It was originally proposed that the model would be prepared by first removing the front and back faces of the strongbox, securing a jig and then using a wire cutter to trim the excavation profile. However, this operation would have required the use of extensive jigs and would consequently delay the model preparation time owing to the sheer number of bolts to be tightened. In addition, the sample was expected to settle by up to 20mm in-flight during reconsolidation at $160g$, which would displace, distort and potentially damage PPT instrumentation in the model. Furthermore, any LVDTs would also be taken beyond their range and the acquisition of useful data during the test would not be possible.

The solution adopted involved consolidating the sample on the swing at $160g$ following $1g$ consolidation. This was the most effective means of producing a dimensionally accurate model within a convenient time frame. This also ensured that the instrumentation was protected from damage and prevented LVDTs from becoming out of range owing to excessive settlements resulting from consolidation.

During the day prior to model making and testing the standing water on top of the platen in the hydraulic press was removed, the drainage taps were closed and the

sample removed from the press. During the first centrifuge test, the extension was unbolted and the front face of the strongbox was removed with extreme difficulty. It was ascertained that consolidating the clay to such a low pressure resulted in large suction forces forming between the front face of the strongbox and the soil model. The need for additional waterproof grease was addressed in the preparation for subsequent tests whilst the suction forces were overcome by sliding the front face along the sample.

At City, clay samples are typically trimmed by clamping a 150mm wide aluminium angle across the front of the model and using a 75mm x 75mm x 3mm thick aluminium box section with tapered edges to remove sections of soil. This approach was initially attempted, however the low strength of clay made it impossible to achieve clean cuts. The adhesion between the box cutter and the clay disturbed the sample as it was pulled away from the back wall of the strongbox irrespective of the amount of silicone oil sprayed onto the surfaces of the box cutters. An improvised trimming process was adapted by scraping soil away using a stiff steel plate. This proved to be more suitable for this soil, however the accuracy of the sample height that could be achieved was unacceptable.

A steel lid which incorporated an LVDT was bolted to the top of the box before the sample was weighed and transferred to the centrifuge swing. A standpipe was connected to the base of the model and provided a water table 10mm above the initial sample height, see Figure 5.3. The LVDT measured the rate of soil settlement as it consolidated and confirmed when the sample could be removed from the centrifuge and model making could commence. The steel lid prevented standing water from drying out in-flight and ensured that the sample remained fully saturated. A typical settlement profile curve during in-flight consolidation is shown in Figure 5.4.

Development of the sample trimming procedure involved fabricating a scraper which could be dragged across the top edges of the strongbox walls before disassembling the box. The scraper constituted a 1mm thick steel plate tapered at the cutting end and mounted between two 50mm aluminium angles. Details of this apparatus are illustrated in Figure 5.5. The angles overhung the strongbox to guide trimming whilst the plate width of 199.5mm accounted for slight horizontal misalignments of the scraper. The plate was secured between the angles with two M5 bolts which ensured

the tip of the plate trimmed the sample to a consistent height of 290mm. Additional holes were drilled into the plate to allow adjustment such that it was possible to produce the final sample height of 255mm thereby reducing the number of modelling tools needed. A photograph of the scraper in the clay sample is shown in Figure 5.6. A sample of clay was routinely recovered from the top of the sample in order to check consistency of water content between tests prior to in-flight consolidation.

5.3.1 Sample preparation of lime-stabilised soil

Preparation of the lime-stabilised kaolin clay was key in this series of tests. Kaolin and distilled water were combined to form a uniform slurry in a small Hobart mixer to a water content of 140%. Hydrated powdered lime was added and this formed a thicker slurry as the lime rehydrated so it was necessary to mix the slurry to a higher water content to improve its workability.

The consolidation box fabricated for consolidating the lime-stabilised clay was lubricated with waterpump grease and assembled, whilst care was taken to ensure that the walls remained perpendicular. The un-anodised aluminium plates had corroded between the preparation of each sample and it was necessary to abrade the surfaces before each sample was prepared to aid the removal of the sample post consolidation. The consolidation box was placed in a tray and a porous plastic sheet and filter paper were positioned at the base. The slurry was carefully placed in the box with a scoop and particular attention was paid to agitating the slurry between each slurry placement to remove air bubbles. A further sheet of filter paper and porous plastic sheet were placed above the sample before sealing the slurry with a lid.

Owing to the various depths of deep soil mixing tested in this series of experiments, and the requirement for consistency between tests, it was decided that the pressure on the sample should equal the vertical in-situ stress at the formation level of the model prior excavation. The samples were consequently normally consolidated to an effective stress of 150kPa at $1g$ for a period of up to 36 hours.

On the morning of model making the lime-stabilised clay consolidation chamber was removed from the press and wrapped in polythene film to prevent it from drying out excessively. The geometry of soil that was required for the test was cut from the main

block and placed in the model. The remaining lime-stabilised clay was resealed and put to one side until the centrifuge model was reconsolidating in-flight.

Investigation into the strength of DSM material was necessary to understand its potential influence on stabilising the formation level and consequently its ability to reduce ground movements. This was achieved through a series of unconfined compression tests carried out on a portion of the soil sample that was not used in the centrifuge model. The test set up is shown in Figure 5.7 and soil samples that were 38mm in diameter and a minimum length of 76mm were taken. Each sample was compressed at a rate of 6mm per minute whilst the applied load and vertical displacements were recorded. Examples of the sample, prior to and post testing are depicted in Figure 5.8. The results from two DSM test samples are compared against the compressive strength of virgin soil in Figure 5.9. There is generally good agreement between the strength of the lime stabilised clay samples in tests JP14 and JP15 giving a UCS of 70-80kPa. Test JPP15a displayed a marginally lower UCS compared with those determined from two separate cores taken from the same sample. It is possible that this was owing to localised shearing within that particular core or the sample being disturbed; which reduced its capacity in the test. The increase in strength is about 35% compared with the 45kPa offered by the kaolin clay. This confirmed that the improved soil samples used in the centrifuge models were of a significantly higher strength than the surrounding soil.

Further tests were conducted to establish the change in strength with time. Cores were tested at the following time periods; 1 day, 7 days, 14 days, 21 days and 28 days. The results were also plotted against a baseline test specimen without any lime to provide a point of reference. The results plotted in Figure 5.10 demonstrate that the longer the duration between consolidating and shearing, the higher the unconfined compressive strength. This is unsurprising owing to the increased pozzolanic activity occurring with the moisture in the sample (Locat *et al.*, 1990), which was demonstrated by the change in measured water contents, see Figure 5.11. Noticeable behaviour included larger peak strengths being recorded with an increased period of time. This supports the theory of stiffer soils being more brittle and developing a higher compressive strengths (Kitazume & Takeyama, 2014), as illustrated in Figure 5.12. By and large, with increasing time there is an increase in strength (Figure 5.13).

Unconfined compressive strength tests are favoured in industry owing to the very simple equipment required and the ability to provide rapid results that are easy to interpret, as presented by Lui *et al.* (2017). These tests can however only be performed on 100% saturated samples that are not fissured or have other significant defects, as this will contribute to early failure of the sample. Whilst the results give a reasonable indication of the strength of the sample, they cannot be used in design as they are unrepresentative of samples in the ground that are confined by lateral earth pressures.

5.4 MODEL MAKING

This section describes the general model making stages employed in the preparation of the centrifuge model. Supplementary details will be given in the following subsections for the additional stages undertaken to manage the range of excavation methods.

5.4.1 General model making method

- i. Following in-flight consolidation the sample was decelerated and base drain closed. The lid was removed from the strongbox and all water on the clay surface mopped using paper towel. The sample was trimmed to a height of 255mm. Clay samples were taken at the surface and just above 255mm to measure the water contents and confirm consistency between tests.
- ii. Silicone oil was sprayed onto the base of the steel template before placing it against the internal edge of the strongbox to mark out the extent of the excavation and retaining wall. A thin layer of PlastiDip, a flexible but durable synthetic rubber membrane, was evenly sprayed across the top of the model. Gorasia (2013) had concluded that PlastiDip was capable of sealing the top surface of the clay more effectively than silicone oil to prevent surface drying. The use of PlastiDip provided good correlation with empirical undrained shear strength solutions for clay and clearly showed an increase in undrained shear strength with depth.
- iii. A scalpel blade was used between the top of the soil model and strongbox front face to prevent the rubber membrane forming continuously against the soil and strongbox front face. The front face of the strongbox was unbolted and slid

across the front face of the model to overcome the high suction forces that had developed between the clay and strongbox. A scraper was used to carefully remove excess waterpump grease from the front face of the soil model to ensure good contrast between the targets and soil for image analysis. A thin layer of low viscosity silicone oil was then applied to the sample to prevent the model from drying out excessively.

- iv. The bespoke cutting shelf was bolted to the front of the strongbox before securing the Perspex guide to the cutting shelf and strongbox back wall, as shown in Figure 5.14. The side channels on the retaining wall prevented it from being pushed directly into the soil. A series of square and circular thin walled brass tubes, 10mm in width and diameter respectively, were used to create voids to the correct depth at the locations of the seals, see Figure 5.15. Silicone grease was smeared along the silicone rubber seals before the retaining wall was embedded into the clay by hand using a solid rectangular plunger, as shown in Figure 5.16. Another layer of PlastiDip was applied directly behind the wall to create a seal at this boundary.
- v. The 10mm thick Perspex sheet of the guide was removed whilst the thicker ribbed Perspex plate was left in place to provide sufficient support to the model cutting shelf. Steel plates were used to systematically cut and scrape layers of soil from the excavation area to produce a clean excavation void (Figure 5.17). Clay samples were taken from the top of the excavation and the layer immediately above the excavation formation in order to determine the water content and subsequently the undrained shear strength profile with depth.
- vi. On account of the spacer required between the wall and the bag, removal of the clay between the ribs in the excavation was particularly important, as shown in Figure 5.18. The spacer, with the silicone layer attached, was aligned with the indentations of the wall and was carefully pushed in place at the base of the excavation.
- vii. The air supply fitting was attached to the latex bag and fastened through the port in the sidewall of the strongbox after which the cutting shelf was removed and the aluminium stiffener bolted in place. It was necessary to place a 3mm thick sheet of porous plastic between the latex bag and the stiffener owing to a number of holes that had been drilled through the base plate for a previous study, shown in Figure 5.19.

- viii. At this point the model was tilted back to enable the application of targets for image analysis. The initial test (JP1) made use of 3mm diameter black acetal bullet shaped targets, as illustrated in Figure 5.20. These targets were arranged in a square grid pattern arranged at 10mm centres. A Perspex template was employed to ensure precise spacing between the targets whilst a brass rod (McNamara, 2001) embedded the targets. This was a time consuming process and typically required in excess of an hour to complete.
- Subsequent tests used GeoPIV-RG, which enabled the modeller to scatter 1mm diameter black glass ballotini across the front face of the model. Care was taken to ensure that the ballotini did not enter into the excavation, as there was a risk that the beads could puncture the latex bag. Once a suitable texture had been achieved in the area of interest the ballotini were gently embedded into the clay surface using a plastic roller, see Figure 5.21.
- ix. The strongbox was then positioned upright in preparation for fixing the instrumentation. This comprised three key elements; the LVDTs on top of the model; the PPTs through the ports in the back of the strongbox and the air pressure transducer housed within the air supply union on the sidewall.
- x. A total of eleven LVDTs were used in this series of experiments which were supported by an LVDT gantry spanning between the walls of the strongbox. In an effort to increase model making efficiency, the LVDTs were already pre-clamped to the gantry prior to model making. Their position had been predetermined during the calibration stage to ensure that they were within range for the height at which they were set above the model.
- xi. Previous researchers at City (McNamara, 2001; Begaj, 2009; Gorasia, 2013; Divall, 2013; Le, 2017; Halai, 2017) typically installed PPTs a day before testing. This saved time during model making. However, owing to the consolidation method adopted in these experiments it was not possible to do this and for this reason the PPTs were necessarily installed during the model making process. This was achieved by de-airing kaolin slurry, mixed to a water content of 120%, for a minimum period of one hour. The plugs from the back wall of the strongbox were removed to provide access to the sample in the chosen areas of interest. An aluminium guide was screwed into the back wall, which had been designed to maintain horizontal installation in the model (McNamara, 2001). A thin walled 7mmOD diameter cutting tube bored out 100mm lengths

- of clay to create a suitable void for the PPTs. Owing to the low strength of clay, it was not possible to achieve a clean bore in one pass. The final bore was achieved in three passes and the cores were recovered to determine the water contents.
- xii. The PPTs, having been calibrated in a pressurised chamber of de-aired water, were ready for installation. PPTs were removed from the chamber one at a time and immediately submerged in de-aired slurry. This was to ensure that the porous stone remained saturated and minimised the entrapment of air. A tool was used to guide the PPT 100mm into the sample, such that the instrument was aligned with the centreline of the strongbox. Each PPT was installed in this manner before all the PPTs were backfilled with the remaining de-aired slurry. Following this the PPT fastenings were screwed into the back wall and tightened.
- xiii. It was crucial that the LVDT gantry was level to ensure that the recorded measurements were vertical displacements. The gantry took support from the topmost part of the stiffener whilst a spacer was fabricated to bolt onto the opposite side of the strongbox. In addition, owing to the sharp corners of the LVDT footings, it became apparent that care was required to avoid the footings cutting holes through the PlastiDip membrane. This was achieved by placing a large sheet of paper across the PlastiDip surface before lowering the gantry onto the model. The LVDTs were aligned perpendicularly to the retaining wall before carefully extracting the sheet of paper; minor adjustments were then made as required.
- xiv. The air pressure transducer was housed within a brass union which also carried an air supply from the centrifuge slip stack and the fitting to supply air to the latex bag. PTFE tape was used to effect a seal between the union and the M8 thread air supply fitting whilst caution was exercised to avoid damaging the transducer cable.
- xv. Following this the model was complete and the final preparation stages followed. High viscosity silicone oil (12,500cs) was applied to the Perspex window to reduce friction at the soil and window interface and all bolts were tightened. A bead of silicone grease was applied along the top of the model that was in contact with the window. This was necessary as the sample tended to shrink slightly during model making and the grease prevented the clay from

drying out further until it had reconsolidated in-flight and had re-established full contact with the Perspex window.

The general model arrangement, representative of a dry excavation, is given in Figure 5.22 and shows the general model dimensions and common apparatus used in all tests.

5.4.2 Model making specific to underwater excavations

The underwater excavation models were produced following an identical process as outlined in the general model making method, however modifications were made to specific pieces of apparatus for these tests.

The spacer separating the latex bag from the retaining wall was adapted to allow water to flow beneath the latex bag. A push fitting was attached to the central solid channel and a 4mmOD pipe secured to it. This pipe was fed through a port in the side channel of the strongbox after the stiffener had been bolted to the model. A sheet of filter paper was also placed on the formation level with a 0.75mm thick sheet of porous plastic to ensure that water could flow across the full formation beneath the latex bag. The general arrangement for underwater excavations is illustrated in Figure 5.23 and a photograph of the model post-test is given in Figure 5.24.

The air actuator linked the standpipe and the 4mmOD pipe and the second standpipe, which allowed the control of water flow to the base of the excavation at the appropriate time in the test.

5.4.3 Deep soil mixing modelling technique

Before the model was removed from the centrifuge swing following in-flight consolidation, the standing water above the lime-stabilised clay sample and the tray was wiped away and the sample extracted from the press. The nuts were loosened to aid in disassembling the small consolidation box and one side panel was slid out of the box. This allowed the lime-stabilised clay block to be extruded without disturbing the sample, as shown in Figure 5.25(a). The sheets of filter paper and porous plastic

were peeled off the sample before sealing the block in plastic wrap to prevent it from drying out.

The excavation model was produced following a similar sequence to the general procedure. After the main 75mm deep excavation had been formed the model cutting shelf was unbolted from the strongbox and a large aluminium angle was clamped across the front of the model to indicate the final depth of the deep soil mixed zone, as shown in Figure 5.25(b).

In the scenario where the full width of the excavation was treated (JP10), a single steel plate was used to scrape away all of the soil below the formation level. However, where a narrow width of deep soil mixing was investigated a small angle was clamped to the large angled shelf to establish the extent of the ground improvement zone. A plate was driven vertically into the soil against the upright angle to cut the interface between the virgin soil and lime-stabilised clay as illustrated in Figure 5.25(b). This prevented excess soil from being removed. Plates were used to remove layers of soil and care was taken to ensure clean perpendicular edges were achieved, shown in Figure 5.25(c) .

Having formed the void for the ground treatment zone, the lime-stabilised clay sample was retrieved and trimmed to the correct width and carefully placed in the model. The block of lime-clay soil was gently pushed into place to ensure that it was in full contact with the rest of the clay sample (Figure 5.25(d)). The angles were removed from the strongbox and replaced with the front face cutting shelf to allow the excavation depth to be accurately cut.

The stages outlined above were undertaken after the standard excavation void had been formed and were in addition to the model making process. Steps following these measures were common with those detailed in the previous subsection and the general schematic DSM geometries of this series of tests is given in Figure 5.26.

5.4.4 Double wall model making procedure

Following installation of the permanent retaining wall and formation of the excavation void, the second Perspex guide was clamped to the back wall of the strongbox and the

front cutting shelf. The outer edge of the guide was in contact with the retaining wall to establish the correct location and this also allowed test repeatability.

The model slurry wall was carefully positioned in the guide and pushed vertically into the soil. The guide was 75mm deep and comprised two blocks spaced 9mm apart, as shown in Figure 5.27. The wall was slowly pushed into the soil until it was flush with the formation level. The cutting shelf and guide were removed and a sheet of 0.75mm thick porous plastic was placed across the base of the excavation. This prevented the latex bag from bursting when it reacted against the top of the wall, as illustrated in the general arrangement scheme (Figure 5.28).

The standard model making procedure was adopted to conclude the model making process and conduct the experiment.

5.4.5 Modelling a bermed excavation

Replicating a bermed excavation was perhaps the most complex and challenging model in the entire test series. This was owing to the use of two latex airbags and the requirement to ensure that there was a rigid containment barrier between the two to accommodate the differential pressures.

Prior to testing a 25mm deep aluminium plate was screwed onto the stiffener that laterally supported the wall. This was to sufficiently restrain the berm bag once the pressure in the excavation bag continued to decrease. Flexible plastic V-seals were adhered to both sides of the bottom edge of the plate as there were concerns that any settlement of the model would result in the bag bulging beneath the plate and potentially fail, as shown in Figure 5.29.

The model was made following the general modelling method but once the excavation had been formed and the spacer pushed into the wall, two bags and unions were installed. Owing to the plate barrier between the two bags considerable difficulty was experienced in positioning the bags so that they were not trapped beneath the plate. Numerous attempts were required to secure both the stiffener and bags. A small amount of air was used to inflate the bags to confirm that they were functional.

Special attention was paid to the fastening of the unions against the strongbox to prevent the risk of pressure loss. After this the remainder of the model was assembled in accordance with the general model making procedure as previously outlined.

5.5 TEST PROCEDURE

Immediately following the general modelling process there were still numerous steps that remained before the model could be tested. For instance, the standpipes and instrumentation connections to the centrifuge were made. Checks were conducted to ensure that the latex bag (or bags) was still intact by applying a small amount of pressure to the bag. Sample images were captured to confirm that the quality of images and lighting conditions were suitable. The amplification gains for all instrumentation were confirmed and all loose cables securely tied before accelerating the model. Model making and preparation on the swing was typically completed within three and a half hours.

With the vertical stresses in the model being a function of gravitational acceleration, depth and soil density, the pressure in the latex bag surcharging the formation level was gradually increased in line with the centrifuge acceleration. It had been determined that the bulk unit weight of the soil was 16.5kN/m^3 and this equated to a pressure of approximately 198kN/m^2 at $160g$.

The pore pressure response and surface settlements were monitored whilst the model reconsolidated in-flight. A large and sudden spike in settlement was observed immediately after spin up owing to the settlement of the LVDT footings in the soil; this was also clearly visible once the sample had been removed from the centrifuge. Ideally, a model is tested when no further changes in pore pressure are observed following initial spin up, however owing to the relatively deep sample and risk of equipment failure at $160g$ it was not considered viable for the sample to remain in-flight to consolidate overnight. When the rate of change in pore pressure was less than 1kPa/hour the excavation simulation began. The model was typically ready for testing approximately five hours after spin up.

A minimum of two people were required to test the model to reduce the pressure in the latex bag, cross reference sample counts from the data logger against the DPI

readings in the control room and record the pressure at which the excavation failed. The standard testing procedure is outlined below and is directly applicable to the dry propped excavation, deep soil mixed ground improvement excavation and the double wall excavation. Details of the additional stages conducted for the underwater and bermed excavations are given in the following subsections:-

- i. Ensure LabView programme was logging
- ii. Check that both cameras were capturing images in synchronicity
- iii. Commence the excavation simulation and record the sample count and image number at this stage
- iv. Commence lowering air pressure in latex bag at a rate of 1kPa/sec
- v. Cross correlate LabView sample count with air pressure readings on the DPI in the control room at five second intervals
- vi. Observe long term ground response in the event of a stable excavation

5.5.1 Underwater excavation test procedure

As the pressure in the latex bag was decreased to commence the excavation, the direct water feed into the excavation area and the air actuator were activated. This began flooding the excavation at a comparable rate to that of the rate of simulated excavation and allowed the soil below the bag to soften owing to unloading combined with contact with free water.

Having completely released the pressure in the airbag, the excavation in all similar tests did not fail and the model was left to further consolidate for up to 30 minutes to observe the long term effects of an unstiffened excavation base on surface settlements.

5.5.2 Bermed excavation

The bermed excavations were carried out by means of two latex airbags. The bag closest to the wall simulated a berm surcharging the formation level and the adjacent bag represented the main excavation area. Feeds from the centrifuge slip ring pressurised each bag independently, therefore allowing independent control of each bag.

To commence, the excavation sequence involved simultaneously decreasing the pressure in both bags, which represented the beginning of the excavation across the site and the formation of a bench across the berm. The total pressure applied from a predefined berm width of 50mm and a battered slope of 1:1 was calculated to be approximately 66kPa. Typically, soft berms are protected and surcharged with a sprayed concrete lining. For simplicity the berm pressure was set at 100kPa. Although the vertical surcharge would in theory vary owing to the irregular cross sectional shape of the berm, the berm was modelled in accordance with the equivalent surcharge method (Fleming, 2008).

Upon reaching 100kPa the pressure in the berm bag remained constant whilst the pressure in the second bag continued to decrease; simulating the main excavation process. The sample counts were noted at the points at which the berm pressure reached 100kPa and the end of the main excavation period.

In the event of a stable excavation under berm loading, the pressure in the berm bag was slowly decreased to observe the influence of a berm on ground movements and failure mechanisms.

5.6 IMAGE ANALYSIS

Subsurface deformations were analysed using particle image velocimetry (PIV). This technique has been well established to visualise unsteady flows in fluid mechanics (Scarano, 2012) by seeding the flow and taking consecutive images for analysis. Its use in analysing soil deformations was developed by White *et al.* (2003) where the area of interest is textured to aid in image analysis. Speswhite kaolin has almost no natural texture therefore it is necessary to apply a flock material or dyed sand to ensure that subsequent image analysis is possible. White *et al.* (2003) explains that this method provides an improvement in accuracy and precision over close-range photogrammetry, with scope for further improvements with the advancement of technology in charge coupled device (CCD) cameras.

PIV works by dividing a reference image into a series of test patches which are essentially pixels defined by an intensity value (White *et al.*, 2003). In the subsequent images the test patch is located within a search patch. The search patch is larger than

the test patch and defines the maximum extent to which the test patch can be located. It therefore needs to be large enough to ensure any movements are captured, but not so large as to prolong computation time. The cross correlation between the two images is referred to as the degree of match. In theory a cross correlation coefficient (CCC) value of 1 indicates that the exact test patch was found within the search patch. However, in practice it is unlikely that the exact patch is located in the following test images, therefore the user defines a CCC threshold. In this series of tests the degree of match was set at 0.8 so that data used in the analysis was of good quality, but also accounted for some tests where there was a higher level of noise or interference was present. Close-range photogrammetry computes soil displacements by converting the image-space deformations in pixel positions into object-space coordinates which in turn gives displacements in millimetres.

The common approach to modelling and observing subsurface movements, particularly around tunnels, uses a camera positioned directly in front of the model; perpendicular to the window (Grant, 1998; Divall, 2013; Le, 2017). This is suitable for applications where a localised field of interest exists. In the case of this research however, it was necessary to measure displacements near to the excavation and in the far field.

Owing to spatial limitations on the centrifuge platform and the hangers within the windshield, it was not possible to position a single wide angle lens camera directly in front of the centre of the model. The bespoke camera bracket originally designed by McNamara (2001) was used, as this allowed the camera to be positioned at an oblique angle to the formation and capture the patterns of movement and magnitude of heave as the excavation progressed. An LED strip was positioned near the top of the model which provided sufficient lighting in the area of interest.

The low undrained shear strength of the soil meant that surface settlements extended far beyond the field of view of one camera hence two were required; with one focussing on the excavation whilst the other captured displacements behind the retaining wall. Calibration of the cameras proved challenging; however the central part of the model was within the field of view of both cameras which enabled cross correlation of image analysis and associated computation.

5.7 SUMMARY

The sample preparation techniques and rationale have been explained in this chapter. Model making processes were developed and optimised to facilitate time efficient and accurate modelling and have been described in detail. Details of additional measures taken to model the range of excavation methods and various testing procedures have been given and are supplemented with photographs as required.

CHAPTER 6 CENTRIFUGE TEST RESULTS

6.1 DETAILS OF TESTS

This chapter details the experiments conducted in this research project and outlines the preliminary results. The turnaround for each test was approximately two weeks, hence time constraints predominantly limited the number of excavation sequences and variables investigated. The influence of wall embedment for various construction methods is briefly assessed. A summary of the experiments undertaken is given in Table 6.1 and comments on the success and failures of each test are also presented.

A total of twenty-two centrifuge tests at $160g$ were completed and are notated in Table 6.2, these comprised:

- Reference tests, where the wall was propped and no stability measures were introduced,
- Underwater excavations; where the excavation void was flooded with water at an equal rate to the level of soil theoretically being removed,
- Double walled excavations; involving a single length of low stiffness wall embedded below formation level in front of the primary retaining wall,
- Ground improvement through deep soil mixing (DSM); where different DSM geometries were investigated,
- Bermed excavations; investigating the influence of berm width on retained ground settlements.

Instrumentation comprising LVDTs, PPTs and air pressure transducers were used across all tests; the positions of which were also common. Trial PPTs were additionally used in the later part of the test series, however the original PPTs were placed in the same location as previous tests to provide a means of direct comparison. A clear Perspex window bolted to the front of the model permitted observation of subsurface movements of the plane strain model, which was primarily focussed on the formation level and retaining wall. As the experimental phase progressed a second miniature USB camera was acquired which provided information about far field

ground movements. Image analysis of deep seated deformations was possible owing to the images captured by the on-board miniature USB digital cameras.

The tests were designed to permit a parametric study on the influence of particular construction sequences on excavation stability and basal heave. Particular attention was paid to controlling wall movements through the use of an extremely stiff propped wall equivalent to a 2m thick reinforced concrete diaphragm wall when considered at prototype scale. Initial tests revealed passive failure of the wall, with rotation occurring about the lowest prop level. Props positioned above this level would therefore have been subject to tension loading. This observation brought about the need for a capping beam to support the top of the wall, which was implemented from test JP12 onwards.

Consistency between samples was achieved by pouring a clay slurry mixed to a water content of $120\% \pm 5\%$ and consolidating it to 100kPa at $1g$ for a period of 10 days. Following this stage, the clay sample was removed from the press, trimmed to a height of 290mm and consolidated in-flight at $160g$ overnight. The same standpipe overflow was used for all samples and an LVDT was clamped in place to record settlement and monitor the degree of consolidation before removing the sample from the centrifuge. The apparatus used to facilitate model making had been designed to predefine the excavation geometry with as much accuracy and consistency as possible. A pressurised latex bag at the excavation formation level initially surcharged the excavation until excess pore pressures had dissipated. At this point the air pressure was gradually reduced to simulate the vertical unloading during an excavation.

In all tests the pressure in the airbag was decreased at a rate of 1kPa/sec, modelling an excavation performed over 3 months at prototype scale. In the event of an excavation failure, the pressure was immediately reduced to 0kPa and the model decelerated. Conversely, if the excavation remained stable following the complete removal of the overburden pressure the model was left to consolidate in-flight to acquire long term ground response data. Details of the successful tests are presented in the following subsections.

6.1.1 Preliminary test; JP1

The proposed sample preparation and model making techniques outlined in the previous chapter were tested. Owing to the lack of experience and various unforeseen problems during preparation of the model, the completed model was accelerated after a very protracted 6 hour period of model making.

A number of issues were highlighted during model making which included the method of trimming the sample. It had been envisioned that the sample would be trimmed using a conventional square section aluminium box cutter, as had previously been adopted amongst other researchers at City, however Chapter 5 details the difficulties in achieving clean cuts in very soft clay with box cutters. This instigated the development of a series of cutters, plates, guides and specialist tools to prepare the model.

The model was transferred to the swing, the instrumentation connected, accelerated to 160g and consolidated in-flight overnight. The extended model making time resulted in excessive swelling of the sample at 1g and considerable settlements of the soil sample, retaining wall, spacer and instrumentation occurred as the model reconsolidated at 160g. The stiffener was bolted in place to the strongbox and consequently the latex bag burst as all other elements settled and the bag established contact with the wall. In addition, the bearing pressure from the conventional 10mm diameter circular LVDT footings was greater than the capacity of the soil at the retained ground surface which resulted in them puncturing through the PlastiDip and clay surface. This prompted the development of 3D printed rectangular footings which were used in subsequent tests.

Although this test did not provide any useable test data, it highlighted inefficiencies and shortcomings of the proposed modelling techniques and prompted further developments of the modelling and testing apparatus.

6.1.2 Preliminary underwater excavation test; JP3

This test intended to model the effects of an underwater excavation on a retaining wall of shallow embedment. However, during the first in-flight consolidation stage, the

pipe supplying water to the standpipe was insufficiently supported and became blocked owing to being kinked under high g . A standpipe pressure transducer had not been employed in the earliest tests, therefore there was no indication that the model was not being supplied with water. Consequently, the sample did not remain fully saturated and any water in the clay gradually drained out of the model. When checked the following morning immediately prior model making it was discovered that the sample was dry and had shrunk. The location of the water table could not be determined without installing multiple PPTs, which was not feasible as it was agreed that the sample would need to be left in-flight to consolidate again. Distilled water was poured on top of the sample before returning it to the swing and adjustments were made to the water pipe to prevent it from folding under acceleration. The model was left to swell under 160g for a further 20 hours, with the water table set 300mm above the base of the sample before commencing model making.

An overconsolidated sample had now been produced irrespective of the saturation of the sample during the second in-flight consolidation stage. The sample was stronger than anticipated and considerable physical effort was required in trimming it to the correct height. After assembling and reconsolidating the model at 160g, the excavation process was simulated by deflating the latex bag. This test was intended to model an underwater excavation. In view of this, as the excavation commenced, water was intended to be supplied to the void. Owing to limited personnel managing the experiment there were difficulties in managing the numerous valves in the control room. The air actuator was activated too early in the excavation simulation however flooding was not initiated until the overburden pressure at formation had been completely removed. For this reason, it is appropriate for the short term results from JP3 to be analysed alongside the reference tests, where no additional measures had been implemented.

Although it was evident that this model would not provide data representative of the intended test series, it was envisaged that the data would give an insight into the robustness and reliability of the apparatus and proposed underwater excavation sequence. This test also contributed to the understanding of soil strength on influencing deformation mechanisms for this excavation geometry.

6.1.3 Underwater excavation tests; JP6 and JP8

Tests JP6 and JP8 successfully investigated the influence of underwater excavations with a 75mm retained soil height. Wall embedment was also varied from 55mm to 75mm to quantify the additional benefit of a deeper wall on mitigating ground movements. Supply of water to the excavation and the formation level commenced simultaneously as the pressure was decreased in the latex bag to replicate an underwater excavation as closely as possible.

6.1.4 Baseline tests; JP7 and JP9

Tests JP7 and JP9 provided a baseline for comparison of the various construction methods which aimed to improve the ground response to deep excavations. These experiments tested the same retained height of soil but, providing 55mm and 75mm wall embedment. The exposed length of wall simply reacted against the aluminium stiffener, simulating an excavation with a very high system support stiffness essentially modelled as a fully propped wall.

Passive failure occurred in both tests as the toe of the wall rotated into the excavation about the bottom of the aluminium stiffener. Although the wall had been fully supported during reconsolidation, the removal of the overburden pressure indicated that props would be subjected to tensile loading. This highlighted the requirement for a method of securing the crest of the wall during the excavation process.

During reconsolidation of the model in test JP7 a power surcharge on centrifuge arm resulted in short circuits of the LVDTs and the air pressure transducers. Owing to the time at which this occurred it was not feasible to spin down and carry out repairs. The PPTs remained responsive and, as the cameras were capturing images, the test was conducted. The pressure in the latex bag was decreased and the DPI display in the control room was manually recorded at five second intervals. This enabled correlation of images and pore pressure responses against changes in overburden pressure.

6.1.5 Tension propping tests; JP11 and JP12

Two methods were tested to address the challenge of providing tensile and compressive restraint to the wall. The first comprised pinning the wall to the stiffener by means of two small thin plates screwed into the stiffener (test JP11). The size of the plates was dictated by the spacing of the ribs, distance between the wall rib and vertical support of the stiffener and the minimum wall upstand, as shown in Figure 6.1. Although this simple solution was effective for restraining small displacements, the overall length of the plate in contact with the wall was unsuitable for securing the wall against the stiffener. Towards the end of the simulated excavation significant wall and soil displacements were observed; the wall consequently moved out of the reach of the pins and the excavation failed.

An aluminium capping beam was developed to restrain the crest of the wall. Initially, this capping beam was secured to the stiffener with no provision for horizontal or vertical displacement (test JP12). However, as the sample reconsolidated the soil settled which resulted in a reduced area of contact between the capping beam and the retaining wall. The capping beam therefore did not perform satisfactorily in this test as it suffered the same problem with movement in excess of that which could be restrained by the pins as in JP11.

Modifications were made to the beam to account for the change in elevation of the wall during both reconsolidation and the simulated excavation stage of the experiment. This was facilitated by providing two L-shaped brackets that were screwed into the top of the capping beam and aligned along the two vertical upstands of the aluminium stiffener. Vertical movements were accommodated by a milling slot along the length of the bracket which guided the capping beam. Verticality was maintained by providing two bolts that were screwed to each bracket, giving $\pm 10\text{mm}$ range of vertical movement. This apparatus was easy to manage during model making because it could be adjusted without disturbing the wall and proved successful when employed in test JP13 and subsequent tests.

6.1.6 Deep soil mixing tests; JP10, JP14 and JP15

The influence of ground improvement construction techniques was investigated in tests JP10, JP14 and JP15. JP10 comprised a raft of improved soil that extended across the full width of the excavation to a depth of $H/2$. The plan dimensions of the improved soil at prototype scale was comparable with many studies that had previously been conducted, as described in Chapter 2.

Model making progressed well in test JPP10; albeit slower than for the previous experiments owing to the additional excavation required in preparing the model. This was the first test in the deep soil mixing test series and the modelling procedure had not been trialled, however no problems were encountered. The model was assembled and placed on the swing before being accelerated and left to reconsolidate in-flight. Problems were faced during this period with interruptions to power supplies on the centrifuge. This was later discovered to have been caused by water damage to the motherboards in the data acquisition system; however the course of action taken at the time was to progress with the experiment. The pressure transducer connected to the base of the standpipe and the LVDTs did not provide any useable data. The PPTs and air pressure transducer were responsive and the cameras continued to capture images; hence subsequent analysis was possible.

Establishing whether there was an optimum geometry of treated soil was thought to be important owing to the lack of publications relating to the influence of ground improvement geometry. With this in mind the plan area of the ground improvement zone was varied between the ground improvement test series. Keller (2017) state it is common practice to treat the area directly in front of the wall as this reduces the overall extent of treatment and subsequent delays in allowing the additive to cure. Considering that ground improvement costs quickly escalate with larger areas, it was decided to maintain a constant volume of lime-stabilised clay, whilst varying the widths and depths of treatment. JP14 modelled an improved zone extending to the toe of the wall which was $2B/3$ wide, whereas the width of treated soil in JP15 was limited to $B/3$ extending to a depth of $3H/2$ below excavation formation level, as illustrated in Figure 5.26. A range of aluminium angles were used as cutting shelves to define the extent of treatment. Care was taken to form a void of the correct dimensions and place the lime-stabilised block without disturbing the surrounding virgin soil.

The cross sectional area of ground improvement in JP15 was sufficiently deep and wide that a PPT was embedded in the lime-stabilised clay zone permitting observations of the dissipation of pore pressures in lime-stabilised soil. This was only possible in JP15 owing to the dimensions of the stabilised block; in tests JP10 and JP14 the location of existing tapped ports in the strongbox back wall precluded such instrumentation.

6.1.7 Double wall tests; JP12, JP13, JP18 and JP20

Modelling of the double wall tests progressed well and the first experiment of this test series was supported with a capping beam. In JP12 the capping beam was fixed in place and as the sample settled during the simulated event the excavation collapsed at approximately 20kPa. JP13 was a repeat of test JP12 with the exception that the top of the wall was restrained by the sliding capping beam, see Figure 5.21.

JP18 was conducted with a more deeply embedded wall to determine the influence of embedment on the magnitude and extent of movements. As the sample was recovered from the swing following in-flight consolidation the surface was found to be merely damp as opposed to flooded with standing water. This lack of standing water resulted from a reduced water flow rate to the standpipe. The flow rate had been reduced owing to a time lag on the data logger and image capture which was suspected to have occurred owing to high levels of moisture in the chamber as a result of large volumes of water evaporating, which subsequently interfered with the apparatus. Consequently, more water was evaporated from the model than was supplied by the standpipe.

Previously, the sample count was used to correlate the excavation pressure against images. Owing to the delay on the data logger and image capture rate matching the sample count and images to view deformations for particular overburden pressures was not a simple exercise. Insufficient amounts of data prevented an illustration of the development of ground movements during the excavation, however the failure mechanism of a double wall excavation with deeper embedment was achieved and could be compared against test JP13.

This test had initially been designed to model the combined effects of a double wall excavation surcharged underwater. Assembly of model JP20 progressed with ease however a number of problems were later encountered during reconsolidation and testing. Firstly, the air pressure transducer was damaged in-flight soon after spinning up. Owing to the lack of additional transducers it was not possible to replace it immediately. The strong correlation between the transducer readings and digital pressure indicator (DPI) readings in the control room from previous tests indicated that it was reasonable to proceed with the test using only the DPI in the control room. As the excavation progressed a number of valves required activation in the control room, which included the air actuator and the feed supplying water directly to the excavation. It was found that the direct feed to the excavation pipe had kinked and therefore was not supplying a sufficient volume of water. At the end of the excavation less than 10mm of water had been deposited into the excavation area and for this reason it was not possible to describe this test as an underwater excavation.

6.1.8 Bermed excavation tests; JP16, JP17 and JP19

An attempt to gain an understanding of the influence of a berm or surcharged area directly in front of the retaining wall was made in tests JP16 and JP17. Test JP16 modelled a 50mm ($B/3$) wide berm, whilst JP17 simulated a berm width of $2B/3$. This test series required the use of two latex bags which were initially pressurised during spin up to provide an overburden pressure of 200kPa, as shown in Figure 4.27. They were simultaneously unloaded to an overburden pressure of 100kPa after which the berm bag remained at this pressure whilst the pressure in the excavation bag continued to decrease at a constant rate. Owing to the use of L-shaped strips of plastic secured to the bottom edge of the divider, the bags were prevented from blowing out and puncturing. Following the failure of the second air pressure transducer located on the strongbox it was necessary to record the pressures displayed on the DPI in the control room. This was deemed acceptable owing to a strong correlation between the pressure measurements and DPI readings for the main air pressure transducer.

JP19 tested a bermed excavation of width $B/3$ and 75mm wall embedment. As with the previous berm tests only one air pressure transducer was available which was used to monitor the pressure in the excavation bag. The DPI readings were manually

recorded to correlate the pressure in the berm bag against the data logger sample count. The images were not captured at regular intervals owing to a fault within the centrifuge computer. This resulted in a six-minute delay during the test, such that images were not taken after the overburden pressure in the excavation bag fell below 20kPa. The pressure in the bags continued to drop at a constant rate of 1kPa/sec. However, owing to the slow connection between the on-board computer and control room computer the delay went unnoticed and the pressure in both bags was completely removed. The instrumentation was responsive and the test continued with surface settlement data obtained from the LVDTs. The lack of images during the test failed to provide the development of movements as the excavation progressed, however it was possible to obtain the final failure mechanism of a bermed excavation with deeper embedment.

6.1.9 Combined excavation method tests; JP21 and JP22

The initial results revealed that underwater excavations were the only construction method explored that were capable of preventing failure; double wall and deep soil mixing excavations provided a reasonable degree of excavation support to reduce surface settlements but ultimately failed. Owing to this discovery, tests JP21 and JP22 were conducted with the aim of assessing whether any additional benefit was afforded by combining underwater excavation with other construction methods.

Test JP21 was a repeat of JP20 and was successful in modelling a deep underwater excavation with an additional low-stiffness wall at formation level. The experimental arrangement of JP21 was akin to that of test JP13, where the secondary wall extended an additional 20mm below the toe of the retaining wall and embedded 25mm away. The retaining wall was supported at the crest by a capping beam on a bracket that permitted vertical displacement. In the final preparation stages prior to reconsolidation, the instrumentation and cameras were checked. It became apparent that attempting to use two cameras resulted in time lags and difficulty in acquiring data at precise time intervals. Consequently, one camera was used to focus on the excavation formation and also as much of the soil behind the retaining wall as could be managed in its field of view. This resolved the problems that had previously been faced with time lags on the data logger and the image capture rate.

JP22 modelled an underwater excavation in conjunction with a lime stabilised block of soil in front of the wall. The geometry of the ground improvement area used in this test was dependent on the quality of results obtained from the DSM test series. Owing to the lack of LVDT data from tests JP10 and JP15, this test modelled a similar DSM block as used in test JP14, for a treatment width of $2B/3$ extending to the toe of the wall. During reconsolidation the air pressure steadily reduced and the on-board camera indicated a developing depression at formation level at the wall/excavation interface. It was assumed that a small tear had formed in the bag, and that this had subsequently sealed itself. The model was left to continue consolidating whilst being carefully monitored. Over the following two hours the depression more than doubled in size and a considerable amount of water collected in the void. It was thought that the bag was embedding itself below the wall spacer along the entire width of the model and there was a risk that it could burst if it was left to further consolidate. In view of this the simulated excavation was performed and the void flooded with water. Upon completion of the test the model was recovered and inspected. It was found that the bag had only bulged at the interface with the window but, if the model remained in-flight much longer, the bag would have slipped under the spacer and punctured. It is thought that as the model reconsolidated the stiffer layer of lime stabilised clay did not compress against the window allowing the bag to expand into a small gap between the window and soil. Seepage around the wall was also noted as water was not prevented from flowing owing to poor contact between the wall spacer and the soil.

6.2 OBSERVATIONS AND RESULTS

In general, observations made from this series of experiments showed a marked improvement in reducing base heave and excavation stability was much increased particularly when a prop had been employed to restrain the top of the wall. Table 6.2 summarises the excavation conditions that were modelled in each of the tests.

6.2.1 Influence of embedment on ground movements

A range of tests were conducted to establish the role of wall embedment in controlling ground movements arising from an excavation. For instance, comparisons were drawn between the reference tests (JP7, JP9 and JP11), the underwater excavation tests (JP3,

JP6 and JP8), the double wall tests (JP12, JP13, JP20 and JP18) and the bermed excavations (JP16, JP17 and JP19).

6.2.1.1 Reference cantilevered tests; JP3, JP7, JP9 and JP11

Reference tests were performed to establish the behaviour of a deep excavation with high propping system stiffness without any additional support, such as ground improvement, and the development of surface settlements as the excavation progressed. Figure 6.2 shows the surface settlement profile of the retained ground at an overburden pressure at formation level of 38kPa, as this was a comparable pressure in all tests. The magnitude of settlement in JP9, with a shallower wall embedment, was more than twice that recorded in JP7 whilst the settlement trough followed the same trend. In comparison, the stronger sample used in test JP3 displayed settlements that were an order of magnitude smaller than those observed in JP9. The maximum vertical displacement was recorded at a distance ranging between $0.5H - H$ behind the retaining wall in all tests.

As expected, surface settlements of the retained ground revealed that a wall of 75mm embedment provided a greater degree of stability to the excavation than a wall with 55mm embedment. Figure 6.3 shows that for a wall embedment of 55mm, the ground rapidly settled when the overburden pressure dropped below 110kPa. This is compared with 75mm wall embedment where the rate of settlement increased after the overburden pressure was reduced below 85kPa. The results from JP7 and JP9 are typical of soft soils. However, the behaviour of the soil model in JP3, which suffered from drying during spinning, was that of a stronger clay sample. The results from JP3 plotted in Figure 6.3 illustrate the retained soil surface response to the vertical unloading immediately behind the retaining wall and are representative of an excavation without any additional support from surcharging. Consistency between tests is evident as the trend and progression of movements is analogous across the results.

6.2.1.2 Underwater excavations supported by cantilever wall; JP6 and JP8

Tests JP6 and JP8 measured the ground response from vertical unloading whilst flooding the excavation void in an attempt to reduce the nett magnitude of vertical stress relief. A direct water feed into the excavation was activated as the excavation

commenced. This applied a head of water equal to the depth of soil that was theoretically being excavated. This means that the change in total vertical stress per metre depth of excavation simulated at prototype scale was 6kN/m^2 compared with 16kN/m^2 if water was not used. Figure 6.4 illustrates that maximum settlements occur between $0.5H$ and H and notable settlements up to a distance of $3.5H$. Beyond this distance the measured ground movements were comparable for deep and shallow wall embedment depths. Twice the magnitude of settlement was observed at H and more than three times at the wall interface in JP6 than in JP8, which indicates that increasing the embedment by approximately a third significantly influences the control of ground movements around an excavation.

The development of vertical displacements immediately behind the retaining wall as the excavation progressed are plotted against the air pressure acting at formation level in Figure 6.5. The settlement profiles show that movements begin to accelerate when the measured air pressure dropped below 125kPa. Following this, settlements begin to stabilise at approximately 80kPa. This trend of movement suggests that the effects of the surcharge from flooding the excavation were not noticeable until the overburden pressure on the formation was reduced to 100kPa. Figure 6.6 demonstrates that the decrease in the air pressure and increase in water pressure acting at formation level were linear. However, the formation level is likely to have experienced a reduction in stress until the water pressure exceeded the air pressure; at this point the formation was reloaded. Consequently, after 120sec of simulated excavation the pressure acting at formation level increased, which coincided with the stabilisation of settlements shown in Figure 6.7. The immediate effect of flooding the excavation was more pronounced in test JP8 owing to deeper wall embedment.

Horizontal (Figure 6.8) and vertical (Figure 6.9) displacement contours were plotted displaying the ground movements immediately after complete removal of the overburden pressure. Whilst horizontal movements were concentrated on the passive side of the excavation adjacent the toe of the shallow wall (JP6), a deeper embedment (JP8) shows that maximum horizontal displacements predominantly occur just below formation level on both sides of the retaining wall. Horizontal movements associated with a shallow wall were about three times larger than those observed in an underwater excavation with deeper embedment. The vertical contours (Figure 6.9) demonstrate

that increasing the embedment of the retaining wall by a third reduced heave by a factor of four and halved the magnitude of maximum settlement.

6.2.1.3 Long term ground movements from a submerged cantilevered excavation; JP3, JP6 and JP8

Following completion of the excavation the models were left submerged in flight for a further 12 minutes, which equates to approximately 7 months at prototype scale. This allowed excess pore pressures to dissipate and the long term ground displacements were observed. Figure 6.10 shows the surface settlement profiles immediately after the excavation and after 12 minutes following complete removal of the overburden pressure. As expected vertical displacements increased following a period of pore pressure dissipation. The stronger soil sample in test JP3 had a deeper settlement trough than those in JP6 and JP8. This was expected owing to the conditions in which the tests were carried out, where test JP3 was flooded following complete removal of the overburden load. Interestingly, however, JP3 exhibited 33% increase in surface settlements compared with the softer samples, in JP6 and JP8 both of which developed additional 20% settlement in the long term. Whilst changes in displacement were less noticeable with distance from the excavation in JP6 and JP8, the pore pressure dissipation effect on surface settlements in JP3 were more apparent in JP3, both 12 and 30 minutes after the excavation. Furthermore, a shallow embedded wall (JP6) accrued more settlement at the soil/wall interface whilst a deeper wall (JP8) developed larger movements at distance H behind the retaining wall.

6.2.1.4 Double walled excavations with wall fixed at crest; JP12, JP13, JP20 and JP18

A series of experiments were conducted to establish the effect of an additional low stiffness wall, defined here as a slurry wall, embedded below formation level. The primary retaining wall was embedded either 55mm or 75mm and the low stiffness wall was positioned 25mm in front of the retaining wall. The total depth of this slurry wall was 75mm, hence in JP12, JP13 and JP20, where the primary wall was embedded 55mm, the toe of the slurry wall was 20mm deeper than the retaining wall. The toe of both the retaining and slurry walls were at an identical horizon in JP18 owing to the deeper retaining wall embedment length of 75mm.

Figure 6.11 illustrates the settlement troughs of four double walled tests, the trends of which are comparable. The maximum settlements consistently occurred at a distance H behind the wall. The results also show that the magnitude of movement at the wall interface was approximately half that of the maximum settlement. Test JP18 performed considerably better than the tests with 55mm embedment as the final settlement profile was half the magnitude of JP13. The settlements recorded in JP12 and JP20 were noticeably larger than JP13 but were seen to converge from $2.5H$. Where the wall was simply pinned at the crest (JP12, see Figure 6.1) vertical displacements developed at 110kPa and continued at a relatively constant rate to 50kPa overburden pressure, as shown in Figure 6.12. Settlements gradually accelerated as the excavation approached completion. On the other hand, adequately securing the top of the retaining wall (JP13) resulted in a more controlled development of settlement with a sudden acceleration in settlement at 5kPa. With deeper wall embedment (JP18) the settlements were better controlled and did not exceed 0.5mm until the overburden pressure had dropped below 20kPa.

Horizontal contours at an overburden pressure of 25kPa are illustrated in Figure 6.13 and compare the results from JP13 and JP18, for 55mm and 75mm embedment respectively. The deeper wall embedment constructed in conjunction with a slurry wall was shown to reduce horizontal movements by a third, with maximum horizontal displacements concentrated at a depth 40mm below formation level. The vertical displacements that had developed at 25kPa, presented in Figure 6.14, show similar patterns of movement but increasing the primary wall embedment reduced vertical settlements by a factor of three.

6.2.1.5 Bermed excavations with wall fixed at crest; JP16, JP17 and JP19

The results plotted in Figure 6.15 present the surface settlement profiles of three bermed excavations at the end of the simulated excavation of the main bag; at this stage the berm bag continued to apply a surcharge of 100kPa. The influence of berm width or retaining wall embedment was shown to be minimal at distances exceeding $2H$. Test JP16 displays a considerably greater settlement profile compared with tests JP17 and JP19, owing to failure of the excavation upon removal of the excavation bag overburden pressure. Comparing the settlement profiles of JP17 ($2B/3$ and 55mm wall embedment) and JP19 ($B/3$ and 75mm wall embedment), little difference in the trend

or magnitudes of displacement exist, suggesting that the berm size is as significant in controlling displacements as wall embedment.

Displacement contours have been plotted to illustrate the ground movements that occurred following complete removal of the overburden pressure of the main excavation and berm. Figure 6.16 presents horizontal contours for tests JP17 and JP19 and illustrates similar magnitudes of displacement. However, the concentration of pressure imposed by a narrow berm (JP19) results in maximum horizontal displacements developing in an area as wide as the applied surcharge. Conversely, a wide berm (JP17) used in conjunction with shallow wall embedment results in a high concentration of horizontal displacement around the wall. Although the berm was shown to have limited influence in reducing the magnitude of vertical settlement adjacent the retaining wall, shown in Figure 6.17, the pressure applied to the formation level was controlled the magnitude of heave post excavation. A wide berm reduced heave by a factor of two across the entire formation level, compared with a narrow berm which was only shown to reduce the magnitude of heave directly below the berm.

6.2.2 Effects of construction methods on displacements

6.2.2.1 Ground displacements of a 55mm deep wall embedment with an unrestrained wall crest; JP3, JP6, JP9 and JP10

These tests sought to observe ground movements arising from a deep excavation with a high stiffness wall that was unrestrained at its crest. Results include a reference test, an underwater excavation, an excavation in firm ground and a ground improved excavation. The results showed that the various excavation methods offered a reduction in ground movements both at formation level and behind the retaining wall.

Figure 6.18 illustrates the retained surface settlements for each of the tests immediately after the simulated excavation. Adjacent the excavation, deep soil mixing (DSM) was shown to reduce maximum settlements by a third compared with those measured in the reference test (JP9). Furthermore, surface settlements measured at the retaining wall in the underwater excavations (JP3 and JP6) were 20 times smaller than the settlement observed in JP9. The trend of movements was similar across all tests with

surface settlements becoming less pronounced at a distance $2H - 2.5H$ from the retaining wall and at $4H$ were negligible.

Vertical displacements directly behind the retaining wall are plotted in Figure 6.19. Ground heave measurements of 0.15mm were observed immediately behind the wall with an overburden pressure of up to 100kPa in the reference test (JP9) before rapidly settling as the excavation continued. Displacements in test JP10 were computed using PIV analysis and showed that the retained soil responded to the excavation once the overburden pressure dropped below 150kPa. The subsequent settlement in tests JP10 occurred at a slower rate than in JP9, which was expected owing to the excavation support systems that had been implemented. Furthermore, the vertical movements from JP6 (underwater excavation) were shown to follow the same settlement trend up to 80kPa as those recorded in JP10. At lower overburden pressures the rate of settlement plateaued with an ultimate settlement immediately behind the wall of 0.53mm at the end of the excavation. The magnitude of settlement was controlled by the surcharge applied to the formation by flooding the excavation, which appears to have had some impact after 100kPa. Finally, in test JP3, the excavation was flooded after the surcharge had been completely removed from the formation level. Owing to the higher strength of the soil sample, vertical movements measured at 50kPa were nine times smaller in JP3 than JP9.

Subsurface horizontal displacements were captured on camera and the contours for each of the tests are plotted in Figure 6.20. The special excavation methods and stronger soil samples all show a marked reduction in horizontal movements at the toe of the wall. Maximum displacement was observed in front of the retaining wall toe approximately 120mm below ground level and the contours show that this was countered by the movement of the crest of the wall into the retained soil. As expected the largest horizontal movement was observed in the reference test (JP9). The presence of the lime stabilised soil (JP10) significantly reduced horizontal movements. Horizontal movements measured in the underwater test (JP6) were again concentrated around the toe of the wall, however the maximum displacements were 0.75mm, almost three times smaller than those seen in the reference test.

Vertical contours plotted in Figure 6.21 show that the underwater excavation zone provided the most support to the excavation and that the magnitude of settlement

behind the retaining wall was almost twice the heave measured at the formation level (Figure 6.21b). The reference test (JP9) exhibited a similar trend, with 2.1mm settlement measured behind the wall and 1.1mm heave at formation (Figure 6.21c). However, the maximum surface settlement was observed over a wider area in the ground improvement excavations compared with the reference test. In addition, the settlements were approximately a third larger than the magnitude of heave, suggesting a wider deformation mechanism owing to the presence of an obstruction at formation level. Whilst the magnitudes of maximum settlement were comparable in the underwater excavation and DSM tests, JP6 and JP10 respectively, the surcharging effects from flooding the excavation reduced the magnitude of heave by a factor of approximately two.

6.2.2.2 Influence of wall fixity through comparisons of reference tests JP9 and JP11

Vertical displacements immediately behind the wall are presented in Figure 6.22 and clearly show that the influence of pinning the crest delays vertical displacement and failure of the excavation. Whilst the settlement trends were generally consistent, the effect of pins was shown to control the magnitude of heave at the early stages of the excavation. Figure 6.23 compares the final surface settlement profiles of similar excavations and was shown to significantly reduce the maximum magnitude of displacement by a factor of about three. This was owing to the pins supporting the crest of the retaining wall and highlighted the significance of properly securing the crest of the excavation to prevent passive failure and rotation about the lowest prop.

6.2.2.3 Comparison of double walled and lime stabilised excavations with 55mm embedment; JP12, JP13, JP20, JP10, JP14 & JP15

Figure 6.24 compares the vertical displacements directly behind the retaining wall during the double walled excavations (JP12, JP13 & JP20) against those measured in the deep soil mixing tests (JP10, JP14 & JP15). Results from test JP9 have also been plotted to provide baseline comparisons for the improvement offered by these construction methods. The retaining wall was embedded 55mm below formation level for all of these tests. The trend and rate of settlement in these tests were comparable across tests suggesting that the presence of the strengthened soil and the additional wall have a similar influence on ground movements. Although the geometry of all three double walled excavation tests were the same, the discrepancy between

settlement readings are a result of the wall fixity conditions and slight variations in soil strength. The wall crest was fixed in test JP12 which meant that as the model reconsolidated in-flight and settled, the area of contact between the wall and the pins reduced. As the excavation progressed the ground behind the wall settled and subsequently failed rapidly. This trend of movement was similar to test JP20 which was likely to have been caused by the discharge pipe in the standpipe base becoming blocked which resulted in a higher water table and softer sample. However, when the double walled excavation was sufficiently restrained the rate of settlement was reduced and more comparable with the trend of movements observed in the DSM series of tests.

The rate of settlements illustrated in Figure 6.24 suggest that double walled excavations provided some degree of control over the accumulation of settlement as there was a lower rate of settlement compared with JP9. However, the DSM tests show that the stronger area of soil in the passive zone was better able to restrain the toe of the wall. Surface settlements therefore developed less rapidly than those in JP12, JP20 and JP9. However, the relatively brittle nature of the lime stabilised soil resulted in more sudden failure at an overburden pressure between 30 – 40kPa.

Figure 6.25 gives the settlement troughs of the double walled and DSM tests immediately after the overburden pressure had been removed. The profiles of JP10 and JP15 were interpreted from PIV analysis whereas the other tests were measured using LVDTs. A wide spread of results was observed for each of the excavation methods and suggests that DSM across the full formation or a narrow and deep (JP15 – B/3) DSM arrangement best controlled settlements, however, this was only marginally better than the double walled excavation in test JP13. Conversely, it appears that the retained ground behaviour of JP14 and JP12 were comparable, where the excavation formation was treated with DSM to the toe of the wall and across two thirds of the excavation width.

The horizontal displacement contours were plotted for each of the tests at an overburden pressure of 25kPa (Figure 6.26). Although the double walled excavation; JP13 had the potential to reduce the magnitude of horizontal movement, fixity conditions are clearly important. With the wall simply pinned at the crest at the

beginning of the excavation (JP12) additional movements were permitted to develop owing to the accumulation of large vertical displacements (Figure 6.27).

However, employing a sliding capping beam restrained the wall crest against excessive rotation into the retained soil and also significantly reduced horizontal soil displacement at the toe of the wall by about half. Surprisingly, comparisons in magnitude were more evident between the DSM (JP14) and the double wall (JP20) tests. The horizontal displacements from the successful double wall test (JP13) were 55% smaller than those observed in JP14.

The vertical contour plots (Figure 6.27) showed that the maximum settlement in both the double wall and DSM series of tests occurred at a distance approximately $B/3$ from the retaining wall, regardless of the width of ground improvement treatment. The proximity of the boundary to the excavation appears to have had a negligible effect on ground movements as displacements were in the region of 0.04 – 0.06mm at a distance of $3H$. Although the secondary wall in JP13 was able to significantly reduce horizontal movements at the toe compared with DSM, the influence of an additional wall or stiffer block of soil on vertical displacements appeared small, with 0.92mm heave measured in JP13 and 1.11mm in JP14.

6.2.2.4 Ground movements arising from a combination of multiple excavation methods of a 55mm embedded wall; JP13, JP14, JP21, JP22

The results from the initial testing phase revealed that of the four special excavation methods, the underwater excavation tests provided the greatest excavation support in terms of minimising adjacent ground movements. The final tests, JP21 and JP22, sought to model the combined effect of an underwater excavation with additional support/stabilisation in place. This was to assess whether further reductions in soil deformations could be gained by combining excavation methods.

Figure 6.28 illustrates the effect combining underwater excavation with alternative construction methods on the development of surface settlements directly behind the retaining wall. The dotted black line illustrates the change in vertical displacement arising from an underwater test (JP6). The progression of settlement in tests JP21 and JP22 are also plotted. JP21 modelled the effects of an underwater excavation in conjunction with a double wall, whilst JP22 combined an underwater excavation with

DSM. Figure 6.28 shows that the underwater and double wall excavation method reduced the overall magnitude of surface settlement by 29%, but also delayed the onset of movement until the overburden pressure was reduced to 125kPa compared with 165kPa in the underwater baseline test (JP6). The overall displacement trend tends to follow that of the underwater excavation, test JP6.

An underwater excavation with a lime stabilised layer of soil exhibited similar behaviour to the underwater baseline test as displacements behind the wall commenced at 165kPa overburden pressure. The rate at which these developed was akin to JP6, however the overburden pressure at which this accelerated was delayed to 100kPa, compared with 140kPa in JP6. Surface settlements continued to follow a trend comparable to that observed in JP6, with only a 4% greater magnitude in ultimate settlement.

Figure 6.29 illustrates the surface settlement profiles of the combined excavation method tests compared with the profiles associated with one particular excavation method. The profiles of JP13 (double wall) and JP14 (DSM) show that the double wall alone resulted in considerably reduced vertical displacements than the DSM arrangement. Figure 6.30 focusses on the effects of combining each of these methods with an underwater excavation. Similar to the trends seen in the tests where only one excavation method was employed, the underwater excavation with double wall arrangement (JP21) resulted in virtually no movement at distance H behind the wall, but the ground heaved by a maximum of 0.1mm with increasing distance from the excavation, which was likely owing to the apparatus set-up. At the soil/wall interface the measured displacement at the end of the excavation was 30% lower than observed in JP6 and JP22. In comparison, the underwater excavation with DSM (JP22) resulted in a settlement trough that essentially replicates the results of the underwater baseline excavation.

6.3 PORE PRESSURE RESPONSES

A minimum of three Druck PDCR81 miniature pore pressure transducers were used in the entire series of tests. These were positioned either side of the retaining wall below the excavation formation and one was placed in the far field, as illustrated in Figure 6.31. These were monitored to establish the point during reconsolidation that

the model reached equilibrium and measured the generation of excess pore pressures during the excavation event. Additional pore pressure transducers were employed towards the end of the test series, however these were not consistently reliable, were eventually damaged and became unusable.

Large excess pore pressures were typically generated directly beneath the pressurised airbag, owing to the unloading of the formation level. A small change in the far field pore pressure was measured indicating that boundary effects were negligible.

Pore pressure responses either side of the retaining wall were plotted and comparisons were drawn for a number of variables. Figure 6.32(a) shows the influence of each of the different construction methods on the development of excess pore pressures during the excavation directly below the formation. As expected, the measurements, with the exception of JP6, follow the same trend as the overburden pressure reduced. Behind the wall, the lowest excess pore pressures were generated in the DSM tests. The pore pressures recorded during the underwater excavation (JP6) gradually increased as the change in overburden pressure reached 100kPa before dissipating as the excavation progressed. This behaviour validates the theory, illustrated in Figure 6.6, that the formation level was reloaded once the water pressure exceeded the air pressure in the latex bag.

The excess pore pressures on the passive side of the excavation (Figure 6.32(b), PPT2) follow similar trends. A slight decrease in pore pressures was typically noted at the start of the excavation. However, as the excavation progressed and more soil displacements occurred excess pore pressures developed. The underwater test (JP6) showed little change in pore pressure up to a change in overburden pressure of 60kPa. Following this there was a large increase in excess pore pressure when the change in overburden pressure reached 100kPa. Further changes in overburden pressure showed a slight increase in excess pore pressure. A comparable magnitude in excess pore pressure at the end of the excavation was observed in the *B/3* bermed excavation test (JP16).

Figure 6.33(a) compares the excess pore pressure response directly below the formation level of the reference tests with a free wall crest (JP7) and pinned crest (JP11). Prior to failure both tests displayed very similar pore pressure response with

a maximum excess pore pressure development of approximately 60kPa towards the end of the excavation. The results suggest that improving the fixity of the wall can marginally reduce the magnitude of excess pore pressure, however the changes are not necessarily significant. Excess pore pressures on the active side of the excavation (PPT, Figure 6.33(b)) are almost identical up to the failure pressure irrespective of the fixity conditions. During the initial unloading stage negative excess pore pressures up to -4kPa developed. These subsequently dissipated as the excavation progressed and reached approximately 5kPa at failure.

The influence of wall embedment on excess pore pressures is illustrated in Figure 6.34, which include results from the two reference tests (JP7 and JP9) modelled as excavations with a free wall crest. Excess pore pressures measured by PPT1 were similar in both tests, shown in Figure 6.34(a), with marginally smaller pressures observed for a wall with deeper embedment. Conversely, Figure 6.34(b) shows that although the magnitude of excess pore pressure prior to failure is comparable for two embedment depths, these excess pores pressures generated earlier in the excavation process for the deeper wall embedment.

An assessment of DSM geometry on excess pore pressures was made in Figure 6.35. PPT1 shows that the geometry of the ground improvement zone has some influence over the excess pore pressure response. Figure 6.35(a) indicates that the wider the area of treated soil the lower the generation of excess pore pressures on the passive side of the excavation. This is consistent with the assumption that the stronger soil at the formation level supports the base of the excavation and limits the magnitude of heave. Tests JP14 and JP15 modelled narrower DSM zones, which would encourage a wider deformation mechanism but continue to permit movements with distance from the wall. Therefore, it is expected that the magnitude of excess pore pressures would be greater for narrower widths of treated soil. Despite observing such a variation in excess pore pressures at the formation level Figure 6.35(b) shows considerable similarities in the excess pore pressures behind the retaining wall. In summary, ground improvement of constant cross sectional area provided excavation support such that subsequent settlements of the retained surface could be expected to be comparable.

During the simulated bermed excavation the surcharge pressure in both bags was reduced to 100kPa. The pressure in the airbag furthest from the wall continued to

decrease whilst the berm bag continued to apply a surcharge of 100kPa. Upon completion of the simulated excavation, the berm was removed by reducing the air pressure at a rate similar to that of the main excavation stage. As the pressure in the excavation bag was reduced the influence of the berm on excess pore pressures was monitored. Figure 6.36(a) shows the generation of excess pore pressures below the formation level. When the pressure in the berm remained at 100kPa, the excess pore pressures plateaued which was expected owing to the comparatively large width of each berm. As the excavation continued excess pore pressures continued to develop with an ultimate excess pore pressure of approximately 40kPa. Excess pore pressures measured by PPT2 on the active side of the excavation (Figure 6.36(b)) showed that deeper wall embedment (JP19) reduced the magnitude of excess pore pressures. For a similar berm width and shallower embedment an alternative trend was observed. At the beginning of the excavation there was a rapid generation of excess pore pressures which started to return to equilibrium after the overburden pressure reduced below 120kPa. In comparison, generation of excess pore pressures attributed to a wide berm (JP17) gradually approached 15kPa towards the end of the excavation.

Figure 6.37 compares the excess pore pressure response between the underwater excavations combined with either a DSM zone or a secondary wall. The PPT below the formation level (Figure 6.37(a)) showed that the presence of two excavation methods significantly reduced the magnitude of excess pore pressures during the excavation. In addition, the pore pressures tended to dissipate when the overburden pressure had been reduced by 75kPa. Towards the end of the excavation positive excess pore pressures had developed. This was probably owing to the rotation of the toe of the wall into the excavation. The excess pore pressures on the retained soil side showed that a double wall (JP21) gave an immediate response to the excavation. Conversely, the presence of a lime stabilised block (JP22) limited the generation of excess pore pressures until the overburden pressure was 70kPa. Subsequent excess pore pressure developed rapidly owing to the nature of a stronger and more brittle zone of soil. Upon completion of the excavation, a similar magnitude of excess pore pressures was achieved.

6.4 CORRELATION BETWEEN AIR PRESSURE TRANSDUCER MEASUREMENTS AND DIGITAL PRESSURE INDICATOR (DPI) READINGS

A pressurised latex bag used to surcharge the excavation formation level required an air pressure transducer to measure and record the applied pressure. The data logger recorded air pressures and their respective LVDT and PPT measurements which provided a simple set of data that was easy to interpret. Whilst PPTs were the only means of measuring pore pressures in the model, an alternative method of measuring surface settlements, in the event of LVDT failure, could be achieved by way of image analysis; discussed in the following section. As this project was central to ground movements around excavations it was vital to have an alternative means of recording overburden pressures. This would assist in establishing whether the measured air pressures were accurate and would also provide a secondary means of recording the overburden pressure should the air pressure transducer fail in-flight.

Compressed air supplied to the model was controlled via a valve located in the control room that was fitted with a digital pressure indicator (DPI). As the model was accelerated the DPI was monitored to ensure the correct pressure was applied to the formation. Similarly, as the excavation was simulated the data logger was programmed to log every second whilst one member of the research group manually lowered the pressure at a rate of 1kPa/sec. Every five seconds the DPI reading was recorded alongside the sample count on the data logging programme. Figure 6.38 demonstrates the high precision between the air pressure transducer and the DPI readings for two individual tests. These results are representative of all the tests in which the air pressure transducer was responsive. In the limited tests where the air pressure transducer had failed (JP7, JP8) and where only one transducer was available for the berm test series (JP16, JP17, JP19), the high consistency between DPI and air pressure transducer readings that had been demonstrated inspired confidence in the subsequent analyses of these tests.

6.5 COMPARISON BETWEEN LVDT MEASUREMENTS AND IMAGE PROCESSING COMPUTATIONS AT THE RETAINED SURFACE

Image analysis was the only means of obtaining subsurface deformation patterns during the excavation process. However, a series of eleven LVDTs was used to monitor surface deformations with measurements taken from the centreline of the model. Comparisons between image analysis data and LVDT output could be used to instil confidence in the accuracy of the two measurement systems.

Modellers at City typically orientated the camera perpendicular to the Perspex window (Grant, 1998; Divall, 2013; Le, 2017), owing to the area of interest being in or near the centre of the strongbox. However, for symmetric half-width excavation projects (McNamara, 2001; Halai, 2018) the area of interest was positioned at one end of the strongbox. It was therefore necessary to view both the excavation event and movements of the retained surface attenuating some distance away from the excavation site. The excavation camera (Figure 6.39) was used in all tests and was located towards the left hand side of the model and angled towards the excavation. Towards the middle of the test series (JP11 – JP15) two cameras were used with the second being angled to capture far field displacements. The common columns of control targets in images from both cameras are indicated by the red and yellow boxes.

A calibration check was performed to first gauge whether the PIV analysis automatically accounted for the new camera position. This was achieved by taking images of a control board with the camera positioned in the centre, perpendicular to the window and repeated with the camera angled towards the window. The Perspex window was put into position and a randomly textured sheet mounted on an acrylic board was pressed against the window. Angles, clamps and slip gauges were used to secure the board in place and provide a reference position, the set-up is illustrated in Figure 6.40. A range of displacements were made in the calibration check for the camera positioned at an angle towards the excavation area and also when the camera was orientated perpendicular to the window. The horizontal displacement contours are presented in Figure 6.41 and Figure 6.42 respectively. Comparisons between the average value PIV computations and LVDTs were made against the slip gauges and are detailed in Table 6.3 and Table 6.4. Although the range of PIV displacements appears to be excessive, there was noise affecting the camera and the slightly uneven

surface of the textured sheet resulted in additional displacements being measured. These are particularly evident in the PIV contour plots in Figure 6.41 and Figure 6.42. Whilst the average error between the LVDT measurements seems unusually high in the calibration of the perpendicular camera, care was taken to calibrate the LVDT prior to use using a screw micrometre attached to an aluminium clamp. It is possible that the footing of the LVDT became loose resulting in a greater degree of freedom and more lateral displacement.

Additional checks at $1g$ were conducted to determine whether measurements taken within the two areas of interest that overlapped by each of the cameras were internally consistent, as shown in Figure 6.43. This was achieved through comparing patches from each camera that either overlapped or were in very close proximity to each other. A similar set up was adopted to that illustrated in Figure 6.39. Table 6.5 summarises the cumulative displacements using slip gauges and the measurements made using an LVDT and the PIV analysis software. The error between the physical measurements and the slip gauge are provided and the results show that, in general, smaller displacements results in a lower magnitude of error. A greater error is noticed for larger displacements, as shown in Figure 6.44 owing to the image processing technique. As explained in Chapter 3, PIV tracks a small patch within the mesh to compute displacements. If the displacement of that single patch is greater than the size of the patch the data is lost and computations cannot progress. This analysis illustrated good agreement between measurements taken in four discrete locations in the overlapping field of view region. The horizontal displacement contour plot is illustrated in Figure 6.45 and similarly with the previous calibration check, slight variations in displacements were found owing to the sheet of paper being adhered to an acrylic board.

Validating the measurements taken at $160g$ was more significant and was performed by comparing PIV measurement with LVDT data. The results from test JP12 have been presented as part of this analysis. Figure 6.46 plots the surface settlement profiles recorded by LVDTs and calculated from PIV analysis at an overburden pressure of 74kPa. LVDTs work over a 10V range and consequently the LVDT resolution of the system at the London Geotechnical Centrifuge facility is $5\mu\text{m}$. The plot demonstrates consistency in displacement trends recorded with both systems however there appears

to be regular peaks and troughs in the PIV measurements that align with the LVDT data. The mesh that was generated for this analysis is illustrated in Figure 6.47, which also provides the control target points and the area of interest. A target mesh generated within an area of interest is perpendicular to the camera frame. However, owing to the obscure angle of the camera, the surface and formation level were not perpendicular to the camera frame therefore the mesh targets representing surface settlements were generated at various elevations. This saw tooth effect resulted in different settlements being recorded with increasing distance from the retaining wall. The x-coordinates of the mesh points at ground surface were interpolated from the location of the control point targets and are indicated in red text in Figure 6.47. These points are represented on the settlement profiles in Figure 6.46 and exhibit a higher level of accuracy of PIV measurements at the surface. Therefore, the PIV results are generally consistent with LVDT data, validating that the PIV system has an accuracy of $5\mu\text{m}$.

Further analysis of the LVDT and PIV data was made between vertical displacements developed at $2H$ with changes in overburden pressure is presented in Figure 6.48. Overall, there is very good agreement between the displacements made using the two systems, however the LVDT shows ground heave occurring at the retained surface for an overburden pressure between 150kPa and 100kPa, as shown in Figure 6.49. This could be owing to a small rotation of the toe of the wall into the formation level which pushed the soil behind the crest of the wall further back, causing it to bulge and heave. This behaviour was not identified in the PIV analysis owing to friction between the soil and the Perspex window.

6.6 SUMMARY

The experiments conducted as part of this project were grouped and details of their successes and failures have been presented. The influence of the various construction techniques on settlements of the retained ground and vertical and horizontal subsurface displacements were presented. The effects on the development and dissipation of excess pore pressures have also been outlined.

6.6.1 Wall embedment and surface settlements

Two wall embedment depths were modelled as part of this series of tests; 55mm and 75mm. The wall profiles were identical and therefore both walls were of equal stiffness. The final surface settlement profile of excavations where a deeper wall embedment was used all showed a noticeable reduction in the magnitude of surface settlements. The accumulation of settlement immediately behind the wall as the excavation progressed was generally reduced by the deeper embedment, however this was not the case for the reference tests and bermed excavations.

6.6.2 Effect of wall fixity on ground movements

Whilst the retaining wall in all excavation simulations was supported by a continuous prop, the wall in the initial series of tests simply rested against the prop which permitted passive failure as the excavation progressed. Later experiments employed a capping beam that secured the wall crest to the prop to assist in delaying failure of the wall. Comparisons between tests indicated that fixing the crest of the wall delayed the accumulation of settlement until at least half of the excavation has been completed. It also reduced the magnitude of heave at the earlier stages of the excavation and reduced maximum settlements by a factor of three.

6.6.3 Influence of construction method on settlements

Five excavation methods were modelled which included a dry excavation; by way of providing a baseline measure, underwater excavation, double walled excavation, bermed excavation and DSM ground improvement at formation level. All methods were shown to offer an improvement over the conventional dry excavation whilst the underwater excavation was the most effective, owing to the largest reduction in nett vertical stress relief. DSM and double walled excavations exhibited comparable behaviour and settlement profiles. A bermed excavation, although developing movements at a rate comparable with the DSM excavation, resulted in a considerably larger settlement profile.

CHAPTER 7 DISCUSSION

7.1 INTRODUCTION

The key findings from this series of centrifuge tests are collated in this chapter to provide an explanation of the behaviour of deep excavations in soft soils with various control measures in place.

Some of the modelled excavation techniques adopted are more commonly used than others. Hence, where appropriate, relevant case studies including; field, experimental and numerical modelling data will be drawn up on as a means of assessing their effectiveness.

7.2 EXCAVATION STIFFNESS SUPPORT SYSTEM

Mitigating deformations associated with deep excavations in soft clay is particularly important in urban areas founded on thick deposits of soft clay. Deformations are governed by factors including the depth of excavation, undrained shear strength of the soil, method of excavation and stiffness of the wall and support system, to name a few. Consequently, the magnitude and extent of ground deformations are a complex combination of basal heave, wall translation, rotation and bending.

Minimising wall deformations is one key measure used to control ground movements and subsequent damage to adjacent buildings (Hsieh *et al.*, 2017). This can easily be achieved by increasing the stiffness of the retaining wall and props. However, in practice, this may not always be regarded as an efficient engineering solution. Hsieh *et al.* (2017) states that auxiliary measures, such as ground improvement and buttresses can be implemented to further reduce wall displacement. Overall, wall deformations can be reasonably well controlled, however the effect of particular auxiliary measures is not clear on controlling heave. Furthermore, surface settlements occurring from an excavation supported by a high stiffness retaining wall can be argued to have occurred entirely from basal heave in the short term undrained case.

This project aimed to investigate the influence of a range of construction methods on heave at formation level and subsequent surface settlements beyond the excavation. It

was therefore necessary for the excavation to be designed with a high stiffness support system which could be installed in a very soft soil sample at 1g. Consequently, the retaining wall was formed from a 10mm stainless steel plate with slots machined along its length so that the final profile consisted of a 1mm thick corrugated wall similar to a sheet piled wall. At prototype scale this wall had the equivalent stiffness of a 1.4m thick reinforced concrete wall. In addition, the wall was uniformly supported with very stiff props along its length from the crest to 25mm above the formation level.

The stiffness of an excavation support system was defined by Clough *et al.* (1989) as

$$S = \frac{EI}{\gamma_w h_{ave}^4}$$

Where S is the system stiffness (kN/m^2), EI is the flexural rigidity (kNm^2), γ_w is the bulk unit weight of water (kN/m^3) and the h_{ave} is the average spacing between props (m). Clough & O'Rourke (1990) proposed a graph, presented in Figure 2.13, that could be used to predict lateral wall deflections based on the system stiffness. In general terms, higher stiffness of the excavation system results in a lower the magnitude of lateral wall deflection, which can further be reduced by increasing the factor of safety against basal heave. Consequently, very high system stiffness of the simulated excavation could arguably eliminate lateral wall deflections.

7.3 EXCAVATION SUPPORT MECHANISMS

7.3.1 Theorised effectiveness of excavation methods

This series of centrifuge tests modelled underwater excavations; deep soil mixing of varying geometries; two berm width excavations and a double walled excavation. A brief definition and summary of the assumed support mechanism for each excavation method is detailed here. Whilst the strength of soil can easily be measured, quantifying the exact influence of each of these methods is not straight forward owing to the variation in stiffness of the ground at formation level. The complex nature and variety of the construction methods used in this series of tests and the interaction between the control measures and soil is difficult to quantify.

7.3.1.1 Underwater excavation

An underwater excavation first involves constructing an embedded retaining wall before excavating the top few metres of soil in a conventional manner. Water is pumped into the void whilst the soil is dredged or jetted underwater and the initial head of water is maintained. A base slab is typically cast in-situ before dewatering the excavation and installing props as necessary.

In theory, this excavation method has the potential to drastically control and reduce ground movements compared to other method as the water in the excavation surcharges the formation level and provides lateral support to the wall. This is shown schematically in Figure 7.1.

During an excavation, the change in vertical stress is a function of the height of excavated soil (H) and the soil bulk unit weight (γ) as defined in equation (7.1). For a head of water equal to the final excavation depth the magnitude of the change in overburden stress will be reduced to equation (7.2). Assuming that the bulk unit weight of soil is approximately 16kN/m^3 and the unit weight of water is 10kN/m^3 , then the unit weight of water is equivalent to 60% of the soil bulk unit weight. Therefore the total magnitude of the change in vertical stress is given by (7.3). To provide context for this, a 12m deep excavation full of water will have undergone a reduction in vertical stress of approximately 75kN/m^2 at formation level compared with 200kN/m^2 experienced during a conventional excavation.

$$\Delta\sigma = \gamma H \quad (7.1)$$

$$\Delta\sigma = (\gamma - \gamma_w) H \quad (7.2)$$

$$\Delta\sigma = 0.4 \gamma H \quad (7.3)$$

In addition to the large reduction in vertical stress relief, the water in the excavation also provides horizontal support to the retaining wall, given by equation (7.4). This acts at a depth of $2/3H$.

$$P_w = 1/2 \gamma_w H_w^2 \quad (7.4)$$

In the context of the model tests conducted the passive resistance afforded to the retaining wall during an underwater excavation for 55mm wall embedment is

illustrated in Figure 7.2. In addition to the 708kN/m lateral pressure 50mm below ground level, there is a combined passive force of 1450kN/m acting approximately 25mm below the formation level. Considering that the active pressure of 1518kN/m acts 87mm below ground level, it is reasonable to assume that the passive resistance provided in this underwater excavation are sufficiently large to counteract overturning moments.

7.3.1.2 Deep soil mixing

Deep soil mixing (DSM) combines a strengthening additive, such as cement or lime, with the soil. The improved zone can comprise columns in various arrangements or as a mass block. The mixing process is carried out in-situ and the depth of treatment typically extends from the formation level to the toe of the retaining wall with the excavation commencing post treatment.

The undrained shear strength of the treated soil improves as DSM ground improvement treatment cures. This in turn increases the stability of an excavation against rotational failure of the retaining wall as the passive resistance below the formation level increases. In addition, the higher unconfined compressive strength of the soil would provide a higher degree of lateral restraint against passive failure along the embedded length of the wall as it behaves like a prop, as illustrated in Figure 7.3.

The passive forces that are provided by an area of DSM ground treatment is entirely dependent on the geometry of the DSM block, see Figure 7.4. Where the DSM zone does not extend across the full width of the excavation, it is assumed that passive pressure develops behind the ground treatment. This is owing to the stiffer behaviour of the lime-stabilised clay block which allows the soil behind it to deform independently. Consequently, a deeper ground improved area could be expected to develop larger passive pressures in the soil behind the lime stabilised block. The horizontal component, considered as a point load prop force, reacts at a greater depth below formation level with a deeper DSM block. Therefore, although there was a negligible difference in the cross sectional area of treated ground, the passive resistance provided by varying the DSM geometry clearly indicates that a significant improvement could be achieved with a deeper and narrower DSM block.

7.3.1.3 *Berm*

A berm comprises a mass of soil that remains against the perimeter wall as the site is excavated, as shown in Figure 2.74. The localised surcharge resulting from the berm on the excavation formation level stabilises the embedded retaining wall as it results in an increase in passive earth pressure along the embedded length of the wall. The height of the soil berm above formation level can also offer lateral support and contribute to the control of wall deflections; as illustrated in Figure 7.5.

Contrary to underwater excavations, berms only surcharge the formation level directly below the soil mass. The effectiveness of the support provided by soil berms of constant volume was reported to be dependent on berm height as opposed to berm width (Potts *et al.*, 1993). The trapezoidal shape of the berm results in an unevenly distributed load across the formation level. In addition, the lateral pressure applied to the wall would also be much less effective at ground level compared with at formation level, with larger lateral pressure developing with depth.

In reality a soil mass exists against the wall, however the berm modelled in these experiments used only a shallow airbag. Therefore, the horizontal component of lateral resistance from a soil berm was not modelled in the centrifuge and is not considered in Figure 7.6. The behaviour of a bermed excavation could potentially be regarded as being similar to a ground improved excavation where the DSM block extends to the toe of the wall and across two-thirds of the excavation.

7.3.1.4 *Double wall*

The term ‘double wall’ is defined in this thesis as an excavation with a secondary lower stiffness ‘slurry’ wall placed in front of the primary retaining wall. The method of construction would involve installing the primary and secondary retaining walls prior to excavating the soil. The plastic deformation mechanism for such a system could be expected to be larger than that of an excavation without any support, illustrated in Figure 7.7. This would increase the stability of the excavation as the undrained shear strength of the soil would be mobilised over a greater perimeter. In addition, the shear strength in the block of soil between the two walls would need to be mobilised before the passive pressure behind the secondary wall is mobilised. This would contribute to stability of the excavation as the overburden pressure was reduced.

The passive resistance mobilised during a double walled excavation are illustrated in Figure 7.8. It was assumed that passive pressure would develop behind the secondary wall and that the soil block between the two would not be mobilised. In view of this, the compressive strength of the internal soil block was assumed to act along the shallowest length of wall whilst the soil mass was assumed to behave as a prop. The magnitude of the passive resistance developed is comparable with that of an underwater excavation, with the exception of the lateral force acting against the exposed length of the wall owing to the pressure of the water.

7.3.1.5 Summary of effectiveness of various excavation methods

In summary, the construction methods outlined above are all though to increase the stability of an excavation. This may be achieved by one or a combination of the following means:

- Increasing the passive pressure in front of the toe of the embedded retaining wall
- Surcharging the formation level
- Providing lateral restraint to the exposed face of the wall.

Considering the assumed deformation mechanisms resulting from each construction method in turn it would be reasonable to assume that an underwater excavation should provide the greatest level of support, owing to the much reduced vertical stress relief. Instinctively, the berm would be expected to provide a degree of support to the excavation owing to the vertical and horizontal stresses applied. The effectiveness of the surcharge decreases with distance from the wall and although the expected failure mechanism may be comparably wider than an excavation without any surcharge, it would not necessarily provide a significant amount of additional support to the excavation. The movements arising from an underwater excavation would intuitively be considerably less than those observed from an excavation supported by a berm.

With respect to increasing the lateral stability of the excavation, it could be argued that ground improvement at the toe of the wall should be more effective than a double walled excavation. This is owing to the strength of the DSM treated soil which would be higher than the strength of the virgin soil. The DSM soil would therefore be better able to resist soil deformations and rotation of the toe of the wall into the excavation.

The relatively low undrained shear strength of the soil in the centrifuge models suggests that a wider plastic deformation mechanism attributed to a double walled excavation (Figure 7.7) would not have significantly influenced the stability of the excavation. A double wall could therefore not be expected to provide comparable results to an excavation treated with ground improvement techniques.

The passive resistance generated during the excavation suggests that construction using a deep and narrow DSM block is potentially capable of developing larger passive pressures at a greater depth than the other DSM geometries. The subsequent failure mechanism would need to be mobilise soil in the treated soil zone, with a higher undrained shear strength, in order to achieve significant deformation. The magnitude of heave measured near to the strongbox walls would be expected to be lower than heave measured nearer to the retaining wall owing to boundary effects.

Image analysis was used to determine displacements across the formation level up to 25mm away from the soil-strongbox boundary interface. This was owing to the angle of the camera which resulted in poor image resolution close to the boundary. It should be noted that in the early analysis the meshes close to the strongbox boundary were omitted as the correlation coefficient factor fell below 80%. Consequently, the deformation profiles of the excavation formation level typically show that there is a progressive increase in the magnitude of heave at greater distances from the retaining wall. This trend of soil displacements at the formation level could be expected and can therefore be said to be a reasonable representation of the soil response to vertical unloading during an excavation.

7.4 HEAVE AT FORMATION LEVEL

Although LVDTs were used to measure settlements of the retained ground, image analysis was the only means of determining the soil displacements at and below the formation level. Results from image analysis were used to monitor heave at the formation level at varying distances from the retaining wall. Displacements measured at an overburden pressure of 50kPa will be presented in this section to provide comparison across all tests.

The excavation process caused significant change in vertical stress at the formation level and resulted in the generation of negative excess pore pressures directly beneath the excavation. As the distance from the excavation increases, the magnitude of excess pore pressure decreased.

Simulation of an excavation was achieved by reducing the air pressure in a latex bag that was surcharged the formation level. Image processing data was used to monitor the development of heave as the excavation progressed. Displacements from test JP18, at varying overburden pressures, have been plotted in Figure 7.9 and gives a clear indication of the development of heave across the formation level at various stages of the excavation. The greatest movements occurred when the overburden pressure was reduced from 100kPa to 75kPa. The formation level appears to have continued to heave as the pressure was further reduced by 25kPa to 50kPa however the change in additional heave was less pronounced. Additional displacements accrued in the final excavation stage although these were negligible.

Soil settlements occurring immediately adjacent the retaining wall were owing to the wall displacements. As the excavation progressed the change in overburden pressure at the formation level decreased and the retained ground settled. Therefore, the expected deformation mechanism would be akin to that illustrated in Figure 7.10.

In addition, the stainless steel wall used in these tests had a much higher bulk unit weight than the soil and could be expected to settle regardless of excavation. The bracket used to hold the crest of the wall in JP18 permitted vertical movements and up to 2mm lateral movement. Therefore, as the net movement of retained soil was down and angled towards the toe of the wall, the crest of the wall could be expected to rotate about the lowest prop into the retained soil, whilst the toe of the wall rotated into the formation level. Owing to the shape of the wall, the interaction between the soil and wall resulted in the soil plugging between the ribs and adhering to the stainless steel surface. As the wall settled and rotated into the excavation the retained soil immediately adjacent the retaining wall settled as it has adhered to the wall during consolidation. Similarly, as the toe of the wall rotated into the excavation, the soil immediately adjacent the wall at formation level settled, as this too had adhered to the wall whilst the soil some distance from the retaining wall heaved; as schematically described in Figure 7.11. This intimate contact area between the soil and wall

essentially extends beyond the physical interface between the two materials which will be defined here as the zone of influence. Referring back to the vertical displacements across the formation level in Figure 7.9, the zone of wall-soil influence appears to extend approximately 20mm into the excavation. Beyond this, the retaining wall no longer influenced the behaviour of the formation level and, as expected, the formation level heaved.

Figure 7.12 shows vertical displacements at extreme positions on the formation level; immediately adjacent the retaining wall and at the far end of the strongbox against the change in overburden pressure. Displacements near to the retaining wall were measured at distances of 13mm and 22mm, whilst the other data points are representative of displacements at distances of 120mm and 130mm into the excavation. Adjacent the retaining wall, the formation level was shown to have settled and heaved within a distance of 9mm. This confirmed that the zone of influence did indeed extend as far as 20mm from the retaining wall. Vertical displacements occurring as the excavation progressed were first observed at an overburden pressure of 140kPa at distances of 13mm, 120mm and 130mm. This suggests that as the wall settled a deep seated mechanism developed relatively early in the excavation. Soil displacements rapidly evolved as the overburden pressure dropped from 100kPa to 70kPa and although additional movements developed as the excavation neared completion they were negligible in magnitude.

The profile of the retained surface and the excavation formation level determined from image analysis as the excavation progressed is given in Figure 7.13. At the end of the excavation, it is clear that the soil in contact and close to the wall was influenced by the presence of the wall. This is particularly evident as the soil either side of the wall settled and the magnitudes of each were similar. As the distance beyond the excavation increases the magnitude of soil settlement increases up to distance H , in keeping with the profile proposed by Hsieh & Ou (1998).

Excavations in clay typically lead to movements first developing at formation level. This is owing to the unloading at formation level which in turn allows the ground to swell. Initially, therefore, displacements at formation level are not necessarily driven by the weight of soil on the active side of the excavation. At the earlier stages of the excavation the undrained shear strength of the clay, particularly in the retained soil, is

not mobilised. Therefore, it is reasonable to expect that as the excavation commences movements would initially be observed at the formation level. In addition to this, the bulk unit weight of the wall, plugged with soil, was approximately 27.5kN/m^3 ; this is 70% higher than the bulk unit weight of soil. Logically the wall would settle before settlements of the retained soil occurred. To assess whether the soil in the intimate contact zone moved prior to the soil extending beyond this zone, displacements at six discrete locations were analysed. These positions are illustrated in Figure 7.14 and Figure 7.15 shows the development of vertical displacements of the crest and toe of the wall in addition to the retained soil and formation level during the simulated excavation. Owing to the position of the on-board miniature camera, the extreme positions across the formation level that were measureable were at $-0.2H$ and $-1.6H$. Taking the retaining wall as a centreline, displacements of the retained surface were also plotted at distances of $0.2H$ and $1.6H$. The magnitudes of settlement of the toe of the wall and soil at formation level ($-0.2H$) were comparable. Similar behaviour was observed at the retained surface with settlements at a distance of $0.2H$ equal to the settlement of the crest of the wall. This was consistent with the assumption that the zone of influence exists on both sides of the retaining wall. Figure 7.15 suggests that the general mechanism of movement illustrated in Figure 7.11 is representative of the displacements recorded in these experiments. The magnitudes of settlement at the toe and crest are not equal owing to the horizontal movement recorded at the toe of the wall (Figure 7.16(b)) which was driven by the active wedge that caused the wall to rotate about the lowest prop. The prop acted below the midpoint of the wall, therefore as the wall settled and rotated about the prop it was displaced laterally by a greater magnitude than the crest of the wall. Consequently, the settlement at the crest could be expected to be larger than those observed at the toe of the retaining wall.

Although the targets appear to show that the wall deformed laterally at a depth of 150mm it is highly unlikely as the apparent deformation profile is grossly excessive for a retaining wall of this stiffness. The typical profile given by O'Rourke (1993) in Figure 7.16(a) shows that a flexible wall deforms below the lowest prop with the maximum deflection at near to formation level. Figure 7.16(b) was obtained from PIV analysis and shows the deformation of the wall at the end of the excavation. It suggests that a maximum deflection of 2.5-3mm occurred 25mm below formation level. Whilst this is plausible for a flexible wall, the retaining wall used in this series of tests was

considerably stiff. Furthermore, if the retaining wall had deflected by this amount it would have resulted in plastic deformation of the retaining wall that would be evident when recovering the wall from the model post-test; this was never observed. The measured wall deformations obtained from image analysis were likely a consequence of the silicone seal deforming as opposed to the wall. This was particularly evident when the model was disassembled and the wall side channel, designed to house the silicone seal flange, was clogged with clay and had obviously allowed the silicone seal a greater degree of freedom to move. Based on this, the predicted lateral movement of the toe of the wall is represented in Figure 7.16(b) by the purple dashed line. This suggests that the toe of the wall rotated by approximately 4mm whilst the crest rotated into the retained soil by 1mm. Whilst the crest of the wall settled by up to 1.5mm the larger horizontal component of movement would result in reduced settlement. As the magnitude of settlement at $-0.2H$ at the formation level was comparable to the settlement of the toe, it is reasonable to assume that the soil in this location was within the intimate contact zone.

Whilst Figure 7.15 investigated the soil and wall response for the duration of the excavation, Figure 7.17 focussed on vertical movements that occurred during early stages of the excavation. The purpose of this was to establish which part of the soil model first responded to the simulated excavation. Having established that the magnitude of displacements between the wall and the soil in the zone of influence were comparable, the displacements of the retaining wall crest and toe have been plotted alongside displacements at $1.6H$ between the start of the excavation and an overburden pressure of 120kPa. There is considerable noise in the analysis and it is not possible to conclusively state whether the wall first settled or the retained ground. The results do however show that the magnitude of settlement at the toe was less than the crest, which is consistent with the theory that toe was displaced laterally more than the crest. It is certainly possible that owing to the very soft soil, the retained ground responded immediately to the excavation and the retaining wall settled simultaneously.

7.4.1 Influence of embedment depth on heave

Irrespective of the construction measures in place, a greater magnitude of heave would be observed at formation level where shallower wall embedment depths exist. The results typically conform to this theory and also show that any of the various construction methods employed offer some means of controlling heave.

For the purpose of evaluating the influence of embedment depth on heave, the effects of an unimproved excavation (reference test) will be compared against excavations with additional stiffening properties (double wall) and surcharging (underwater) at formation level. Plots of the magnitude of heave from the formation level to depths and varying distances across the formation level are given in the following figures.

Although the quality of images taken for the use of PIV analysis in experiment JP7 were not high-quality and the mesh generated in the analysis was limited (Figure 7.18) data from the second row below formation level were used in the analysis. Figure 7.19(a) and (b) gives the magnitude of heave from formation level to a depth of about 100mm at varying distances from the retaining wall. A wall embedment depth of 55mm resulted in excessive settlement adjacent the wall but this was quickly reversed as the distance into the excavation increased. The analysis of vertical movements below formation level in JP7 at an overburden pressure of 50kPa showed very little settlement close to the wall whilst the trend was generally to heave. As expected, the magnitude of vertical displacement at depth was less than at formation level for both deep and shallow wall embedment. Owing to the lack of additional support from surcharging or ground improvement, the vertical displacements of the soil with depth were linear. Interestingly the rate at which the magnitude of vertical displacements developed for shallow wall embedment was twice that of an excavation with deeper embedment. Consequently, maximum heave measured in these experiments for 55mm and 75mm embedment were approximately 1.5mm and 1mm respectively.

Figure 7.20 compares the heave profiles of the reference tests at an overburden pressure of 50kPa. Although the results from JP7 tend towards a constant value from $0.5H$ onwards, the heave measured in JP9 reaches a peak at around $0.8H$ before plateauing at a value similar to that measured in JP7. This decrease in heave towards the edge of the strongbox is probably a result of friction effects at the boundary.

The soil response of the underwater tests highlighted that deeper wall embedment restricted the magnitude of heave at the formation level by about 50%, as illustrated in Figure 7.21. The trend of movement was typical of soil displacements during an excavation with significant heave at formation level, owing to soil softening, however little was observed at depth as a result of the magnitude of surcharge. Flooding an excavation with water reduced the magnitude of heave, measured in JP6, by approximately 30% compared with that measured in a reference test with comparable wall embedment (JP9). As the change in vertical stress in the underwater excavation was 40% of a conventional excavation it is reasonable to state that surcharging an excavation formation level is a very effective means of controlling ground movements. The heave observed in an underwater excavation may be construed as excessive, however the very soft state of the soil and the addition of water into the excavation is likely to have contributed to this magnitude of heave. This however was only observed at the formation level but did not continue to progress with depth below the excavation.

To observe the influence of increasing the stiffness of the soil at formation level, the results from JP13 and JP18 were plotted at the same scale, see Figure 7.22(a) and (b) respectively. The analysis shows comparable settlement immediately in front of the retaining wall irrespective of the primary wall embedment depth. As expected, the trend of movements is such that a greater magnitude is observed at formation level, decreasing with depth. Owing to the spread of displacements in Figure 7.22(b) an obvious change in the magnitude of heave at a depth of 75mm was noted. Below 75mm there is a constant value of heave, however as the depth to formation level decreases the magnitude of heave steadily increases. This indicates that the presence of the secondary wall can reduce the development of movements at depth.

The heave profile at the end of the excavation was plotted in Figure 7.23 and shows that soil displacements in close proximity to the primary retaining wall were smaller for deeper embedment, however with increasing distance from the retaining wall the embedment of the primary wall had a negligible effect on controlling the development of heave.

7.4.2 Impact of fixity conditions on ground movements

Owing to the low strength of soil, the stiffness and weight of the retaining wall it was expected that settlements should be observed close to the retaining wall. However, an evaluation of the influence of fixity conditions on the development of heave at formation level was established using data from tests JP7 and JP11. Figure 7.24 illustrates vertical soil displacements below formation level plotted on the same scale. The results show that at a comparable overburden pressure the heave in a cantilevered excavation linearly increased at a rate of 0.01mm per 1mm depth below formation. However, fixing the crest of the wall significantly controlled heave such that the displacements at depth were comparable to those at formation level. Figure 7.24 indicates that very little settlement was recorded adjacent the wall in test JP7 compared with that measured in JP11. As such, it can be argued that restraining the crest of the wall reduced the magnitude of heave by up to 20%.

However, Figure 7.25 (test JP7), illustrates the heave profiles at 50kPa for both tests and show that settlement adjacent the wall gradually reverses and heaves with distance into the excavation. On the other hand, the magnitude of soil displacements in tests JP11 at 50kPa are $\pm 100\mu\text{m}$ and fluctuate between heave and settlement. At an overburden pressure of 25kPa the excavation in JP7 failed and the formation displacements are plotted (Figure 7.26). The formation level continued to heave in JP7 but little additional movement was observed in JP11, with the exception of some settlement adjacent the wall; this was owing to the settlement of the wall at the low overburden pressure.

7.4.3 Limiting the width of ground improvement or surcharge on excavation formation level

Two of the excavation methods; including DSM and berms, involved varying the control measure widths to ascertain its effect on ground movements. The vertical displacements with depth and distance from the wall are plotted in Figure 7.27 and Figure 7.28 respectively.

Where the control measure acted across the formation level (test JP10, Figure 7.27(a)) comparable heave was observed at depths of up to 40mm below formation level. This aligns with the underside of the lime-stabilised zone. Vertical displacements above this level are shown to rapidly increase which is expected owing to the stiffening effects offered by the DSM block which controlled excessive displacements that would otherwise develop at depth. In addition, the magnitude and trend of heave were generally consistent across the formation level. However, for ground improvement $2B/3$ wide the trends of movements were comparable to the reference test, as settlements were observed adjacent the wall and gradually increased with distance into the excavation. Further reducing the width, but deepening the level of treatment to 112mm below formation level, prevented vertical movements at depth but up to 3.5mm of heave was recorded at the surface. This indicates that the presence of a lime-stabilised block of soil supporting twice the embedded length of a retaining wall influences the deformation mechanism of the wall and the associated heave is a direct result of the vertical unloading during the excavation.

Figure 7.29 presents heave profiles at an overburden pressure of 80kPa for the DSM geometries. Similar trends are noted for treatment widths of B and $2B/3$ suggesting that deformation mechanisms are not influenced by these geometries. However, there is a clear increase in the magnitude of heave at approximately a third of the width of the formation in test JP15. This is evidence of the influence the deep DSM block has on controlling heave, particularly in close proximity to the retaining wall.

Owing to the apparatus and electrical failures experienced during the berm tests data has been plotted when the overburden pressure in the main excavation bag reached 80kPa. The magnitude of heave across the entire formation level was smaller for a narrower berm width, consistent with the findings of Potts *et al* (1993). However, the presence of a berm resulted in large settlements adjacent the wall as illustrated in Figure 7.30. This suggests that a concentrated surcharge placed directly in front of the wall supports the toe of the wall, preventing rotation into the excavation and subsequently reduces the magnitude of heave at formation level.

7.5 SOIL SETTLEMENTS OF RETAINED SURFACE

Controlling surface settlements is perhaps the most crucial factor when performing excavations. Displacements of the retained ground are influenced not only by the excavation process but also by the construction methods in place to mitigate them and the stiffness of the support system. Greater surface settlements occur during an excavation with a flexible cantilevered wall compared to an excavation with a stiffer propped retaining wall. The surface settlements measured in this series of tests will be discussed in this section.

Of the construction methods explored the underwater excavation offered the most efficient solution in terms of limiting surface settlements of the retained ground, as illustrated in Figure 7.31 where the profile is indicative of the retained ground after full removal of the overburden pressure. This method was also shown to be more effective at mitigating surface settlements with shallow embedment compared with other methods where a deeper retaining wall embedment existed. This was expected owing to the significant reduction in overburden pressure where nett unloading was equivalent to an excavation 4.6m deep, applying a surcharge of 74kPa to the excavation formation level. It is though that considering the final surface settlement profile of the underwater excavations against the profiles of other methods subjected to an overburden pressure of 74kPa would provide a suitable basis for comparable results of the efficacy of the various excavation methods.

Comparisons between surface settlement profiles of the underwater excavation and reference tests at an overburden pressure of 74kPa are plotted in Figure 7.32. As expected, the results show a greater magnitude of settlement for the reference tests with the exception of JP3. The much reduced settlement profile of JP3 was owing to the higher strength of the sample than the average strength. This variation in undrained shear strength occurred because of failures in supplying water to the sample during the initial in-flight consolidation stage. At an overburden pressure of 74kPa the trend of the settlement profile in test JP3 was remarkably similar to that of test JP8 for an embedment depth of 75mm. The maximum settlement occurred at distance H behind the wall which steadily reduced up to a distance of $3H$; settlements were negligible beyond this. In reference tests JP7 and JP9, of 75mm and 55mm embedment respectively, marginally greater settlements were observed for the shallow wall

embedment. This is surprising as the influence of the deeper wall embedment was shown to result in heave approximately a third of the magnitude of that measured in the 55mm wall embedment tests (Figure 7.20). A narrower settlement profile was obtained from data in test JP7 owing to LVDT failure and poor resolution images, but suggests that the settlement profile is wider with a less defined peak at distance H behind the wall. Therefore, it could be expected that the movements associated with an excavation without construction support systems in place would be noticeable beyond $3H$. On the other hand, the settlement profiles for 55mm wall embedment for the reference and underwater excavations followed a similar trend where displacements at the soil and wall interface were nominally smaller than the maximum displacement at H . The influence of pinning the crest of the wall (JP11) was shown to significantly reduce settlements immediately behind the wall, which was owing to a more stable excavation and settlements were comparable with those observed from an underwater excavation of equal wall embedment.

Comparing the passive forces acting on the retaining wall in tests JP6 and JP9 provide an explanation to the trend in the surface settlements of these two methods. Figure 7.33 illustrates the pressures and it was noted that the passive pressure acts at similar depths below the retained surface. The magnitude of the reference test passive pressure in test JP9 was approximately 20% lower than that of JP6 which resulted in a 55% increase in surface settlements. The correlation suggests that for a reduction in lateral force acting at the same depth there is approximately twice as much settlement.

Figure 7.34 and Figure 7.35 illustrate the influence of increasing the stiffness of the formation level on surface settlement troughs arising from double walled and DSM improved excavations. The influence of the two methods of fixing the retaining wall crests on settlements are also illustrated in Figure 7.34. The similarities between the settlement profiles of JP12 and JP13 for a pinned and capped wall is owing to the small magnitude of vertical displacement. At lower overburden pressures the wall settled and in test JP12 lost contact with the pins. Therefore, the ultimate settlement profiles differ; however, at 74kPa the comparable profiles were attributed to the consistency of the modelling and sample preparation techniques. The settlement profiles of the double walled tests and the underwater excavation JP6 were within $\pm 25\mu\text{m}$ and this may be owing to the location at which the measurements were taken. In the

underwater test LVDT data was used whereas the higher quality of images taken in the latter part of the experimental testing stage meant PIV analysis could be performed with confidence. Therefore, at the Perspex window there would inevitably be boundary effects and this could result in the difference in measurements. Considering the passive forces acting in each scenario, it is surprising that comparable settlements were observed as a result of doubling the passive resistance in the double walled tests. Attempts were made to flood the excavation in test JP20 and consequently the magnitude of settlements followed the same trend and were approximately half of that measured in test JP6. However, owing to a blockage in the direct water feed the correct rate of flooding was not achieved. Consequently, the exact pressure applied to the formation is not known. However, the images show that at an overburden pressure of approximately 90kPa the airbag had deflated sufficiently to allow the standing water to seep through to the base of the excavation. Hence, it can be said with certainty that at an overburden pressure of 74kPa the formation level was partially surcharged which explains the reduced settlement profile of test JP20.

Where a slurry wall was installed in front of a deep retaining wall (JP18), the magnitude of the settlement profile was approximately half that of the underwater test with similar embedment. The lateral forces in the double wall would be slightly larger than those developed for a shallow wall embedment owing to the same embedment of the primary and secondary walls employed in all tests. Therefore, this shows that the embedment of the primary wall plays a significant role in controlling the magnitude of the settlement trough, although the extents of movement were similar.

Figure 7.35 illustrates the influence of a lime-stabilised block of soil at formation level on the retained soil settlement profile. The profiles from all DSM arrangements indicate that they have an equal or improved effect on reducing the magnitude of surface settlement. Test JP10, in which shallow treatment extended across the formation level, showed a settlement profile similar to the reference test from distance H beyond the wall. This was expected as this arrangement developed lateral forces that were approximately 25% lower than those developed in the underwater excavation JP6. Increasing the passive resistance in JP14 by 5% of those in JP6 reduced the magnitude of the settlement profile by an average of 30% with a significant reduction at large distances from the excavation. In test JP15 the largest

lateral forces were developed and consequently the settlement adjacent the wall is half the magnitude of those measured in JP6. However, as the distance from the excavation increased, the vertical displacements did not continue to decrease at a constant rate. Instead, the settlement trough was shown to be more level and followed the trend of movements observed in JP6 at a distance of $1.5H$. This is not necessarily illustrative of a less effective construction technique as differential settlements can ultimately be more controlled and subsequent damage to neighbouring structures less severe.

Although the bermed excavations heave profiles were inconclusive, the observed settlement profiles show interesting results in Figure 7.36. The settlement profiles are representative of the ground movements associated with the unloading of the main excavation to an overburden pressure of 80kPa, whilst the berm bag applied a surcharge of 100kPa. Vertical displacements of the retained soil for berm widths spanning a third of the excavation model, for both deep and shallow wall embedment, showed a very strong correlation to those measured at the end of the underwater excavation. This is owing to comparable passive forces acting at the same elevation in both excavation scenarios. However, the behaviour of the soil in response to a wider berm was shown to result in larger settlement. Only data from PIV analysis could be used owing to water damage of LVDT instrumentation and electrical equipment, including the lighting and data logger. Issues with the lighting led to an increase in exposure (Figure 7.37) hence the surface settlement data obtained from the analysis was substandard and of poor quality. For this reason, data from test JP17 will be omitted, however it is expected that a larger berm would help reduce the magnitude of settlements of the retained ground.

Evidence of the effectiveness of underwater excavations became apparent early in the test series and an attempt was made to ascertain whether an additional control measure could be implemented with the underwater excavation to further reduce vertical displacements of the retained surface. Owing to difficulties faced in modelling berms it was deemed unfeasible and unrealistic to model a submerged bermed excavation. Therefore, double walled and DSM excavations were modelled with a 55mm embedded retaining wall. Their effect on surface settlements are illustrated in Figure 7.38 and show that where a double wall is present the settlements developed beyond H are akin to those in the underwater test with 75mm embedment. The fact that the

settlement profile of JP21 closely follows that of JP8 gives validity to test JP20, where a double wall was tested and a small surcharge of water was applied to the formation level (Figure 7.34). Tests JP22 suggests that additional benefits can be obtained by combining double walled construction methods with an underwater excavation, as the magnitude of settlement immediately behind the retaining wall would be reduced. However, test JP21 suggests that DSM used in conjunction with an underwater excavation has little to offer in terms of mitigating surface settlements.

7.6 SOIL MODEL SHEAR STRENGTH PROFILE

The primary aim of this research was to investigate heave and ultimately settlement profiles in very soft ground resulting from deep excavations. It was therefore of paramount importance that the soil model was subjected to an appropriate stress history in order to achieve a low strength sample.

The behaviour of soil is governed by its stress history and current stress. Empirical formulae have been published as a means of estimating the strength profile of Speswhite kaolin; these are given below in Equations (7.5) to (7.8).

$$\text{Phillips (1987):} \quad S_u = 0.19 \sigma'_v (OCR)^{0.67} \quad (7.5)$$

$$\text{Stewart (1989):} \quad S_u = 0.22 \sigma'_v (OCR)^{0.57} \quad (7.6)$$

$$\text{Springman (1989):} \quad S_u = 0.19 \sigma'_v (OCR)^{0.71} \quad (7.7)$$

$$\text{Garnier (2002):} \quad S_u = 0.19 \sigma'_v (OCR)^{0.59} \quad (7.8)$$

Alternatively, the undrained shear strength of soil can be physically obtained from shear vane readings. Gorasia (2013), Divall (2013) and Halai (2018) had successfully reported the consistency of shear strength profiles using this method.

Owing to the model requirements it was necessary to produce a very soft sample, however it was equally critical to form accurate and consistent models as part of this project. Achieving clean square cuts in a very soft sample would not be possible. Therefore, following 1g consolidation up to 100kPa the sample was trimmed to a height of 290mm and left to consolidate in-flight at 160g overnight. A water table was established 10mm above the soil sample which ensured that the sample remained

saturated and a lid was bolted to the top of the model to prevent any standing water from evaporating. During model making the soil sample was trimmed again to give a final sample height of 255mm. The effective stresses and the trimming heights of the sample were presented in Figure 5.1.

Equations (7.5) to (7.8) were used to predict the strength of a soil sample that had been subjected to these stresses. These were compared against the actual shear strengths in each test measured using a shear vane in four locations behind the retaining wall. The purpose of taking up to four shear vane readings was to obtain a representative undrained shear strength profile through the model rather than rely on a single set of data that could potentially be erroneous. All four empirical formulae over-predicted the undrained shear strength of the soil models however Garnier (2002) and Phillips (1987) provide an upper envelope for the soil strengths. This was similarly noted by Mair (1979) and Le (2017) whose models were also consolidated to very low stresses. Mair (1979) explained that the lower measured strength was a consequence of cavitation, which developed from the complete removal of the overburden stress when the model was decelerated to $1g$. The sudden reduction in total stress on a clay model results in the generation of negative pore pressures. These should equal the mean total stress in order to maintain the same effective stress. There is however a negative pore pressure limit which the soil can sustain (Powrie, 2004). Mair (1979) explained that cavitation occurs when the pore fluid in samples consolidated to pressures less than 100kPa are unable to sustain the negative pore pressures and some of the air in the soil evaporates. This factor contributes to the reduction in the undrained shear strength of the soil. The S_u/σ'_v ratio obtained from the measured undrained shear strengths was calculated to be between 0.15-0.2 and is annotated in Figure 7.39. This value is consistent with field data taken from soft clays (Low *et al.*, 2010).

The computed S_u values from Phillips (1987), Stewart (1989), Springman (1989) and Garnier (2002) consistently estimated higher undrained shear strengths than those measured. Therefore, using critical state soil mechanics (Schofield & Wroth, 1968) an estimate for the strengths was made;

$$S_u = \frac{M}{2} \exp\left(\frac{\Gamma - v_0}{\lambda}\right) \quad (7.9)$$

where M , Γ and λ are soil properties of Speswhite kaolin and are given in Table 3.2. The specific volume, v_o , was computed from water contents taken at three depths in the model. Comparisons between measured shear vane readings and computed undrained shear strengths from a selection of the various tests are presented in Figure 7.40. Reasonable agreement was demonstrated between the water content calculations and shear vane readings, indicating that the empirical formulae are not representative of undrained shear strengths in soft ground where evaporation during in-flight reconsolidation has been eliminated through the use of PlastiDip.

7.7 FAILURE MECHANISMS

Part (a) of Figure 7.41 to Figure 7.43 are photographs of the excavation formation level taken post-excavation. These illustrate the shear planes that had formed in the clay model at failure during the simulated excavation. Images include the reference test (JP7), a double walled excavation (JP12) and all three DSM tests (JP10, JP14 and JP15). The visible shear planes were traced onto a clear sheet of acetate and these are presented as thick black lines in part (b) of Figure 7.41 to Figure 7.43.

Compatible failure mechanisms were sketched over these failure surfaces in an attempt to establish whether the various methods of excavation affected the mechanism. The same driving mechanism exists for each method of excavation however the extent of the mechanism is influenced by the method of excavation. For a conventional unimproved excavation a fan mechanism developed through the soil, from ground level through to the formation level, with the centre of the fan being immediately adjacent the retaining wall at the formation level. The radius of the fan is equal to the height of the excavation, therefore the fan mechanism is entirely present in the soil, as shown in Figure 7.41(b). For an improved excavation, a 270° fan mechanism also exists, however the radius of the fan can reasonably be expected to extend as far as the corner of the secondary wall, illustrated in Figure 7.42(b). In these tests, the embedment and distance of the double wall from the retaining wall remained constant, therefore at prototype scale the minimum radius is 13.5m. Where DSM is present, the mechanism extends further to avoid shearing through the stronger soil. In test JP14, the failure mechanism clearly demonstrated this and subsequently, the

radius of the failure mechanism was defined as the width of the treated zone, as shown in Figure 7.43.

The mechanisms have been analysed as upper bound solutions using a series of fans with a common centre. The radius of each of the mechanisms is dependent on the method of construction and can be defined as Equation (7.10);

$$H_c = \frac{2\pi R \left(S_{u1}/2 + S_{u2} \right) - N}{R\gamma} \quad (7.10)$$

Where H_c is the height of soil excavated at failure, H_{exc} is the intended formation level, S_{u1} is the average undrained shear strength above the intended formation level, S_{u2} is the average undrained shear strength below the formation level, N is the load factor determined from the external work done based on the radius of the mechanism (R) and γ is the bulk unit weight of the soil. The general failure mechanism is illustrated in Figure 7.44.

For each of the various excavation methods estimated failure heights that were between 10-50% greater than those simulated by centrifuge model tests. Details can be found in Appendix A.

Comparisons were drawn between the actual depth, at prototype scale, of soil excavated at failure in the centrifuge models, the theoretical depth based on the new stability number determined from the upper bound mechanisms described in the previous paragraph; where the radii was dependent on the method of excavation, and the failure depth based on the stability number defined by Peck (1969). The results, presented in Table 7.1, demonstrate that the stability number defined by Peck is not appropriate for use in this simulation as the ratio of estimate to actual failure excavation height is less than unity. Consequently, the mechanism that was developed following various excavation simulations was shown to be more representative of the actual behaviour observed in the tests.

7.8 EXCAVATION FAILURE PRESSURE

Whilst the main aim of this study was to investigate the influence of specific excavation techniques on ground movements developed at the retained surface, it was

found that, owing to the incredibly soft soil, excavation failure often occurred. For this reason, it was important to ascertain the overburden pressure at which the excavation failed. This is usually achieved by construction of tangents on an overburden pressure vs. settlement curve and taking the point of intersection as the collapse pressure, as illustrated in Figure 7.45. Determining this pressure, however, is open to interpretation and the tangents can be drawn at any point along the settlement curve; consequently, it is difficult to achieve consistency in excavation failure analyses. For context the results from JP12 have been plotted in Figure 7.46 and the overburden failure pressure was estimated to be in the region of 70kPa.

Le (2017) stated that the method of tangents was not particularly suited for small displacements as the change in the rate of settlement may not be detected. Subsequently, Le (2017) devised a procedure in which a more obvious failure pressure could be identified by plotting the rate of settlement against the overburden pressure, as shown in Figure 7.48. The rate of settlement was calculated using the settlements that had accrued at a distance H beyond the wall, as this was typically the location of maximum displacement. An example of this technique is shown in Figure 7.47 for test JP12 and suggests that the overburden pressure at failure is approximately 55kPa. This method provided a more consistent and quantitative approach to observing the efficiency of a particular excavation technique.

The rate of settlement curves clearly show the improvement afforded to the excavation when the crest is restrained. Similar rates of settlement are achieved for double walled and DSM excavations. As expected, the deeper wall embedment tests typically slowed the rate of settlement by up to 20kPa, however in the case of a double walled excavation the additional support was shown to reduce the rate by an order of magnitude.

7.9 SUMMARY

A series of 22 centrifuge tests were conducted to model ground deformations arising from a range of excavation techniques. A parametric study involving centrifuge modelling was completed to investigate a number of limited but significant factors. This series of tests controlled wall deflections and consequently focussed on the

influence of various excavation methods on ground movements occurring as a result of vertical stress relief at formation level.

High quality data was obtained to permit comparisons to be drawn between different methods of construction, which has enabled an assessment to be made of the efficacy of various excavation techniques compared with a reference excavation. Although some instrumentation, the data logger or image capturing devices occasionally failed during reconsolidation in-flight, sufficient systems were in place to facilitate the acquisition of data.

Results from the centrifuge tests have been critically reviewed, discussed and explanations of particular behaviours have been provided. Quality of data has been considered and the accuracy of different data acquisition methods, in particular the use of PIV and LVDTs, has been assessed.

Two excavation techniques were employed; surcharging the formation and stiffening the soil in the passive zone. All excavation measures tested showed a marked improvement in the control of ground displacements and were also shown to improve the stability of the excavation by delaying failure. In general, surcharging the formation level was more effective at minimising surface settlements as a consequence of controlling the magnitude of heave. Although complications arose during the bermed excavation test series, analysis of the data at an overburden pressure equal to the weight of water from a fully submerged excavation presented similar surface settlements to a fully surcharged formation level. Ground improvement through the use of deep soil mixing (DSM) was modelled using various geometries to investigate whether greater benefits could be achieved. Whilst theory assumes that a deeper but narrower area of soil treatment provides a greater degree of resistance, the analysis suggested that the volume of treatment was more critical to controlling ground movements than the geometry. A double walled excavation, whether used in collaboration with a wall of deep or shallow embedment resulted in comparable magnitudes of heave at formation level. However, increasing the depth of embedment in all cases was shown to offer a reasonably significant reduction in surface settlement.

CHAPTER 8 CONCLUSIONS, LIMITATIONS OF RESEARCH AND RECOMMENDATIONS FOR FURTHER WORK

8.1 INTRODUCTION

There is a need for the construction of deep excavations in soft soil to be properly managed and ground movements minimised. This is particularly prevalent in congested towns and cities where surface settlements can have a detrimental impact on neighbouring structures.

This thesis detailed the work that was conducted to investigate the influence of a range of construction methods on controlling ground movements around deep excavations in very soft soil. The construction methods are relatively simple to employ and some techniques, particularly DSM, are currently used for a variety of applications. The construction methods modelled in these tests demonstrated a marked reduction in the development of surface settlements beyond the excavation site.

This chapter summarises the experimental approach that was adopted in modelling the various construction methods, draws conclusions from the project, discusses the limitations and implications of the work and suggests recommendations for future work.

8.2 EXPERIMENTAL APPROACH

A total of twenty-two centrifuge tests were undertaken at the London geotechnical centrifuge facility. Bespoke apparatus and equipment were fabricated to facilitate model making and testing. The sample preparation technique had been developed and tailored to produce a very soft clay sample in a short period of time that was essentially normally consolidated. The equipment was designed to simulate a 12m deep open cut excavation with very high system stiffness. The excavation was performed by reducing air pressure in a latex bag that surcharged the formation level. The experimental equipment comprised a stiffener that provided lateral support to the wall as well as a reaction plate for the pressurised airbag and a stainless steel wall that was

fabricated to be extremely stiff but thin enough to push into the soil with minimal disturbance.

Comparisons were drawn between reference tests, where no special construction measures had been implemented and excavations with additional support or stiffness. The modelled construction methods included underwater excavations, berms, double walls and DSM. The influence of wall embedment and fixity conditions were also briefly investigated.

The models were largely normally consolidated Speswhite kaolin samples that were produced in a consolidation press at $1g$ for a period of about 10 days before being further consolidated at $160g$ on the centrifuge overnight. The models were made the following morning within 3.5 hours before being reconsolidated in-flight at $160g$ for 5 hours to achieve pore pressure equilibrium prior to simulating the excavation.

A minimum of three miniature PPTs measured the development of excess pore pressures either side of the retaining wall and also at a distance of $4H$ from the excavation to monitor the far field pore pressure response. A series of eleven LVDTs were used to measure surface settlements of the retained ground at predefined locations with one measuring settlement immediately behind the retaining wall. At least one miniature USB camera was angled towards the excavation area to capture subsurface deformations and validate surface settlement measurements recorded by the LVDTs. Some experiments towards the end of the test series employed an additional camera to capture displacements in the far field.

An extensive literature review was carried out concerning ground movements in soft soils arising from deep excavations, expected deformation mechanisms, background on the special construction methods and field studies on their performance. Attempts have been made to predict ground movements in soft soils however owing to the variability in ground conditions, excavation geometry and construction it is difficult to accurately predict displacements. Instead, settlement profiles have been normalised and simplified and are therefore referenced in this project. Vertical settlements of the retained surface are a function of wall displacements and basal heave. This project assumes that in controlling the lateral wall displacements the respective surface settlements are solely a function of basal heave. The construction methods employed

in this series of tests aim to limit the magnitude of heave and in doing so, reduce surface settlements.

8.3 CONCLUSIONS

This research project focussed on limiting basal heave whilst eliminating lateral wall displacements. In doing so, it was possible to isolate the resultant settlement troughs to have occurred from basal heave. A series of centrifuge tests were conducted carefully to ascertain the comparable efficacy of a range of construction measures in mitigating ground movements at the retained surface arising from a deep excavation in soft ground. Deep soil mixing (DSM), underwater, double walled and bermed excavations have all been conducted with a range of embedment depths and fixity conditions.

The behaviour observed in the centrifuge tests were largely consistent with theoretical expectations and permit a number of statements to be made about the influence of the construction techniques on controlling soil deformation.

In soft ground maximum settlements were observed between $0.5H$ and H behind the retaining wall, where H is the final excavation depth. Significant settlements were observed up to $3H$ from the excavation irrespective of whether additional construction measures had been implemented or not. The construction methods were shown to have a degree of influence on reducing settlements compared with the baseline tests, with some proving more effective than others.

Typically, the largest change in the rate of settlements occurred between 100kPa and 75kPa which represents the point after half of the excavation was completed. Following this change in vertical stress, the accumulation of displacements generally continued at a similar rate. Displacements occurring between the start of the excavation and an overburden pressure of 100kPa accounted for less than 10% of the ultimate settlement. However, the underwater excavation displacements commenced earlier in the test at around 150kPa before plateauing at 50kPa.

The retaining wall employed in each of the centrifuge tests was representative of 1.4m thick reinforced concrete diaphragm wall. This eliminated the risk of wall bending

during the test but consequently resulted in rotational failure of the excavation at low overburden pressures.

In all experiments the retaining wall was supported along $\frac{2}{3}$ of its exposed length by a stiff aluminium block that essentially provided a continuous incompressible rigid prop. This afforded lateral support to the wall during reconsolidation and during the simulated excavation process. This system supported the wall in compression however with increasing settlement the wall was displaced downward and rotated about the lowest prop into the excavation. Therefore, the support afforded to the wall was only suitable for minimal displacements. Consequently, securing the crest of the wall was shown to further stabilise the excavation and minimise the magnitude of settlement. Where the crest was supported by a sliding capping beam the settlement trough was reduced by approximately a third.

Surcharging the formation proved to be an important factor in minimising the development of heave and subsequently reducing the settlements of the retained surface. During the underwater excavations, the entire formation level was surcharged and the ultimate change in vertical stress was 40% of the total weight of soil removed in the other reference test. Consequently, the maximum displacements were almost twenty times smaller. In the long term, a submerged excavation exhibited up to a 20% increase in the magnitude of the settlement profile but these plateaued as excess pore pressures dissipated. Underwater excavations were therefore revealed as the most efficient method of constructing deep excavations in very soft ground and limiting the magnitude of settlements arising from the construction process.

Bermed excavations, following a similar concept to the underwater excavation but over a reduced area, were also shown to be effective in reducing settlements to a third of the displacements measured in the reference test. Berms also demonstrated that they could widen the settlement trough so the potential for differential settlement related damage to neighbouring structures would be reduced.

The introduction of a stiffer material at formation level also demonstrated an improvement in the soil response and a reduced settlement profile. The use of DSM created stiffer zones at formation level and all geometries were shown to have an equal or improved response compared with the final underwater excavation settlement

profile. The shallowest settlement profile was observed for a treatment area extending $2B/3$ across the formation level and to the toe of the wall. Low excess pore pressures were generated on the passive side where a shallow DSM raft was cast across the formation, however comparable responses were seen on the active side for the range of DSM treatment geometries.

Similarly, the presence of a low stiffness wall embedded 25mm deeper than the permanent retaining wall reduced the maximum surface settlement by 63%. Constructing the secondary wall to the same depth as the retaining wall showed additional benefits. The maximum settlements where a double wall had been installed were 28% lower than those observed in the reference test of similar embedment.

When the main excavation area was surcharged with 80kPa and the narrow berm applied a 100kPa surcharge across a formation width equal to $B/3$, the settlement profile tended to follow the same trend as the final underwater excavation. Although the entire formation was not surcharged there appeared to be some benefit in leaving a soft soil berm against the retaining wall whilst performing a deep excavation.

Further reductions in surface settlements were observed by combining the underwater excavation with either a double wall or a DSM block. The combined effects from the underwater excavation with 55mm wall embedment developed surface settlement profiles comparable with an underwater excavation with 75mm wall embedment.

Figure 8.1 draws on data from the entire test series to depict the efficacy of each of the various construction methods in controlling settlement behind the retaining wall. The greatest magnitude of settlement from each test, typically taken at distances of $0.5H$ or H , and measured at a common overburden pressure between tests of 74kPa are normalised against the maximum settlement recorded in the reference test at 74kPa. Effectiveness is defined as the inverse of the load factor, developed in equation (7.10). This has been rearranged and magnified by a factor of 1000 for ease of comprehension, as defined in equation (8.1).

$$N = 2 \pi R \left(S_{u1}/2 + S_{u2} \right) + \Delta H R \gamma \quad (8.1)$$

The graph demonstrates that the four distinct construction methods offer benefits compared with the reference tests. Partially or completely submerging the excavation

void was shown to offer the greatest improvement in reducing the magnitude of maximum settlement. At an overburden pressure of 74kPa settlements measured in the combined underwater excavation and double walls or DSM treated zone were both shown to reduce settlements by approximately 35% compared with those measured in the tests without a submerged excavation formation level.

Based on the typical load-settlement curve, presented in Figure 7.45, the change in settlement would be expected to attenuate for a smaller load factor. The data conforms to the behaviour that could be expected when loading a shallow foundation.

8.4 LIMITATIONS AND IMPLICATIONS OF THIS PROJECT

One of the major limitations of this research relates to the simplicity of the model. The excavation void was cut at $1g$ rather than being performed at $160g$ with in-flight excavators. The sample will have been in suction during model making having been recently removed from the centrifuge following in-flight consolidation. This is not representative of an excavation conducted in the field and no attempts were made to establish the effects of excavating at $1g$ and simulating the excavation at high- g . However, the model was reconsolidated post-model making to allow the excess pore pressures to dissipate prior to testing. In addition, this project was designed as a parametric study and internal consistency between tests was achieved. Comparisons of results could be made owing to the repeatable modelling techniques and excavation geometry.

Underwater excavations were considered a novel excavation technique during the construction of the station box at Marina Bay in Singapore. They were also seen as a high-risk construction activity owing to the need for divers to assist in casting a level ground slab. However, with recent developments in self-levelling concrete the risks to human life are less of a concern and the benefits of performing submerged excavations are significant. In addition, the lateral pressures that develop with depth through the submerged excavation would contribute to supporting the retaining walls and potentially reduce the need for propping.

Some hesitancy exists around the use of deep soil mixing to improve the soil as this is sometimes perceived as a time consuming process that does not contribute to the actual

structure. However, in areas where the ground is very soft and large movements are likely this is one of the faster methods of strengthening the ground. DSM is also versatile as the desired strengths, plan area, depth and precise locations can be adjusted to suit the site and application. It is easy to carry out deep mixing in very soft ground compared with stiffer soils and eliminates the need for drilling and installing drains and mass surcharging. This project has demonstrated that the same volume of treatment arranged in various DSM cross sectional geometries can all contribute to an improved settlement profile. The ground improvement test series conducted as part of this research project produced lime-stabilised soil samples that had only cured for a period of up to 36 hours. In reality, the treated soil will be left for a period of up to a week before excavation commences. Therefore, a stronger block of soil would exist and the soil displacements arising from the excavation can be expected to be reduced.

Double walled excavations are relatively simple to construct and could be constructed in sequence with the primary retaining wall. Whilst these tests were constrained to one wall of a particular length, the depth, stiffness and location can be varied in the field to suit the site constraints.

Although experimental failures occurred during the bermed excavation tests, the preliminary results suggest that there is some validity in surcharging the soil directly in front of the wall. The berms were very simplistically idealised as an equal surcharge across a pre-defined part of the formation. In reality however berms are trapezoidal and the surcharge applied at the toe of the berm would be significantly lower than that immediately adjacent the wall. In addition, forming a berm in very soft soil would need careful planning, monitoring and protection to ensure stability throughout the excavation.

There is a notable lack of long-term data from this series of centrifuge tests, with the exception of the underwater excavations. This is owing to the failures of each excavation during the unloading of the formation level. Although the excavation process was conducted over a period of about three months at prototype scale a time delay may exist between the end of the excavation and construction. Establishing the long-term influence of these various construction methods would provide an understanding of how movements develop with the dissipation of excess pore pressures and assist with programming construction of the superstructure.

8.5 RECOMMENDATIONS FOR FURTHER WORK

Owing to the wide range of construction methods modelled in this three-year research project time constraints restricted the number of variables that could be investigated within each test series. Therefore, two embedment depths were studied, two fixity conditions were planned, three DSM geometries were modelled whilst the cross sectional area remained constant and one embedded depth of double wall was analysed.

The results from these tests showed that all of these methods have some influence on controlling movements of the retained surface. However, further investigations could be conducted to establish the optimum excavation design parameters for each or a combination of the construction methods.

Further tests on DSM block geometry and columns should be conducted to determine a more efficient DSM solution that minimises the volume of treatment but achieves a suitable reduction in surface settlements. Furthermore, an investigation into the influence of zoned excavations i.e. compartmental excavations, each segregated with low stiffness walls, could be conducted with a shallow retaining wall. If proving successful in controlling ground movements this would also assist in construction programming whilst reducing the requirement for expensive specialist equipment.

It was established that combining underwater and double walled excavations can further reduce settlements that could be expected for an excavation that was carried out using only underwater techniques. In view of this, whilst it might be costly and time consuming to undertake a completely submerged excavation, benefits could be gained in understanding whether a balance could be struck between partially submerging an excavation and constructing a double walled formation to achieve similar magnitudes of settlements at the retained surface.

Engineers are tasked with designing efficient and economical excavations. Therefore, it is unreasonable to state that all support systems should be designed as rigidly as possible to eliminate wall bending. In reality the retaining wall will have some degree of flexibility and so it is important to establish a link between this research and an excavation with some known wall flexibility. This would enable the application of this study to other sites.

REFERENCES

- Abedi, H., Porter, T.G., Lien, B.H. & Ramos, J.A., 1992. Performance of a flexible earth retaining structure in soft clays – comparisons between finite element method and field measurements. *Proceedings of the Retaining Structures conference, Cambridge 20-23rd July*, Thomas Telford, London, pp. 281-290.
- Allersma, H.G.B., 1988. Development of cheap equipment for small centrifuges. In *Proceedings of the International Conference Centrifuge '88, Paris*, Balkema, Rotterdam, pp. 85-90.
- Almeida, M.S.S., Santa Maria, P.E.L., Martins, I.S.M., Spotti, A.P. & Coelho, L.B.M., 2000. Consolidation of a very soft clay with vertical drains. *Géotechnique*, 50(6), pp. 633-643; Discussion. 52(2), pp. 148-154.
- Al Tabbaa, A., 1987. Permeability and stress-strain response of speswhite kaolin, PhD thesis, University of Cambridge, UK.
- Atkinson, J., 2007. The mechanics of soils and foundations, 2nd edition, Chapman & Hall, London.
- Atkinson, J.H., Brown, E.T., Potts, M., 1975. Collapse of shallow unlined tunnels in dense sand. *Tunnels and Tunnelling* 3, pp. 81-87.
- Azevedo, R.F., 1983. Centrifuge and analytical modelling of excavation in sand, PhD thesis, University of Colorado, Boulder, USA.
- Begaj-Qerimi, L., 2009. Geotechnical centrifuge model testing for pile foundation reuse, PhD thesis, City, University of London, UK.
- Bell, A.L., 2012. Chapter 90: Geotechnical grouting and soil mixing. *Institution of Civil Engineers Manual of Geotechnical Engineering*, Thomas Telford, London, pp. 1323-1341.
- Bjerrum, L., Moum, J. & Eide, O., 1967. Application of electro-osmosis to a foundation problem in a Norwegian quick clay. *Géotechnique*, 17(3), pp. 214-235; Discussion 18(2), pp. 276-278.

- Boardman, D.I., Glendinning S. & Rogers, C.D.F., 2001. Development of stabilisation and solidification in lime-clay mixes. *Géotechnique*, 50(6), pp 533-543.
- Bolton, M.D. & Powrie, W., 1987. The collapse of diaphragm walls retaining clay. *Géotechnique*, 37(3), pp. 335-353.
- Bolton, M.D. & Powrie, W., 1988. Behaviour of diaphragm walls in clay prior to collapse. *Géotechnique*, 38(2), pp. 167-189.
- Brooker, E.W. & Ireland, H.O., 1965. Earth pressures at rest related to stress history. *Canadian Geotechnical Journal*, 2(1) pp. 1-15.
- Casagrande, L., 1949. Electro-osmosis in soils. *Géotechnique*, 1(3), pp. 159-177.
- Charles, J.A., 2002. Ground improvement: the interaction of engineering science and experience-based technology. *Géotechnique*, 52(7), pp. 527-532.
- Clarke, P.J. & Prebaharan, N., 1987. Marina Bay Station, Singapore excavation in soft clay. In *Proceedings of Case Histories in Soft Clay*, NTU, Singapore, pp. 95-107.
- Clayton, C.R.I., Woods, R.I., Bond, A.J. & Milititsky, J., 2014. Earth pressure and earth-retaining structures, 3rd Edition, Taylor & Francis Group, Boca Raton.
- Daly, M.P. & Powrie, W., 2001. Undrained analysis of earth berms as temporary supports for embedded retaining walls. In *Proceedings of the Institution of Civil Engineers - Geotechnical Engineering*, 149(4), pp. 237-248.
- Davidson, R.R., 1977. Effects of construction on deep excavation behaviour, PhD thesis, Stanford University, California.
- Divall, S., 2013. Ground movements associated with twin-tunnel construction in clay, PhD thesis, City, University of London, UK.
- Dong, Y.P., Burd, H.J. & Houlsby, G.T., 2016. Finite-element analysis of deep excavation case history. *Géotechnique*, 66(1), pp. 1-15.
- Elshafie, M.Z.E.B., Choy, C.K.C. & Mair, R.J., 2013. Centrifuge modelling of deep excavations and their interaction with adjacent buildings. *Geotechnical Testing Journal*, 36(5), pp. 1-12.

Femie, R., St John, H.D. & Potts, D.M., 1991. Design and performance of a 24m deep basement in London Clay resisting the effects of long term rise in groundwater, *Proceedings of 10th European Conference on Soil Mechanics and Foundation Engineering 26-30 May, Florence*, Balkema, Rotterdam, pp. 699-702.

Finno, R.J. & Nerby, S.M., 1989. Saturated clay response during braced cut construction. *ASCE Journal of Geotechnical Engineering*, 115(8), pp. 1065-1084.

Finno, R.J., Atmatzidis, D.K. & Nerby, S.M., 1988. Ground response to sheet pile installation in clay. In *Proceedings of Second International Conference on Case Histories in Geotechnical Engineering, June 1988*, St Louis pp.1297-1301.

Fleming, E.G.K., Weltman, A.J., Randolph, M.F. & Elson, W.K., 2008. Piling Engineering. Surrey University Press, Glasgow and London.

Fuglsang, L.D. & Ovesen, N.K., 1989. The application of the theory of modelling to centrifuge studies. *Centrifuge in Soil Mechanics*. Edited by Craig, James & Schofield. Balkema, Rotterdam, pp. 119-138.

Gaba, A., Hardy, S., Doughty, L., Powrie, W. & Selemeas, D., 2017. CIRIA C760; Guidance on embedded retaining wall design. CIRIA, London.

Garnier, J., 2002. Properties of soil samples used in centrifuge models. *Physical Modelling in Geotechnics: ICPMG '02*, Phillips, Guo & Popescu (eds.) Swets & Zeitlinges Lisse, 1. pp 5-19.

Goldberg, D.T., Jaworski, W.E. & Gordon, M.D., 1976. Lateral support systems and underpinning Volume 1, Federal Highway Division, Washington DC, USA.

Gorasia, R.J., 2013. Behaviour of ribbed piles in clay, PhD thesis, City, University of London, UK.

Grant, R.J., 1998. Movements around a tunnel in two-layer ground, PhD thesis, City, University of London, UK.

Hsieh, P.G. & Ou, C.Y., 1998. Shape of ground surface settlement profiles caused by excavation. *Canadian Geotechnical Journal*, 35, pp. 1004-1017.

Hsieh, H.S., Huang, Y.H., Hsu, W.T. & Ge, L., 2017. On the system stiffness of deep excavation in soft clay. *Journal of GeoEngineering*, 12, pp. 21-34.

Hui, L.C., 2006. Centrifuge modelling of wet deep mixing processes in soft clay, PhD thesis, National University of Singapore, Singapore.

Kantarzo, C., 1993. Ground movements during diaphragm wall installation in clay. PhD thesis, Queen Mary and Westfield College, London, UK.

K. Karlsrud & L. Andresen, 2008. Design and Performance of deep excavations in soft clays. (August 11, 2008). In *Proceedings of the 6th International Conference on Case Histories in Geotechnical Engineering*. Paper 9

Keller, D., 2017. Private communication.

Kimura, T., Takemura, J., Hiro-oka, A., Okamura, M. & Park, J., 1994. Excavation in soft clay using in-flight excavator. *Proceedings of International Conference Centrifuge '94*, Singapore, pp. 649-654.

Kitazume, M. & Takeyama, T., 2014. Centrifuge model tests on failure pattern of cement treated ground. In *Proceedings of International Conference for Physical Modelling in Geotechnics*, Perth, Australia, pp. 1113-1118.

Kusakabe, O., 1982. Stability of excavations in soft clay. PhD thesis, University of Cambridge, UK.

Ladd, C.C. & Varallyay, J., 1965. The influence of stress system on the behaviour of saturated clays during undrained shear. *Research in Earth Physics*, Report 1, Part 2, Massachusetts Institute of Technology, USA.

Lam, S.S.Y., 2010. Ground movements due to excavation in clay: physical and analytical models, PhD Thesis, University of Cambridge, UK.

Lam, S.Y., Elshafie, M.Z.E.B., Haigh, S.K. & Bolton, M.D., 2012. A new apparatus for modelling excavations. *International Journal for Physical Modelling in Geotechnics*, 12(1), pp 24-38.

Lam, S.Y., Haigh S.K. & Bolton, M.D., 2014. Understanding ground deformation mechanisms for multi-propped excavation in soft clay. *Soils and Foundations*, 54(3), pp 296-312.

Le, B.T., 2017. The effect of soil reinforcement of tunnel face stability in clay, PhD thesis, City, University of London, UK.

Lee, S.L. & Yong, K.Y., 1991. Grouting in substructure construction. In *Proceedings of the 9th Asian Regional Conference on Soil Mechanics and Foundation Engineering, 9-13th December*, Bangkok, Thailand.

Liang, F.Y., Chu, F., Song, Z., 2012. Centrifugal model test research on deformation behaviors of deep foundation pit adjacent to metro stations. *Rock and Soil Mechanics*, 33(3), pp. 657-664.

Lim, G., 2003. Stabilisation of an excavation by an embedded improved soil layer, PhD thesis, National University of Singapore, Singapore.

Liu, J.Y., 1999. Centrifugal model test in soft soil foundation pit, PhD thesis. Tongji University, China.

Liu, Y., Jiang, Y.J., Xiao, H. & Lee, F.H., 2017. Determination of representative strength of deep cement-mixed clay from core strength data. *Géotechnique*, 67(4), pp. 350-364.

Locat, J., Berube, MA. & Choquette, M., 1990. Laboratory investigations on the lime stabilization of sensitive clays: shear strength development, *Canadian Geotechnical Journal*, 27, pp. 294-304.

Long, M.M., 2001. Database for retaining wall and ground movements due to deep excavation. *Journal of Geotechnical and Geoenvironmental Engineering*, 127(3), pp. 203-224.

Long, M.M. & O'Riordan, N.J., 2001. Field behaviour of very soft clays at the Athlone embankments. *Géotechnique*, 51(4), pp. 293-309.

Low, H.E., Lunne, T., Andersen, K.H., Sjursen, M.A., Li, X. & Randolph, M.F., 2010. Estimation of intact and remoulded undrained shear strengths from penetration tests in soft clays. *Géotechnique*, 60(11), pp. 843-859.

Lyndon A. & Pearson, R., 1984. Pressure distribution on a rigid retaining wall in cohesionless material. In *Proceedings of the Application of Centrifuge Modelling to Geotechnical Design Symposium, Manchester 16-18 April* (ed. Craig W.H.), Balkema, Rotterdam, pp. 271-281.

Lyndon, A. & Schofield, A.N., 1970. Centrifugal model test of a short-term failure in London Clay, *Géotechnique*, 20(4), pp. 440-442.

Ma, X.F. & Xu, J.W., 2018. Centrifuge model tests on excavation in Shanghai clay using in-flight excavation tools. In *Proceedings of the 9th International Conference for Physical Modelling in Geotechnics – (eds. McNamara et al.)*, London., Volume 1, pp. 419-424.

Ma X.F., Zhang H.H., & Zhu W.J., Zheng, Y. & Xu, Q., 2009. Centrifuge model tests on deformation of ultra-deep foundation pits in soft ground. *Chinese Journal of Geotechnical Engineering* 31(9): 1371–1377.

Mayne, P. & Kulhawy, F.H., 1983. K-OCR relationships in soil. *International Journal of Rock Mechanics and Mining Sciences & Geomechanics*, 20(1), pp. 851-859.

McCabe, B.A. & Egan, D., 2010. A review of the settlement of stone columns in compressible soils, *In Proceedings of the GeoShanghai International Conference, 3-5 June*, Shanghai, China.

McGown, A. & Hughes, F.H., 1981. Practical aspects of design and installation of vertical drains. *Géotechnique*, 31(1), pp. 3-17.

McNamara, A.M., 2001. Influence of heave reducing piles on ground movements around excavations, PhD thesis, City, University of London, UK.

McNamara, A.M., Goodey, R.J. & Taylor, R.N., 2009. Apparatus for centrifuge modelling of top down basement construction with heave reducing piles. *International Journal of Physical Modelling in Geotechnics*, 9(1), pp. 1-14.

Mitchell, J.M. & Jardine, F.M., 2000. A guide to ground treatment, CIRIA Report C573. London.

Nadimi, S., Fonseca, J., Barreto, D. & Taylor, R.N., 2016. A new approach to investigate the particle size effects in centrifuge modelling. *3rd European Conference on Physical Modelling in Geotechnics, 1-3 Jun 2016, Nantes, France*.

Nash, D.F.T. & Ryde, S.J., 2001. Modelling consolidation accelerated by vertical drains in soils subject to creep. *Géotechnique*, 51(3), pp. 257-273.

Ng, C.W.W., Hong, Y., Liu, G.B. & Liu, T., 1992. Ground deformations and soil-structure interaction of a multi-propped excavation in Shanghai soft clays. *Géotechnique*, 62(10) pp. 907-921.

Ng, C.W.W., Van Laak, P.A., Zhang, L.M., Tang, W.H., Li, X.S. & Xu, G.M., 2001. Key Features of the HKUST Geotechnical Centrifuge. *Proceedings of the International Symposium on Geotechnical Centrifuge Modelling and Networking: Focusing on the Use and Application in the Pan-Pacific Region*: pp. 66-69.

Ng., C.W.W., 2014. The state-of-the-art centrifuge modelling of geotechnical problems at HKUST. *Journal of Zhejiang University (Applied Physics & Engineering)*, 15(1), pp. 1-21.

Ong, D.E.L., Leung, C.F. & Chow, Y.K., 2006. Pile behaviour due to excavation induced soil movement in clay. *Journal of Geotechnical and Geoenvironmental Engineering*, 132(1), pp. 36-44.

O'Rourke, T.D., 1993. Base stability and ground movement prediction for excavation in soft clay. *Retaining Structures*, Thomas Telford, London, pp. 657-686.

Osman, A.S. & Bolton, M.D., 2006. Design of braced excavations to limit ground movements. *In Proceedings of the Institution of Civil Engineers Geotechnical Engineering*, 159(GE3), pp. 167-175.

Ou, C.Y., Wu, T.S. & Hsieh, H.S., 1996. Analysis of deep excavation with column type of ground improvement I soft clay, *ASCE Journal of Geotechnical Engineering*, 122(9), pp. 709-716.

Ou, C.Y., Liao, J.T. & Lin, H.D., 1998. Performance of diaphragm wall constructed using top down method. *Journal of Geotechnical and Geoenvironmental Engineering*, 124(9), pp. 798-808.

Padfield, C.J. & Mair, R.J., 1984. CIRIA Report 104; Design of retaining walls embedded in stiff clay. CIRIA, London.

Panchal, J.P., McNamara, A.M. & Stallebrass, S.E., 2018. Physical modelling of lime stabilisation in soft soils around deep excavations. *DFI Journal - The Journal of the Deep Foundations Institute*,

Phear, A.G. & Harris, S.J., 2008. Contributions to Géotechnique 1948-2008: Ground improvement. *Géotechnique*, 58(5), pp. 399-404.

Potts, D.M., Addenbrooke, T.I. & Day R.A., 1993. Soil berms as temporary supports for retaining walls. *Proceedings of the Retaining Structures conference, Cambridge 20-23rd July*, Thomas Telford, London, pp. 440-447.

Potts, D.M. & Fourie, A.B., 1984. The behaviour of a propped retaining wall: results of a numerical experiment. *Géotechnique*, 34(3), pp. 383-404.

Powrie, W., 1986. The behaviour of diaphragm walls in clay, *PhD thesis*, University of Cambridge, UK.

Powrie, W., 2004. Soil mechanics: concepts and applications (2nd edition), Taylor & Francis, UK.

Powrie, W., & Daly, M.P., 2002. Centrifuge model tests on embedded retaining walls supported by earth berms. *Géotechnique*, 52(2), pp. 89-106.

Powrie, W. & Daly M.P., 2007. Centrifuge modelling of embedded retaining walls with stabilising bases. *Géotechnique*, 57(6), pp. 485-497.

- Powrie, W., Davies, J.N. & Britto, A.M., 1993. A cantilever retaining wall supported by a berm during temporary works activities. *Proceedings of the Retaining Structures conference, Cambridge 20-23rd July*, Thomas Telford, London, pp. 418-428.
- Powrie, W & Kantartzzi, C., 1996. Ground response during diaphragm wall installation in clay: centrifuge model tests. *Géotechnique*, 46(4), pp. 725-739.
- Richards, D.J. & Powrie, W., 1998. Centrifuge model tests on doubly propped embedded retaining walls in overconsolidated kaolin clay. *Géotechnique*, 48(6), pp. 833-846.
- Sato, E., Aoki, M. & Maruoka, M., 1992. Large excavation with cantilever type continuous walls. *Proceedings of the Retaining Structures conference, Cambridge 20-23rd July*, Thomas Telford, London, pp. 270-280.
- Scarano, F., 2013. Tomographic PIV: principles and practice. *Measurement Science and Technology*, 24(1).
- Schofield, A.N. & Wroth, C.P., 1968. Critical State Soil Mechanics. McGraw-Hill, London.
- Simpson, B. & Powrie, W., 2001. Embedded retaining walls; theory practice and understanding, *Perspective lecture at the 15th International Conference on Soil Mechanics and Geotechnical Engineering, Istanbul*.
- Smethurst, J.A. & W. Powrie, W., 2008. Effective-stress analysis of berm-supported retaining walls. *In Proceedings of the Institution of Civil Engineers - Geotechnical Engineering*, 161(1), pp. 39-48.
- Springman, S.M., 1989. Lateral loading on piles due to simulated embankment construction. PhD thesis, University of Cambridge, UK.
- Stanier, S.A., Blaber, J., Take, W.A. & White, D.J., 2015. Improved image-based deformation measurement for geotechnical applications. *Canadian Geotechnical Journal*, 53(5), pp. 727-739.
- Su, J.Q. & Wang, Z., 2003. The two-dimensional consolidation theory of electro-osmosis. *Géotechnique*, 53(8), pp. 759-763.

Sun, Y., Zhou, S. & Luo, Z., 2017. Basal-heave analysis of pit-in-pit braced excavations in soft clay. *Computer and Geotechnics Journal*, 81, pp. 294-306.

Takemura, J., Kondoh, M., Esaki, T., Kouda, M & Kusakabe, O., 1999. Centrifuge model tests on double propped wall excavation in soft clay. *Soils and Foundations*, 39(3), pp 75-87.

Tamaro, G.J. & Gould, J.P., 1992. Analysis and design of cast in situ walls (diaphragm walls). *Proceedings of the Retaining Structures conference, Cambridge 20-23rd July*, Thomas Telford, London, pp. 343-352.

Taylor R.N., 1995. Chapter 2; Modelling principles. Geotechnical centrifuge technology (R.N. Taylor (ed.)). Blackie Academic & Professional, pp 19-33.

Tomlinson, M.J., 1956. Telford and soil mechanics. *Géotechnique*, 6(3), pp. 99-105.

Wallace, J.C., Ho, C.E. & Long, M.M., 1992. Retaining wall behaviour for a deep basement in Singapore marine clay. *Proceedings of the Retaining Structures conference, Cambridge 20-23rd July*, Thomas Telford, London, pp. 195-204.

Wang, J.H., Xu, Z.H. & Wang, W.D., 2010. Wall and ground movements due to deep excavations in Shanghai soft soils. *Journal of Geotechnical and Geoenvironmental Engineering*, 136(7), pp. 985-994.

White, D.J., 2002. An investigation into the behaviour of pressed-in piles. PhD thesis, University of Cambridge, UK.

White, D.J., Take, W.A. & Bolton, M.D., 2003. Soil deformation measurement using particle image velocimetry (PIV) and photogrammetry. *Géotechnique*, 53(7), pp. 619-631.

Wu, B.R. & Lee, C.J., 2003. Ground movement and collapse mechanisms induced by tunneling in clayey soil. *International Journal of Physical Modelling in Geotechnics*, 3(4), pp. 13-27.

Yu, F., Xie, Z., Duan, N., Liu, N. & Shan, H., 2018. Performance of double-row piles retaining excavation beneath existing underground space. *International Journal of Physical Modelling in Geotechnics*, ICE publishing, pp. 1-14.

Zhu, W. & Yi, J., 1988. Application of centrifuge modelling to study a failed quay wall. *In Proceedings of the International Conference Centrifuge '88, Paris*, Balkema, Rotterdam, pp. 415-419.

TABLES

Characteristics of hardening agent

- Type of hardening agent
 - Quality
 - Mixing water and additives
-

Characteristics and conditions of soil (especially clays)

- Physical chemical and mineralogical properties of soil
 - Organic content
 - pH level of pore water
 - Water content
-

Mixing conditions

- Degree of mixing
 - Timing of mixing/re-mixing
 - Quality of hardening agent
-

Curing conditions

- Temperature
 - Curing time
 - Humidity
 - Wetting/drying or freezing/thawing
-

Table 2.1 Factors affecting increase in strength of DSM treated soil (after Bruce *et al.*, 1998)

Ultimate compressive strength (UCS)	0.2-5.0 MPa
Permeability	$10^{-4} - 10^{-9}$ m/s
Modulus of Elasticity (laboratory)	350-1000 times greater
Modulus of Elasticity (field)	150-500 times greater
Direct shear strength	40-50% of UCS
Tensile strength	1.4-1.5 times greater than 7-day UCS in clays
28 day UCS	1.5 times the 28-day UCS

Table 2.2 Typical values of DSM treated soil (after Bruce *et al.*, 1998)

Description	Model	Prototype
Length	1	N
Self-weight stress	1	1
Force	1	N^2
Strain	1	1
Young's Modulus	1	1
Moment of inertia	1	N^4
Bending stiffness	1	N^3

Table 3.1 Scaling laws for centrifuge tests (Powrie, 1986)

Symbol	Parameter	Value
A	coefficient in relationship for $G'_{\max(nc)}$	1964
N	exponent in relationship for $G'_{\max(nc)}$	0.65
M	exponent in relationship for $G'_{\max(oc)}$	0.2
κ	average gradient of swelling line in $v:\ln p'$ space	0.035
λ	gradient of compression line in $v:\ln p'$ space	0.18
M	stress ratio at critical state ($q':p'$)	0.89
Γ	specific volume at critical state when $p'=1\text{kPa}$	2.994
N	specific volume on INCL when $p'=1\text{kPa}$	3.05
ϕ'_c	critical state angle of shearing resistance	23°
Γ	unit weight of soil (saturated for clay)	17.5 kN/m ³
G_s	specific gravity	2.61
γ_w	unit weight of water	9.81 kN/m ³

Table 3.2 Properties of Speswhite kaolin clay (after Grant, 1998)

Test ID	Date	Embedment	Excavation method	Comments
JPP1	24/05/16	55mm	Underwater	Airbag burst during overnight consolidation – no data collected
JPP2 a	28/06/16	-	-	Sample prepared for first pre-consolidation spin up. Slip ring stack seized during spin-up. Sample returned to press after 1.5 hours after being flooded with distilled water.
JPP2 (failed)	09/08/16	-	-	During first pre-consolidation phase on swing a power outage occurred after an hour of acceleration. The sample was left on the swing for 3.5hours before spinning again. The sample was consolidated overnight and model making commenced on 10 th August as planned. After model was retrieved from the swing the chamber was flooded from the AC vents above and PXI computer suffered irreparable water damage – the model unusable.
JPP3	21/09/16	55mm	Dry excavation Area flooded post excavation for long term swelling	Sample put on the swing on Tues 20/09/16 and left to consolidate overnight. No water was fed to the standpipe during first pre-consolidation phase as pipe became kinked therefore the sample dried out overnight. Sample left on swing to consolidate during the day and overnight on Wed 21/09/16. Model making commenced in the morning of 22/09/16 with the plan to test on Thursday evening. The PXI crashed on Thursday evening and the model spun down and left on the swing overnight. Base drains were closed and the clay surface had been sprayed with PlastiDip to prevent drying out. The fibre optic (FO) cable had sheared which ceased the connection from the control room to the PXI. FO was fixed on Fri 23/09/16 morning and the model was spun up again and PPTs were monitored until the sample had come into equilibrium. The test was conducted on Friday afternoon.
JPP4	13/10/16	55mm	-	In-flight pre-consolidation stage was successful. After model making and during reconsolidation there was a suspected air bag leak. The union had not been secured tightly and was resealed on the swing. 100kPa air pressure was unknowingly supplied to the bag at the time and after successfully tightening the bag the high pressure caused passive failure. No useable data was obtained from the test
JPP5		55mm	-	In-flight pre-consolidation stage was successful. After model making and reconsolidation the air bag burst against a sharp unprotected corner resulting in active failure. No useable data was obtained.
JPP6	09/11/16	55mm	Underwater excavation	Preconsolidation in flight - standpipe provided 10mm standing water above soil. Test progressed well

Table 6.1 Summary of centrifuge tests conducted including comments on successes and failures

<i>Test ID</i>	<i>Date</i>	<i>Embedment</i>	<i>Excavation method</i>	<i>Comments</i>
JPP7	07/12/16	75mm	Dry excavation	During reconsolidation the LVDT, standpipe and air pressure transducers were non-responsive. PPT responded to the excavation and overburden pressures recorded from DPI in control room during excavation
JPP8	21/12/16	75mm	Underwater excavation	Air pressure transducer damaged in flight - readings taken from DPI in control room at 5s intervals
JPP9	06/01/17	55mm	Dry excavation	Test progressed well - excavation failed at approximately 30kPa
JPP10	19/01/17	55mm	DSM 37.5	Power outage to the LVDT and standpipe transducers. Air pressure transducer and PPTs were responsive. PIV necessary for surface settlements.
JPP11	08/02/17	75mm	Dry propped excavation	First test where the crest was pinned. New camera lenses (5MP) and 2no cameras were also used. LVDT footing came loose during initial pre-consolidation stage - no data obtained. During the test the pins help the wall in place until all overburden pressure had been removed.
JPP12	22/02/17	55mm	Double wall	Newly machined capping beam was screwed to stiffener. Beam provided insufficient restraint as model consolidated in flight and settled. Test progressed well and excavation appeared to fail at approximately 20kPa
JPP13	07/03/17	55mm	Double wall	Repeat of JPP12. Capping beam fixed to a bracket to permit vertical movement during reconsolidation Test completed, excavation prevented from passive failure
JPP14	28/03/17	55mm	DSM 55; 2B/3	Test okay - excavation failed at approximately 20kPa. Air pressure transducer appeared to that airbag applied 125kPa to formation level however PPTs showed similar response to other tests. DPI used in analysis.
JPP15	20/04/17	55mm	DSM, 112.5, B/3	Power outage to LVDT and standpipe transducers and cameras froze for 1 minute during the simulated excavation. Excavation appeared to fail at approximately 7kPa
JPP16	04/05/17	-	<i>Trim preflight</i>	During in-flight consolidation, stater on electrical slip ring sheared and all electrical cables were torn. No model making done. Sample was returned to press following morning
JPP16b	23/06/17	55mm	Berm B/3	Following repair of centrifuge and electrical cables a second attempt to make the model using the same sample. During initial pre-consolidate stage the centrifuge spun down overnight after approximately 8 hours of spinning. The out of balance trigger had been exceeded. The sample had swelled for approximately 5 hours until modeller arrived at 0800. The sample was left to reconsolidate on swing from 0830 to 1300. Test progressed reasonably well. Only one air pressure transducer was used to record the pressure in the main excavation bag. The other air bag was controlled using the DPI in the control room. Image capture froze at approximately 60kPa for a period of 30 seconds.

Table 6.1(cont'd) Summary of centrifuge tests conducted including comments on successes and failures

<i>Test ID</i>	<i>Date</i>	<i>Embedment</i>	<i>Excavation method</i>	<i>Comments</i>
JPP17	06/09/17	55mm	Berm 2B/3	The chamber was flooded from overhead AC vent and no air pressure transducer was available for the secondary airbag. Time lags on PXI were suspected owing to the hardware being damp and affecting the signals or wifi connection
JPP18	28/09/17	75mm	Double wall	The water flow to the standpipe had been adjusted by another operator prior to this test. Therefore, during in-flight pre-consolidation, a lower water level was supplied to the sample. No significant problems were noted relating to the performance of the excavation. A time lag on LabView existed.
JPP19	10/10/17	75mm	Berm B/3	The time lag on LabView persisted and timestamps checks were required to match LabView data and the images
JPP20	25/10/17	55mm	Underwater & Double wall	The water feed to the excavation void became kinked and therefore supplied insufficient water to the formation level. Time lag on SC and images
JPP21	14/11/17	55mm	Underwater & Double wall	Test progressed well, only one camera used which seemed to eliminate the time lag on the camera capture rate and data logger
JPP22	08/12/17	55mm	Underwater & DSM 2B/3	During reconsolidation bulging of bag was observed around the front block of DSM adjacent the wall. The model was carefully monitored and bulge continued to grow. Test was conducted early. The standpipe also appeared to have a lower level of water. Post flooding, model continued spinning inflight to monitor long term effects – post spin down the water in excavation seemed to have drained out.

Table 6.1(cont'd) Summary of centrifuge tests conducted including comments on successes and failures

	Free at crest		Fixed at crest	
Embedment depth	55mm	75mm	55mm	75mm
Excavation method	Test reference number			
Reference test	JP9	JP7		JP11 (pinned)
Underwater excavation	JP6 JP3 (strong sample)	JP8		
Double wall excavation			JP12 (fixed at crest) JP13 (sliding beam) JP20 (underwater attempt)	JP18
Deep soil mixing (DSM)	JP10 (B)		JP14 ($^{2B}/3$) JP15 ($^{B}/3$)	
Bermed excavation			JP16 ($^{B}/3$) JP17 ($^{2B}/3$)	JP19 ($^{B}/3$)
Combined excavation methods	Underwater + Double wall		JP21	
	Underwater + DSM		JP22 ($^{2B}/3$)	

Table 6.2 Centrifuge test series and notation

<i>Slip gauge (mm)</i>	<i>LVDT reading (mm)</i>	<i>LVDT vs slip gauge error (μm)</i>	<i>Average PIV measurement (mm)</i>	<i>Average PIV vs slip gauge error (μm)</i>	<i>Minimum / maximum PIV values (mm)</i>	<i>Range of PIV values (μm)</i>
0.5	0.502	2	0.473	27	0.319 / 0.759	439
1	1.021	21	0.985	15	0.612 / 1.431	811
1.1	1.101	1	1.059	41	0.912 / 1.369	457
1.2	1.235	35	1.177	23	1.057 / 1.516	459
1.3	1.317	17	1.268	32	1.126 / 1.462	337
1.4	1.407	7	1.330	70	0.919 / 1.783	863
1.5	1.509	9	1.438	62	0.979 / 1.859	880
2	2.006	6	1.959	41	1.593 / 2.444	851
4	4.035	35	3.931	69	3.803 / 4.083	280
5	5.03	30	4.927	73	4.809 / 5.238	429
Average of errors		16		45		

Table 6.3 Excavation camera (angled) calibration check

<i>Slip gauge (mm)</i>	<i>LVDT reading (mm)</i>	<i>LVDT vs slip gauge error (μm)</i>	<i>Average PIV measurement (mm)</i>	<i>Average PIV vs slip gauge error (μm)</i>	<i>Minimum / maximum PIV values (mm)</i>	<i>Range of PIV values (μm)</i>
0.5	0.591	91	0.504	4	0.382 / 0.566	184
1	1.083	83	1.002	2	0.882 / 1.077	195
1.1	1.187	87	1.104	4	0.971 / 1.174	203
1.2	1.299	99	1.204	4	1.078 / 1.279	201
1.3	1.406	106	1.3	0	1.195 / 1.324	129
1.4	1.531	131	1.402	2	1.307 / 1.429	122
1.5	1.598	98	1.487	13	1.361 / 1.544	184
2	2.098	98	1.986	14	1.829 / 2.165	336
4	4.138	138	3.989	11	3.857 / 4.048	192
5	5.144	144	4.976	24	4.704 / 5.060	356
Average of errors		108		8		

Table 6.4 Straight camera (perpendicular) calibration check

Slip gauge step	1.35	1.4	1.5	1.75	2	2.5	6	10	15	25
Displacement	<i>Reference</i>	0.05	0.15	0.4	0.65	1.15	4.65	8.65	13.65	23.65
<i>LVDT reading (mm)</i>	0	0.030	0.380	0.367	0.612	1.096	4.410	8.288	13.519	23.173
<i>Slip gauge error (μm)</i>		20	-230	33	38	54	240	362	131	477
<i>Slip gauge diff (%)</i>		-67%	-153%	-9%	-6%	-5%	-5%	-4%	-1%	-2%
PIV	R1	219.9544	219.8995	219.5095	219.5788	219.3471	218.846	215.4156	211.4484	206.5194
	R2	220.2477	220.2389	219.8659	219.8464	219.5849	219.1066	215.6504	211.7377	206.8333
<i>Disp. (mm)</i>	R1	0	0.0549	0.4449	0.3756	0.6073	1.1084	4.5388	8.506	13.435
	R2	0	0.0088	0.3818	0.4013	0.6628	1.1411	4.5973	8.51	13.4144
<i>Slip gauge error (μm)</i>	R1	-	5	295	24	43	42	111	144	215
	R2	-	41	232	1	13	9	53	140	236
<i>Average difference from slip gauge (%)</i>	-	-523.86%	-16.53%	-6.84%	-9.14%	-2.95%	-1.29%	-0.05%	-0.15%	-0.24%
PIV	Y1	233.4988	233.4664	233.1016	233.0947	232.8542	232.3687	228.9243	224.9998	220.1024
	Y2	233.7714	233.7272	233.3526	233.395	233.1507	232.6474	229.2195	225.2751	220.3756
<i>Disp. (mm)</i>	Y1	0	0.0324	0.3972	0.4041	0.6446	1.1301	4.5745	8.499	13.3964
	Y2	0	0.0442	0.4188	0.3764	0.6207	1.124	4.5519	8.4963	13.3958
<i>Slip gauge error (μm)</i>	Y1	-	18	247	4	5	20	75	151	254
	Y2	-	6	269	24	29	26	98	154	254
<i>Average difference from slip gauge(%)</i>	-	-36.42%	-5.44%	-7.36%	-3.85%	-0.54%	-0.50%	-0.03%	0.00%	-0.01%
PIV	G1	332.143	332.1232	331.7488	331.7933	331.5288	331.0183	327.5885	323.629	318.7014
	G2	332.686	332.6602	332.2762	332.2763	332.0213	331.5409	328.0864	324.1456	319.2332
<i>Disp. (mm)</i>	G1	0	0.0198	0.3942	0.3497	0.6142	1.1247	4.5545	8.514	13.4416
	G2	0	0.0258	0.4098	0.4097	0.6647	1.1451	4.5996	8.5404	13.4528
<i>Slip gauge error (μm)</i>	G1	-	30	244	50	36	25	96	136	208
	G2	-	24	260	10	15	5	50	110	197
<i>Average difference from slip gauge(%)</i>	-	-30.30%	-3.96%	-17.16%	-8.22%	-1.81%	-0.99%	-0.31%	-0.08%	-0.05%

Table 6.5 Comparison between PIV analysis, LVDT and slip gauge results for all excavation camera and far camera data

Slip gauge step	1.35	1.4	1.5	1.75	2	2.5	6	10	15	25	
Displacement	Reference	0.05	0.15	0.4	0.65	1.15	4.65	8.65	13.65	23.65	
<i>PIV</i>	P1	357.8744	357.8521	357.4623	357.47	357.2108	356.7044	353.2544	349.3264	344.3759	334.5837
	P2	357.8453	357.8222	357.4578	357.5026	357.2277	356.7398	353.2635	349.2731	344.3426	334.5074
<i>Disp. (mm)</i>	P1	0	0.0223	0.4121	0.4044	0.6636	1.17	4.62	8.548	13.4985	23.2907
	P2	0	0.0231	0.3875	0.3427	0.6176	1.1055	4.5818	8.5722	13.5027	23.3379
<i>Slip gauge error (μm)</i>	P1	28	262	4	14	20	30	102	152	359	
	P2	27	237	57	32	44	68	78	147	312	
<i>Average difference from slip gauge(%)</i>		-3.59%	-6.35%	-18.00%	-7.45%	-5.83%	-0.83%	-0.28%	-0.03%	-0.20%	

Table 6.5(cont'd) Comparison between PIV analysis, LVDT and slip gauge results for all excavation camera and far camera data

	S_{u1}	S_{u2}	Actual depth at collapse (centrifuge model)	$H = \frac{N S_u}{\gamma}$ (Peck, 1969)	Factor Peck : Actual	$H_c = \frac{H_{exc} \left(\frac{S_{u1}}{2} + S_{u2} \right) - C}{R \gamma}$ Upper bound solution (UB)	Factor UB : Actual
Reference	(kN/m ²)	(kN/m ²)	(m)	(m)		(m)	
JP7	7	14	7.5	7.5	1	11.2	1.49
JP11	8	16	8.7	6.9	0.79	10.2	1.17
JP9	7	16	7.2	6.9	0.96	10.4	1.44
Double wall						Radius = 12m, N = 1160	
JP12	9	17	8.4	6.5	0.77	11	1.31
JP13	10	17	9.9	6.5	0.66	10.8	1.09
JP18	11	21	8.4	5.3	0.63	9.2	1.1
DSM						Radius = 16m, N = 1717	
JP10	9	15	8.4	7.2	0.86	13	1.55
JP14	9	15	9.6	7.2	0.75	13	1.35
JP15	10	17	9.9	6.5	0.66	12.2	1.23
Berm						Radius = 15m, N = 1500	
JP19	10	18	4.7	6.2	1.32	10.8	2.3
JP16	10	18	9.6	6.2	0.65	10.8	1.13

Table 7.1 Comparisons between excavation depths at failure calculated from the Peck (1969) stability number, the UB developed solution and the depth at failure measured from overburden pressure in the centrifuge tests.

FIGURES

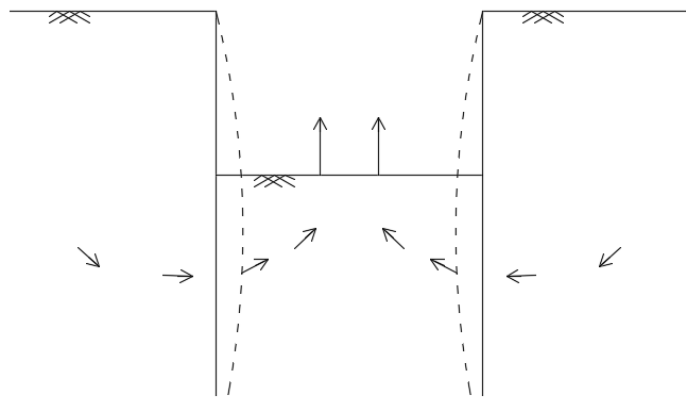


Figure 2.1 Deep seated inward displacement due to excavations (after Burland *et al.*, 1979)

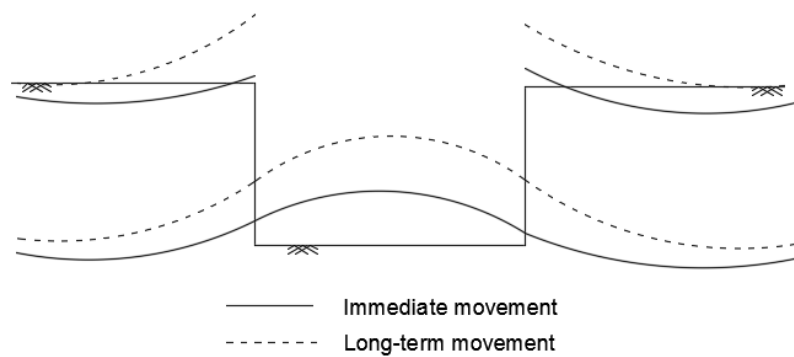


Figure 2.2 Vertical stress relief at the base of an excavation (after Burland *et al.*, 1979)

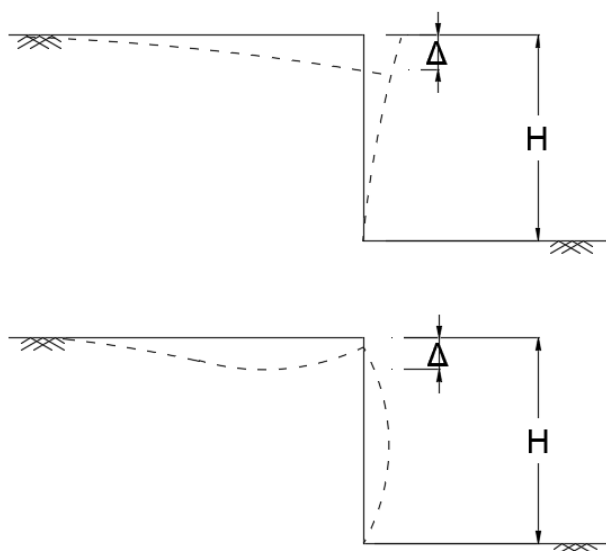


Figure 2.3 Movements occurring from horizontal stress relief (after Burland *et al.*, 1979)

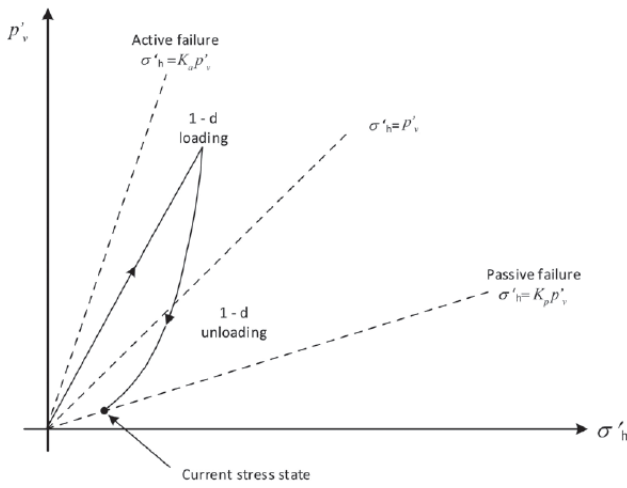


Figure 2.4 Influence of stress history on the relationship between horizontal effective stresses and the effective overburden pressure in clays (Gaba *et al.* (2017) after Burland *et al.*, 1979)

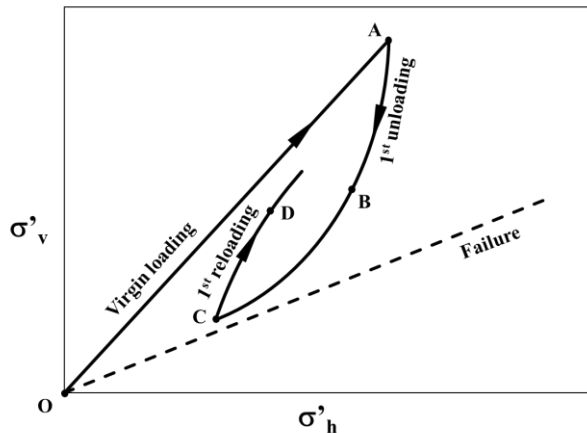


Figure 2.5 Simplified soil stress history under K_0 conditions (after Mayne & Kulhawy, 1982)

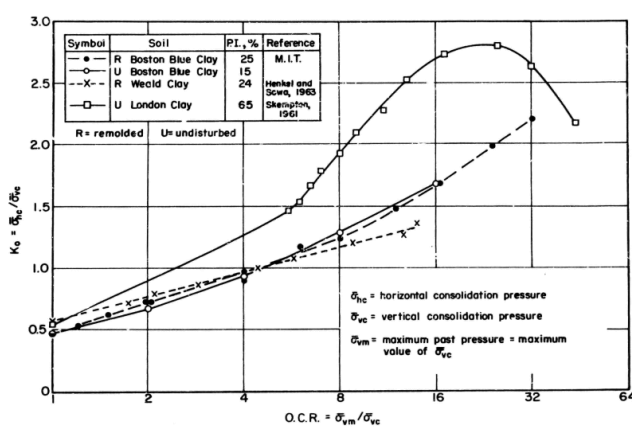


Figure 2.6 Variation in K_0 against overconsolidation ratio for three clays (Ladd & Varallyay, 1965)

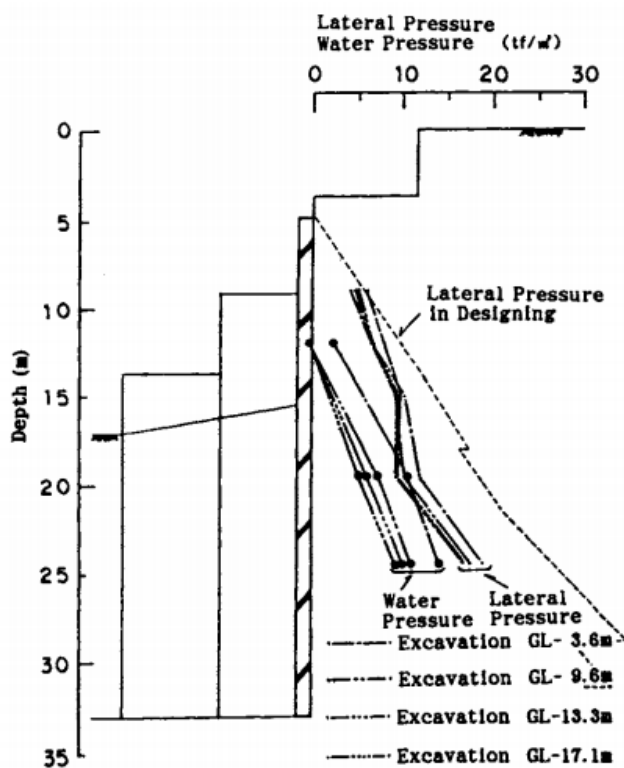


Figure 2.7 Measured lateral earth pressures on a diaphragm wall during excavation of a 17m deep basement in soft silty clay (Sato *et al.*, 1992)

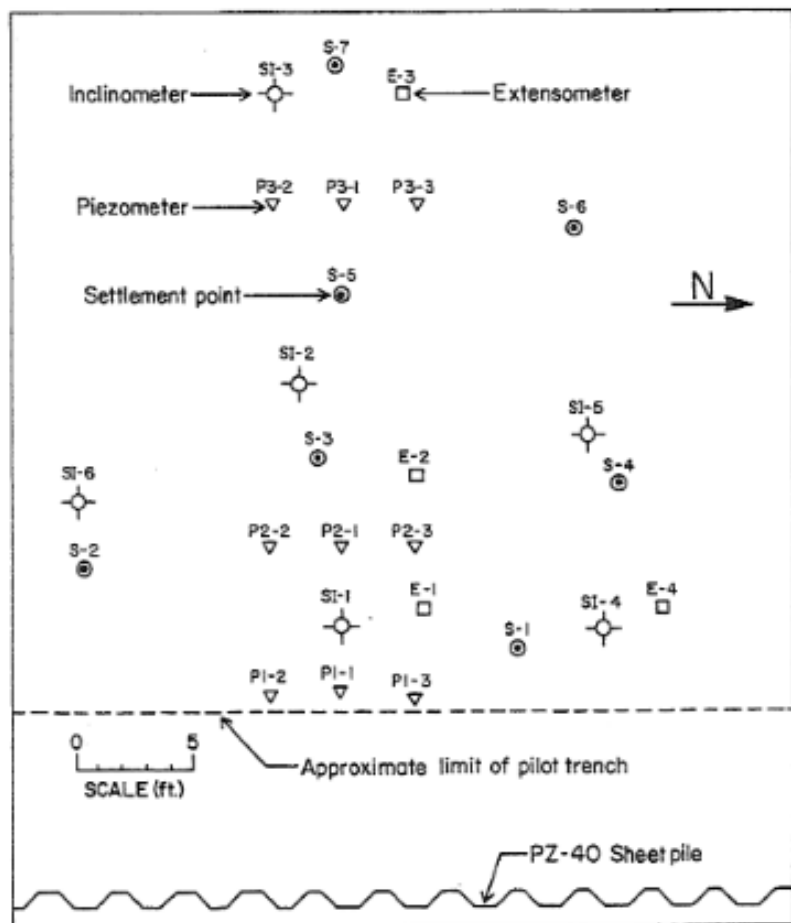


Figure 2.8 Plan of instrumented site (Finno *et al.*, 1988)

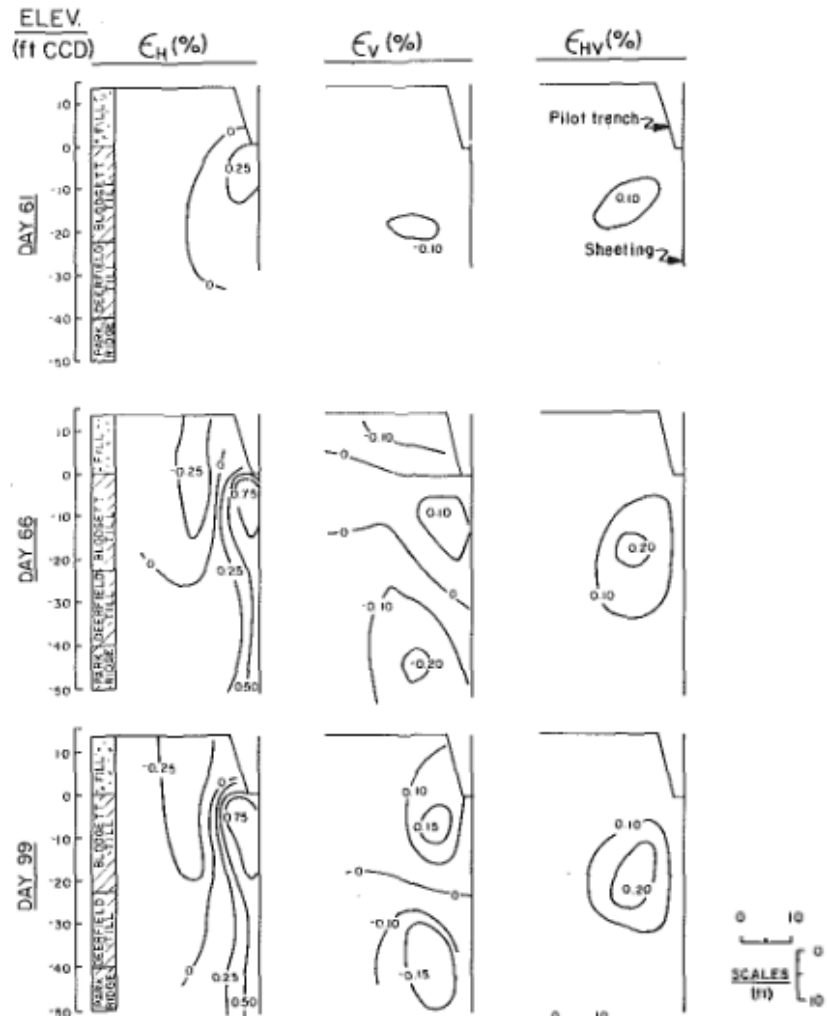


Figure 2.9 Development of strains during and after sheet pile installation (Finno & Nerby, 1989)

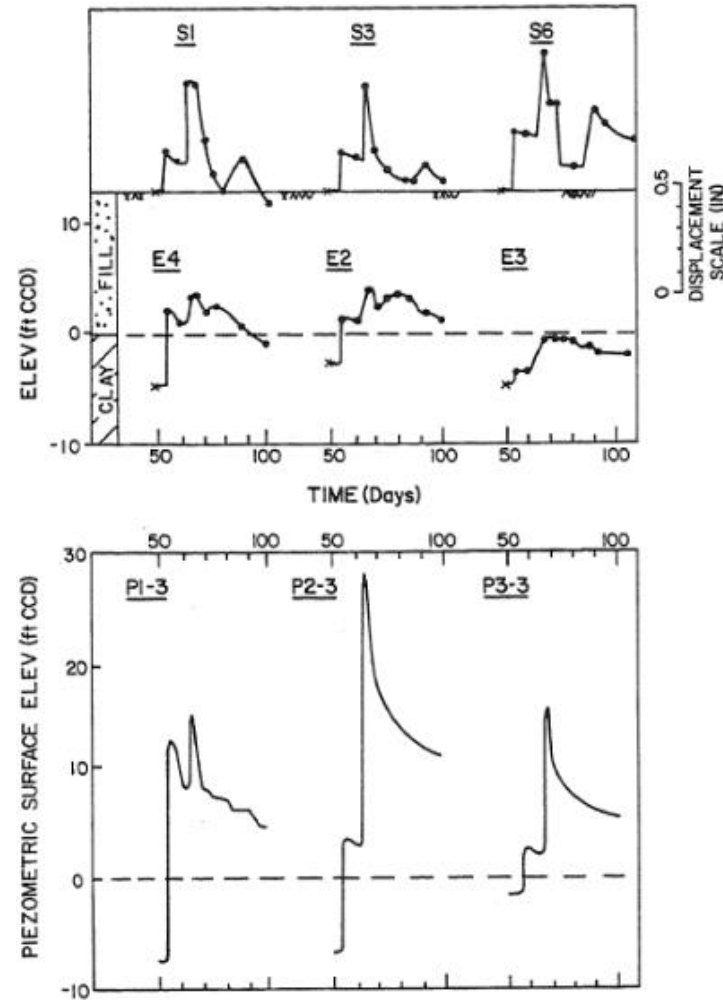


Figure 2.10 Pore pressure and settlement responses during pile driving and vibration (Finno *et al.*, 1988)

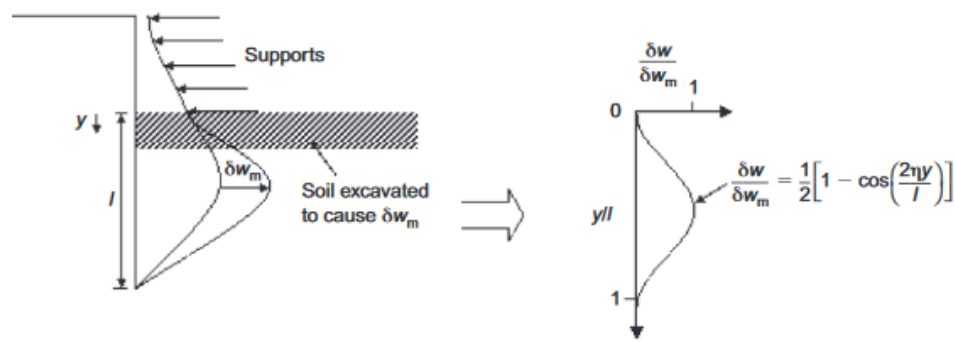


Figure 2.11 General lateral deformation pattern (after O'Rourke, 1993)

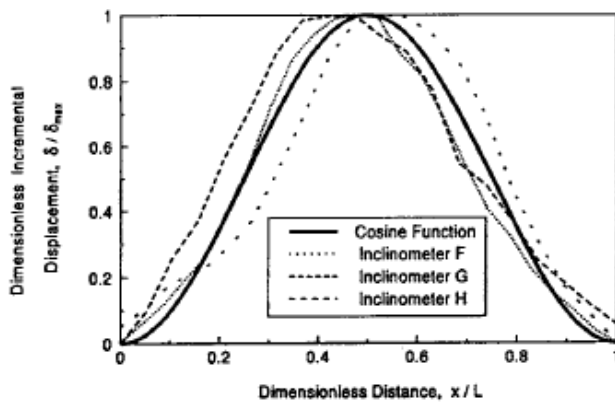


Figure 2.12 Comparison between field measurements and the computed incremental displacements (O'Rourke, 1993)

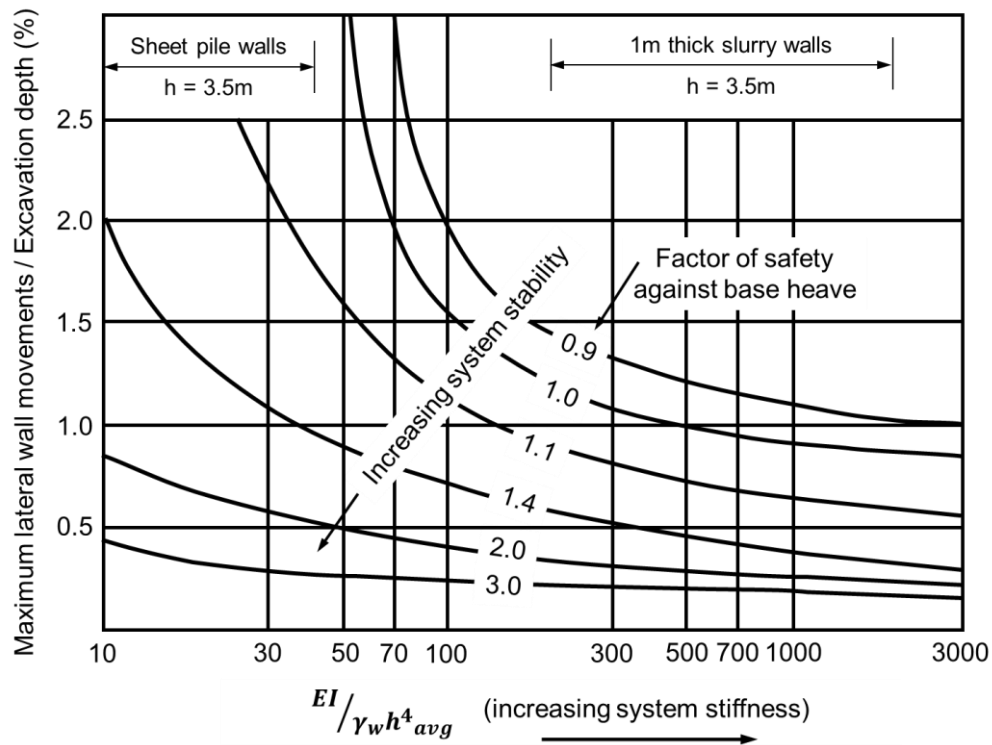


Figure 2.13 Proposed method for predicting wall displacements based on FOS against basal heave and system stiffness (after Clough & O'Rourke, 1990)

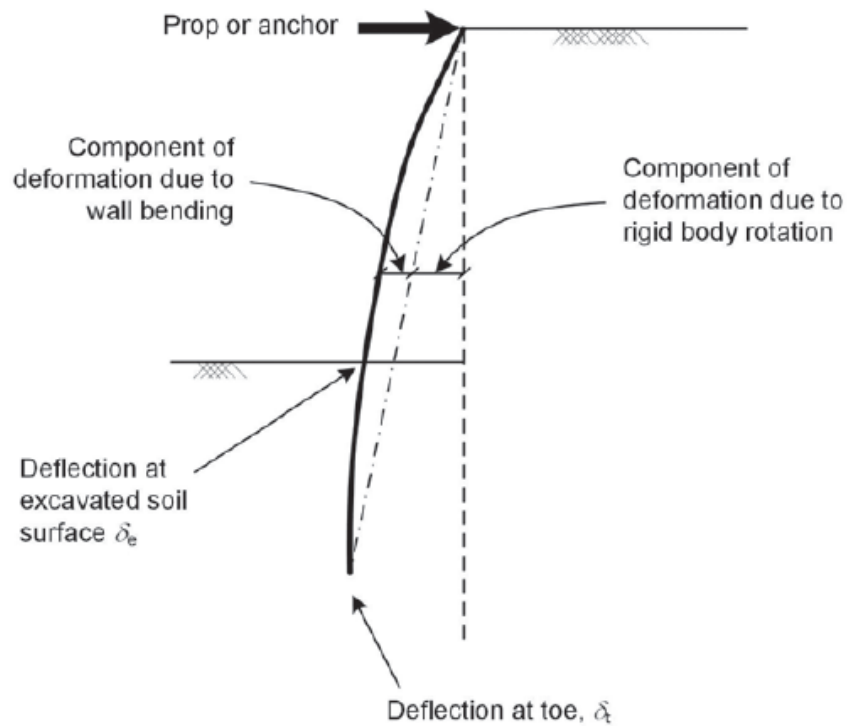


Figure 2.14 Wall displacements of a stiff retaining wall (Gaba *et al.*, 2017)

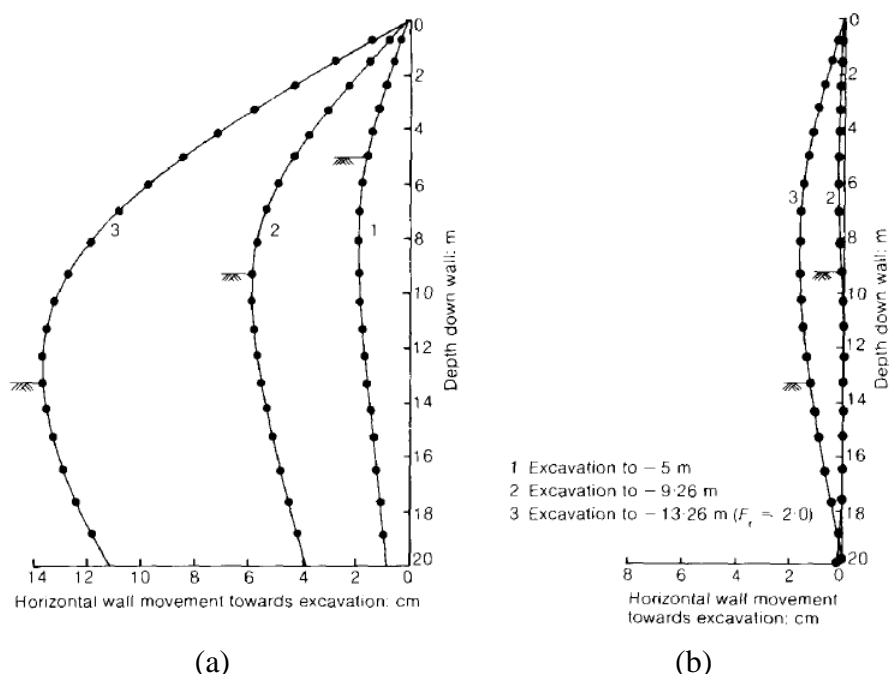


Figure 2.15 Lateral wall displacements for a factor of safety of 2 during excavation where (a) $K_0 = 2$ and (b) $K_0 = 0.5$ (Potts & Fourier, 1984)

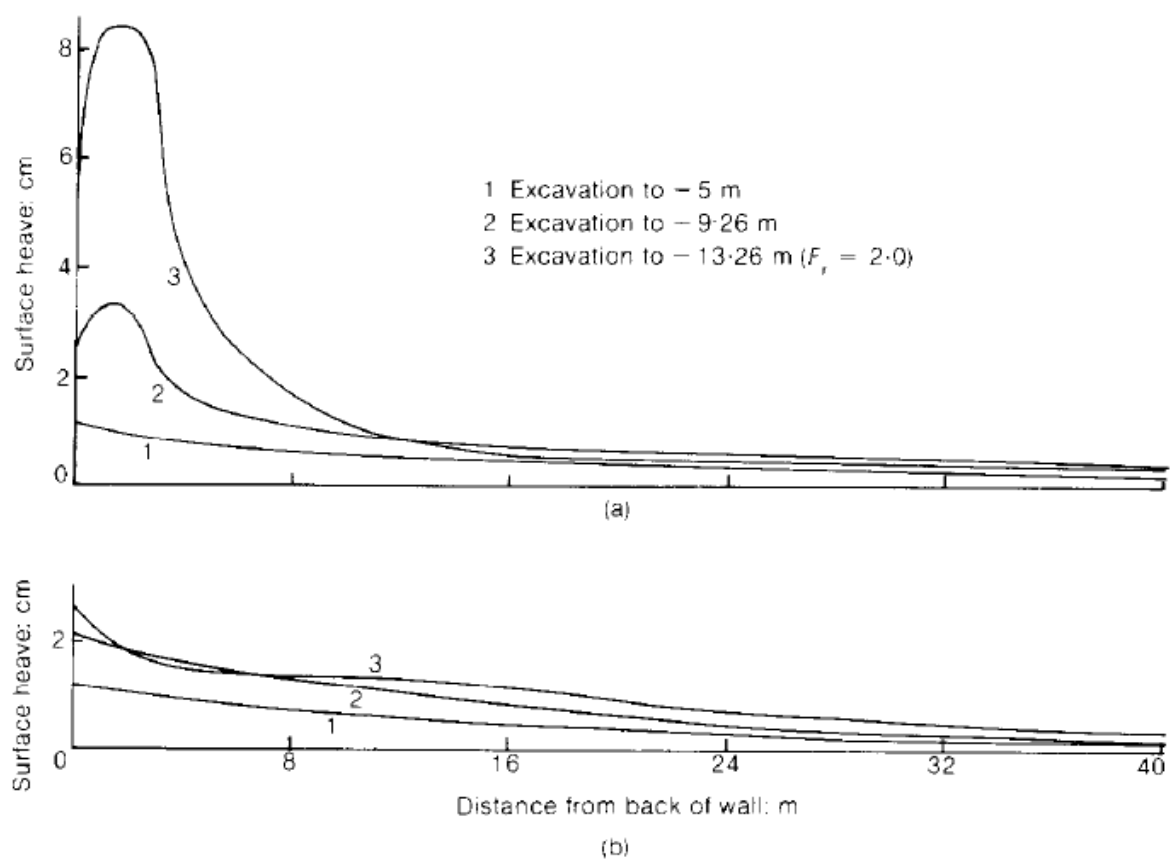


Figure 2.16 Corresponding surface settlement profiles for a factor of safety of 2 during excavation where (a) $K_0 = 2$ and (b) $K_0 = 0.5$ (Potts & Fourier, 1984)

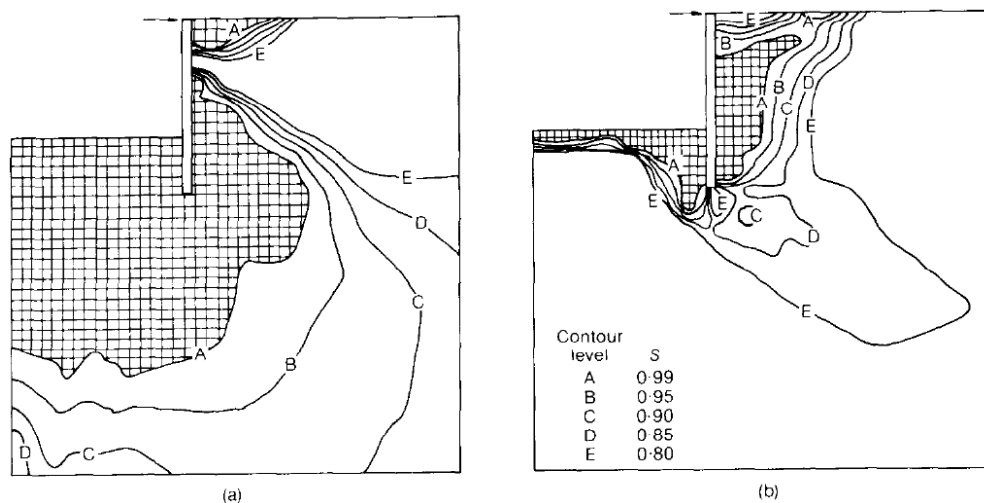


Figure 2.17 Stress contours after 13m excavation in (a) $K_0 = 2$ and (b) $K_0 = 0.5$ (Potts & Fourier, 1984)

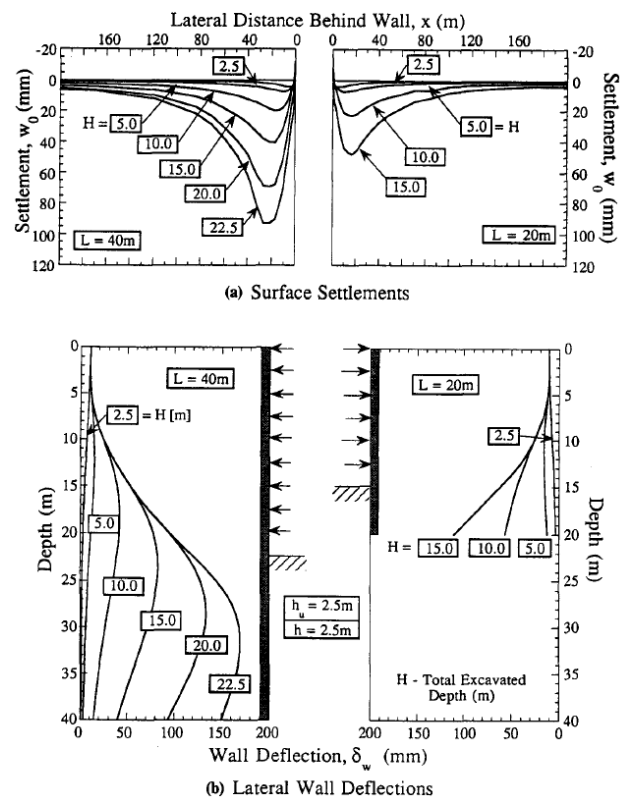


Figure 2.18 Influence of wall embedment on surface settlements and lateral wall deflections in normally consolidated soil ($\text{OCR} = 1$) (Hashash & Whittle, 1996)

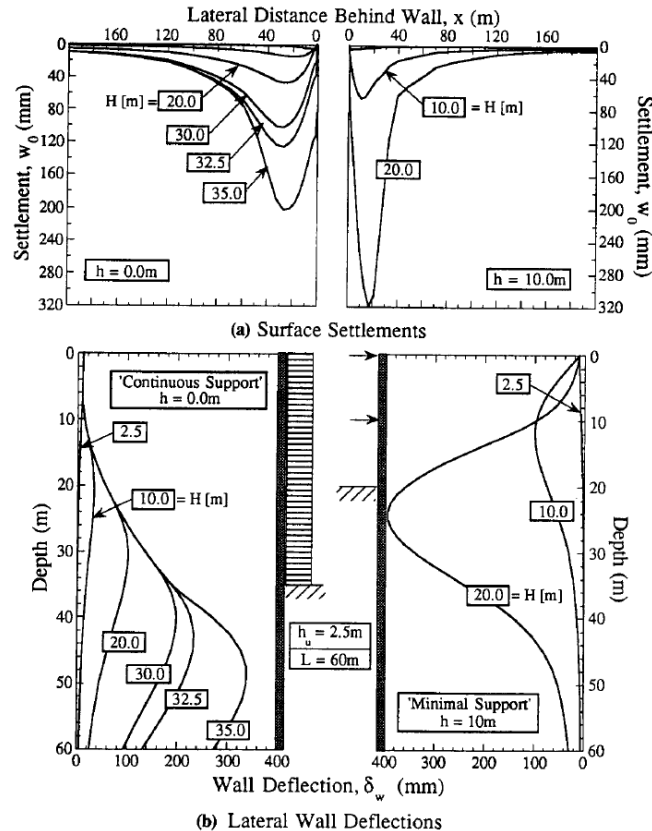


Figure 2.19 Influence of prop spacing (h) on surface settlements and lateral wall deflections in normally consolidated soil ($\text{OCR} = 1$) for wall embedment of $L = 60\text{m}$ (Hashash & Whittle, 1996)

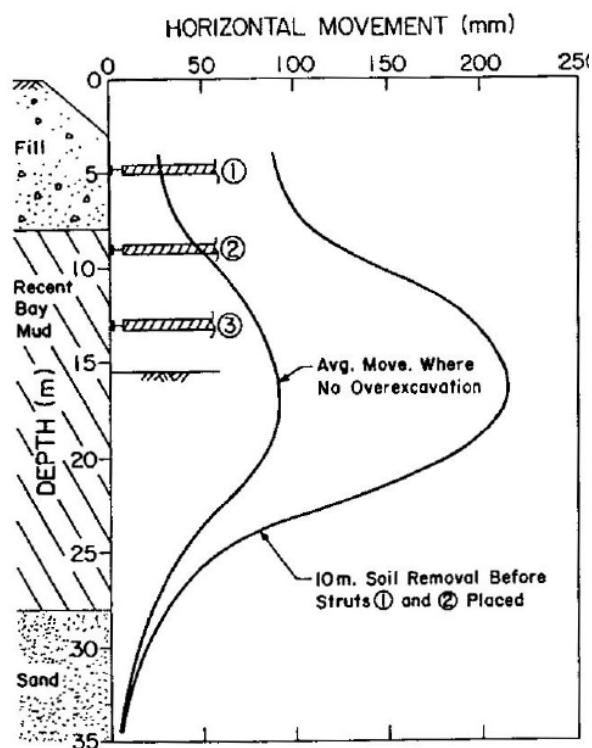


Figure 2.20 Lateral wall deflections arising from good construction sequencing and over-excavation prior to installing props (after Davidson, 1977)

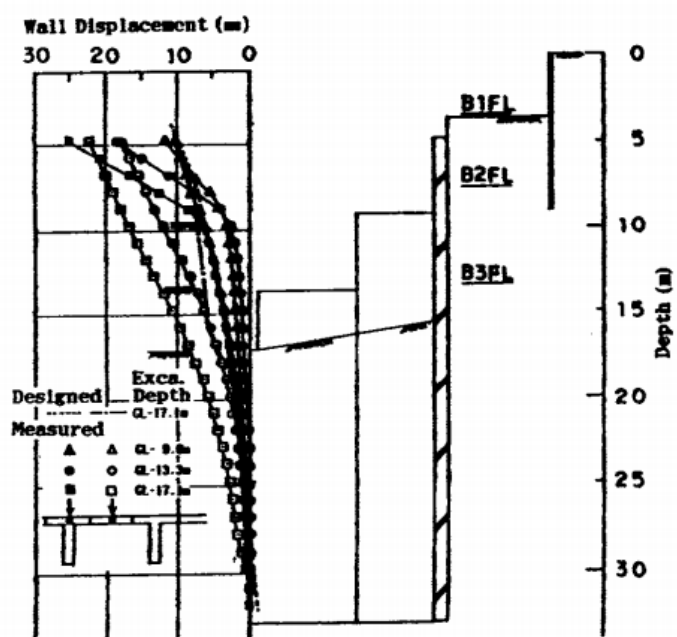


Figure 2.21 Measured and computed wall displacements of a cantilevered excavation comprising T-section diaphragm wall panels (Sato *et al.*, 1992)

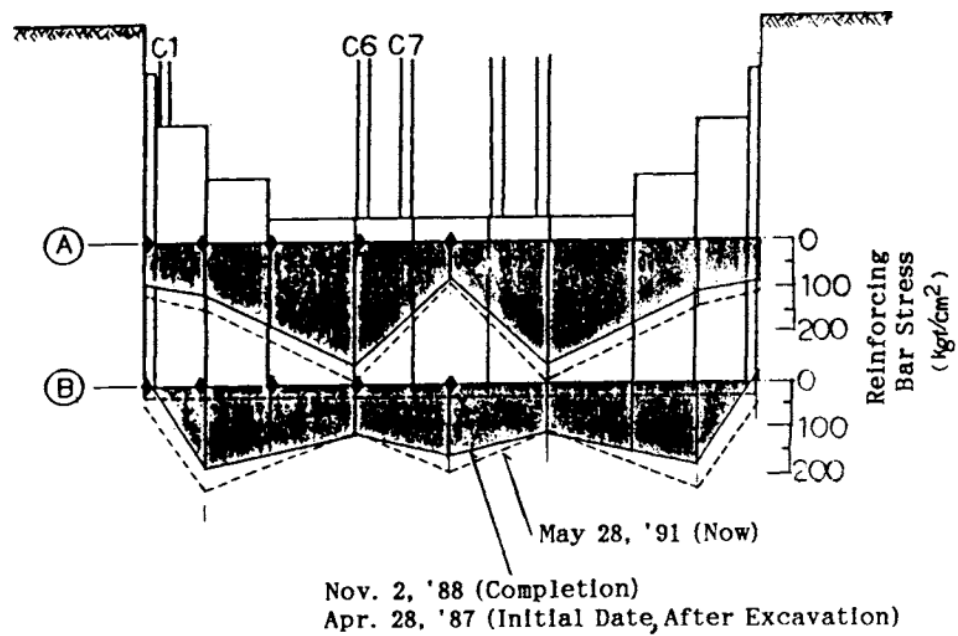


Figure 2.22 Stress distribution of reinforcement bars along the diaphragm walls (Sato *et al.*, 1992)

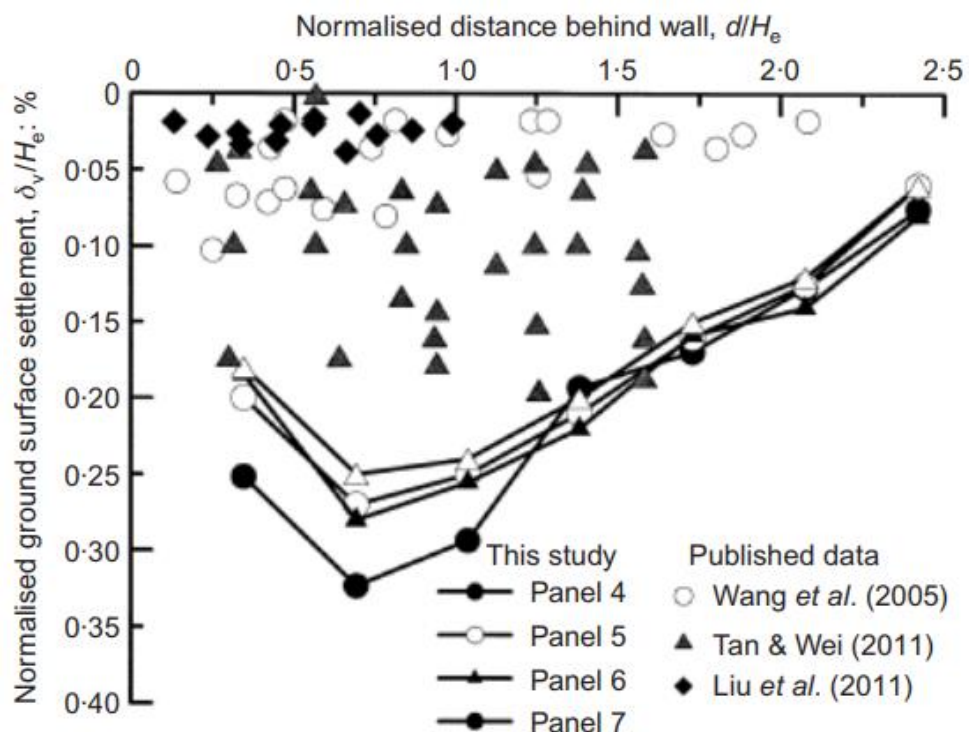


Figure 2.23 Comparison of vertical displacements between greenfield site and those measured in densely developed areas (Ng *et al.*, 2012)

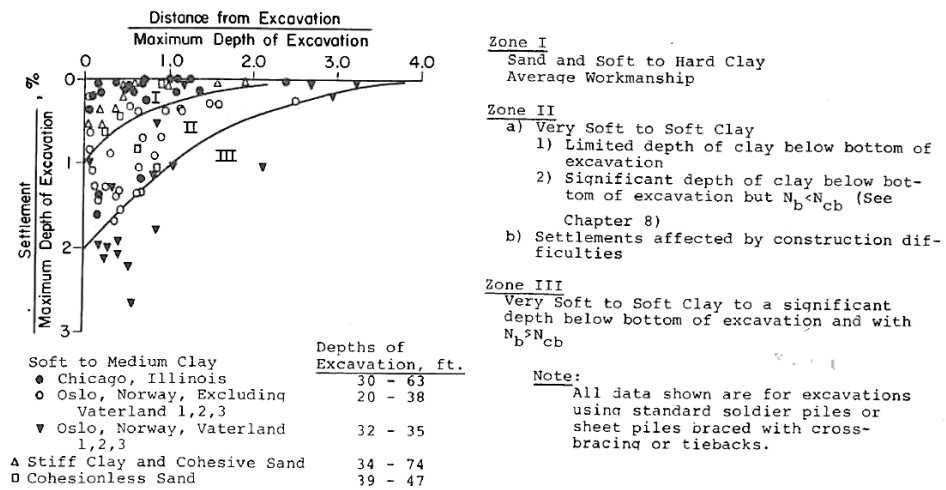


Figure 2.24 Database of settlements of retained surface across various excavations in a range of ground conditions (Peck, 1969)

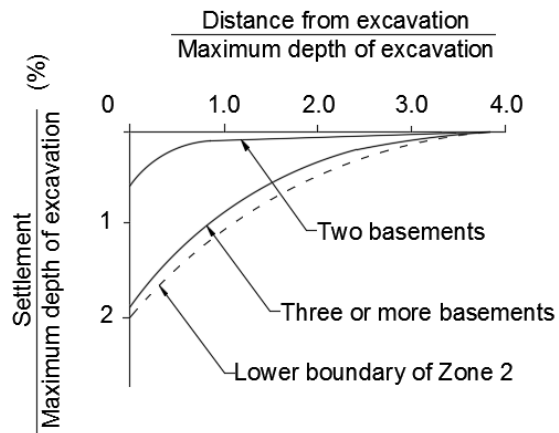


Figure 2.25 Influence of basement level on settlement profile in Chicago (after Peck, 1969)

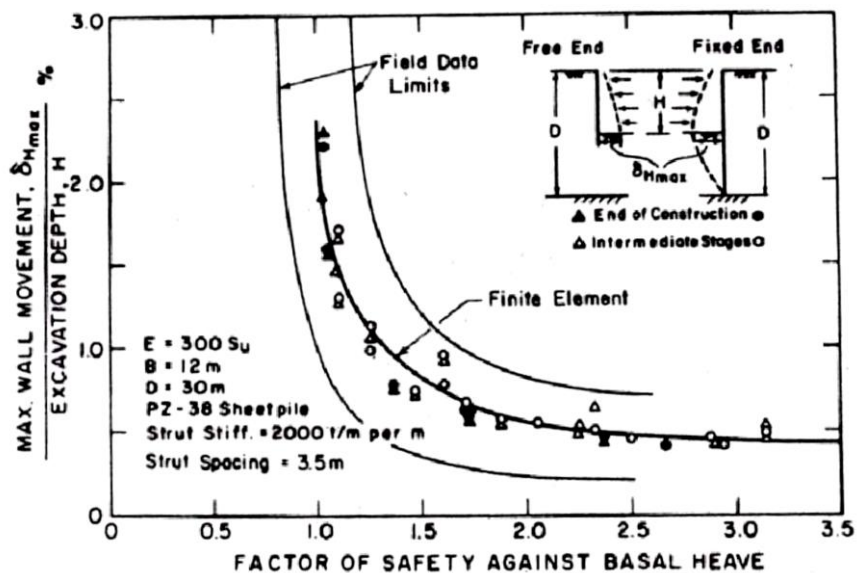


Figure 2.26 Influence of FOS against basal heave on lateral wall displacements (after Mana & Clough, 1991)

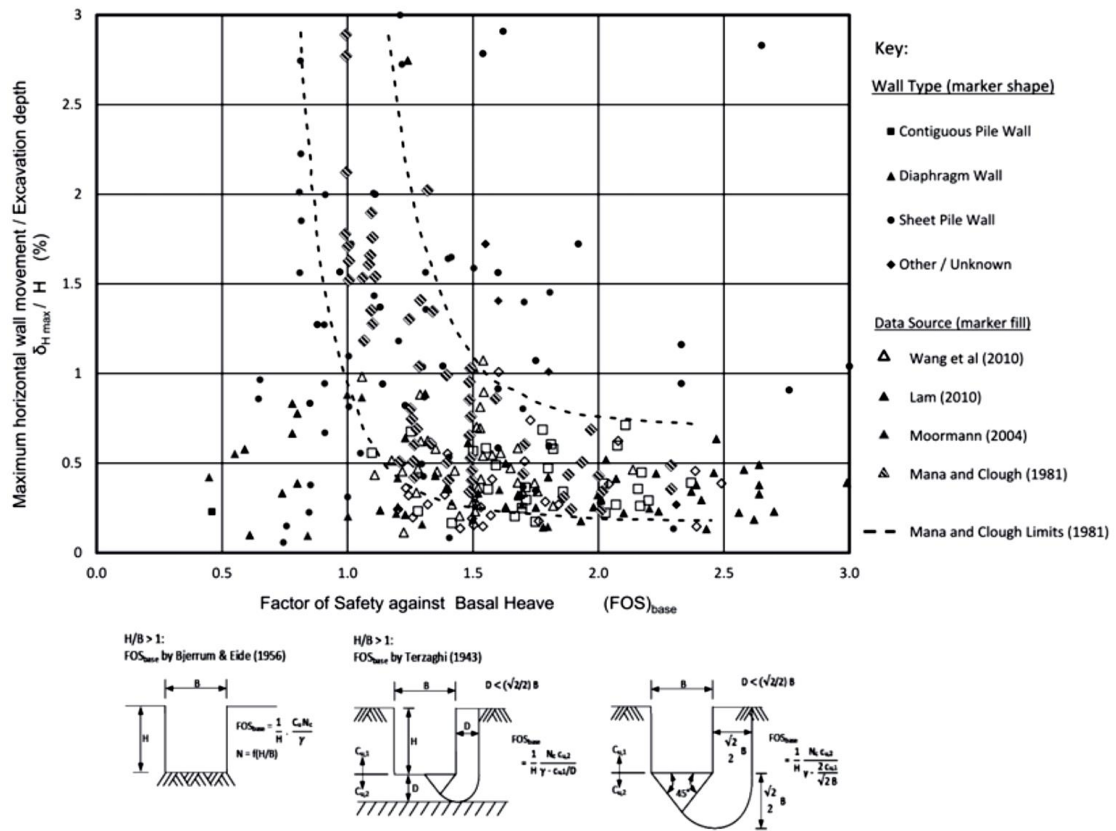


Figure 2.27 Additional data superimposed onto the original Mana & Clough (1981) graph (Gaba *et al.*, 2017)

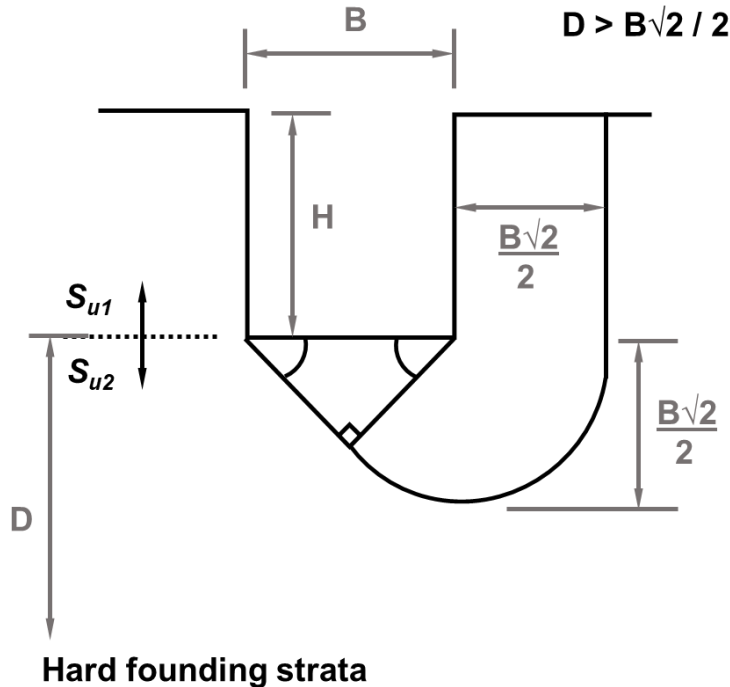


Figure 2.28 Excavation geometry in soft soil used to calculate the factor of safety against base heave

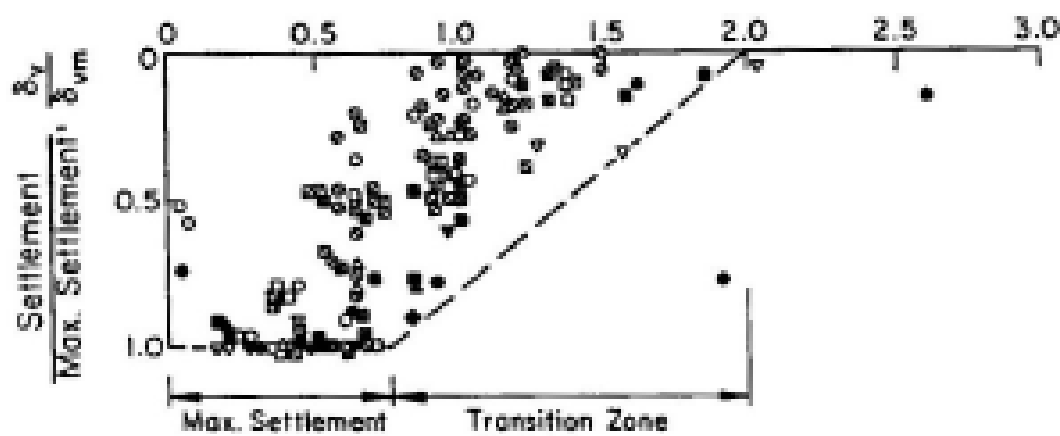


Figure 2.29 Settlement at various distances beyond excavation normalised against the maximum recorded settlement (Clough & O'Rourke, 1990)

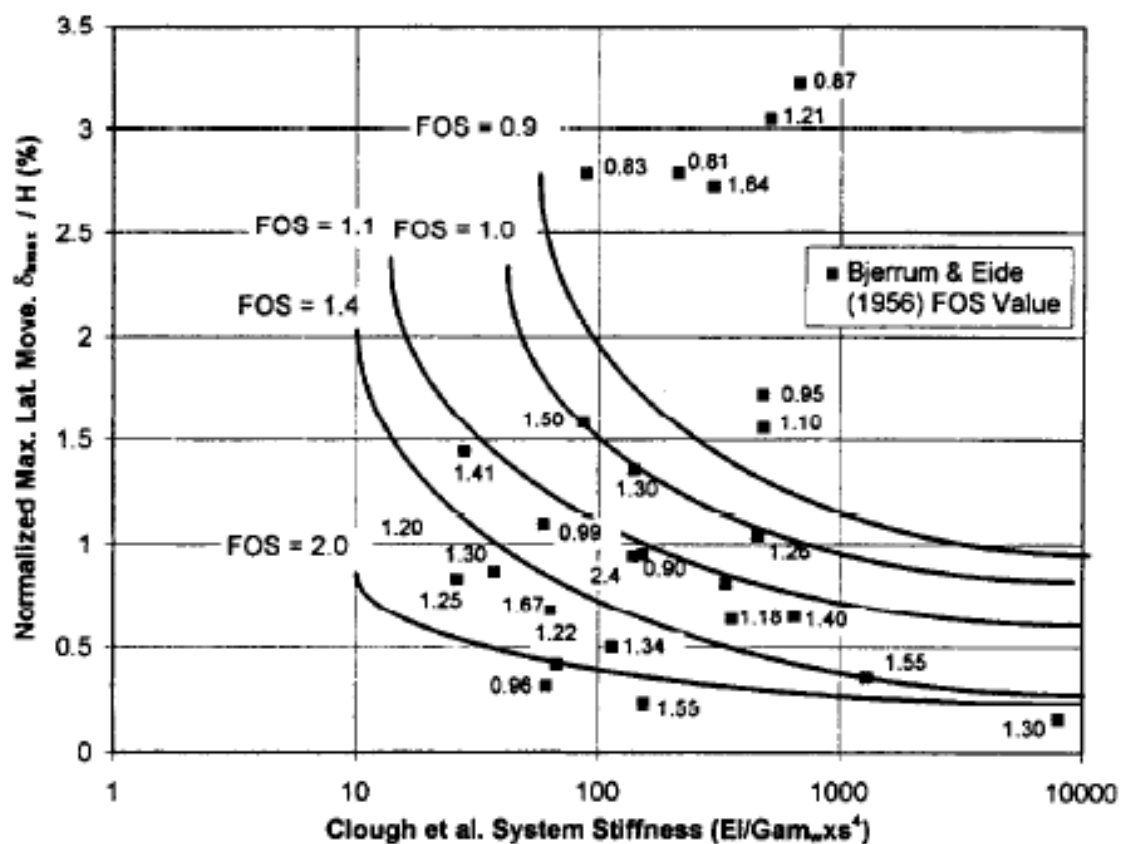


Figure 2.30 Case studies included in the Long (2001) database replotted on Clough *et al.* (1989) graph

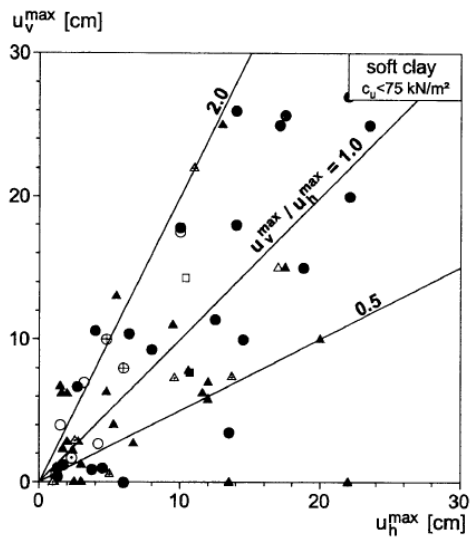


Figure 2.31 Maximum vertical and horizontal displacements arising from deep excavations in soft clay ($S_u < 75 \text{ kN/m}^2$) (Moormann, 2004)

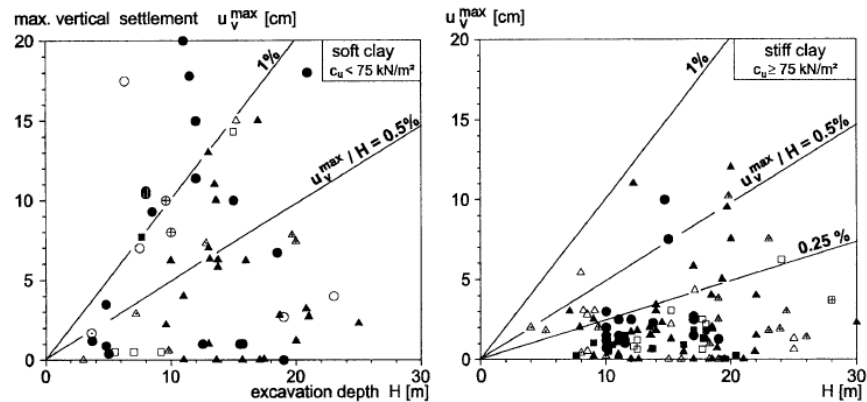


Figure 2.32 Comparison between maximum vertical displacements in soft and stiff ground (Moormann, 2004)

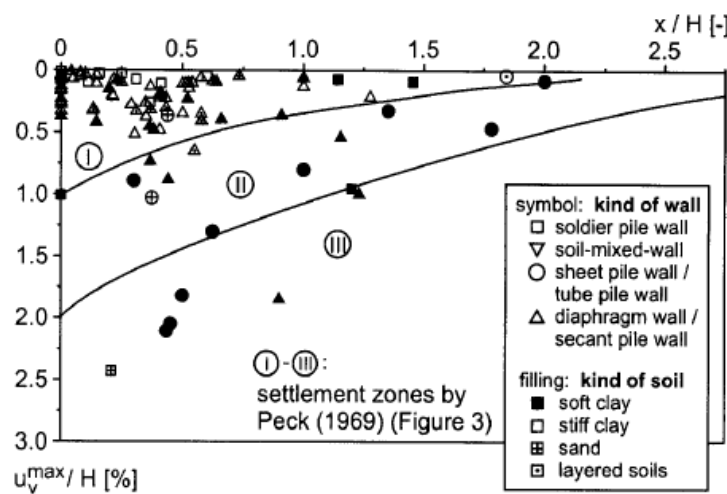


Figure 2.33 Moormann (2004) data superimposed on the Peck (1969) graph

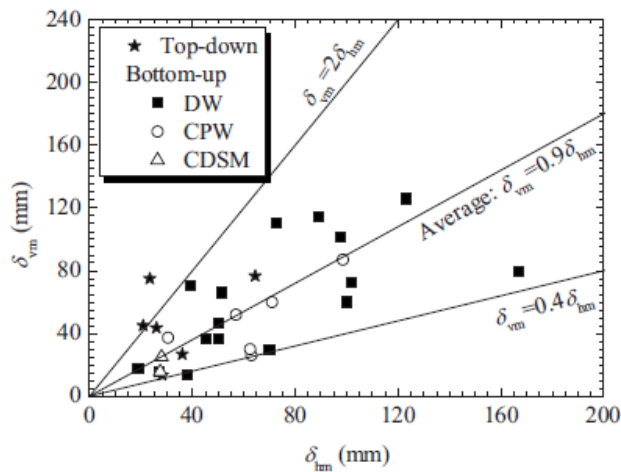


Figure 2.34 Maximum vertical and horizontal displacements arising from deep excavations in soft clay ($20\text{kN/m}^2 < S_u < 40\text{kN/m}^2$) (Wang *et al.*, 2010)

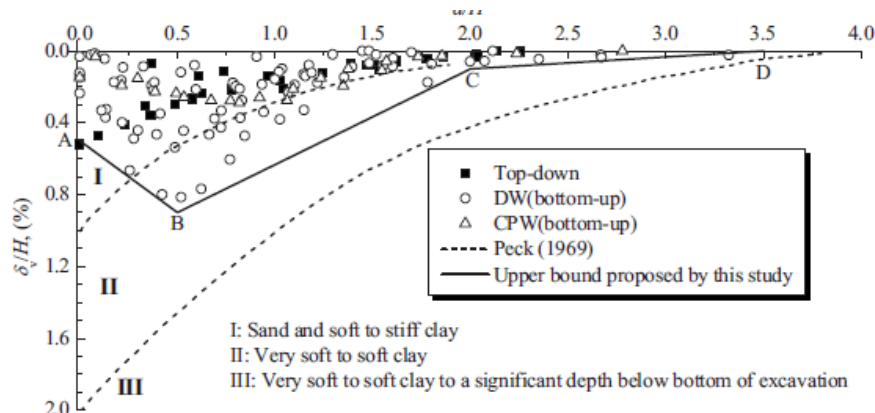


Figure 2.35 Wang *et al.* (2010) data plotted on the Peck (1969) graph

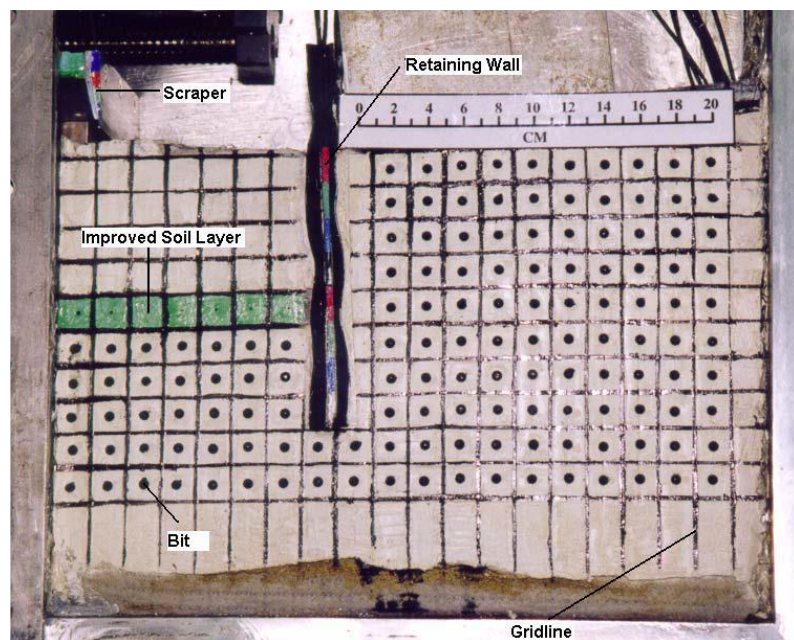


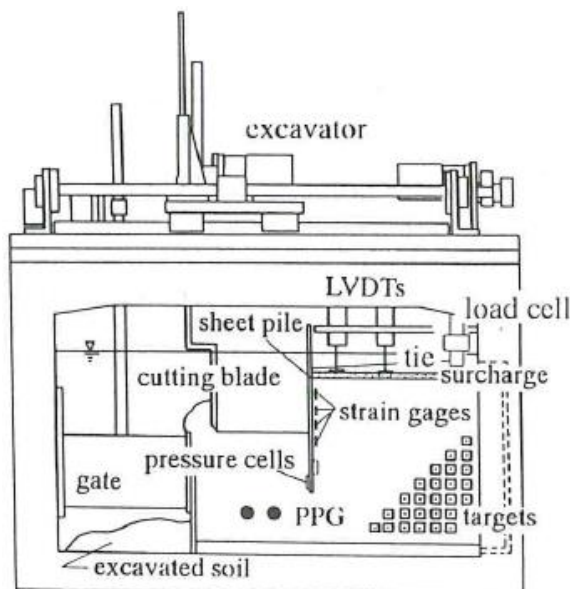
Figure 2.36 Image of excavation produced by in-flight excavator (Lim, 2003)

Test No.	Model Ground	Acceleration	P_{c0}	P_0	Sheet Pile
SP00	uniform	50g	50kPa	10kPa	unsupported
SP01	NC	50g	10kPa	10kPa	without
SP02	OC	50g	30kPa	10kPa	without
SP03	NC	50g	10kPa	10kPa	unsupported
SP04	OC	50g	30kPa	10kPa	unsupported
SP05	NC	50g	10kPa	10kPa	tie backed
SP06	OC	50g	30kPa	10kPa	tie backed

P_{c0} : pre-consolidation pressure at the surface

P_0 : surcharge pressure during test

(a)



(b)

Figure 2.37 (a) centrifuge test series and (b) experiment set up (Kimura *et al.*, 1994)

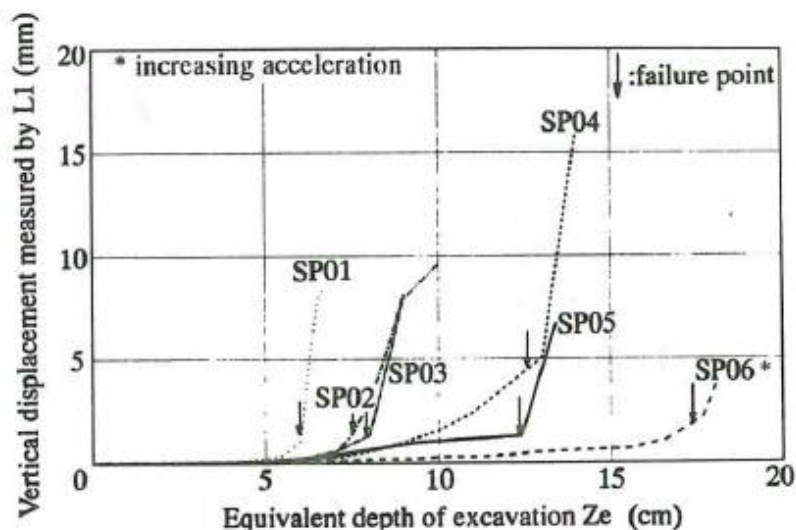


Figure 2.38 Surface settlements measured 25mm from excavation (Kimura *et al.*, 1994)

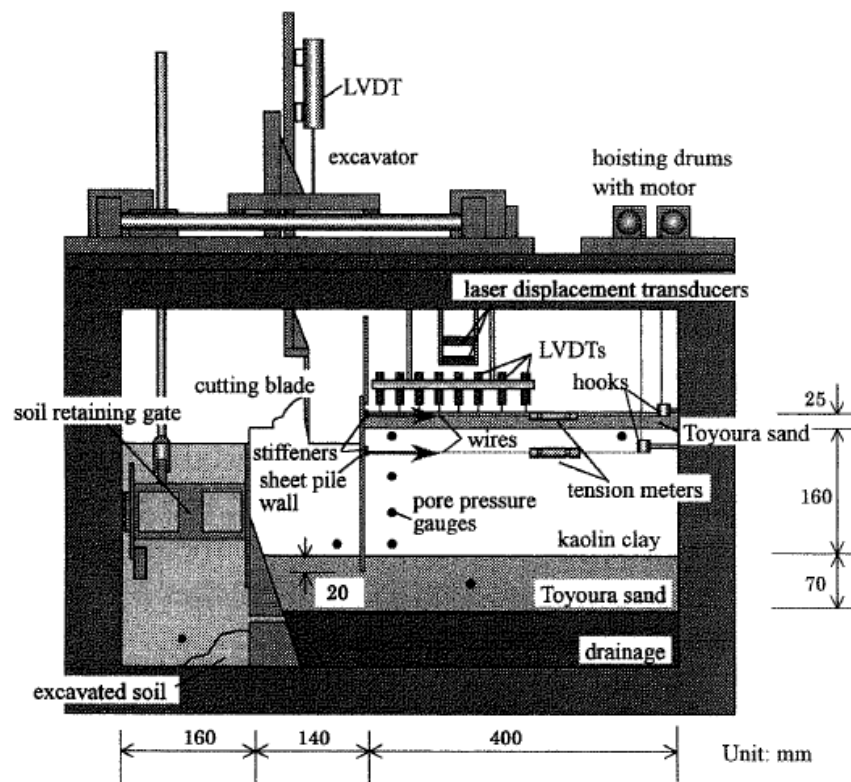


Figure 2.39 In-flight excavation test set up (Takemura *et al.*, 1999)

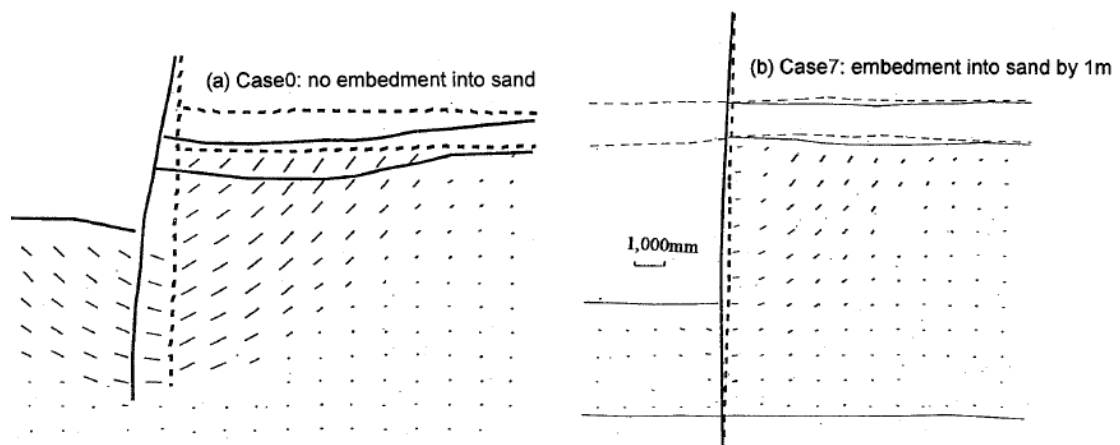


Figure 2.40 Observed deformations for a 5.5m deep excavation illustrating the effect of embedment in sand and a floating wall (Takemura *et al.*, 1999)

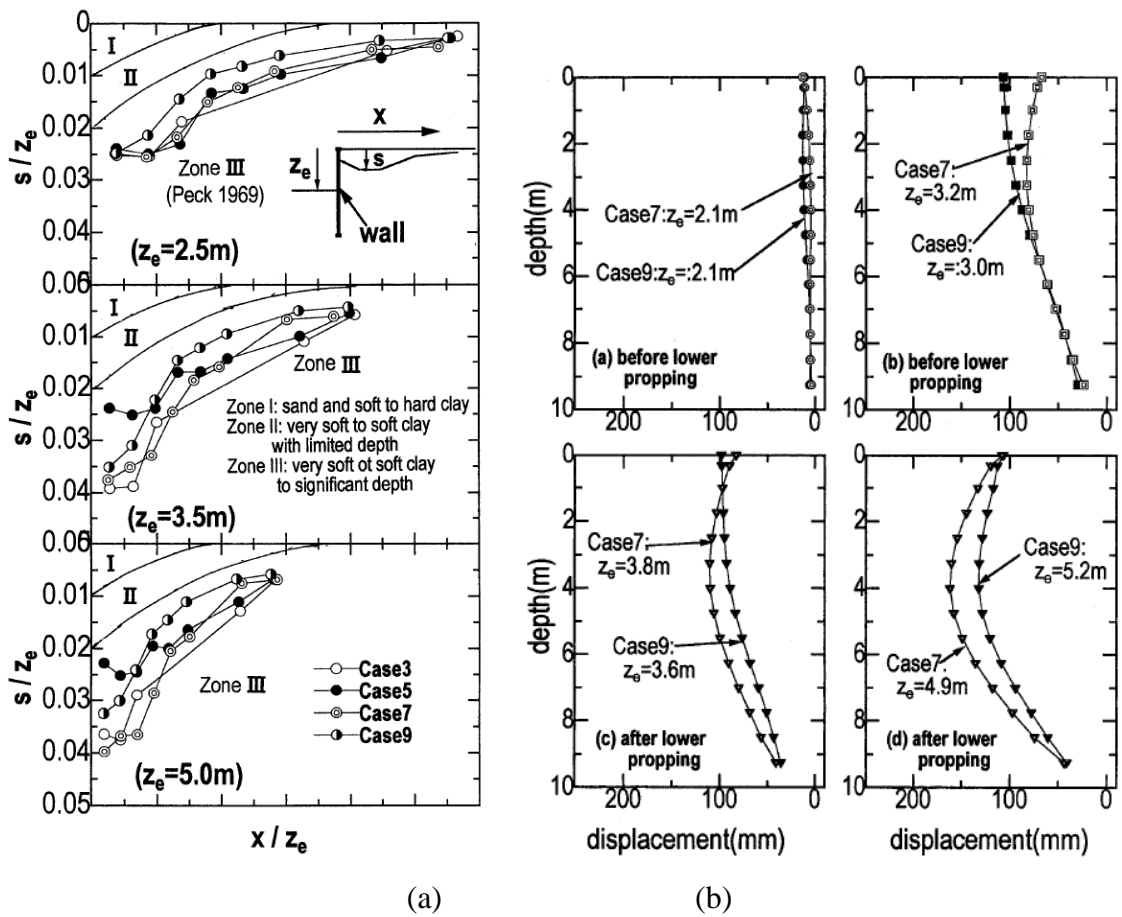


Figure 2.41 (a) normalised surface settlements for various tests as excavation progresses and (b) corresponding lateral wall deflections (Takemura *et al.*, 1999)

Test code	Wall length	Final excavation depth	Flexural rigidity of sheet pile wall	Exca. depth at lower propping	Upper propping force*	Lower propping force*	Remark
Case 0	8.25 m (16.5 mm)	3 m (60 mm)	5.9 MPa·m ⁴ /m (0.05 kPa·m ⁴ /m)	—	3.7 kN/m (11 N)	—	No lower sand Failure before lower propping
Case 3	10.25 m (20.5 mm)	5 m (100 mm)	20 MPa·m ⁴ /m (0.16 kPa·m ⁴ /m)	3.0	3.1 kN/m (9.4 N)	35 kN/m (105 N)	
Case 5	10.25 m (20.5 mm)	5.1 m (102 mm)	20 MPa·m ⁴ /m (0.16 kPa·m ⁴ /m)	2.6	8.0 kN/m (24.3 N)	49 kN/m (146 N)	
Case 7	10.25 m (20.5 mm)	5.5 m (110 mm)	20 MPa·m ⁴ /m (0.16 kPa·m ⁴ /m)	3.2	6.3 kN/m (19.0 N)	44 kN/m (131 N)	
Case 9	10.25 m (20.5 mm)	5.6 m (112 mm)	20 MPa·m ⁴ /m (0.16 kPa·m ⁴ /m)	3.1	3.1 kN/m (9.5 N)	58 kN/m (175 N)	

Note: values in prototype scale are given in the table and model scale in parenthesis

* Total propping forces applied to two wires are shown for model scale.

Figure 2.42 Centrifuge test series (Takemura *et al.*, 1999)

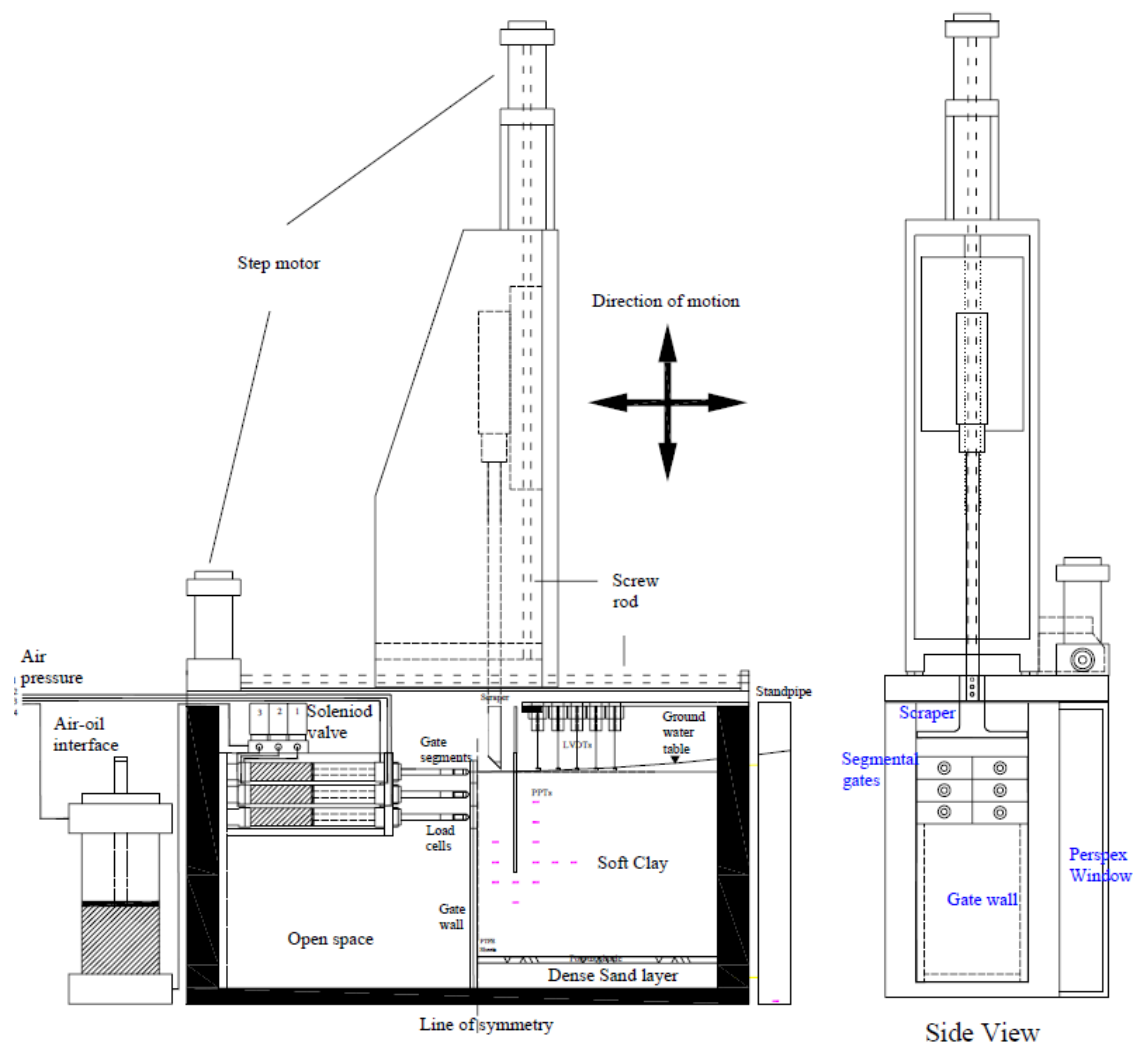


Figure 2.43 Apparatus set up for simulating in-flight excavation (Lam, 2010)

Centrifuge tests	1	2	3	4	5
Objectives	Floating rigid wall with stiff props	Floating flexible wall with stiff props	Fixed-base flexible wall with base grout	Floating rigid wall with soft props	Fixed-base flexible wall in shallow clay
Depth of clay stratum, D (mm)	Baseline test	Wall stiffness	Fixed-wall toe condition	Prop stiffness	Clay thickness
(kN/mm)	300	300	300	300	160
System stiffness $E/I/\gamma_w^4$	1.66	1.66	1.66	0.55	1.66
Toe fixity	Free	Free	Fixed	Free	Free

Figure 2.44 Centrifuge test series (Lam *et al.*, 2014)

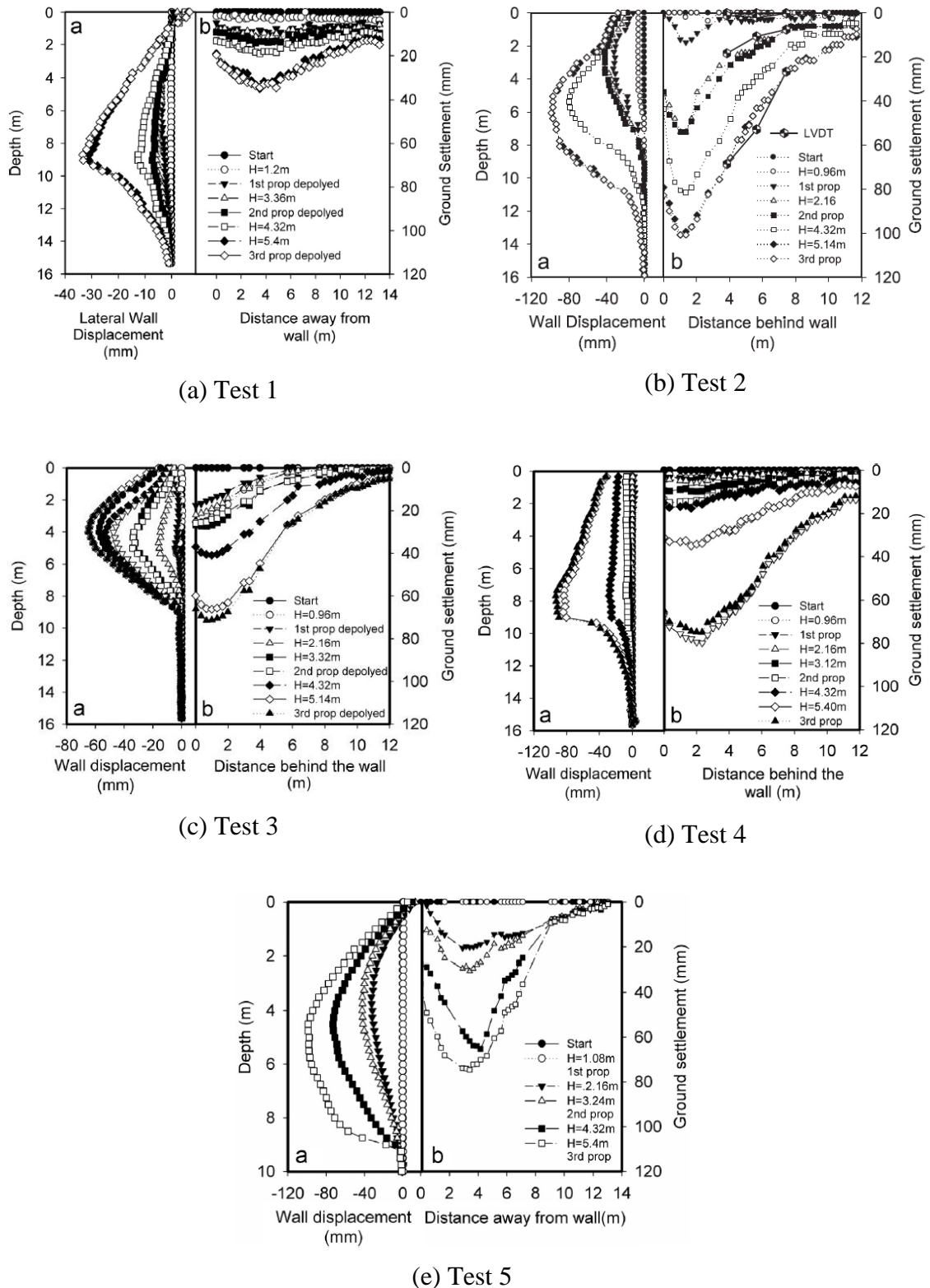


Figure 2.45 Lateral wall deflections and surface settlements recorded in centrifuge tests (Lam *et al.*, 2014)

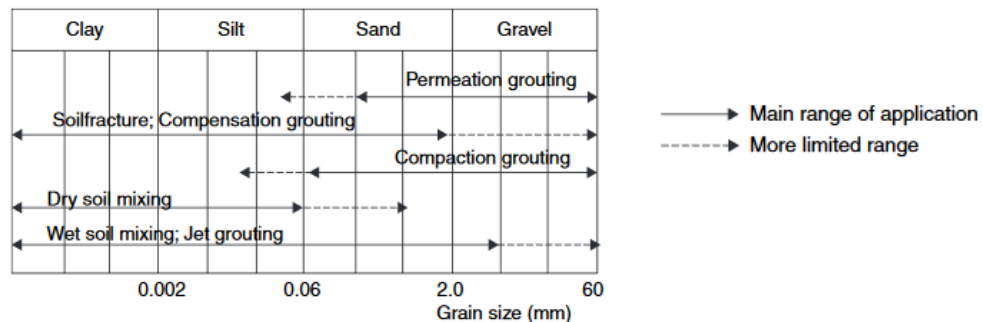


Figure 2.46 Applicability of grouting processes for various soils (Bell, 2012)

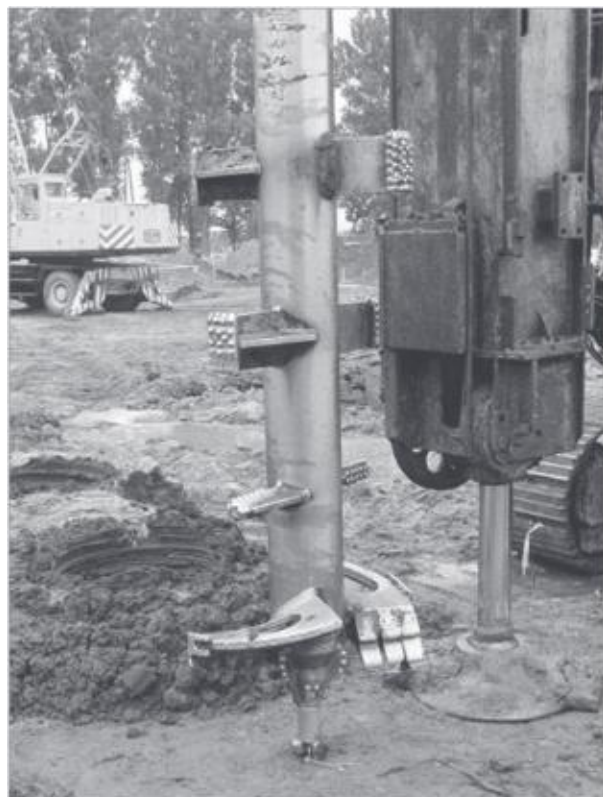


Figure 2.47 Deep soil mixing auger (Bell, 2012)

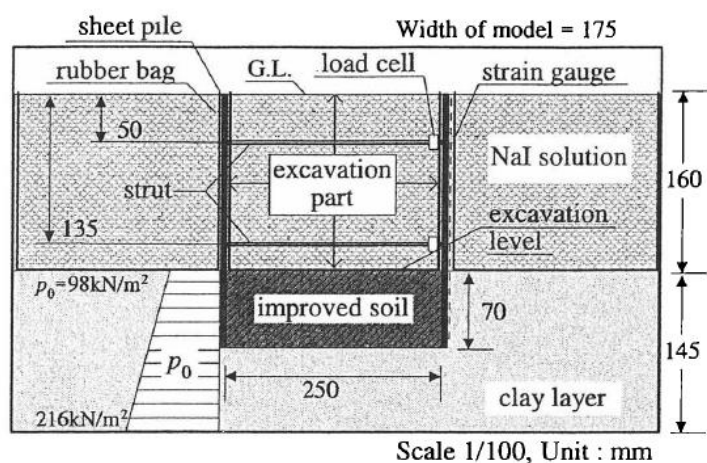


Figure 2.48 Centrifuge set up on DSM ground improvements beneath excavation (Ohnishi *et al.*, 2000)

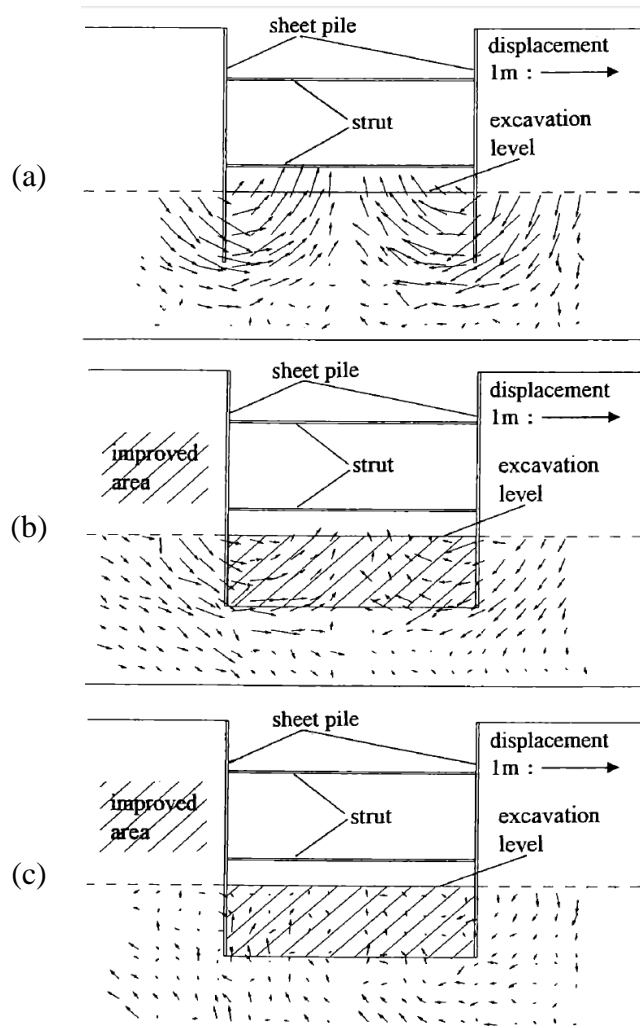


Figure 2.49 Ground deformations for (a) Reference test were bearing capacity of soil is 60kPa (b) improved soil with 100kPa bearing capacity (c) improved soil with 400kPa bearing capacity (Ohnishi *et al.*, 2000)

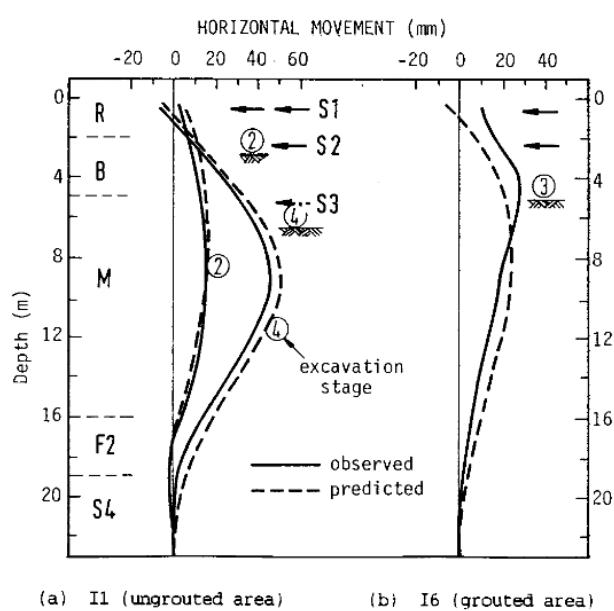


Figure 2.50 Lateral wall deflections in the untreated and ground improved sites (Lee & Yong, 1991)

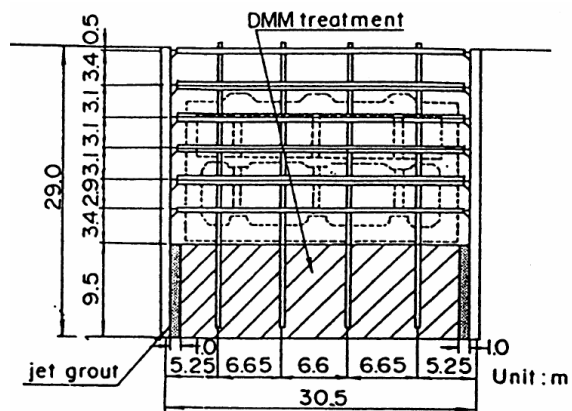


Figure 2.51 Cross section of site and proposed treatment (Tanaka, 1993)

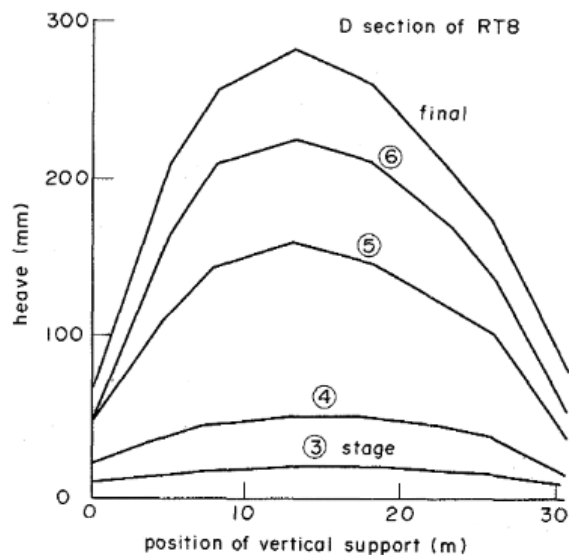


Figure 2.52 Heave measured during each stage of excavation across the entire formation level (Tanaka, 1993)

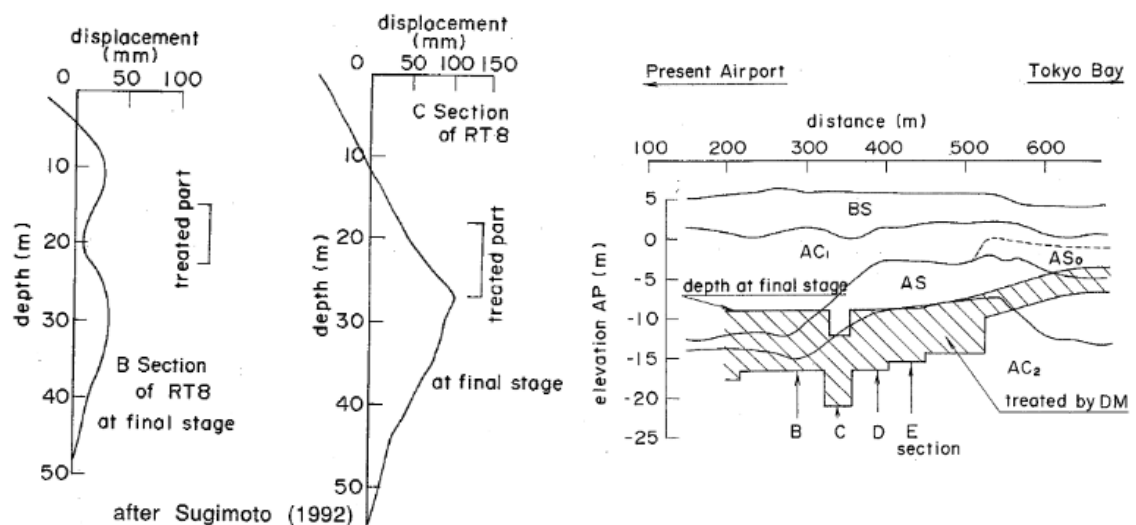


Figure 2.53 Lateral deflections measured at two adjacent locations at end of excavation and section illustrating soil strata, final formation levels and depths of DSM treatment.

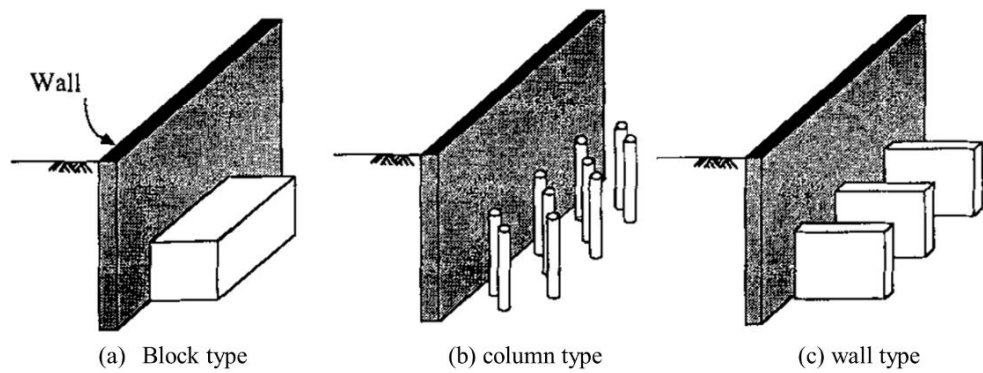


Figure 2.54 Typical DSM patterns for use in excavations (Ou *et al.*, 1996)

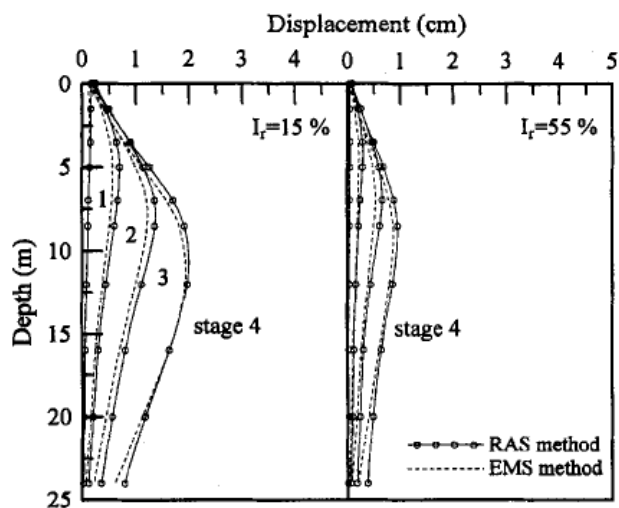


Figure 2.55 Comparison between EMS and RAS simulations (Ou *et al.*, 1996)

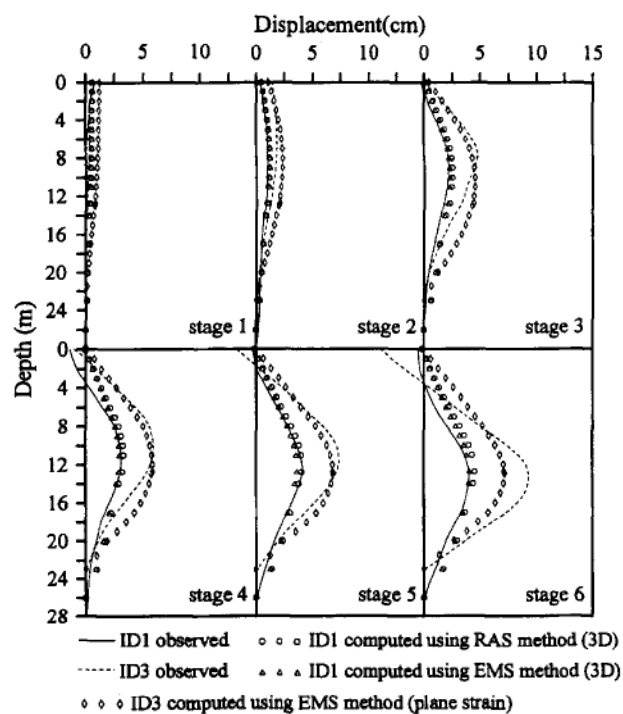


Figure 2.56 Comparisons between field measurements on site in Taipei with the 3D RAS, EMS and 2D EMS models (Ou *et al.*, 1996)

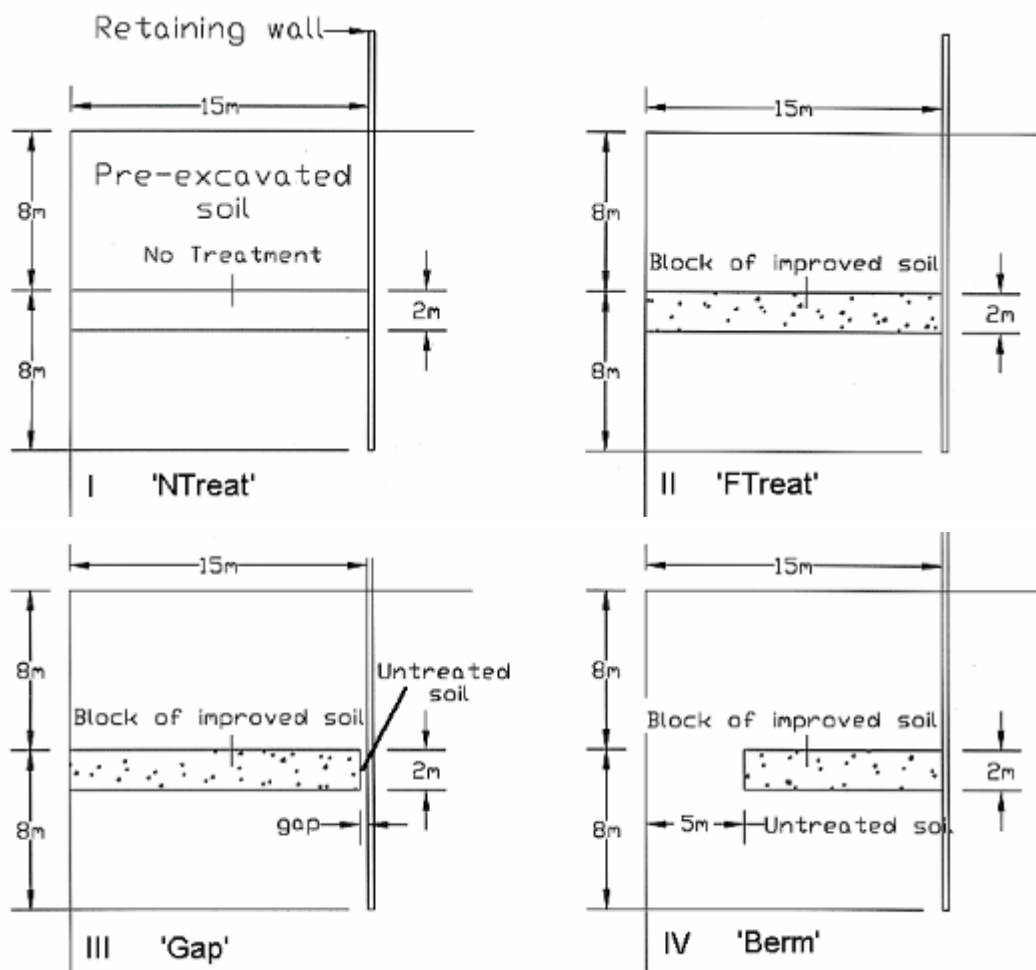


Figure 2.57 Experiment set up to model; (I) reference test; (II) treated strut across entire formation (III) improved soil with the presence of a gap and (IV) an improved soil berm (Lim, 2003)

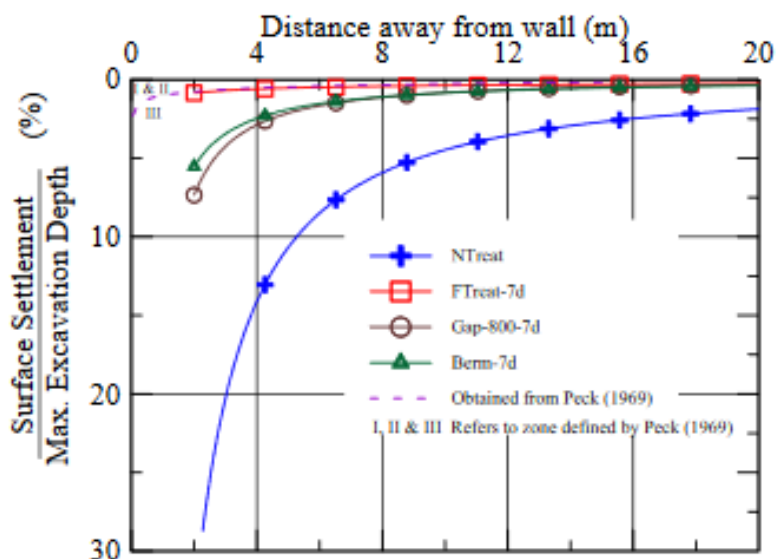


Figure 2.58 Typical results from centrifuge tests (Lim, 2003)

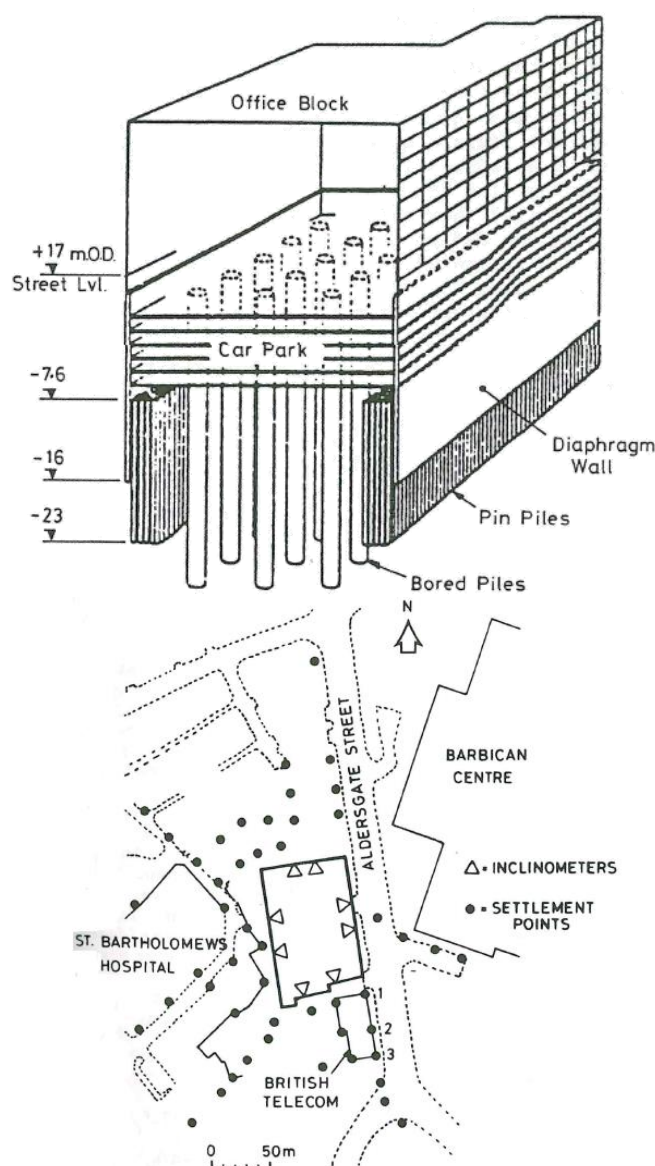


Figure 2.59 Schematic of pin piles used in construction of deep excavation in London Clay and plan of site (Fernie *et al.*, 1991)

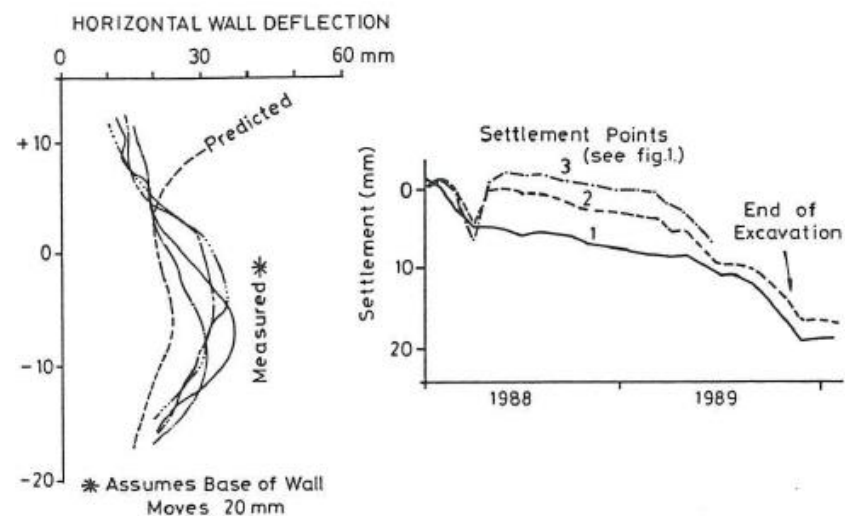


Figure 2.60 Measured displacements after excavation (Fernie *et al.*, 1991)

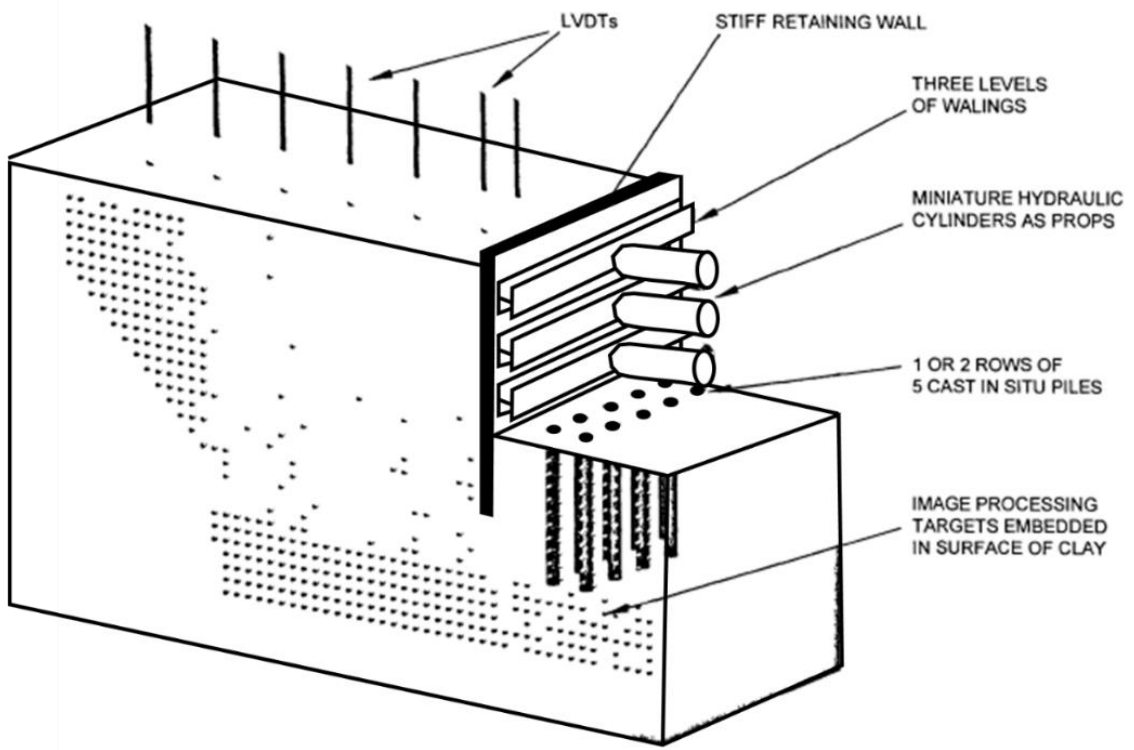


Figure 2.61 Schematic of heave reducing pile model (after McNamara, 2001)

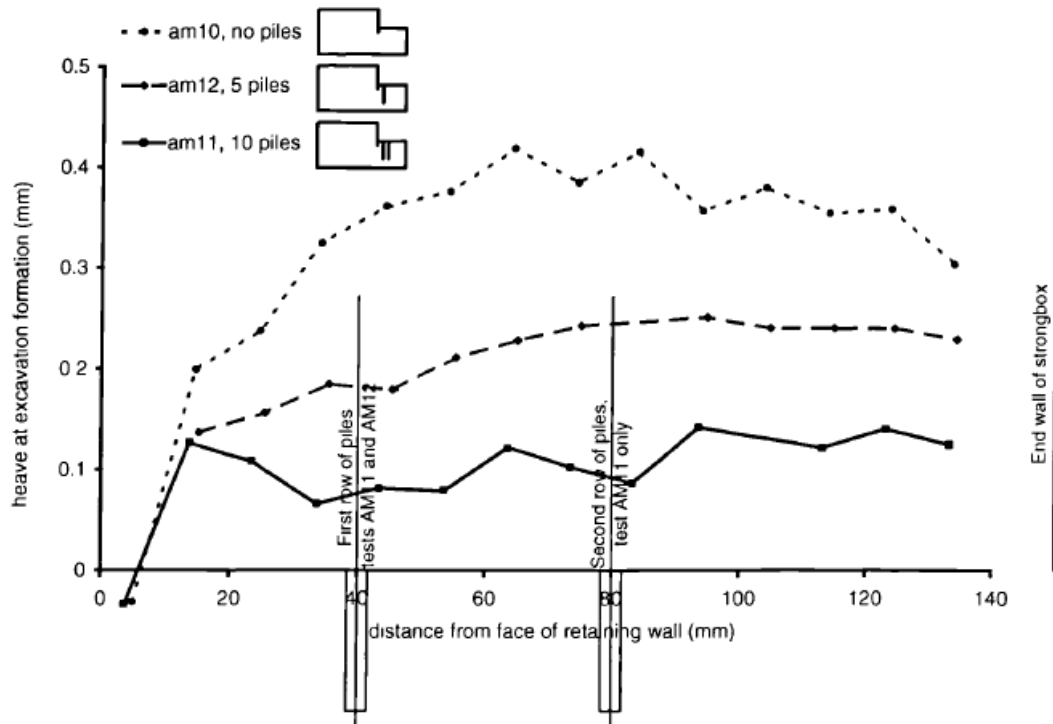


Figure 2.62 Comparable heave developed at formation (McNamara, 2001)

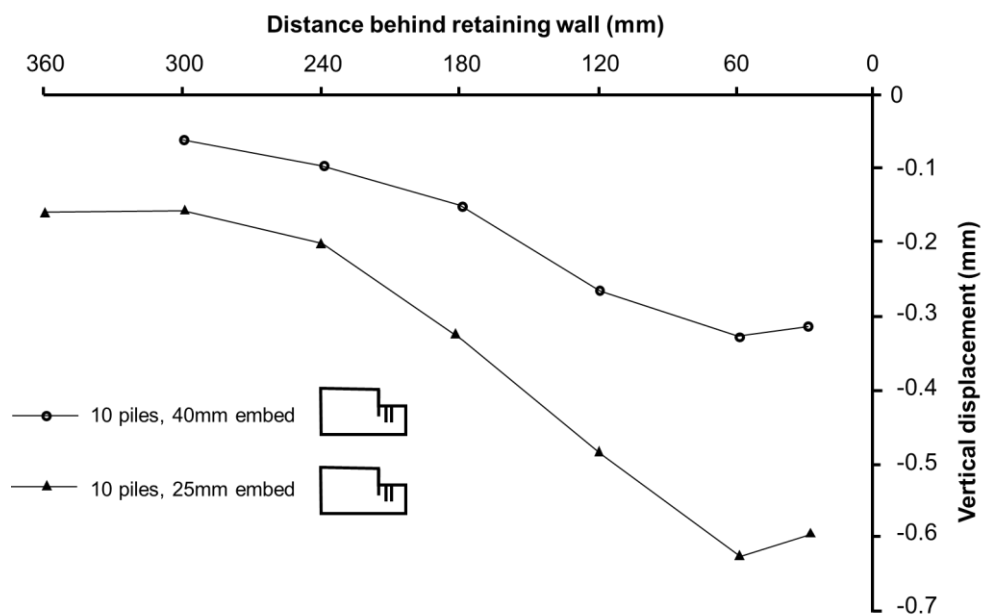


Figure 2.63 Influence of embedment on ground movements (after McNamara, 2001)

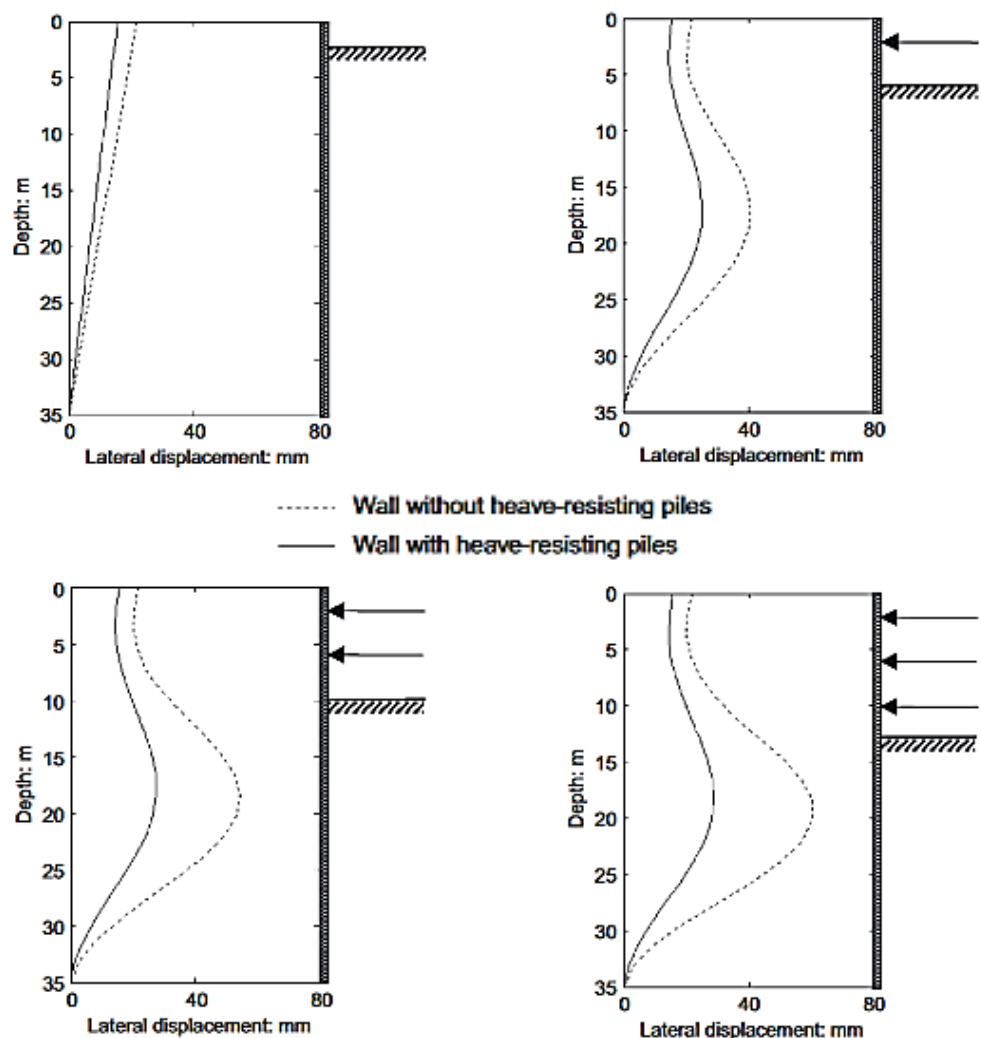


Figure 2.64 Comparative influence of heave reducing piles on predicted lateral deflections for braced excavation as excavation progresses (Osman & Bolton, 2006)

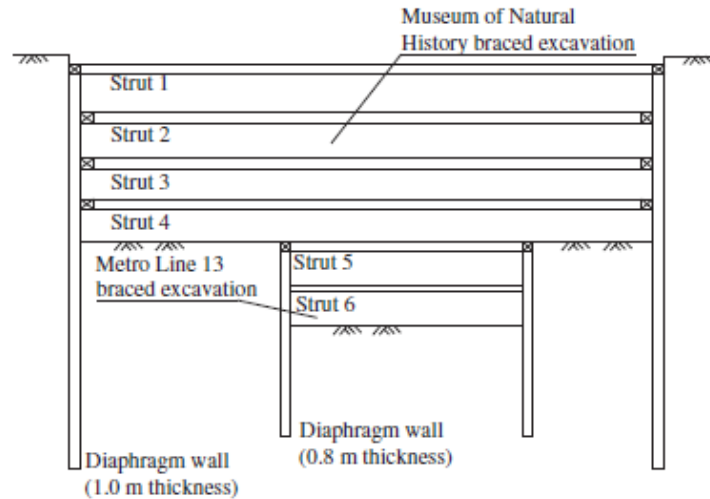


Figure 2.65 Pit-in-pit excavation (Sun *et al.*, 2017)

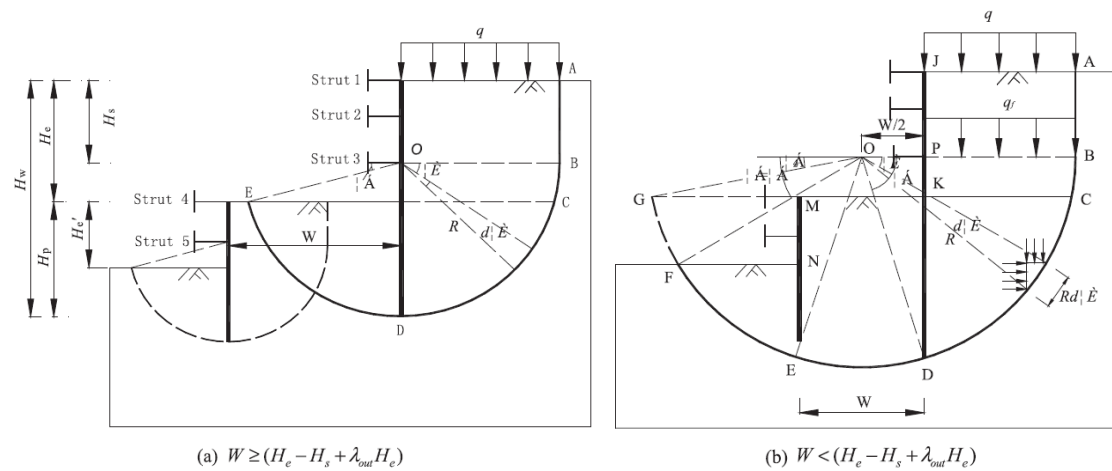


Figure 2.66 Failure mechanisms of varying wall spacing for pit-in-pit braced excavations (Sun *et al.*, 2017)

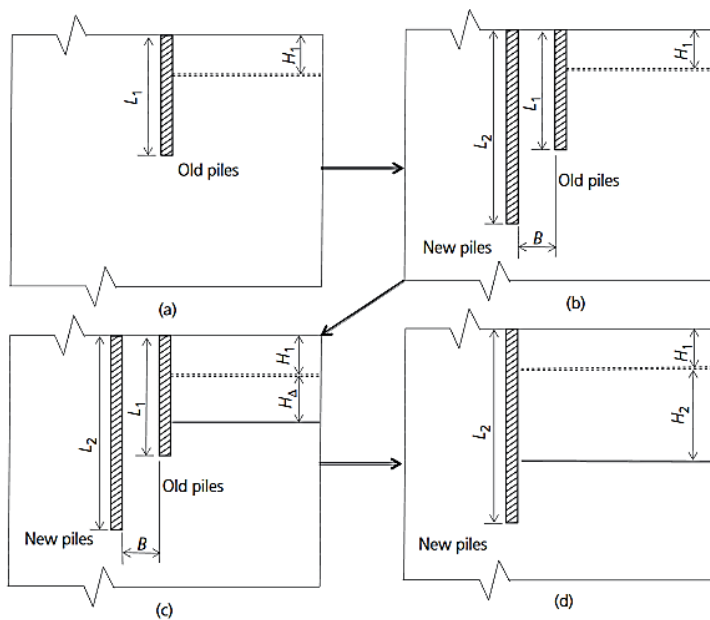


Figure 2.67 Sequence of double walled excavations (Yu *et al.*, 2018)

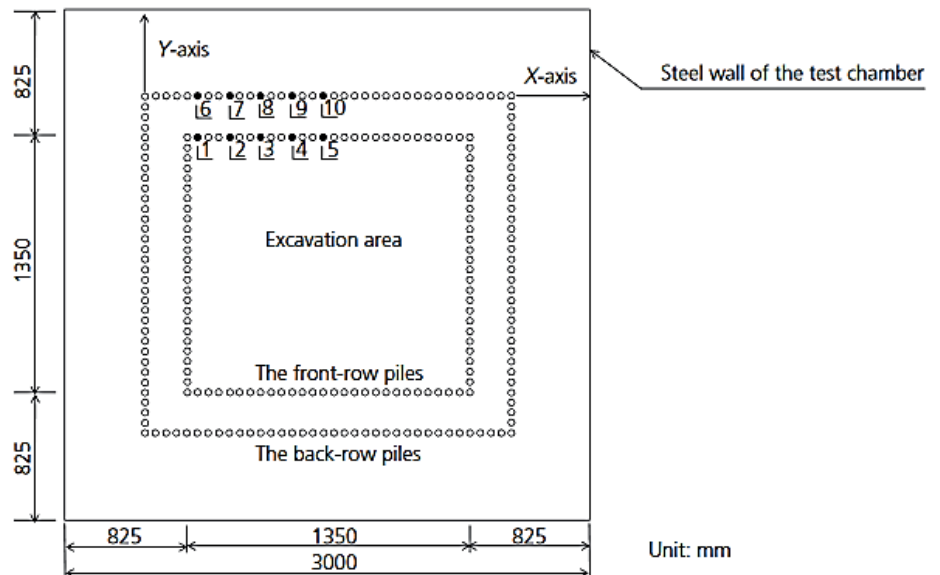


Figure 2.68 Plan of modelled tests (Yu *et al.*, 2018)

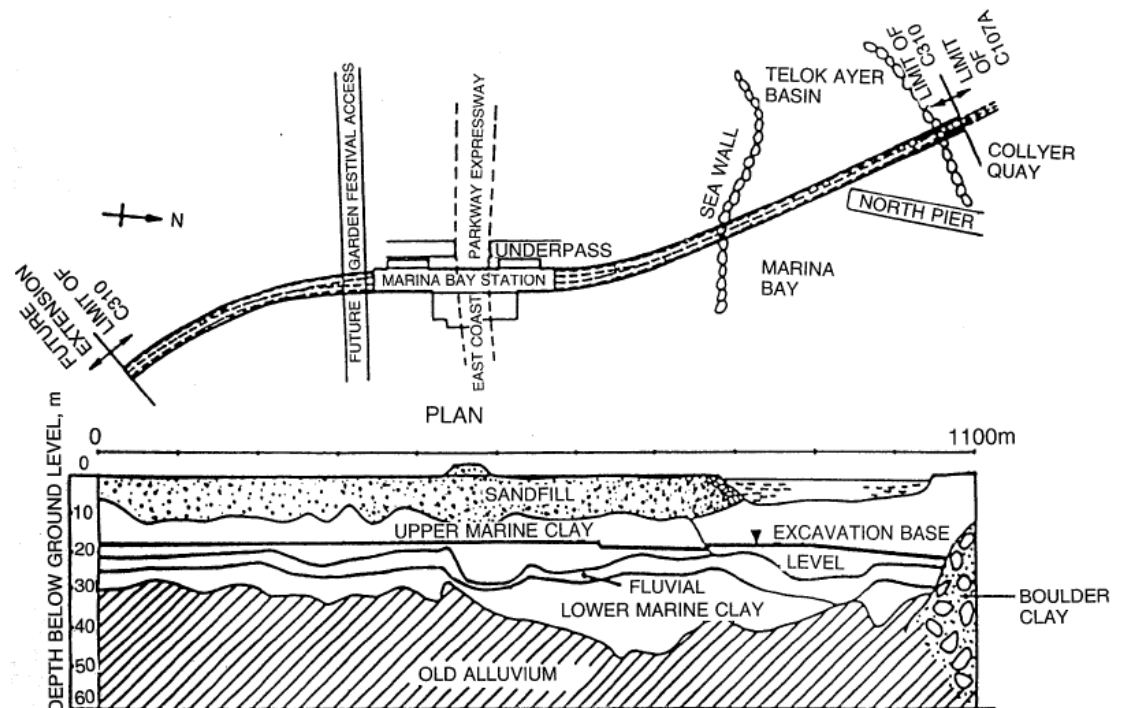


Figure 2.69 Singapore Marina Bay station location and cross section (Denman *et al.*, 1987)

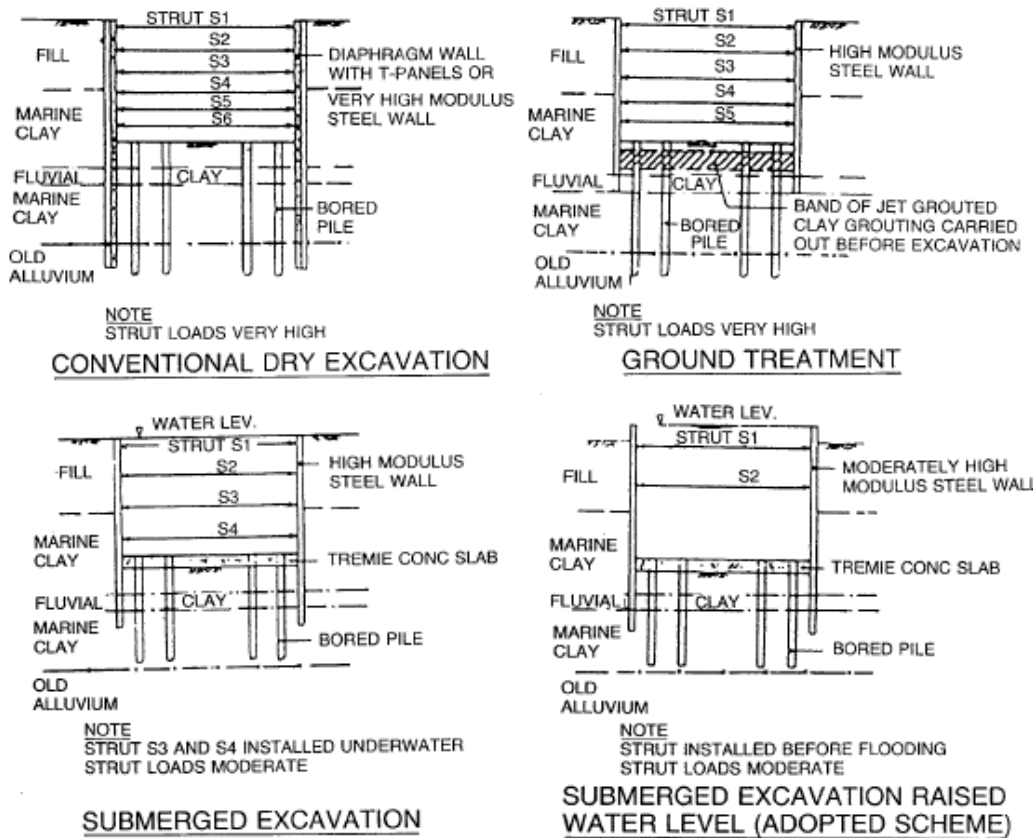


Figure 2.70 Excavation schemes considered for the construction of the Marina Bay station box (Denman *et al.*, 1987)

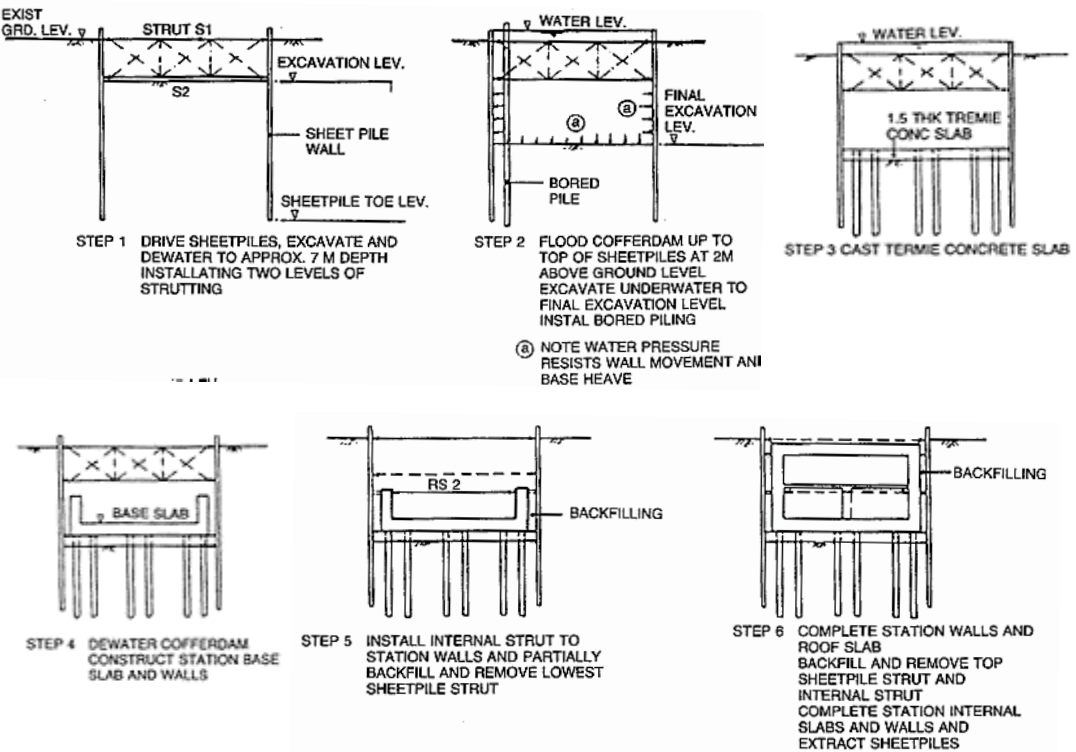


Figure 2.71 Excavation sequence at Marina Bay, Singapore (Denman *et al.*, 1987)

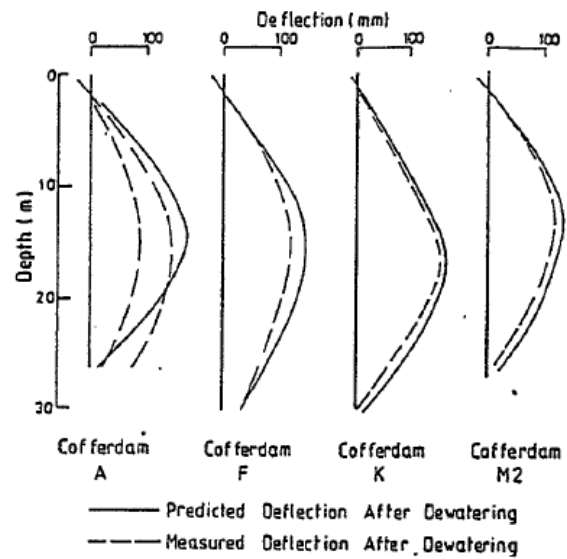


Figure 2.72 Comparisons between measured and predicted deflections (Clarke & Prebaharan, 1987)

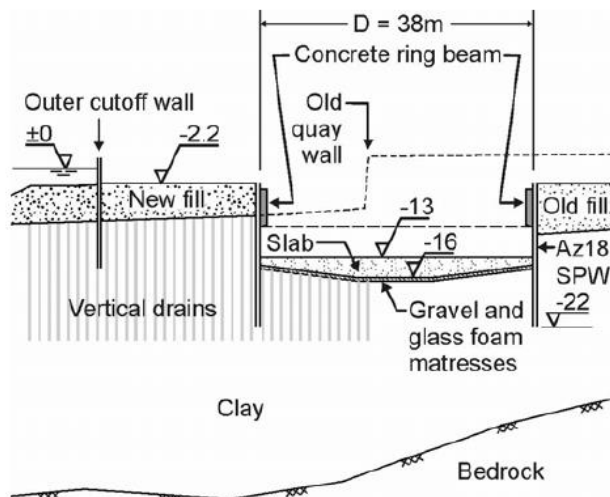


Figure 2.73 Cross section through Oslo Opera excavation site (Karlsrud & Andresen, 2008)

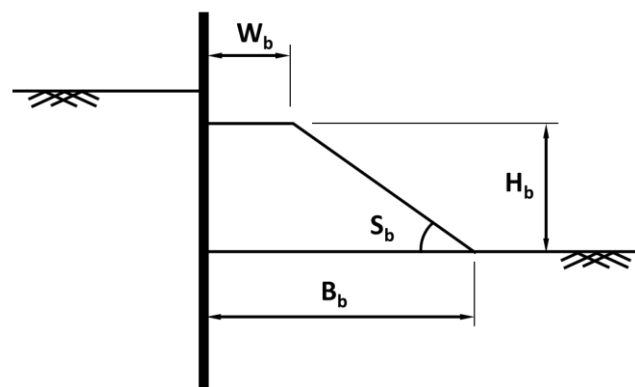


Figure 2.74 Typical berm geometry

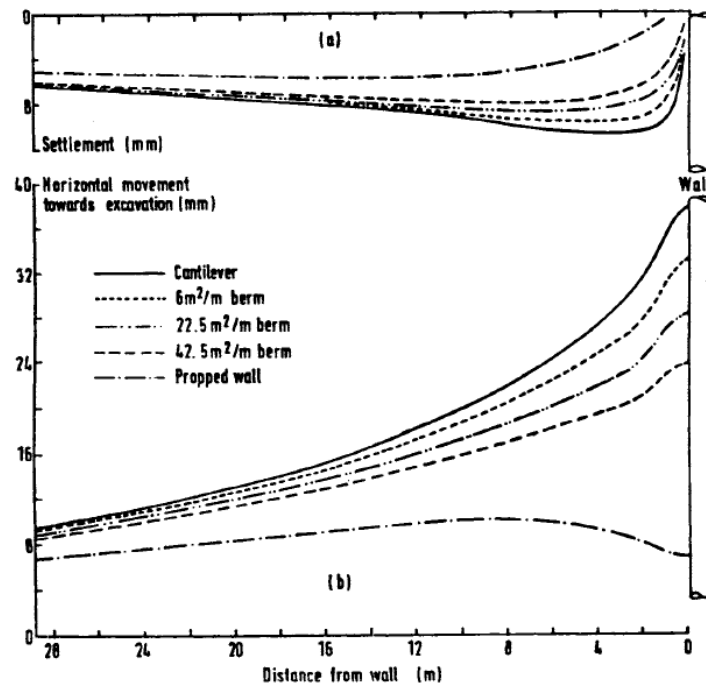


Figure 2.75 Influence of berm volume on settlements and lateral deflections compared with a cantilevered and propped excavation (Potts *et al.*, 1993)

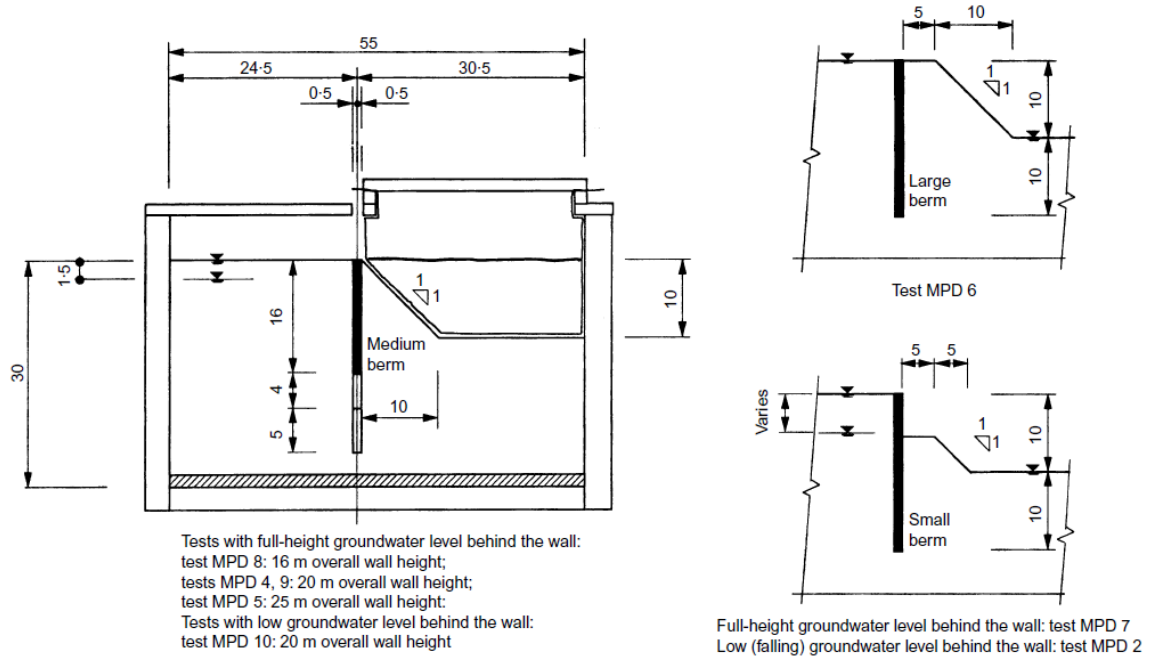
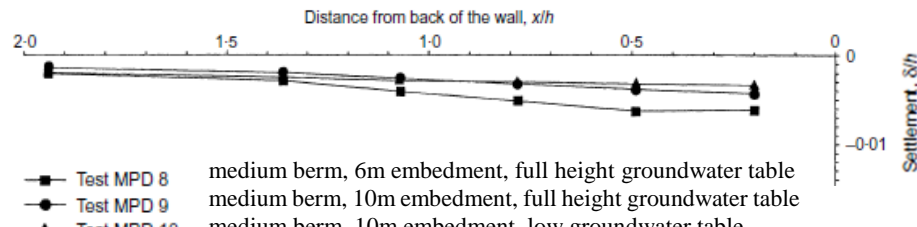
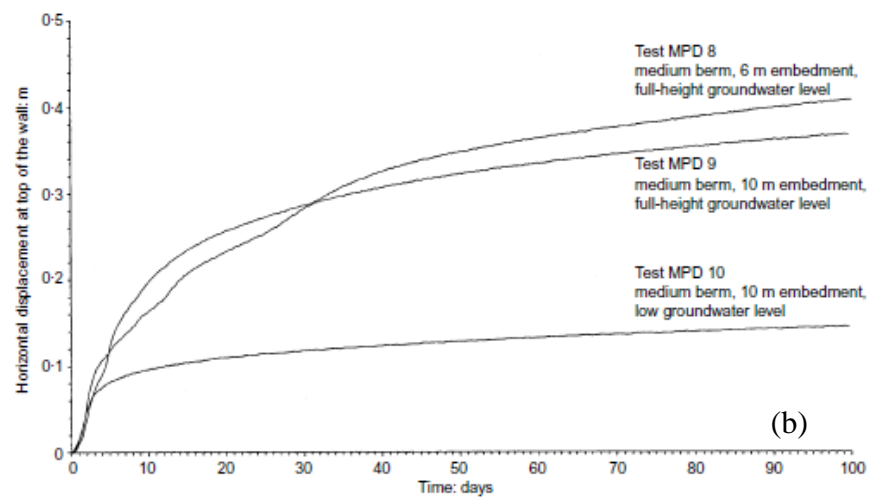


Figure 2.76 Experiment set up (Powrie & Daly, 2002)

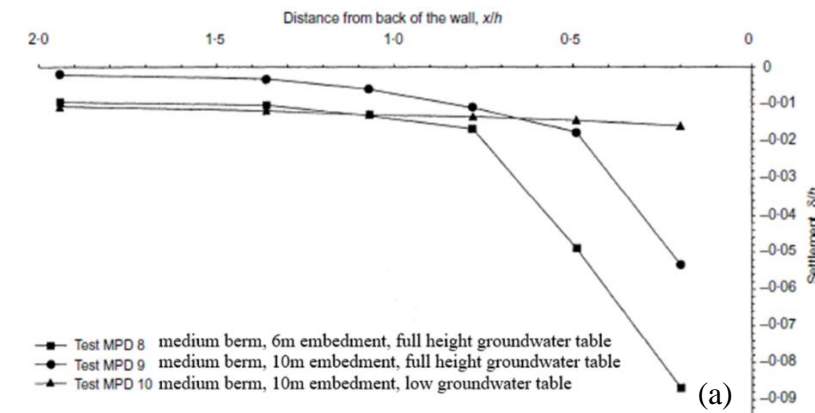


(a)

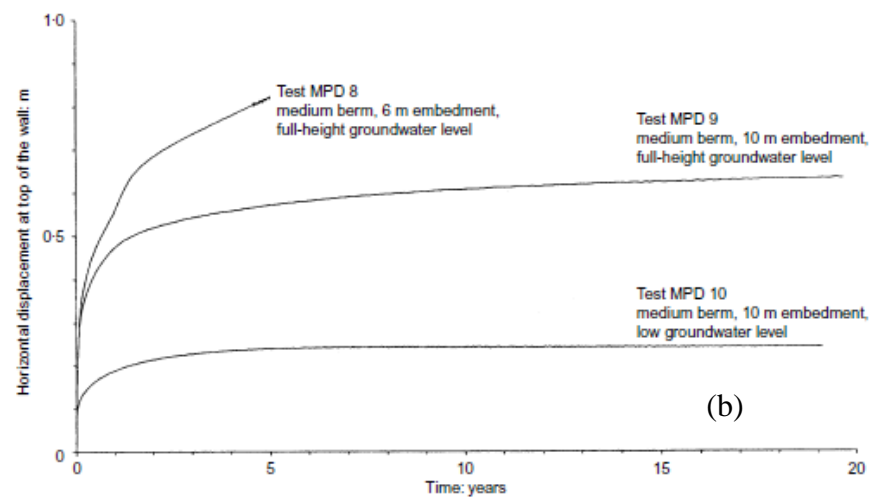


(b)

Figure 2.77 Short term behaviour on (a) surface settlement profile (a) lateral displacements of wall crest immediately after excavation (Powrie & Daly, 2002)



(a)



(b)

Figure 2.78 Long term behaviour on (a) surface settlement profile 5 years after excavation (a) wall crest lateral displacements between 0-20 years (Powrie & Daly, 2002)

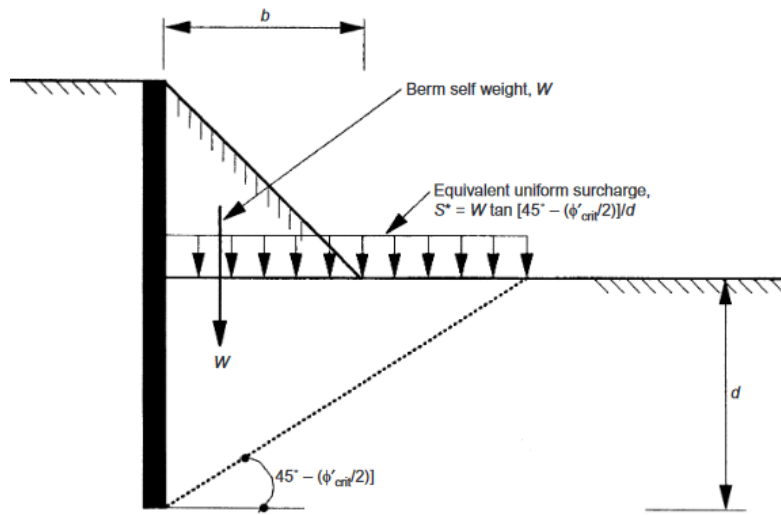


Figure 2.79 Equivalent surcharge method (Daly & Powrie, 2001)

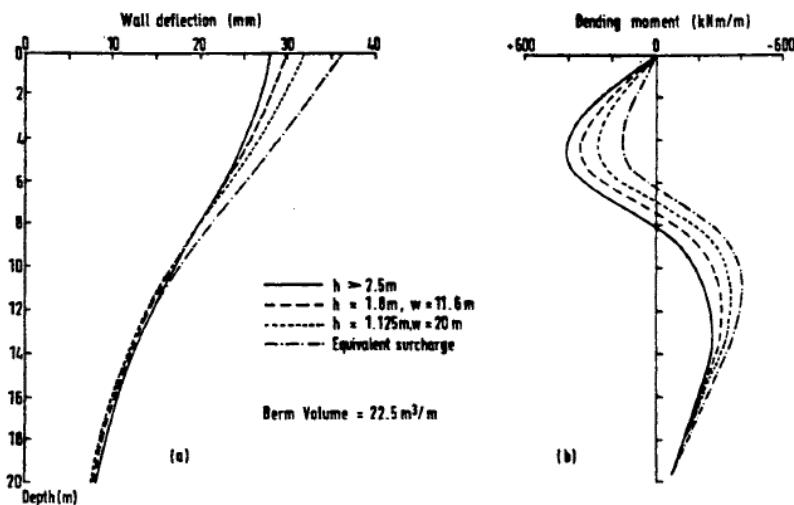


Figure 2.80 Comparison between modelled and equivalent surcharge method berms on wall deflections and bending moments (Potts *et al.*, 1993)

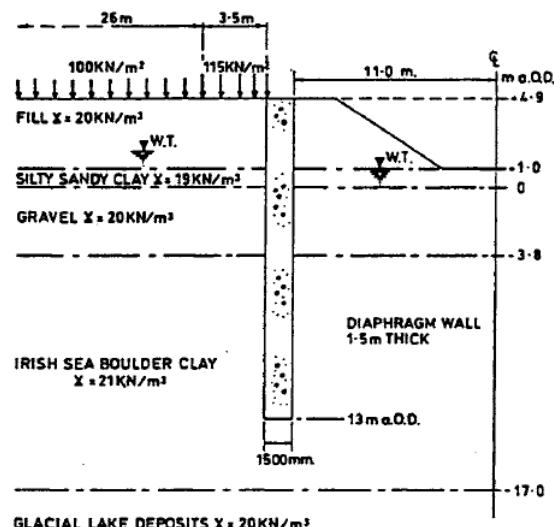


Figure 2.81 Berm geometry and soil profile (Powrie *et al.*, 1993)

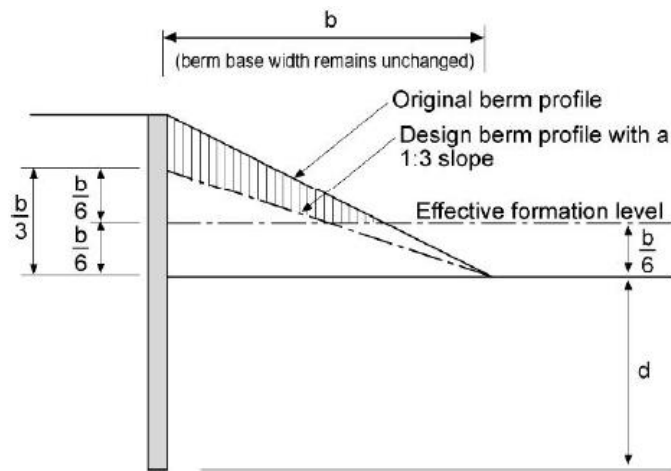


Figure 2.82 Raised effective formation level method (Gaba *et al.*, 2017)

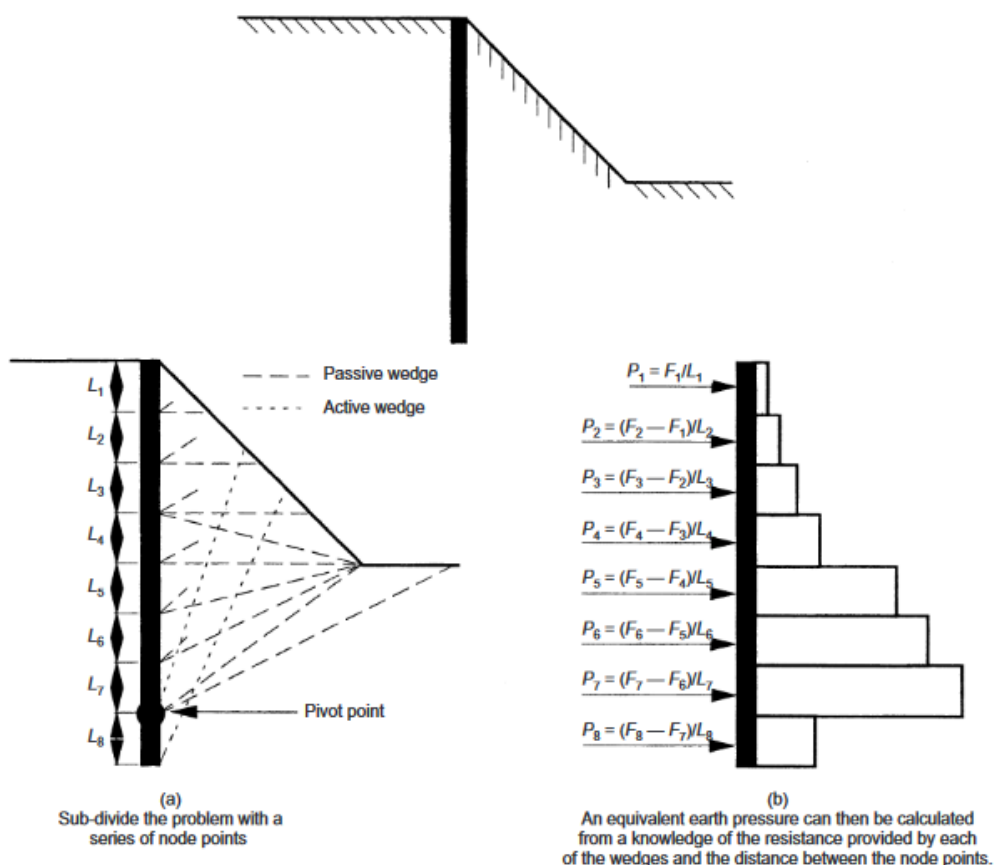


Figure 2.83 Modified limit equilibrium method (Daly & Powrie, 2001)

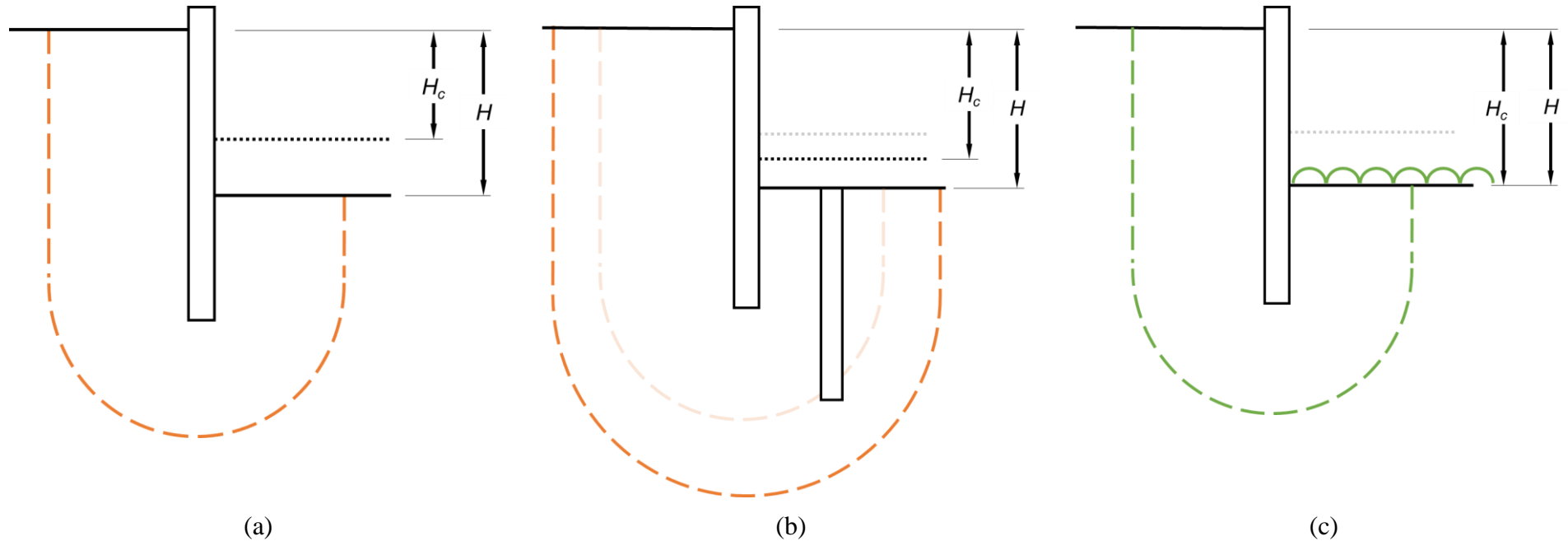


Figure 2.84 (a) Classic deformation mechanism where H_c is the critical height that the excavation reaches prior to failure and H is the design excavation depth (b) influence of construction techniques designed to interrupt the classic deformation mechanism and (c) effect of reducing the vertical stress change

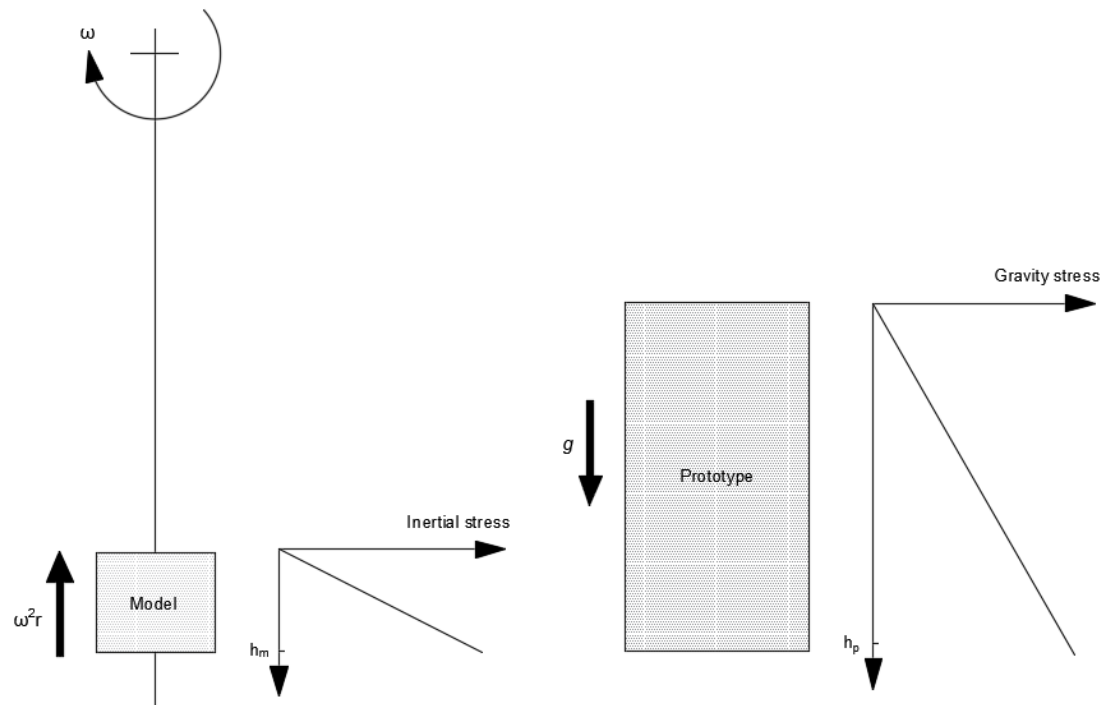


Figure 3.1 Gravitational stress in prototype modelled by inertial stresses induced by rotational acceleration in centrifuge (after Taylor, 1995)

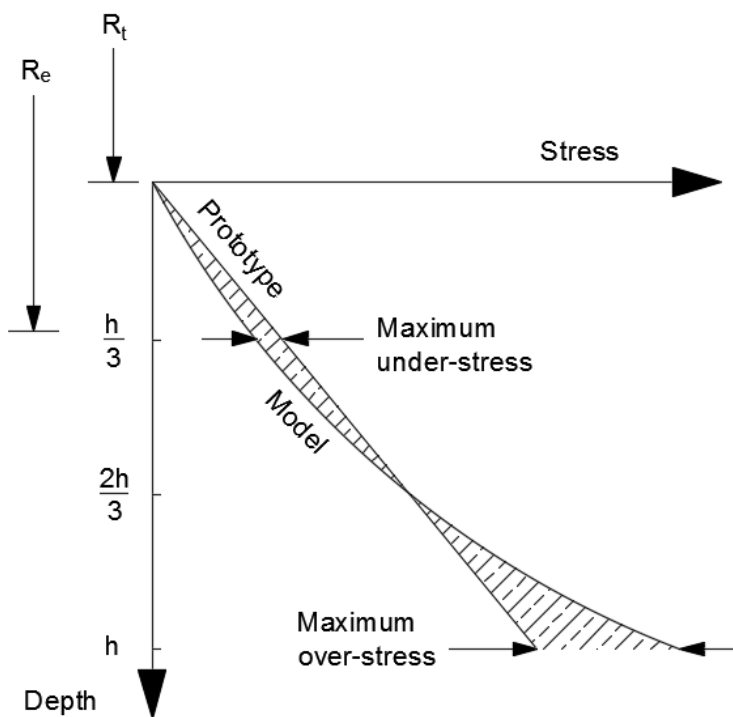


Figure 3.2 Under and over stress in the centrifuge model (after Taylor, 1995)

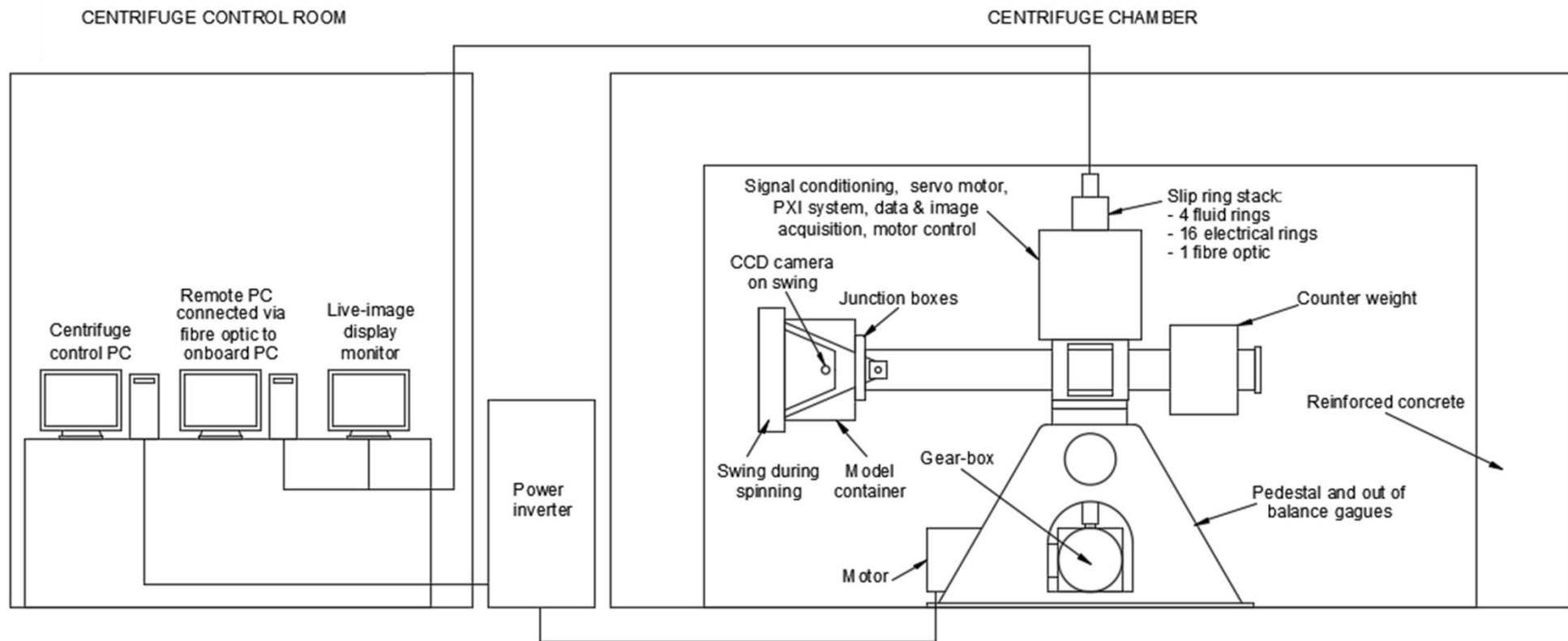
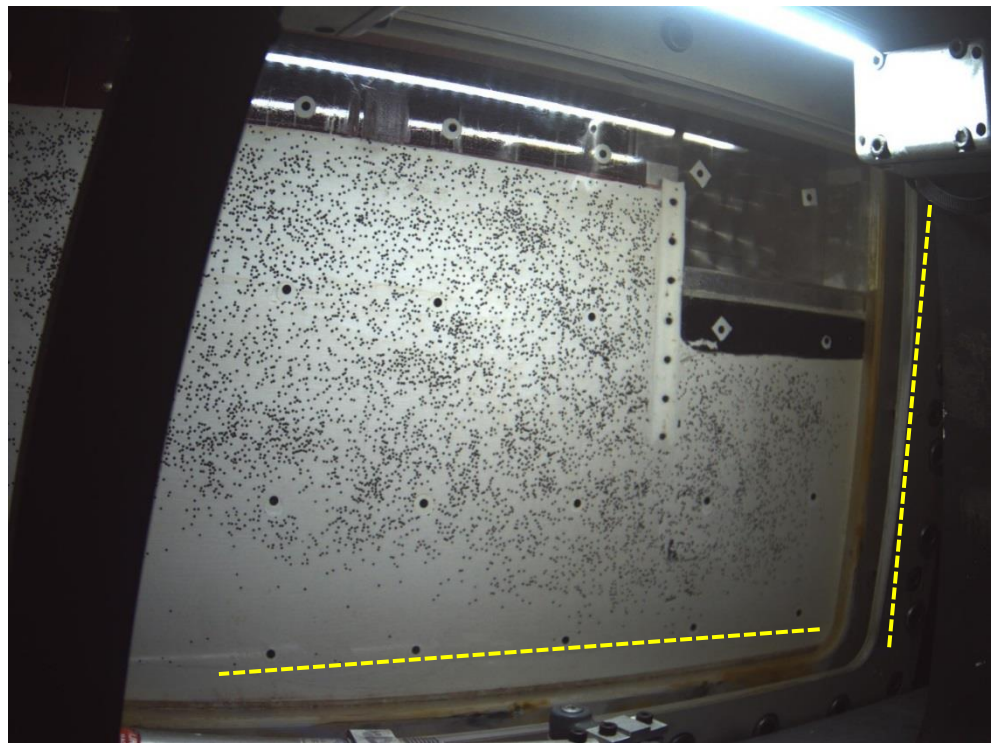
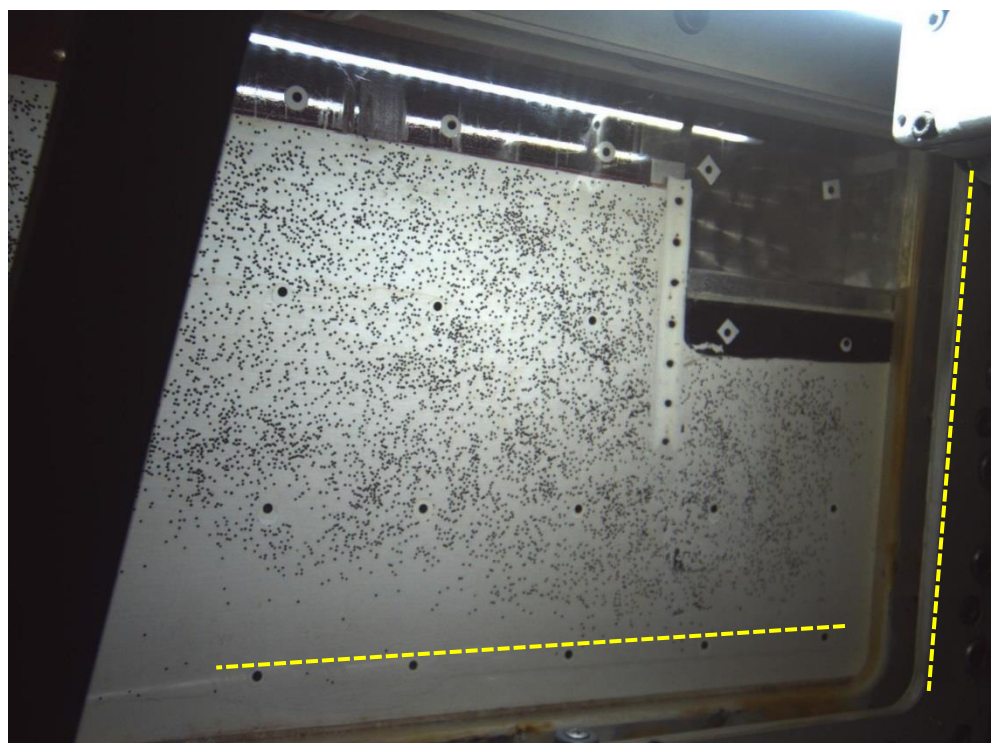


Figure 3.3 Schematic diagram of the Acutronic 661 centrifuge at City, University of London (after Le, 2017)



(a)



(b)

Figure 3.4 (a) Original image taken with miniature USB camera and (b) undistorted image, curvature removed, used in Geo_PIV image analysis

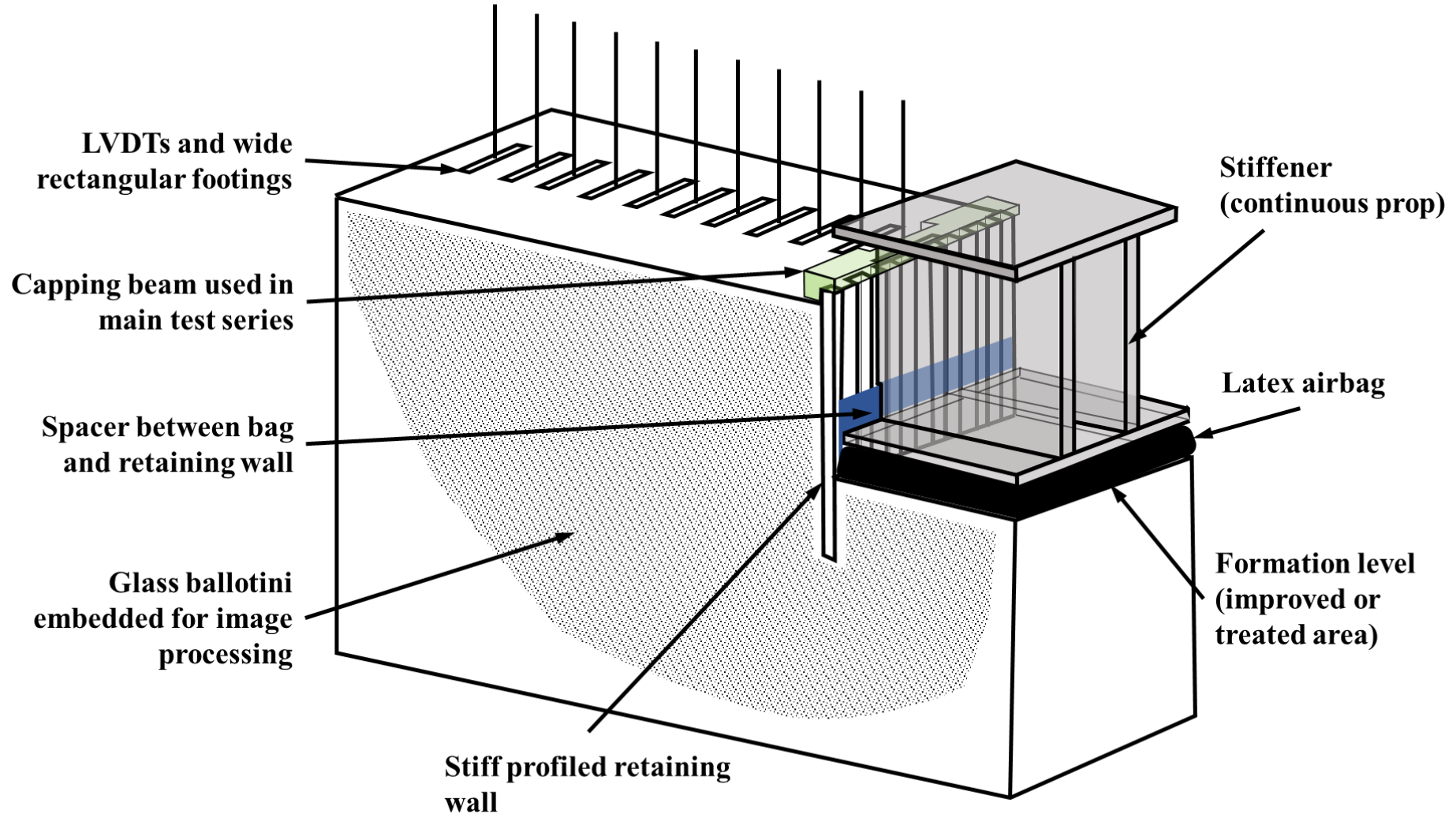


Figure 4.1 General centrifuge test arrangement

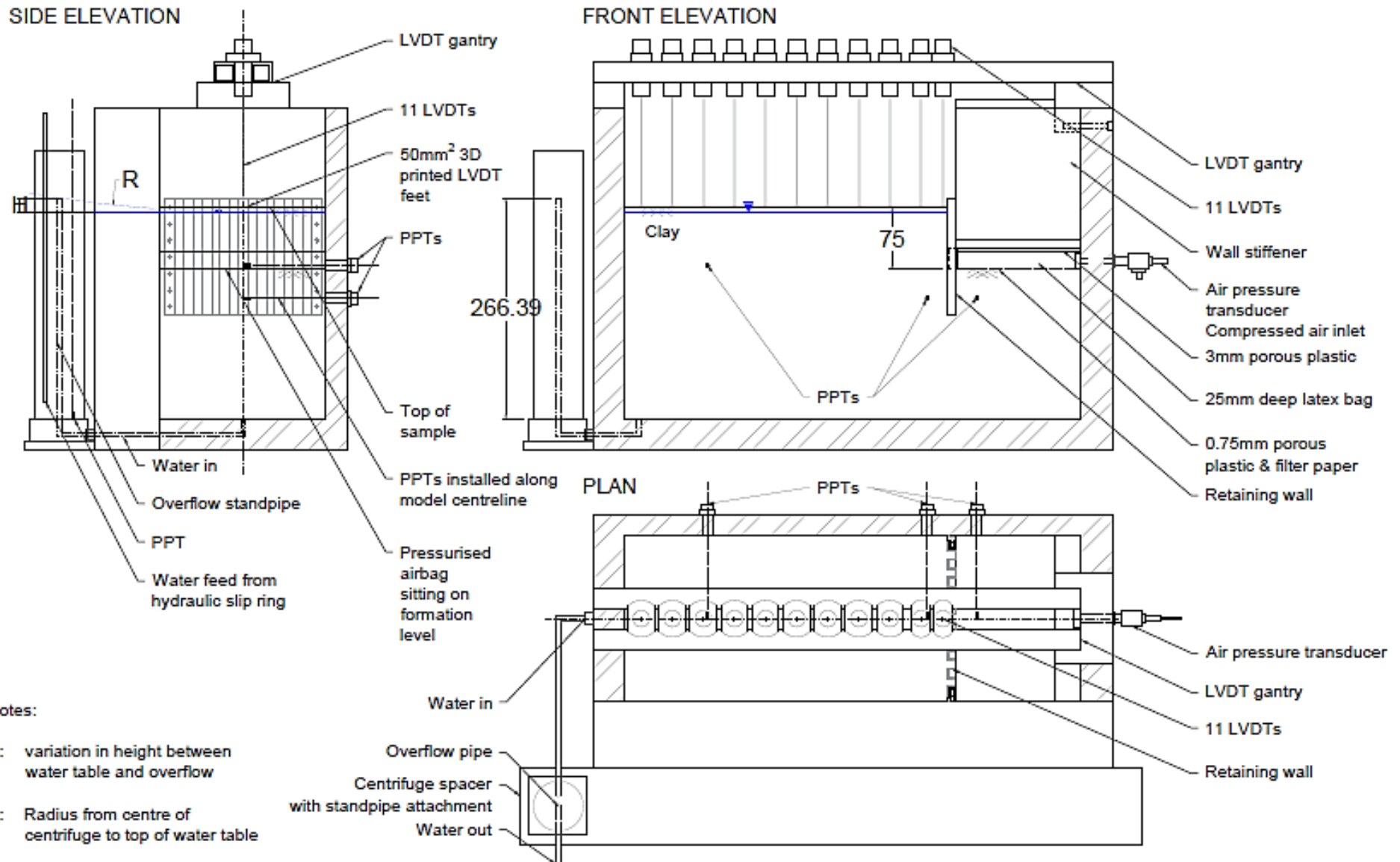


Figure 4.2 Typical apparatus set up



FRONT ELEVATION



Figure 4.3 Images of retaining wall with tapered toes

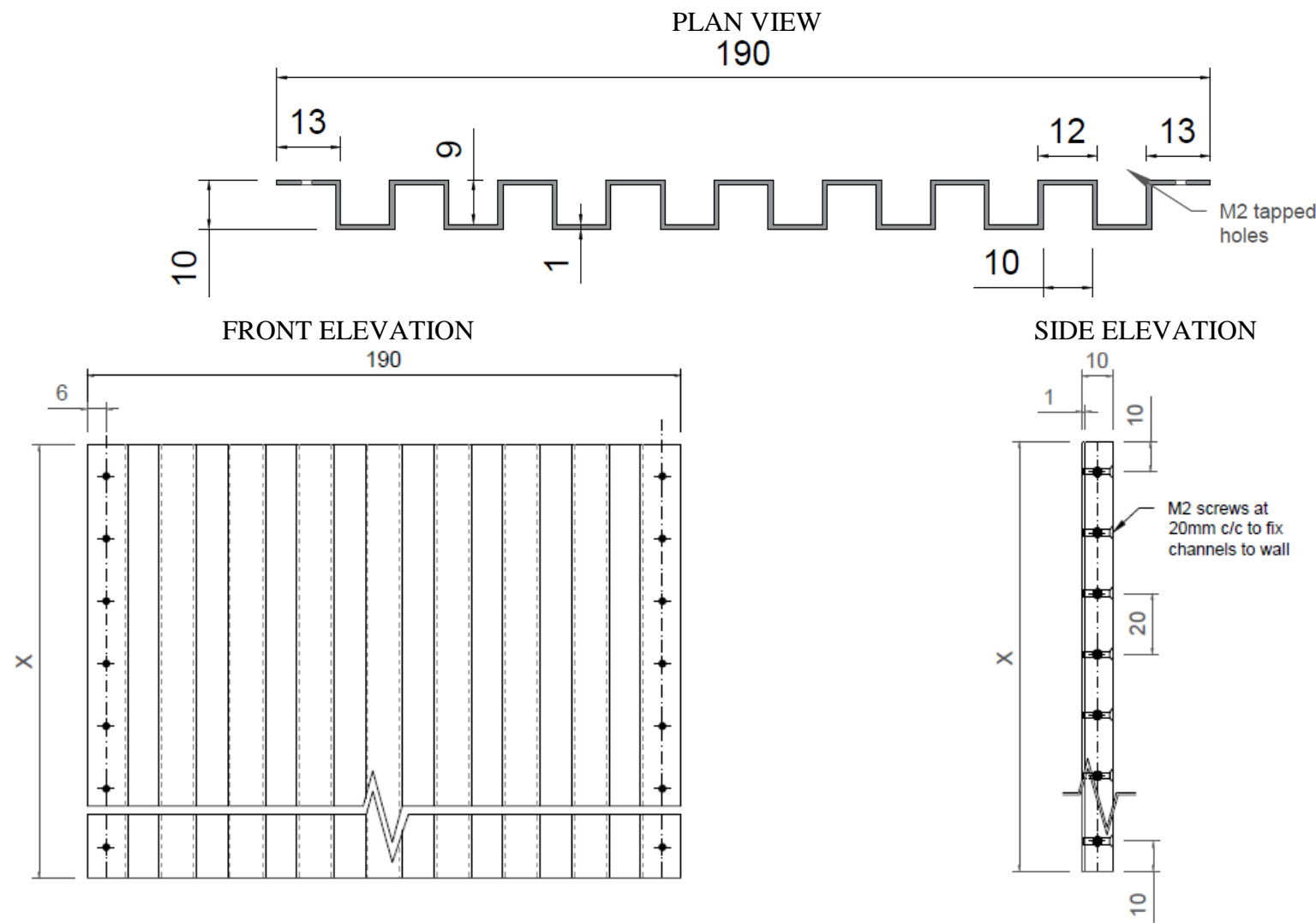


Figure 4.4 Retaining wall details, where X is the length of the retaining wall

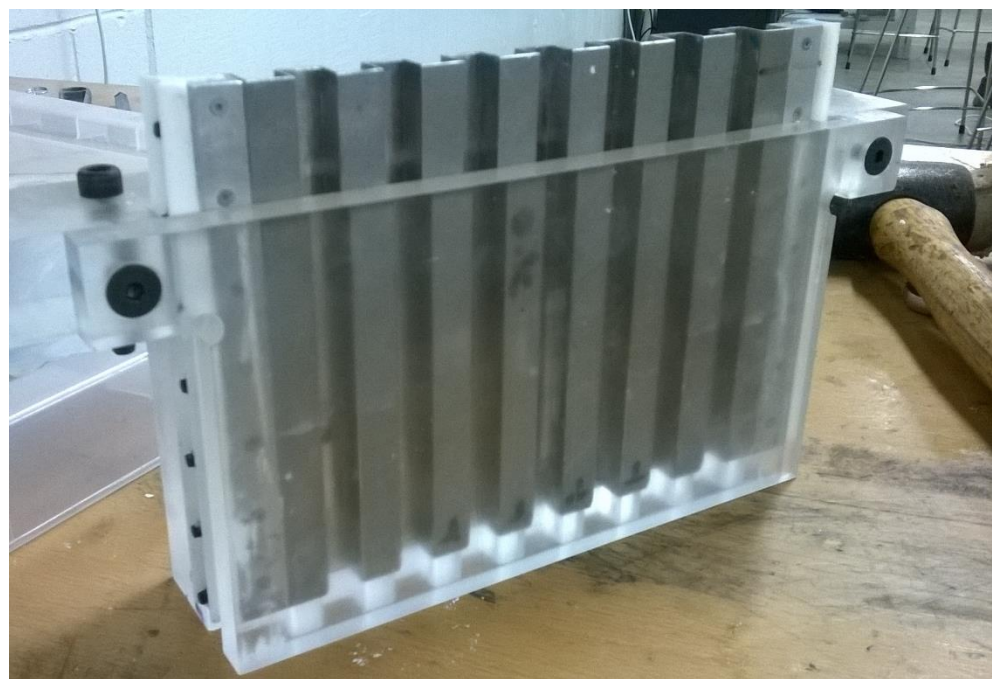


Figure 4.5 Perspex guide for installation of retaining wall

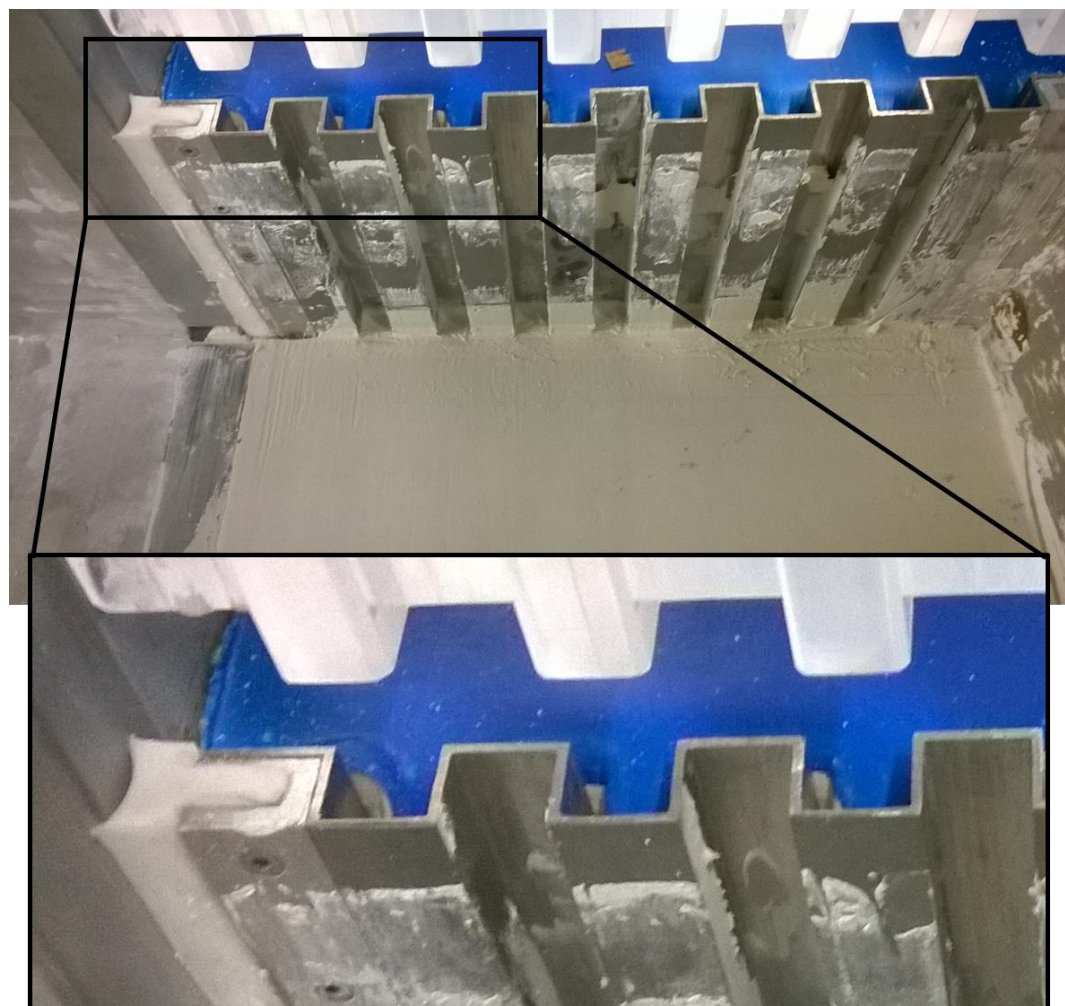


Figure 4.6 Gaps forming behind retaining wall owing to rubber membrane being pulled into soil



Figure 4.7 Template used to prevent application of PlastiDip rubber membrane to excavation void and outer edge of retaining wall

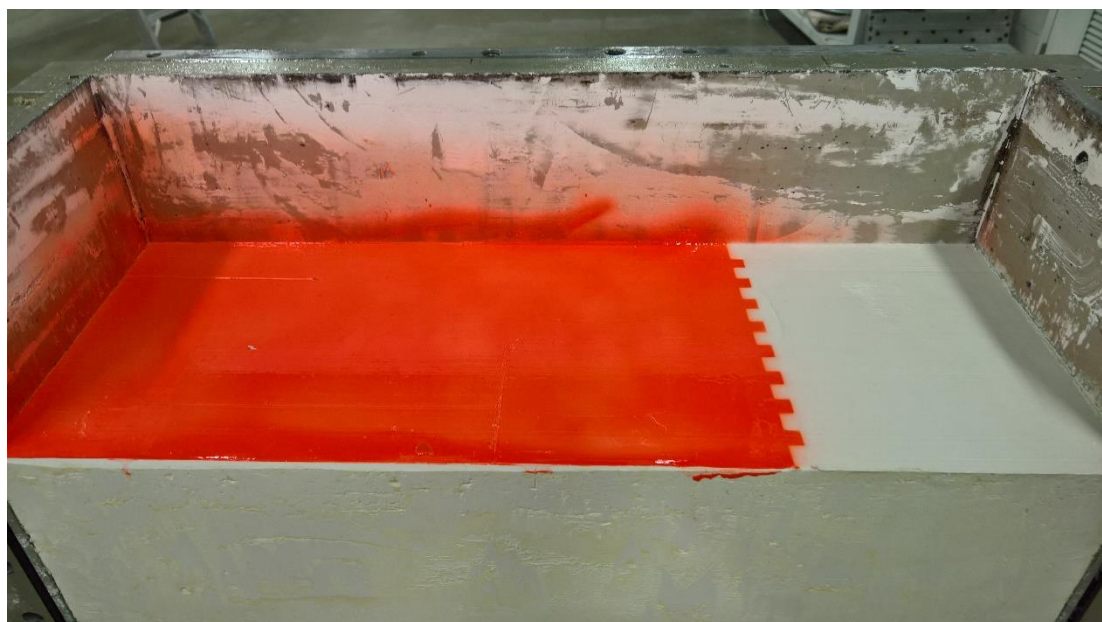


Figure 4.8 Final PlastiDip layer on surface of clay model

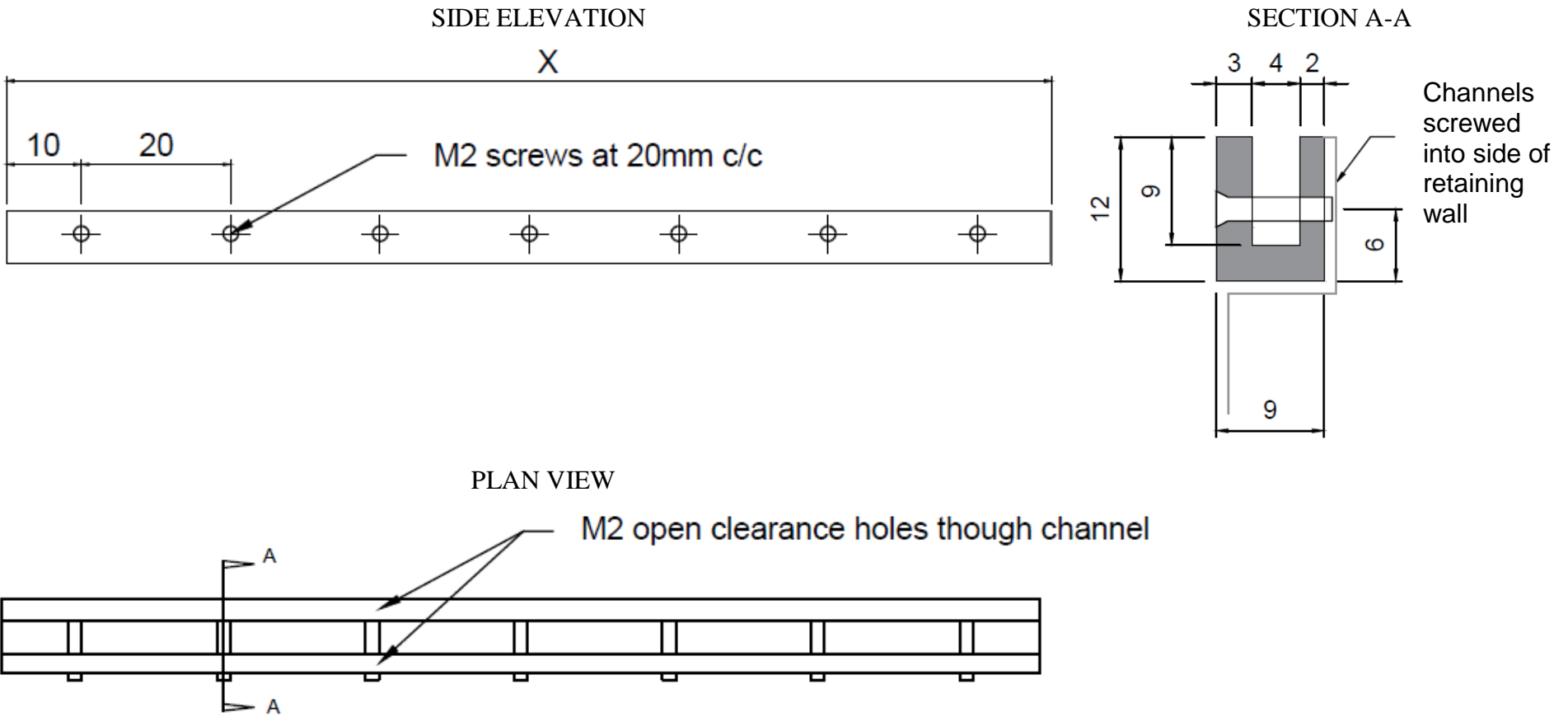


Figure 4.9 Aluminium channel design to secure silicone seal to retaining wall

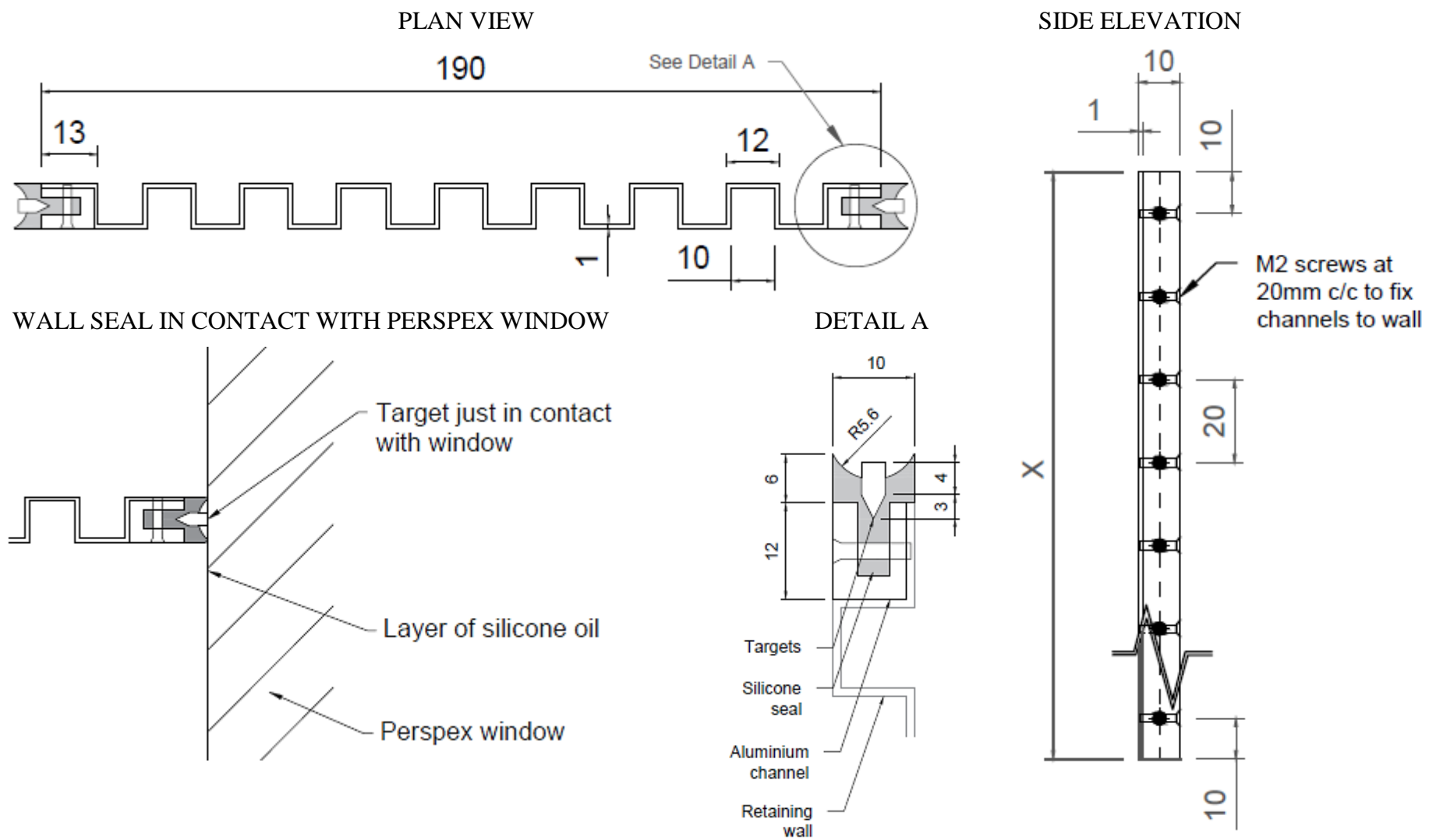
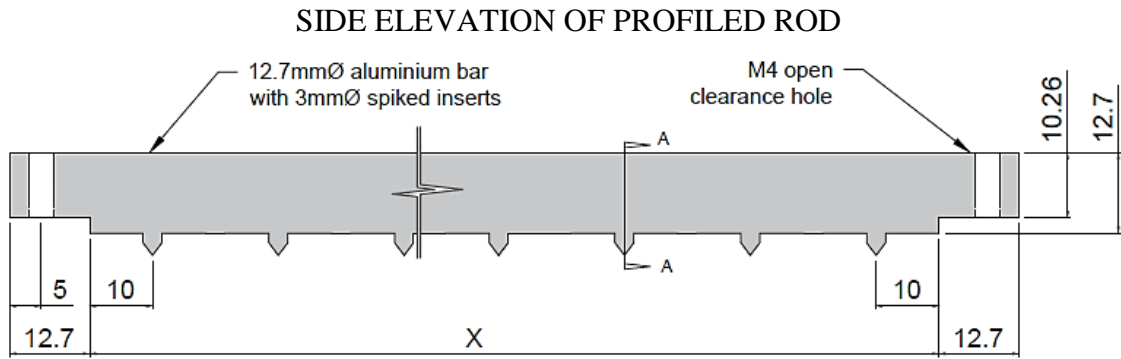
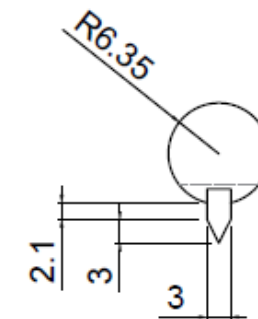


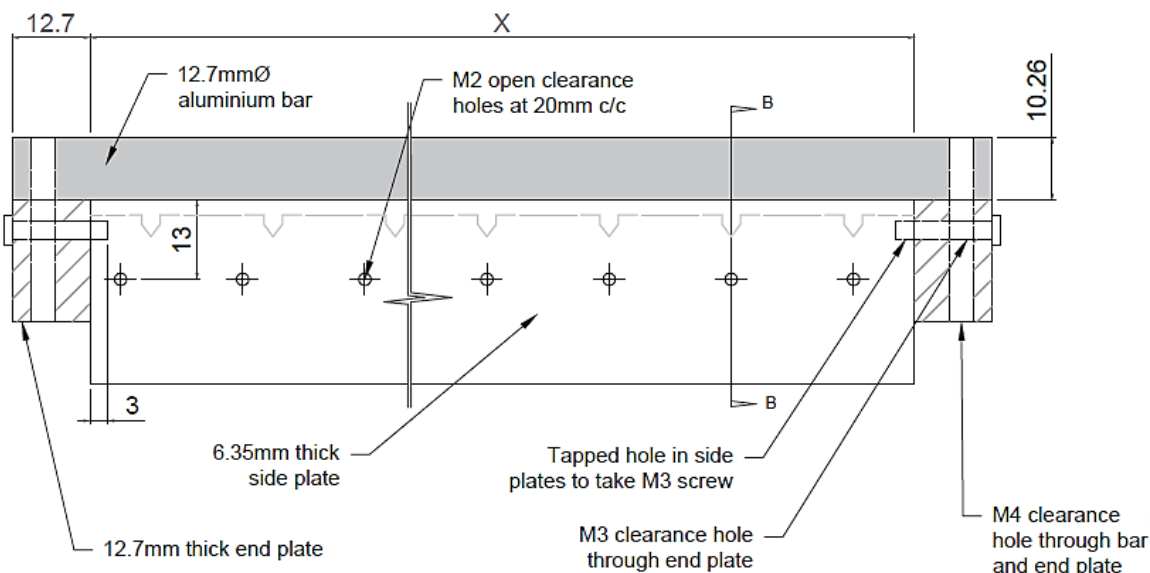
Figure 4.10 Details of silicone seals cast on retaining wall



SECTION A-A



SIDE ELEVATION OF BAR AND SIDE PLATES



FRONT ELEVATION

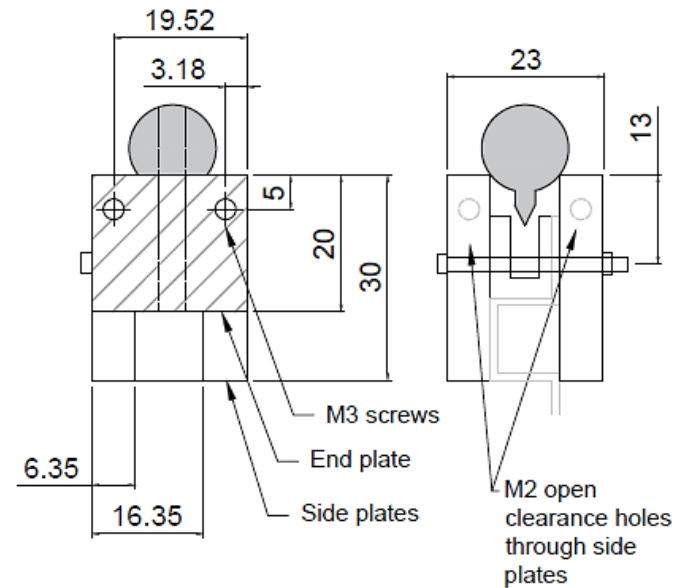


Figure 4.11 Aluminium mould used to form silicone seals on retaining wall

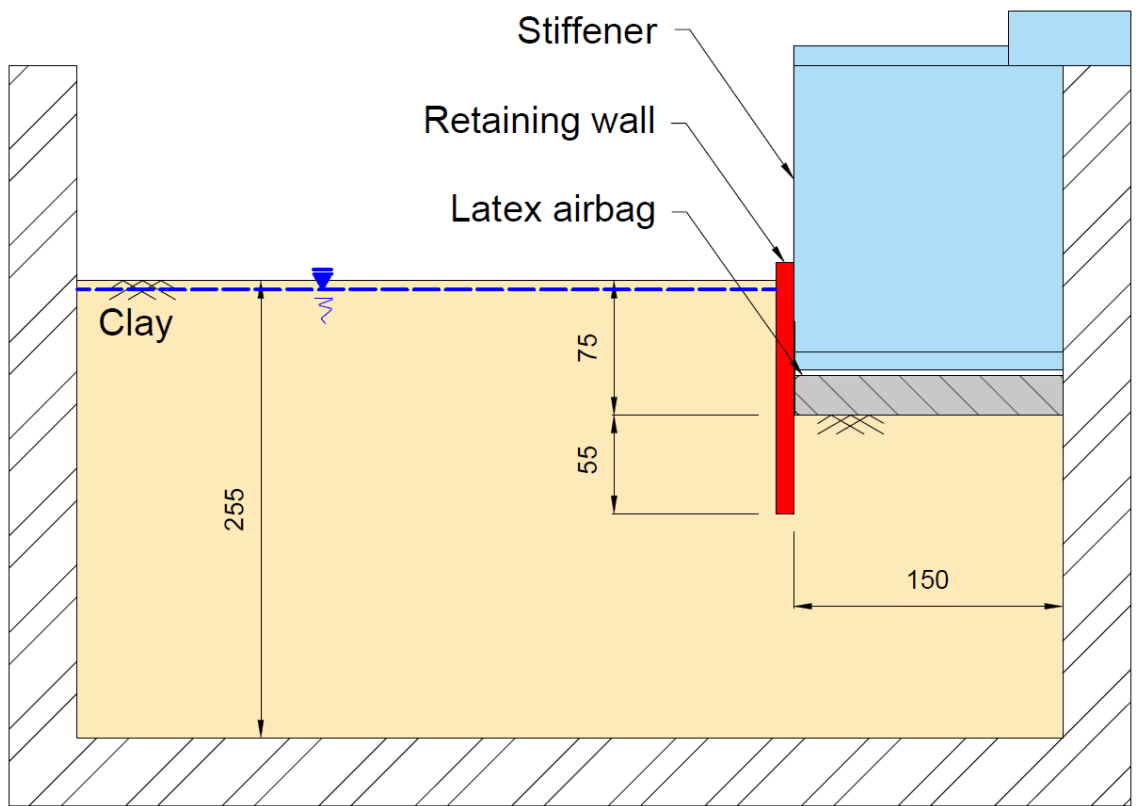


Figure 4.12 General centrifuge model configuration with retaining wall, stiff excavation support (stiffener) and latex airbag

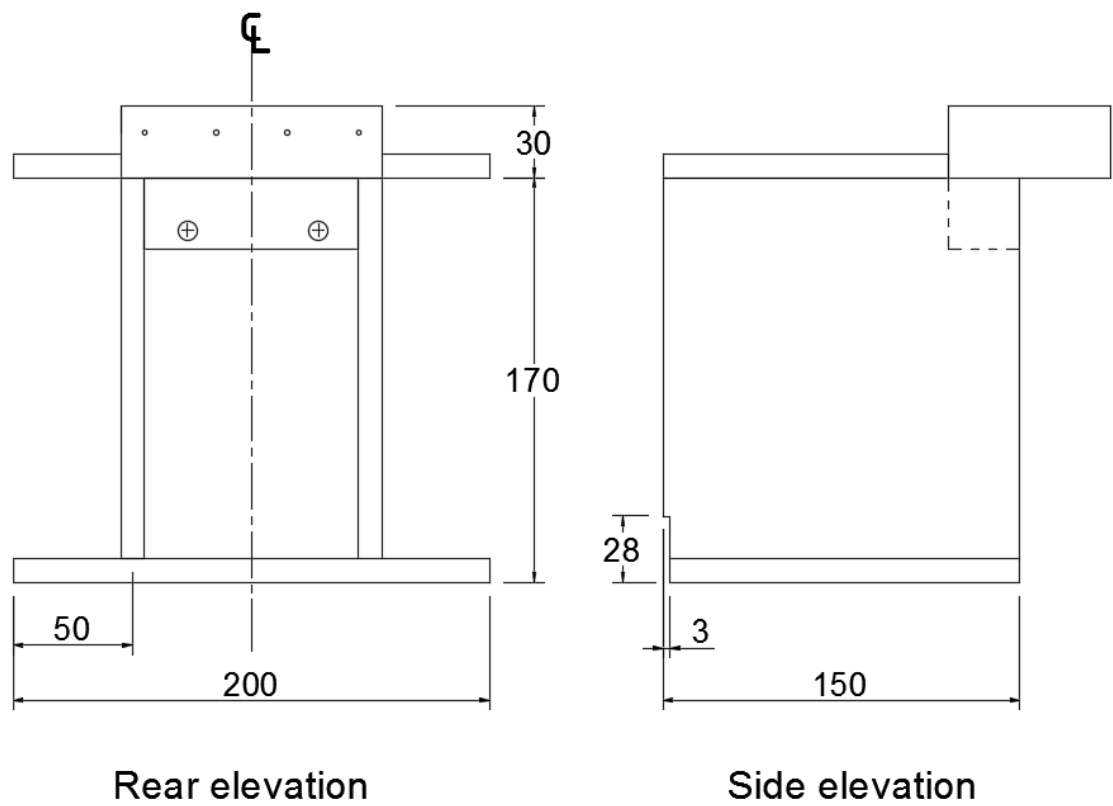
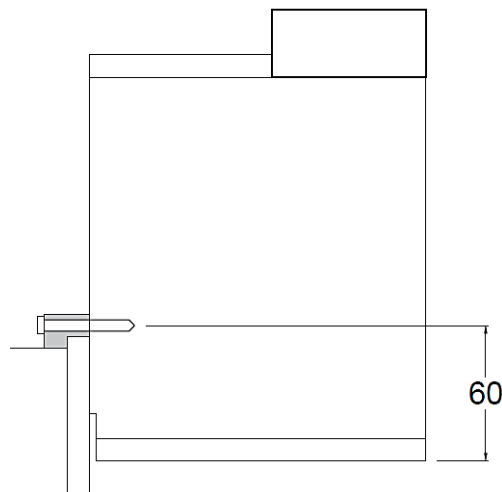
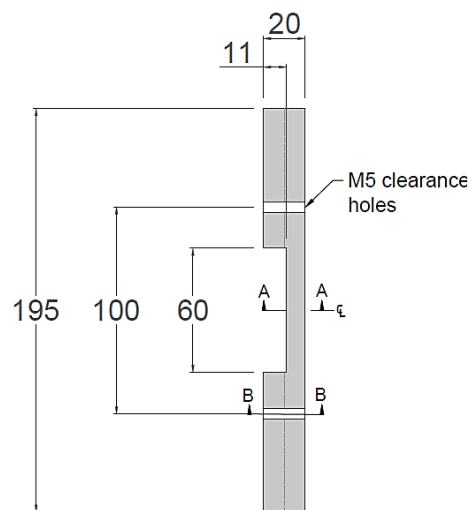


Figure 4.13 Excavation stiffener details

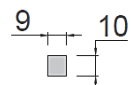
SIDE ELEVATION OF STIFFENER
AND CAPPING BEAM



PLAN



SECTION A-A



SECTION B-B

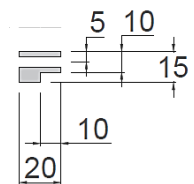


Figure 4.14 Capping beam details

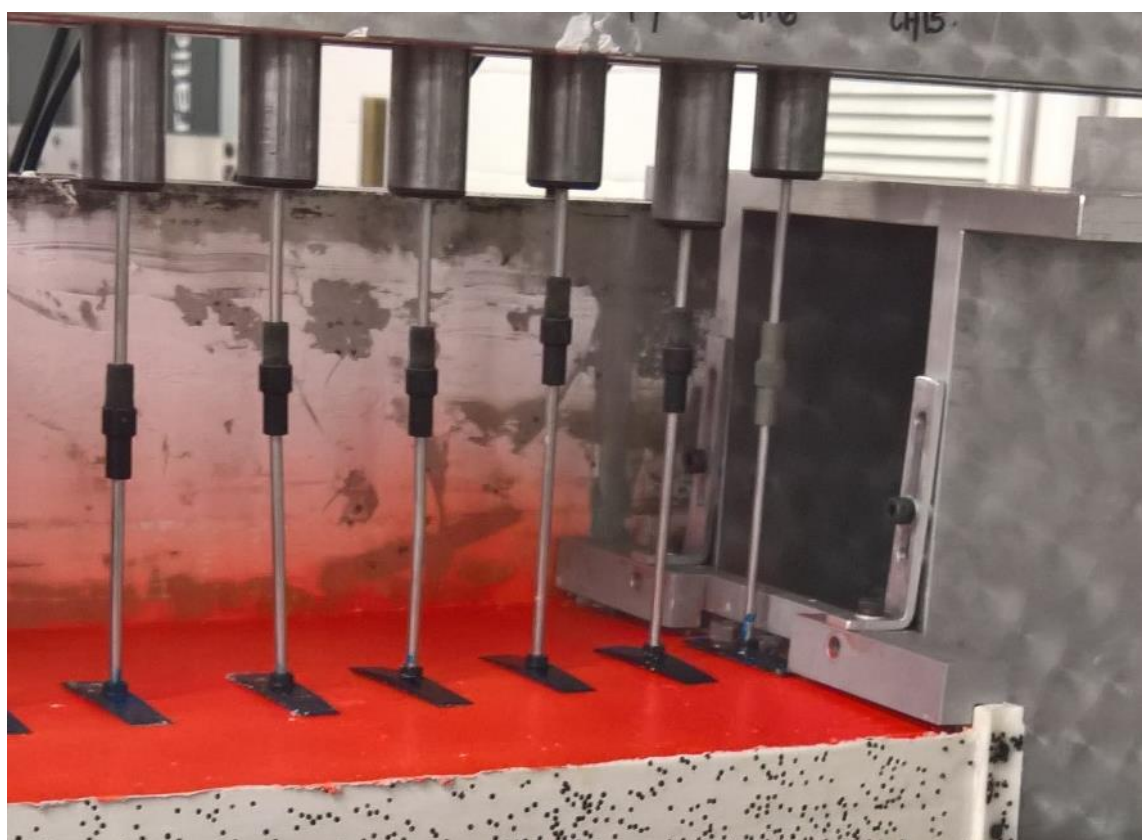


Figure 4.15 Space in capping beam to accommodate LVDT footing

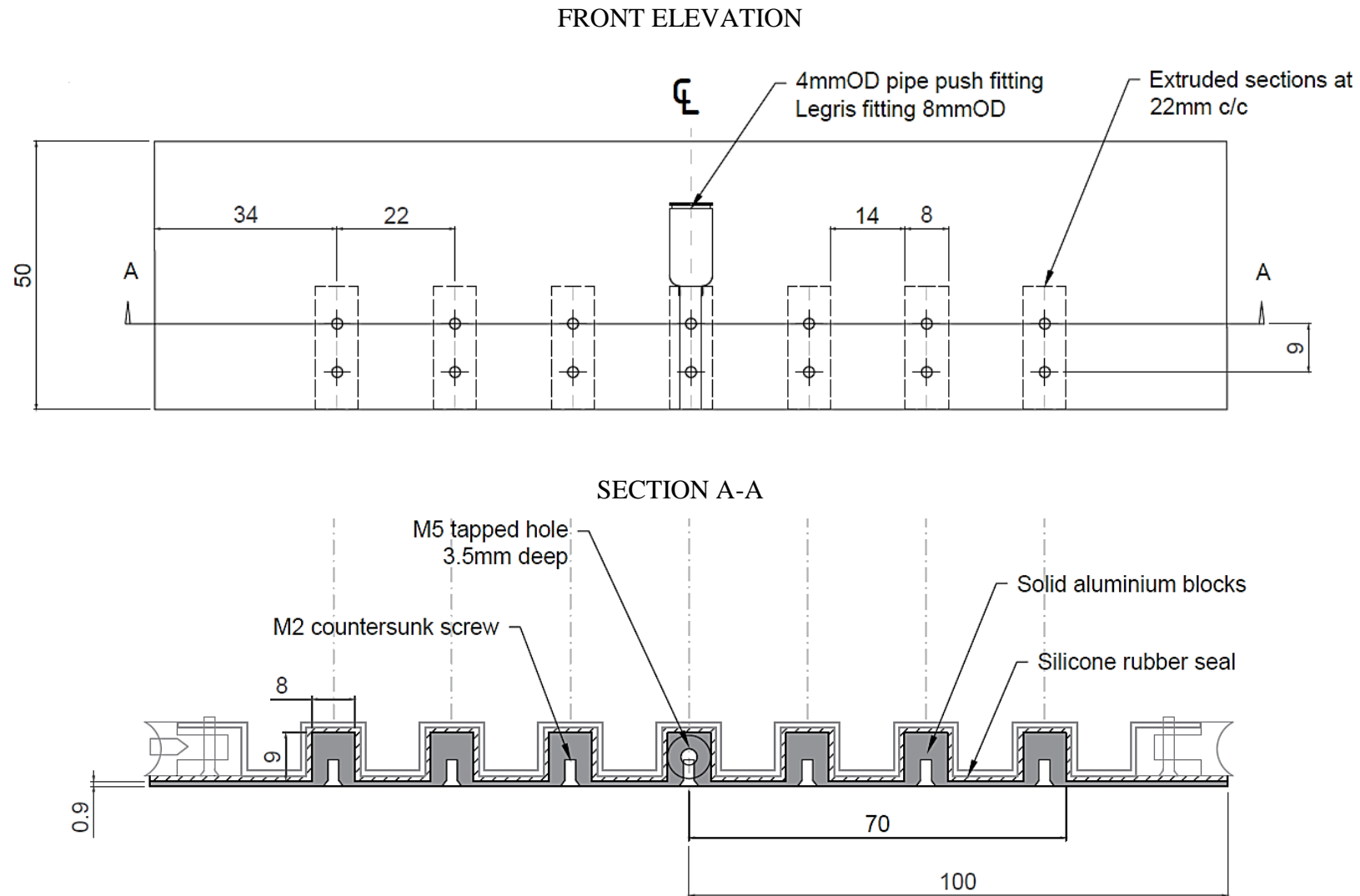


Figure 4.16 Airbag spacer details



Figure 4.17 Photograph of airbag spacer with push fitting attachment for underwater test series and silicone rubber seal

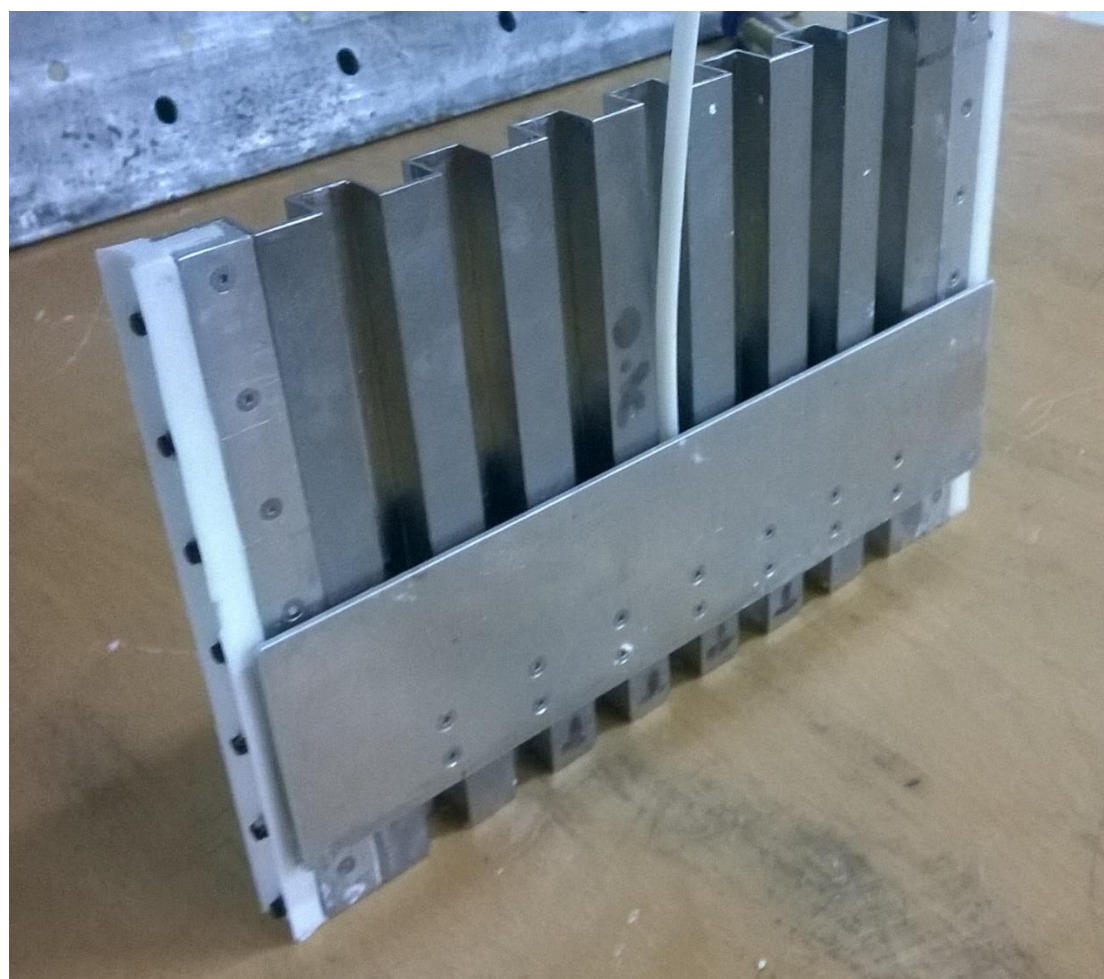


Figure 4.18 Photographs of airbag spacer sealed against retaining wall



Figure 4.19 Bespoke LVDT footings for soft soil models, 50 x 10mm in plan and 2mm thick in the centre tapered to 0.5mm at the ends



Figure 4.20 Image taken post-test showing that LVDT footings had settled in sample during reconsolidation

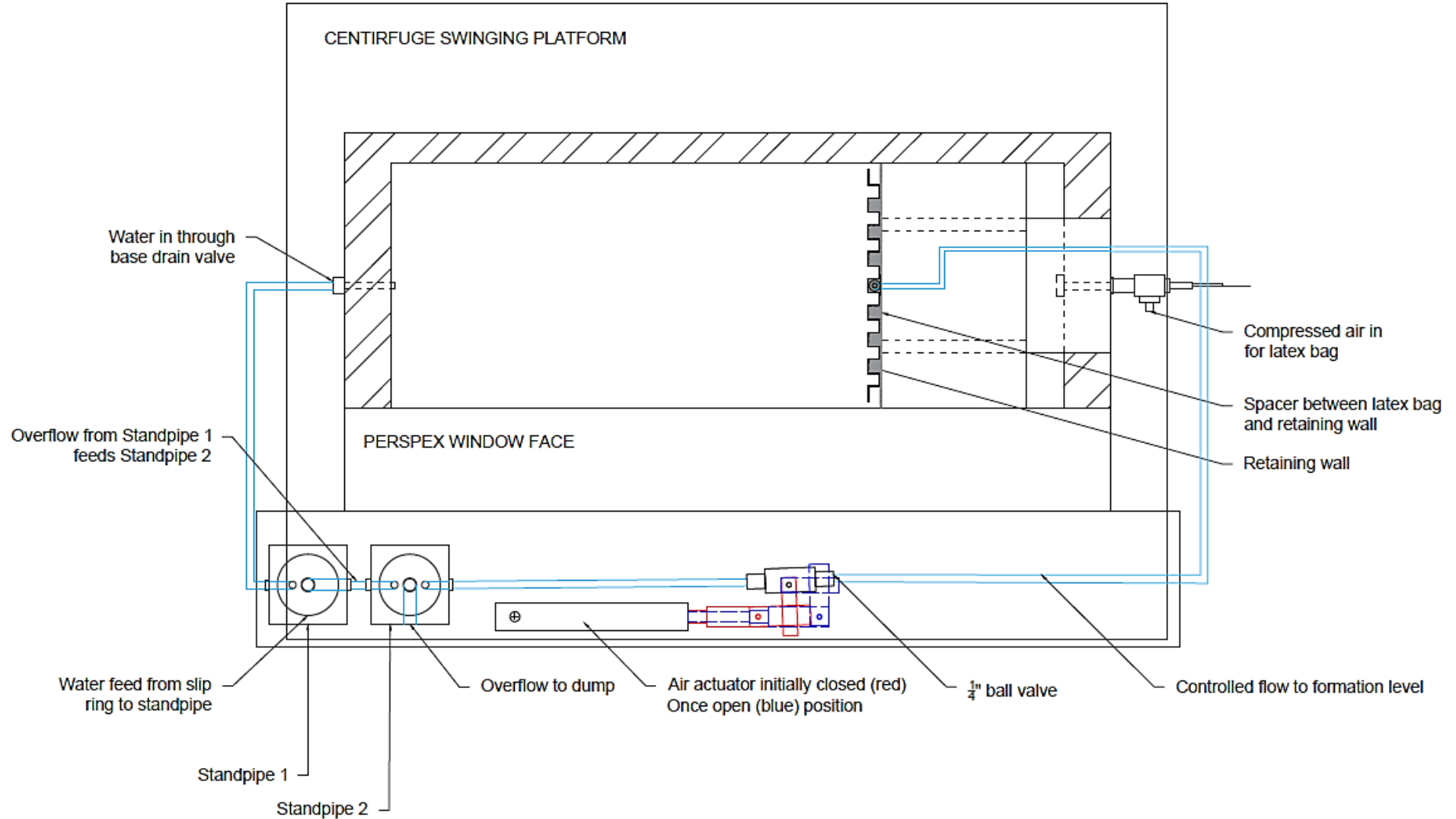


Figure 4.21 Standpipe arrangement used in underwater excavation test series

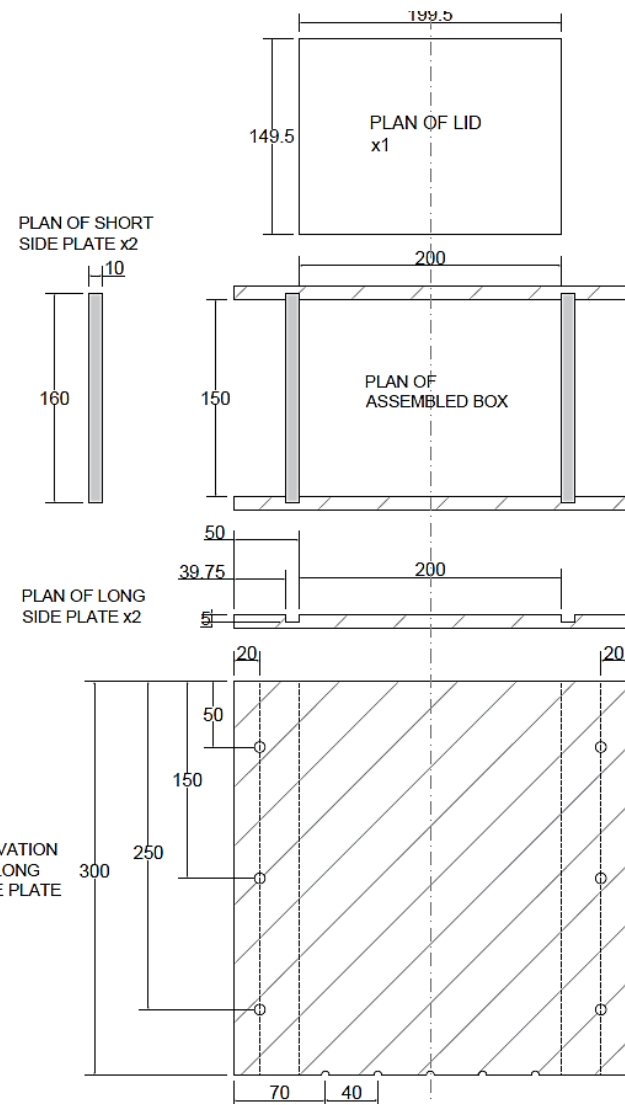


Figure 4.22 Details of consolidation box for lime stabilised clay sample



Figure 4.23 Photograph of consolidation box being disassembled by sliding out front plate

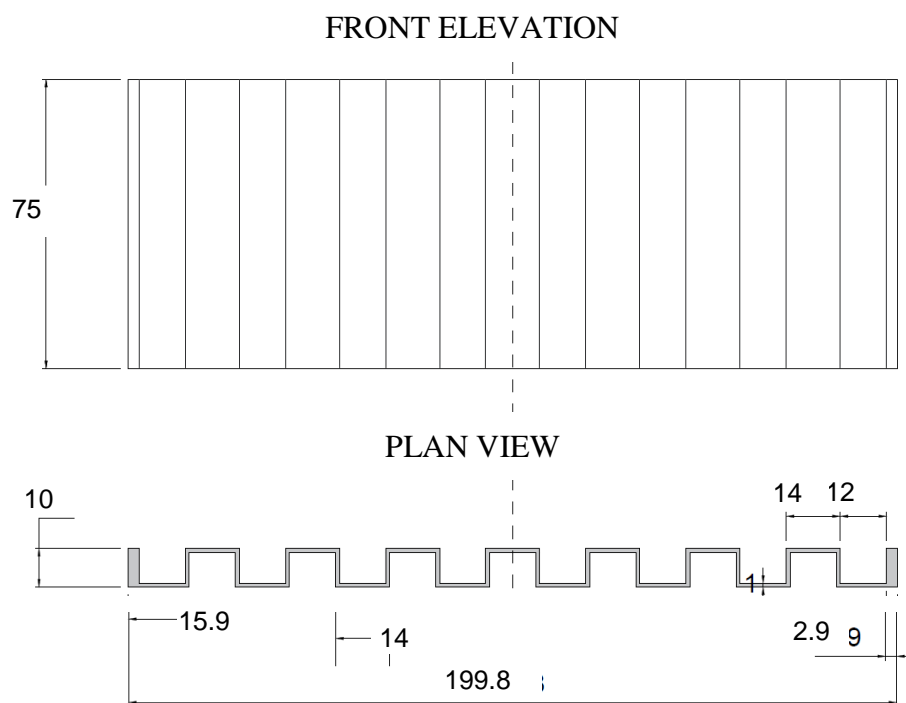


Figure 4.24 Details of lower stiffness cut off wall used in double wall series of tests

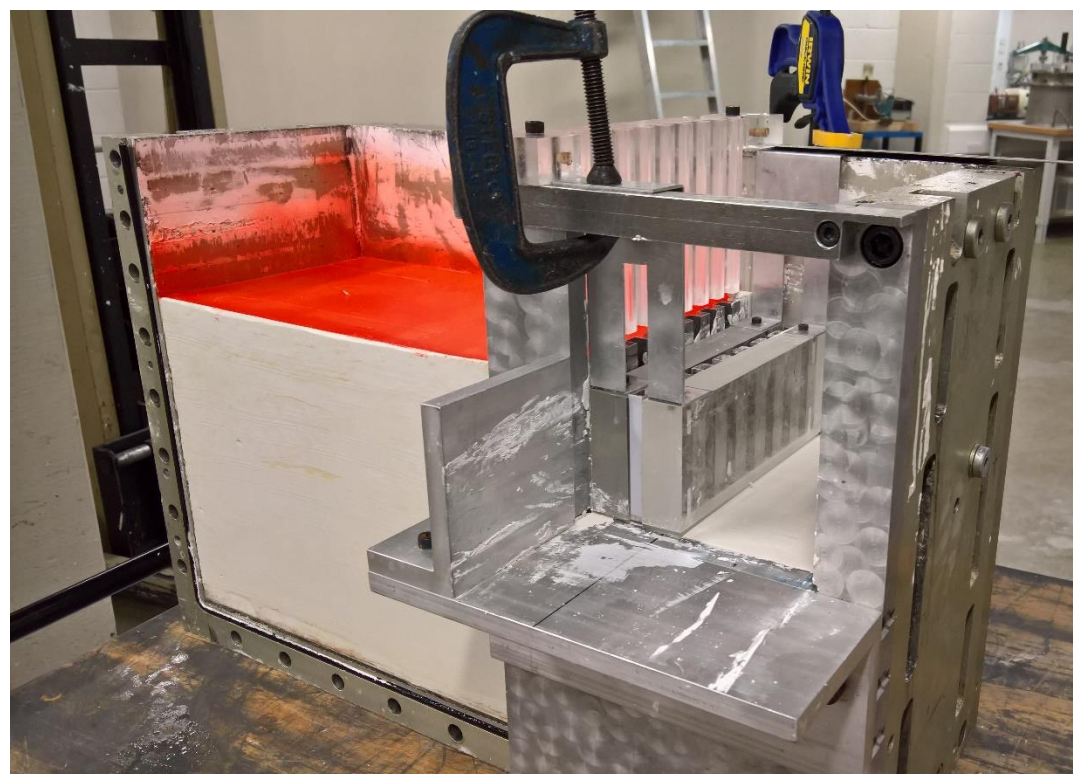


Figure 4.25 Guide used for double wall installation clamped to strongbox



Figure 4.26 Photograph of double wall at formation level

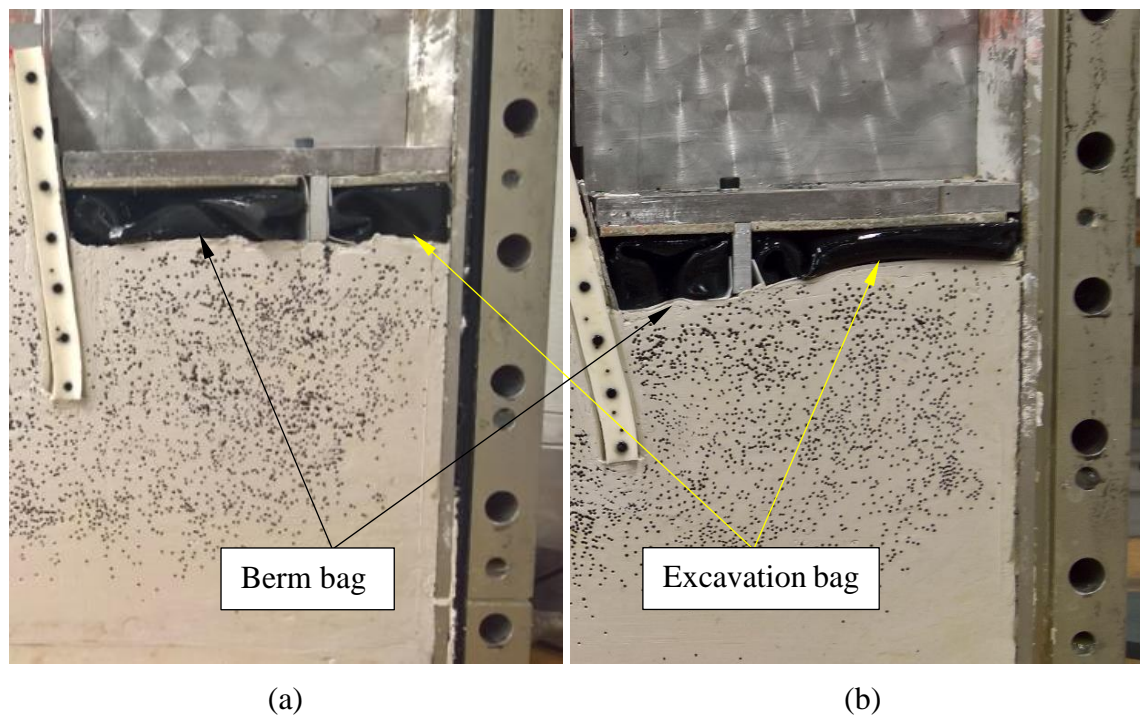


Figure 4.27 Photographs post simulated excavation of the two positions of vertical support used to model two independent berm widths; (a) 100mm wide berm and (b) 50mm wide berm

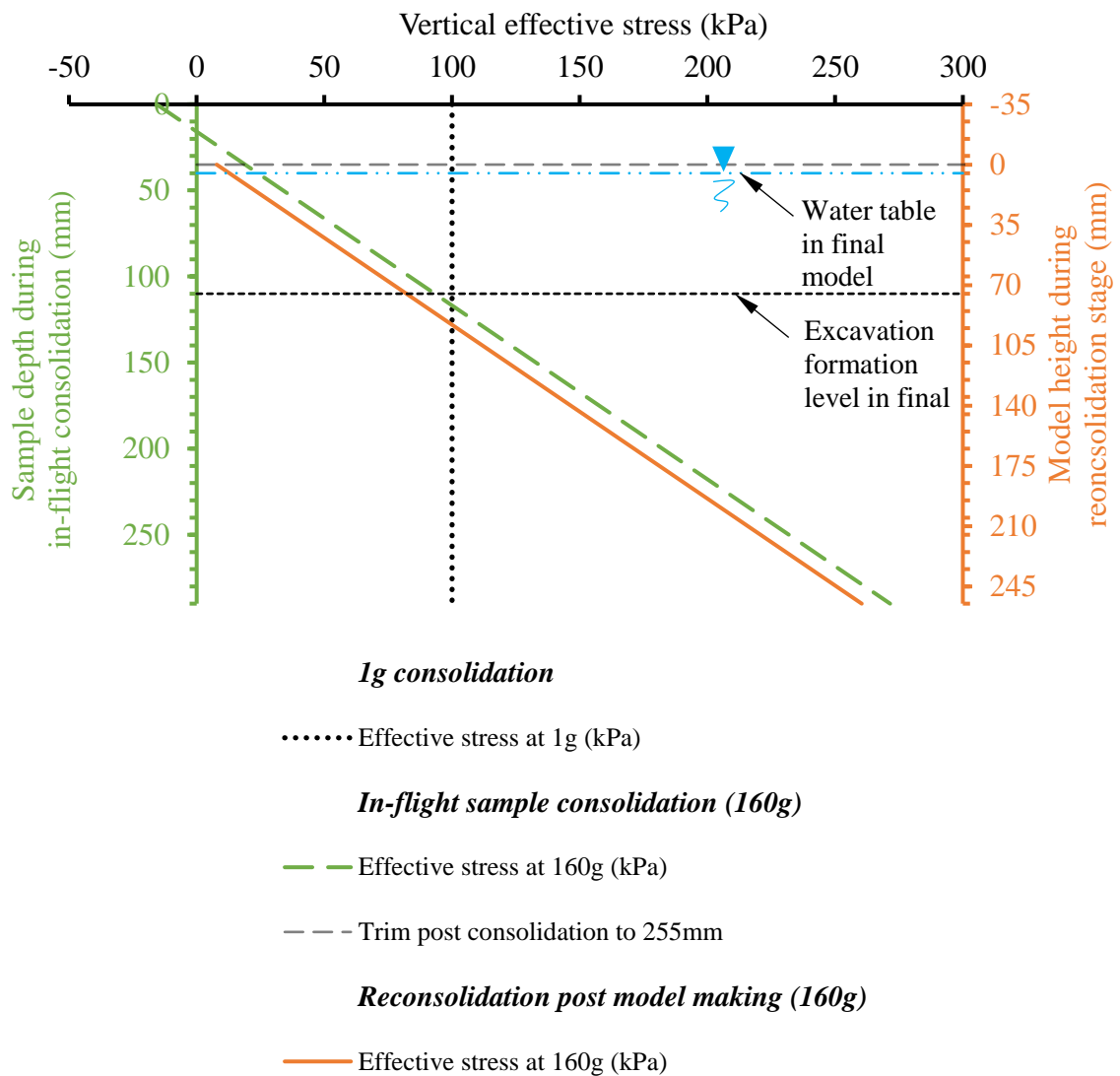


Figure 5.1 Stress profile through sample following 1g and 160g consolidation

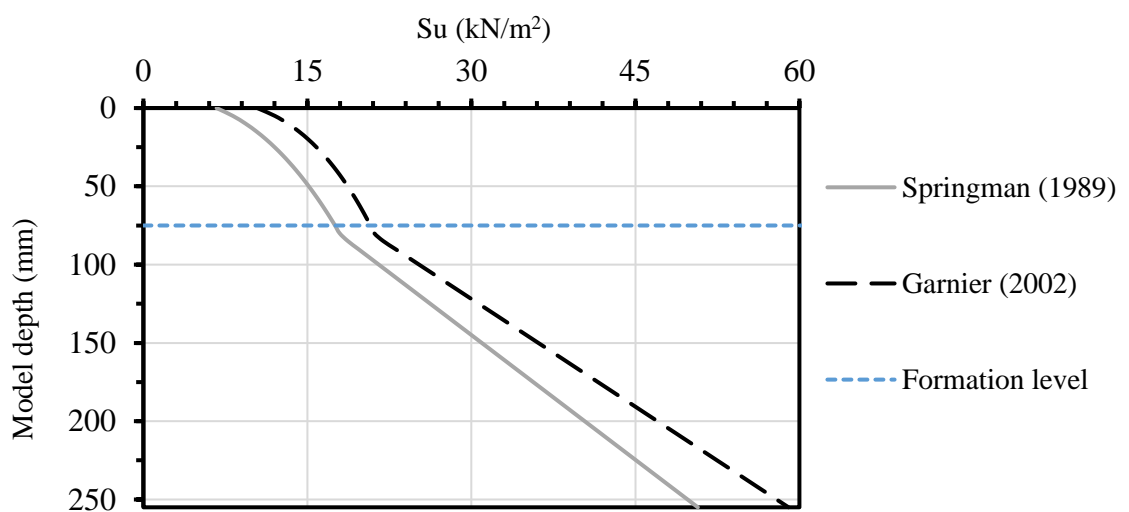


Figure 5.2 Estimated undrained shear strength profile of soil following in-flight consolidation

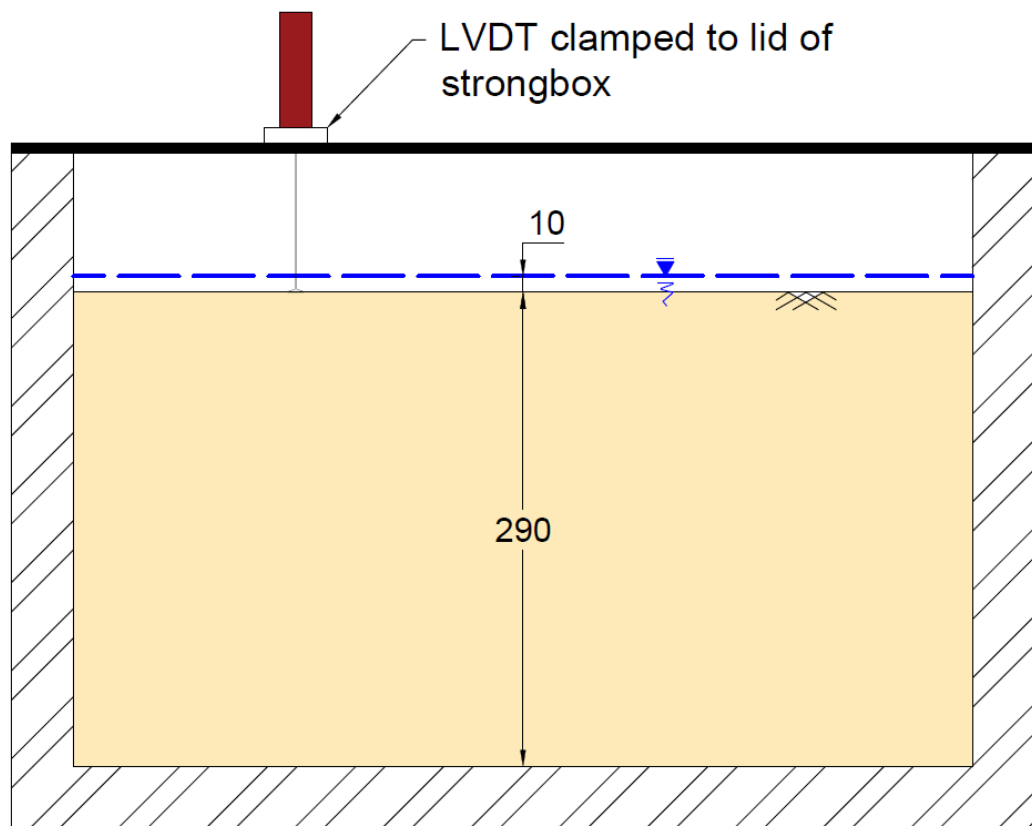


Figure 5.3 Soil sample consolidation set up at 160g

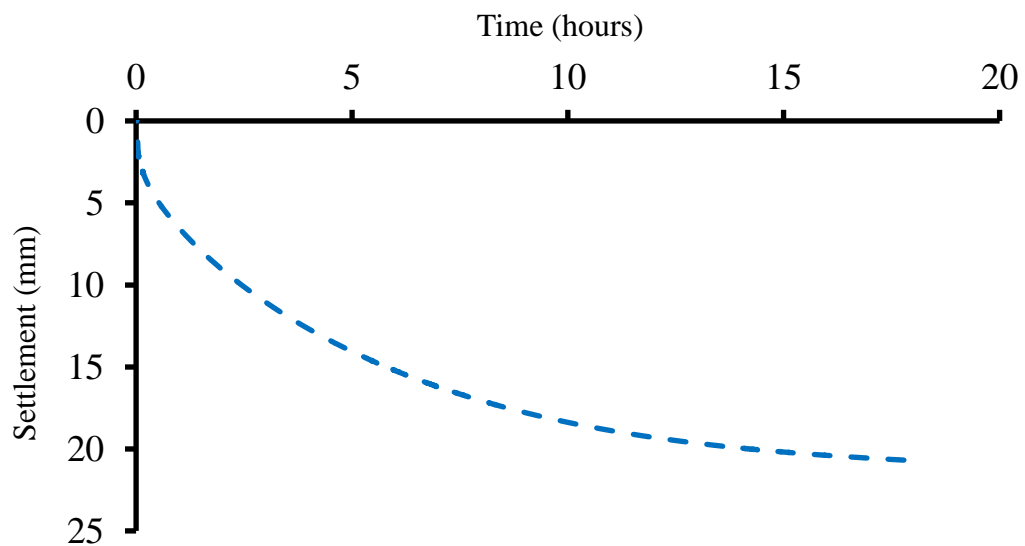


Figure 5.4 Typical settlement curve during in-flight consolidation at 160g

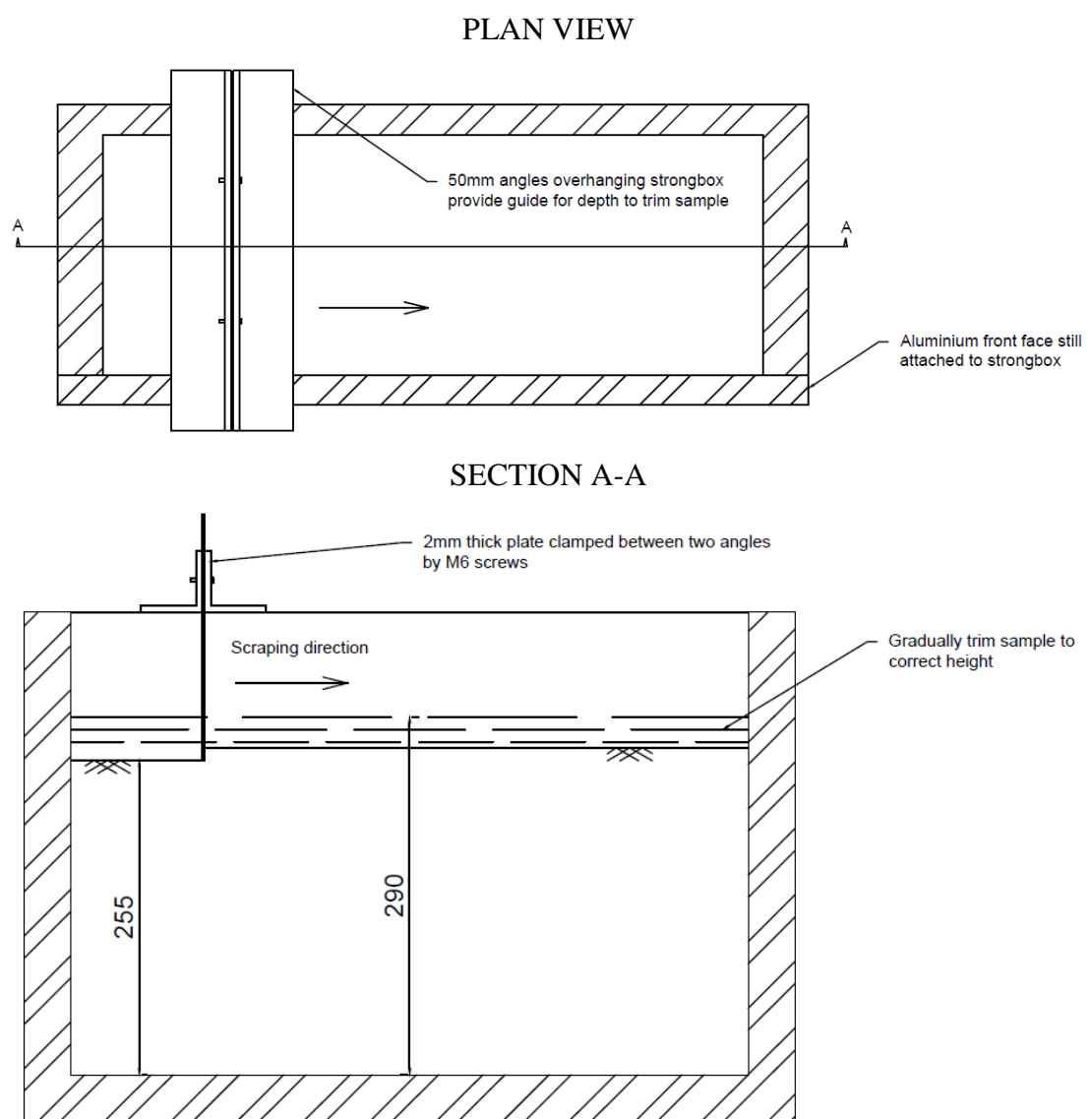


Figure 5.5 Details of scraper used for trimming soft soil clay samples



Figure 5.6 Photograph of scraper in model in preparation for the first trim

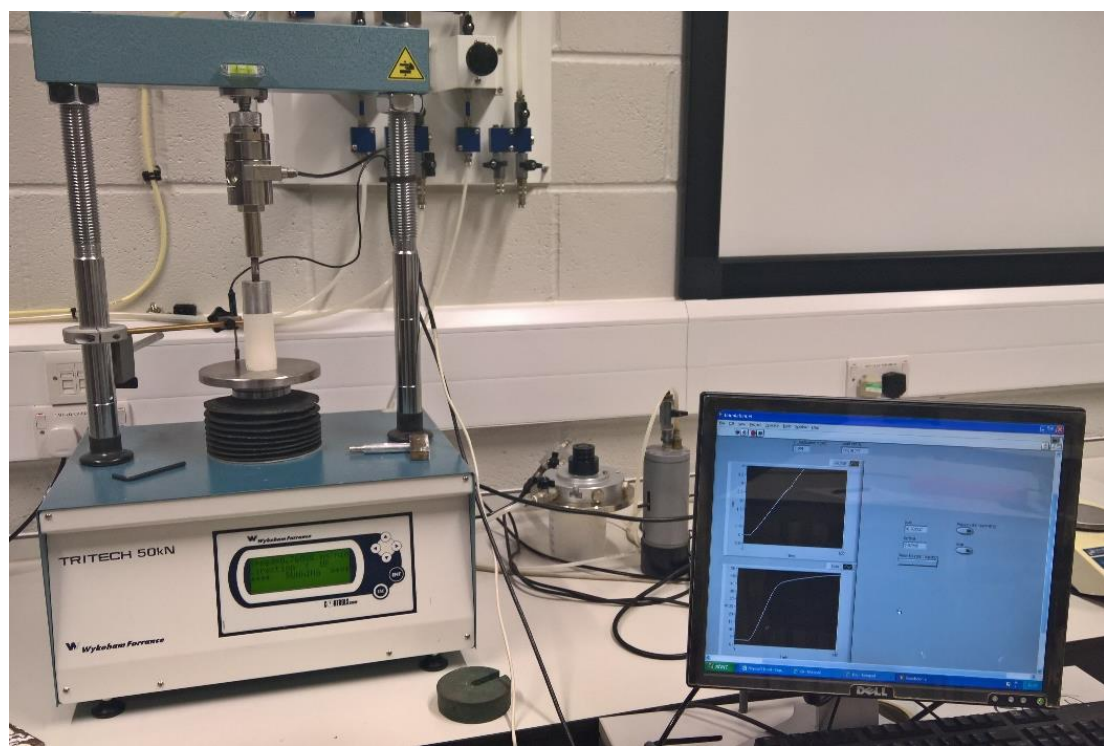


Figure 5.7 Unconfined compression test set up illustrating data logging programme, test specimen, loading frame, LVDT and load cell

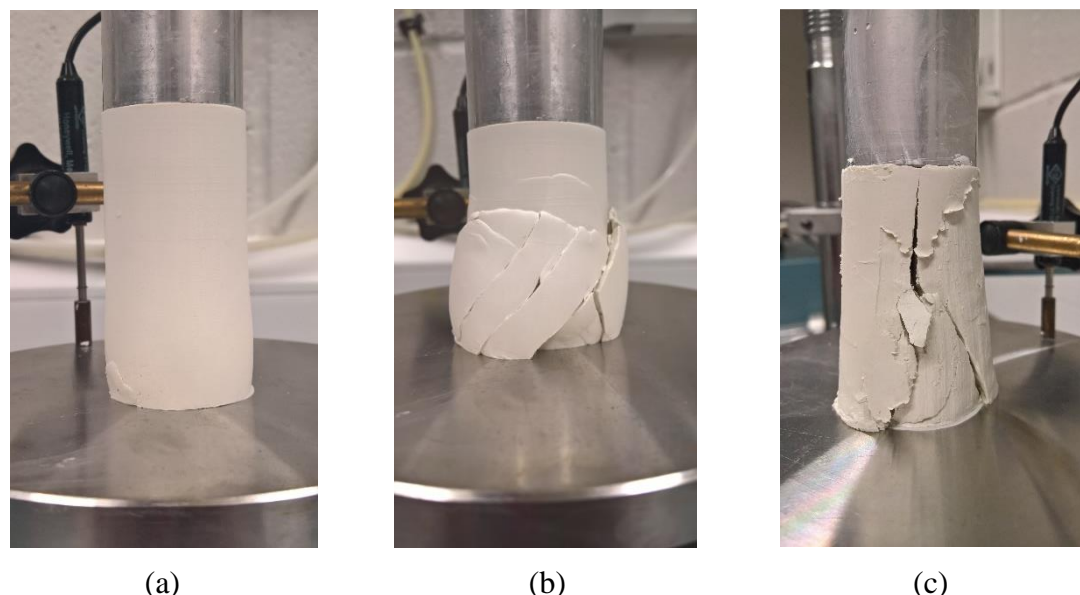


Figure 5.8 Images of lime-stabilised soil samples (a) prior to testing and (b) and (c) at failure after developing multiple shear planes in two independent samples

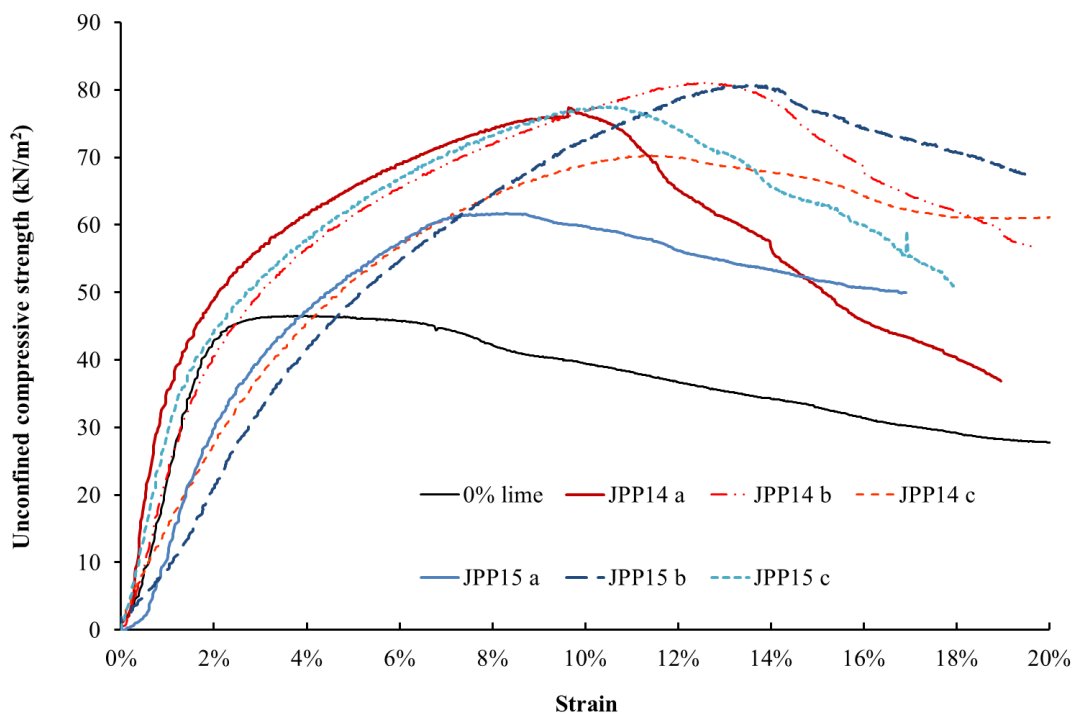


Figure 5.9 Unconfined compressive strengths of lime-stabilised clay samples compared with a virgin clay sample from centrifuge test samples

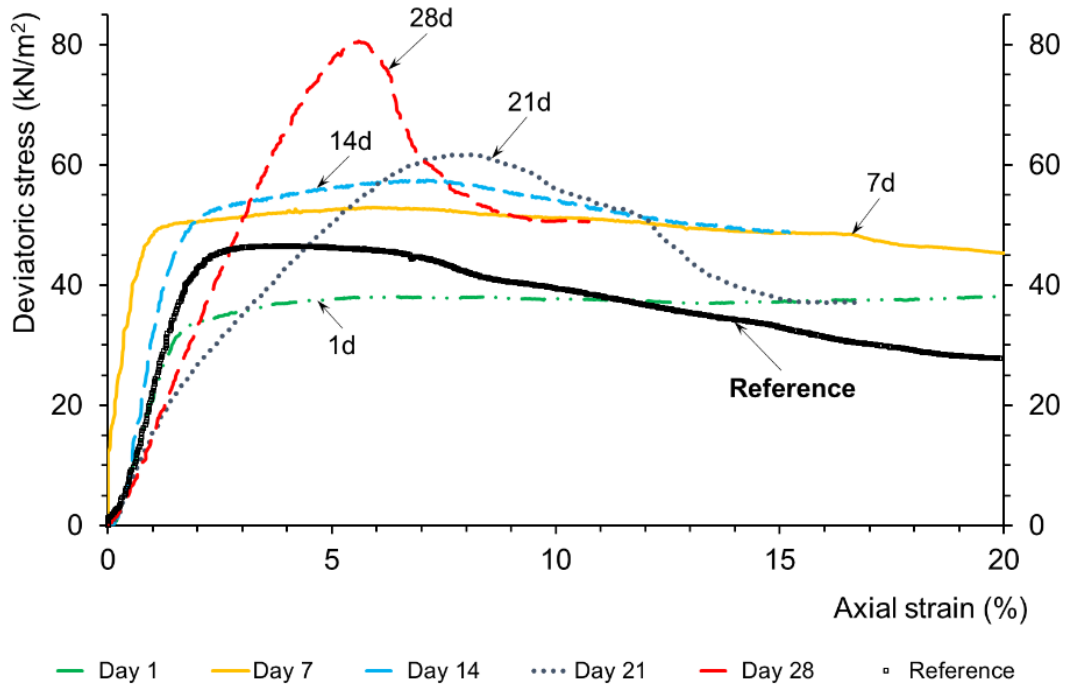


Figure 5.10 Unconfined compressive strengths of lime-stabilised soil after varying time periods (Panchal *et al.*, 2018)

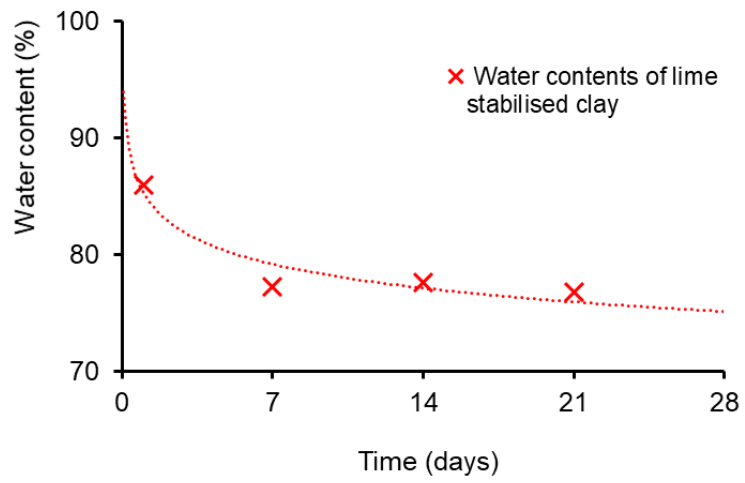


Figure 5.11 Change in measured water contents of lime stabilised soil with increasing time (after Panchal *et al.*, 2018)



(a) Relatively low strength (b) Relatively high strength

Figure 5.12 Failure patterns of cement treated soil (Kitazume & Takeyama, 2014)

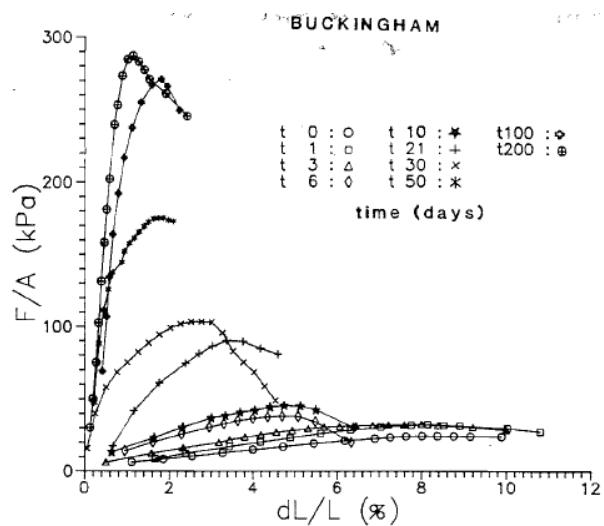


Figure 5.13 Influence of time on unconfined compressive strengths (Locat *et al.*, 1990)

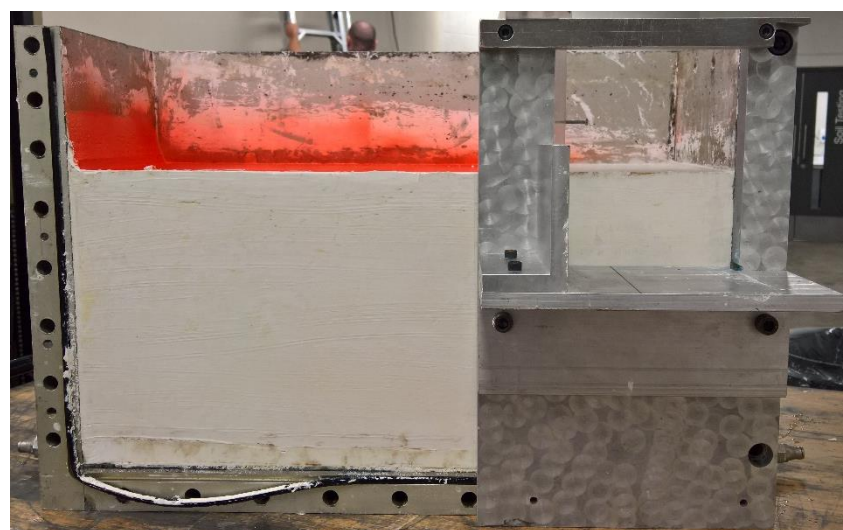


Figure 5.14 Bespoke cutting shelf and guide used for establishing extent of excavation

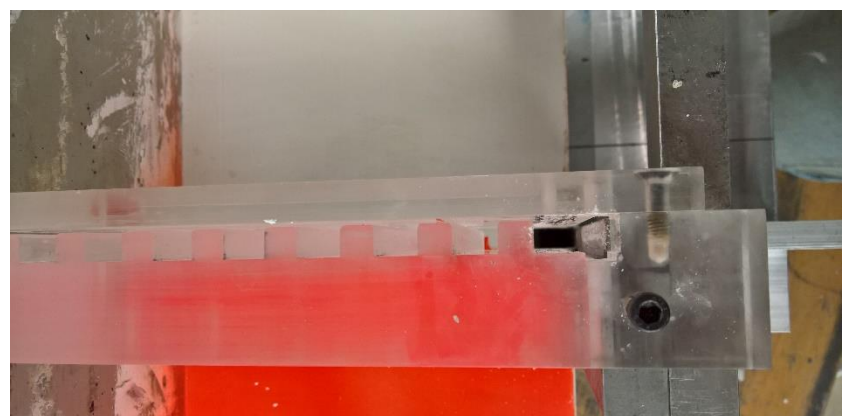


Figure 5.15 Voids formed at both ends of the retaining wall to accommodate silicone seals prior to wall installation

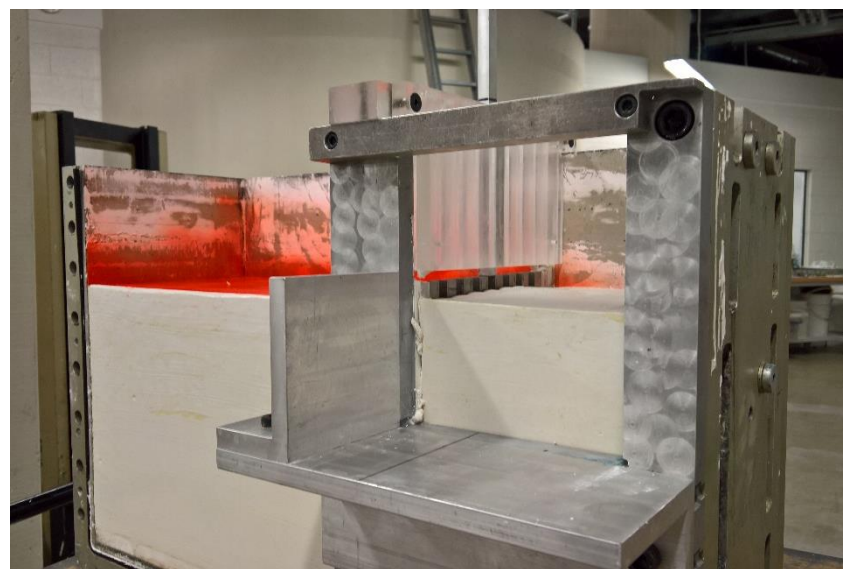
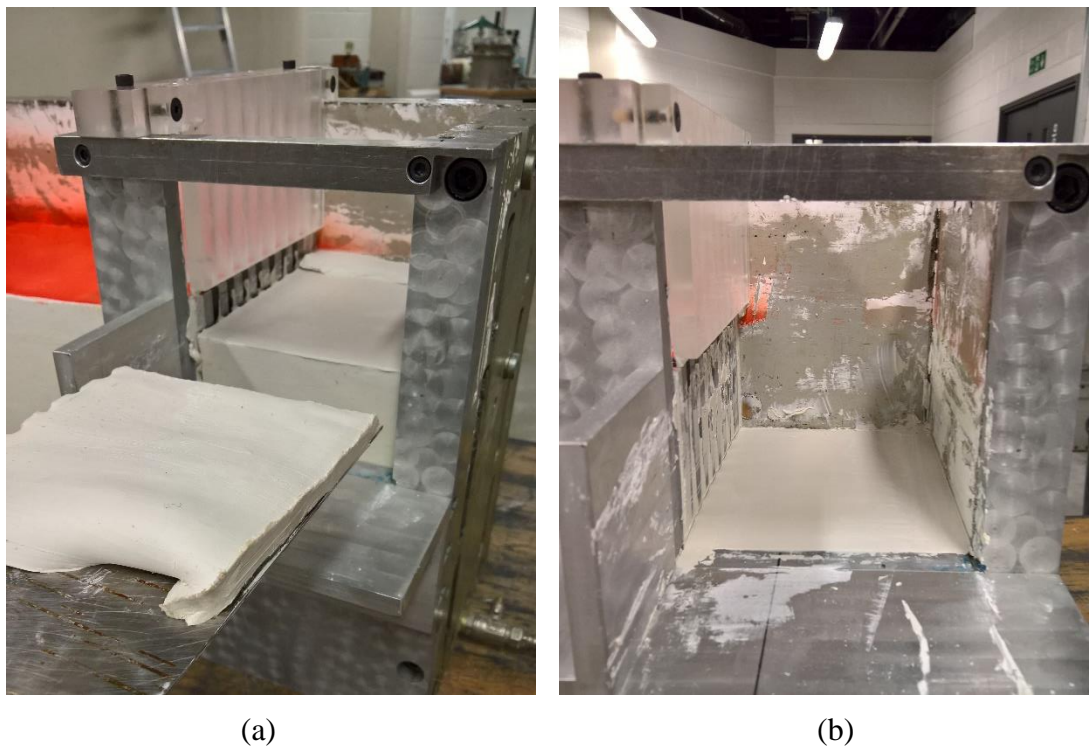


Figure 5.16 Embedment of retaining wall by hand using rectangular plunger



(a)

(b)

Figure 5.17 Formation of the excavation (a) using plates to scrape away material and (b) final excavation void



Figure 5.18 Removal of clay from between the ribs of the retaining wall



Figure 5.19 Sheet of filter paper, latex airbag, porous plastic and aluminium stiffener placed after formation of the excavation void

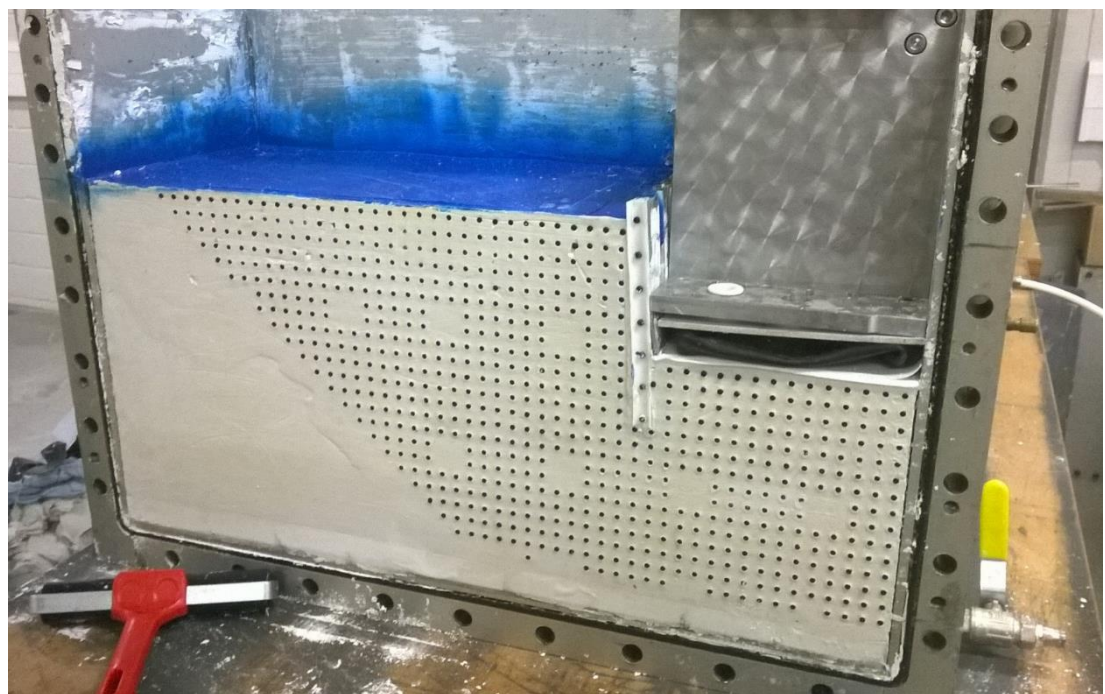


Figure 5.20 3mm acetal targets embedded in model with propping system and latex airbag in test JP1

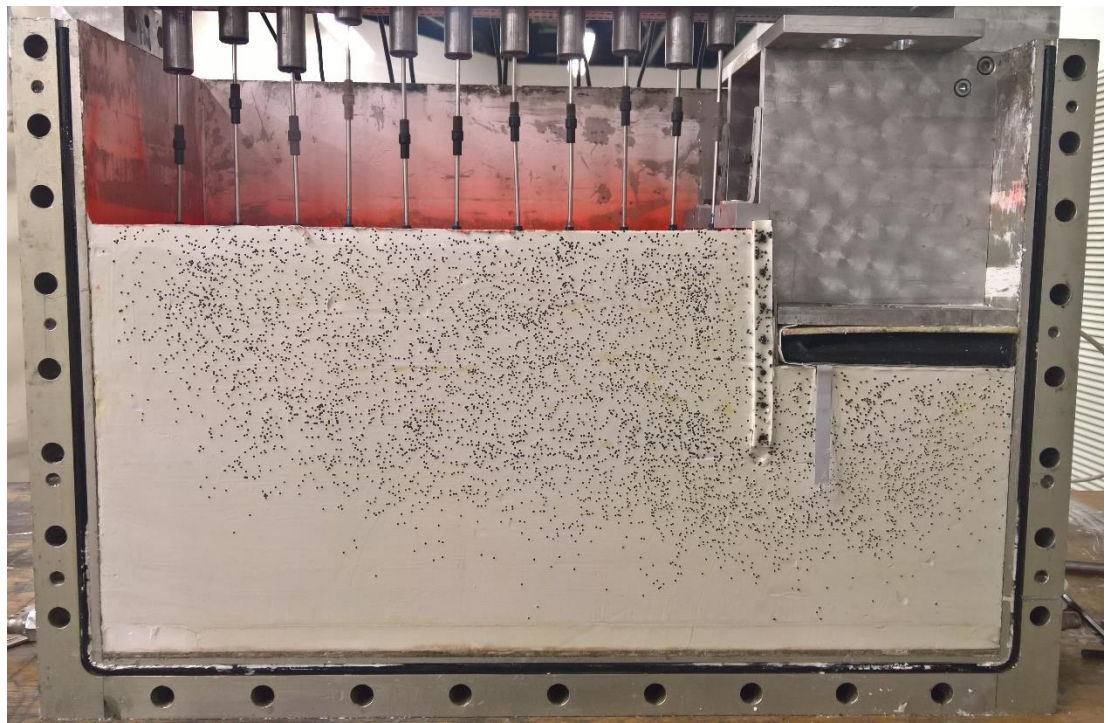


Figure 5.21 Typical texture of black ballotini applied to models in main experimental test series

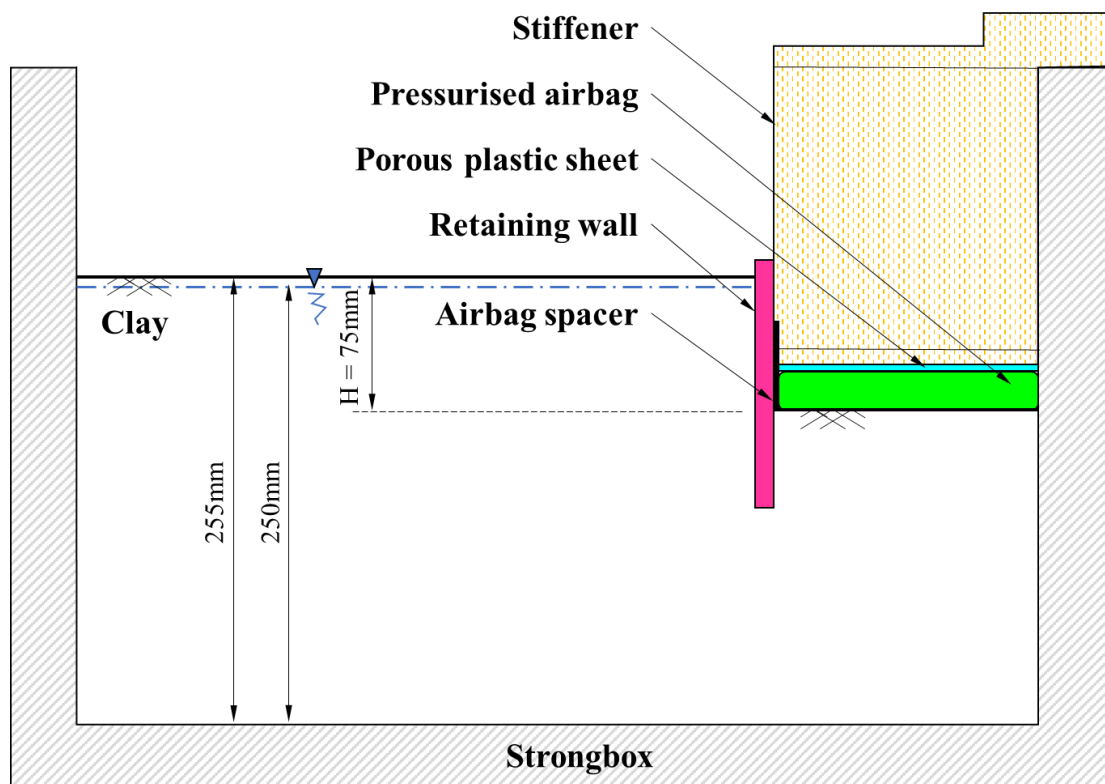


Figure 5.22 General centrifuge arrangement for dry excavations

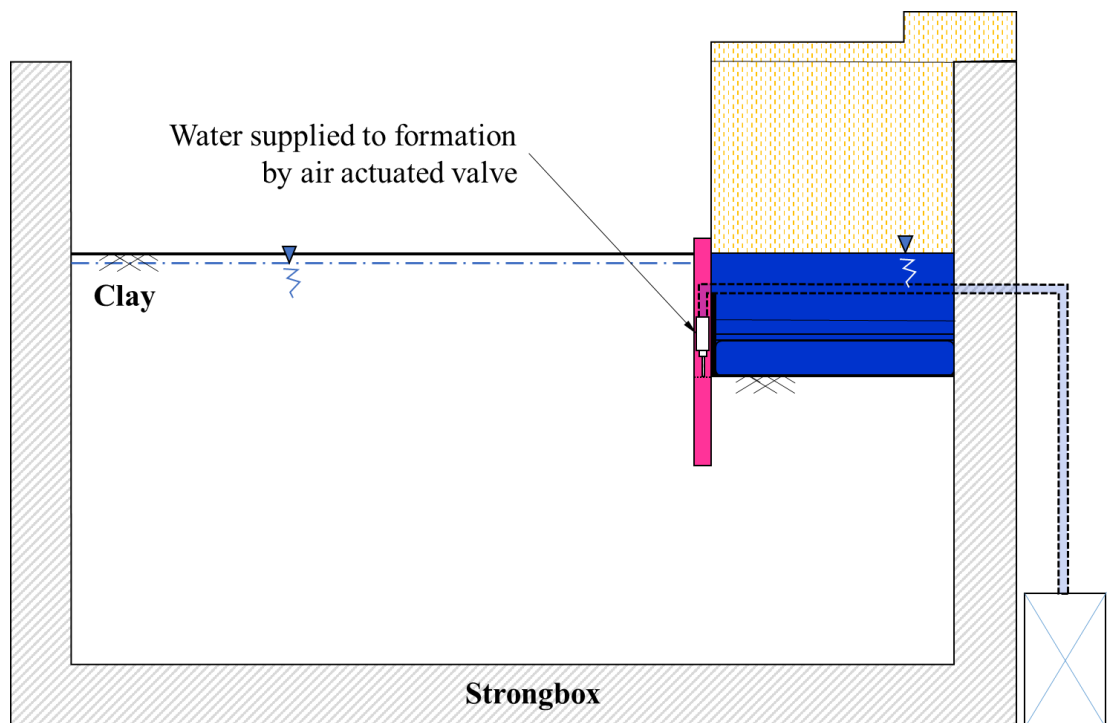


Figure 5.23 General arrangement of an underwater excavation test

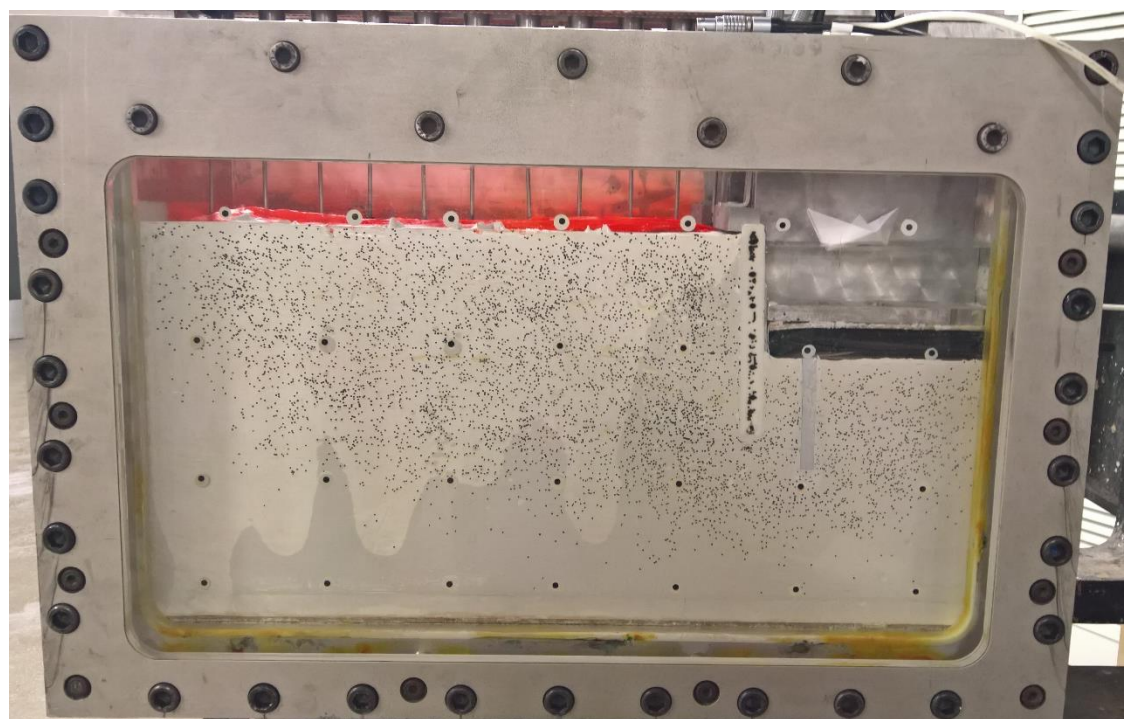


Figure 5.24 Photograph post underwater excavation test with excavation void full of water

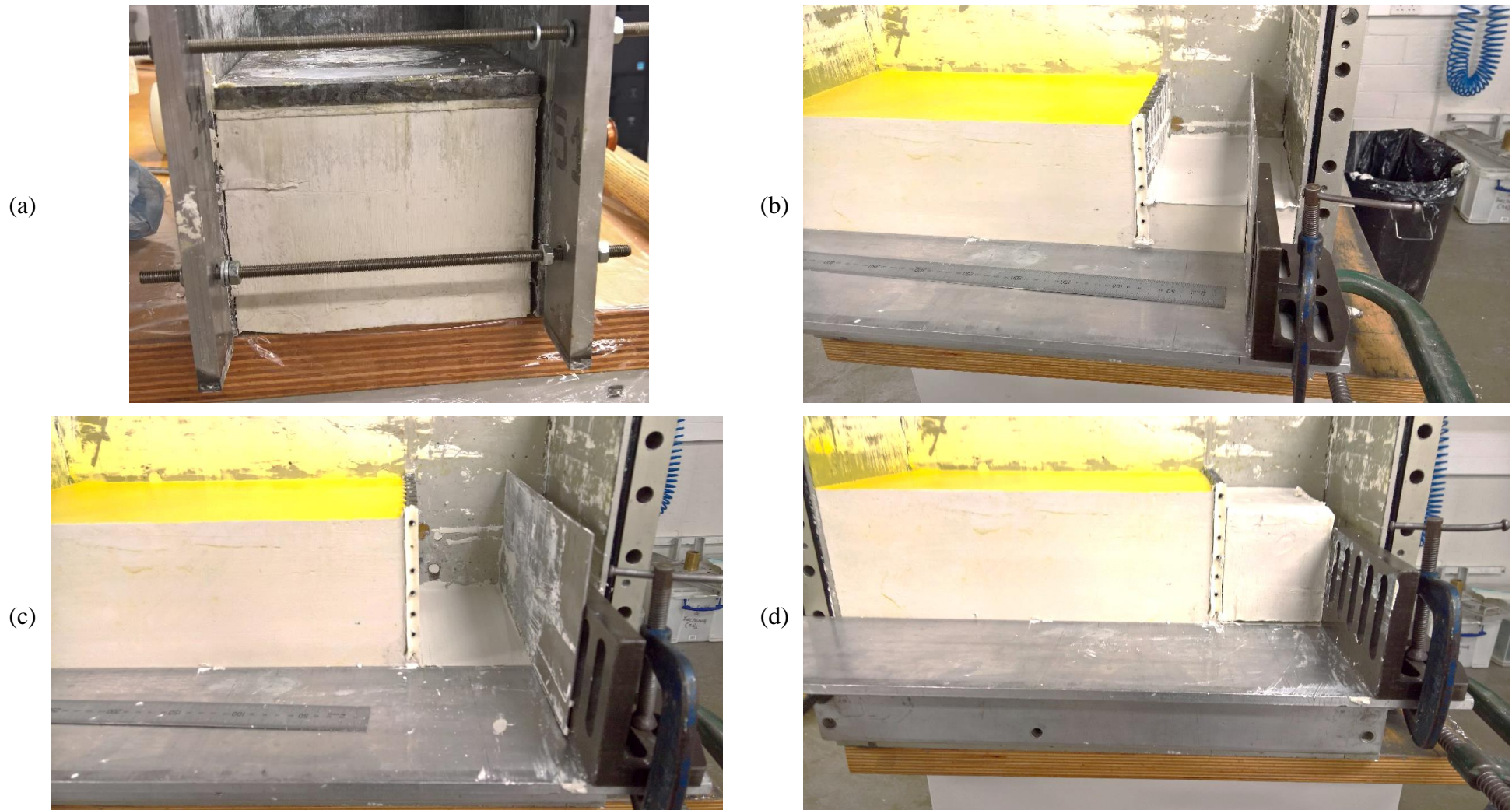


Figure 5.25 (a) Removal of treated soil from consolidation box, (b) series of angles clamped to model to accurately establish extent of ground treatment, (c) plates used to excavate virgin soil and (d) installation of lime-stabilised clay soil block

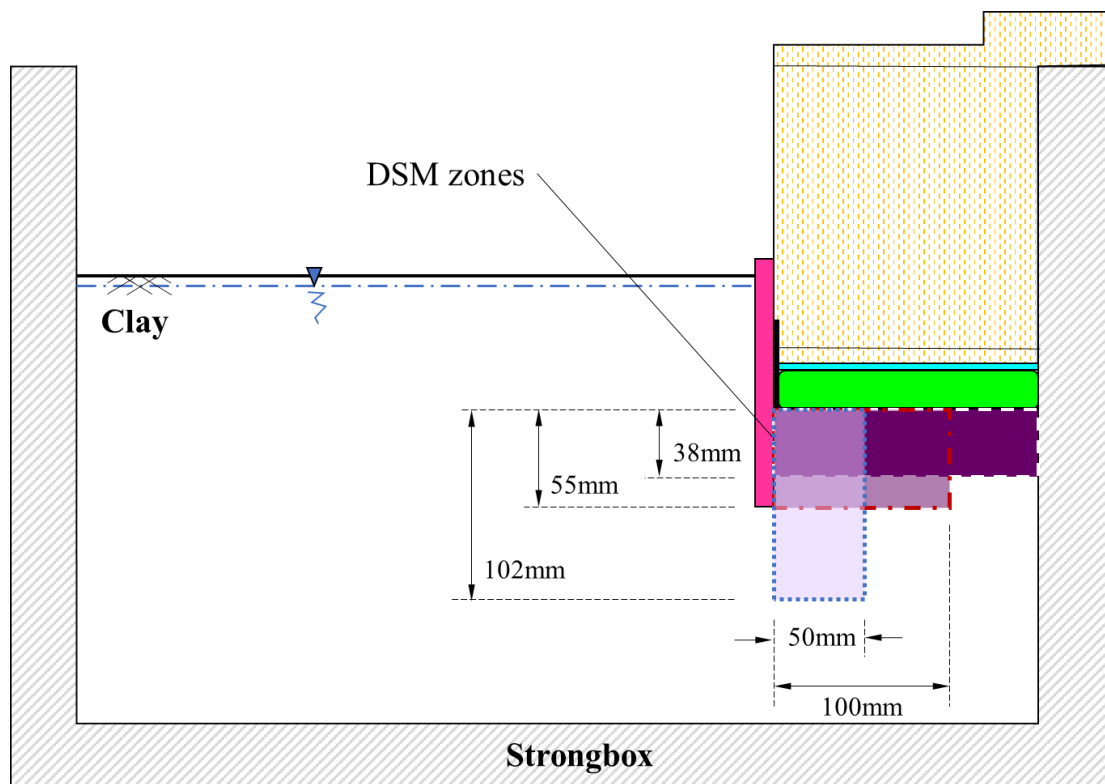


Figure 5.26 General arrangement of DSM ground improvement tests

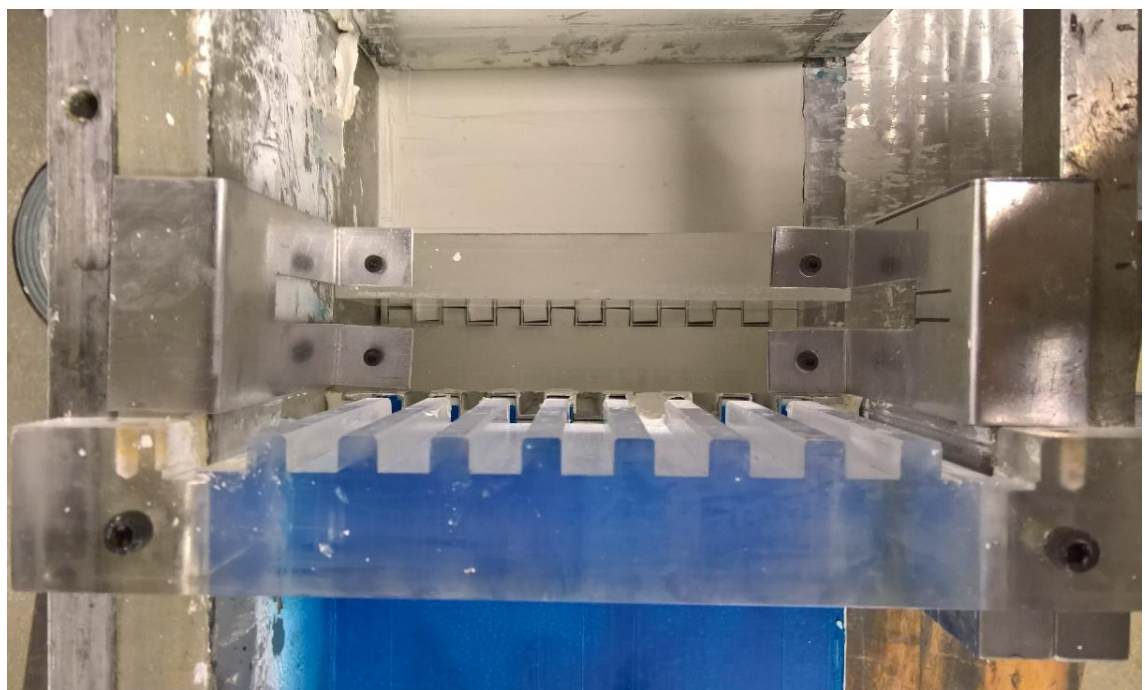


Figure 5.27 Plan view of double wall after installation

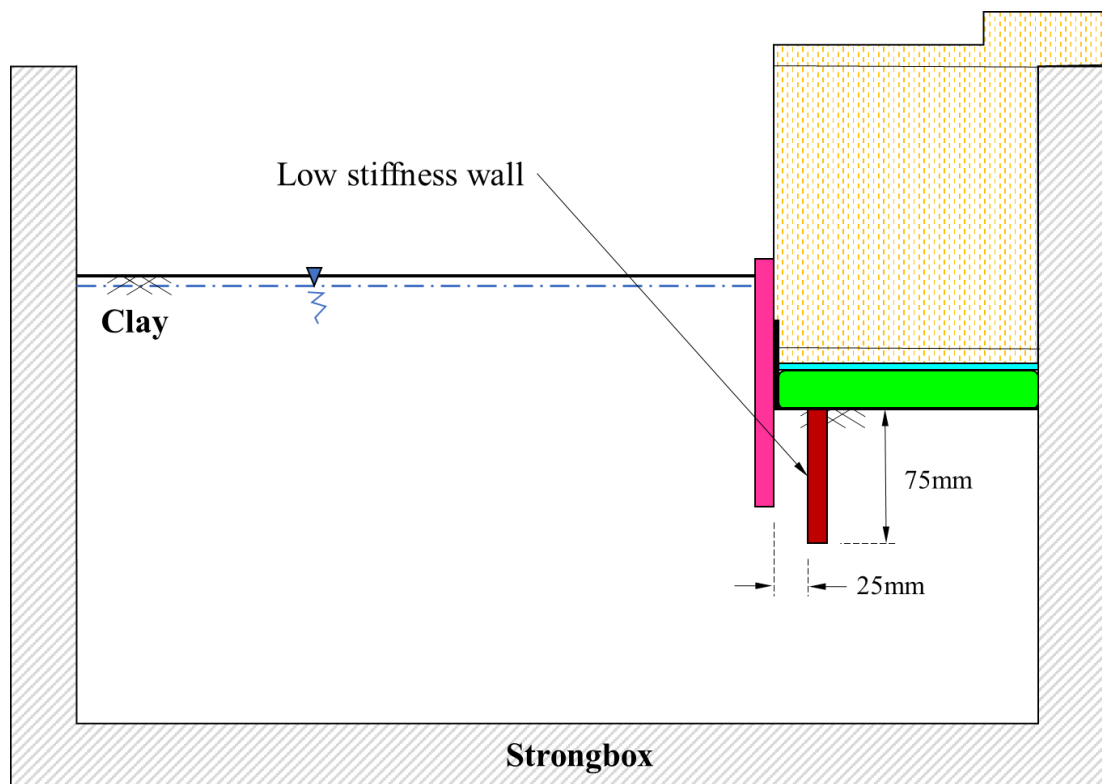


Figure 5.28 General arrangement of a double walled test

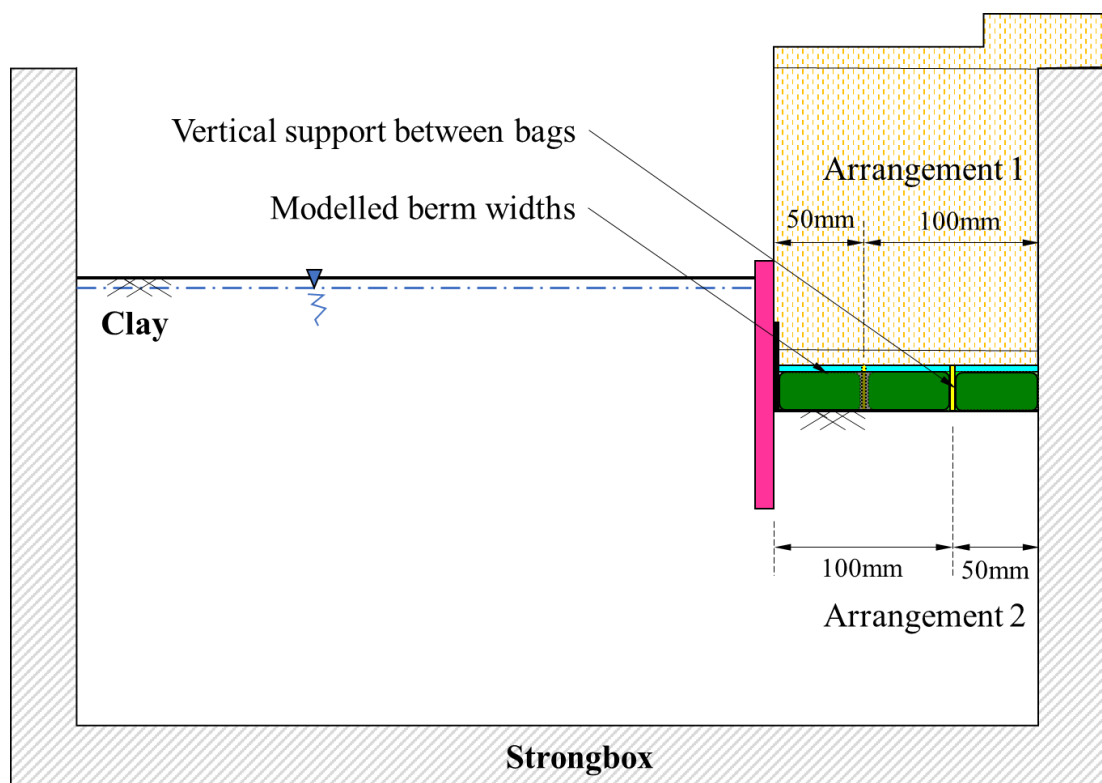


Figure 5.29 General arrangement of bermed excavation tests

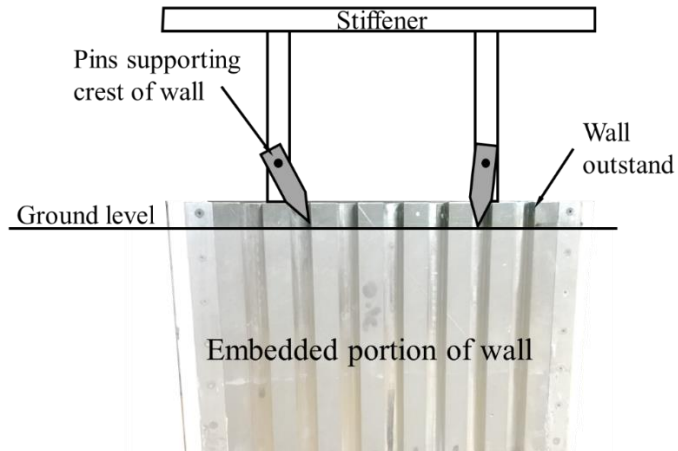


Figure 6.1 Schematic diagram of pins used to fix crest of wall in test JP11

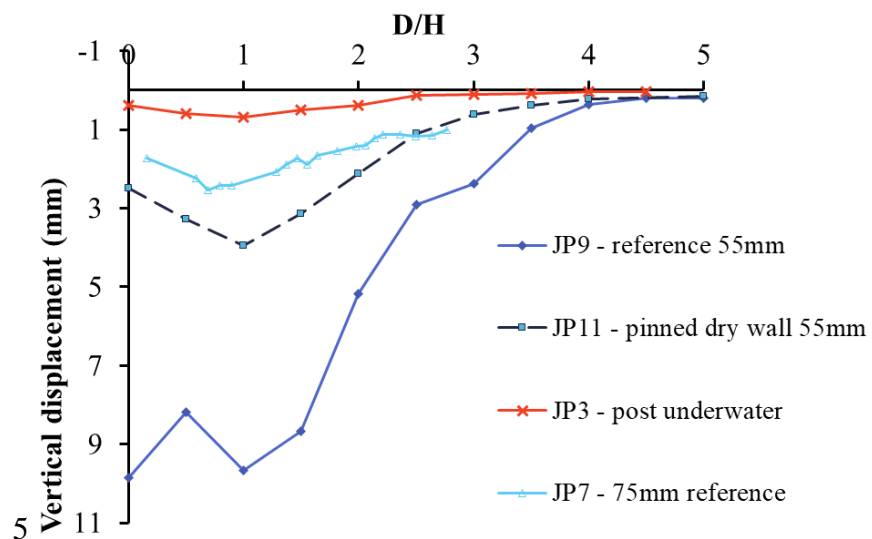


Figure 6.2 Settlement profile of retained ground at an overburden pressure of 38kPa

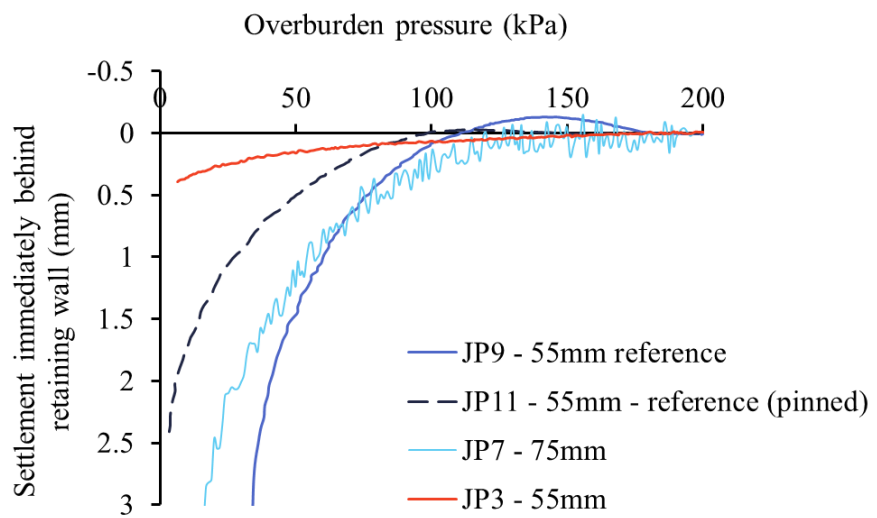


Figure 6.3 Vertical displacement immediately behind retaining wall during reference test excavations

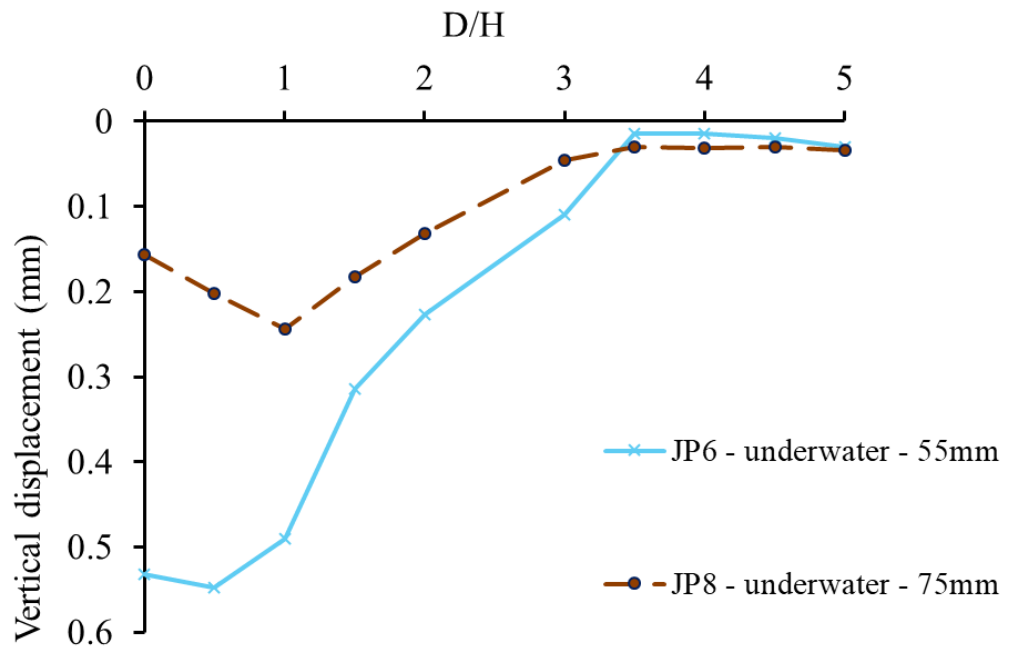


Figure 6.4 Settlement profile of retained ground at end of excavation

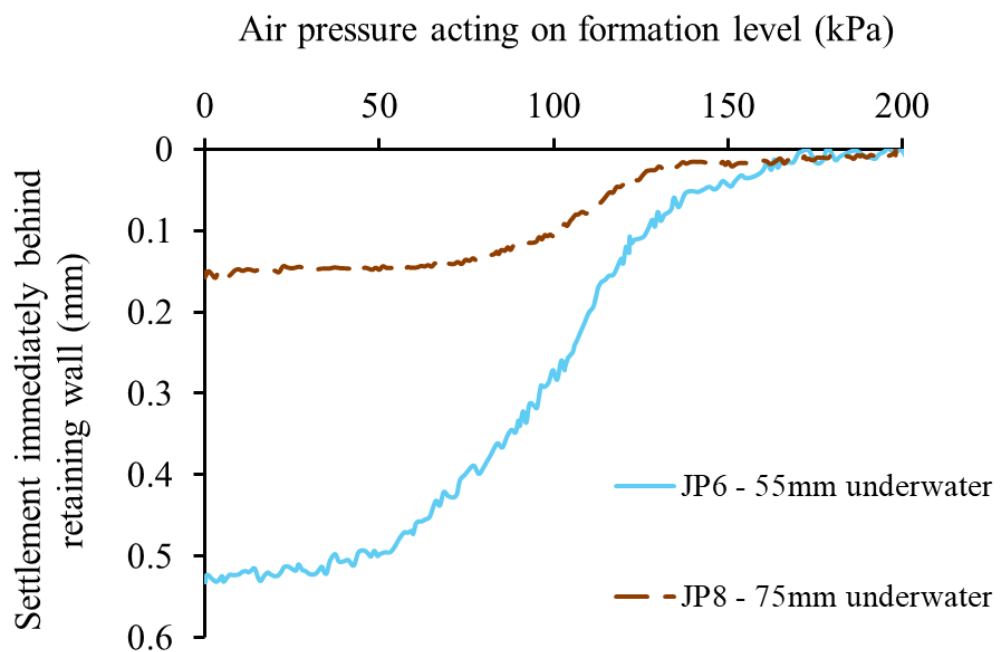


Figure 6.5 Vertical displacement immediately behind retaining wall during underwater excavation tests

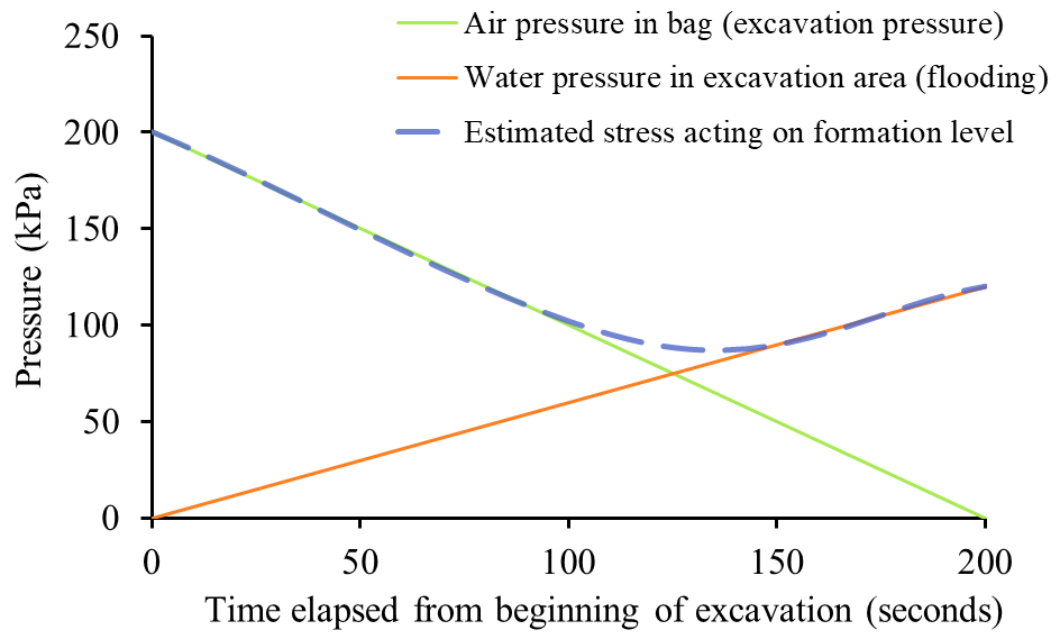


Figure 6.6 Loading history on formation level owing to reduction in air pressure and flooding of excavation area

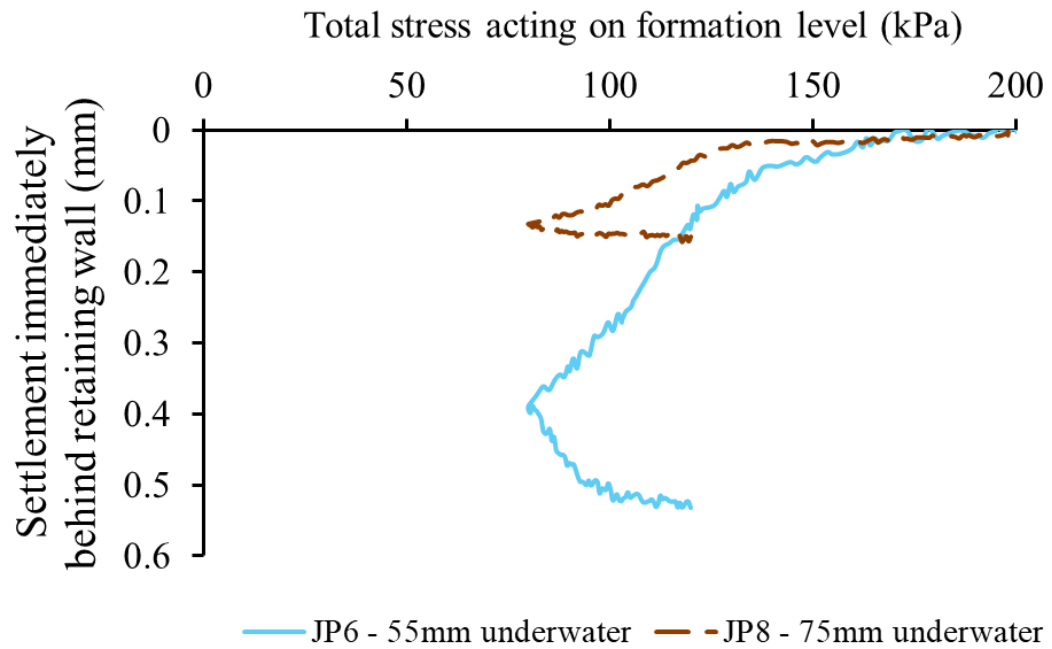
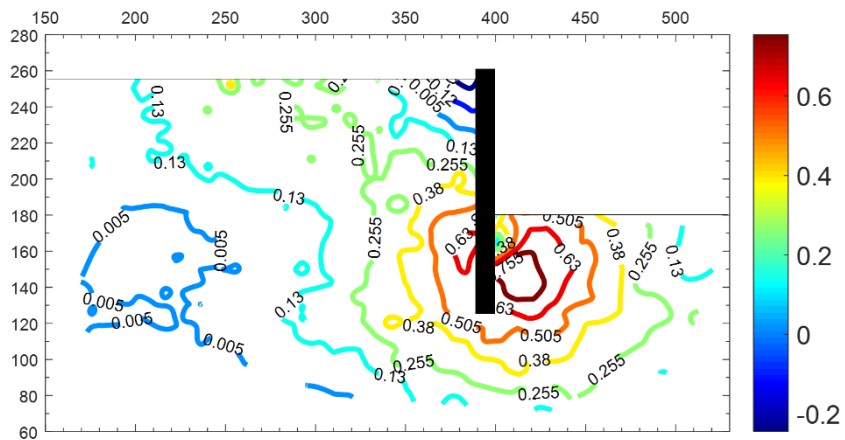
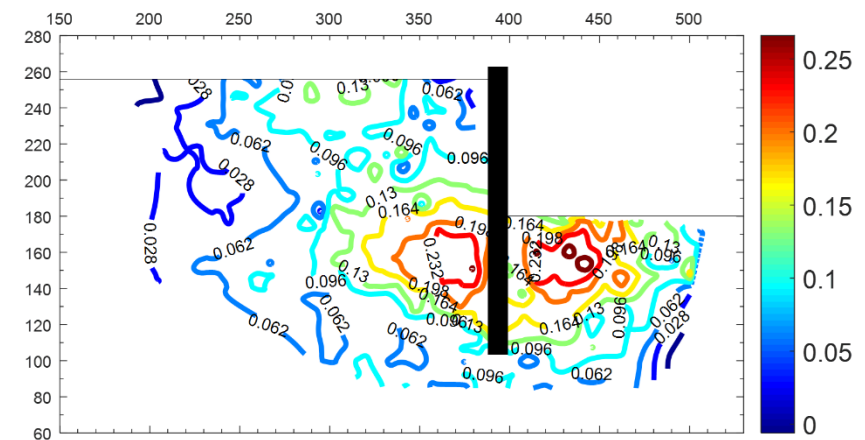


Figure 6.7 Development of settlements owing to total stress acting on formation level

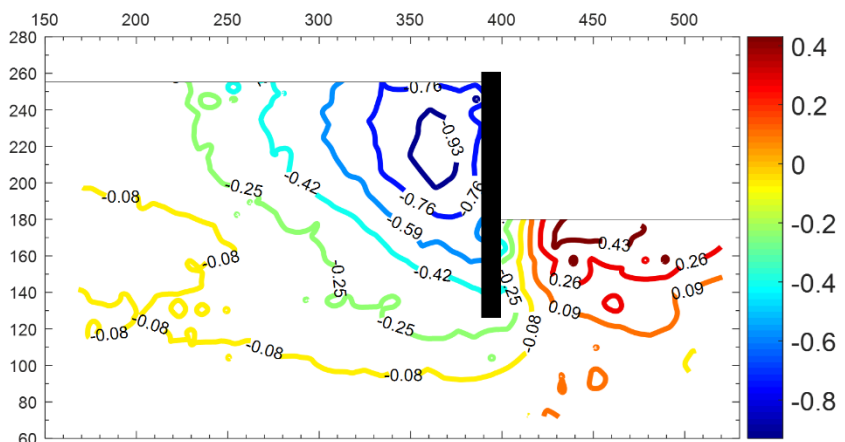


a) Test JP6, underwater excavation 55mm embedment

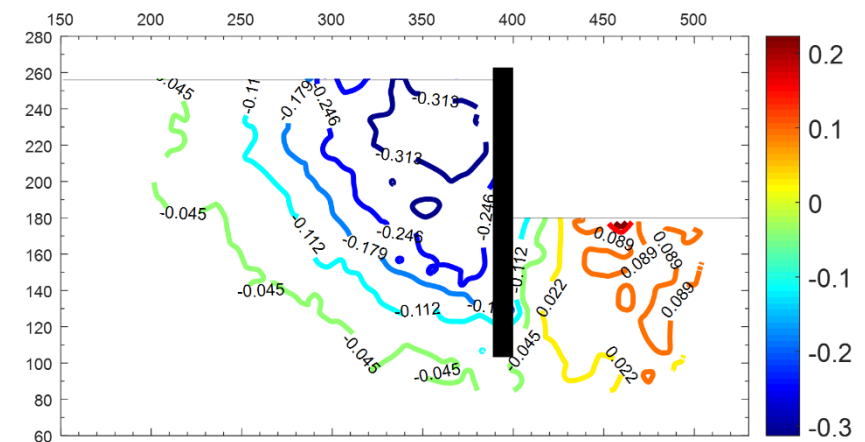


b) Test JP8, underwater excavation 75mm embedment

Figure 6.8 Contours of horizontal movements at end of excavation (OkPa) (displacement in mm)



a) Test JP6, underwater excavation 55mm embedment



b) Test JP8, underwater excavation 75mm embedment

Figure 6.9 Contours of vertical movements at end of excavation (0kPa) (displacement in mm)

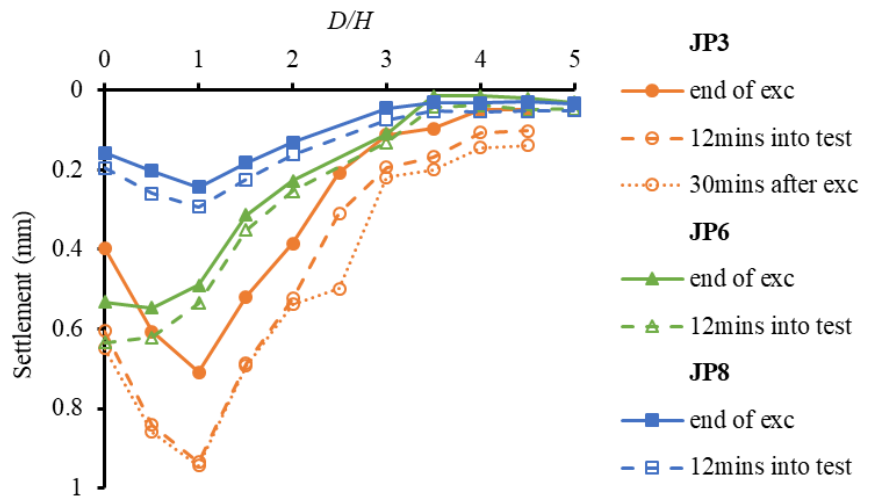


Figure 6.10 Change in surface settlement profile 12 minutes post excavation

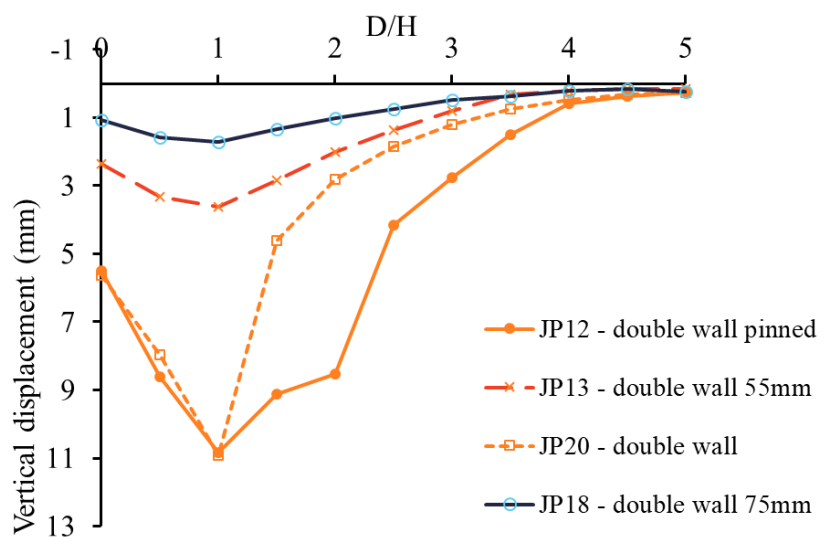


Figure 6.11 Settlement profile of retained ground at end of excavation

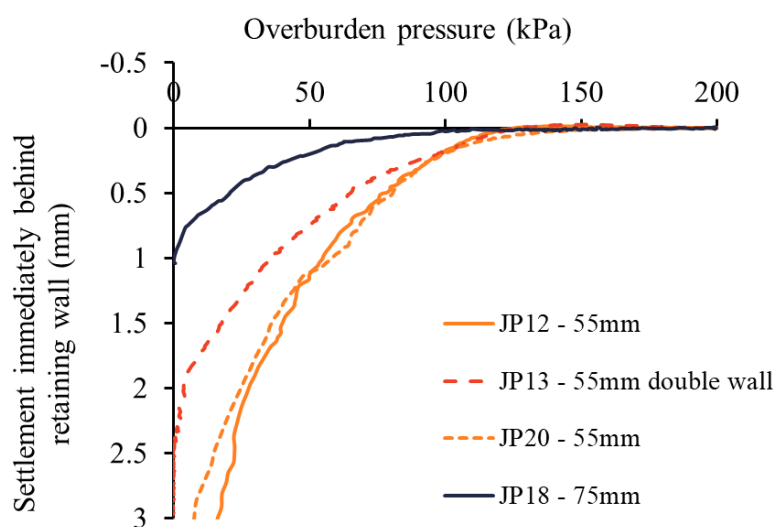
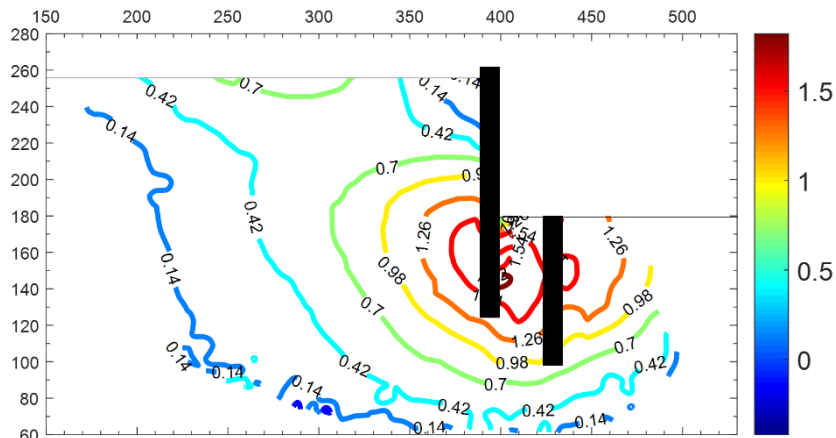
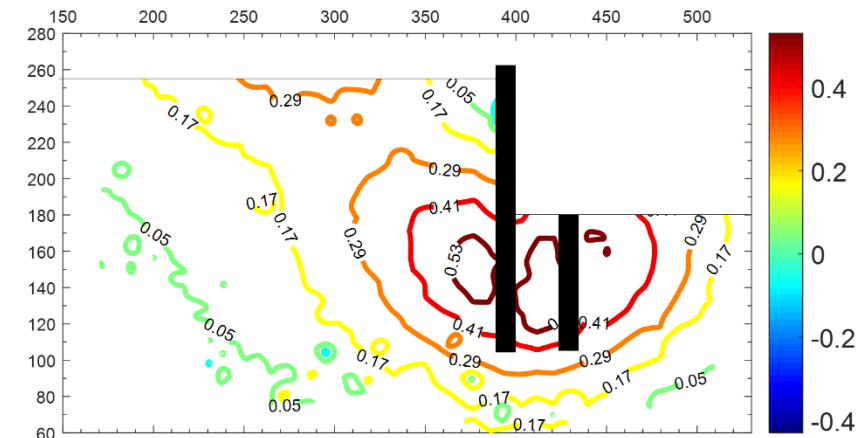


Figure 6.12 Vertical displacement at immediately behind the retaining during double walled excavation tests

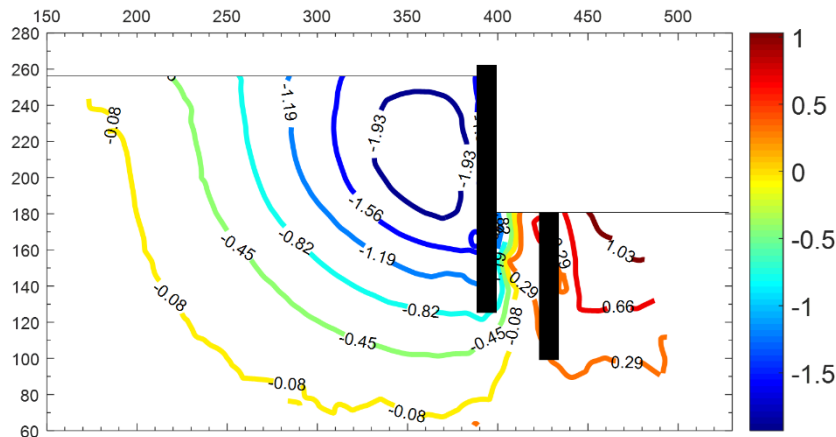


a) Test JP13, double wall with 55mm embedment

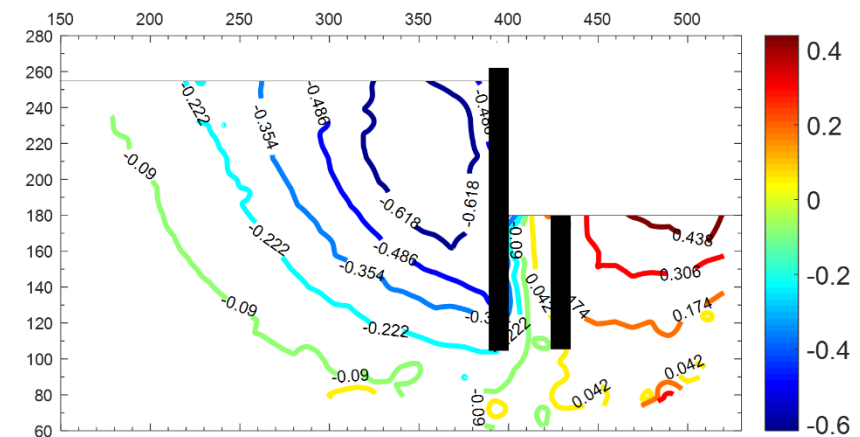


b) Test JP18, double wall with 75mm embedment

Figure 6.13 Contours of horizontal movements at 25kPa overburden pressure (displacement in mm)



a) Test JP13, double wall with 55mm embedment



b) Test JP18, double wall with 75mm embedment

Figure 6.14 Contours of vertical movements at 25kPa overburden pressure (displacement in mm)

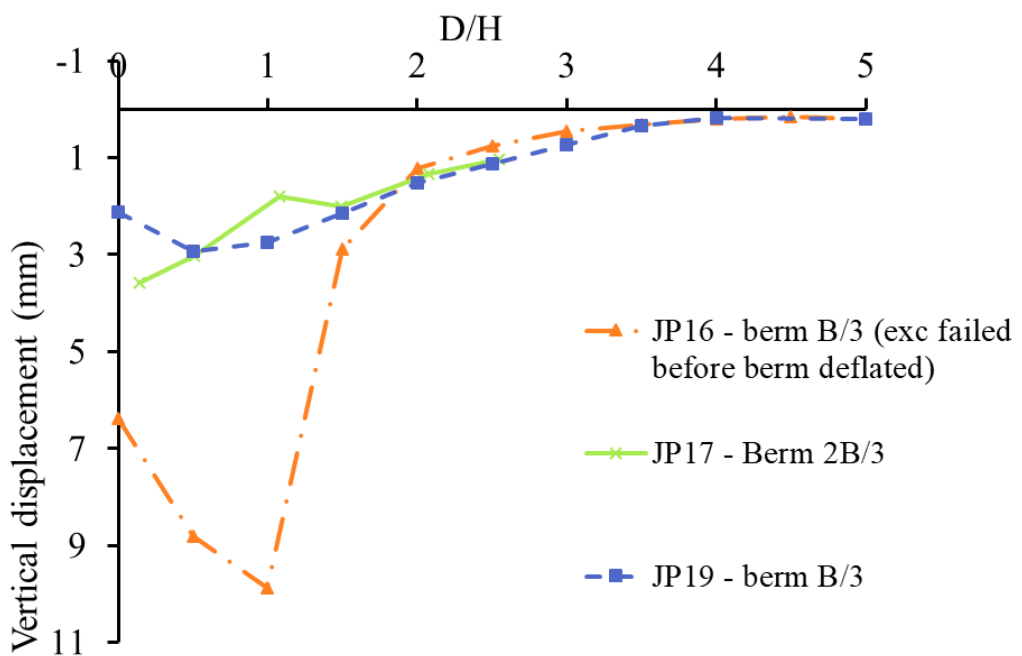
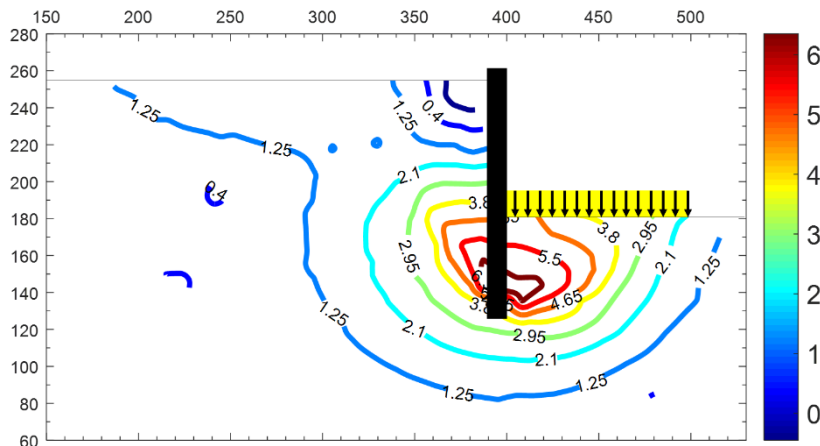
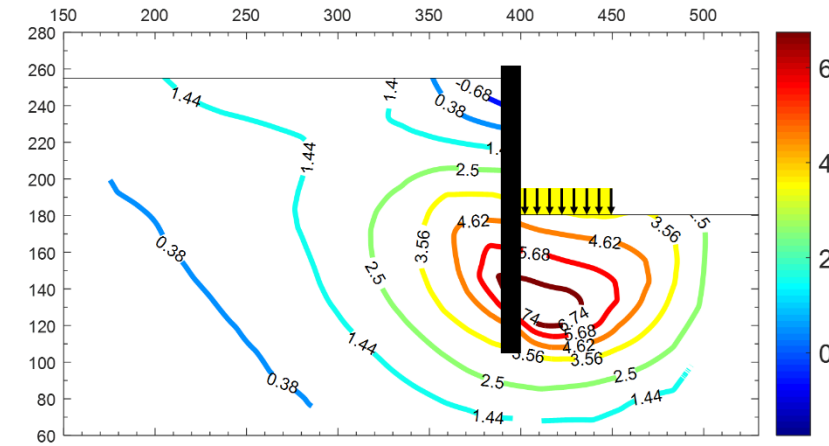


Figure 6.15 Settlement profile of retained ground at end of excavation

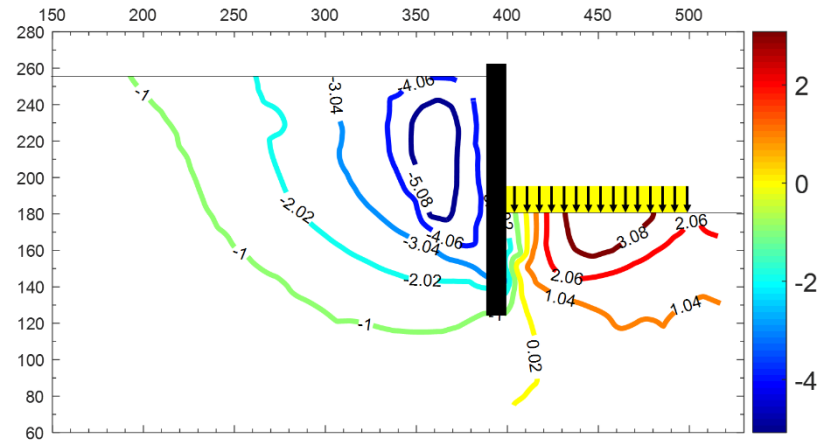


(a) JP17, bermed excavation 2B/3, 55mm wall embedment

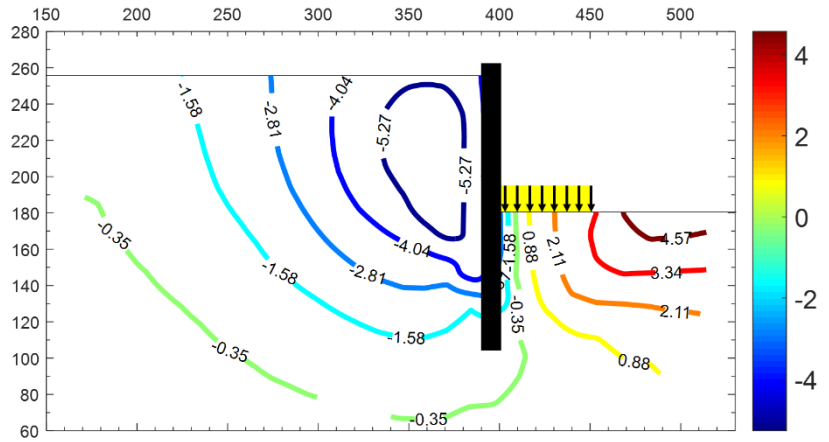


(b) JP19, bermed excavation B/3, 75mm wall embedment

Figure 6.16 Contours of horizontal movements at end of excavation and complete removal of berm pressure (displacement in mm)



(a) JP17, bermed excavation 2B/3, 55mm wall embedment



(b) JP19, bermed excavation B/3, 75mm wall embedment

Figure 6.17 Contours of vertical displacement at end of excavation and complete removal of berm pressure (displacement in mm)

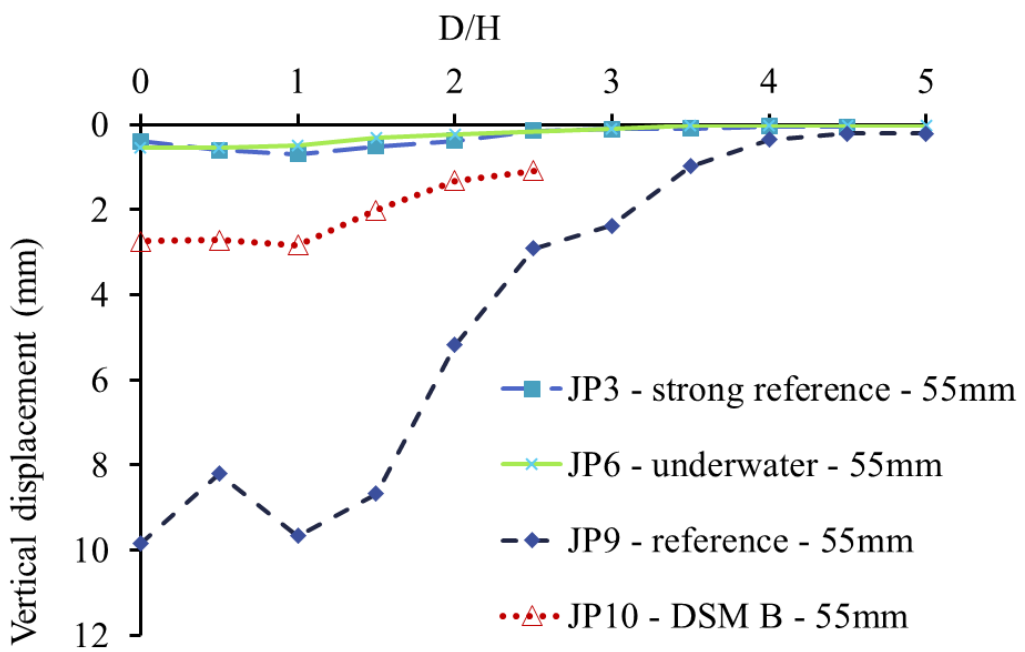


Figure 6.18 Surface settlements immediately after excavation

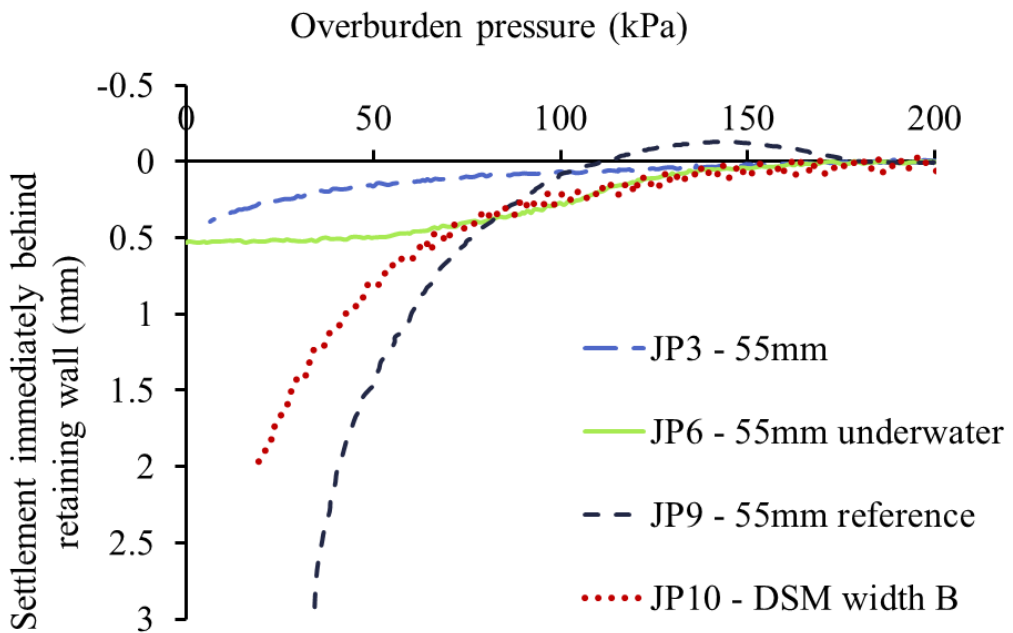
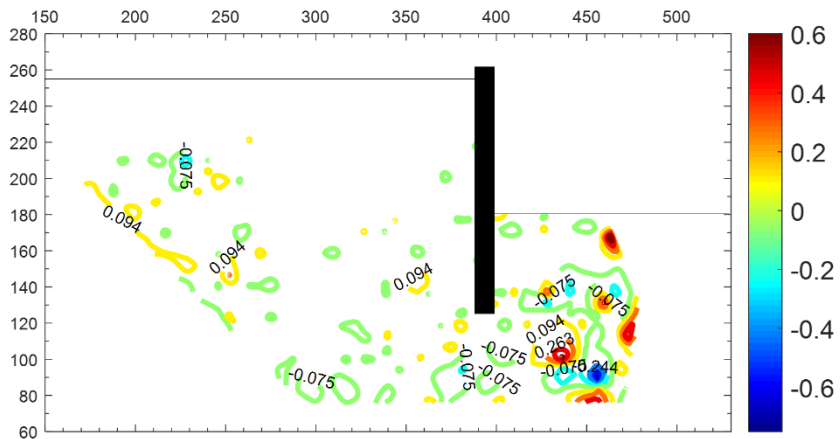
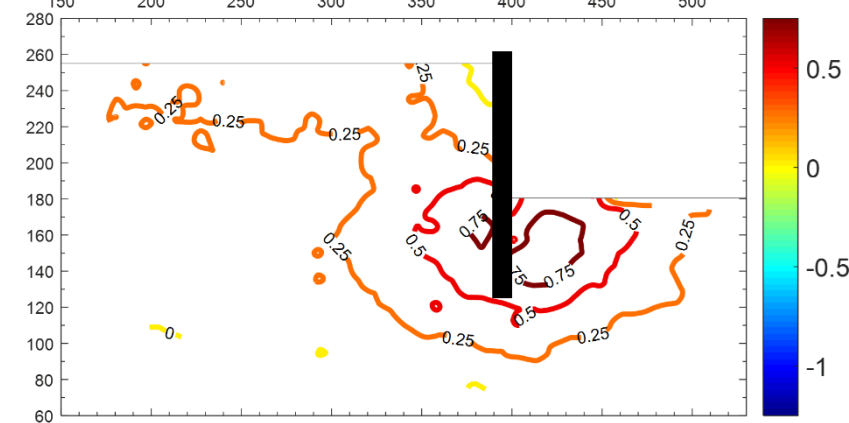


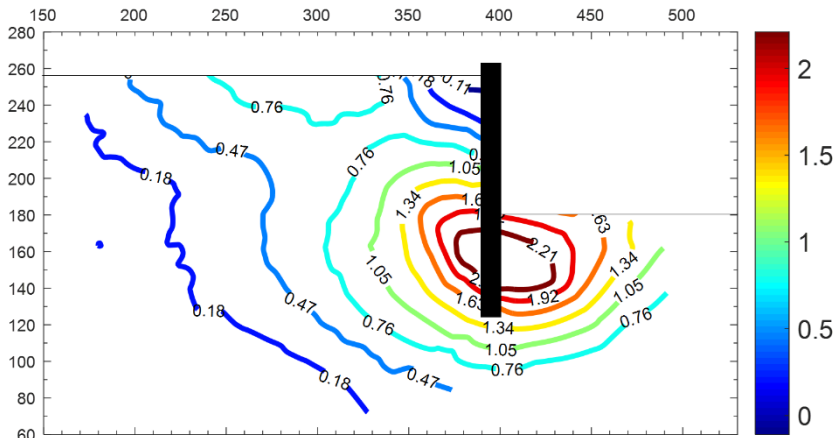
Figure 6.19 Progression of vertical displacements during excavation immediately behind retaining wall



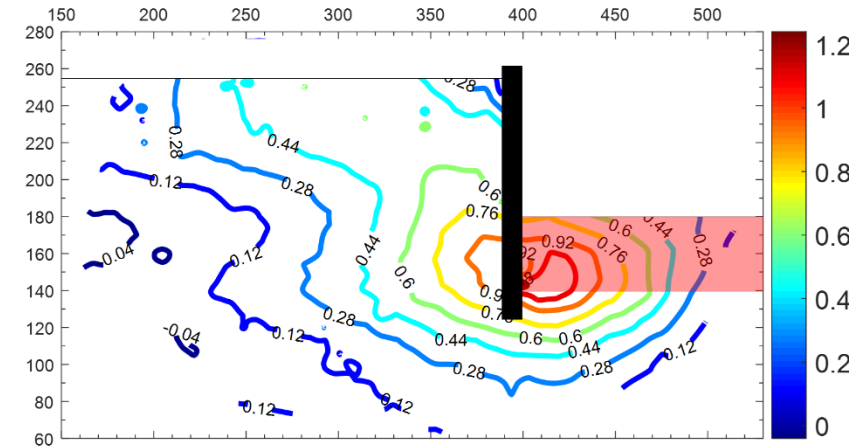
a) Test JP3, excavation flooded post removal of overburden pressure



b) Test JP6, underwater excavation

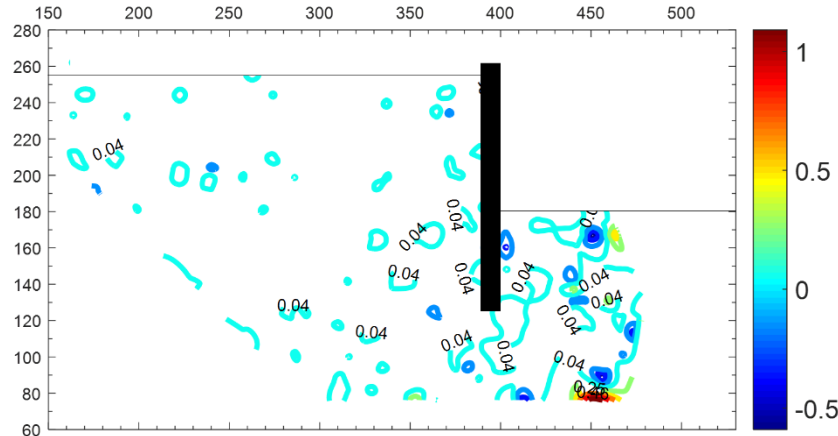


c) Test JP9, reference test

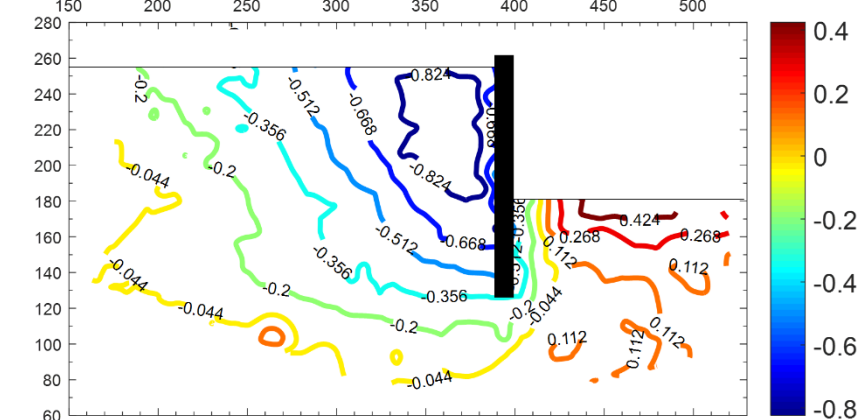


d) Test JP10, DSM ($H/2$)

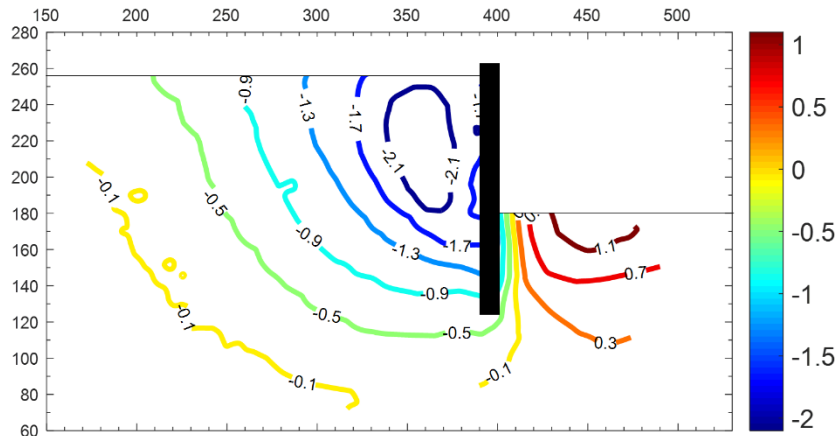
Figure 6.20 Contours of horizontal movements at 50kPa (displacements in mm)



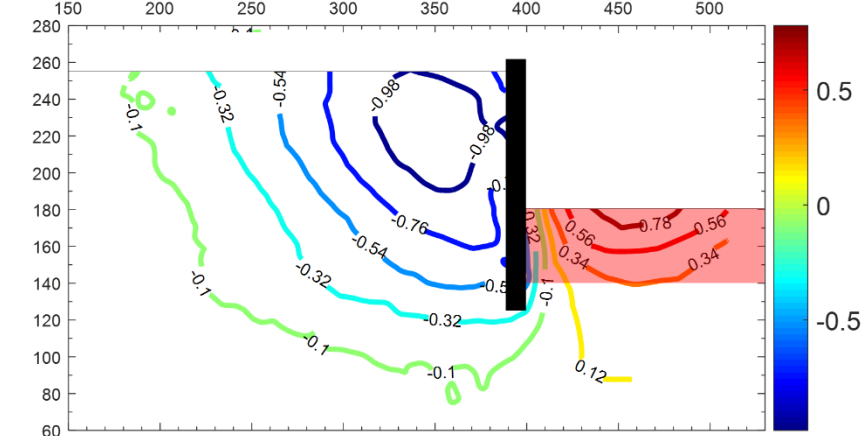
a) Test JP3, excavation flooded post removal of overburden pressure



b) Test JP6, underwater excavation



c) Test JP9, reference test



d) Test JP10, DSM ($H/2$)

Figure 6.21 Contours of vertical movements at 50kPa (displacements in mm)

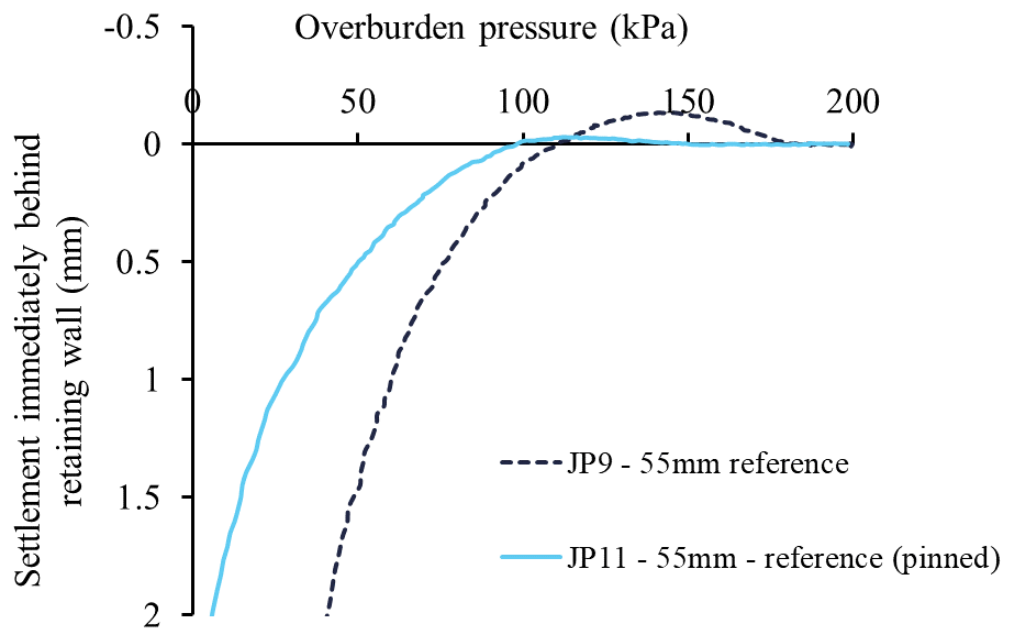


Figure 6.22 Settlement during removal of overburden pressure immediately behind retaining wall for a fixed wall crest and an unrestrained wall

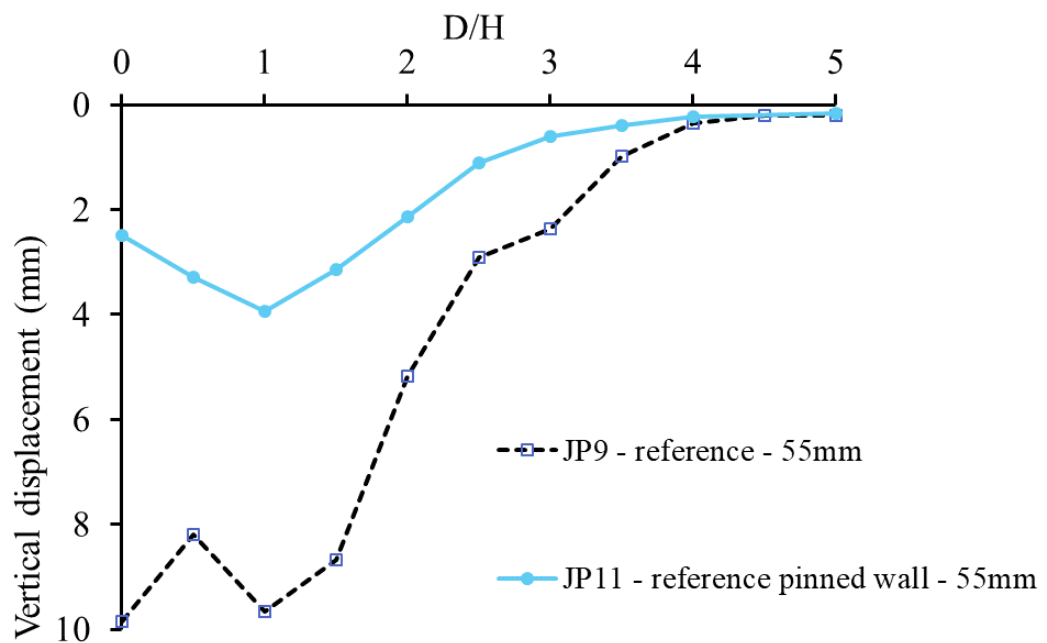


Figure 6.23 Surface settlement profiles at end of excavation for a wall fixed at the crest and an unrestrained wall

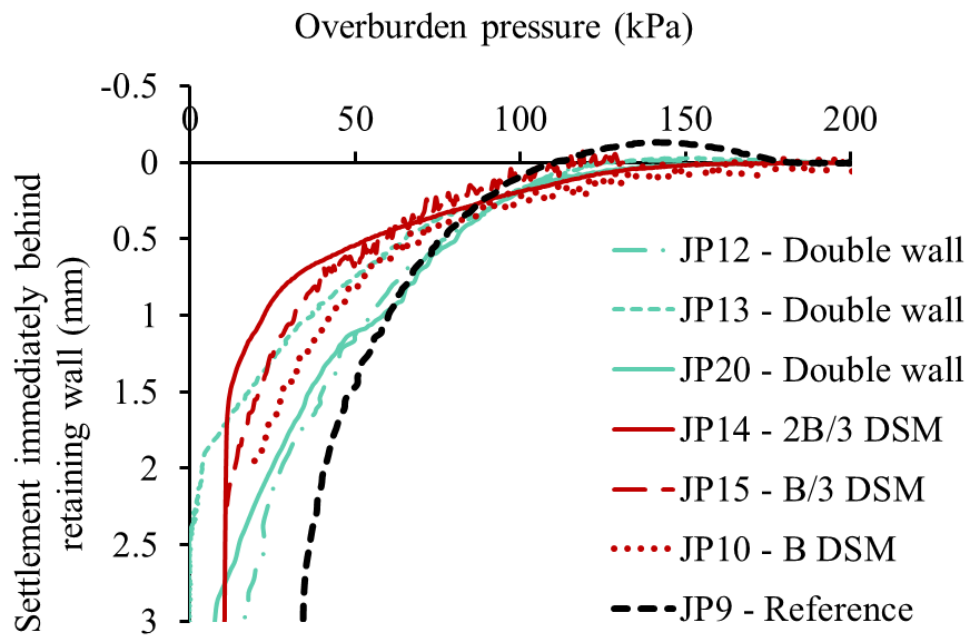


Figure 6.24 Settlement during removal of overburden pressure immediately behind retaining wall for double walled and DSM tests

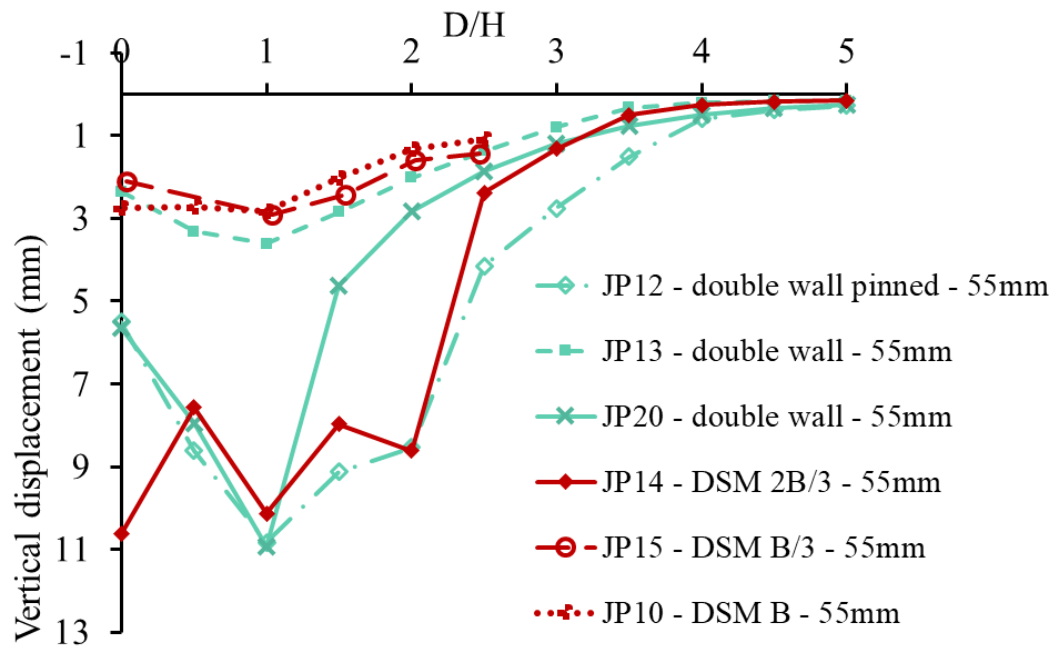
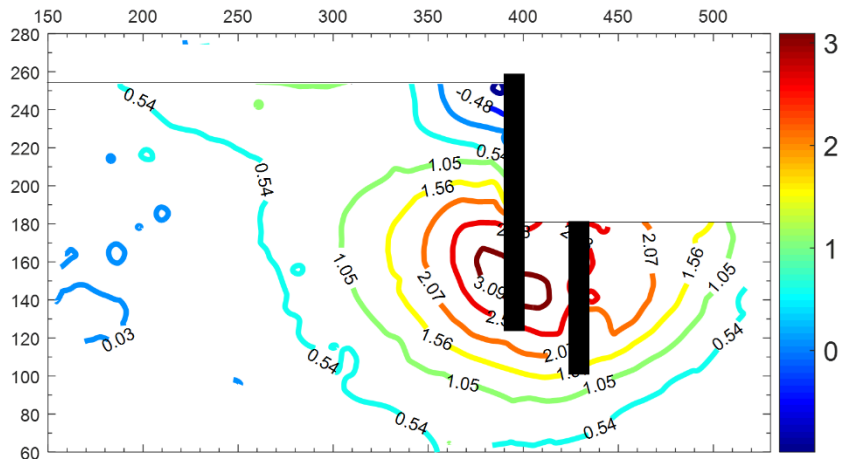
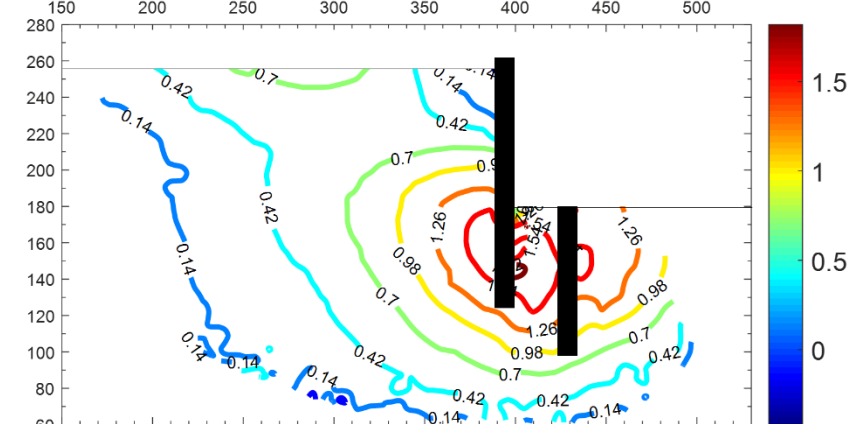


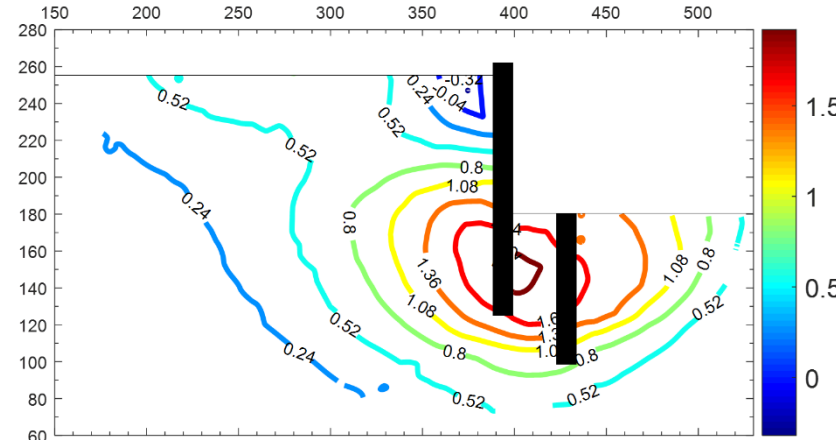
Figure 6.25 Settlement troughs at end of excavation for double walled and DSM tests



a) Test JP12, double wall pinned at crest

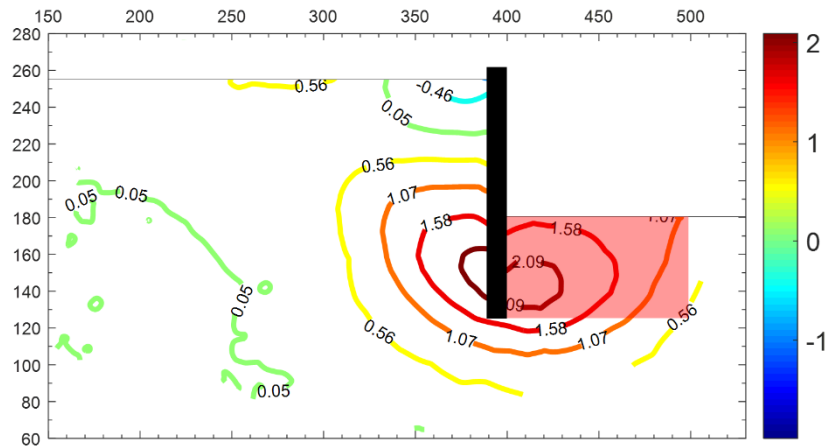


b) Test JP13, double wall (sliding bracket)

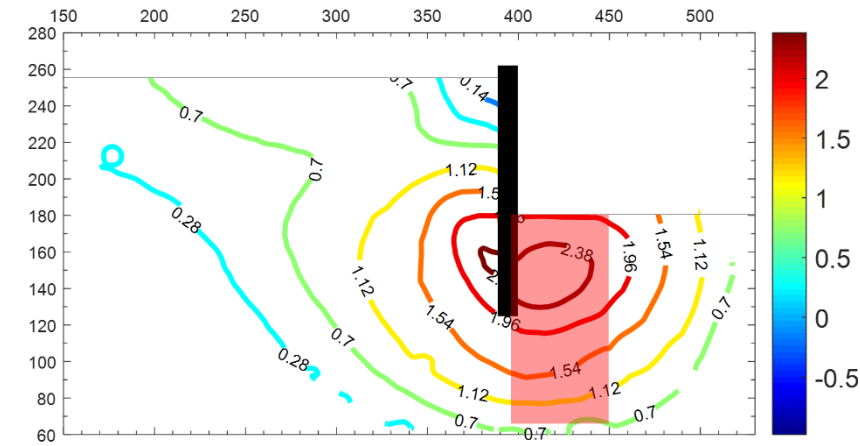


c) Test JP20, double wall with sliding bracket

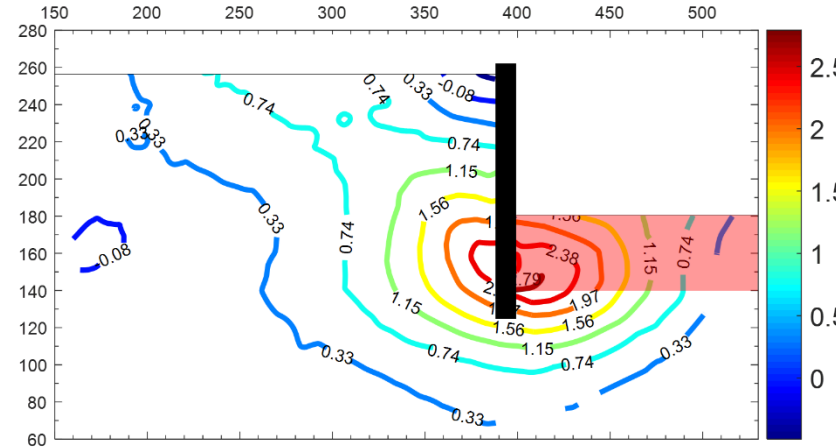
Figure 6.26 Contours of horizontal movements at 25kPa overburden pressure (displacement in mm)



d) Test JP14, DSM (2B/3)

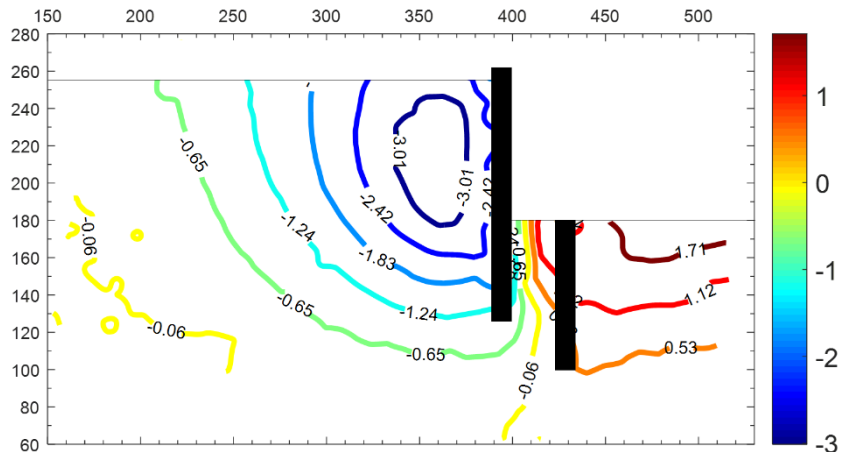


e) Test JP15, DSM (B/3)

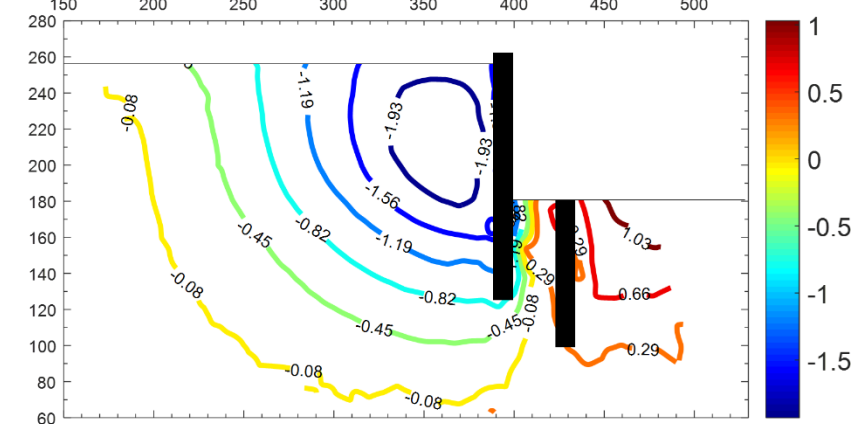


f) Test JP10, DSM (B)

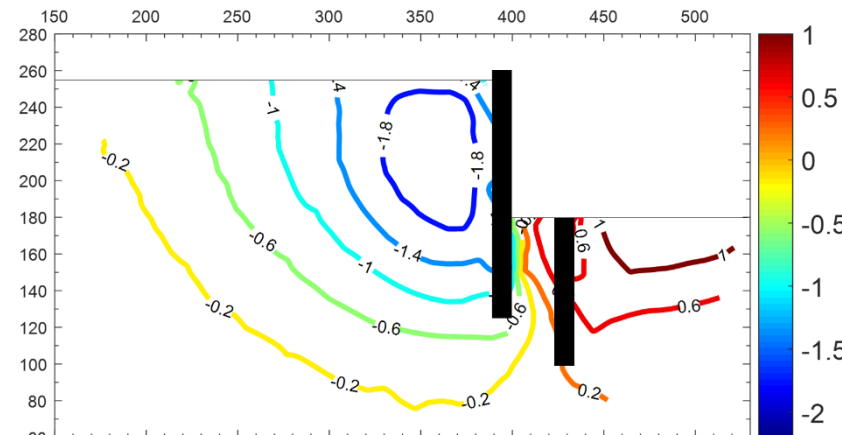
Figure 6.24 (cont'd) Contours of horizontal movements at 25kPa overburden pressure (displacement in mm)



a) Test JP12, double wall pinned at crest

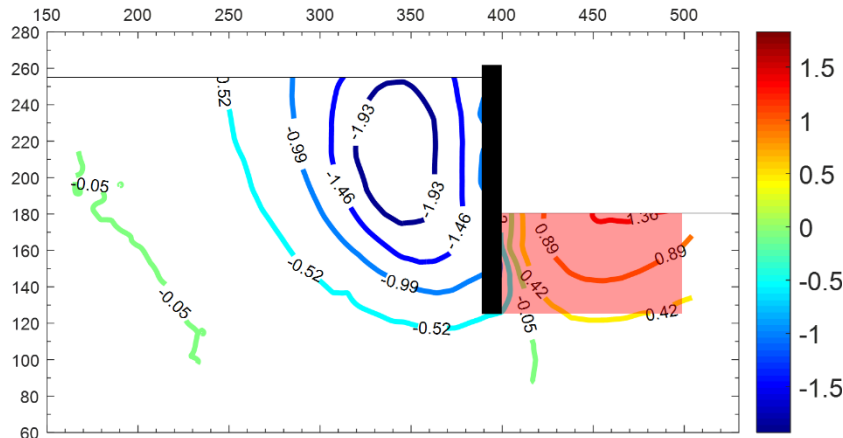


b) Test JP13, double wall with sliding bracket

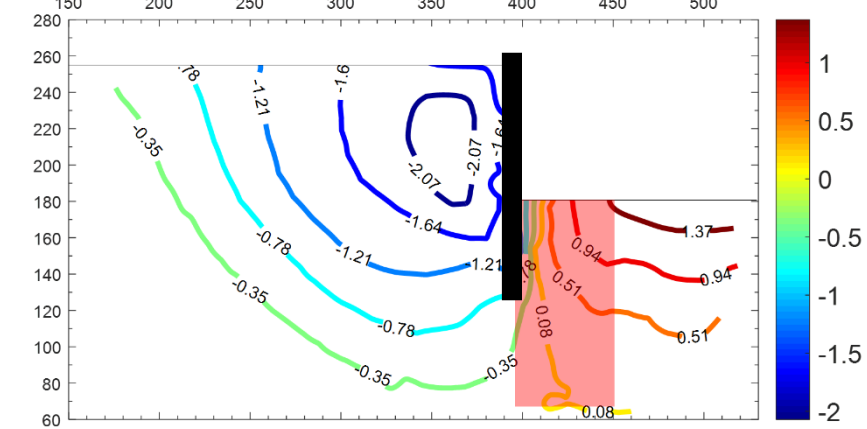


c) Test JP20, double wall with sliding bracket

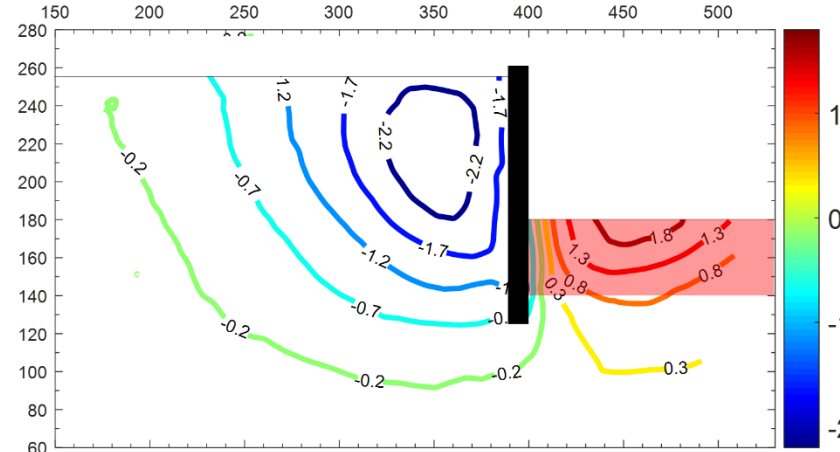
Figure 6.27 Contours of vertical movements at 25kPa overburden pressure (displacement in mm)



d) Test JP14, DSM (2B/3)



e) Test JP15, DSM (B/3)



f) Test JP10, DSM (B)

Figure 6.25 (cont'd) Contours of vertical movements at 25kPa overburden pressure (displacement in mm)

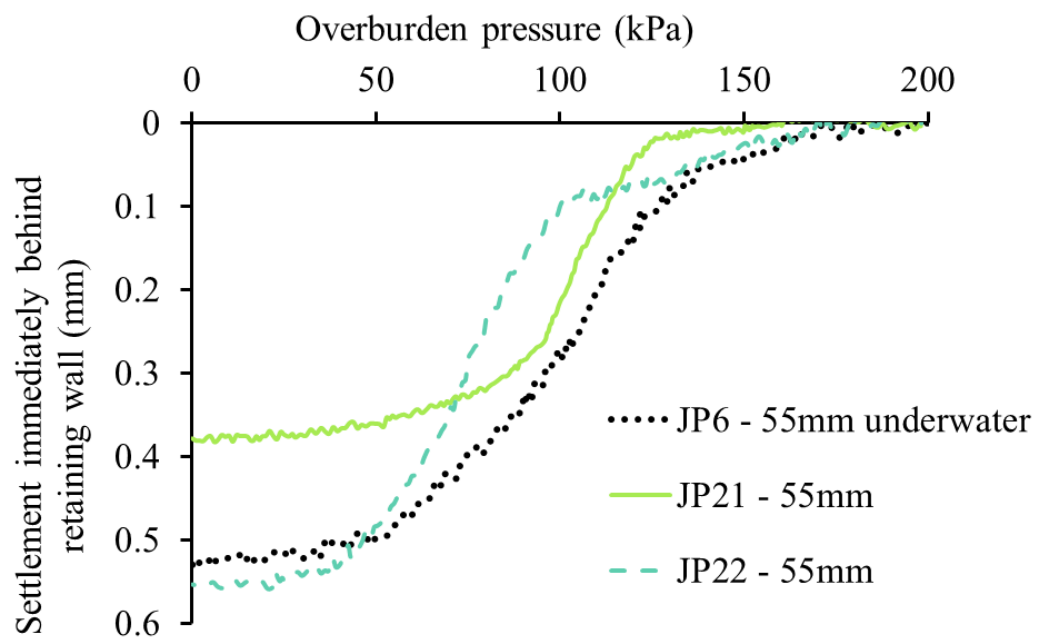


Figure 6.28 Settlement during excavation immediately behind retaining wall for underwater excavation and a double wall or DSM zone

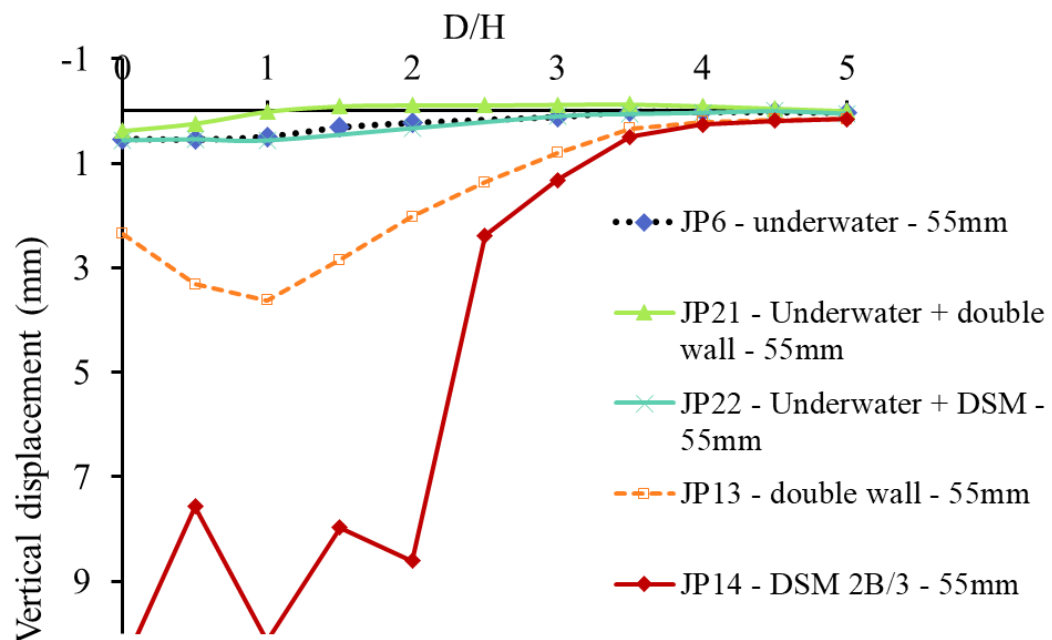


Figure 6.29 Surface settlement profiles of combined tests (JP21 and JP22) compared with individual tests (JP6, JP13 and JP14)

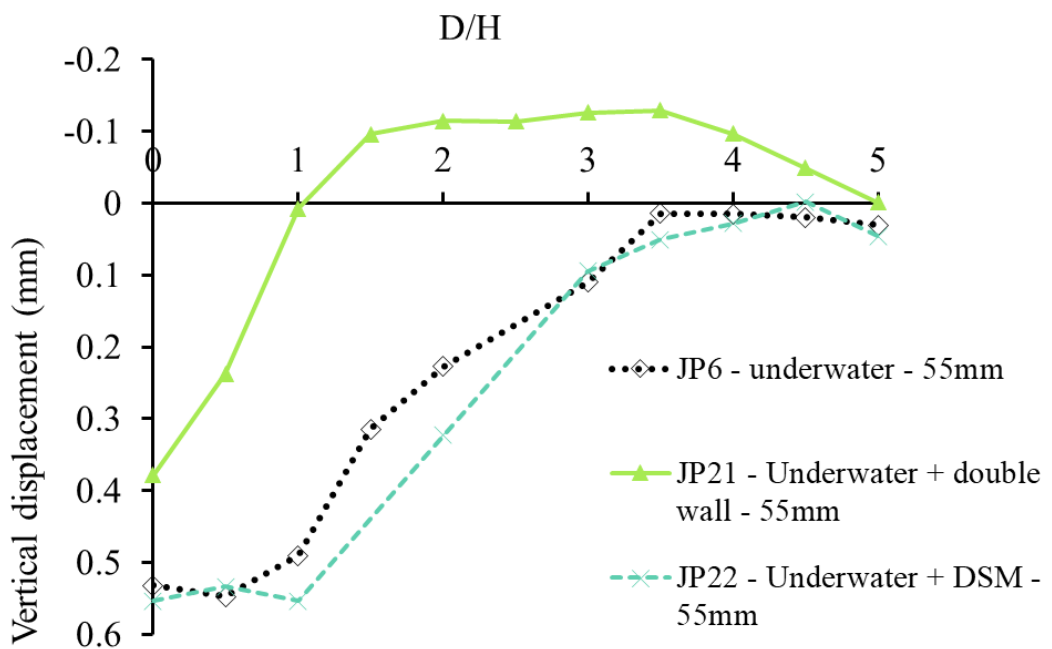


Figure 6.30 Influence of combining construction methods with underwater excavation at end of simulated excavation

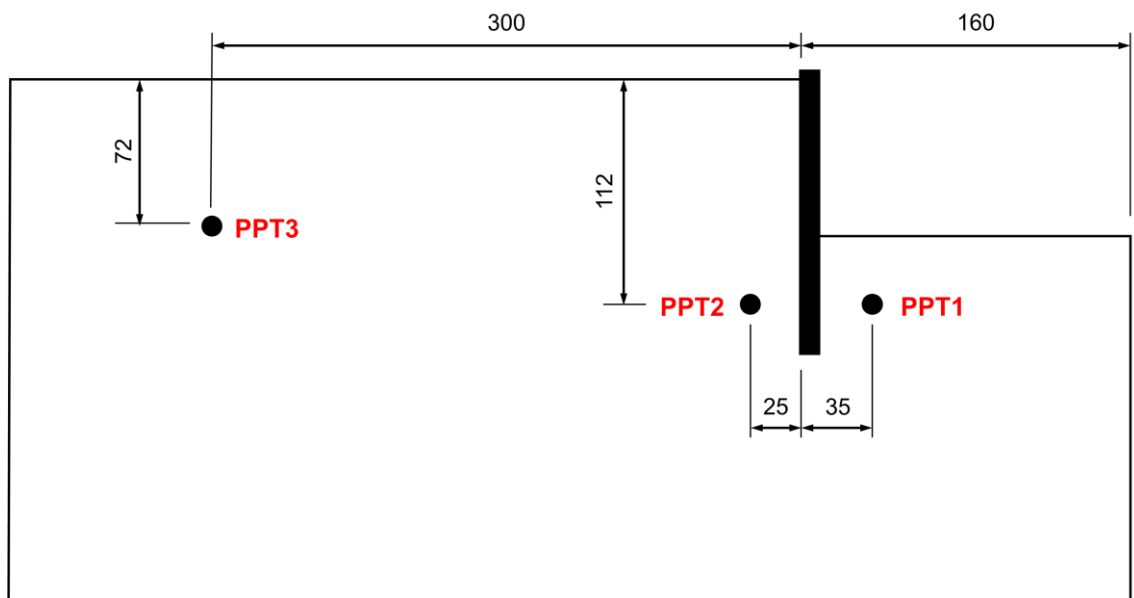


Figure 6.31 Location of pore pressure transducers

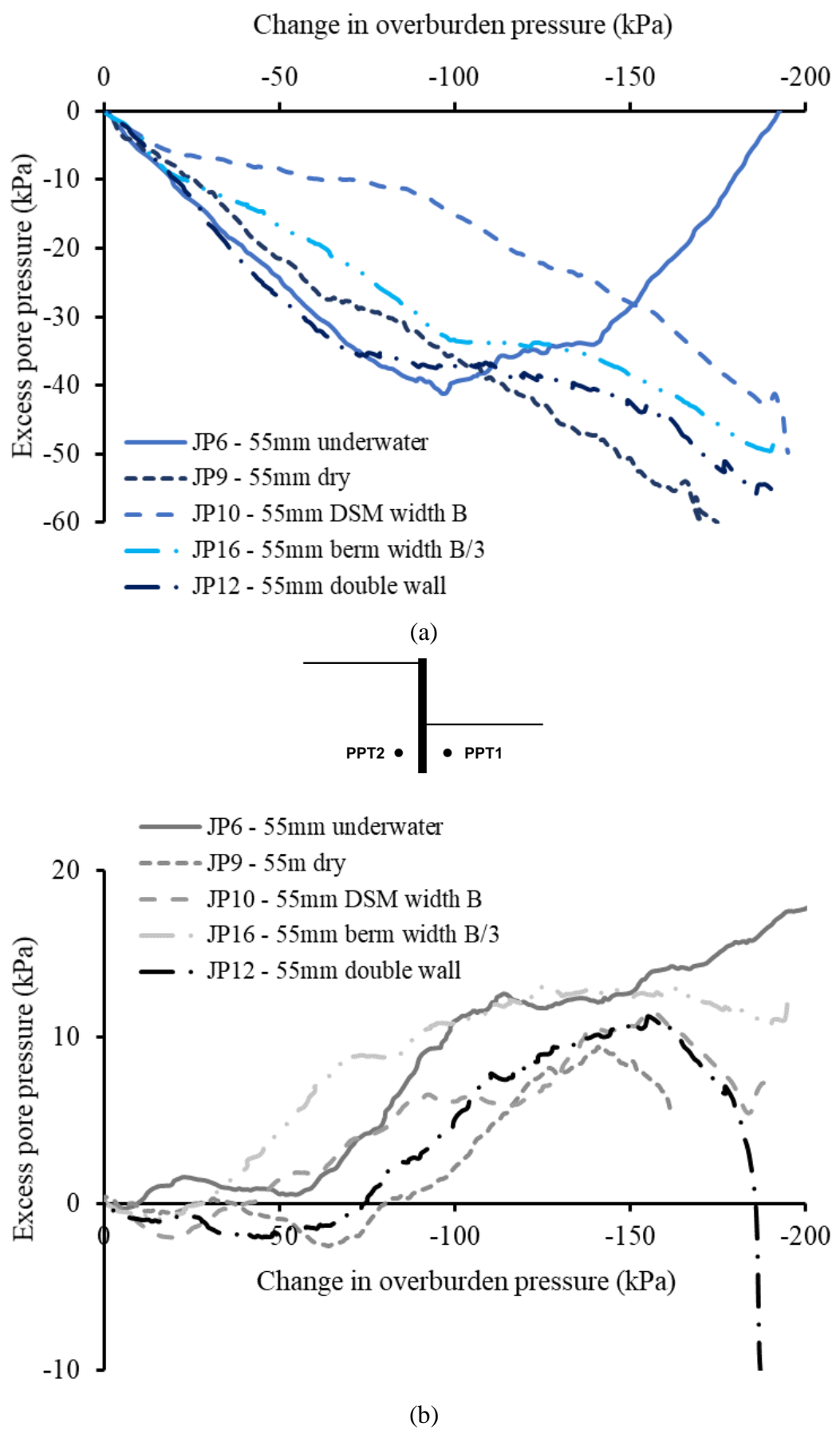
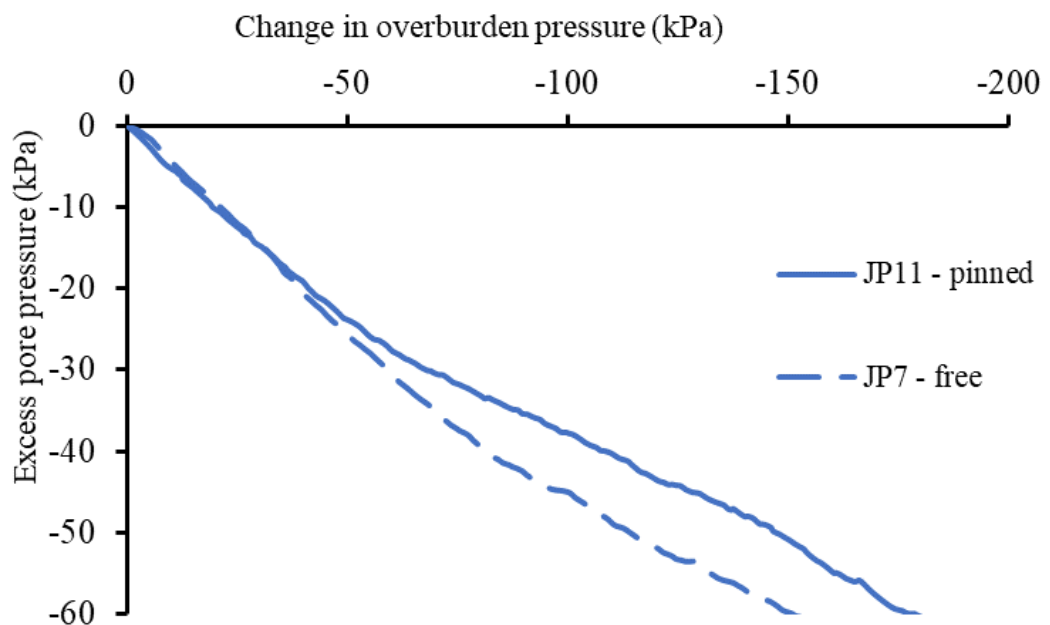
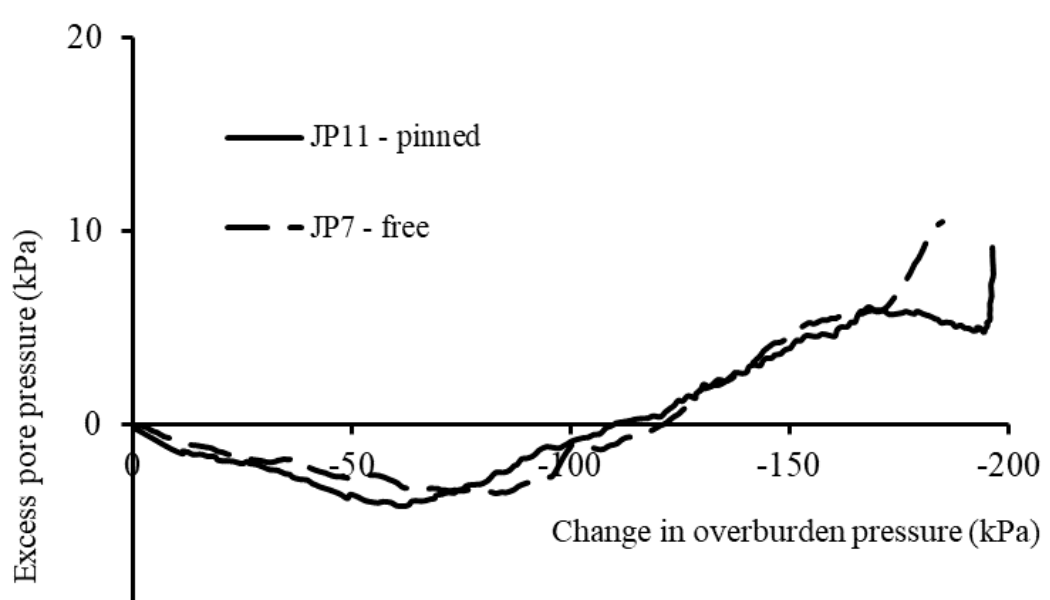


Figure 6.32 Influence of excavation methods on excess pore pressures (a) PPT1 and (b) PPT2



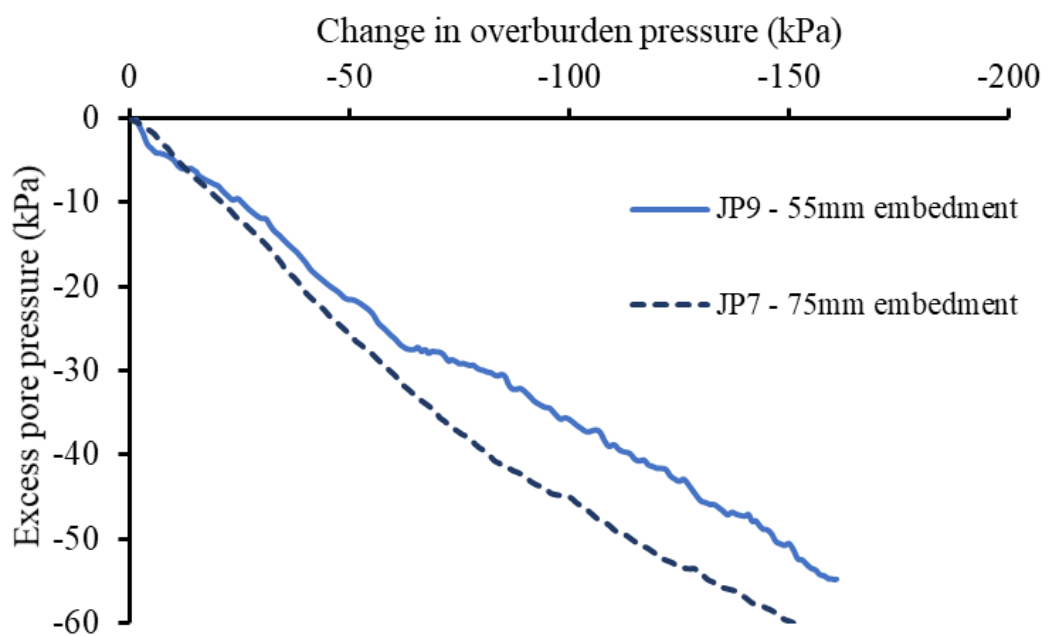
(a)

PPT2 • PPT1



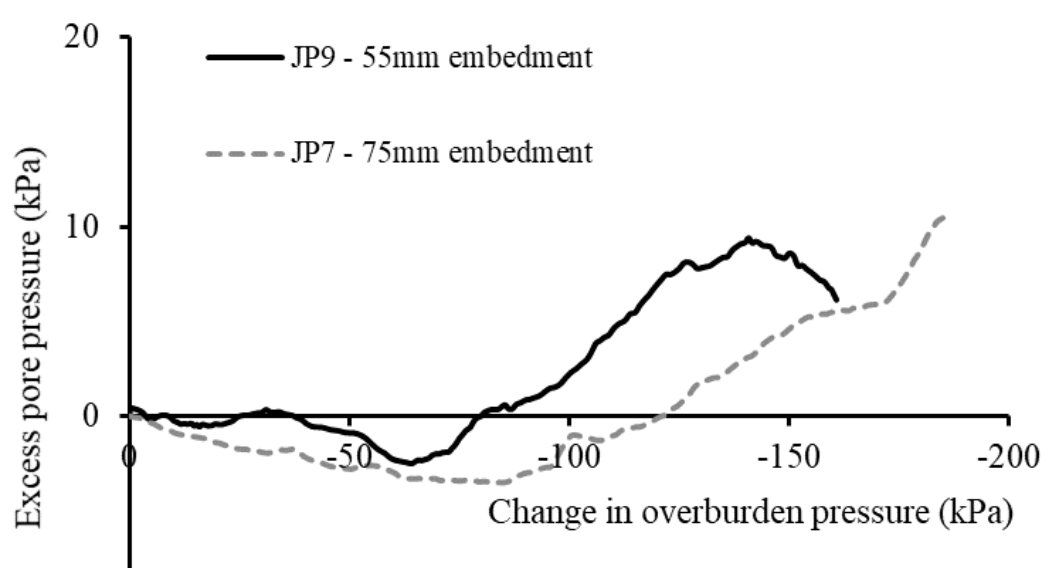
(b)

Figure 6.33 Influence of fixity conditions on excess pore pressures (a) PPT1 and (b) PPT2



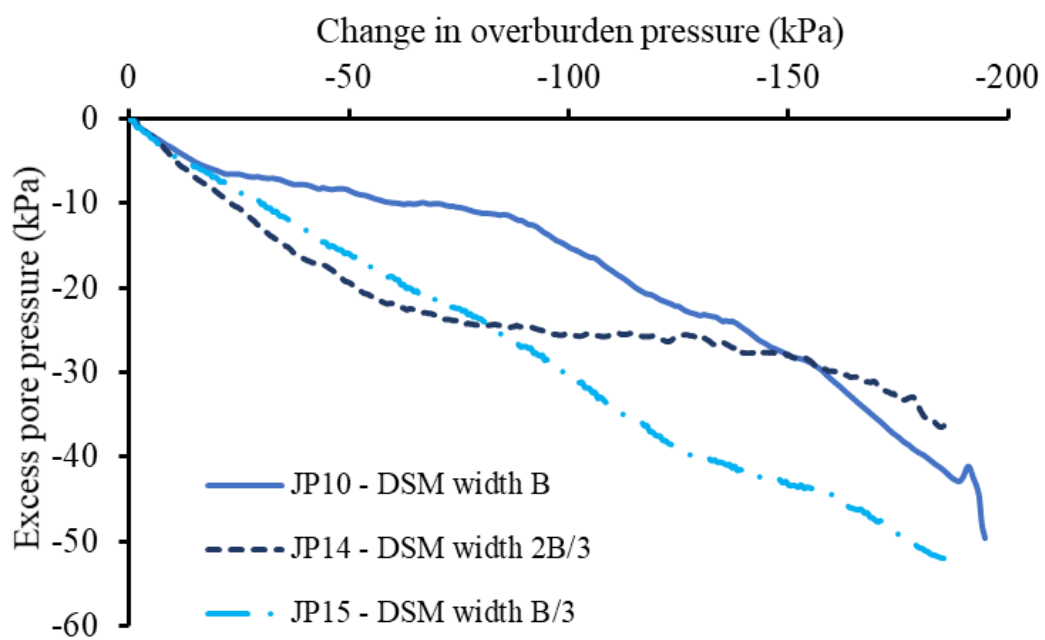
(a)

PPT2 • PPT1



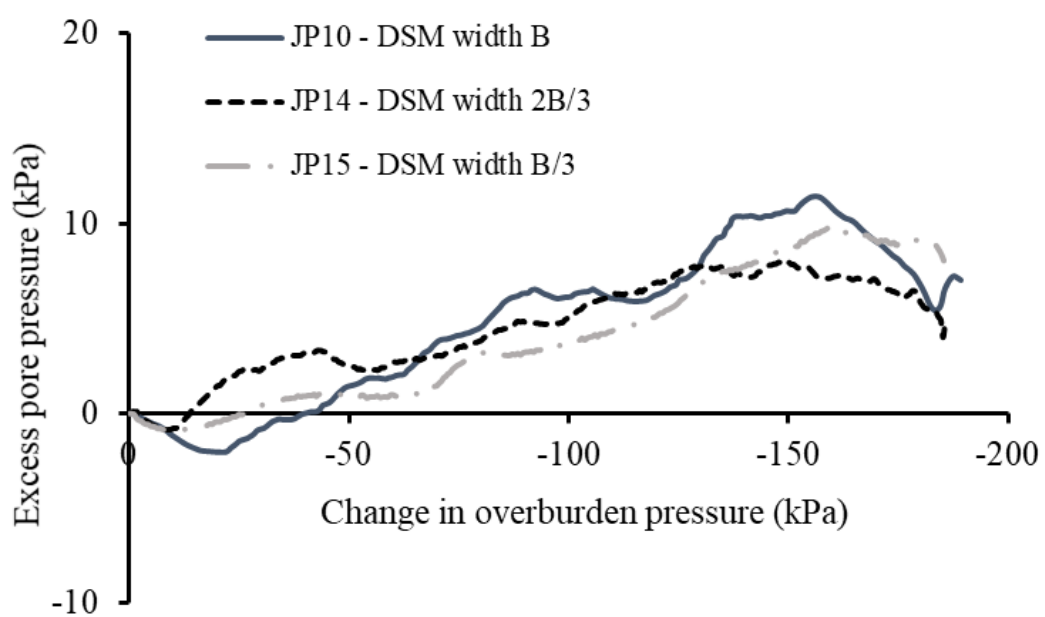
(b)

Figure 6.34 Influence of wall embedment on excess pore pressures (a) PPT1 and (b) PPT2



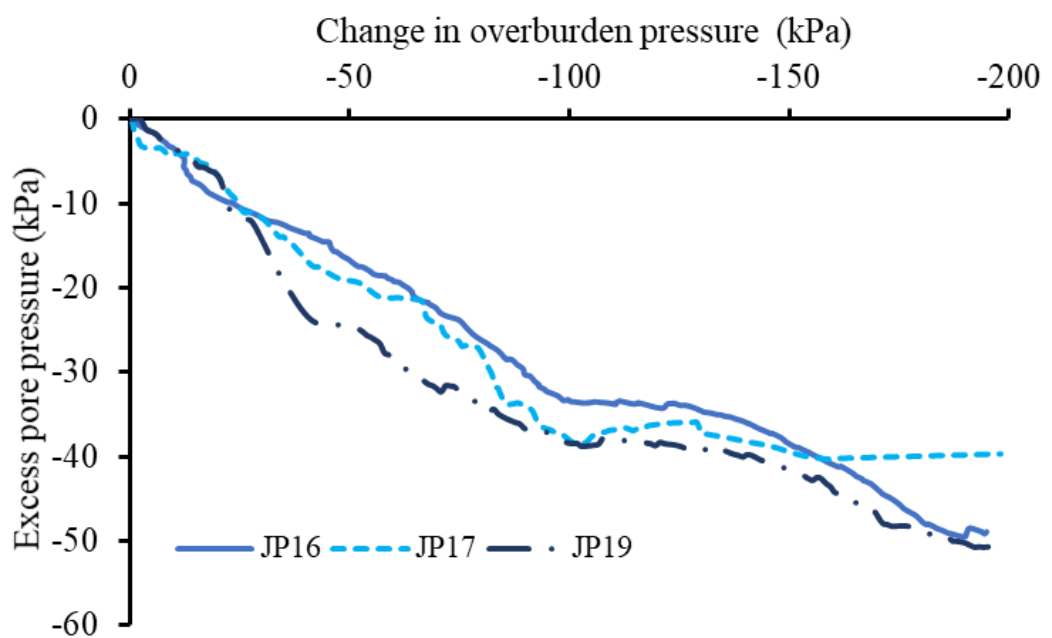
(a)

PPT2 • PPT1



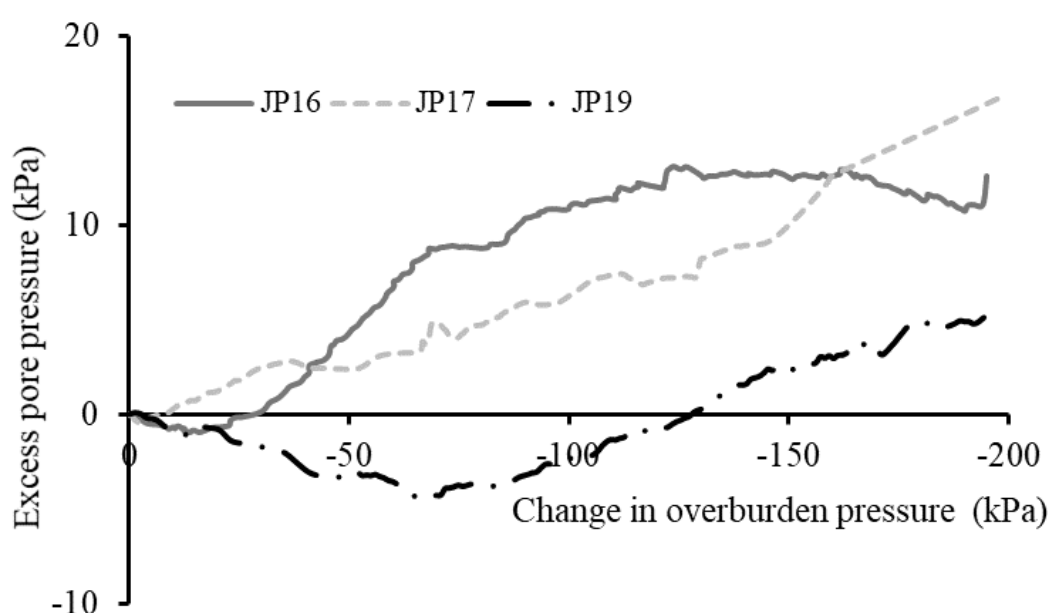
(b)

Figure 6.35 Influence of DSM geometry on excess pore pressures (a) PPT1 and (b) PPT2



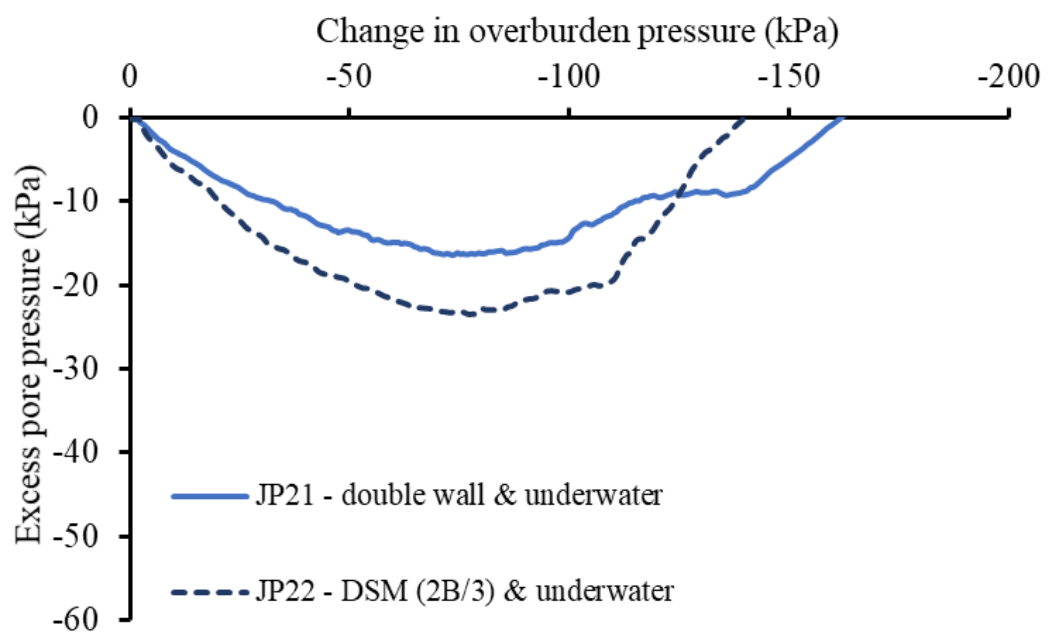
(a)

PPT2 • PPT1



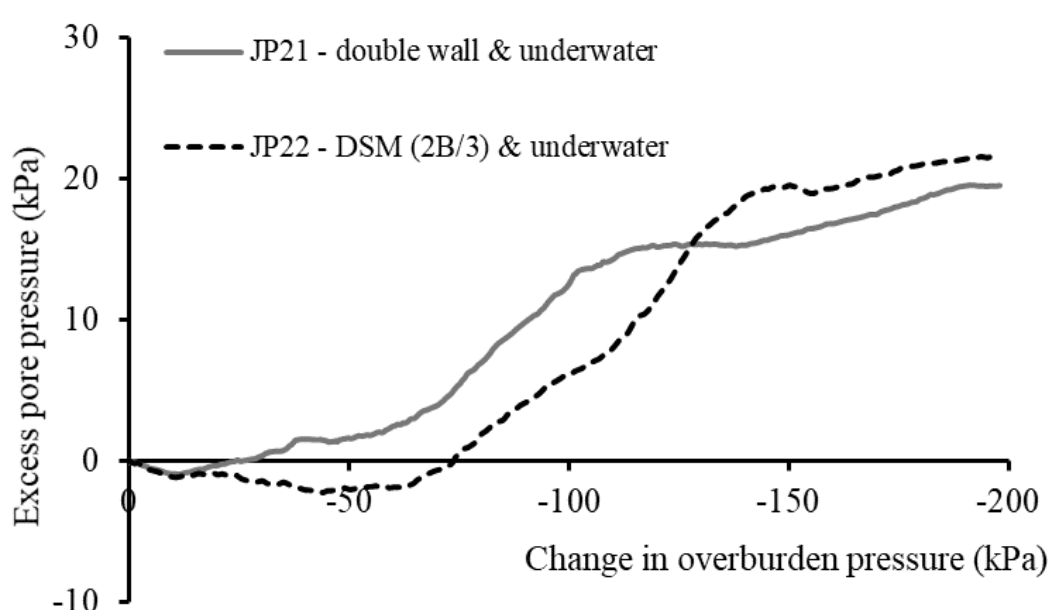
(b)

Figure 6.36 Influence of berm geometry on excess pore pressures (a) PPT1 and (b) PPT2



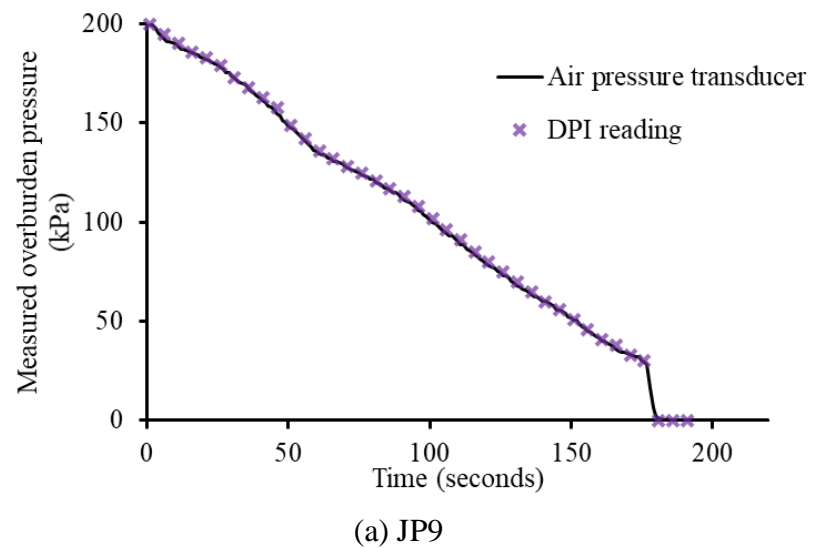
(a)

PPT2 • • PPT1

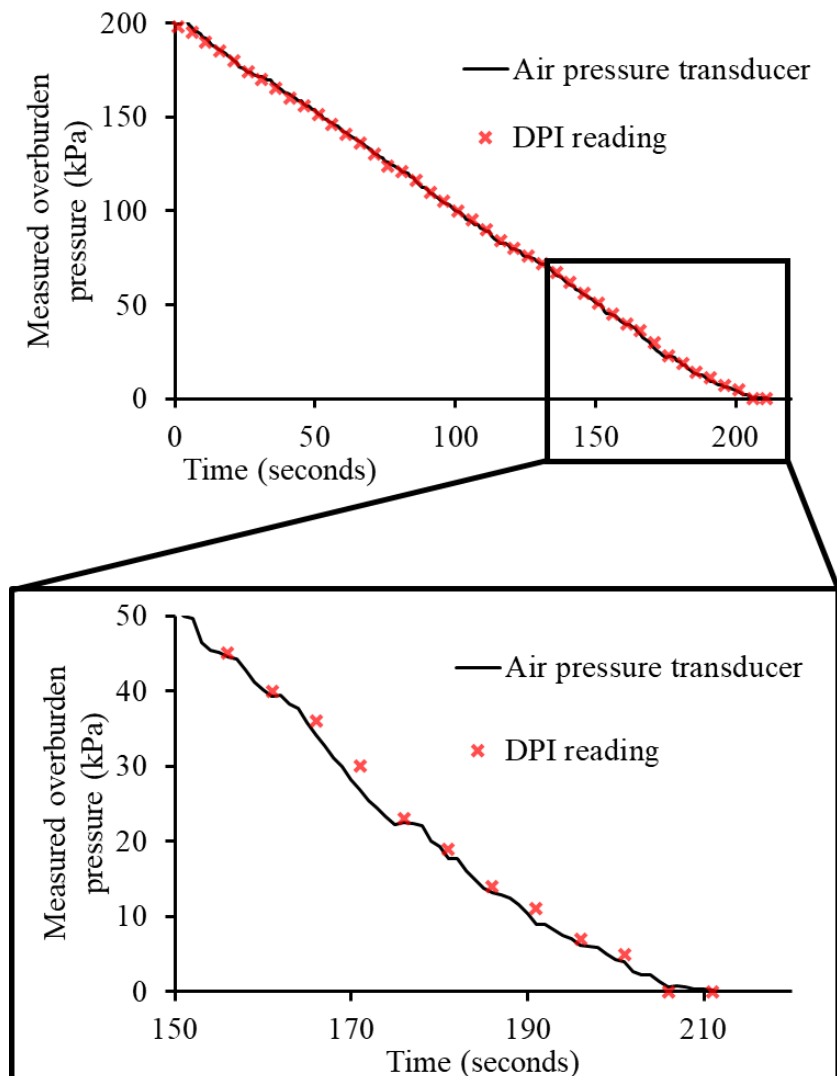


(b)

Figure 6.37 Influence of combining a construction method with an underwater excavation on excess pore pressures (a) PPT1 and (b) PPT2



(a) JP9



(b) JP12

Figure 6.38 Comparisons between DPI readings and air pressure transducer recordings

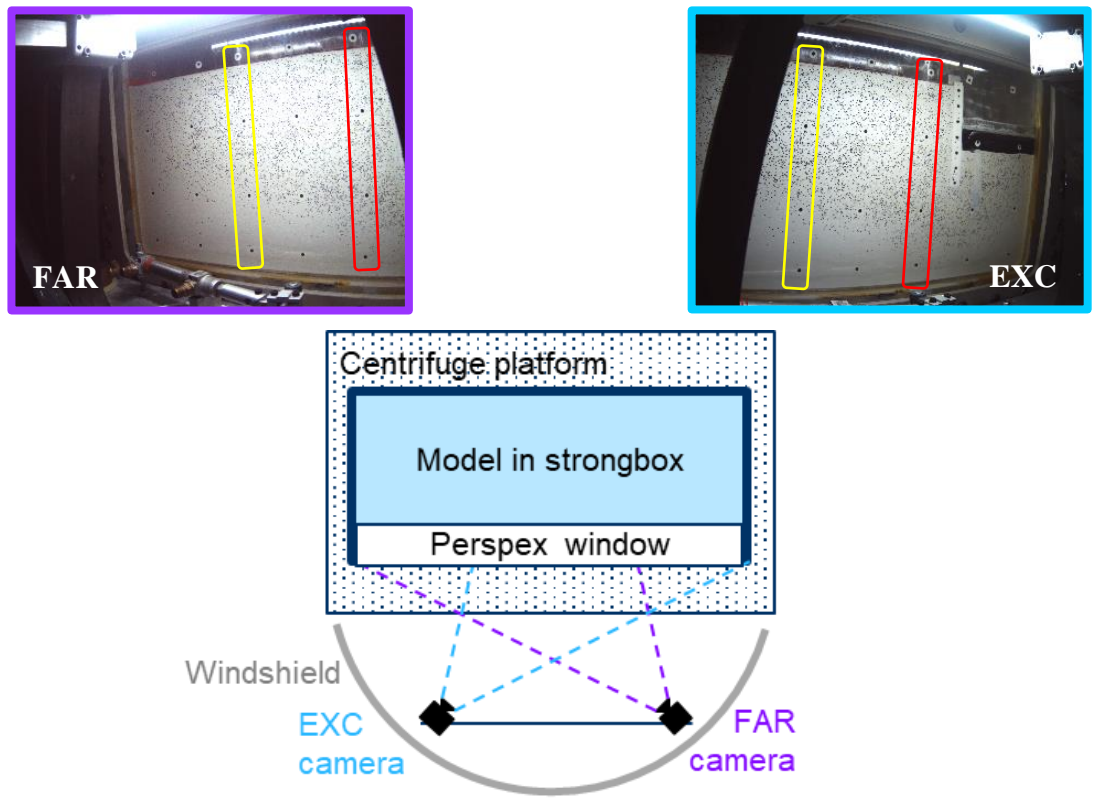


Figure 6.39 Schematic orientation of cameras on centrifuge swing, areas of model captured by each camera and common columns of control point targets

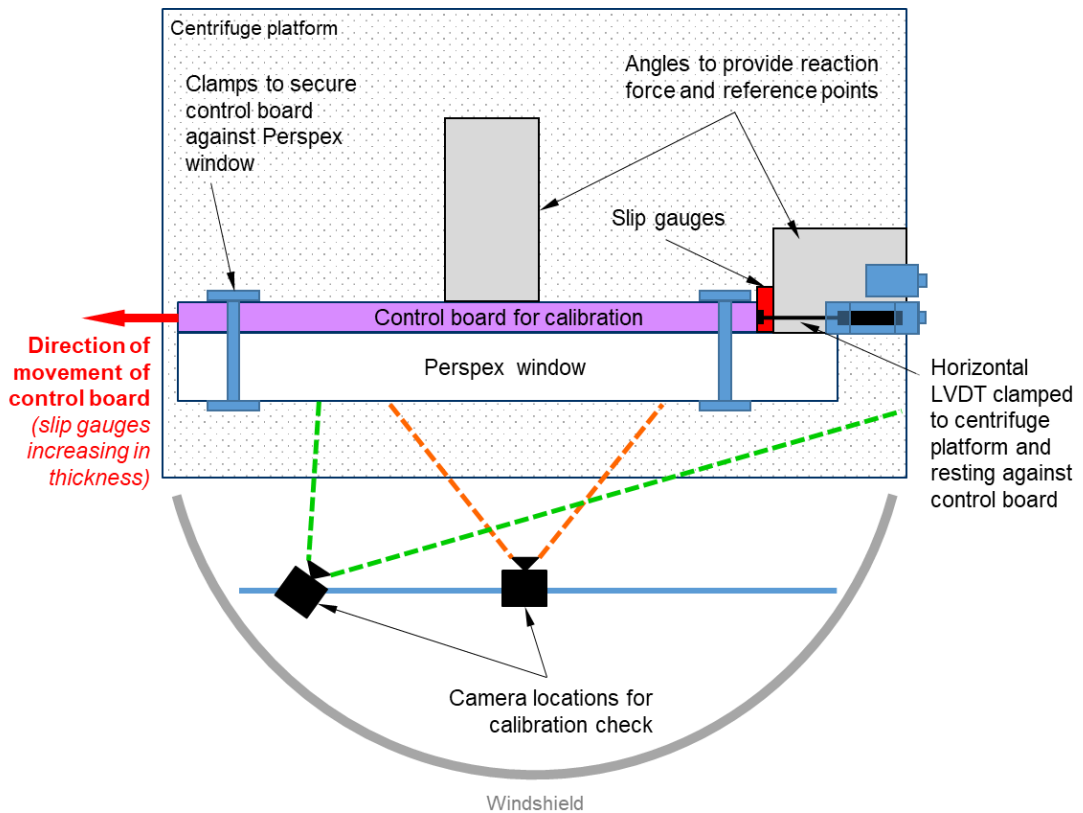


Figure 6.40 Plan of general arrangement for calibration checks using slip gauges, an LVDT and control board

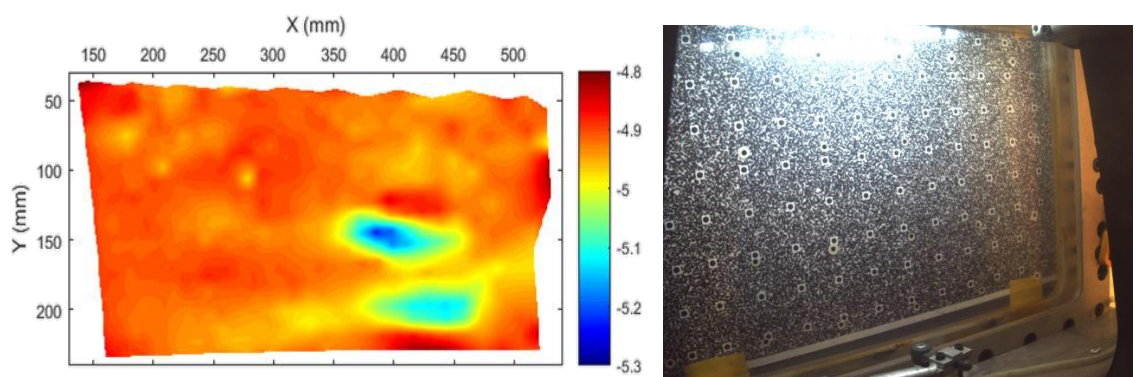


Figure 6.41 Horizontal contours from the angled calibration series (camera orientated towards location of excavation) at 5mm displacement and example of field of view

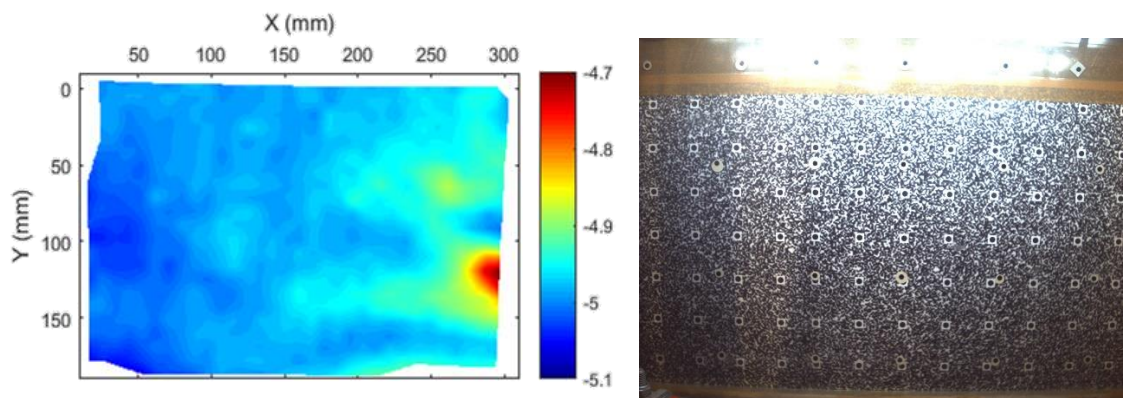


Figure 6.42 Horizontal contours from the straight calibration series (perpendicular to window) at 5mm displacement and example of field of view

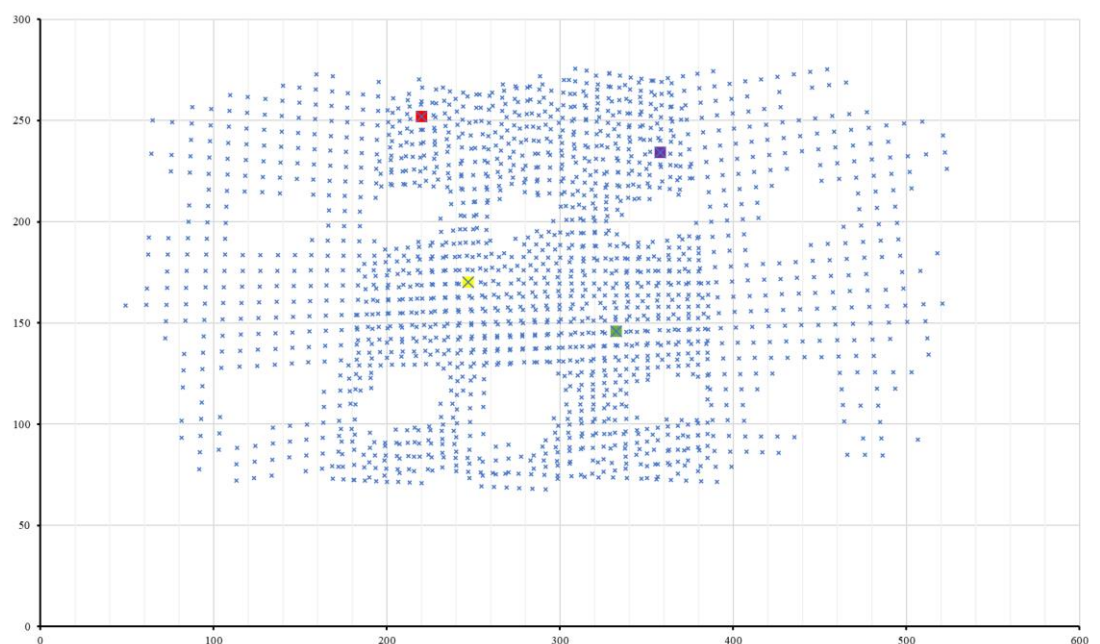


Figure 6.43 Overlapped data from two cameras and four points used in comparative analysis

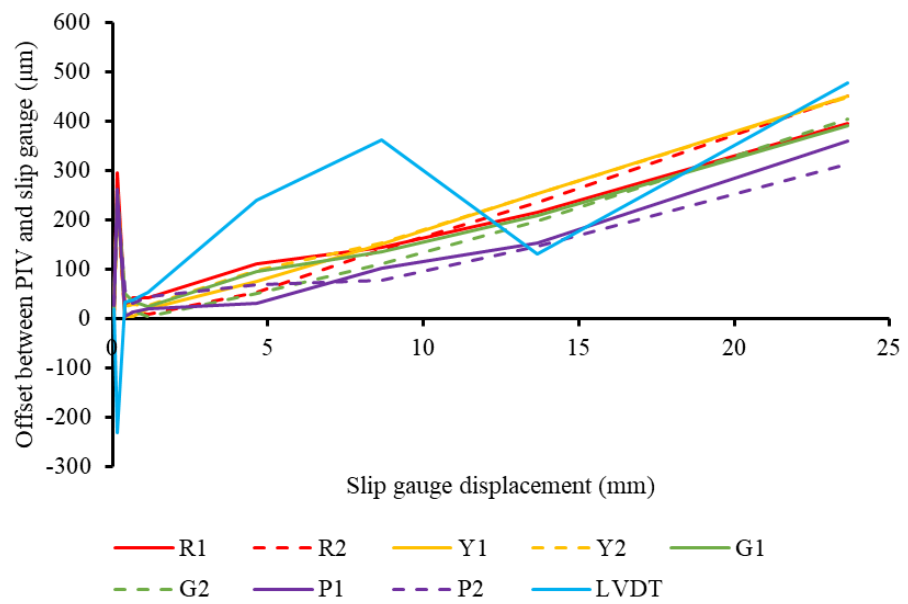


Figure 6.44 Accumulation of errors as displacement increases

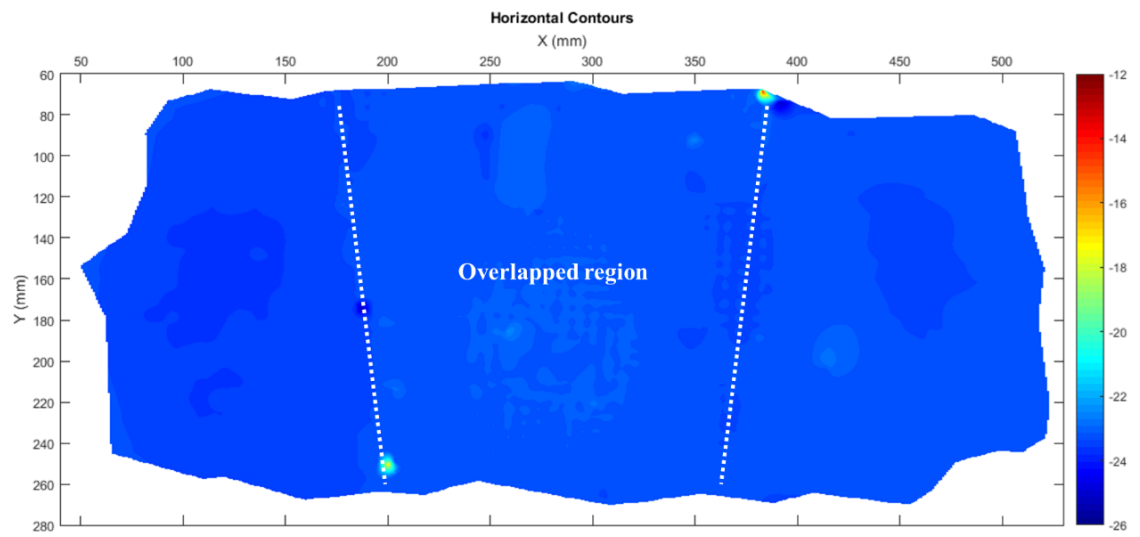


Figure 6.45 Horizontal displacement contours plotted from two cameras

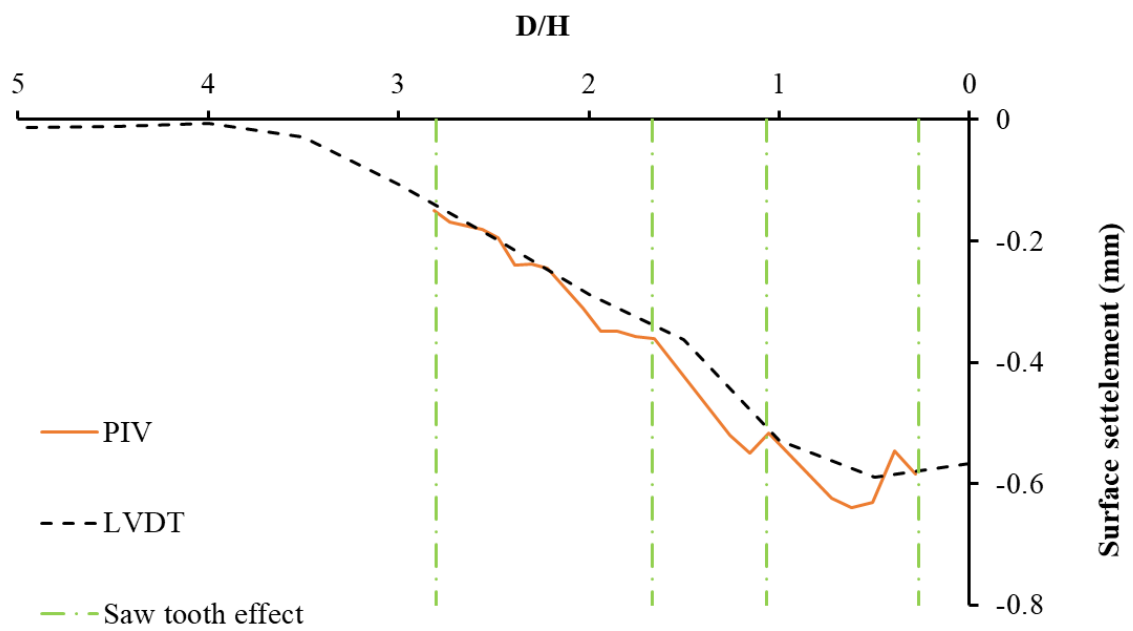


Figure 6.46 Comparisons between LVDT and PIV surface settlements

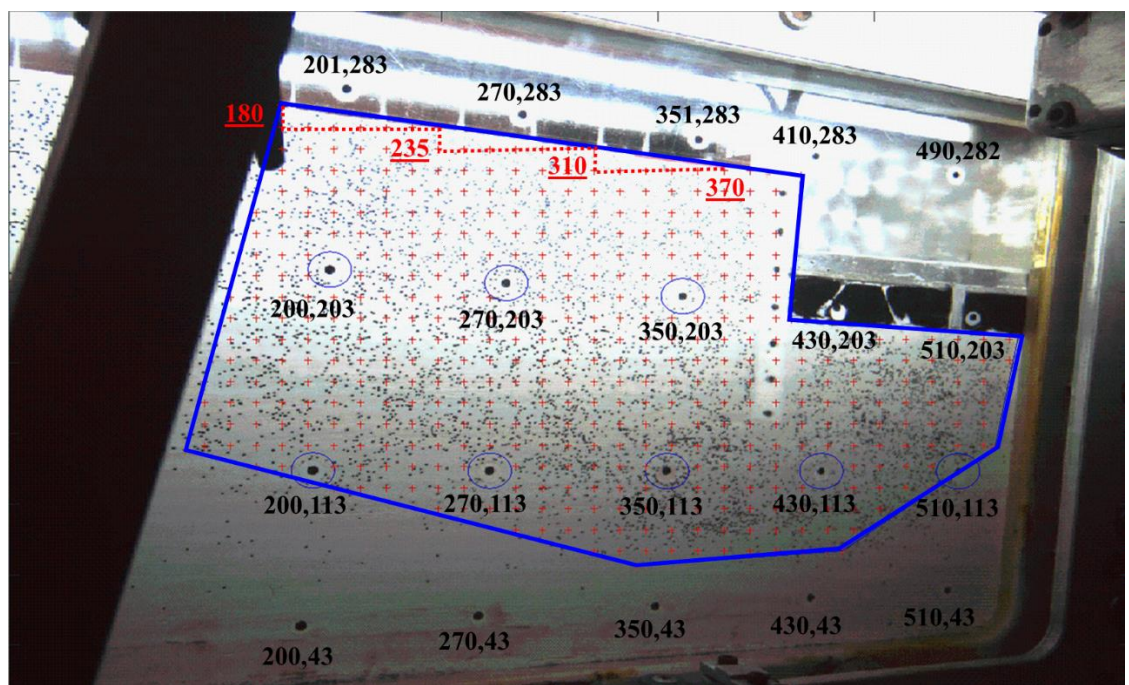


Figure 6.47 Example of mesh generated for PIV analysis and emphasis on the points used as surface targets

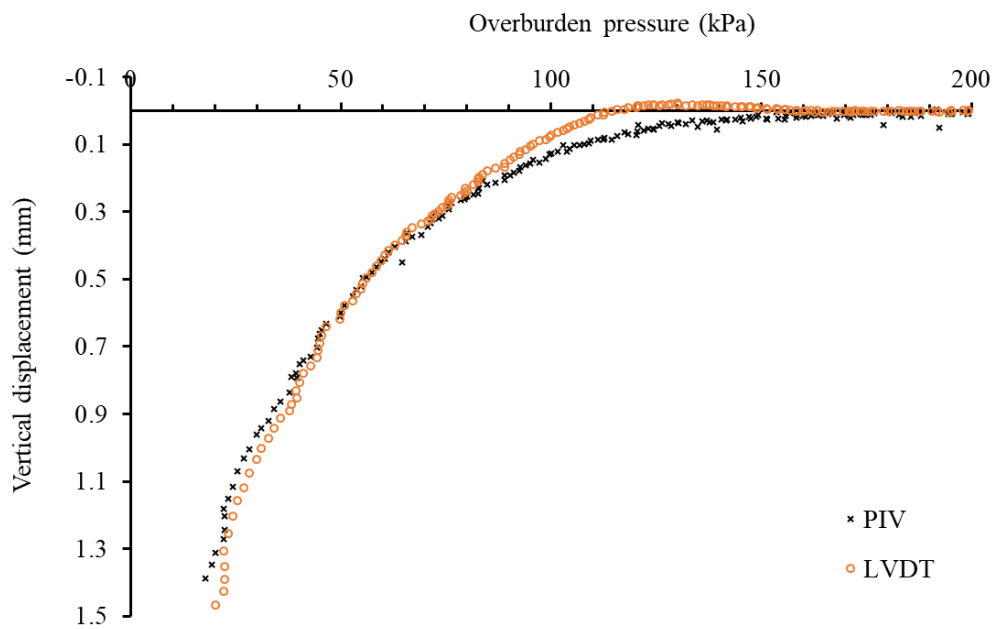


Figure 6.48 Comparisons between PIV and LVDT data at distance $2H$ behind the retaining wall

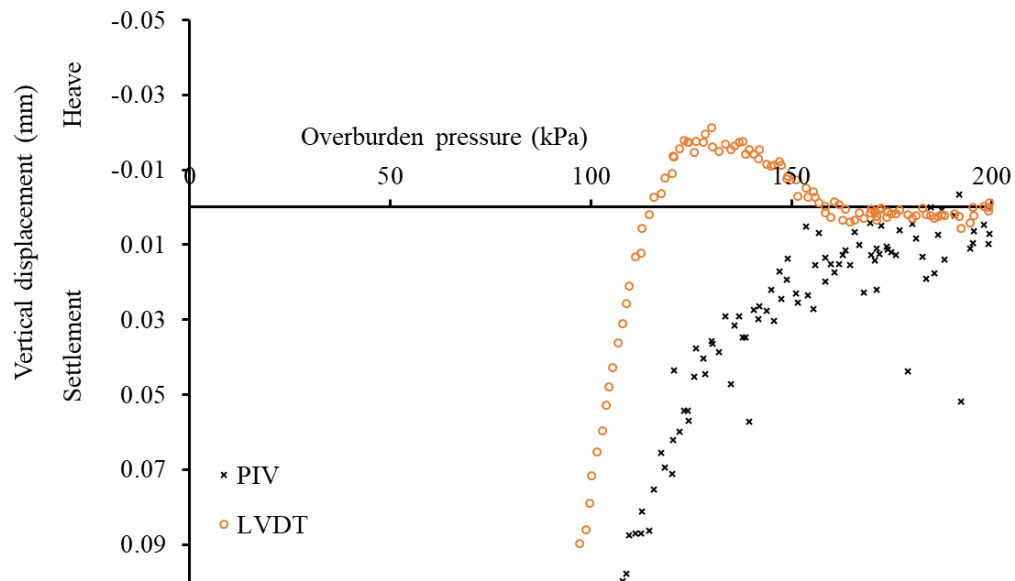


Figure 6.49 Surface displacements at early stages of excavation simulation recorded at distance $2H$ behind the retaining wall.

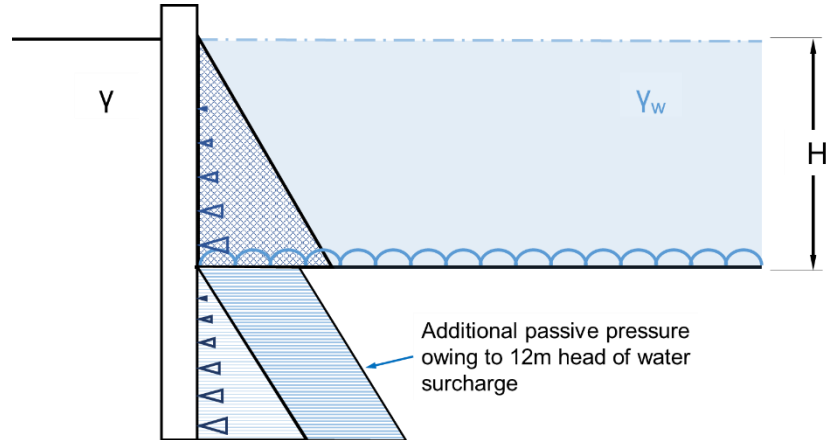


Figure 7.1 Support offered by underwater excavation method

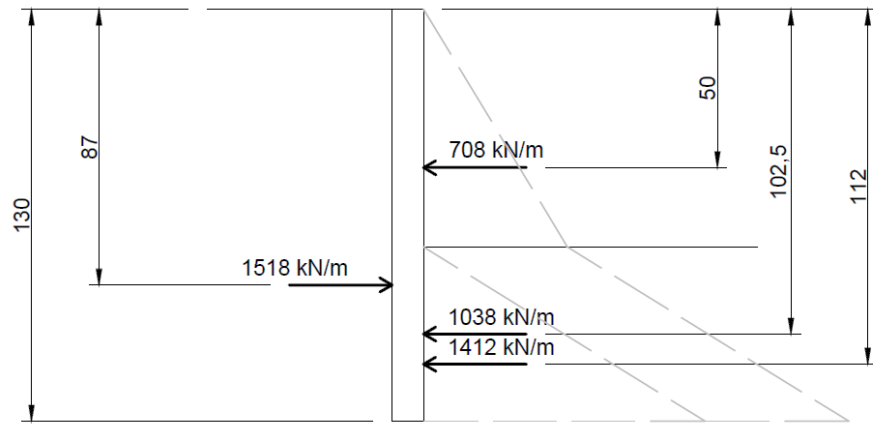


Figure 7.2 Passive resistance during underwater excavation method

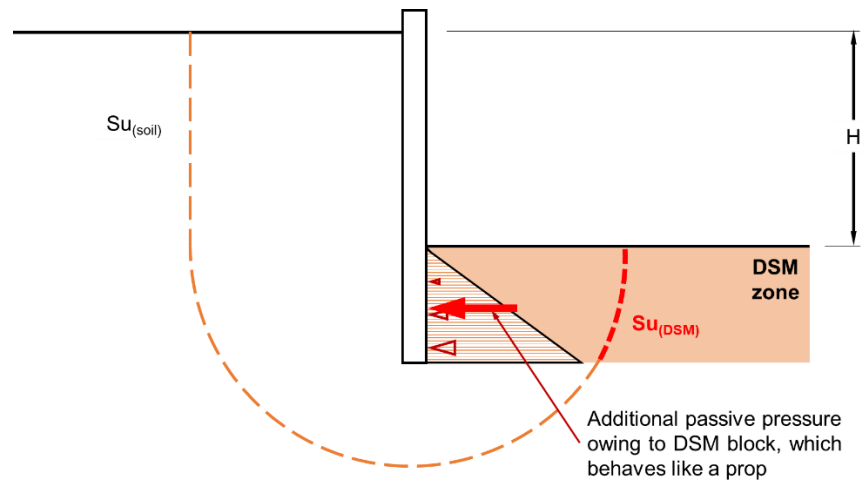
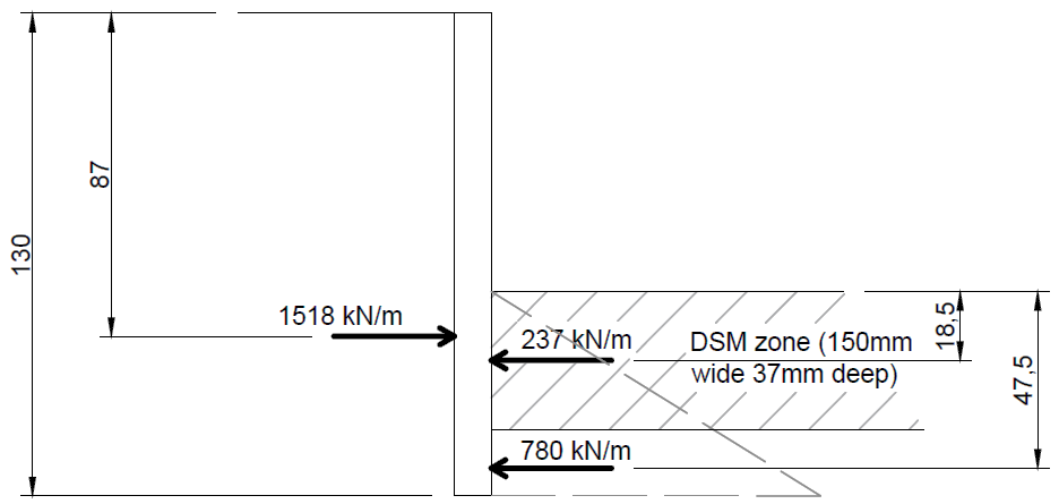
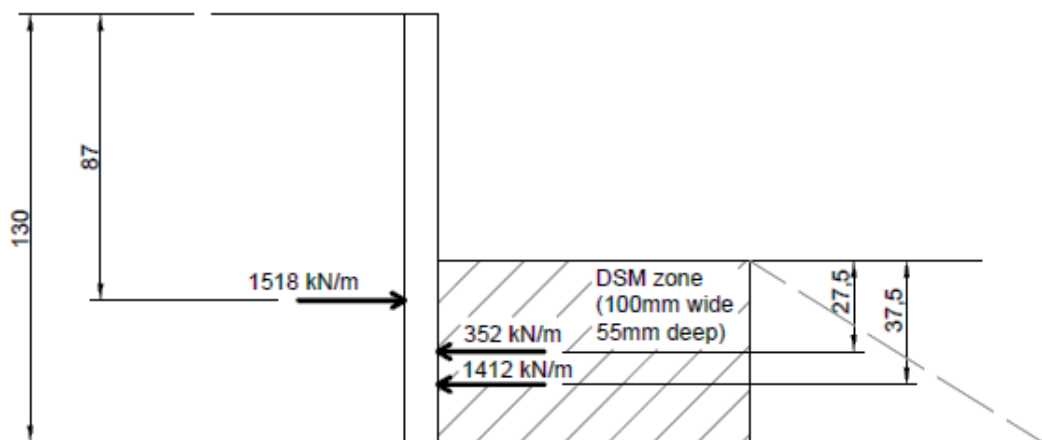


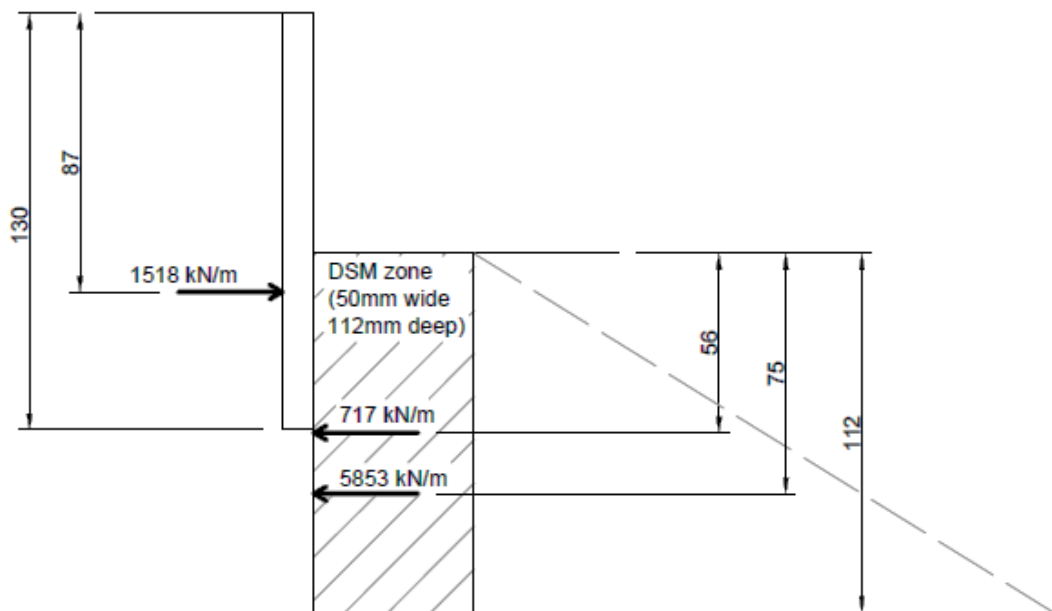
Figure 7.3 Comparative support offered from deep soil mixing treatment



(a)



(b)



(c)

Figure 7.4 Passive resistance during DSM treatment across (a) full width of formation, 37mm deep (b) 100mm wide and 55mm deep and (c) 50mm wide and 112mm deep

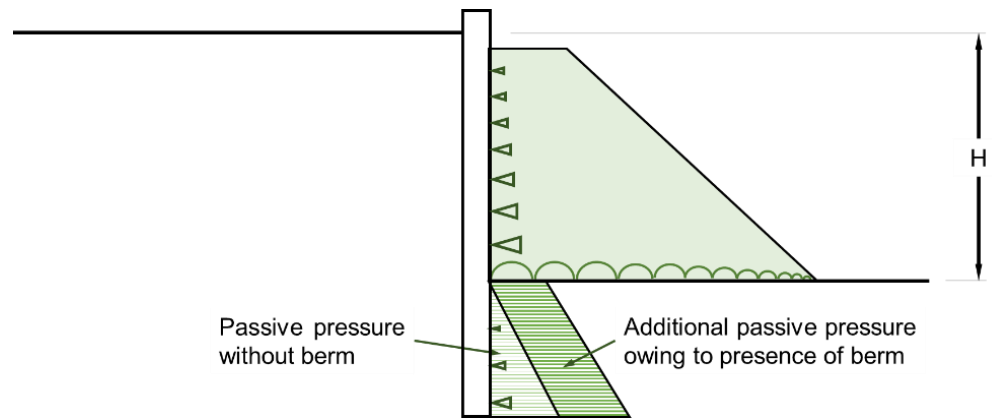


Figure 7.5 Increase in passive pressure afforded to excavation from soil berm

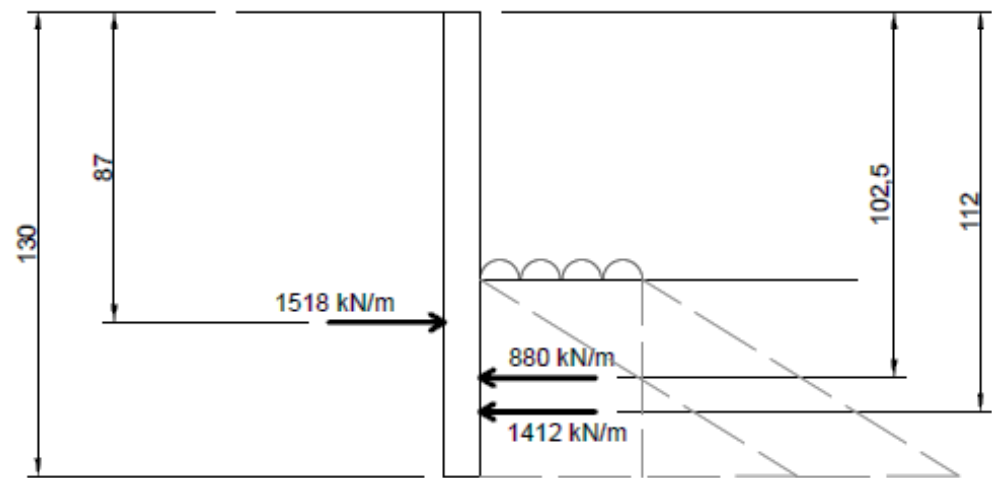


Figure 7.6 Increase in passive pressure afforded to excavation from soil berm

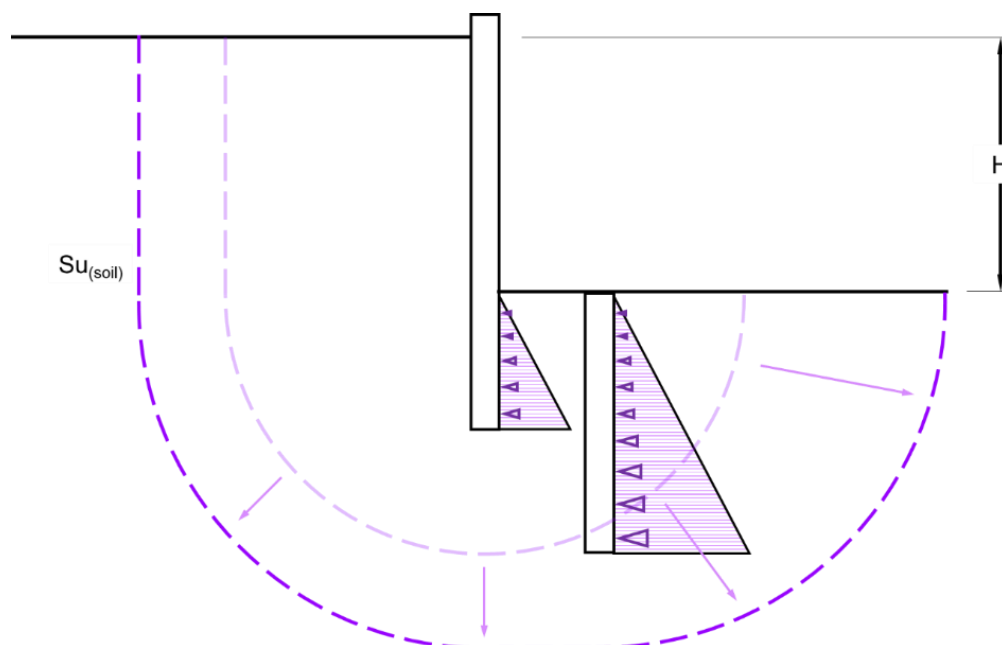


Figure 7.7 Increase in passive pressure and mobilised undrained shear strength as a result of a double walled excavation

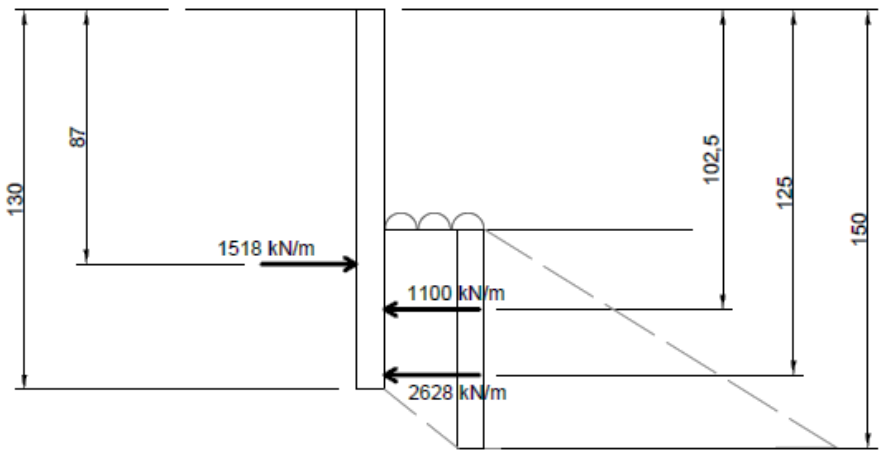


Figure 7.8 Increase in passive pressure afforded to excavation from a double walled excavation

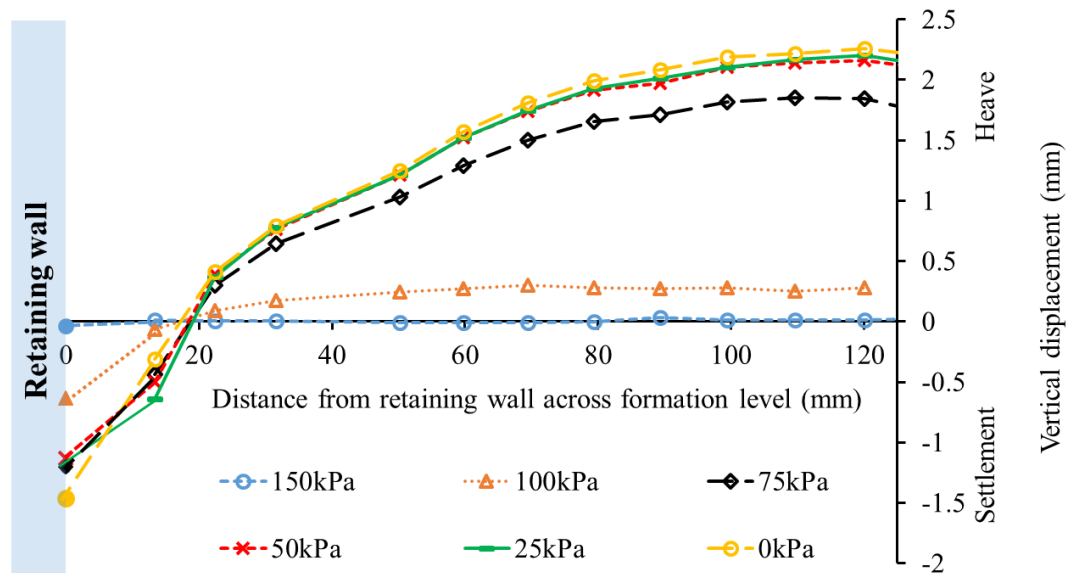


Figure 7.9 Vertical displacements across formation level during various stages of the simulated excavation in test JP18

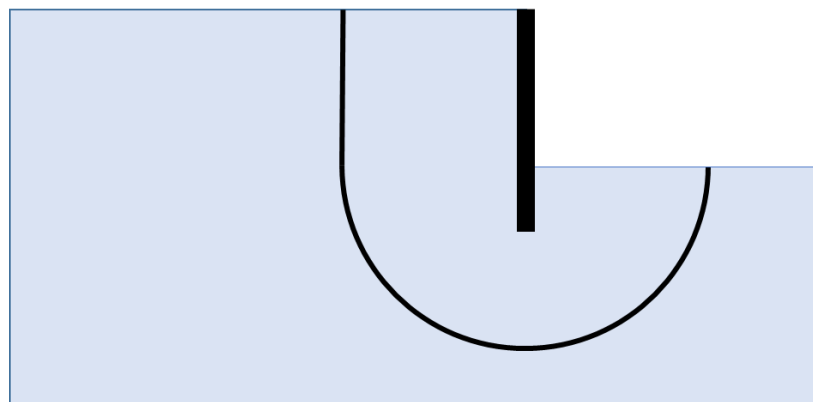


Figure 7.10 Expected deformation mechanism during excavation

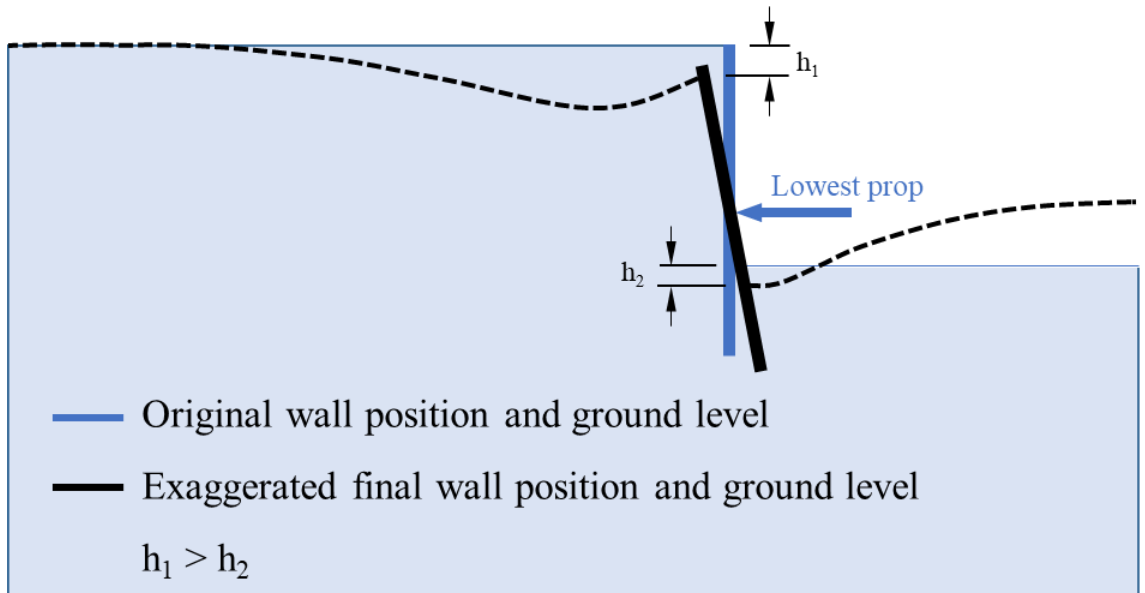


Figure 7.11 Expected settlement and heave profiles during excavation owing to soil-wall interaction and settlement of retaining wall

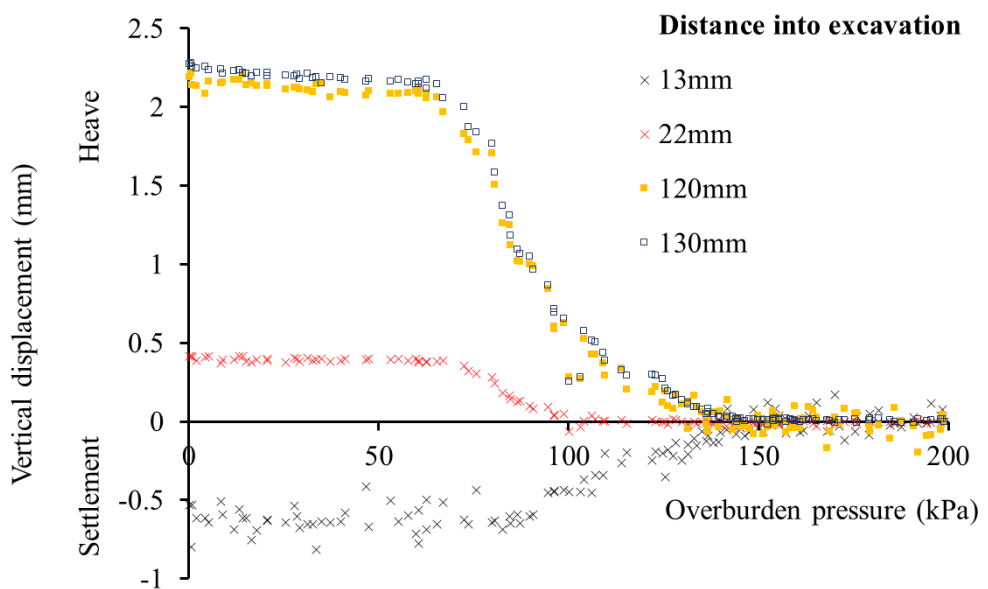


Figure 7.12 Maximum and minimum measured vertical soil displacements at formation level in test JP18 from PIV analysis of mesh points nearest to and furthest from the retaining wall

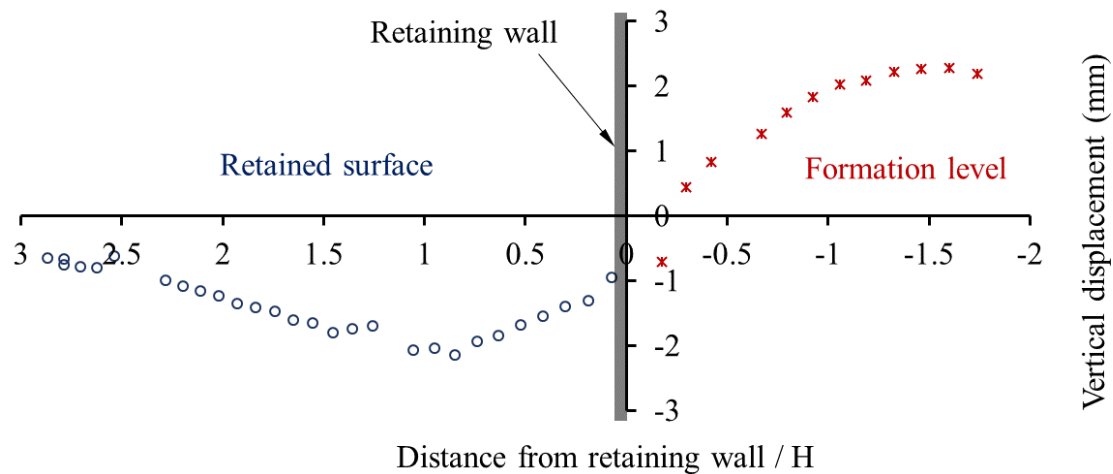


Figure 7.13 Settlement profile of retained soil upon completion of excavation

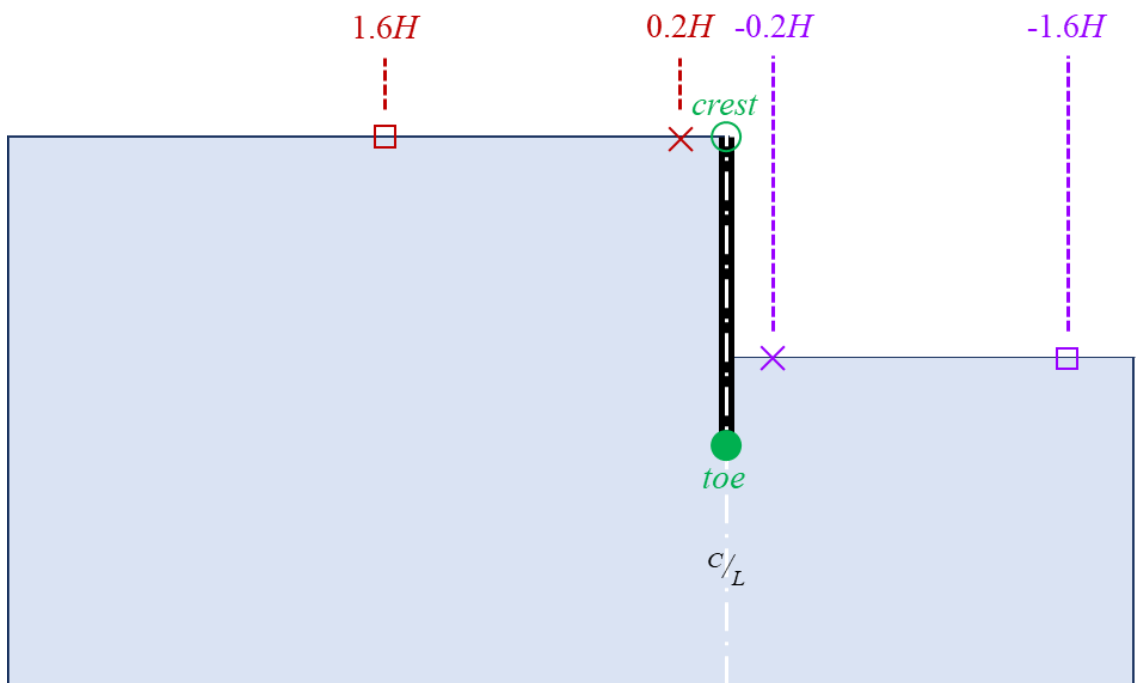


Figure 7.14 Positions analysed to determine location where displacements first occurred

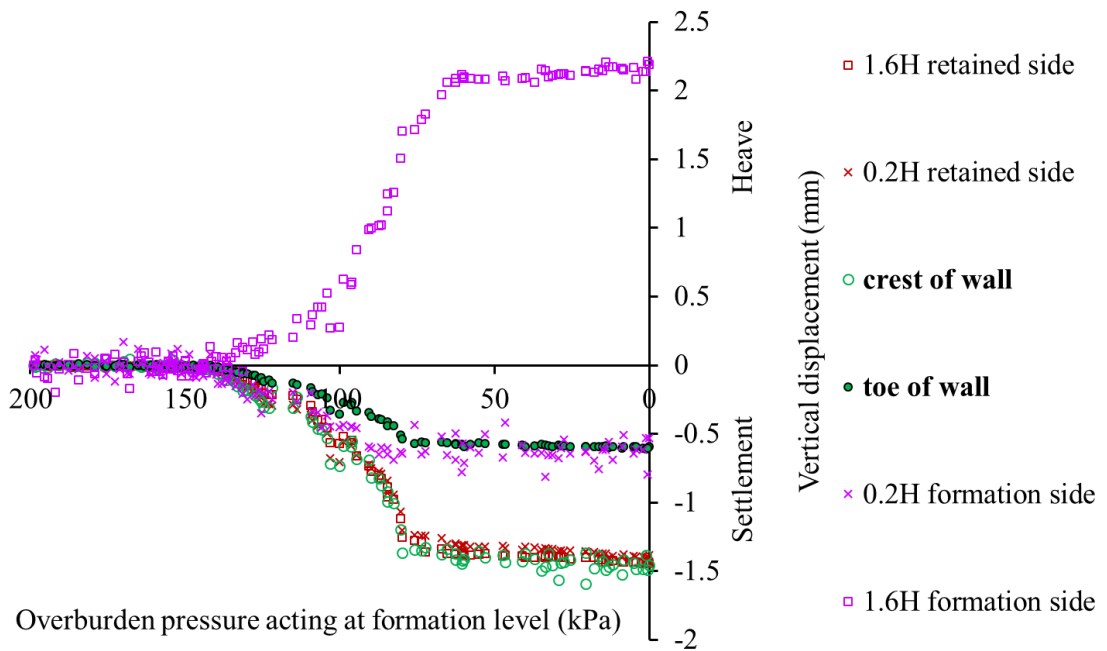


Figure 7.15 Wall crest response and soil response at retained surface and formation level during the removal of the overburden pressure.

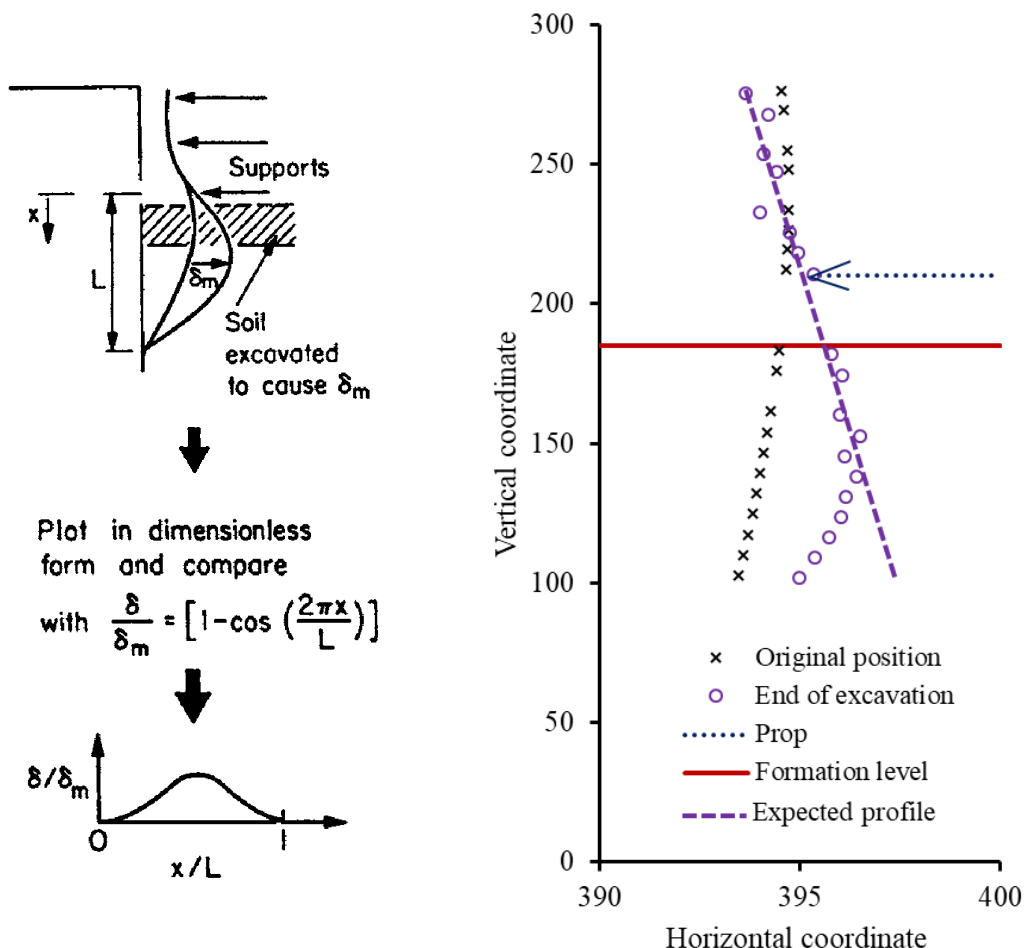


Figure 7.16 (a) typical cosine curve of flexible walls (O'Rourke, 1993) and (b) original and final position of the wall measured from PIV analysis at the end of the excavation

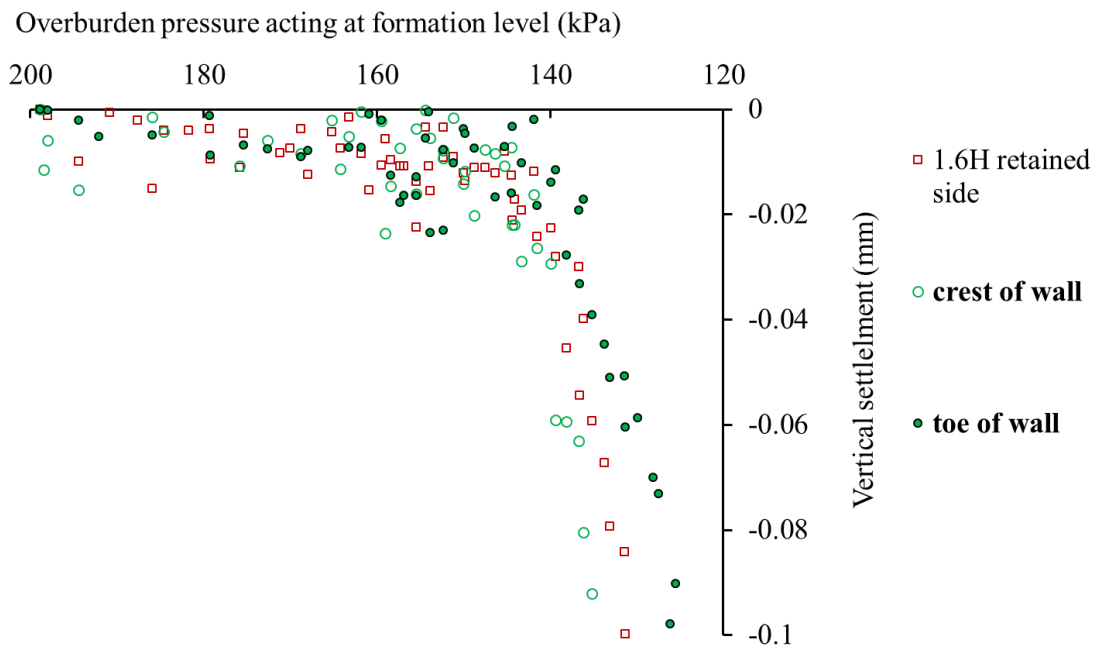


Figure 7.17 Vertical movements developing from beginning of the excavation to an overburden pressure 120kPa

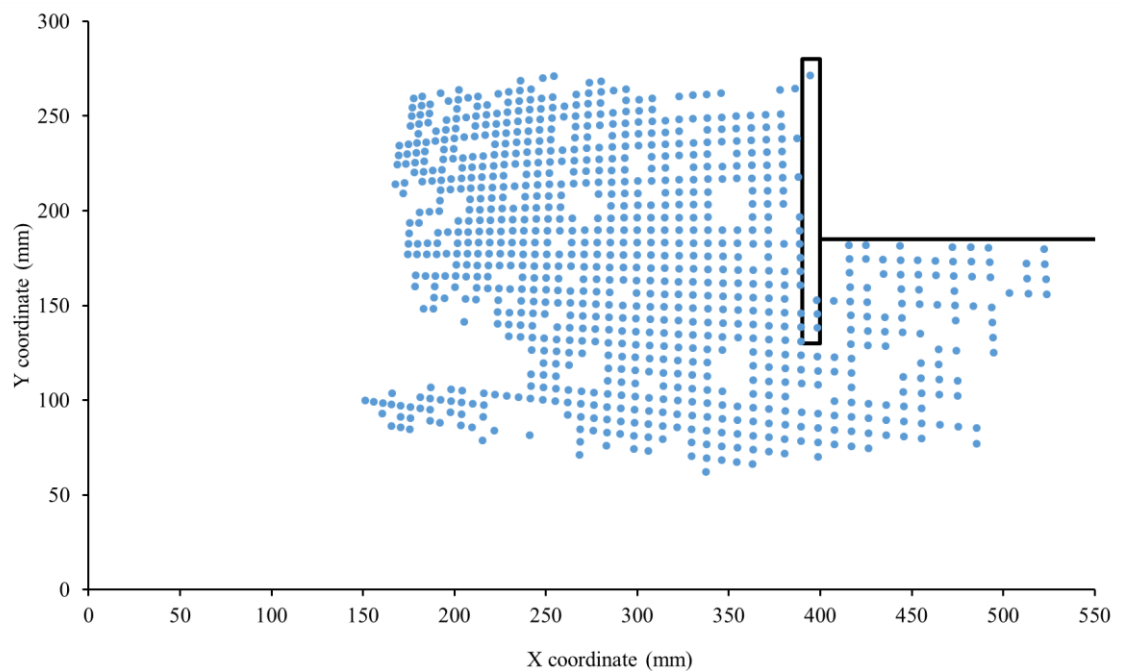


Figure 7.18 Mesh points used in the PIV analysis of test JP7

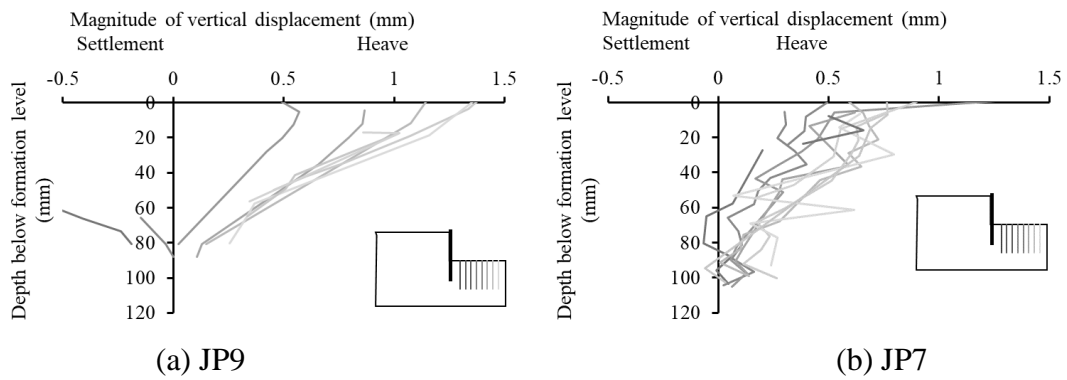


Figure 7.19 Vertical movements across the formation level of a reference test at varying depths plotted at an overburden pressure of 50kPa where (a) illustrates vertical movements in JP9 (55mm embedment) at 50kPa; (b) JP7 (75mm embedment) at 50kPa plotted on the same scale

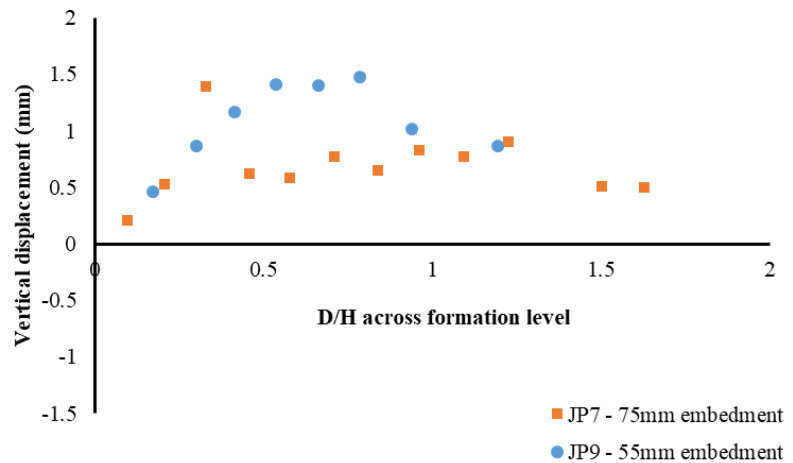


Figure 7.20 Heave profile of formation level at 50kPa overburden pressure for varying wall embedment depths

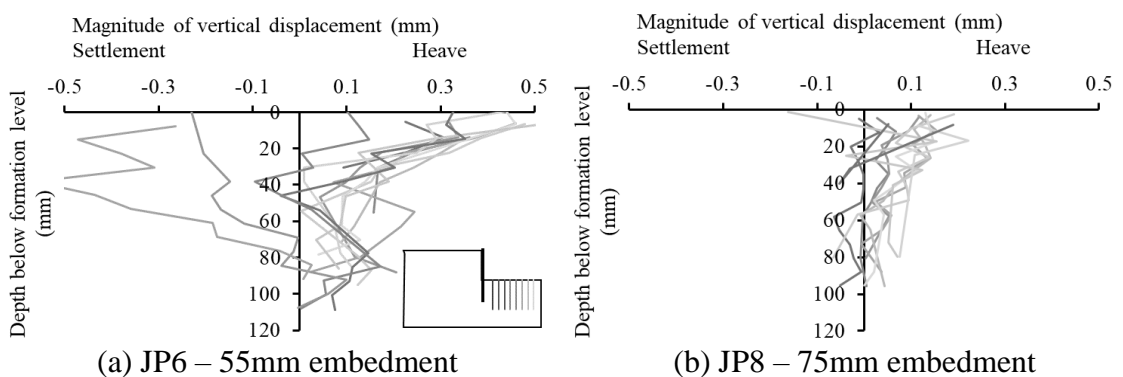


Figure 7.21 Vertical movements across the formation level of an underwater excavation at varying depths plotted at an overburden pressure of 50kPa.

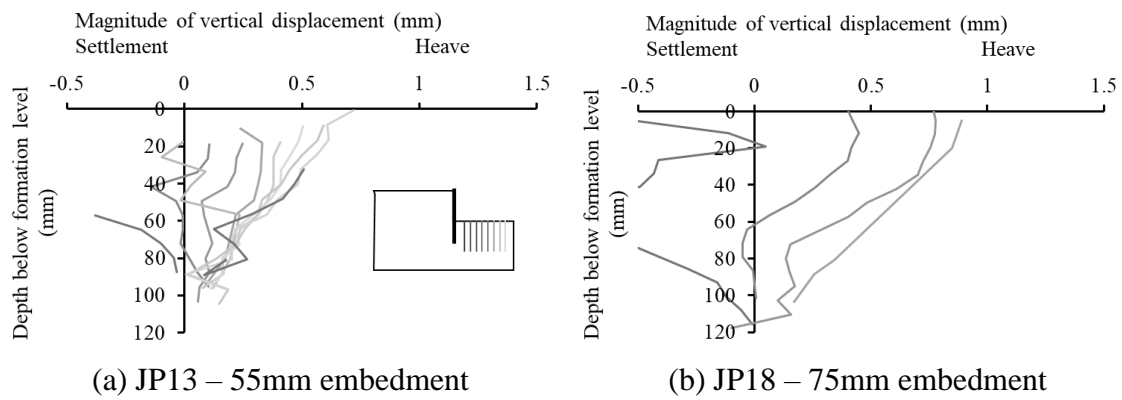


Figure 7.22 Vertical movements across the formation level of a double walled excavation plotted at an overburden pressure of 50kPa

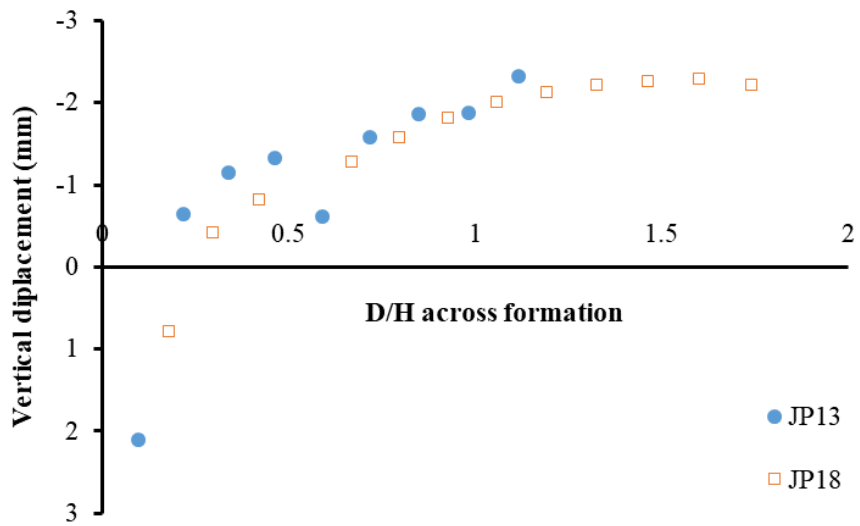


Figure 7.23 Heave profiles at the end of the excavation for a shallow and deep primary retaining wall in tests JP13 and JP18 respectively

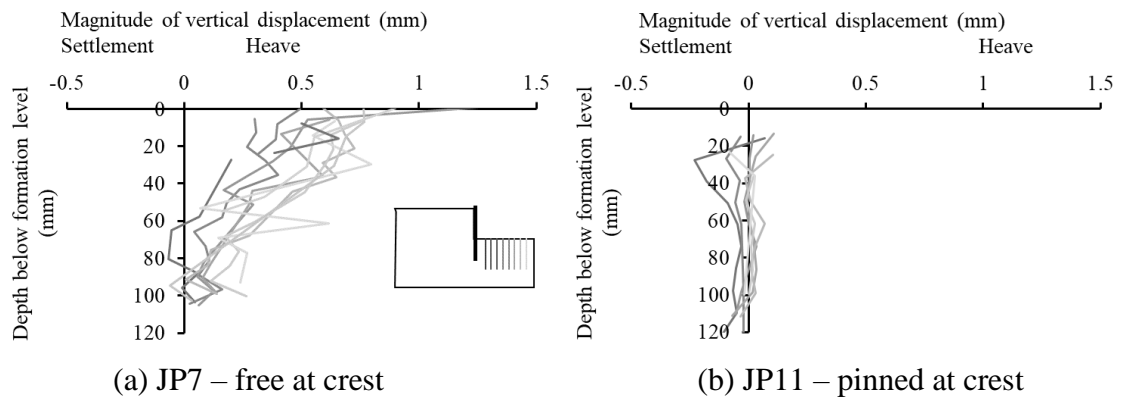


Figure 7.24 Vertical movements across the formation level of reference excavations plotted at an overburden pressure of 50kPa showing (a) free unrestrained wall crest; (b) wall fixed at crest

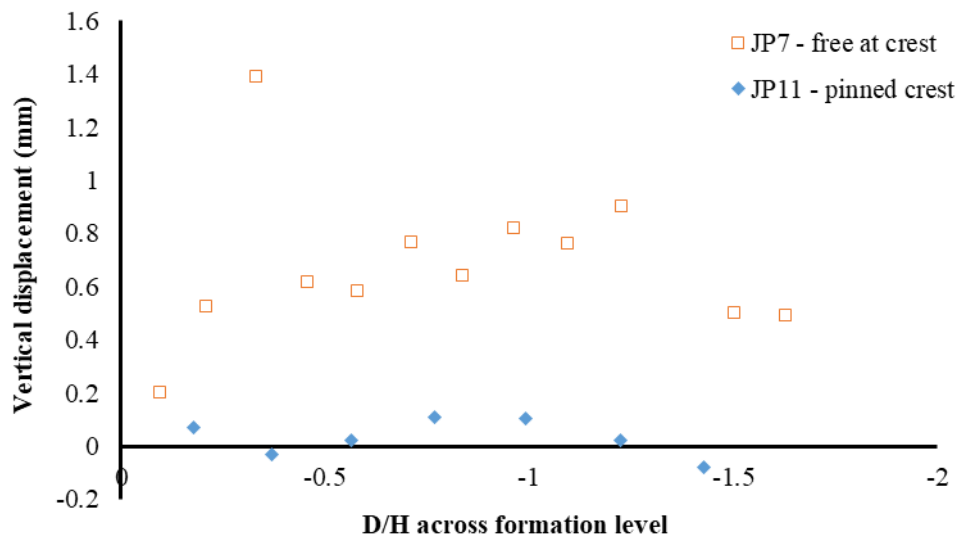


Figure 7.25 Heave profile at 50kPa overburden pressure illustrating the vertical displacement across the formation level for excavations with free and fixed crests

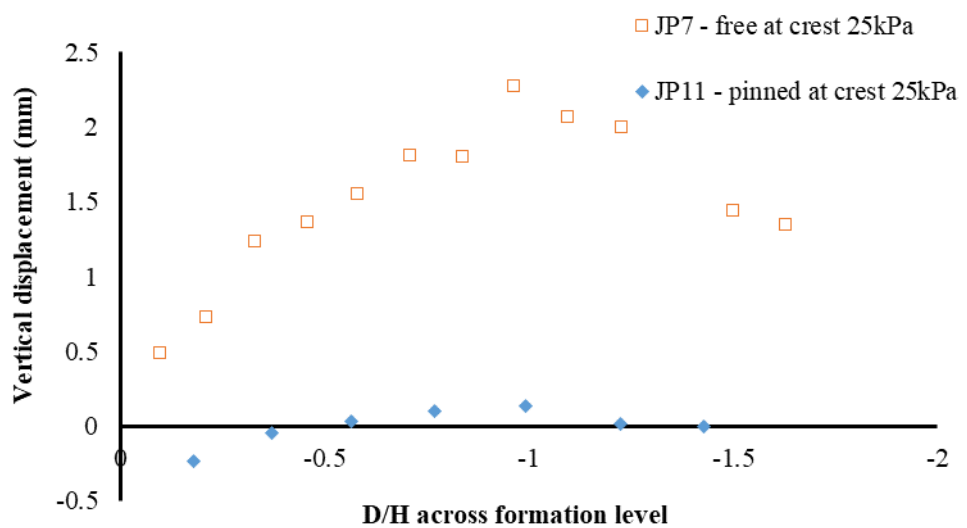


Figure 7.26 Heave profile at 25kPa overburden pressure illustrating the vertical displacement across the formation level for excavations with free and fixed crests

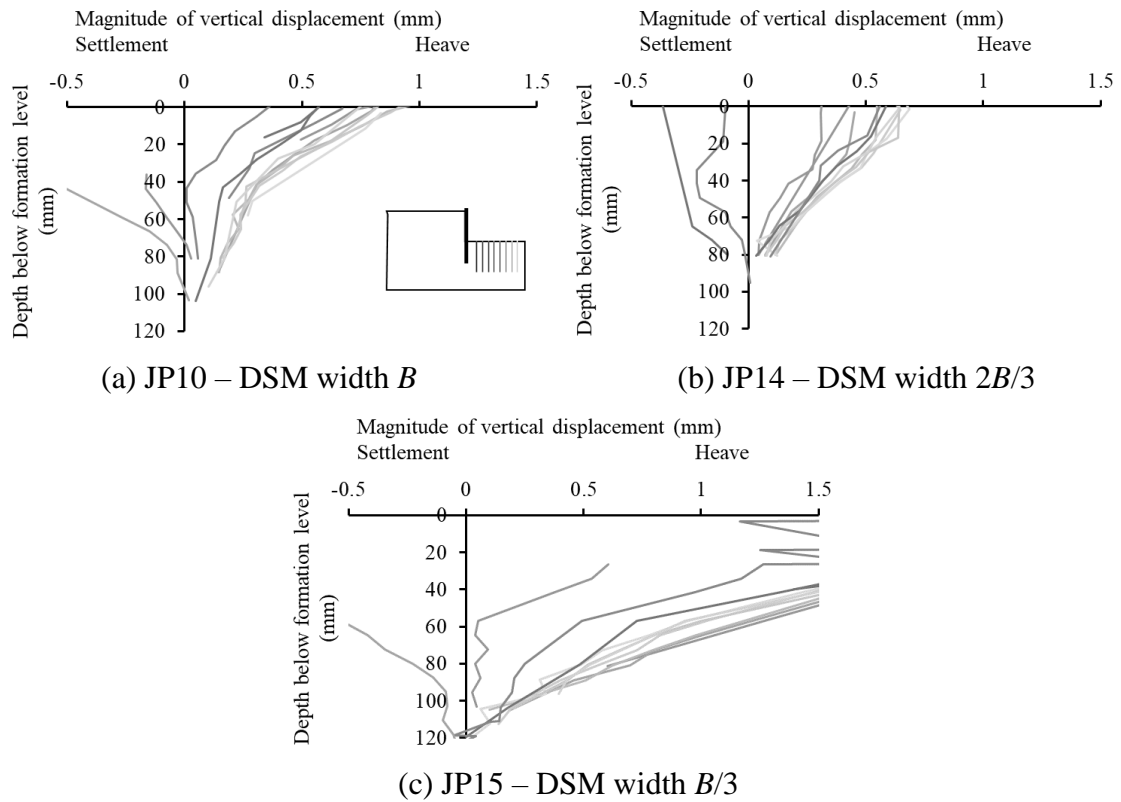


Figure 7.27 Vertical displacements for DSM excavations of the following widths (a) B , (b) $2B/3$ and (c) $B/3$

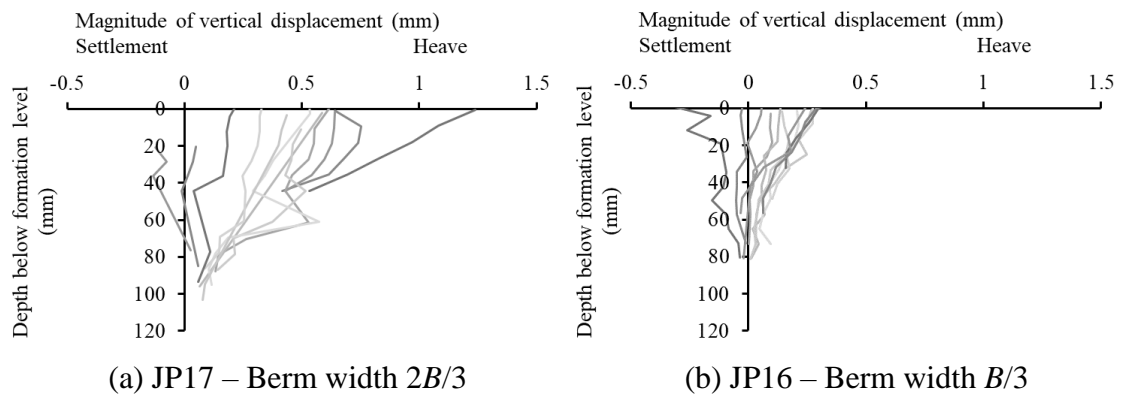


Figure 7.28 Vertical displacements for bermed excavations of widths (a) $2B/3$ and (b) $B/3$ all of which were taken at an overburden pressure of 80kPa in the main excavation area

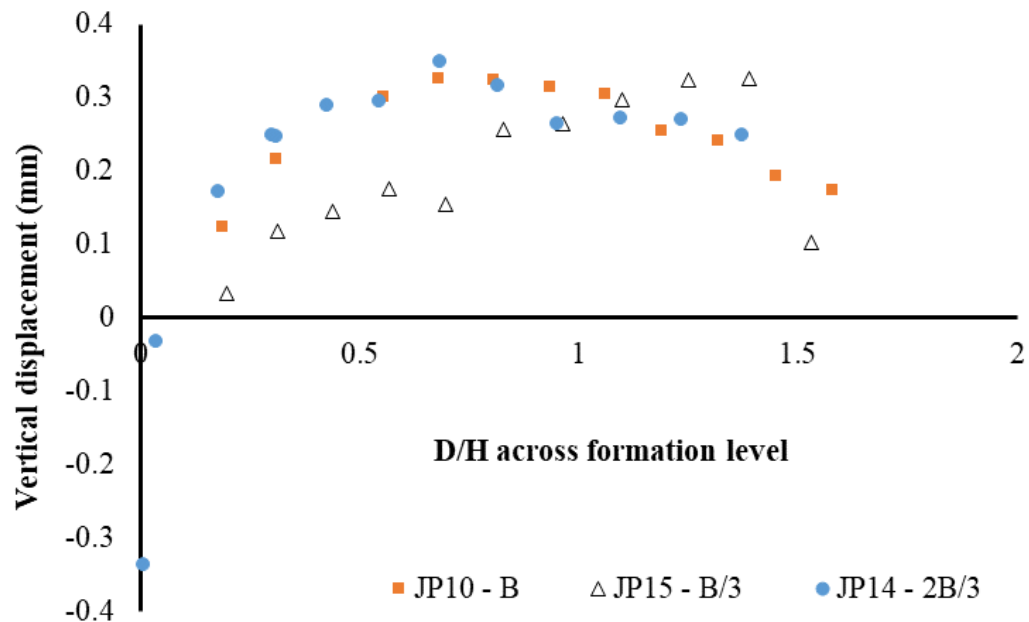


Figure 7.29 Heave profiles of various DSM geometries at 50kPa overburden pressure

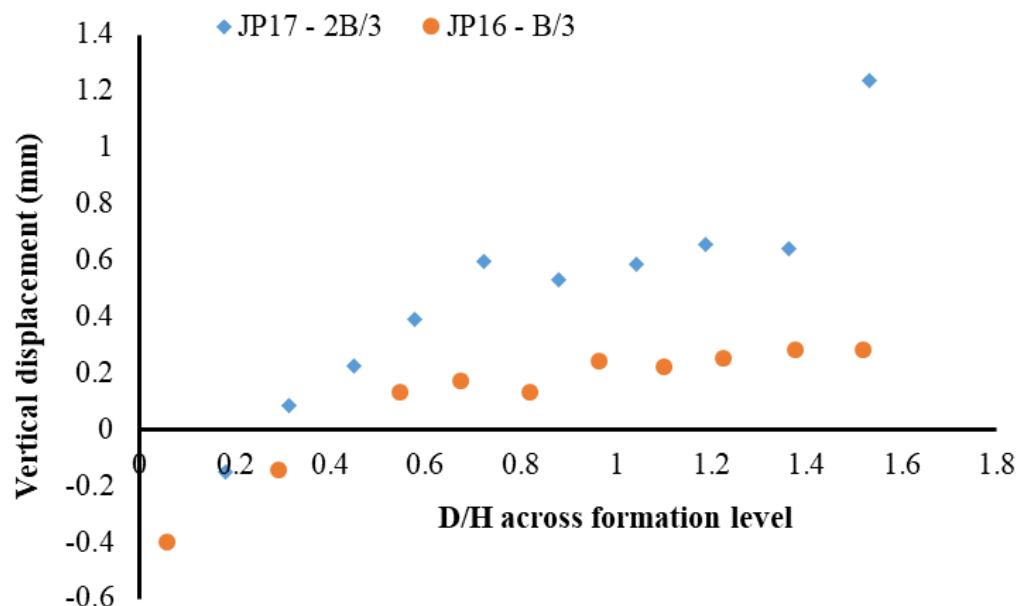


Figure 7.30 Heave profiles of the two bermed excavation widths recorded when the overburden pressure in the main excavation reached 80kPa

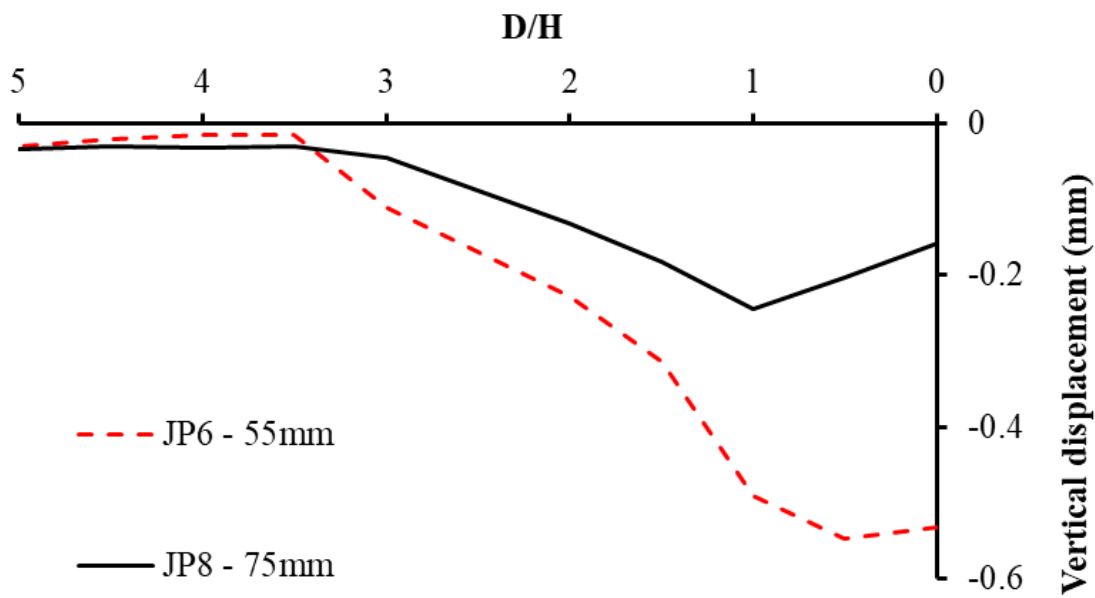


Figure 7.31 Surface settlement profile of the underwater excavations upon complete removal of the overburden pressure

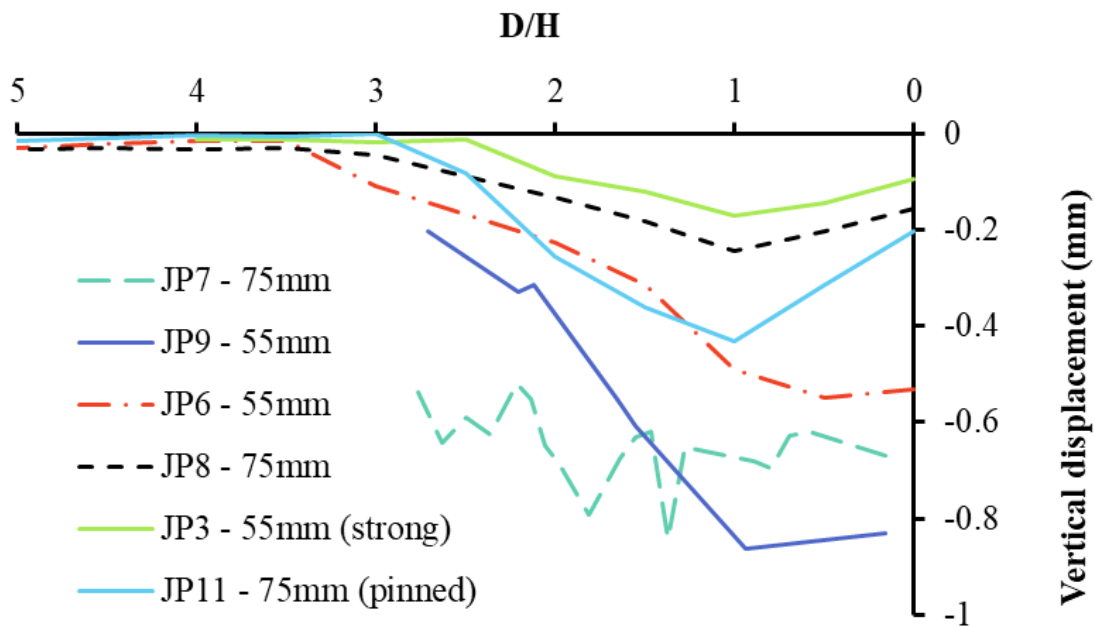


Figure 7.32 Surface settlement profile of reference tests at an overburden pressure of 74kPa

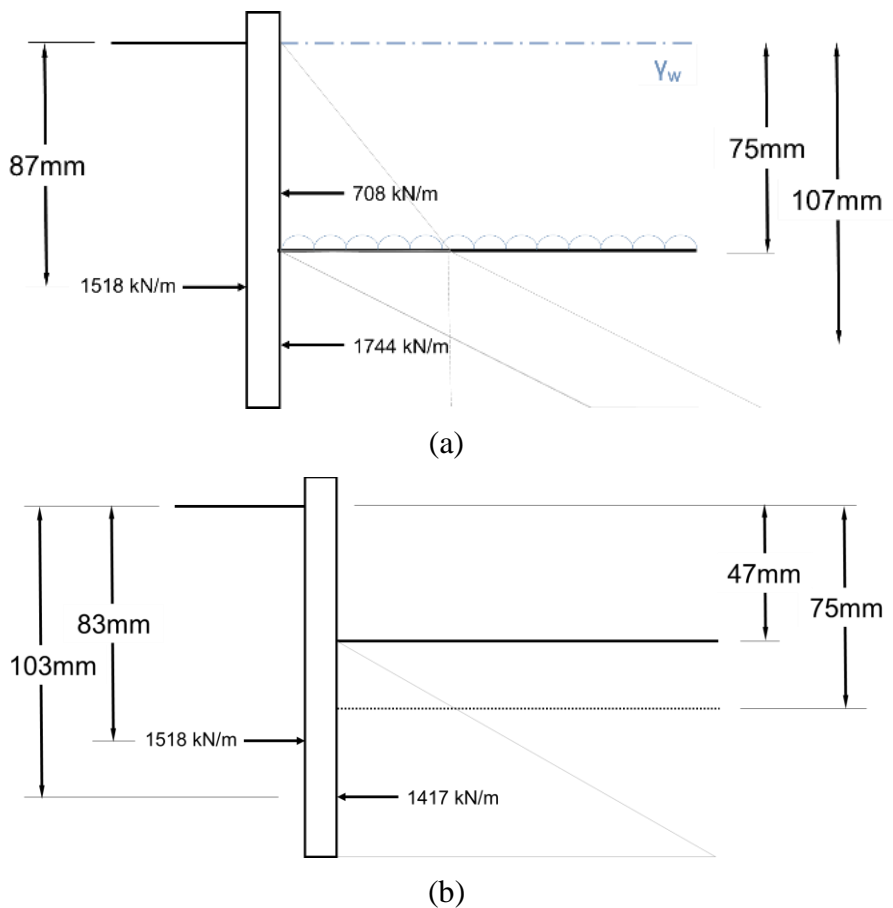


Figure 7.33 Comparison of passive pressures acting on wall of 55mm embedment in the underwater excavation and the reference test with an overburden pressure of 74kPa acting at the formation

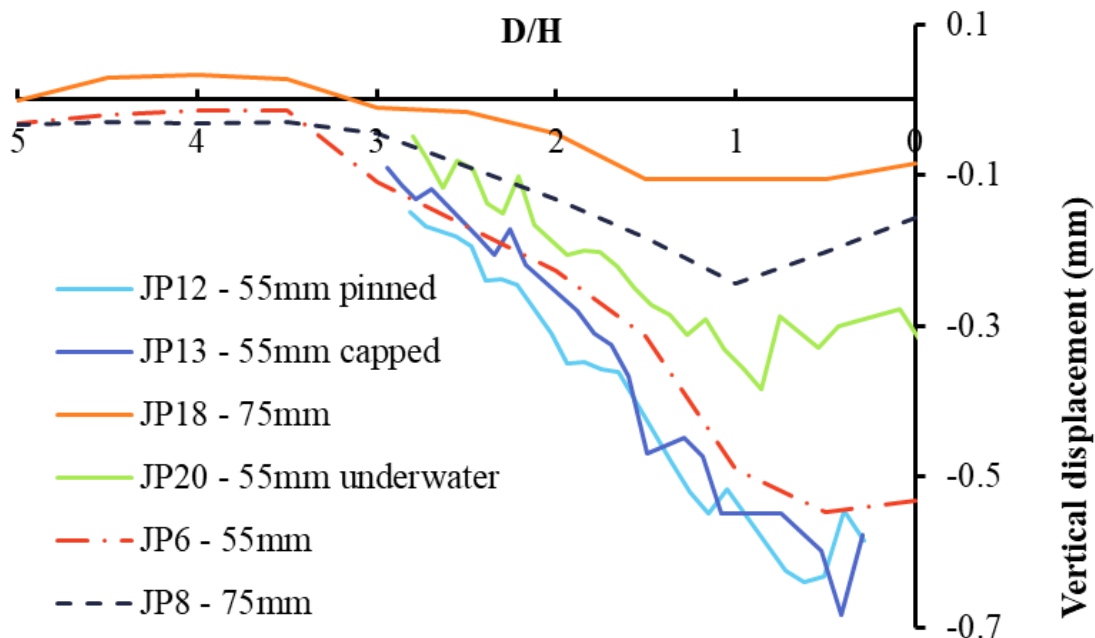


Figure 7.34 Surface settlement profiles of various double wall tests under a 74kPa overburden pressure plotted in relation to the underwater surface settlements at the end of the excavation

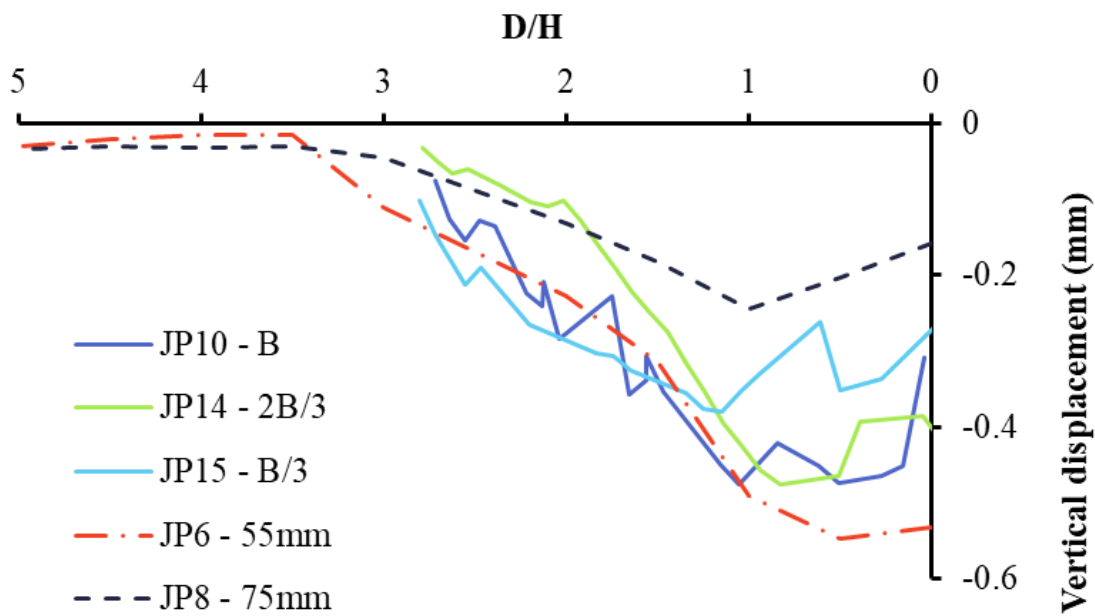


Figure 7.35 Surface settlement profiles of the different DSM geometries under a 74kPa overburden pressure compared the underwater surface settlements at the end of the excavation

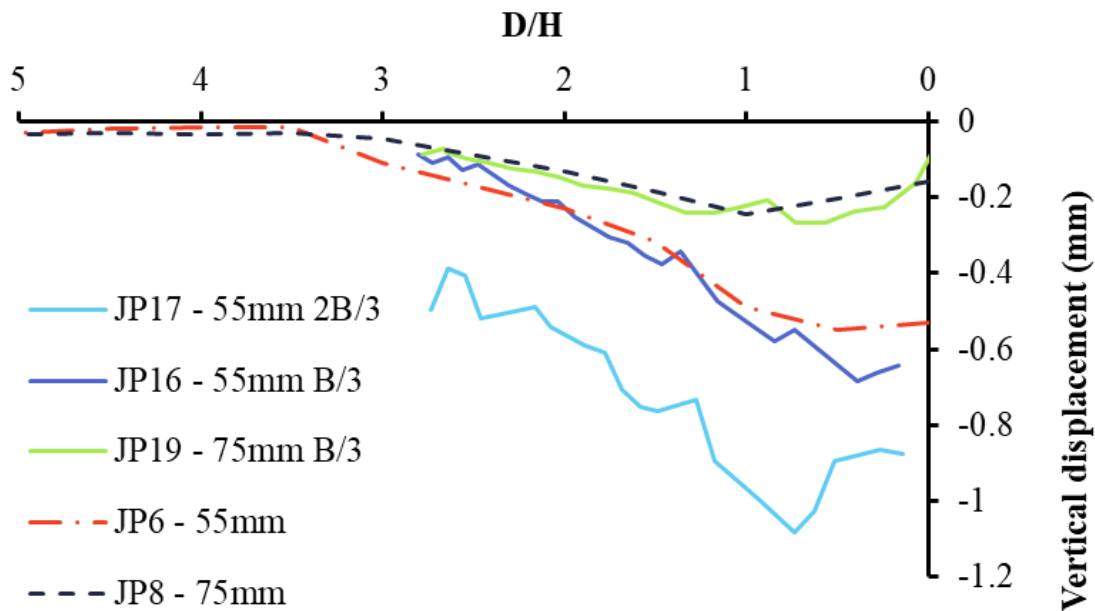


Figure 7.36 Surface settlement profiles of the bermed excavations where the pressure in the main excavation bag was 80kPa and the berm applied a surcharge of 100kPa

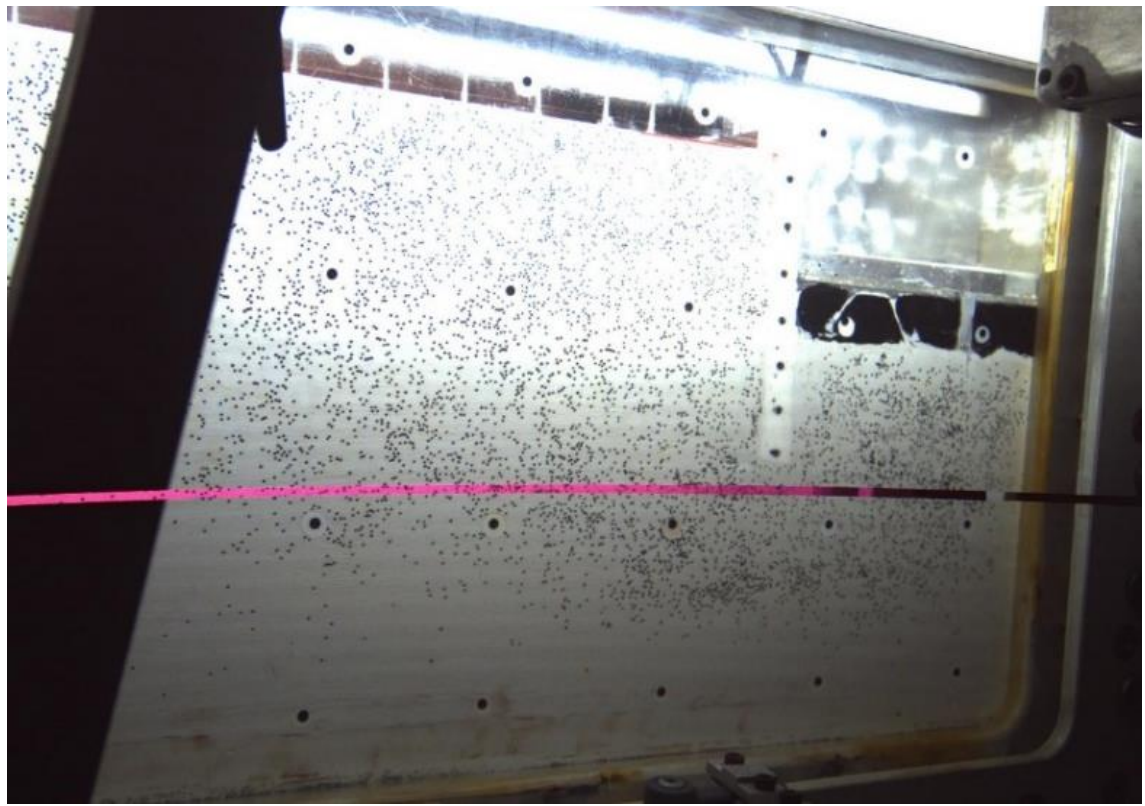


Figure 7.37 Example of the quality of images obtained from test JP17 showing extreme light exposure and interference

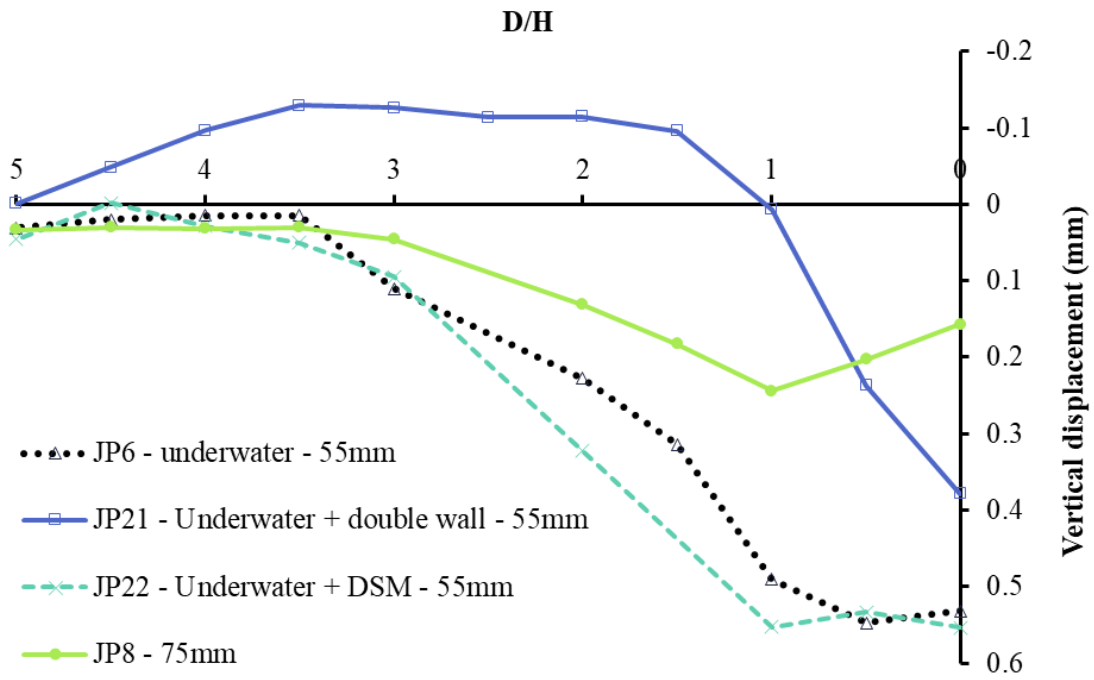


Figure 7.38 Surface settlement profiles of underwater excavations combined with a double wall or DSM configuration all taken at the end of the excavation

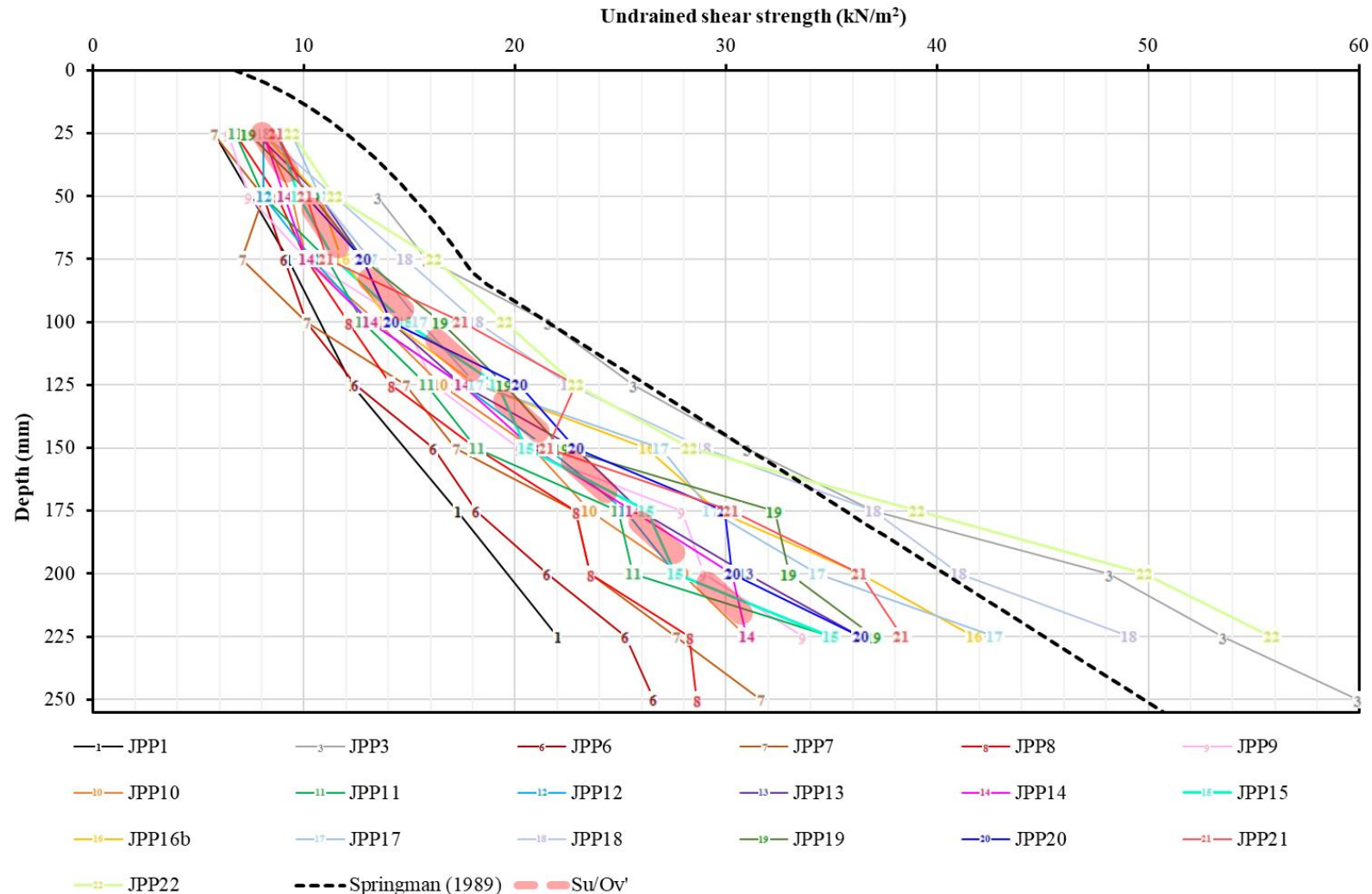
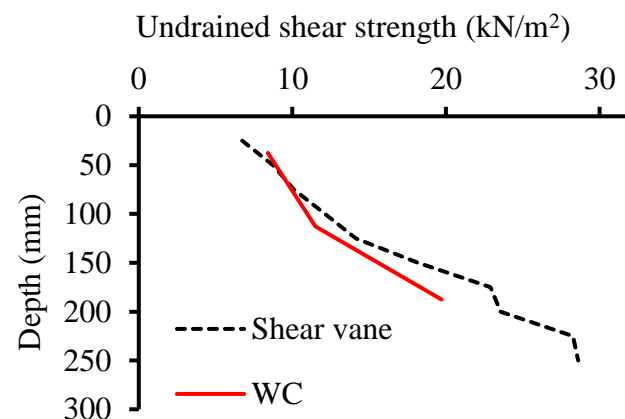
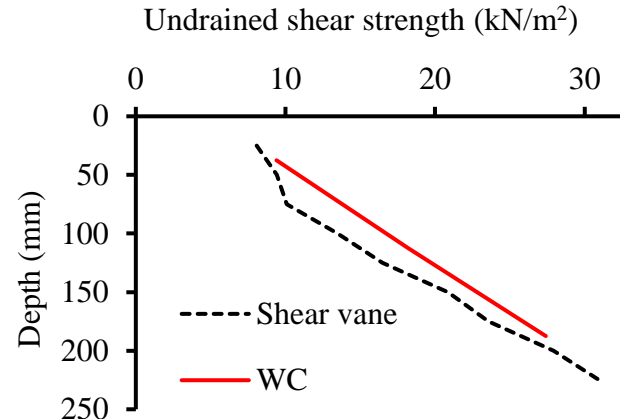


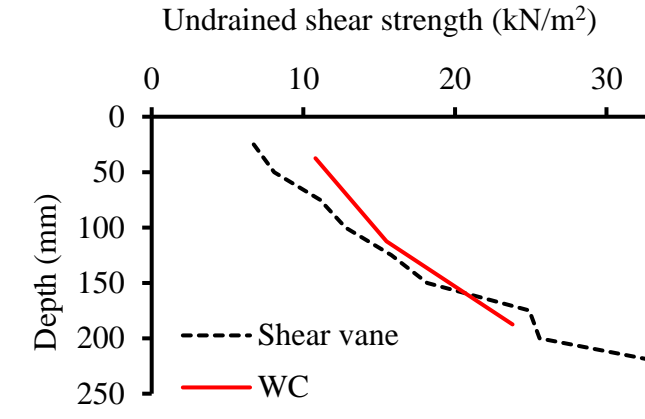
Figure 7.39 Undrained shear strength profiles from centrifuge tests and theoretical profile based on Springman (1989) empirical formula and S_u/σ_v' ratio for soft clays



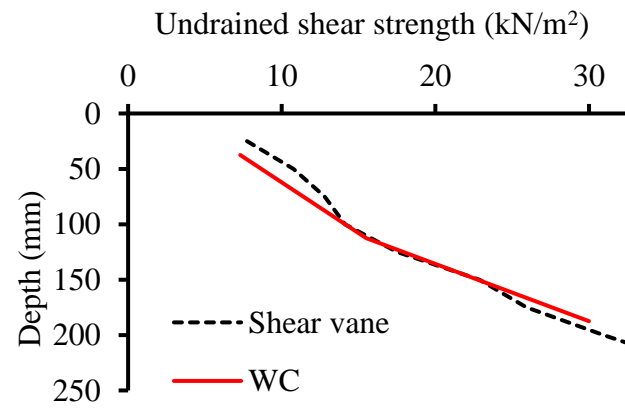
(a) JP8 – underwater, 75mm embedment



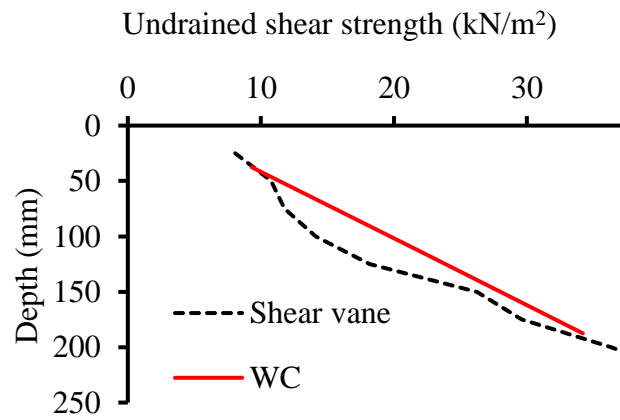
(b) JP10 – DSM, B, 55mm embedment



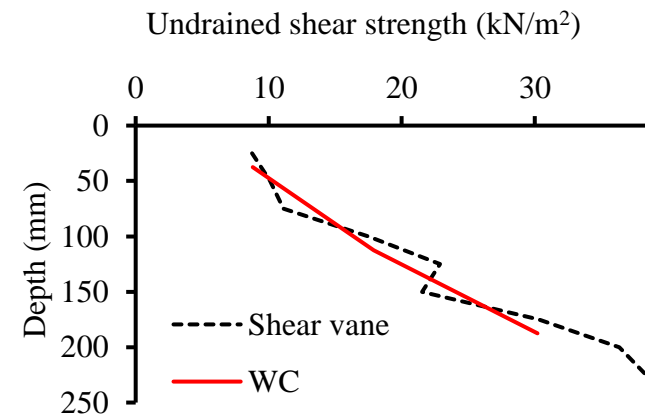
(c) JP11 – reference test, pinned, 75mm embedment



(d) JP13 – double wall, fixed at crest, 55mm embedment

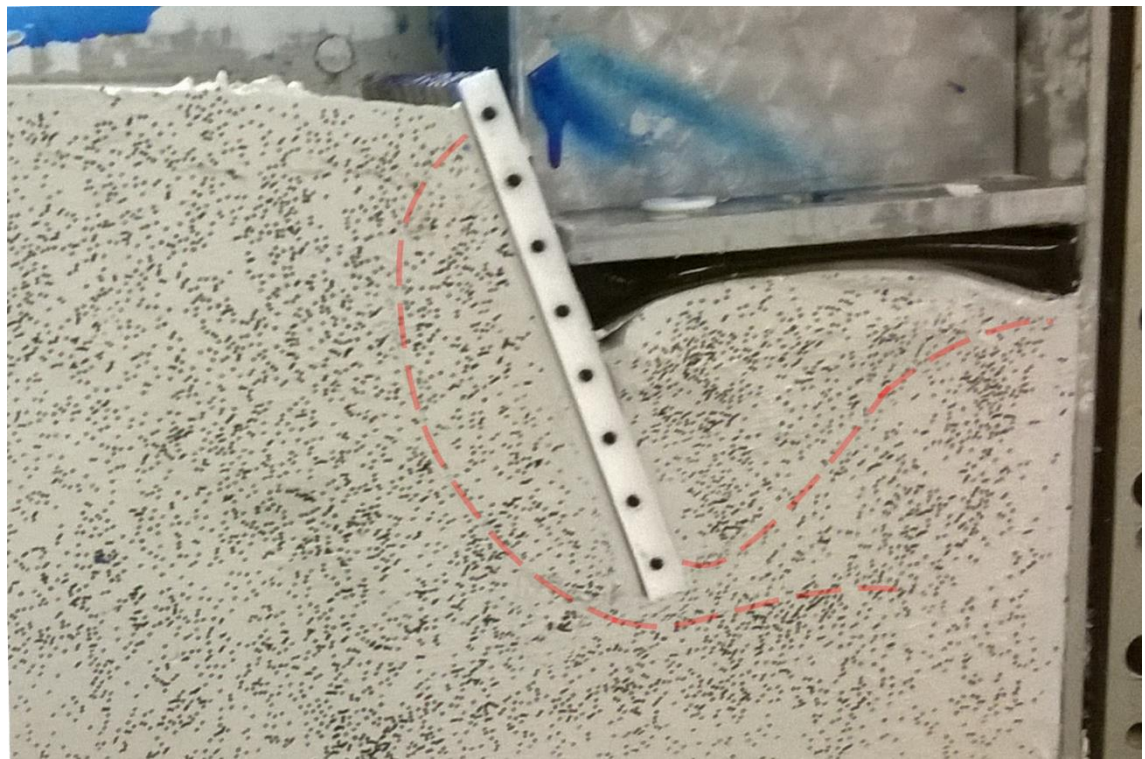


(e) JP16 – Berm, B/3, 55mm embedment

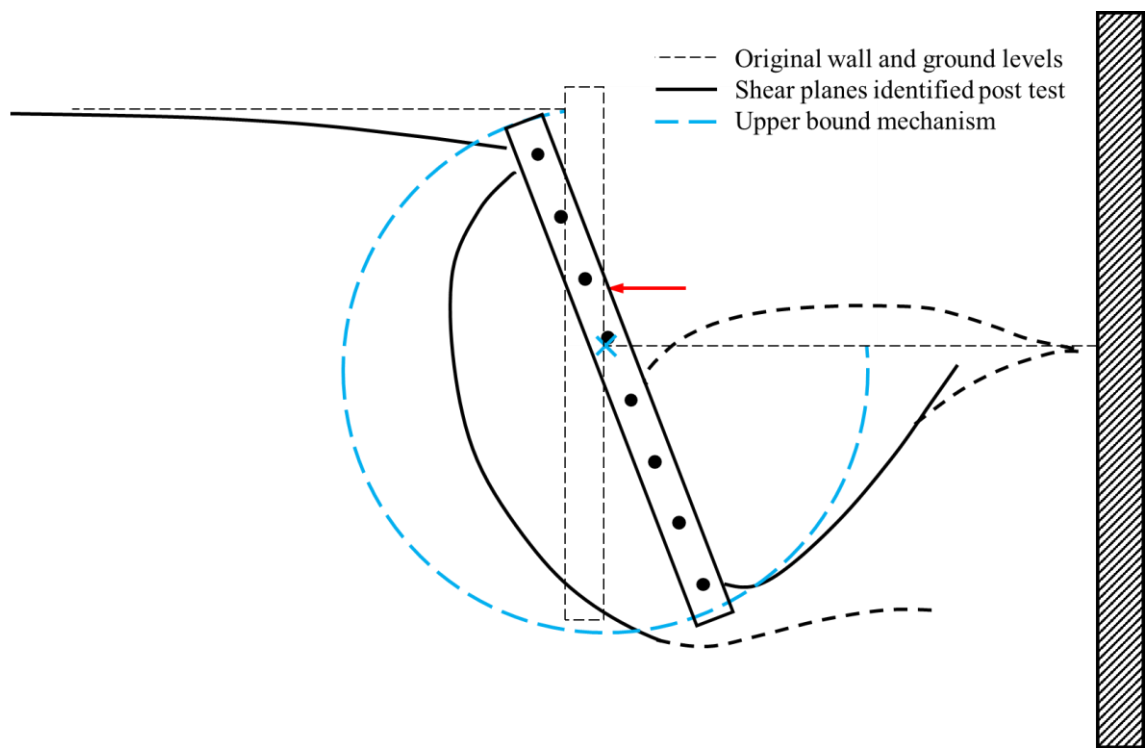


(f) JP21 – combined underwater and double wall, 55mm embedment

Figure 7.40 Comparison between undrained shear strengths measured with shear vane and computed from water contents (WC)

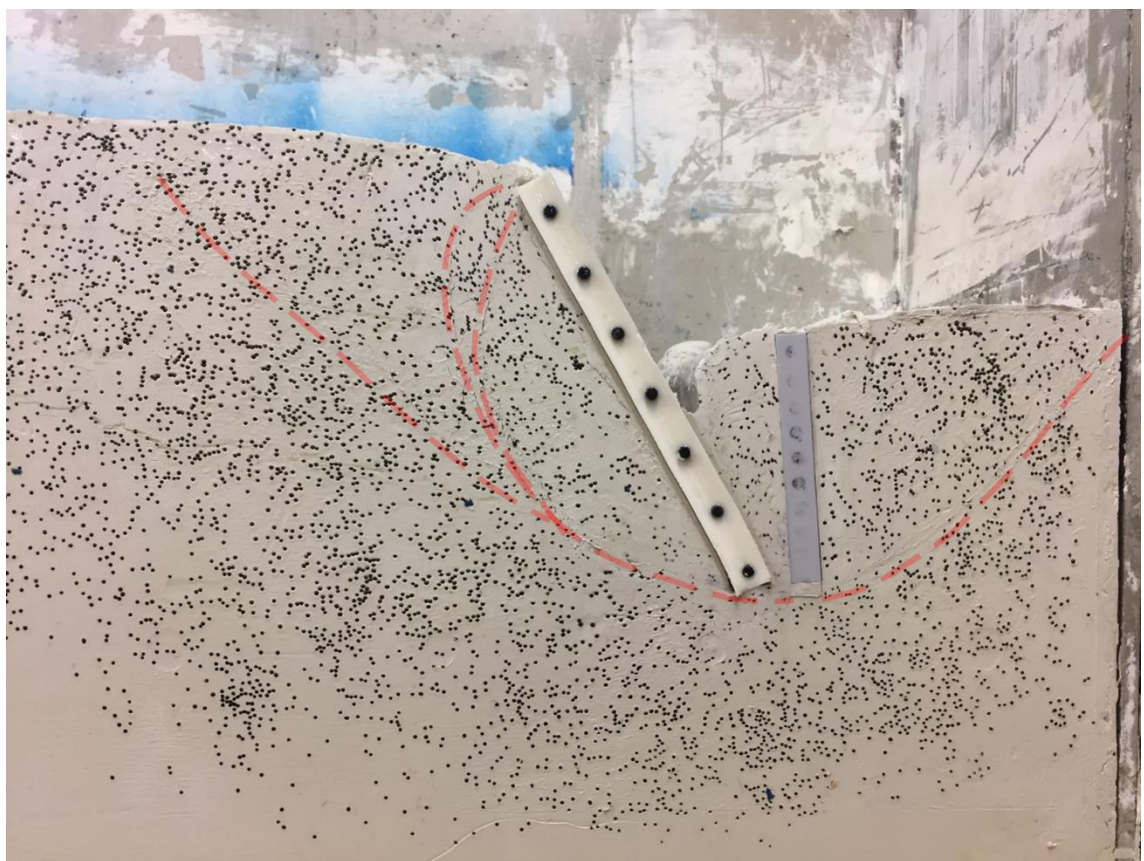


(a) Photograph of excavation formation and shear planes in soil

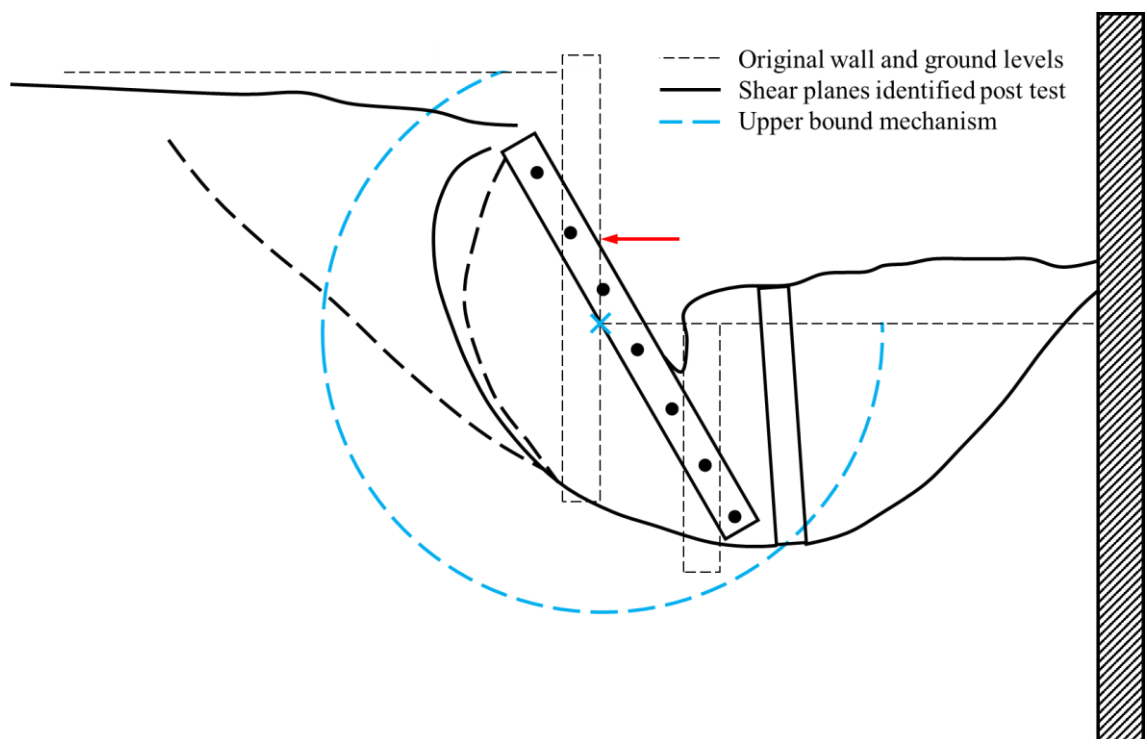


(b) Shear planes and upper bound mechanism

Figure 7.41 JP7 - Reference test with 75mm wall embedment

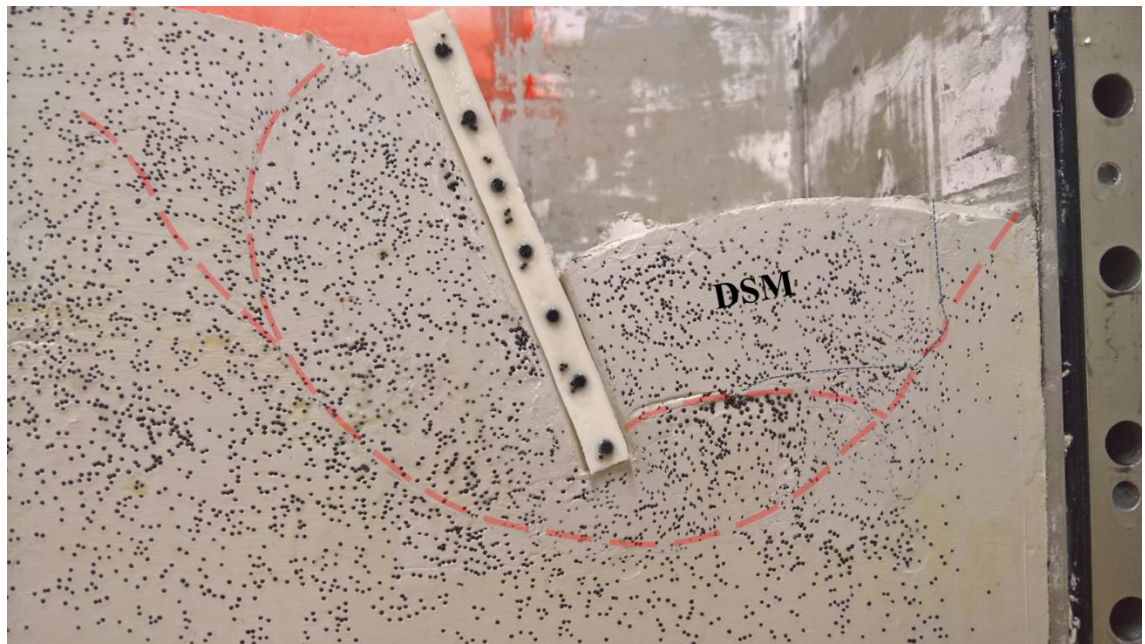


(a) Photograph of excavation formation and shear planes in soil

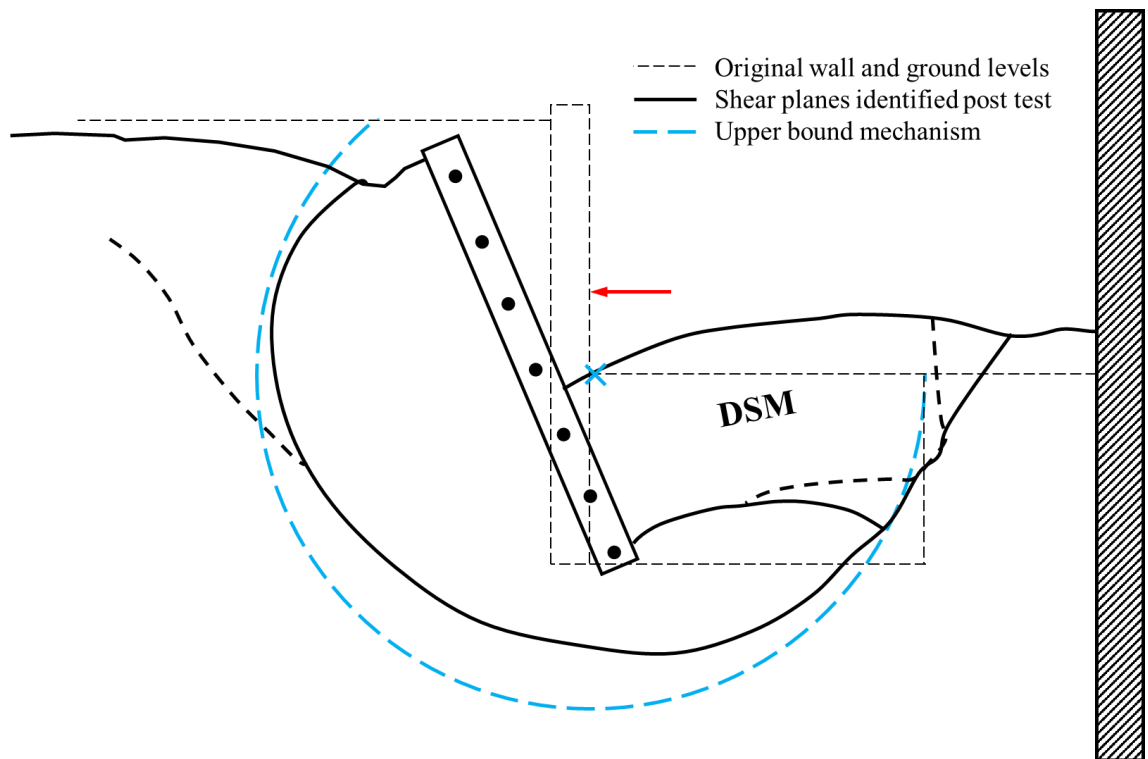


(b) Shear planes and upper bound mechanism

Figure 7.42 JP12 – Double wall test with 55mm wall embedment



(a) Photograph of excavation formation and shear planes in soil



(b) Shear planes and upper bound mechanism

Figure 7.43 JP14 – DSM of width $2B/3$ with 55mm wall embedment

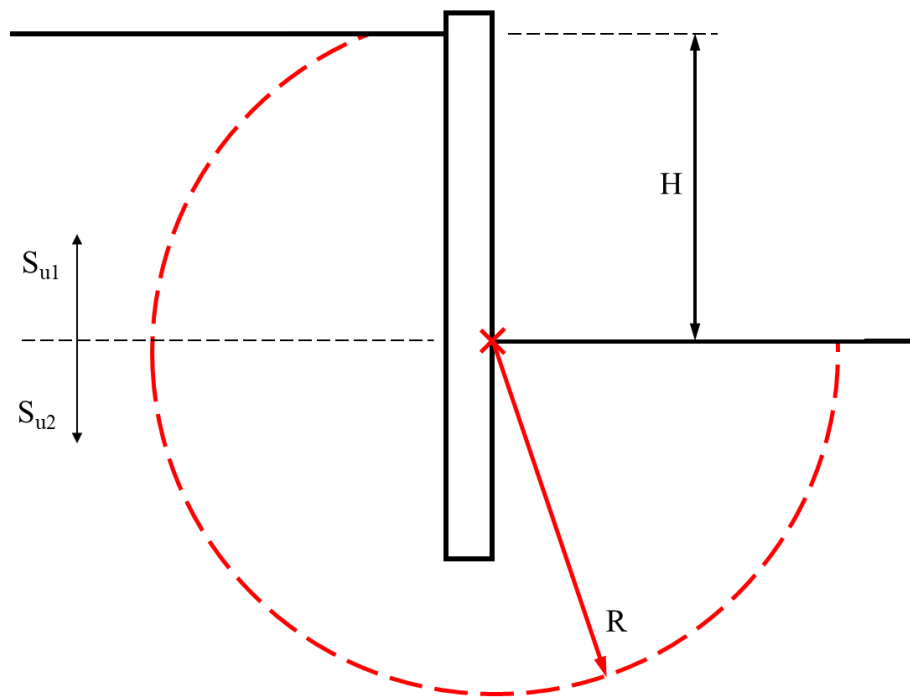


Figure 7.44 General failure mechanism identified in centrifuge tests

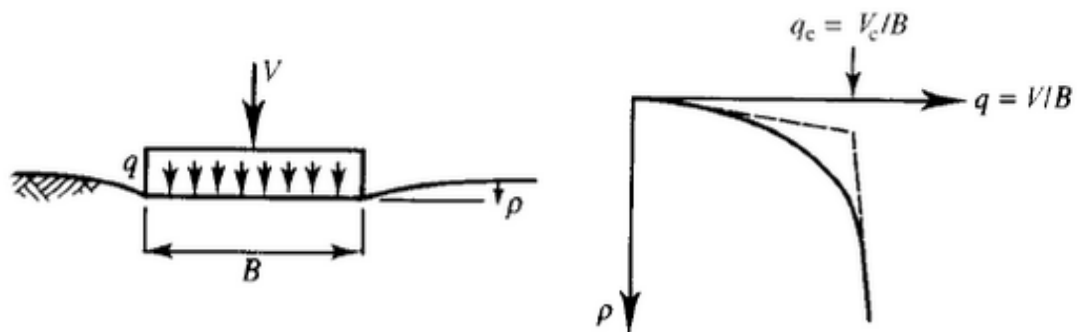


Figure 7.45 Interpretation of bearing capacity at collapse of a simple foundation (Atkinson, 2007)

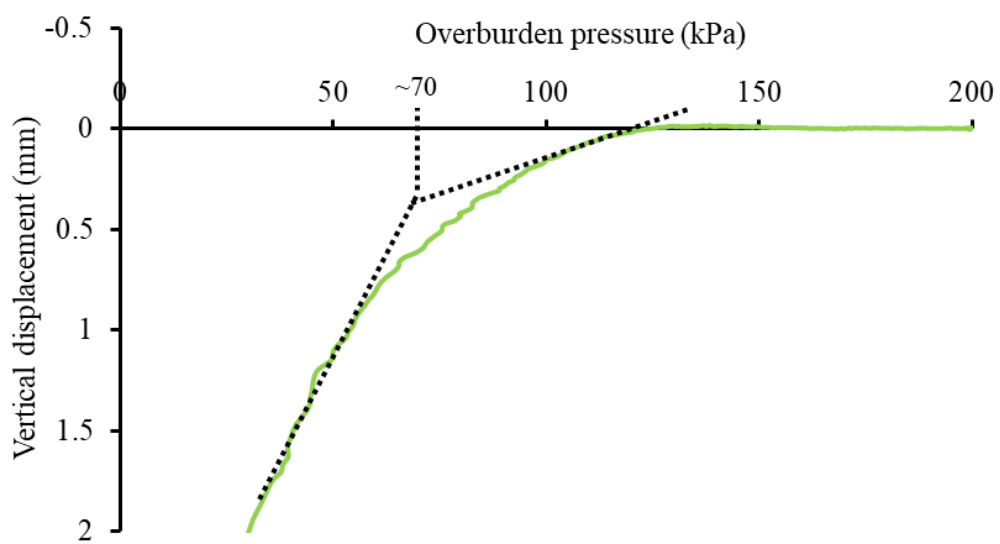


Figure 7.46 JP12 settlement against overburden pressure at distance H

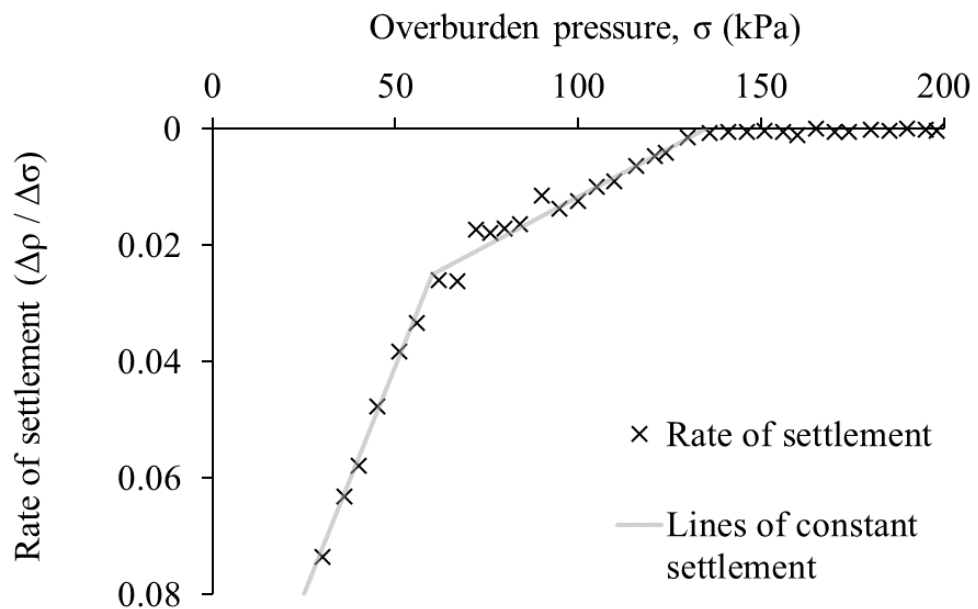


Figure 7.47 Rate of settlement plotted against overburden pressure in test JP12

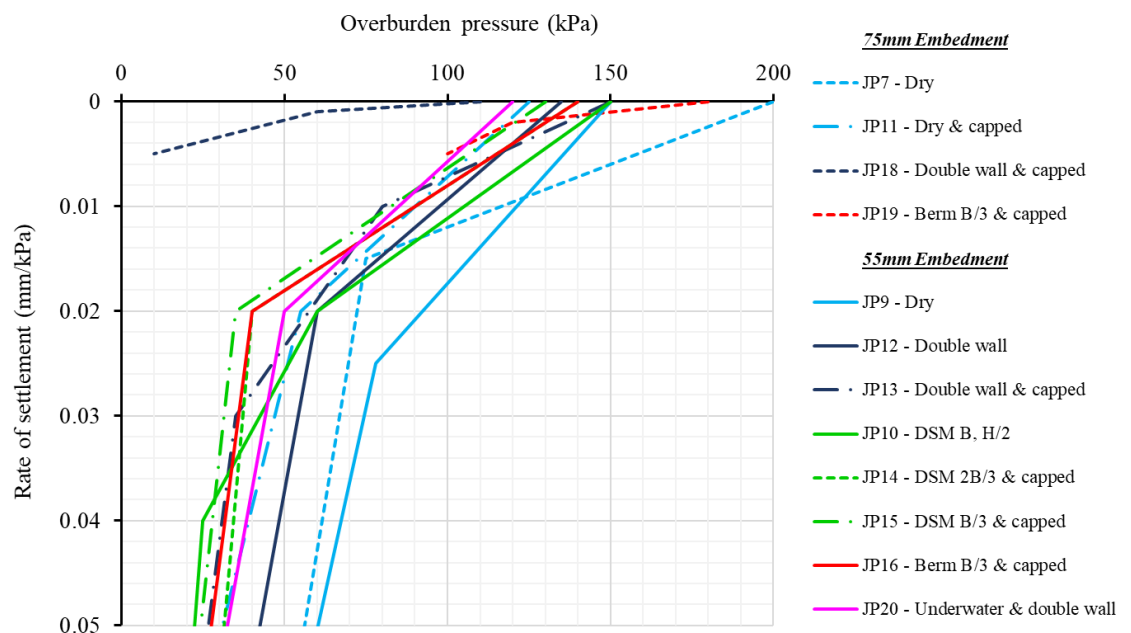


Figure 7.48 Rate of settlement against overburden pressure

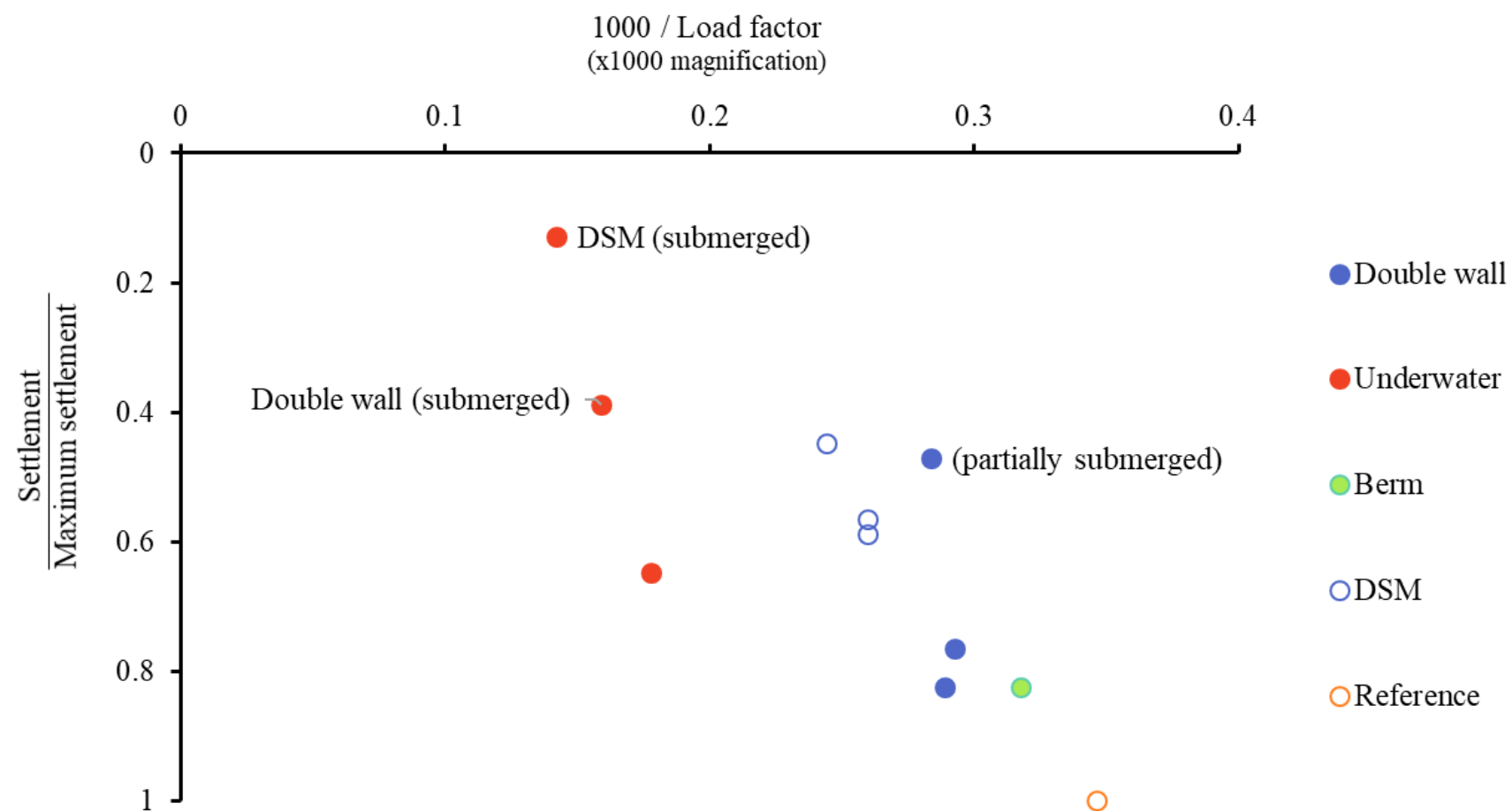
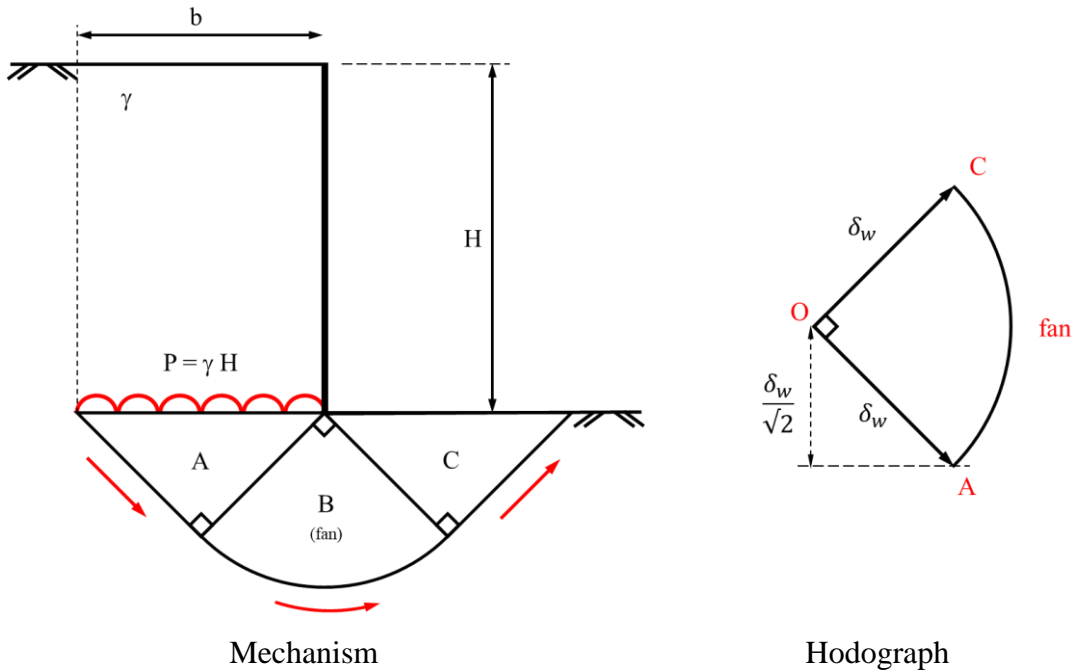


Figure 8.1 Graphical representation of relative effectiveness of influence of the retaining wall embedment and wall crest fixity on various excavation methods at an overburden pressure of 74kPa

APPENDIX A

A.1 CLASSIC FAILURE MECHANISM



External work done (E):

$$E = P b \frac{\delta_w}{\sqrt{2}}$$

Internal work done (W):

$$W = \left(S_u \frac{b}{\sqrt{2}} \delta_w \right)_{OA} + \left(S_u \frac{b}{\sqrt{2}} \delta_w \right)_{OC} + \left(2S_u \frac{b}{\sqrt{2}} \frac{\pi}{2} \delta_w \right)_{fan}$$

$$\therefore W = 2S_u \frac{b}{\sqrt{2}} \delta_w (1 + \frac{\pi}{2})$$

Equating work done; $E = W$ to evaluate P

$$P b \frac{\delta_w}{\sqrt{2}} = 2S_u \frac{b}{\sqrt{2}} \delta_w (1 + \frac{\pi}{2})$$

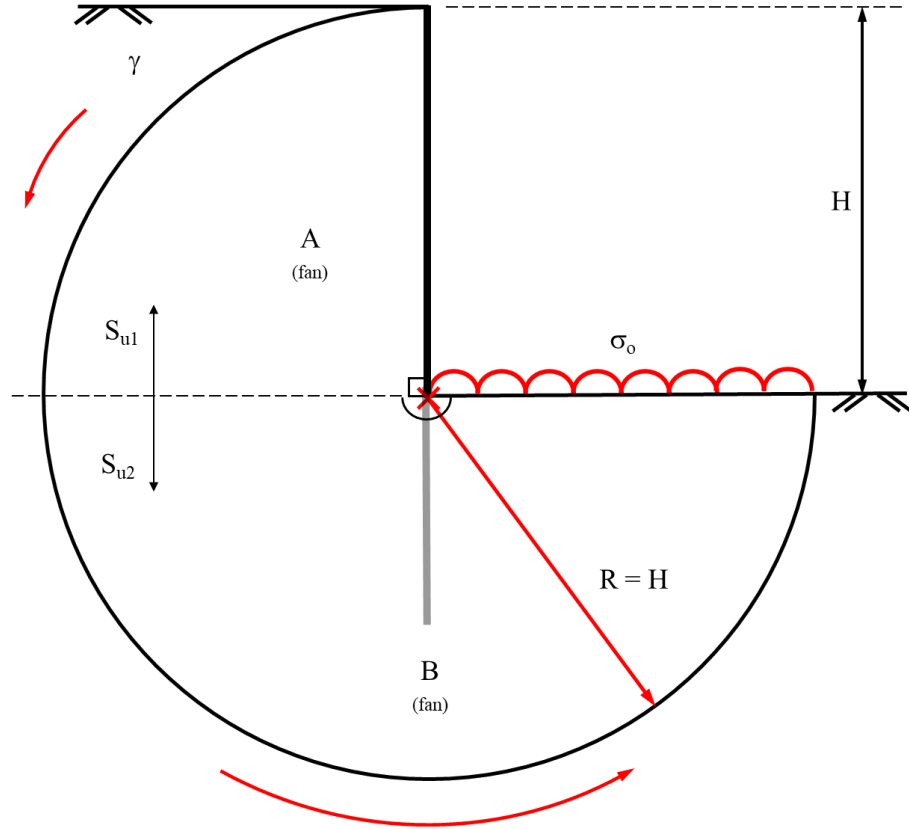
$$P = 2S_u (1 + \frac{\pi}{2}) \quad \text{where } P = \gamma H$$

$$\gamma H = 2S_u (1 + \frac{\pi}{2}) = S_u (2 + \pi)$$

$$\therefore H = \frac{5.14 S_u}{\gamma} = \frac{N S_u}{\gamma}$$

A.2 UPPER BOUND MECHANISM BASED ON CENTRIFUGE TEST OBSERVATIONS

A.2.1 Reference test:



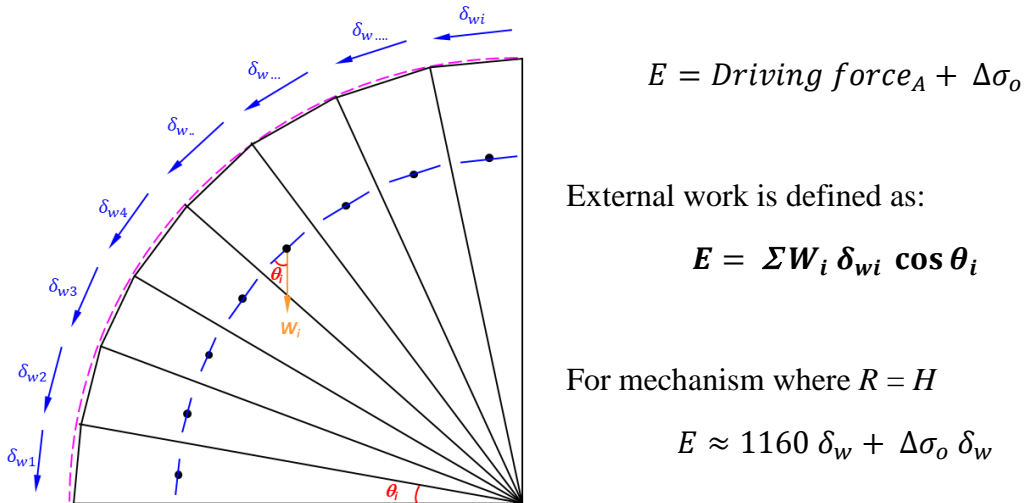
Internal work done (W):

$$W = (\Sigma S_u r \delta_w \delta\theta) + (\Sigma S_u r \delta_w \delta\theta) = \Sigma (2S_u r \delta_w \delta\theta)$$

For 2 different fans:

$$W = \left(2 S_{u1} R \delta_w \frac{\pi}{2} \right)_A + (2 S_{u2} R \delta_w \pi)_B$$

External work done (E) considered as a series of small wedges:



Note that $\Delta\sigma_o = \gamma \Delta H R$

Equating E = W

$$1160 \delta_w + \Delta\sigma_o \delta_w = \left(2 S_{u1} R \delta_w \frac{\pi}{2} \right)_A + (2 S_{u2} R \delta_w \pi)_B$$

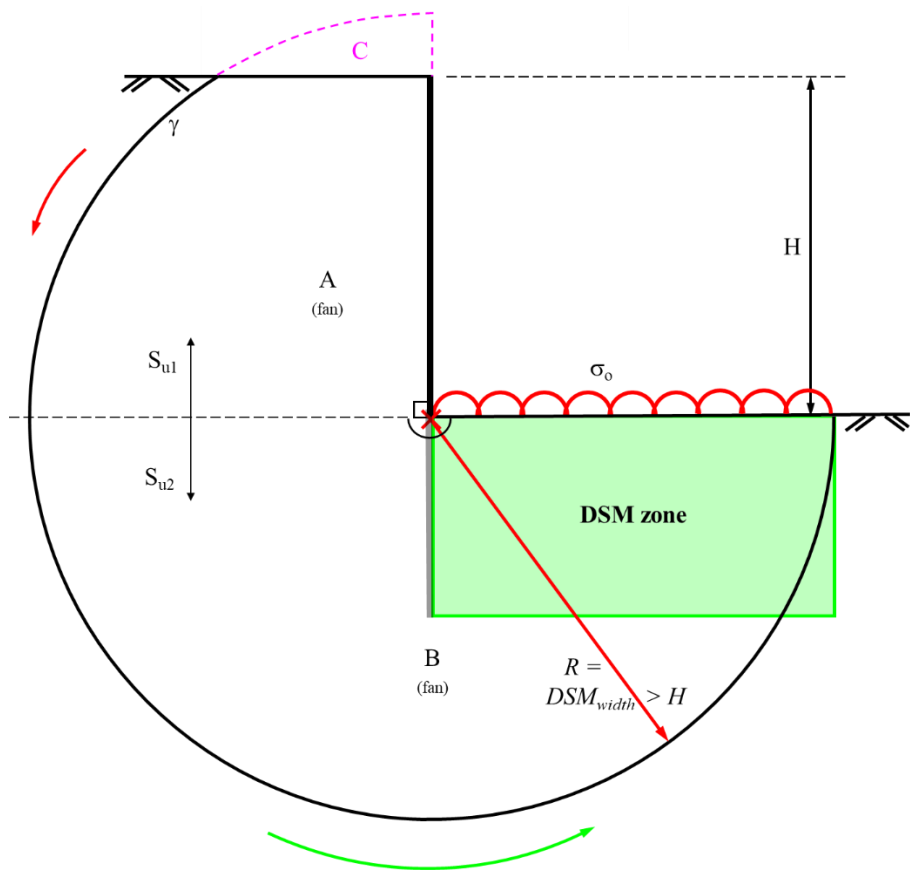
$$1160 + \gamma \Delta H R = 2 R \pi \left(\frac{S_{u1}}{2} + S_{u2} \right)$$

$$\therefore \Delta H = \frac{2 R \pi \left(\frac{S_{u1}}{2} + S_{u2} \right) - 1160}{R \gamma}$$

In the reference test, $R = H = 12\text{m}$ (at prototype scale) and $\gamma = 16\text{kN/m}^2$

$$\Delta H = \frac{24 \pi \left(\frac{S_{u1}}{2} + S_{u2} \right) - 1160}{12 \times 16}$$

A.2.2 DSM test:



Internal work done (W); assumed as approximately equal to that of the reference test*;

$$W = 2S_u b / \sqrt{2} \delta_w (1 + \pi/2)$$

*Overestimation of internal work done at section C is countered by the failure mechanism passing through the small area of increased undrained shear strength of the DSM block.

External work done (E):

$$E = (\Sigma W_i \delta_{wi} \cos \theta_i) + \Delta\sigma_o - C$$

$$\therefore E = (\Sigma W_i \delta_{wi} \cos \theta_i) - \left(\gamma/2 [R - H] \sqrt{R^2 - H^2} \right) + \Delta\sigma_o$$

For $R = 16\text{m}$ (width of DSM in JP14 at prototype scale)

$$E = 1717 \delta_w + \Delta\sigma_o \delta_w$$

Equating $E = W$

$$1717 \delta_w + \Delta\sigma_o \delta_w = \left(2 S_{u1} R \delta_w \frac{\pi}{2} \right)_A + (2 S_{u2} R \delta_w \pi)_B$$

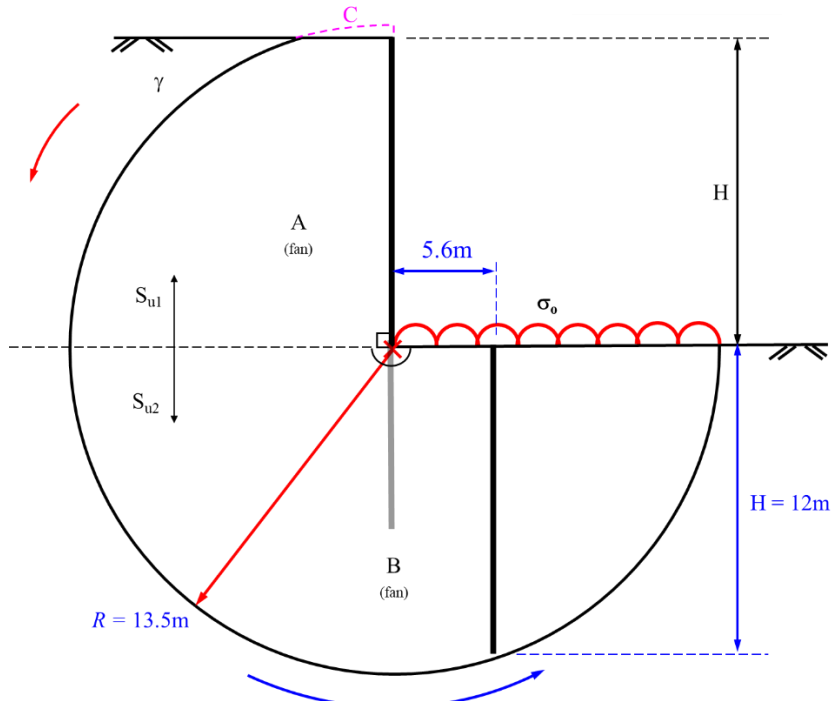
$$1160 + \gamma \Delta H R = 2 R \pi \left(\frac{S_{u1}}{2} + S_{u2} \right)$$

$$\therefore \Delta H = \frac{2 R \pi \left(\frac{S_{u1}}{2} + S_{u2} \right) - 1717}{R \gamma}$$

In the DSM test, $R = 16\text{m}$ (at prototype scale) and $\gamma = 16\text{kN/m}^2$

$$\Delta H = \frac{32 \pi \left(\frac{S_{u1}}{2} + S_{u2} \right) - 1717}{16^2}$$

A.2.3 Double wall test:



Internal work done (W); assumed as approximately equal to that of the reference test*;

$$W = 2S_u b / \sqrt{2} \delta_w (1 + \pi/2)$$

*Overestimation of internal work done at C is negligible.

External work done (E):

$$E = (\Sigma W_i \delta_{wi} \cos \theta_i) + \Delta\sigma_o - C$$

$$\therefore E = (\Sigma W_i \delta_{wi} \cos \theta_i) - \left(\gamma/2 [R - H] \sqrt{R^2 - H^2} \right) + \Delta\sigma_o$$

Radius of mechanism is constant owing to the secondary wall length and position being constant across all tests hence, $R = 13.5\text{m}$ at prototype scale.

$$E = 1400 \delta_w + \Delta\sigma_o \delta_w$$

Equating $E = W$

$$1400 \delta_w + \Delta\sigma_o \delta_w = \left(2 S_{u1} R \delta_w \frac{\pi}{2} \right)_A + (2 S_{u2} R \delta_w \pi)_B$$

$$1400 + \gamma \Delta H R = 2 R \pi \left(\frac{S_{u1}}{2} + S_{u2} \right)$$

$$\therefore \Delta H = \frac{2 R \pi \left(\frac{S_{u1}}{2} + S_{u2} \right) - 1400}{R \gamma}$$

In the double wall test, $R = 13.5\text{m}$ (at prototype scale) and $\gamma = 16\text{kN/m}^2$

$$\Delta H = \frac{27 \pi \left(\frac{S_{u1}}{2} + S_{u2} \right) - 1400}{16 \times 13.5}$$

A.2.4 Bermed excavation test:

Similarly, for a bermed excavation, assume that $R = 14.25\text{m}$

Therefore,

$$\Delta H = \frac{28.5 \pi \left(\frac{S_{u1}}{2} + S_{u2} \right) - 1500}{16 \times 14.25}$$